SCIENTIFIC BASIS OF MODERN TECHNOLOGIES: EXPERIENCE AND PROSPECTS

Edited by

Y.I. Shalapko

L.A. Dobrzanski

JAREMCHE 2011

SCIENTIFIC BASIS OF MODERN TECHNOLOGY: EXPERIENCE AND PROSPECTS. Monograph: edited by Shalapko Y.I. and Dobrzanski L.A. - 2011. – 628 p.

Monograph prepared at the Department of Principles of Engineering Mechanics of Khmelnitsky National University

Ukraine, 29016, Khmelnytsky Str. Institutskaya 11,
Khmelnitsky National University,
e-mail: shalapko@yahoo.com

5. NEW ASPECTS IN TECHNOLOGIES OF PROCESSING OF MATERIALS 398

PREFACE

The idea of this monograph emerged for the year to 50-year anniversary of Khmelnitsky National University. Nearing the time not only to summarize the half-century history of the University, but also the election of new areas of research, and creating new educational programs to solve technological problems of modern society.

This collective work is a reflection of fruitful scientific collaboration, which conduct scientific centers of Ukraine, Poland, Slovakia and Russia. Publication of a monograph entitled "Scientific basis of modern technology: Experience and Prospects" embracing several major trends that are subject to interest and methods for achieving results have a "language of purpose" - man-made solutions and humanitarian problems in society. This took advantage of editors who picked up and lined of books materials so that it provided an opportunity to the reader find out with a broad specificity of the industrial development of Eastern Europe, about new technological solutions in production and new methods of building materials, tasks of tribology , processing of materials, processes, measurement , mathematical modeling. In our view substantial interest the reader may cause material devoted to the problems in bioengineering and biomechanics. In addition the book may be useful for young researchers, graduate, masters to formulate new ideas in the field of new technologies and calculating their cost-effectiveness. The book consists of seven chapters:

1. Regional trends of innovative technologies for industrial development
2. Mathematical modeling of processes
3. Technology management quality and strength of engineering structures
4. Practical experience of the decision of problems tribologia
5. New aspects in technologies of processing of materials
6. New principles of technology of measurement
7. Experience of bioengineering technologies

The logic of the first chapter reflects the social problems of industrial society, connected with the history of the regions, the construction of economic relations, ecology, and quality of human life. Due to the different causes of problems and different goals towards their solution, they consist of multi-

directions activities of scientists. Some of these trends reflected in next six chapters of the monograph.

At present it is difficult to overestimate the methods of mathematical modeling and use of information technologies in all spheres of human activity. Along with impressive achievements in this area, recently there is quite a great problem in assessing the correct calculation errors. Development of the element base of modern computers and numerical modeling techniques have led to the paradoxical situation: on one hand may find the most difficult decision boundary problems, and the other - to practice persists difficulties in the reliable estimation error of numerical calculations. Exit from mathematical crisis could seek further development of analytical methods based on detection of new patterns of phenomena and effects on quality experimental data. On the other hand, is the development of information technology in the creation of artificial intelligence and neuroinformatics. Examples of processes of formalization of mathematical knowledge and its use in mathematical models of applications are presented in chapter 2.

Exhaustion of natural resources and saving energy costs requires a reduction of specific weigth of structures, on the other hand leads to their overloading. The last requires processing and hardening materials. In chapter 3 represented of laser and electric-sparks technologies, cold-spray of nanopowders, detonation spraying of carbide, ion nitriding. In chapter 4 dealt with aspects of the tribological contact interaction of structural materials and the problems of lubricating surfaces. It is important information relating to the processing of metals and metal alloys, textiles, plastics and building materials placed in chapter 5. Some fundamental decisions in the processes of measuring technology by radio engineering methods and electronic sensors are shown in chapter 6.

The last chapter is devoted significant achievement in the creation of new biomaterials for use in bioengineering and biomechanics. The basis of this section is a fragment of many-year works made in the Institute of Engineering Materials and Biomaterials of the Silesian University of Technology in Gliwice, Poland, enabling further works to improve many materials design methodology activities changed because of changes of expectations and contemporary

requirements of manufacturing of materials having required structure and utility properties. At present modeling, simulation and prediction of both the technological processes of manufacturing, processing, and forming their structure and properties, and especially of the service and use properties of materials, including those after long time service in the complex conditions, the development of safe materials and products technologies, the standardization of materials testing procedures, the development of the prediction methodology of the new materials behavior in service is necessary. The development of materials engineering and materials science features also one of the most essential elements of the scientific-, scientific and technical-, and innovative policy within the framework of the knowledge based economy, consisting in knowledge generation, treated as production, and in distribution and practical use of knowledge and information.

The editors express their sincere gratitude to the Rector of Khmelnitsky National University to Professor Mykola Skyba, Rector of Kielce University of Technology to Professor Stanislaw Adamczak, Rector of Cracow University of Technology to Professor Kazimierz Furtak, to the Director of the Institute of Mechanics and Computer Science of Khmelnytsky National University Ass. Professor George Drapak and Deans of the Mechanical Faculties of Kielce University of Technology to Professor Leszek Radziszewski, AGH University of Science and Technology to Professor Janusz Kowal and Cracow University of Technology Professor Leszek Wojnar for their support and cooperation in preparing for publication of monographs, as well as the entire editorial board and respected reviewers.

Khmelnitsky – Gliwice – Jaremche, October 2011

Ass. prof. dr hab. Ing. **Yuriy. I. Shalapko**
Institute of Mechanics and Computer Science,
Khmelnitsky National University, Ukraine

Prof. dr hab. Ing. **Leszek. A. Dobrzanski dr h.c.**
Institute of Engineering Materials and Biomaterials,
Silesian University of Technology, Gliwice, Poland

1. REGIONAL TRENDS OF INNOVATIVE TECHNOLOGIES FOR INDUSTRIAL DEVELOPMENT

1.1 CLASTERS IN FORMATION OF COMPETITIVE ABILITY OF REGIONAL ECONOMY

Voynarenko M.[1], Rybchynska L.[1]

Realization of enterprises network form of cooperation in assistance with local authorities and innovation infrastructures is an important element of innovation development and competitive ability increase in regions of Ukraine. Intensification of world integration processes influence on formation of innovation potential of territory makes it difficult to reach competitive benefits by certain market participants and stimulates formation of different forms of network cooperation. Creation of clusters is considered to be one of the most efficient forms of innovation cooperation of enterprise merging. Cluster is a voluntary unification of enterprises in which competitive benefits can be reached by means of the most efficient cooperation choices of power structures, enterprise sector and innovation infrastructure elements. Diversities of cluster forms, opportunities of their approbation in intersectional dimension and at different levels of territorial organization for economic system competitive ability increase have led formation of wide management toolkit of regional cluster development [1].

Considering peculiarities of cluster approach application in developing and advanced countries, we can state that universal and general approaches and schemes of clusters development don't exist. Each country, depending on its national policy of enterprise activity and economic systems competitive ability stimulation, develops its own approaches to clusters formation and management of their activity. The common feature in innovation development of cluster policy realization and competitive ability increase is the fact that every separate country finds the ways of increase (unique goods, services, deposits, branch and territorial advantages) which could lead regional economy and economy of the

---

[1] National university of Khmelnitsky

whole country to the highest level of civilization development and growth of national prosperity [2].

Analysis of theoretical studies and problems of national and regional competitive ability achievements allowed Pylypenko I.V. to come to the conclusions which prove the necessity of cluster policy implementation. Firstly, all the researchers agree that competitive advantages are formed and realized on the regional level. Secondly, they underline leading significance of economic entities whose incidence is limited by certain region, and who are principal indicators of economic systems competitive ability increase. Thirdly, different researchers acknowledge that such forms of regional level production organization as industrial regions of different types, local clusters connected by regional chain of added value distribution, become the indicators of competitive ability of different fields of economy of the country [3,p.5-6]. Fourthly, the primary object of competitive ability increase policy should be the regions which form regional innovation systems by means of competitive clusters creation. It proves gist and role of clusters as regional unifications which, according to Michael Porter, are concentrations of interdependent enterprises and institutions within certain branch in geographical region [4, p.78].

Implementation of cluster policy makes it possible to concentrate on solution of several important problems of domestic economy:

1. Cluster policy aims at development of competitive market and support of competitive ability of enterprises which are considered to play substantial part in regional economy competitive ability increase. The state cluster initiatives should be concentrated on support of powerful and creative companies and creation of welcoming business climate in which weaker market participants could fulfill their competitive advantages;

2. Cluster policy deals with micro- and macro economy, namely, it analyses local markets and enterprises whose competitive benefits are not inherited (raw materials etc.) but are based on created factors of production (skilled personnel, available infrastructure etc.). Micro- and macroeconomic approaches in cluster policy permit to take into account territorial peculiarities of development and create efficient programs contributing to innovation development and regional competitive ability increase;

3. Cluster policy is based on interaction of the institutions of state authority and local government, business and scientific organizations in order to coordinate innovation growth of production and services, that contribute to intensification of synergetic effects within network structures and their work efficiency;

4. Cluster policy is directed to development stimulation and innovation potential increase of small-scale and average-scale enterprises that take passive part in innovational transformations of Ukraine [5, p.78].

It is necessary to take into account that competition between the regions differs much from competition between the countries. Countries usually compete on the basis of comparative benefits and they don't actually have the lower level of compatible ability; regions compete on the basis of absolute benefits on account of increased mobility of majority natural and created factors of production. Moreover, a region, to the contrary of a country may not find its specialization in interregional labor distribution in case it possesses only comparative benefits. Regions may be deprived of possibility to make use of currency and credit or revenue and tariff policy tools in case of territorial competitive ability decrease (on account of labor output decrease, loss of target market that are reflected on the population incomes and well-being). In order to support living standards a region should apply for subsidy and this can lead to capital and employable population runoff to another, more favorable regions [6, p.6].

According to the structure and potential, cluster policy is the very complex of undertakings that can contribute to the principal task solution: it can increase competitive ability of regional economic systems by means of competitive markets development, economic branches innovations, fast development of small scale and average scale businesses, stimulation of government, business and scientific cooperation.

The high level of the territory competitive ability is possible only under the terms the developing strategies of a region and developing strategies of separate clusters are agreed. It should be stated that necessity of a certain cluster development must be taken into account in strategic and industrial policy of the region as well as there should be an agreement between business and

administrative representatives of the region. The functions to be performed by the authorities and businesses in cluster development are different but complementary. Cluster approach primarily used in research of national competitive ability, is implemented to solve more tasks nowadays:

- Analysis of competitive ability of a region or branch;
- Background of regional industrial policy;
- Regional development program planning;
- Background of innovation activity stimulation;
- Instrument of small scale and big scale businesses interaction [7].

Table 1 - Classification of forms of production dimensional organization

Method of creation / Size of enterprise	Created independently structures	Structures, created by authorities
Small and average enterprises	– industrial regions – local and regional clusters (e.g. Italian industrial districts)	– techno parks – scientific parks – business incubators – innovation technological centers – territorial and branch clusters
Small, average and big enterprises	– industrial regions with a big enterprise and small and average suppliers and subcontract companies around; – industrial regions with a state enterprise and independent suppliers and subcontract companies around	– techno polis – territorial and branch clusters
Average and big enterprises	– groups of big and average enterprises which are not connected technologically, structural subdivisions of TNC	– territorial and production complexes
Big enterprises	– agglomerations of vertically integrated enterprises; – clusters in old industrial regions	– territorial and production complexes

No doubt, cluster approach is one of the most efficient tools of innovation development of the region, at the same time it is necessary to realize that cluster

system cannot be considered as a complex of one or several clusters. Difficulty of regional innovation systems planning on the basis of cluster approach is in the cluster activity which is directed to coordinate and agree interests of different sides involved in the process of clusterization, stimulate their development taking into account diverse (sometimes contradictory) interests of the participants of the unification. It should be mentioned once again that clusters are organizational structures able to form both independently and in a natural way in certain conditions. In case of absence of historical or economical conditions for formation of unnatural cluster in the region, other forms of dimensional production organization will be created. Their classification which is based on the size of enterprises-participants and manner of formation is introduced in Table 1.

According to Rodionova L.M., and Highrulling R.F., application of cluster technologies for competitive benefits of regional economy is possible only if cluster activity is directed to new investments generation, i.e. formation of the so called 'added investments' which will create a source for innovation development of the territory [8, p.3].

It is necessary to evaluate periodically influence of cluster on investment potential development of the region for assessment of applied activities efficiency. Koloshyn A. suggests evaluation of cluster influence on investment attraction of regional economy by means of investment resources transfer analysis, dimensional growth concentration and effects of investment redistribution in economic system (Table 2) [9, p. 29]

Efficient cluster policy makes it possible to form competitive network structures and increase competitive benefits of economic system in general. Traditionally, it's impossible to introduce the results of cluster activity and its influence on formation of competitive benefits of regional economy as mechanical sum of enterprises activity results of organizations-participants of the unification.

Peculiar feature of a cluster is synergetic effect obtained by means of internal cluster cooperation. This means it's possible not to form a cluster but a social or enterprise network. In 1994 in Portugal 33clusters were distinguished by a group of scientists led by M. Porter. In several years of their activity it

became clear that low state policy results of national economy clusterization were caused by noncompetitive clusters or unifications of enterprises which were not connected [3, p 10].

Table 2 - Assessment of cluster influence on development of the regional investment potential

Cluster influence on economy of a region	Influence measurement	Assessment methods
Investment resources transfer	Improvement of access to investment resources in other branches of economy	Study of enterprise investment attraction sources which are not cluster participants. Analysis of investment resources value for a cluster and its separate participants.
Dimensional concentration of investment attraction growth	Dimensional distribution of growth effects of investment attraction for enterprises-participants of a cluster	Data formation for analysis of investment attraction growth concentration inside of a cluster
Investment transfer effects in a region	Direct or indirect effects of cluster influence on development of other participants on regional economic system	Study of enterprises – participants of a cluster but don't belong to the unification. Formation of 'added investment' chain

Thus, as we see, clusters 'branding' may lead to unreasonable state expenses on inefficient state policy and mislead potential private investors. Consequently, as it was mentioned, regional innovation system formation and cluster creation should be considered as constituent mechanism of regional policy competitive ability implementation, and every part of the constituent mechanism should be a catalyzer of interregional integration.

Chainykova L., and Chainykov V., consider cluster competitive ability as means of macro technology potential implementation for obtaining multiplicative effects in regional economic system and cluster competitive benefits growth on account of leadership in production technology, optimization of dimensional organization forms and sales management [10, p 24]. So we can agree to some extent with Skoch A., who says that it isn't necessary to connect

cluster competitive ability with a rhombus of competitive benefits of Mr. Porter, who separated determinants of competitive ability on the basis of advanced countries analysis. Thus, not all the factors may be applied for developing countries. It's much better to analyze traditional factors of labor, land and capital for determination of cluster competitive ability in developing countries [11, p.11].

Koloshyna A., says that regional economy competitive ability growth and formation of cluster competitive potential are possible if an enterprise unification possesses the following features:

- Stable position on a regional market: cluster competitive ability depends both on its share on a regional market and on share accumulation;

- Technological leadership in the branch and innovation ability: ability to make scientific and technical research, transfer technological benefits into successful production are typical for all efficient clusters (including those which are at the stage of maturity or decrease where technological changes rate is limited);

- Renovation ability: clusters should be active in self-support and self-management [9, p.29].

Division of the above mentioned features into elements simplifies the process of evaluation of competitive ability of a cluster and provides an opportunity to find out competitive benefits of regional economy. The above mentioned elements for cluster competitive ability evaluation and cluster influence on regional economy competitive benefits formation are reflected in Table 3.

Our research shows that in conditions of competition for investment resources attraction between regions the first and foremost task is search of new tools of competitive benefits of regional economy. The state authority and enterprise structures are interested in active implementation of world initiatives in creation and realization of cluster concepts of regional innovation development. It was mentioned that competitive benefits of a country are created and implemented on the regional level. The regions become a major object of state innovation policy by means of creation of the system of competitive clusters

Table 3 - Elements for evaluation of cluster competitive ability and influence of its activity on regional economy competitive benefits formation

Type of cluster competitive ability	Data for cluster competitive ability evaluation	Cluster influence on regional economy competitive benefits formation
Position on the market	Leading cluster positions on the regional market	Increase of regional enterprises competitive benefits on the local and national markets
	Assimilation of new product markets by cluster members	New market research by regional enterprises.
	Cluster appearance on the national and world markets	Growth of domestic and foreign export of final goods by regional enterprises
Technological leadership and innovation ability	Growth of scientific research development by cluster participants	Growth of demand in internal scientific research on the regional market of innovation product from the side of the enterprises which don't belong to a cluster
	Growth of innovation implementation and new goods production ability	Growth of new products made by the enterprises of a region; possibility to increase competitive benefits of enterprises - cluster nonmembers by means of implementation of new products; growth of new products demand
	Growth of cluster members ability to technical modernization and innovation implementation in production process	Growth of new technological lines, processes, innovation approaches implemented by the enterprises – cluster nonmembers
Renovation ability	Attraction and creation of new enterprises in a cluster	Creation of new enterprises
	Attraction of foreign participants to a cluster	Increase of foreign investment to the economy of a region
	Growth of regional cluster members economic activity rate	Growth of specific gravity of gross regional product in gross national product

We should agree that implemented in all the regions of Ukraine cluster policy is not an additional tool of state management of regional economy competitive potential, but, on the contrary, it's a new approach of implementation of existing toolkit. According to its potential and structure cluster policy is a complex of technologies which contributes to solving of the major task: providing of investment attraction increase, formation of competitive regional systems by means of competitive markets development, intensification of small and average businesses development, stimulation of initiatives at places and interaction of state, business and scientific organizations.

References

1. Войнаренко М.П. Использование кластерного инструментария для повышения уровня инвестиционной привлекательности и конкурентоспособности региональной экономики / М.П.Войнаренко, Л.А.Рибчинская // Украина и ее регионы на пути к инновационному обществу : монография [в 4 т.] / Под общей ред. В.И.Дубницкого, И.П.Булеева. - Донецк: Юго-Восток, 2011.– Т.4. – 372 с. (С.188-200).

2. Войнаренко М. Кластери як полюси зростання конкурентоспроможності регіонів // Економіст. – 2008. - №10. – С.27-30.

3. Пилипенко И.В. Проведение кластерной политики в России (Приложение 6 к Ежегодному экономическому докладу 2008 года Общероссийской общественной организации «Деловая Россия» «Стратегия 2020»: от экономики «директив» к экономике «стимулов») / И.В. Пилипенко // Электронный ресурс. Режим доступа: http://www.biblio-globus.ru/docs/Annex_6.pdf

4. Porter Michael E. Clusters and the New Economics of Competition // Harvard Business Review.- 1998.- November-December.- P. 77-90.

5. Меньшенина, И.Г. Кластерообразование в региональной экономике : монография / И. Г. Меньшенина, Л. М. Капустина ; Федер. агентство по образованию, Урал. гос. экон. ун-т. – Екатеринбург: Изд-во Урал. гос. экон. ун-та, 2008. – 154 с.

6. Производственные кластеры и конкурентоспособность региона [Текст]: монография / колл. авт. под рук. Т.В. Усковой. – Вологда: Ин-т социально-экономического развития территорий РАН, 2010. – 246 с.

7. Трофимова О.М. К вопросу о формировании инновационных кластеров в региональной экономике / О.М. Трофимова // Научный вестник Уральской академии государственной службы. – 2010. – № 2 (11). – Электронный ресурс. Режим доступа: http://vestnik.uapa.ru/issue/2010/02/10/

8. Родионова Л.Н. Кластеры как форма интеграции инвестиционных ресурсов / Л.Н. Родионова, Р.Ф. Хайруллин // Нефтегазовое дело. Электронный научный журнал.

Вып. 1/2006. – Электронный ресурс. Режим доступа: http://www.ogbus.ru/authors/Rodionova/Rodionova_4.pdf

9. Колошин А. Анализ зарубежного опыта повышения отраслевой, региональной и национальной конкурентоспособности на основе развития кластеров / А.Колошин, К.Разгуляев, Ю.Тимофеева, В.Русинов // Электронный ресурс. – Режим доступа: http://www.politanaliz.ru/articles_695.html

10. Чайникова Л.Н. Конкурентоспособность предприятия : учеб. пособие / Л.Н. Чайникова, В.Н. Чайников. – Тамбов : Изд-во Тамб. гос. техн. ун-та, 2007. – 192 с.

11. Скоч А.В. Место кластеров в современных концепциях формирования региональной экономической политики / А.В. Скоч // Электронный ресурс. Режим доступа: http://independent-academy.net/science/tetradi/12/skoch.html

1.2 DEVELOPMENT OF MODERN TECHNOLOGIES IN THE AREA OF THE OLD POLISH INDUSTRIAL REGION. TRADITION FOR MODERNITY

Szot-Radziszewska E[1]

Introduction

Do engineering achievements, solutions and innovations of our ancestors contribute in any way to the development of modern science and society in the era of rapid technological progress and unusual discoveries? Does tradition stimulate the development of science or is it rather a burden of the past, suppressing the progress of civilization, and needs therefore to be rejected? How is heritage perceived today? This paper is an attempt to analyze the role of heritage in the modern world. Until recently, the predominant approach in the long discourse on this subject was to reject tradition. In the late 20th century, progress was considered the highest value, not at all dependent on the past models. Tradition was identified with backwardness, thus referring to it was not in vogue. Progress was regarded to be attributable to the achievements of science performed only here and now. There was no need to learn from the experiences of our predecessors. The rejection of tradition was global in character. Searching for modern solutions in isolation from the roots, tradition, history or religion leads to the disintegration of cultural systems, destruction of

---

[1] Politechnika Świętokrzyska

social bonds, and, accordingly, alienation in societies. Now it has been proved that societies without heritage are like trees without roots. The academic discourse emphasizes that, in traditional societies, religion, culture, science and technology all overlap and derive from one another, forming a coherent, harmonious system. Supporters of the respect-to-heritage approach claim that tradition and modernity only seem to be mutually exclusive. They emphasize that new generations do not have to start from scratch; they may make use of the achievements of their predecessors. Enginnering progress with innovations and achievements is a constant process, involving selection, improvement and adjustment to the requirements of the times we live in. What is tradition, then? How should we define tradition contributing to the cultural integrity or tradition without which, as it has turned out, progress and development cannot be achieved? The key definitions useful for the considerations here are as follows.

"Tradition is any heritage that one generation passes down to the next" [1]. "Tradition has many meanings. The Latin origin of the word – traditum – is the most important. It is anything transmitted or passed down from the past to the presence. At least two records of cultural goods made by three generations are necessary if the goods are to be regarded as tradition. The elements given the status of tradition generally have their values estimated; it is assumed that they are particularly worth accepting." [2]

"Taking a new look at tradition and modernity requires liberating oneself from deep-rooted thinking patterns. A critical insight should be taken into the stereotype of traditional society, frequently presented as one in a state of stability and inner harmony, and the concept of social and cultural development and a social and cultural change, treated as a process of exchange of traditional elements into modern ones" [3].

For over twenty years, tradition has been perceived as an evolutionary process during which some elements of the heritage being passed on become rejected as the archaic ones and others are given a new meaning by the next generations, causing that tradition significantly contributes to our contemporary activities.

Why has tradition become an object of interest to scientists and ordinary people recently? In my opinion, the intensive studies on the role of tradition and

cultural heritage in the development of science and contemporary societies and the lively academic discourse on the subject are attributable to the accelerated social, cultural and technical development. Of importance is also the disappointment concerning modernity and its achievements, for example, in the field of the arms, chemical and pharmaceutical industries as well as medicine. Inappropriately-used scientific discoveries are posing an increasingly large threat to the coexistence of nature and humans. Very many negative experiences, ecological crises, terrifying weapons used in incomprehensible wars have disturbed the belief in social progress and safe and harmonious development without imposing social patterns or control. The patterns of the Euro-American, industrial and post-industrial, culture, treated as symbols of modernity, have lost their attractiveness. Over the last twenty years, it has become fashionable to derive from the heritage of our ancestors. There is a revival of interest in natural products, products based on old recipes, searching for the cultural roots or applying natural therapies and technologies that are friendly to the environment and the people living in it. Tradition has become a brand that guarantees safety and harmonious continuity. The fundamental values of heritage are being verified both in science and everyday life. The past inspires scientists working, for example, on renewable energy technologies. Like the builders of wind and water mills in the past, they make use of the energy of wind and water. Pharmacologists, too, are investigating the healing properties of plants used for natural remedies. Scientists are trying to rediscover and utilize the great potential of nature. Today's businesses make use of local natural resources and improve the good old recipes to produce goods labelled traditional, local or home-made with a view to gaining confidence of their customers.

The Kielce region (Kielecczyzna), with beautiful landscapes, rich history, ancient mining and metallurgical traditions and unique industrial heritage structures and sites of the Old Polish Industrial Region, is a place where tradition inspires modernity. This area has been selected to illustrate how the history of a place and its community boosts the development of modern science and technology and the growth of local businesses.

The Old Polish Industrial Region, located in the Holy Cross Mountains (Góry Świętokrzyskie), covering the area of the Vistula-Pilica-Nida river system, is probably the oldest mining, metallurgical and metalworking centre in the territory of Poland. The abundant mineral deposits, especially iron, lead and copper ores, flintstone, limestone, sandstone, marble, loam, clay, marl, glass-making sand, as well as various river and forest products, e.g. charcoal, have provided favourable conditions for the development of the mining and manufacturing industries in the north of the Kielce region. For many centuries, smelting furnaces, forge shops, mills, blast furnaces, finery forges, puddling mills, rolling mills and other production facilities have been built along the Czarna, Kamienna and Bobrza rivers.

Stone mining is one of the oldest industrial activities in the Holy Cross Mountains (Góry Świętokrzyskie). Numerous chocolate flint artefacts from the Paleolithic Era have been found in the chocolate flint mines at Wierzbica (the Radom Powiat) and at the archaeological site of Rydno. Banded flint was mined at Krzemionki Opatowskie as early as the Neolithic times [4]. The development of stone mining and quarrying contributed to the construction of many early medieval and later Renaissance **religious and secular buildings.** For example, the limestone from the Pińczów quarry was used for a number of Romanesque buildings, including Wiślica Church, and the Kunów sandstone was used in the construction of the Collegiate Church in Opatów.

There is also a long tradition of **metal mining and metallurgy**, especially in the vicinity of Chęciny, Karczówka Hill in Kielce, Moczydło Hill at Jaworznia near Piekoszów and Łagów. Lead mining and metallurgy in the Chęciny area date back to the 14th century, while copper metallurgy is as old as the year 1479. The origins of metallurgy in the Świętokrzyski Region are mainly attributable to the hematite deposits at Rudki near Święty Krzyż[5]. The area of the Holy Cross Mountains (Góry Świętokrzyskie) emerged as the largest mining and metallurgy centre in Central and Eastern Europe about two thousand years ago, and developed intensively during the early first millennium A.D. Archaeological investigations have revealed 114 iron smelting furnace sites, frequently with more than several furnaces [6]. Ore roasting required using charcoal, which is still considered to be an ideal fuel for any metallurgical

processes. The depletion of forest resources caused that charcoal was replaced with coke [7].

Studies on the history of mining and metallurgy in this area depict the technological evolution of local production facilities. The 12th century witnessed the introduction of the waterwheel, which was soon commonplace not only in flour mills but also forge shops, sawmills (saws), fulling mills (for fulling cloth and processing oak bark used for leather tanning), paper mills as well as lead, copper and glass works. In the 13th century, a mechanical blower was applied to operate, for example, bellows, which used the energy of water. Bellows powered by hydropower were used in smelting furnaces in forge shops.

The term forge shop was used to denote a group of workshops in an iron works, including a smelting furnace, a power hammer and a forging furnace (*kowalicha*), and in other iron processing works producing metal wire, axes and sabres. All those workshops were powered by water energy, generated by damming up small rivers. In the early 16th century, 142 out of 321 forge shops operating in Poland were located in the Old Polish Industrial Region. Forge shops became commonplace in Poland at the end of the 13th century. Until the 18th century, they were the predominant type of iron works. After that time, they were gradually replaced by complexes of blast furnaces [8] and finery forges [9]. Iron was produced in two stages: first, liquid pig iron was obtained in a blast furnace, and then the iron was further processed in a finery forge. A finery forge was a furnace for fining pig iron by decarburization and oxidation of impurities at high temperature by burning charcoal [10].

The first blast furnaces in the Old Polish Industrial Region were built in the 17th century at Bobrza (1610-1613), Cedzyna (1636-1640) and Samsonów (1641-1644). In 1790, there were 70 blast furnaces and 40 smelting furnaces in the territory of Poland. The advancements in the technology of blast furnaces throughout the 17th century led to a significant increase in their capacity [11]. The 17th century saw also the development of the arms industry in the Kielce area. There were many places manufacturing cannons, scythes, sabres, bullets, bombs, grenades and canister-shots. In the 19th century, on the initiative of Stanisław Staszic, measures were taken to industrialize the Kingdom of Poland so that the ancient traditions of mining and metallurgy could be continued in the

Kielce region. The project was launched in 1816 and continued until 1824. It involved, for instance, constructing several iron works along the Kamienna [12], Czarna and Bobrza rivers to create the so called cascades of metallurgical and processing facilities in the vicinity of each water dam, according to the stages of the production process. Damming up the rivers made it possible for waterwheels to operate various machines and devices. According to that plan, the production facilities of the Old Polish Industrial Region were to operate using the local natural resources only. The buildings and structures built in the first stage of the project included the industrial buildings and housing estates for workers in Starachowice, Białogon, Rejów (a district of Skarżysko Kamienna now), Bzina, Mostki, Michałów, Brody and Nietulisko, the impounding reservoir at Kunów and a number of canals, dams and water locks. The plan was fully accomplished only after the state-owned mining and metallurgical facilities were taken over by the Polish Bank (Bank Polski). In the late 19th century, some of the industrial complexes were converted into public limited companies, e.g. the Starachowice Society of Mining Companies (1875), the Ostrowiec Society of Blast Furnaces and Works (1886) and the Bodzechów Society of Mining and Metallurgical Companies (1897-1912). In the years 1870-1879, the Old Polish Industrial Region produced as much as 72-90% pig iron in the Kingdom of Poland (*Fig 6*).

The evidence of the existence of the 19th century large industrial complexes of the Old Polish Industrial Region, spanning alongside three picturesque rivers, are the remains of mine shafts, iron works with blast furnaces, rolling mills, puddling mills, industry-related stone structures such as those displayed in the Museum of the Old Polish Industrial Region in the village of Sielpia Wielka, the museum at Maleniec, the Museum of Ancient Metallurgy of the Świętokrzyski Region in the town of Nowa Słupia and the sites viewed as permanent ruins at Bobrza, Brody, Samsonów, Nietulisko and other places of the Kielce region [13]. The industrial landscapes alongside the three working rivers, Kamienna, Czarna and Bobrza, are evidence of the rich history of the Old Polish Industrial Region, to which today's businesses and research institutions operating in the Kielce region frequently refer to.

1.2.1. Historic post-industrial landscape along the Kamienna river

The historic landscape along the Kamienna river includes the remnants of numerous industrial sites, such as the iron works with blast furnaces in Starachowice, Skarżysko Kamienna, Ostrowiec Świętokrzyski, Bodzechów and Brody Iłżeckie, the puddling and rolling mills at Brody and Starachowice-Michałów, and the last link of the metallurgical chain, the rolling mill producing small-size profiles and thick sheet metal at Nietulisko Fabryczne. The industrial complex spanned 20 km, occupying the banks of the Kamienna river. The stormy histories of the particular facilities add to the unique value of the Starachowice complex.

The central facility was the works in Starachowice with a state-owned iron rolling mill (1818) and three blast furnaces (1841). In the years 1897-99, the facility was modernized and a new coke blast furnace was installed. The iron works and rolling mill operated until 1968. The blast furnace complex was declared a historical monument as early as 1966, and, for this reason, the Museum of Natural History and Technology (*Ekomuzeum im. Jana Pazdura)* was established. The centrepiece of the museum is the blast furnace from 1899 with a unique metallurgical process line and a huge steam engine. The Starachowice blast furnace complex included the rolling and puddling mills (1836-1841) in the nearby village of Starachowice Michałów, which were destroyed by flood in 1903. Another complex of iron works along the Kamienna river was that in the village of Brody Iłżeckie [14], where in the years 1834-1841 puddling and rolling mills were built. The flood of 1903 destroyed almost the entire water system.

An impressive iron rolling mill, designed by Karol Snake, was built at Nietulisko near Ostrowiec Świętokrzyski in 1834-46 [15]. It was owned by the Polish Bank (Bank Polski). A reservoir, a canal, and a rolling mill were built along the so called production axis. The other buildings, including the drying shop, two guardhouses, two stables, the head office, the warehouse, and the housing estate for the factory workers, were built along the so called communication axis. The main production facility was supported by 14 columns. It was equipped with two lines of rolling mills (40 pairs of rollers, different in size), shearing machines, a turning shop and heat furnaces. The

machinery was powered using one of the first water turbines in the Kingdom of Poland and a large breast waterwheel. The modernization project involved installing a locomobile and three power turbines, which allowed producing not only bar iron but also sheet metal and small-size profiles.

The second ironworks was built in Ostrowiec Świętokrzyski in 1837. It was frequently modernized, thus, in the 1860s, it had two blast furnaces with elements powered by two waterwheels producing 40 HP. The plant comprised 17 buildings. Further plant modernizations involved rebuilding one of the blast furnaces and the machine-shop, where a hot blast stove and steam engines with a capacity of 98 HP were installed. The railway line built in 1885 linked the Kingdom of Poland with the whole empire and enabled bringing in raw materials and fuels (e.g. coal from Silesia). The link also helped to sell products in remote markets. In the late 19th century, the works had 2 new blast furnaces, 12 open-hearth furnaces, 4 rolling mills, an iron foundry, a hammer shop, a forge shop as well as a power station and a laboratory. The company had their freight forwarding offices in Warsaw, Moscow and St. Petersburg. After WW1, the steelworks was given another chance; it received government orders for steel products. In the years 1922-1928, the Ostrowiec area belonged to the so-called *safety triangle* zone, which included arms plants, continuing the 17th century traditions of armament engineering. The Ostrowiec works was to support the production of grenades in Skarżysko and rifles in Radom. In 1933, the company made bullet and bayonet steel, aerial bomb parts, goods wagons and depth bombs. Steel and steel products, such as rails, electrodes or wheels, were exported to the Soviet Union, Czechoslovakia, Bulgaria, Yugoslavia, Romania, Finland, Latvia, Holland and India. The new facilities built in those days included a blast furnace, a rolling mill, a press shop, a pipe foundry and a goods wagon assembly plant. After 1945, the factory produced metallurgical machinery, steel structures, tower cranes, gantry cranes, goods wagons and wheel sets for goods wagons. The remnants of the glory days are a fragment of the water canal and the industrial, office and residential buildings from the 19th and 20th centuries. Fragments of the blast furnace (1829) and the rolling mill can be found in the nearby village of Bodzechów .

An important element of the complexes of iron works along the Kamienna river was the town of Skarżysko Kamienna. In 1836, the government built a new blast furnace there and, two years later, a housing estate for workers, canals, a large-size foundry, a bullet foundry and an enamel shop.

1.2.2. Historic landscape alongside the Czarna river

In the 19th century, production facilities were built also along the Czarna river. They included a state-owned impressive rolling mill at Sielpia Wielka (the Końskie Powiat) and a private-owned works in the nearby village of Maleniec (the Końskie Powiat).

The construction of the iron works at **Sielpia Wielka** started in 1821 by damming up the river and digging an 8-km long canal to carry away the operating water. After the defeat of the November Uprising (in 1831), the investment project was continued by the Polish Bank (Bank Polski). It involved building a rolling mill and a puddling furnace. In 1843, the first water turbine in the Kingdom of Poland was installed there. The plant was shut down in 1921, because the forest resources and iron ore deposits were exhausted. The rooms with the rolling mill and the puddling furnace were converted into the Regional Museum of Engineering and Metallurgical Industry in 1934. The exhibits included puddling furnaces, a hammer for shaping puddled balls, a blooming mill, shearing machines, a faggoting machine, heat furnaces, two bar milling machines, a jobbing mill, two waterwheels and a well-preserved water turbine, which is a centrepiece of the museum. During the Second World War, German occupants looted 72 wagons of iron and machinery, part of which they destroyed. The museum was reopened in 1962, and renamed The Old Polish Industrial Region Museum. The only original facility left is a huge iron waterwheel, 8 m in diameter, situated on the deep canal, for powering the machinery of the old iron works. The rest of the exhibits were brought from other production facilities of the Old Polish Industrial Region [16].

The well-preserved works at Maleniec, consisting of a rolling mill, a nail mill and a spade mill from the 19th century, is an example of numerous private industrial initiatives. In 1782, the contemporary owner of Maleniec, Jacek Jezierski, the castellan of Łuków, built a flour mill, a sawmill, a wire mill and a finery furnace with eleven hammers there. Iron ore was delivered from the

nearby villages of Machory, Kołoniec and Ruda Maleniecka. Pig iron was produced in blast furnaces in his other works located in the nearby villages of Miedzierza, Kawęczyn and Cieklińsk. The Maleniec facility produced hatchets, axes, wire, saws, files, flat irons, coffee mills and metal combs, scoops and spoons. The next owners changed and modernized the works. No changes, however, were made to the hydropower system and the production line for the iron forming process. Because of the reliability and simplicity of the hydropower system and the engineering solutions applied in the works, the operation continued for 180 years [17]. The well-preserved production line, including sheet mills, tool making machinery and a hydropower system with a large wooden wheel, a transmission gear and a flywheel, has a particular historic value. Other unique exhibits include a well-preserved rolling mill, made in the Starachowice works in 1834, a power transmission system for the transmission shaft in the cut nail machine, a gear train, a wooden drill structure and two cut nail machines from 1840. In 1967, the iron works at Maleniec was inscribed on the national industrial heritage list, and converted into a museum.

For many years, the museums at Sielpia, Maleniec and Stara Kuźnica have held an annual joint event, the Engineering and Tourist Festival, called "Kuźnice Koneckie", during which the old machinery is started up.

1.2.3. Historic post-industrial landscape along the Bobrza river

The third complex of the industrial heritage landscape of the Old Polish Industrial Region comprises the works at Białogon (today, a district of Kielce), Bobrza and Samsonów, all located along the Bobrza river.

Białogon, an old metallurgical settlement, had a copper works already in the 16th century. Later, the factory smelted ores from the nearby mines into copper, lead and silver. In the years 1816-1820, the place was extended and modernized by building a new furnace, a rolling mill, a hammer shop, brass melting furnaces and a foundry. In 1827, after the copper ore deposits were exhausted, the copper works was converted into the largest machine works, which was equipped with five steam engines and four waterwheels. The machines made there included reaping machines, chaff cutters, potato ploughs, winnowing machines, threshing machines, as well as various production machines and equipment for the other works of the Old Polish Industrial Region.

In 1945, the factory at Białogon was renamed into the Białogon Machine Works and Iron Foundry, and in 1966 it became the Kielce-Białogon Pump Manufacturer, operating at full capacity until today.

There was a gigantic project of building another big iron works on the Bobrza river but it was never completed. The historic remains at the village of Bobrza include the picturesque ruins of the impressive retaining wall [18], the workers' houses, the foundry master's house, the storage buildings, the production building and the coal storage building. The Bobrza complex had a pond and canals [19]. The project, started in 1826-1827, assumed building five blast furnaces on the natural terrace overlooking the east bank valley of the River Bobrza [20]. On the adjacent hill terrace, a long new production building and a foundry were to be constructed. To support the hillside, a stone retaining wall was erected. The construction work had to be stopped due to an enormous flood in 1828 and the November Uprising (in 1830-31). It has never been completed.

Another industrial site on the Bobrza river was the iron works at Samsonów (the Kielce Powiat), with a modern (at that time) charcoal blast furnace, built in 1818 [21]. The facility included forge shops, finery forges, pattern shops, drying shops, an enamel shop and a foundry. Moreover, there were rolling mills to produce large-size iron, copper, brass, zinc and lead sheets. The works produced mainly to meet the army's needs [22]. During its modernization, a steam engine with a capacity of 6 HP was delivered from Miedziana Góra (the Kielce Powiat), the old piping bellows were replaced with modern cylindrical ones, powered by a waterwheel, and a better hoisting mechanism was installed in the elevator tower.[23] All the machines were powered by water carried through a canal from the Bobrza river. The facility also included underground canals, water intakes, a dyke and sluices. It was destroyed by fire in 1866.

A revolution in iron metallurgy was attributable to several innovations, one of which was the use of steam engines, instead of waterwheels. After 1828, the finery forge process was replaced by puddling [24]. Of importance was also the propagation of rolling as an effective metal forming method. Replacing charcoal with coke (which was first done at the Ostrowiec ironworks in 1886)

made it possible to apply new technologies and build open-hearth furnaces (the first was built in Ostrowiec in 1889).

The industrial complexes of the Old Polish Industrial Region were built in the times of difficult political and economic changes. Frequent floods, fires, uprisings, wars, changing trends in the market, and, finally, the exhaustion of ore deposits and forest resources were the major causes of their closure. It was also necessary that they should constantly change, improve or modernize their production profiles. As a result, the metalworking and metallurgical companies operating once in the Kielce region (Kielecczyzna) represent all the links of the development chain of the iron and steel metallurgy from the Middle Ages to the modern day. The iron works situated alongside the three rivers can be regarded as the transition phase to today's spatially concentrated industrial clusters. The old factories with well-preserved complete production lines, forging machinery, water systems, coal blast furnaces, rolling mills and puddling mills are unique heritage sites offering a fascinating insight into the history of metallurgy in Poland and Europe.

1.2.4. Modern technologies in the Old Polish Industrial Region – dialogue with tradition

Looking at the history of the heritage sites of the Old Polish Industrial Region, we learn about the traditions of this post-industrial landscape related to the mining and processing of stones and metals, for example, copper, lead, silver and iron ores in the northern part of the Kielce region (Kielecczyzna). The industry of the Świętokrzyski Voivodship has been shaped by a long tradition of metallurgy, mining, quarrying and ceramics making. The rich mineral deposits (e.g. gypsum, limestone and quartzite) have made the area become the heart of Poland's cement and gypsum industries. The gypsum mines provide raw materials for gypsum products, and the large limestone and marl deposits contribute to the growth of the cement industry. Almost 90% of Poland's production of gypsum is from the Świętokrzyski Voivodship. The region is also the source of a large production of cement, lime and construction aggregate. At Wola Morawicka there is marble quarry. Ożarów has a cement plant (Cement Ożarów). Biofuels are produced in the nearby village of Bidziny, and Stąporków (Henkel Bautechnik) offers construction chemistry products. The largest foreign

investors in the region, e.g. French Lafarge Cement Polska SA in Małogoszcz, German Dyckerhoff in Nowiny, Belgian Group Lhoist at Bukowa, Austrian Rigips Austria GmbH at Stawiany, are the world's leaders in the mineral and construction materials industries.

Today, many companies continue the tradition of industrial activity, with a focus on the metal, engineering, construction materials, glass making, paper making and cardboard packaging industries. These traditional industries contribute to the development of the towns in the northern part of the Kielce region (Kielecczyzna). In picturesque Sandomierz, there is a prosperous glassworks (Pilkington Sandoglass from the UK) producing tempered and laminated automotive glass. The steelworks in Ostrowiec Świętokrzyski is a manufacturer of stainless steel, propeller drive shafts and a wide range of rolled and wrought products. The predominant industrial activities of Skarżysko-Kamienna are still related to the production of metal and arms (Mesko S.A., a manufacturer of ammunition and missiles). Starachowice is a hub of metal, metallurgical, engineering, wood, automotive (buses produced by MAN Truck & Bus) and construction materials industries. The Kielce-Białogon Pump Manufacturer (Kielecka Fabryka Pomp „Białogon" S.A.) in Kielce equipped with modern machinery produces impeller pumps, positive-displacement pumps and grey iron castings. Moreover, large companies such as Barlinek, Centrostal, Cersanit, Echo Innvestment, Exbud Skanska and Lafarage have their headquarters there. For a few years, companies based in this region have been assessed and awarded for their innovativeness, launching of new products and contribution to the promotion of the Kielce region in a competition called Region's Leader.

Good industrial traditions, specialization and the potential for economic diversity help the region attract foreign investors, mainly from Belgium, France, Japan, Germany, Great Britain, and recently also from the Far East, i.e. China. The companies investing in the engineering and metal industries include NSK-RHP Europe Ltd. from Japan and Schmidt Holland BV from Holland .

The glory years of the Old Polish Industrial Region have contributed to the development of today's businesses and research institutions.

The most important research institution of the region is the Kielce University of Technology (Politechnika Świętokrzyska), originating from the first technical university in Poland, the Academic School of Mining, founded by Stanisław Staszic in Kielce in 1816 and operating until 1827. The Academic School of Mining had enormous influence on the industrialization of the Kingdom of Poland. In a similar way, the Kielce University of Technology (Politechnika Świętokrzyska) is involved in various research projects and cooperates with other research institutions all over the world with a view to providing state-of-the-art technologies to be used by local businesses.

The establishment of the Świętokrzyski Innovation Council (Świętokrzyska Rada Innowacji - ŚRI) and five clusters – the Kielce Fair Cluster (Grono Targowe Kielce), MedCluster, the Energy Cluster (Klaster Energetyczny), the Industrial Cluster (Kom-Cast) and the Construction Cluster (Klaster Budowlany) – aimed at maintaining the social and economic coherence in the fields of innovation and building a knowledge-based economy. A sixth cluster, labelled the Design Cluster (Klaster Wzorniczy), is still in the development phase. In my considerations, I focus on the activities that contribute to the continuation of traditional industries, specific to the region, such as metallurgy and construction, as well as the transfer of modern technologies and cooperation between the local businesses and universities.

The economic pride of the region is the Kielce Fairs (Targi Kielce), the second largest fair and exhibition centre in Poland. The Kielce Fair Cluster (Grono Targowe Kielce) provides engineering professionals with the latest technological and structural solutions. By developing a modern Internet network and building hotels and restaurants offering traditional local food, the region is able to attract businessmen, capital investors and tourists. The Association of Cast Component Manufacturers - Innovative Industrial Cluster, Kom-Cast (Stowarzyszenie Producentów Komponentów Odlewniczych Innowacyjny Klaster Przemysłowy, Kom-Cast) comprises 26 companies from the Świętokrzyski, Podkarpacki and Lubelski Voivodships. Their market share in the foundry industry accounts for over 20 %, whereas their metalworking exports amount to 30 %. As a result of the cooperation with the local university, the cluster members can be up to date with the trade-related issues.

The Świętokrzyski and Podkarpacki Construction Cluster called Innovator (Świętokrzysko-Podkarpacki Klaster Budowalny Innowator) was founded in January 2010 by small and medium-sized construction companies from the Świętokrzyski and Podkarpacki regions. Like Kom-Cast, it is to become a platform for the transfer of knowledge and state-of-the-art technologies. The cluster is involved in organizing training sessions, seminars and conferences to enhance and develop competencies, as well as purchasing and implementing modern technologies, management systems and quality systems.

The Design Cluster (Klaster Wzorniczy) was established to intensify and popularize design activities in the Świętokrzyski region. The cluster initiatives will be realized by the Kielce Technological Park (Kielecki Park Technologiczny) – a platform for cooperation in industrial and utility design. It is assumed that by combining the activities and cooperation on the project between many business, scientific, cultural and self-governing institutions, it will be possible to create a good atmosphere for the development of design in the whole region. The Kielce Technological Park (Kielecki Park Technologiczny KPT) is a research and industrial complex with an area of 14 thousand square metres. It will consist of two parts: the Technological Incubator (Inkubator Technologiczny) and the Technological Centre (Centrum Technologiczne). The Technological Incubator (Inkubator Technologiczny - IT) covers an area of over 4.6 thousand square metres of office, commercial and laboratory space. It is addressed mainly at academic-related and start-up businesses. Young and beginner entrepreneurs, members of the Incubator, will be offered a specially-developed programme which will prepare them to operate successfully under competitive conditions. One of the floors in the Incubator office will be occupied by Design Laboratories, realizing the regional design support programme. The aim of LabDesign is to combine art with business as well as support cooperation between designers and entrepreneurs specializing in industrial design. One of the advantages of the Kielce Technological Park (Kielecki Park Technologiczny) is the fact that it is strategically connected with the Special Economic Zone in Starachowice, a place with a long industrial tradition. The Kielce Technological Park will definitely contribute to the

implementation of the latest technologies and improvement of competitiveness of the small and medium-sized businesses in the region.

The Regional Centre for Innovation and Technology Transfer, Ltd. (Świętokrzyskie Centrum Innowacji i Transferu Technologii Sp. z o.o. - ŚCIiTT) was established on the initiative of the authorities of the Świętokrzyski Voivodship, the Kielce Town Council and the Kielce University of Technology (Politechnika Świętokrzyska). The concept of synergic organization with different specialists advising on regional competitiveness is considered to be very promising. The centre can offer small and medium-sized businesses a number of IT, consulting, training and professional services, which will help them reduce costs and increase effectiveness. Many services are provided free of charge, as a result of the participation of the Regional Centre for Innovation and Technology Transfer, Ltd. (Świętokrzyskie Centrum Innowacji i Transferu Technologii Sp. z o.o. - ŚCIiTT) in national and international networks of cooperation, such as the National Service System (Krajowy System Usług - KSU), the National Innovation Network (Krajowa Sieć Innowacji - KSI), the Network of Regional and Contact Points of EU Research Programmes (Sieć Regionalnych i Punktów Kontaktowych Programów Badawczych UE) or the Enterprise Europe Network (EEN). The cooperation between researchers, particularly those from the Kielce University of Technology (Politechnika Świętokrzyska), and businesses operating in the area of the Old Polish Industrial Region gives hope of sustainable development and effective utilization of the marketing potential of this region.

The dialogue of science and modernity with tradition may have a beneficial effect on the remnants of the Old Polish Industrial Region. There is hope that the dynamic businesses of the region will offer support to preserve and protect the endangered historic places, which are actually the achievements of their predecessors. The value of the post-industrial heritage of the Old Polish Industrial Region needs to be looked at in a wider, cultural context. By showing how important tradition is in the building of the modern world, we need to remember that the heritage and the material evidence in the form of historic sites and structures are significant not only for the history of science but also for the collective memory of successive generations inhabiting these areas. From the

social point of view, the historic space, full of meanings and symbols, plays an important role in the building of regional ties and identity. The attitude, activity and initiatives of the inhabitans have a considerable effect on the preservation of the national and regional heritage and development.

Promoting tradition and recognizing its value and merits to the modern world may help preserve the historic sites and structures of the Old Polish Industrial Region.

References

1. K. Dobrowolski, Studia nad życiem społecznym i kulturą (Studies on social life and culture), Wrocław 1966, p. 77.

2. Słownik etnologiczny terminy ogólne (Dictionary of ethnology – general terms), Z. Staszczak (edit.), Warszawa-Poznań 1987, p. 355.

3. Tradycja i nowoczesność (Tradition and modernity), J. Kurczewska, J. Szacki (edit.), Warszawa 1984.

4. Krzemionki Opatowskie is a site with a well-preserved Neolithic and Early Bronze Age flint mine, used from the mid 3rd to the mid 2nd millenia B.C., mainly by the Funnelbeaker culture peoples. It provided banded flint, which was very much in demand as a primary material for making stone tools. Over a thousand shafts (up to 10 m deep) with galleries (up to 30 m long) and chambers were discovered at the site. Flint nodules were extracted using deer antler picks, hammers and chisels. Flint tools produced in that area reached as far as Rugen, Sambia, Volhynia and Moravia, being exchanged for other goods. The Encyclopaedia of Economic History of Poland until 1945 (Encyklopedia Historii Gospodarczej Polski do 1945 roku), Vol. I Warszawa 1981, entry on Krzemionki Opatowskie, written by S. Krukowski, p. 395. Today, Krzemionki near Ostrowiec is an archaeological site with an archaeological museum.

5. The oldest known open-pit hematite mine operated in the villages of Łyżwy and Grzybowa Góra near Skarżysko-Kamienna from the 11th to the 4th millenia B.C. In 1986, the Rydno archaelogical site was established there. While examining the ancient hematite mine named after Staszic at Rudki, Bielenin came across vertical shafts and horizontal galleries at a depth of 36 meters from the surface in the layers explored in the first centuries of our era. In the 18th and 19th centuries, shafts were dug using percussion drilling to a depth that allowed water and air flow. Ore was extracted from the shaft by widening it to several meters in radius. This type of mining was used until World War One. There are still sites in the region where depressions left by collapsed shafts can be seen. Traces of similar shafts, called dooks, are found in the prehistoric flint mine at Krzemionki Opatowskie.

6. Explorations of the Holy Cross Mountains (Góry Świętokrzyskie) to search for ancient iron slag started in 1955 and were continued for many years on the initiative of and under supervision of Mieczysław Radwan, a docent of the Academy of Mining and Metallurgy (AGH) in Cracow at that time. The archaeological investigations were conducted by Kazimierz Bielenin from the Archaeological Museum in Cracow. cf. K. Bielenin, Starożytne górnictwo i hutnictwo żelaza w Górach Świętokrzyskich (Ancient iron mining and metallurgy in the Holy Cross Mountains), Kielce 1992.

7. The last charcoal blast furnace in Poland was started up in the Pokój Steelworks (Huta „Pokój") at Chlewiska in 1939. Furnaces fuelled with charcoal produced higher-quality metal.

8. A blast furnace is a chimney-like structure lined with refractory brick which was filled with the layers of ore, flux and fuel charged into the top of the furnace in a defined order. At the bottom part, there were tapholes for tapping pig iron and slag (a by-product of smelting ore formed by combining the flux with the gangue material). The blast furnace process is a continuous process during which air is artificially blown into the bottom part of the furnace using bellows or blowers. Pig iron is tapped every several hours. The blast furnace was invented in Western Europe in the 15th century by gradually extending and changing the shape of the primitive smelting furnace (dymarka) and required using the energy of water to power the bellows. The blast furnace was much more efficient than a primitive smelting furnace (dymarka). In a primitive smelting furnace, 5.2 tonnes of ore and 5.1 tonnes of charcoal were used to smelt 1 tonne of iron. Obtaining a tonne of pig iron in a blast furnace required using 3.3 tonnes of ore and 1.9 tonnes of charcoal. The furnace capacity increased from 50 to 90 %.

9. See: Encyklopedia; entry on "kuźnica" (forge shop), written by B. Zientara, p. 400; cf. by the same author Dzieje małopolskiego hutnictwa żelaznego XIV-XVII wiek (The history of iron metallurgy in Little Poland from the 14th to the 17th century), Warszawa 1954.

10. Finery forges were developed by converting smelting furnaces. They had inside walls lined with cast iron plates and side nozzles supplying air. The pig iron was placed on white hot charcoal. One finery forge had a capacity of approximately 500 kg of iron per day. In Europe, they were known from the 14th century, whereas in Poland they appeared in the early 17th century.

11. The changes in this technology started in England in 1735. Charcoal was replaced by coke, the blow system was improved (from 1768 cylindrical blowers were powered by steam engines, and in 1828 hot-blast stoves were introduced). The first blast furnaces were about 7 m in height and 10 m in volume; in the 19th century they had a height of 30 m and a volume of about 500 m. In Poland, the last charcoal blast furnace was decommissioned in 1893. The lack of coking coal required improving the technology of charcoal blast furnaces. The first steam engines appeared in 1804. Blowers and hot-blast stoves (Samsonów) were introduced in 1805 and 1836, respectively. It was only in 1880 that a modern coke blast

furnace was started up in the Kingom of Poland. The number of old-type blast furnaces decreased from 22 to 1 (Chlewiska), with the latter being decommissioned only in 1925. In the late 18th century, the annual output of a blast furnace amounted to about 200 t. of pig iron, and in the mid-19th century it reached over 700 t.

12. The basins of these rivers were a place of intensive development of settlement and industry.

13. In 1994, a Plan of Location of the Historic Industrial Sites and Structures of the Old Polish Industrial Region was issued. The map shows the location of ore mines, forge shops, blast furnaces and other iron mining and making facilities. It presents many historic industrial sites and structures and even more remains of such facilities starting from the Paleolithic and Neolithic Eras and ending with the early 20th century.

14. In the 17th century, there was a water-powered forge shop there. Later, an iron smelting furnace was built. Finally, a blast furnace and finery forges were erected in 1784 and continued in operation until the floods of 1812-1813.

15. The construction of the hydropower facilities started in 1924.

16. The exhibits from the Białogon works include a 19th century steam blower, a steam engine from 1858 and a face lathe. A unique press forging machine and a waterwheel were saved from the now non-existent forge shop at nearby Drutarnia.

17. The system consisted of an old pond (now an impounding reservoir with an area of 27 ha), a side dyke, a face dam (1625 m in length and 3 m in average height) and seven relief weirs and a fire bridge.

18. The retaining wall actually consists of two parallel walls made of irregularly arranged broken stone, with the voids filled with coarse stone in order to create ballast. The lengths of the face, the south side and the north side were about 328 m, 80 m and 112 m, respectively. The wall width was 5 m, while the maximum height was approx. 15 m.

19. The products of the forge shops and iron works operating at Bobrza from the 16th century included cannons and cannon balls.

20. The factory was designed by the Mining Counsellor in the Government of the Kingdom of Poland, Fryderyk Lampe, a professor of the Academic School of Mining in Kielce. The business was expected to have a yearly production output of 5000-9000 tonnes of pig iron.

21. The traditions of iron mining and making at Samsonów date back to the 16th century, when there was a water forge there. Later, in 1641, Jan Gibboni was granted permission by Bishop Tomasz Zadzik to build a blast furnace at Samsonów and a forge shop at Ćmińsk. The factories produced field cannons, cannon balls, guns, armour, backswords, pikes and helmets. In the early 17th century, the contemporary owners of the iron works purchased forges in the nearby villages of Humer, Światełko and Suchyniówek, which formed the so-called Samsonów Complex (klucz samsonowski). In 1814, the property was transferred to be managed by the Internal Affairs Commission (Komisja Spraw Wewnętrznych).

22. Apart from ammunition and cannons, they produced candlestics and candlabra, crucifixes, frames, reliefs, grave crosses, commemorative plaques, anvils, etc..

23. A blast stove, known as the Calder stove, was installed to heat cold air blown by the bellows into the blast furnace. The vertical elevator supplying ore into the furnace was powered by a separate mechanism connected with the waterwheel.

24. Puddling is a process invented in 1784 by Englishman Henry Cort. It involved decarburizing pig iron in an oxidizing atmosphere. Puddling furnaces were more efficient than finery forges. As they separated fuel from pig iron, it was possible to use hard coal. The first puddling mill in the territory of Poland was opened in the Baildon ironworks in Upper Silesia (Górny Śląsk). The first puddling furnaces in the Kingdom of Poland were built in 1833. It was only after 1882 that the first large coal-fuelled puddling mills appeared in the Dąbrowa area (Zagłębie Dąbrowskie). Puddling became less popular with the development of steel metallurgy. The puddling process was commonly applied in the 1830s in the areas of Machory and Starachowice. In 1839, the Irena puddling mill was built near Zaklików, where pig iron was delivered from the Ostrowiec iron works (1837). There were about 75 puddling mills in the Polish Commonwealth (Rzeczypospolita) in the late 18th century and 150-180 in the Kingdom of Poland between 1823 and 1838, whereas Upper Silesia had 170-190 facilities of this type , cf. Encyklopedia Historii…, p. 167.

1.3. TECHNOLOGICAL DEVELOPMENT OF INDUSTRIAL ENTERPRISES OF UKRAINE: PRIORITIES AND EFFECTIVENESS
Yokhna M.[1]

Problem setting. Growth potential of modern social-economic systems depends much on the level of development of their industrial sphere. However today many traditional branches of industry have depleted not only extensive, but also intensive possibilities of their development. That's why in many countries begin to lead branches of industry, based on innovative technologies. They are a powerful lever, thanks to which countries not only overcome their economic downfall, but also implement structural renovation of economy, filling industrial sector by resource-saving and ecology-friendly technologies and raising the level of competitiveness of national economies. The problem of

---

[1] National university of Khmelnitsky

technological renovation of industrial sector for Ukraine is very important because capital assets of most of branches have exhausted their resource.

Technological changes in every economic system happen under influence of changes in social needs, and their intensiveness and effectiveness depend on conditions of functioning of institutional environment (which depends on state government policy and regulations). It is impossible to implement a very important task for national economy – growth of its competitiveness on world market, without creation of proper legislative background, which would favor innovations. That's why an important role gain questions of effective management of technological renovation processes on enterprise (on micro and macro levels). At the same time technological renovation should happen according to ecology and energy-saving standards, what will assist in environment preservation and soften the question of energy resources price growth.

The search of optimal ways of technological renovation of production implementation on innovative basis (that expects growth of resource-preservation and ecology-friendliness level) becomes very important. That's why many Ukrainian and foreign scientific publications are aimed on this question. In Ukraine researches on this topic were made by O.Amosha, V.Shevchenko [1], V.Aleksandrova [2], A.Galchinskiy, A.Kinah, V.Seminozhenko [3], L.Fedulova [4], O.Dmitryk [5], T.Tsihan and many others. Own considerations about influence on these processes were also made by author of this article [6]. However the question of estimation of effectiveness of technological development did not find sufficient reflection in scientific References, what makes this research vital.

Goal of article is to analyze the effectiveness of technological development of Ukrainian industrial enterprises.

Essence of research. First of all it is necessary to underline, that industry of Ukraine has suffered major losses of its economic potential in period of

restructuring. It happened because of incompetence of management in managing new methods of cooperation with customers and deformation of owners' goals (maximize short-time profit). Also many Ukrainian industrial enterprises (especially machine-building) were intermediate sections of technological chains and did not create final production (which maximizes value added). Moreover the development of market mechanism in Ukraine happened under influence of wrong conception (restraining the state from intervention in market economy and its regulation and investment). It stopped development of big part of Ukrainian industrial enterprises. Critical capital assets wear took place on many enterprises, not allowing renovation of technological basis. Some investment help gained only those enterprises, production of which was competitive on external markets. Unfortunately they were enterprises of metallurgy and chemical industry, activity of which harms much the environment.

Generally, transformation processes in the domain caused extension of structural deformation – increase of number of 3-rd and 4-th technologic levels enterprises [4; 6]. However production of these enterprises is needed mainly in periods of economic growth, and in period of crisis demand on it falls at once. Consequences of world economic crisis of 2009 show it. In January 2009 in Ukraine comparing to January 2008 the volumes of production and realization of production has fallen twice (in metallurgy it was 58,3% fall; in chemical – 49,1%) [8]. Only because of quick devaluation of Ukrainian currency enterprises of this domain became to get back on external markets.

Losses were great in machine-building as well. Comparing to 2008 machines production index in 2009 was only 54,9%, generally in industry – 78,1%. It means that decrease in production and sales volume in machine-building was almost twice bigger than in industry [9]. It is necessary to underline, that machine-building enterprises produce products for technological renovation of other enterprises. In order to maintain their competitiveness they

have to produce science-absorbing production and be innovatively-active. But their innovative activity mainly concerns their own technological renovation and production decreases year after year.

It means that investments in technological renovation do not bear systematic character and do not support the decision of main task – raising the ability of enterprises to create new production according to changes in demand. The part of innovative production in general volume of industrial production decreases through last years (from 6,7% in 2005-2006 to 3,8% in 2010). Among product innovations a part of new equipment decreased. Their quantity has fallen from 881 in 2007 to 669 in 2010 (in 2009 there was only 641pieces) [10].

Moreover during crisis enterprises started to spend less on technological renovation. In 2008 investments in machines and equipment were 98426 thousands grivnas throughout Ukraine. In 2009 this number has fallen to 65340 (decreased by 1/3 and were 33,9% from general amount of investments (36,2% in 2008 and 38,2% in 2005) [11]. In 2010 technological renovation investment continued to decrease (figure 1). It means that technological renovation of Ukrainian economy slowed down sharply.
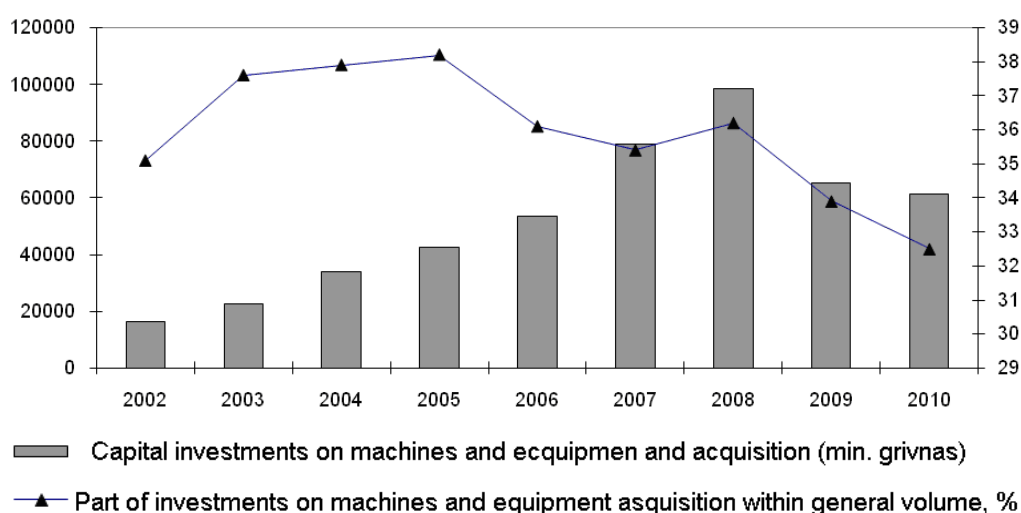
Fig. 1. Dynamics of capital investments in technological renovation of economy of Ukraine in 2002-2010

Sources: State committee of statistics of Ukraine: Capital investments in 2010/ http://www.ukrstat.gov.ua/operativ/operativ2010/ibd/kinv/kinv_u/kinv_u04_10.htm (19.07.2011); own calculations

Analyzing processes of technological renovation investment it is reasonable to compare costs of equipment acquisition with costs of technological innovations implementation. It can give ground for conclusions about innovative character of this renovation. On fig.2 the dynamics of costs on technological innovations (sum of costs on machines, equipment, software and new technologies acquisition) and general sum of capital investments, which were directed on machines and equipment acquisition during 2005-2010 is shown. As it is visible from fig.2, technological renovation is generally made on old technological basis. In 2010 the correlation of innovative costs with general sum of investments into machines and equipment acquisition was 1: 11,8.
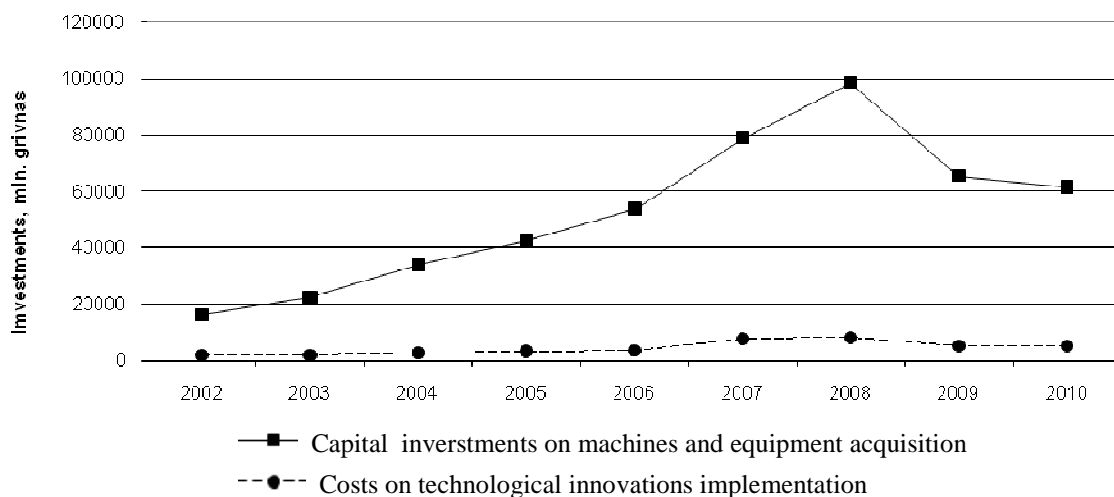
Fig. 2. Comparative dynamics of capital investments, directed on machines and equipment acquisition and technological innovations costs

Sources: State committee of statistics of Ukraine: Capital investments in 2010/ http:/www.ukrstat.gov.ua/operativ/operativ2010/ibd/kinv/kinvu/kinvu04_10.htm(19.07.2011); State committee of statistics of Ukraine: Scientific and innovative activity (1990-2010) / http://www.ukrstat.gov.ua/operativ/operativ2005   /ni/ind_rik/ind_u/2002.html   (19.07.2011); own calculations

Costs on new technologies (resource-saving) are many times lower that costs on technological innovations acquisition. In 2010 innovative costs on machines, equipment and software were 2021,7 mln. grivnas, but on new technologies acquisition – only 141,6 mln. grivnas.

It can be assumed that management of enterprises, which implement new technologies, gives priority to resource-saving technologies, seeing in them the biggest possibilities of production systems competitiveness growth. A large part of such technologies in general amount of technologies implemented through last 10 years shows it (figure 3). The processes of technological renovation themselves do not expect drastic technological changes in production systems.
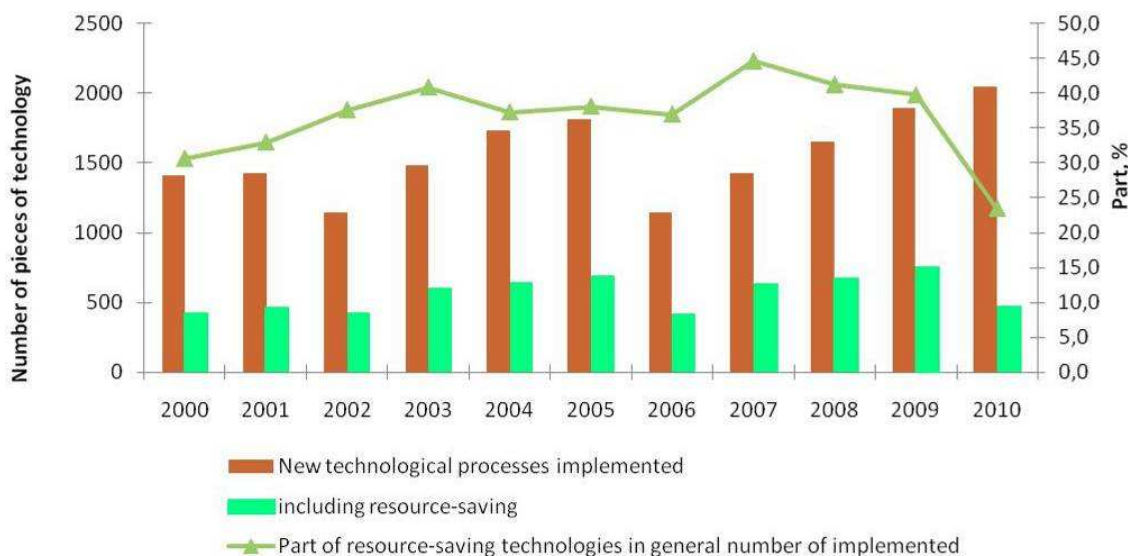
Fig. 3. Comparative dynamics of innovative technologies implementation indexes in Ukraine

Sources: State committee of statistics of Ukraine: Scientific and innovative activity/ http:// www.ukrstat.gov.ua/ operativ/ operativ2005/ ni/ind_rik/ind_u/2002.html (19.07.2011); own calculations

According to results of survey of technological renovation of industrial enterprises in Ukraine, held in 2009 (2407 enterprises observed, 31,5% of them showed that renovation has been implemented), it was discovered that almost quarter of enterprises have made only improvement of available technologies, almost 50% showed that they have acquired new equipment for new products manufacturing. Just a small part of enterprises did a research and implementation of qualitatively new technologies. 10,5% have made it by themselves and 6,2% - together with other enterprises and organizations. The

smallest part of enterprises was oriented on licenses acquisition (5%). Among those, who prefers new equipment acquisition 25,5% are food producers and 11,2% - machine builders [12].

So, analysis of statistical data about technological renovation of enterprises of Ukraine shows their insufficient innovative direction. At the same time it is obvious, that technological development of Ukrainian industrial enterprises should be implemented in a way to overcome technological backwardness, which causes low competitiveness of products.

It is obvious that state must assist in it by appropriate economic policy. And priorities of state investment support of technological renovation should be directed in such spheres of production activity, which refer to higher technological levels. It will create conditions for "technological push" model realization in Ukraine. Unfortunately in Ukraine 70% of state support is directed onto lower technological levels (50% go into fuel and power industry and metallurgy) [4]. Moreover the amount of state financing is very low, being only couple of percent from all amount of investments in technological renovation (figure 4).
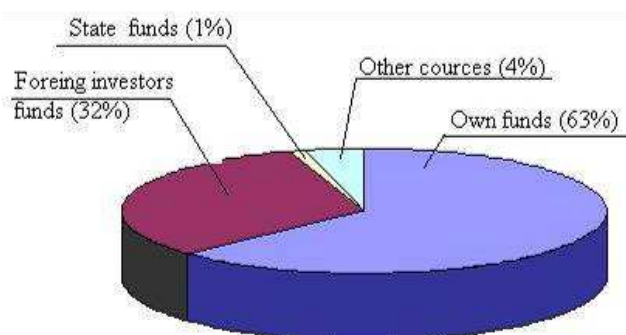
Fig. 4. Structure of technological innovations investments in industrial sector of economy of Ukraine in 2010

Sources: State committee of statistics of Ukraine: scientific and innovative activity/ http:// www.ukrstat.gov.ua/ operativ/ operativ2005/ ni/ ind_rik/ind_u/2002.html (19.07.2011); own calculations

Considering the fact, that qualitative technological renovation requires a lot of funds (which are not sufficient in majority of Ukrainian enterprises), management of enterprises tries to find strategic investors. However foreign investors' funds have not been directed onto production systems renovation for a long time. Main accent has been placed on cheap labor force in Ukraine and on possibility to transfer environment-unfriendly production to the territory of Ukraine.

From general amount of invested by foreign investors in 2008 funds on technological innovations were only 1%. On previous years they were 3-4%, being lower in absolute values [10]. However for today the situation has slightly changed – foreign investors' funds in 2010 have exceeded 30% from their general amount, which were invested in technological innovations (figure 4). But we can surely say that it is reinvestment from offshore zones, where large amounts of funds were placed by Ukrainian big business holders in order to avoid high taxation rates and political risks.

Analyzing processes of technological renovation of industrial sector of Ukraine it is important to estimate not only its successfulness (which is shown in number of innovations or new equipment implementation), but also its effectiveness. Of course it is best to estimate effectiveness of investment processes by economic activity profitability indexes. However considering existing taxation scheme (which induces to maximum possible concealment of positive financial results during statistical report composition), such comparative analysis would be made incorrectly. That's why it is reasonable to estimate effectiveness of processes of technological renovation investments through growth dynamics of sales volumes. On figure 5 tempos of growth of industrial production are compared with tempos of investment into technological renovation.
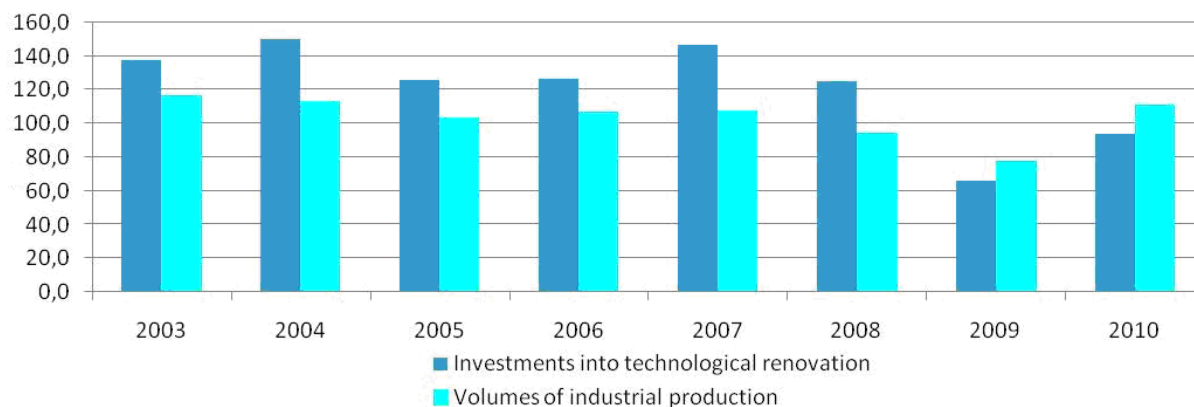
Fig. 5. Comparative dynamics of growth tempos of production volumes of industrial products in Ukraine and tempos of investment of technological renovation.

Sources: State committee of statistics of Ukraine: capital investments in 2010 http://www.ukrstat.gov.ua/operativ/operativ2010/ibd/kinv/kinvu/kinvu0410.htm(19.07.2011); State committee of statistics of Ukraine: Industrial production indexes (2002-2010);http://www.ukrstat.gov.ua/operativ/operativ2007/pr/rm_ric/prm_ric_u/ipv2006_u.html (19.07.2011); own calculations

Indexes dynamics shows, that investment in technological development of enterprises happens with higher tempos than production volumes growth. It can be explained by the fact that investments have been made generally into change of worn capital assets. And just in 2010 such regularity has changed to opposite. It means that return on investments in technological renovation began to grow, being reflected in sales growth.

Let's now compare the effectiveness of new technologies implementation. As it is visible from figure 6, a significant time lag is observed between their implementation and effective usage. So, just after three years of active implementation (2003-2005) indexes of industrial production began to grow. And even now growth was not strong. In 2008 volumes of production lowered significantly, what is explained by influence of world economic crisis. In 2010 growth tempos of industrial production have raised significantly, however volumes did not reach pre-crisis level.
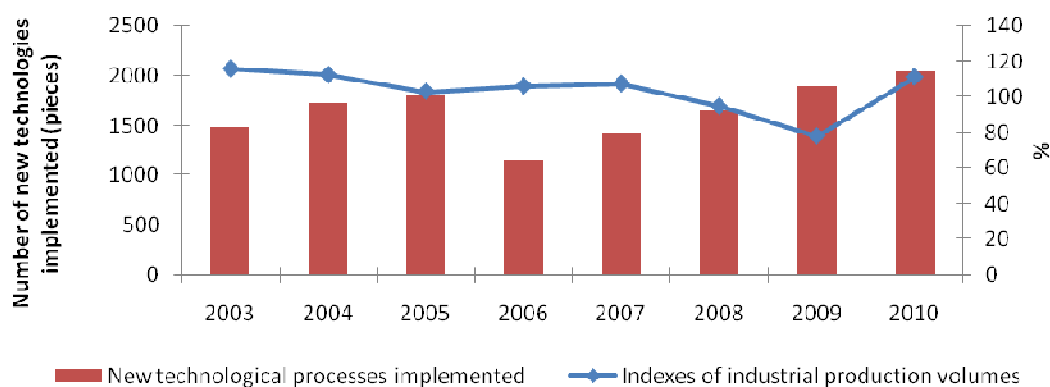
Fig. 6. Comparative dynamics of new technologies implemented and industrial production growth tempos

Sources: State committee of statistics of Ukraine: Industrial production indexes (2002-2010):http://www.ukrstat.gov.ua/operativ/operativ2007/pr/prm_ric/prm_ric_u/ipv2006u.html (19.07.2011); State committee of statistics of Ukraine: scientific and innovative activity (1990-2010): http://www.ukrstat.gov.ua/operativ/operativ2005 /ni/ind_rik/ind_u /2002.html (19.07.2011); own calculations

It can be assumed, that such dependence is a result of insufficient competitiveness of implemented technologies, their insufficient flexibility, which should form their wide technological possibilities.

That's why industrial mastering of new production samples is happening not very actively. Moreover, the number of implemented samples of new technology (machine-building production, which takes main place in process of technological renovation of Ukrainian economy) is much lower (table 1).

The greatest value (over 36%) it has reached in 2007, when production of 881 samples of new products has been mastered. During last years, when machine-building enterprises were under influence of world economic crisis, mastering of new equipment production worsened significantly, reaching minimum in 2009 (648 pieces, 24,1%). In 2010 the situation started to get better (669 (27,8%) pieces mastered).

Table 1 - Structure of new goods production by industrial enterprises of Ukraine in 2001-2010.

Index	Data by years									
	2001	2002	2003	2004	2005	2006	2007	2008	2009	2010
New types of products mastered	15323	19484	22847	7416	3978	3152	2408	2526	2685	2408
Including new samples of equipment	610	520	710	769	657	786	881	758	648	669
Part of innovative equipment in general amount of innovative production, %	4,0	2,7	3,1	10,4	16,5	24,9	36,6	30,0	24,1	27,8

Sources: State committee of statistics of Ukraine: scientific and innovative activity Державний (1990-2010): http://www.ukrstat.gov.ua/operativ/operativ2005/ni/ind_rik/ind_u / 2002.html (19.07.2011); own calculations

However technological renovation of capital assets is needed not just because of ageing of equipment, but also because of objective needs in its replacement with new and progressive samples. It is important that renovation processes in production systems happen under laws of diversified production. It means that each phase of technological renovation should widen market possibilities of an enterprise, rising its ability to manufacture production, which satisfies consumer needs now and will be in future.

Conclusions. This research shows that technological renovation of industrial sector of Ukrainian economy is put into practice not very effectively. Generally investment costs go into reproduction of production systems on slightly modified technological basis, which is improves in a direction of increasing of level resource-preservation. It only allows to raise competitiveness in traditional branches of economy of Ukraine and hold positions on internal market.

According to researches, the volumes of innovative renovation are insufficient for national economy to overcome technological backwardness by accumulating critical mass of innovative technologies, which would permit to

implement the model of "technologic push". In conditions of globalization it is important to provide innovative break in high-technology branches. It is needed to implement such technologies, which have significant innovative potential and can grant maintenance of innovative leadership throughout long time.

Significant role in acceleration and raising the level of innovativeness of technological renovation should play the state by forming priorities of technological development in shift onto higher technological levels and supporting these priorities by appropriate institutional preferences. Justification of directions of such shifting should be the theme of following researches.

References

1. Амоша А.И. К формированию концепции государственного регулирования ускоренной адаптации предприятий к изменениям экономической среды/ А. И. Амоша, В.В.Шевченко // Наукові праці Донецького національного технічного університету. Сер.: економічна. – Донецьк: ДонНТУ. – 2008. – Вип. 33-1(128). – С.5-10.

2. Гальчинський А. Інноваційна стратегія українських реформ / А. Гальчинський, В.Геєць, А.Кінах, В.Семиноженко. – К.: Знання України, 2002. – 336с.

3. Александрова В.П. Технологічне оновлення вітчизняного виробництва в умовах трансформації економіки / В.П. Александрова// Проблеми науки. – 2005. – № 9. – С. 16-22.

4. Федулова Л.І. Технологічний розвиток економіки / Л. І. Федулова // Економіка України. – 2006. – № 5. – С. 4-10.

5. Дмитрук О.Я. Технічне оновлення як складова розширеного відтворення підприємств машинобудівного комплексу в умовах інтеграції / О.Я. Дмитрук // Вісник Хмельницького національного університету. Економічні науки. – 2010. – № 2, т. 1. – С.97-100.

6. Цихан Т.В. О концепции технологических укладов и приоритетах инновационного развития Украины [Электронный ресурс] / Т.В. Цихан // Центр политических технологий. – [Электронный ресурс] / Режим доступа : http://www.politcom.ru.

7. Йохна М. А.Трансфер технологій: форми і методи ефективного здійснення: моногр. / М. А. Йохна, П.Г. Іжевський, В.В. Стадник. – Хмельницький: ХНУ, 2007. – 230 с.

8. Державний комітет статистики України: Індекси промислової продукції (2002-2010рр.) – [Електронний ресурс] / Режим доступу: www.ukrstat.gov.ua/operativ/operativ2007/pr/prm_ric/prm_ric_u/ipv2006_u.html (19.07.2011)

9. Державний комітет статистики України: Про соціально-економічне становище України за 2009 рік [Електронний ресурс] / Режим доступу: http://www.ukrstat.gov.ua/

10. Державний комітет статистики України: Наукова та іновaційна діяльність (1990-2010рр.) [Електронний ресурс] / Режим доступу: http://www.ukrstat.gov.ua/operativ/operativ2005/ni/ind_rik/ind_u/2002.html (19.07.2011)

11. Державний комітет статистики України: Капітальні інвестиції за 2010 рік [Електронний ресурс] / Режим доступу: http://www.ukrstat.gov.ua/operativ/operativ2010/ibd/kinv/kinv_u/kinv_u04_10.htm (19.07.2011)

12. Обстеження потенціалу виробництва високотехнологічної промислової продукції за період 2005-2007рр. [Електронний ресурс] / Режим доступу: //www.ukrstat.gov.ua/operativ/operativ2008 /ibd/obstej.htm

1.4 AN APPROACH TO DEVELOPING AND IMPLEMENTATION OF QUALITY MANAGEMENT SYSTEMS IN LOCAL ADMINISTRATION BODIES

Dubiniewicz W.[1], Drapak G.[1], Tabor A.[2]

Introduction

Quality Management System (QMS) implementation in Ukrainian local administration is a complex problem to solve. Its complexity rises from methodical and perceptual issues that have both external – environmental and internal – structural origin.

---

[1] Khmelnitsky National University, Khmelnitsky, Ukraine
[2] Tadeusz Kościuszko Krakow University of Technology, Krakow, Poland

Organizational environment of local administration bodies comprises of statutory and regulatory requirements, as well as of current general tendencies in management practice.

Ukrainian legislation is mostly conforming European requirements concerning management systems on the whole and quality management systems particularly. But there are few methical sources explaining contents and consequence of activity aimed to QMS implementation. At the same time there is an obvious lack of qualified quality management specialists. Moreover, there are examples illustrating distorted representation of quality management concept and its implementation.

Structurally organization in Ukraine, no matter they are public or private, are very similar to western ones. Thus, one could say, that spreading of quality management philosophy and technologies will follow the same pattern as it has in Europe. However, external movers, as well as internal motivation of such processes are quite different and need additional exploration.

Besides that, Ukrainian enterprises are poorly equipped with computers and techs, skilled enough to use information and statistical technologies effectively.

1. Method

Experimental activity comprised of series of methical, pedagogical, practical and business actions designed to accomplish research program "Implementation of Quality Management Systems in Podillya region of Ukraine", adopted in by Ukrainian and Polish Center of Khmelnitsky National University.

Experimental data that had been obtained due to trying a generic method of QMS implementation stated in ISO 9001 4.1, [1] were used for its improving by adjusting of appropriate activity.

Experimental data, gathered through observing the effects of actions that has been carried out, were measured against planned process performance. Then, results of measurements were analyzed with use of cause-and-effect methodology in order to find out essential interconnections and choose the improvement method (Figure 1).
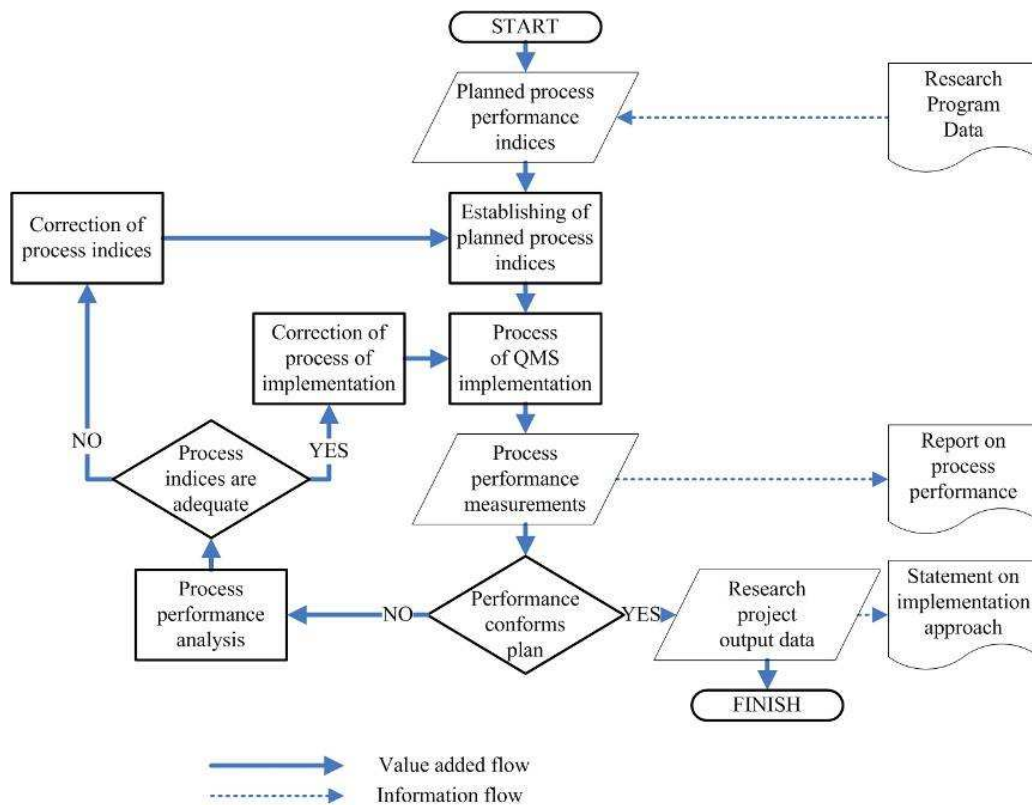
Fig. 1. Process of gathering and processing of experimental data

1.1. Participants

The research program has been designed due to cooperation between Ukrainian and Polish Center (CUP) of Khmelnitsky National University and Center for Quality Management Systems Training and Organization (CJ) of Tadeusz Kościuszko Krakow University of Technology. The program has been incorporated into overall plan of scientific work of University since 2004.

Researcher group, leaded by Prof., dr eng. G. Drapak, includes its permanent members: Prof. h. c., dr, eng. A. Tabor and eng. W. Dubiniewicz.

At different stages of the program the group were assisted or consulted by mgr J. Sierkowa, mgr R. Balicka, mgr eng. A. Repecki, mgr. A. Pieczonka, eng. W. Gerasymczuk, gr eng. O. Dubiniewicz, Prof., dr hab., eng. J. Shalapko, dr T. Kosianczuk, dr A. Krasilnikowa, mgr L. Bondar, W. Bardaczenko (Fig. 2).
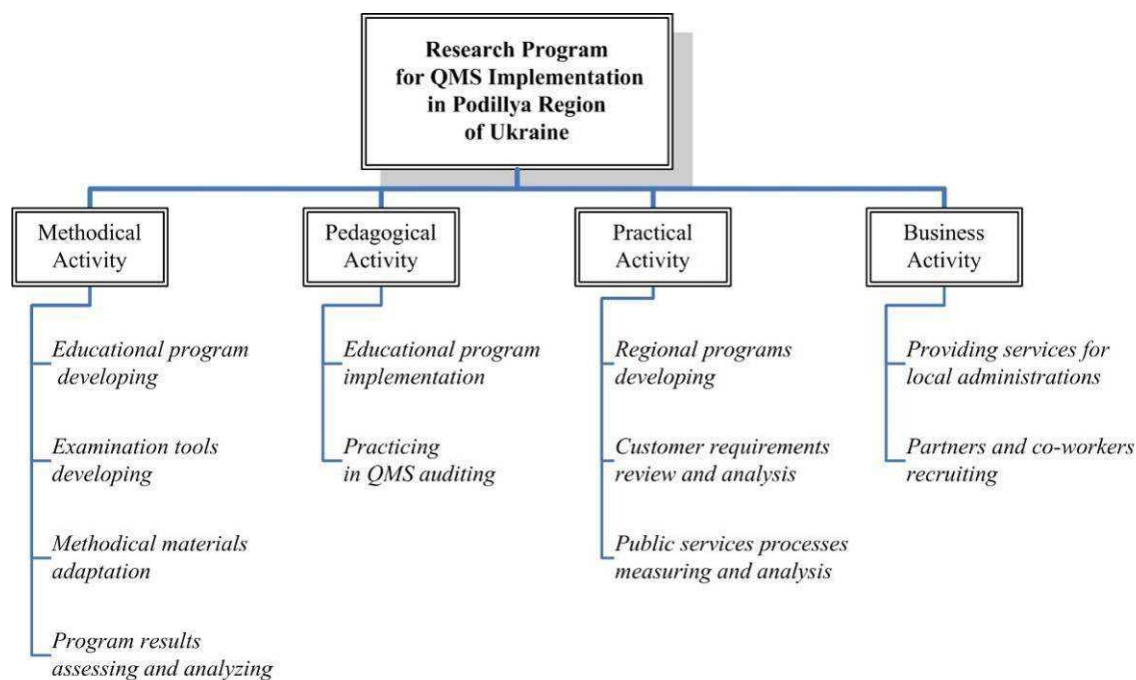
Fig. 2. Research Program Composition

Research works were conducted with the participation of local administration bodies of Khmelnitsky region, as well as business and governmental authorities.

1.2. Apparatus

Research works were based on quality management principles and methodology stated by series ISO 9001 standards. Improving overall approach to developing and implementation of QMS research group were using ISO 9004 recommendations.

Experimental processes performance measured has been analyzed with use of cause-and-effect methodology set forth by dr eng. M. Rączka in collective work edited by A. Tabor and M. Rączka. [2]

Experimental data referring to customer requirements and his perception of their fulfillment were explored by means of adjusted Kano model and SERVQUAL methodology [3][4]

Experimental data gathered were analyzed and presented in graphical view with use of Microsoft Office 2003 programs Excel and Access. Aiming at maximum simplicity, convenience and costs of analysis instruments there has been software based on Excel tools designed, approbated and implemented. They were programs:

- for automated generation of competency tests;

- for automated verifying of competency tests;

- for automated result analyzing of competency tests;

- for automated accounting of use of working hours;

- for automated generation of questionnaires for customer requirements review;

- for automated analyzing of customer requirements review results;

- for automated accounting and analyzing of process performance.

1.3. Procedure

During period from 2004 till now there has been accomplished series of methodical, pedagogical, practical and business actions as follows:

- developing educational program for training of internal auditors for QMS conforming ISO 9001 requirements (2004) and its improving (2008-2010);

- developing, approbation, implementation and improving of methodology, and instruments for estimation and approval of internal auditors' competence (2004-2007);

- developing Regional Program for Production Quality Improvement (2005);

- adaptation of methodical materials belonging to CJ for the purposes of educational program implementation (2005-2008);

- approbation and implementation of Regional and educational programs (2005-2010);

- developing, approbation, implementation and improving of methodology and instruments for customer requirements reviewing with use of Kano model and SERVQUAL methodology (2009-2010);

- performing of the analysis of customer requirements connected to services provided by local administration bodies (2010-2011);

- developing, approbation and implementation of methodology and instruments for measuring of public services process performance (2010-2011);

- performing of the analysis of process performance measurements (2011);

- practicing in internal (2004-2011) and certification auditing (2009)of QMS conforming ISO 9001 requirements;

- developing and approbation of methodology for local administration bodies process definition and the processes' matrix for QMS conforming ISO 9001 requirements (2010);

- developing, approbation and implementation of Regional Program for small and medium enterprises development (2010);

- assessing of the results of Program realization at methodical, pedagogical, practical and business activity levels and at different stages of their realization (2005-2011);

- designing of generalized approach for QMS implementation (start 2011).

Scientific cooperation between Ukrainian and Polish university in Podillya region had begun with the signing in 2002 of agreement defining framework for collateral activity of Khmelnitsky National University and Tadeusz Kościuszko Krakow University of Technology. Latter in 2003-2004, series of additional detailing articles signed allowed their parties to initiate and animate scientific program with intention of propagation knowledge about modern, progressive management technologies.

In 2004, under the conduction of A. Tabor, the processes of future project were defined. Also there were elaborated educational and business program which should facilitate research processes. The latter was intended to draw attention of business circles to the Program and to facilitate its activity with necessary funds. In order to realize business part of the program there were used mass media, as well as national and local scientific and civil information systems.

Next, the foundation of permanent scientific discussion on quality management has been the first step, which presented the possibility to approbate and adjust appropriate methodology for QMS implementation. Regular Ukrainian and Polish Conference, which afterwards got an international status, has been the animator and the catalyst that brought regional development to the upper stage.

At the very moment the implementation of pedagogical part of the program has started. It had been directed primarily to local administration authorities, as well as to pedagogical, scientific and management cadres. Most preferred form of educational activity was seminary.

In 2005 the Program for improving quality of Khmelnitsky region production was initiated. Being subjected to continual improvements the Program for the next 5 years (up to 2010) has became a frame for any enterprises concerning quality management in a region. After the Program has been discussed by local legislative organ Regional Rada, it was adopted as a local statutory order.

In order to facilitate Ukrainian and Polish scientific and educational cooperation there was founded collateral dialogue on a governmental and consular level. It resulted in agreement between Khmelnitsky National University, "Wspólnota Polska" Society and Society of Polish Teachers of Ukraine initiated and promoted by Ambassador Extraordinary and Plenipotentiary of Poland, Consul General of Poland and Senate of Poland. This allowed to provide in 2006 and 2007 necessary infrastructure and to create conditions needed for detailed elaboration of the project and of its proper execution.

Legal assisting should be considered as an independent part of scientific work because of its specific nature. It has begun in 2005 when the problem connected to licensing appeared. Later this part of the Program was incorporated into business activity.

Methodical part of the Program was designated to facilitate pedagogical and practical activity with appropriate and approbated manuals and tools. Its realization lasts until recently and is planned to be continued up to 2012. In order to provide the Program with up-to-date and most demanded materials there were established scientific and methodical dialogue with leading auditors of certification organizations namely: Polish Center for Testing and Certification, British Standardization Institute, TÜV NORD (Poland) and KEMA.

Results of the Program realization were gradually, as they have been acquired, approbated at Ukrainian and Polish and international conferences in 2006-2009.

2. Results

The Program is mostly completed, but several activities are still being executed. These are activities connected to the Regional Program for small and medium enterprises development.

Realization of the Program's methodical part resulted in appearing of methodical manual which was used for facilitating of educational seminaries. That manual was reprinted twelve times and total number of printed copies amounts more than 200. Students have noted that the manual had a lot of different forms and examples of work documents used in QMS.

Educational activity has as an it's effect more than 200 persons, which have passed qualification tests for internal auditor. Among the many parties recognized effectiveness of the Program are Regional Center for Officers' Social Rehabilitation acting in the framework of NATO Program Partnership for Peace, Regional State Administration etc.

Most informative results were obtained during practical activity to develop and implement of QMS in a town government.

Due to legislation regulations local administration bodies are encouraged to develop and implement Quality Management Systems (QMS), pointing, first of all, on a sustained need in quality products. [5] However, practice shows, that the main cause for using of quality management technology in Ukraine is a minor aim of gaining an attractive image in the face of investors.

In order to establish integrated approach in local administration Ukrainian law defines:

- any service, local administration bodies should supply to their citizens; [6]

- requirements to executive documentation; [7]

- requirements to administrative and management processes connected to correction and corrective action. [8]

Above all, there is a special organization, which is to help local administration bodies in modernizing their management systems in order to

comply European Union requirements – Center for Adaptation of the Civil Service to the Standards of the European Union. [9] The Center maintains a Register of State and Administrative Services [10] and provides information services and consulting.

In addition, Main Department of Civil Service of Ukraine has developed generic methodical recommendations for QMS implementing at local administration bodies, [11] and offered samples of procedures required.

But presently, we could talk about only a dozen of implemented QMS in local administration bodies. They are deployed mostly in local town governments at a region level and their number states about of 3 to 4% of its overall quantity.

Moreover, implementing of new versions of ISO standards has been holding over due to protracted process of translation into Ukrainian, so therefore some implemented QMS are considered as outdated.

Besides that, Ukrainian translations of series ISO 9000 standards contain mismatches that could lead to faults in the interpreting of requirements and therefore to nonconformities.

Ukraine has its own system named as UkrCEPRO (Ukrainian Certification of Production) designated for assessing conformity of production and management systems. UkrCEPRO functions in compliance with a considerable number of national standards named DSTU (State Standard of Ukraine). Essential distinctions of these standards, that differ them from European and international ones, make organizations in Ukraine to use exceeding resources in order to save conformity to UkrCEPRO and ISO requirements.

Local administration bodies lack definitions of customer requirements and use of systematic approach both in its establishing, and analyzing. Even when customer requirements review had been made, there were very few evidences that such data has been used for planning and programming.

After studying of customer requirements to services of local administration there were revealed that town citizens pay extreme attention to:

1) continual communication with local administration authorities;

2) sustainable understanding of services content, characteristics, as well as their forms and transparency.

Motivation of local administration bodies' personnel is focused rather on being threatened by a perspective of loosing their jobs than on an enhancing customer satisfaction. Therefore personnel of local administration bodies feel mostly skeptical about any innovations in management. They prefer hiding effectiveness of their work rather than participating in organization development. Results of process performance measurements that have been analyzed afterwards showed that activity appeared effective where it's planning was duly executed.

Being biased in motivation, top management authorities of local administration bodies often act in a passive way that is, evidentially, strongly depending on lack of quality management training and experience. Such a gap in an appropriate education causes local authorities to delegate their leadership role in QMS development, implementation and improvement to poorly authorized representatives. That effects in an overspending of human and infrastructural resources.

There were few local administrative organs that have had an experience of using a process approach as a generic management philosophy, as well as a particular method of managing. And all of them are connected to public finance administration or finance services. Neglecting of process approach leads to loosing control of processes (Figure 3).
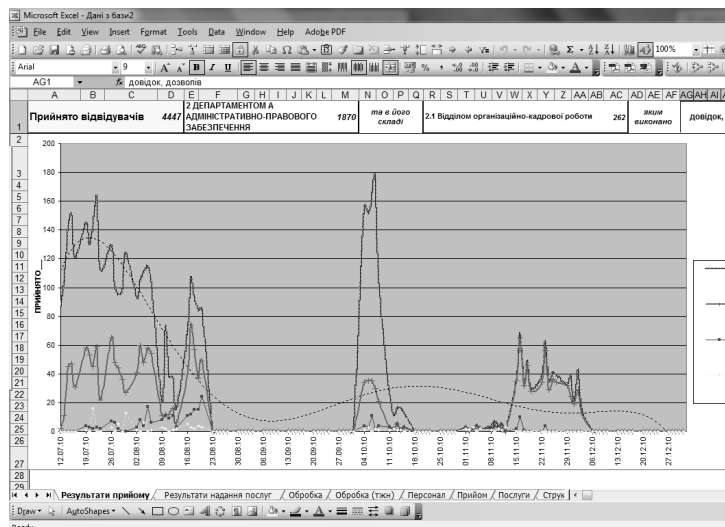
Fig. 3. Example of process performance analyzed

Central element of process approach is the process defining. A formalized method for process defining was presented and approbated. Scheme of process definition is showed on Figure 4.
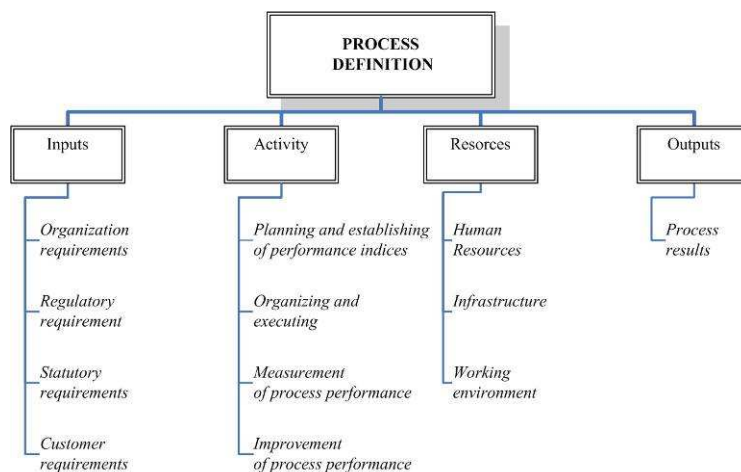
Fig.4. Scheme for process defining

Local administration bodies prefer functional differentiation of responsibilities, paying little attention to defining of personnel and organizational substructures authorities. Resources management in fractioned by functional differentiation organs is based on residual and internal reserves, and therefore this process lacks transparency.

Processes' performance, appropriate metrics and statistical process control (SPC) are out of managers' attention, so they could hardly get an adequate process appraisal, as well as its due correction or improvement. This and the fact that Ukrainian legislation is quite fluctuant compel local administration should assign additional resources:

- to meet statutory requirements;

- to keep quality policy adequate;

- to maintain personnel due competence and

- to distribute infrastructural resources duly.

Summarizing, it should have been sad, that, presently, implementation of QMS in local administration bodies uses excessive resources with little or few effect. Thus, the aim of the research was the formulating of effective and cost efficient approach for the QMS developing and implementation in Ukrainian local administration bodies.

Discussion

Results of The Program accomplishment analysis allows to state that implementation of Quality Management Systems in local administration bodies should be oriented on customer requirements fulfillment.

Most important elements of QMS implementation are:

- local administration authorities need to participate in educational programs in order to get acquainted with quality management philosophy and methodology;

- propagation of the "best practice" in quality management will allow shortening of human resources used for process approach implementation;

- process of QMS implementation should refer to quality management principles;

- special attention should be paid to process performance indices, measurements and metrics;

- planning is essential for ensuring that the process is controllable;

- during process of planning customer requirements review and results of it's analysis should be considered.

Appreciation

Authors would express their appreciation to Prof., dr hab. eng. M. Skyba, Prof., dr h. c., dr hab. eng. J. Gawlik, Prof. dr hab. eng. L. Wojnar, Prof dr h.c., dr hab. eng. L. Dobrzański, Prof. dr hab. M. Jochna, dr eng. S. Truś for their unprecedented and invaluable helping, assistance and consulting which allowed the discussed program to become realized.

Reference

1. Національний стандарт України. Системи управління якістю. Вимоги ДСТУ ISO 9001:2009 (ISO 9001:2008, IDT)

2. Nowoczesne Zarządzanie Jakością, collective work edited by A. TABOR and M. RĄCZKA, Tom II, Metody i Narzędzia Jakości, ISBN 83-919887-4-0, p. 87-118.

3. Wan Zahari, Wan Yusoff and Maziah Ismail (2008). Fm-Servqual: A New Approach Of Service Quality Measurement Framework In Local Authorities, Pacific Rim Real Estate Society

4. Landrum H., Prybutok V., Zhang Xiaoni, Peak D. (2009) Measuring IS System Service Quality with SERVQUAL: Users' Perceptions of Relative Importance of the Five

SERVPERF Dimensions, the International Journal of an Emerging Transdiscipline Volume 12, 2009

5. Concept of State Policy in Quality Management // Офіційний вісник України від 06.09.2002 - 2002 р., № 34, стор. 238, стаття 1620, код акту 23050/2002

6. The Law of Ukraine On Local Self-Government in Ukraine // Офіційний вісник України – 1997 р., № 25, стор. 20, код акту 1051/1997

7. Уніфікована система організаційно-розпорядчої документації // ДСТУ 4163-2003

8. The Law of Ukraine On Citizens' Appeals // Відомості Верховної Ради України, 19.11.1996 – 1996 р., № 47, стаття 256

9. http://www.center.gov.ua

10. http://reestr.center.gov.ua

11. http://www.guds.gov.ua/control/uk/publish/category?cat_id=53688

1.5 SOME ECOLOGICAL PROBLEMS OF MANUFACTURING PROCESSES

Matuszewski M.[1], Musiał Ja.[1], Styp-Rekowski M.[1]

Introduction

Every manufacturing process generates imminence for natural environment. Degree of that imminence, first of all depends on technical level of plant: the higher level – the less negative influence on environment. The imminence depends also and in great part on ecologic consciousness of staff that creatively work at the plant. It is because the ecologic hazard appears already in the stages previous to manufacturing process – as a result of machine design and working out of processing for the machine elements. These imminences materialize themselves during production.

Rapid development of human activities in a lot of industrial branches provokes situation that growth of this activities negative effects runs ahead of ability in removal them. Therefore it is rationally to endeavour after prevent their formation and does not react only when they appear. Realization of this correct way of work requires identification of the imminences, location of places

---

[1] University of Technology and Life Sciences, Bydgoszcz, Poland,

where they are generate and work out minimizing methods of their negative effects. These problems are presented in below consideration.

1. Environmental hazards induced by manufacturing processes

In cybernetic system one can assume manufacturing process as the system with three paths of inputs (i) and outputs (o):

- mass (M),

- energy (E),

- information (I).

On the input of the mass path (M) – see Figure 1, there are materials from whom final products are made, basic means of production: tools and operating fluids and auxiliaries means, e.g.: containers for interoperation transport and for finished products. On the output at this track there are, first of all final products, wasted (partially or completely) tools and operating fluids and their by-products (vapour and dusts), mentioned above containers and residual materials.
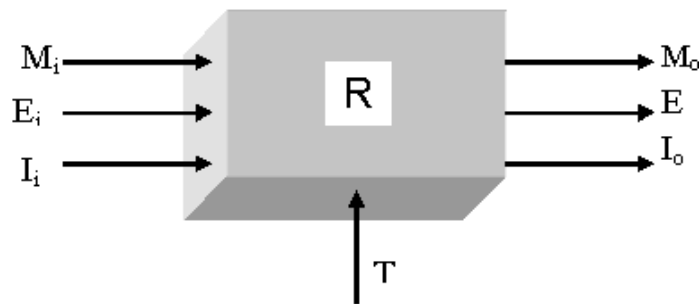
Fig. 1. Manufacturing process in cybernetic formulation

On the input of energy path (E) there is energy directly necessary to realization of manufacturing processes and also for auxiliary activity (feeding, washing and the like). Energy output the most often is difficult to unambiguous identify. On the output of energy path there is heat generated among other things as a result of friction processes. There is also some amount of heat that is supplied to manufacturing processes (e.g. in plastic processing) for assurance their regular run and than, together with medium at mass path is carried away to surroundings. Energy is in general dissipated on the output and energy output partially coincides with mass output.

On the input of informative path (I) there are parameters of manufacturing process that ensure correct run of the process which guarantee high quality

products. These features, mainly of basic product but also of by-products, are identified as informative output. At this path may also exist information files recorded on the diskettes, CD-ROM or other data carriers and then outputs of mentioned data carriers will also exist on information output of manufacturing process.

Manufacturing process is not isolated from surroundings system, therefore on its outputs there are also interferences (T) which are able to change relations (R) between inputs and outputs.
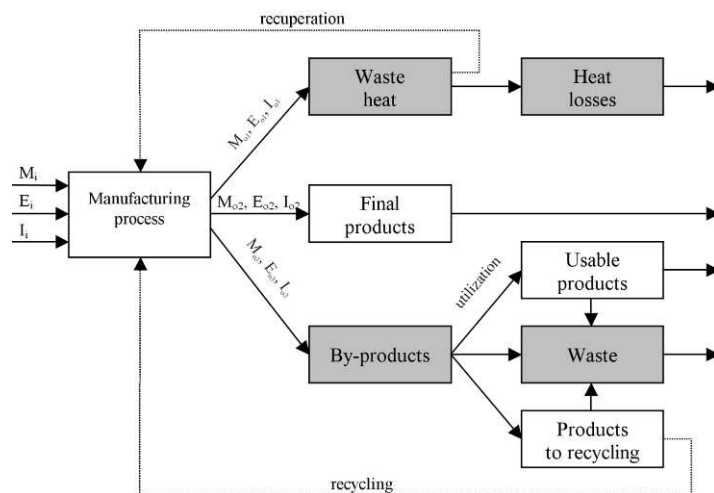
Fig. 2. Scheme of manufacturing process and places where environmental hazards are generated with indicated ways of minimizing

Existing in machine-building industry manufacturing processes the most often have very complex structures. For elements production, which are sometimes characterized by many different features, manufacturing process with a lot of operations is necessary. In such complicate process it is possible to distinguish two type of basic processes: mechanical, thermal.

In Fig. 2 there is shown the block diagram of typical manufacturing process with marked (darken) places where environmental hazards are generated. According to process character all specified in scheme elements or some of them only, can exist. Shares each of them are different.

1.1. Imminences in manufacturing processes mechanical type

As a manufacturing process mechanical type, the process in which mechanical decrementless treatment (e.g. plastic working) or machining (e.g. turning, milling or grinding) are dominant is understood.

Analyzing earlier identified three path of mentioned process it was found that imminences are generated mainly at mass path but there are the greatest possibilities of minimize their effects. As by-products, always present in this type of processes, there are waste of material in the form of chips or blanking scraps, which after waste recovery in steel mill as a full value materials return to other manufacturing process. Blanking scraps can also be directly used as input-material to other useful goods production.

On the mass input there are also various kind of operating medium. In professional References one can find a lot of information about methods of environmental hazards minimization, e.g. by recycling or utilization [7, 11] therefore they are not analyzed in this paper. More and more attention is paid to using lubricants, hydraulic, fluids and coolants, harmless for environment [1, 3]. It is a good example of correct prevention.

Cycle of some tools at mass track we can also present as the example of recycling. Replaceability of their cutting edges and possibilities of regeneration – are the features which increase tool time of life, thus they are very desirable features from point of view of ecology.

Imminences generated at energy track of mechanical manufacturing process are not dangerous for human surrounding. It is the reason that possibilities of their suppressing methods are not searched hard. Electric energy (mainly in this form energy is supplied to mechanical type of manufacturing processes) during machining in a great part is changed to heat energy and then it dissipates by out of control means to surroundings. There are known examples that heat generated during machining is used again to cementation realized directly in machining zone.

1.2. Imminences in thermal type of manufacturing processes

Process in which thermal processes, both exo- and endothermic, are dominant, e.g. plastic or pulp and paper processing, is understood as thermal type of manufacturing process.

At mass path of this process among other things there are plastics. Plastics wastes storage at waste dump can be a great ballast for natural environment. It is the cause that utilization is very often applied for this imminence minimizing. In

recycling process physic-chemical and mechanical properties are used. It is the sphere in which recycling is the most often.

On the mass input of manufacturing processes, no matter what type, there are also machine- tools. In this case recycling is possible too, both – the machine as a whole and as the elements set.

Worn out elements after regeneration are possible to use again and it is the form of recycling possibility of machine-tool as the elements set. Simultaneously regenerability of elements designate ability of usage to them the recycling process.

Because manufacturing processes thermal type are energy-consuming processes the natural matter is attentiveness about the best, if possible, advantage of input energy. One of this way is heat recovery.

At informative path of thermal manufacturing process, similar as of mechanical one, imminences for environment are not so important and in further parts of this paper they will not consider.

2. Pro-ecologic activities

Since a long time is generally well-known that prevention of harmful phenomena is more effective than removal their consequences, therefore more and more attention is paid to environmental protection. There are several prevention methods but the most often are applied:

pro-ecological designing,

minimizing of working media amount.

biodegradable materials applying,

2.1. Pro-ecological designing

Mentioned above notice indicate that the best results in the domain of environment protection one get already in designing stage – just before manufacturing. That is why strong trend towards pro-ecologic designing exists. It is possible to distinguish two following domains:

constructional – previous to manufacturing processes,

technological – basic for manufacturing processes.

In the first field a choice of constructional features: geometric, material and dynamical is realized. For environmental protection particular influence has material constructional features, i.e. features which describe characteristic

properties of material used to production of machine elements. These features decide about machine's performance. One of basic material property ought to be its recycling compliance in utilization processes of machines on this way protect (or minimize influence) natural surrounding against impurity owing to worn elements storage. It is possible to obtain the same or similar effect of designing the elements in the way that their regeneration will be possible and profitable.

In the second field of pro-ecologic designing – technological, in which manufacturing processes are worked out, imminences are generated mainly in the following areas:

- rising by-products (in the solid or fluid form),

- heat dissipation to surrounding,

- gas and dust emission,

- vibration and noise accompanying to manufacturing processes.

In all above mentioned cases it ought to be aimed to minimize of these factor reaction by choice of machining process kind in which mass of generated waste is the smallest, e.g. wasteless cutting or dry turning, possible thanks to application of better and better tools and machine-tools [6, 8].

Mentioned above fields very often interpenetrate, therefore both are very important for considering problem. During designing of machine-tools which will realize assumed manufacturing processes it ought to be considered possibility to equip them with units which minimize negative results of realized manufacturing process, e.g. with units making possible recycling of operating fluids.

2.2. Minimizing of working media amount

The factors that could be potential hazard for natural environment were mentioned above. Ones of the most ecological danger (great amount) are waste materials. In this group among others are cooling and lubricating fluids, necessary in machining, as well as – media in operating processes. Reduction of cooling-lubricating fluids amount in machining process causes faster wear of cutting tool but on the other side – smaller medium amount has possibility to penetrate to surrounding – directly and indirectly. Exemplary of investigations results in mentioned range are presented in Fig. 3.
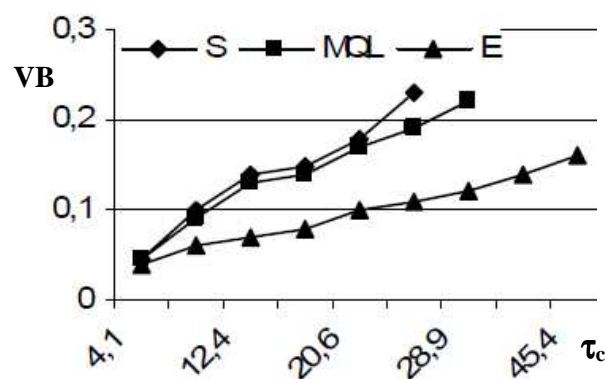
Fig. 3. Changes in the time of volumetric wear coefficient VB of cutting tool edge during turning: S – dry, MQL – minimal quantity lubricating, E – emulsion 4 dm^3/min [4]

Visible greater intensity of wear process or smaller environmental hazard it is problem for solving by technical staff but necessary is also the help from scientists. Results of investigations in mentioned range are published in publications, e.g. [4, 5, 9].

2.3. Biodegradably materials in technical processes

Influence of lubricating media on environment in which technical objects are operating, the most often has unfavourable character. First of all it results from chemical constitution of lubricants. As the mixtures of hydrocarbons, produced from rock-oil products (mineral greases) or synthetically, they penetrate into environment and cause its pollution and, in further consequence – its degradation.

In practice it is impossible fully eliminate any contact of lubricants with surrounding, therefore biodegradable lubricants are applied. Under influence of natural environmental factors they have ability to biodegradation onto environmentally harmless components. This feature concerns whole lubricant or some of their fractions; concerns lubricant additives too.

Biodegradability is tested by several tests. One of the modern is CONCAWE test [2]. It should be noted that CONCAWE biodegrability test is essentially ISO 14593, with modifications that are permitted in the International Standard. Biodegrability degree of some oil product is compiled in Table 1. For comparison measurements were made using CONCAWE and standard OECD

301B tests. One can see that both tests give similar results(test CONCAWE – little bit greater values).

Table 1 - Biodegradability of exemplary oil products in different tests, acc. t o [2]

No.	Oil product	Biodegradation in the test	
		CONCAWE (% ThIC after 56 days)	OECD 301 B (% ThIC after 28 days)
1	Octadecane	88	81
2	Environmentally acceptable hydraulic fluid (rapeseed base oil)	77	82
3	Hexadecane	72	74
4	Synthetic diester	65	31
5	Mineral base oil (solvent-dewaxed heavy paraffinic oil)	65	23
6	Mineral base oil (hydro treated slack wax)	50	48
7	White oil	21	11

Biodegradation degree ≥60% ThIC (Theoretical Inorganic Carbon) indicates that the product under test possesses is inherent ultimate biodegradability. A test result <20% ThIC indicates that the test substance is not inherent biodegradable under test conditions, and biodegradation degree in the range ⟨ 20, 60⟩ ThIC indicates that the product is capable of undergoing partial biodegradation.

3. Exemplary activities on behalf of environment protect

Interesting effects in the domain of environmental protection was get as a result of realization of special ecologic program which prefers continuous put into practice complex preventive strategy of environment protection. This strategy reduces imminences for people and their surrounding generated by production of consumer goods and their existence. Findings of results of program realization were compiled below – in Table 2.

For manufacturing processes realization of this program means saving of mineral raw materials, by-product elimination and reduction of waste and impurities amount.

Table 2 - Changes of emitted waste amount as result of pro-ecologic program realization

No.	Medium	Units	Quantity		Change	
			before	after	quantitative	%
1	Solid waste	Mg	372520	356870	15650	4,2
2	Fluid waste	m^3	1533630	1432337	101293	6,6
3	Gaseous waste	Mg	6122709	6005962	116747	1,9
4	Water	m^3	8787213	7064038	1723175	19,6
5	Energy	GJ	1932000	1613370	318630	16,5
Total economical effect of 71 implementations: ca. 3.000.000 EUR						

Towards consumer goods, results of program concentrate on reduction of their influence on environment in whole cycle of goods existing, beginning from raw materials getting, on worn products storage – ending. Such strategy of natural environment management limits expensive removal of production influences, and thereby makes manufacturing processes more effective.

During the program there were improved management and control process of production at more than 50 industrial plants. Results of these activities were very significant, both – in ecologic and economic meaning.

Closure

Presented above theoretical considerations and described practical example prove that environment protection is not only proper activity but it can be profitable job.

Pro-ecologic activities not always need great cost for technical equipment. Sometimes to this aim it is possible to apply the machines designed to other job (but similar character). Mentioned above the practical example shows also that when pro-ecologic activities needs costs, they fast paid back. In described examples the time was from 3 to 36 months.

Such great and fast economic effects are unfortunately also the sign that realized in industry manufacturing processes are far from perfection.

References

1. Bartz W.J.: Synthetic Hydraulic Fluids – A Survey. Proceedings of 7th Intern. Conference on „*Tribology*", Budapest (Hungary) 2000, pp. 9÷32.

2. Battersby N.S.: The CONCAWE Biodegradability Test for Oil Products.

Proceedings of the 12th International Colloquium „*Tribology 2000 – Plus*". Esslingen (Germany) 2000, pp. 113÷116.

3. Fodor J.: Environmentally Acceptable Lubricants. Proceedings of 12th International Colloquium „*Tribology 2000-Plus*", Esslingen (Germany) 2000, pp. 131÷134.

4. Leppert T.: Tool-edge Wear in Dry and MQL Turning. Proceedings of the 3rd Conference „*Machining. Advances Technics*". Bydgoszcz 2009, pp. 163÷169 (in Polish).

5. Li K.M., Liang S.Y.: Modelling of Cutting Forces in Near Dry Machining under Tool Wear Effect. International Journal of Machine-tools and Manufacture No. 47/2007, pp. 1292÷1301.

6. Oczoś K.E.: Nature, Importance and Development of Hybrid Metal Removal Processes. Proceedings of VIth Conference „*EM2000 (Electromachining)*", Bydgoszcz – Wenecja (Poland) 2000, pp. 145÷164 (in Polish).

7. Potrykus J.: Replenishment of Lubricating Materials and Water-Oil Coolants, Proceedings of VIIth International Conference on „*Machinery Recycling*", Bydgoszcz (Poland) 1997, pp. 171÷177 (in Polish).

8. Sahm D., Schneider T.: Geht es auch ohne? Werkstatt und Betrib, No. 1-2/1995. pp. 17÷24.

9. Styp-Rekowski M., Ozimina D.: Environmental Conditioning of Rolling Bearings Pairs Lubrication. Proceedings of IVth International Conference "„*Advances in Production Engineering*". Warsaw (Poland) 2007, pp. 384÷391.

10. Styp-Rekowski M.: Recycling in Some Manufacturing Processes. Proceedings of VIIth Intern. Conference on „*Machinery Recycling*", Bydgoszcz (Poland) 1997, pp. 171÷177 (in Polish).

11. Styp-Rekowski M.: Operational and Constructional Problems of Working Fluids Recy-cling in Erosive Machines. Scientific Publications of Technological and Agricultural University No. 229, s. Mechanics vol. 47, Bydgoszcz (Poland) 2000, pp. 31÷42 (in Polish).

1.6 NEW TECHNOLOGIES FOR INTENSIFICATION OF SEWAGE TREATMENT FACILITIES

Andreev S.[1], Demydochkyn V.[1]

Discharge of domestic and industrial wastewater into open water bodies is a significant factor leading to deterioration of their condition. The scale of

[1] Penza State University of Architecture and Construction

human impact is currently exceeded the permissible limits due to the ability of water to cleanse itself. This led to an increase in water sources of background values as the total content of organic matter and some toxic components.

Russian demands on the quality of wastewater discharged into the reservoir, are among the most stringent in the world. For example, the requirements for the quality of wastewater discharged into open waters, the EU member states on the BOD and suspended solids are 15-20 and 20-30 mg/l, and for Russia, respectively, 3-6 and 6-15 mg/l. Rigid requirements for the quality of wastewater to exist on the face of limited financial capacity of enterprises that have on its balance sheet treatment facilities. All this necessitates the use of new technological and design solutions for wastewater treatment.

At the Department of Water Supply and Sewerage "of Penza State University under the supervision of the author has developed a number of new technological solutions to significantly improve the efficiency of sewage treatment facilities. One such solution has been realized in the technology of the return activated sludge aeration tanks flow through its serial processing in the ejector device and electrohydrodynamic (EGDU).

Pumping return sludge in the aeration tanks at the station's head of biological wastewater treatment, as a general rule, airlift facilities or centrifugal pumps. When pumping sludge centrifugal pumps excess energy flux is not used and is irrevocably lost. This circumstance allowed to offer new technology, providing for utilization of excess energy flux return activated sludge by its serial processing in the ejector and EGDU. The proposed technology makes it possible to implement the following methods of exposure to the sludge mixture: 1) saturation of the activated sludge oxygen excited spirit, 2) effects on the activated sludge of high turbulence, and 3) electric treatment sludge.

When pumping through the ejector flow return sludge is sucking air, resulting in the withdrawal of the ejector is formed siltaired mixture. To intensify the process of saturation of silt mixture with atmospheric oxygen and the implementation of its technology electroactivation of design electrohydrodynamic device consisting of two coaxially connected camera: input (diameter D) and trunk (diameter d).

In the trunk EGDU created intensive rotational-translational motion mapping siltaired mixture, characterized by elevated round lence. EGDU can be regarded as a very perfect mixer, which considerably intensify the process of mass transfer siltaired mixture mixture formed after the ejector. In order to intensify the activation process sludge mixture trunk EGDU divided insulating sleeves on the cathodic and anodic areas, which supplied the electric potential. In contrast to previously used technologies electroactivation sludge mixture in electrolyzers with a traditional plane-parallel electrode system, processing the mixture in the barrel siltaired mixture. EGDU is a system of coaxial tubular electrodes, does not involve the simultaneous finding her in the anodic and cathodic areas. The siltaired mixture.having a rotational-translational motion, in turn passes the cathode and anode zones, which significantly modifies the re presses her treatment.

All variety of effects of electric field and electric current on bacterial cells is reduced to the following consequences: 1) increased microbial activity due to increased membrane permeability, and 2) activation of microorganisms due to increased activity of extracellular enzymes and a number of superficial receptors of cells, 3) intensification of the processes of intracellular metabolism.

Studies have been conducted on the pilot plant.

The installation includes an experienced and two control intermittent aeration tank with a capacity of 0.1 m^3 each. Sludge mixture from the secondary clarifiers is pumped into experimental and control aeration. Before serving in the test sludge aeration tank mixture is treated in the ejector and EGDU. Mixture of silt flowing into the first control aeration tank are processed only in the ejector, a second test came aeration untreated sludge mixture. As a criterion for defining the general state of sludge mixture and its ability to oxidize organic pollution of wastewater was accepted indicator of the general dehydrogenase ac Noah efficiency. Dehydrogenase activity was determined by a standard technique based on the restoration of colorless 2 -, 3 -, 5-triphenyltetrazolium chloride (TTC) dehydrogenases in colored threephenilformazan.

Depending on changes in dehydrogenase activity (DHA) in the treated sludge mixture from EGDU polarization voltage V, B, and type of the electrode system shown in Fig. 1.
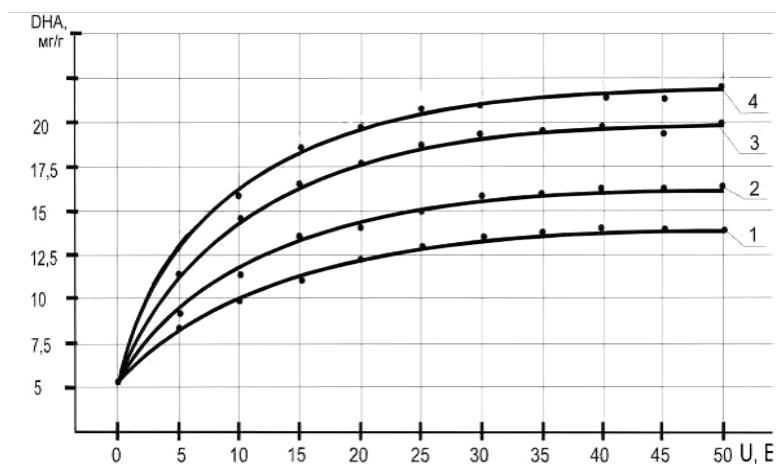
Fig. 1. Depending on changes in dehydrogenase activity treated in EGDU sludge mixture from the polarization voltage and the type of electrode system at $v = 1,5$ m/h: 1 - block electrode (the cathode-anode), . $l_к = 0,2,l$ $l_а = 0,4$ m; 2 - block electrode (the cathode-anode), $l_к = 0.4$, $l_а = 0,2$ m; 3 - block electrode (anode-cathode-anode) $l_к. = 0.2$, $l_а = 0,4$ m; 4 - block electrode (the cathode-anode-cathode), $l_к = 0.4$, $l_а = 0,2$ m

The first phase of research follows dovany revealed that:

1) is the optimal electrode sheath EGDU "cathode-anode-cathode" with the ratio of the lengths of the cathode to the anode of 2:1, 2) flow rate ilovozdushnoy mixture through the barrel EGDU of conditions to ensure maximum DHA should be taken within the $v = 1,5$ -2.5 m/s, and 3) the most significant increase in enzymatic activity in the treated sludge mixture EGDU occurs at higher voltages the polarization of the coaxial electrode system stem EGDU from 0 to 30V.

For the second stage of the research samples from the pilot and pin role of Nogo aeration tanks was filtered and analyzed the following to ka indicators of quality of wastewater: COD, BOD_5, ammonia nitrogen, phosphates. Depending on changes in the concentration of organic pollutants in the process of biological treatment in experimental and control aeration tanks on the duration of aeration pre sented in Fig. 2.

Our study showed that: 1) sequential processing of sludge mixture in the ejector and EGDU to significantly increase its activity, 2) the concentration of pollutants in wastewater, transmitted large biological treatment for 5 h using a mixture of sludge treated by the proposed technology, decreases compared with the concentration of pollution of wastewater, untreated activated sludge with a

mixture of factors: COD - 2,3 times; BOD_5 - in 1,7 times - in 1,2 times - in 1,6 times.
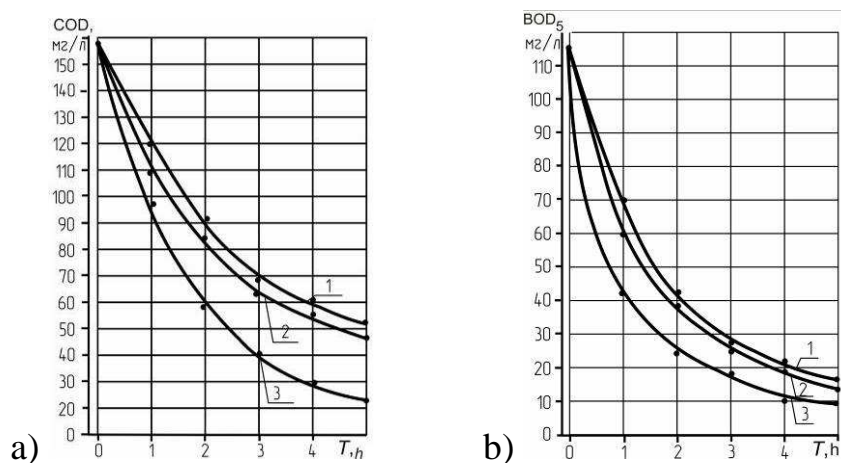
Fig. 2. Depending on the changes: a - BOD_5 **, b - COD wastewater in the process of biological treatment in an experimentalaeration tanks and control the duration of aeration: 1 - untreated sludge mixture, 2 - silt mixture was treated in the ejector; 3 - silt mixture was treated in the ejector and EGDU**

Activation technology flow return sludge aeration tanks by utilizing its excess energy introduced:

- To sewage treatment plants Togliatti Samara Region $290,000 \, m^3 / day$ capacity. Average annual economic effect of the introduction amounted to 13.5 $m\ln$. in prices of 2011;

- To sewage treatment plants Zarechny Penza region capacity $30,000 \, m^3 / day$. Average annual economic effect of the introduction amounted to 2.2 $m\ln$. in prices of 2011.

Technology intensifying biological wastewater treatment in the aeration tanks was in 2004 awarded the bronze medals of the International Fund for biotechnology Academician Blokhin I.N. and the All-Russian scientific-industrial forum "United Russia - 2004" (GN-Novgorod).

Under the leadership of the author has also been developed and brought to the stage of practical implementation of new technology flotation for treating industrial waste water, including the use thinly dispersed water-air mixture.

The finely dispersed effective removal of oil emulsions is possible only if the size of air bubbles 0.1-1 mm. Currently, water-air mixture so the degree of dispersion obtained by the method of allocation of gas from the supersaturated

liquid. The value of gas saturation of the flotation volume in this case depends on the maximum concentration of dissolved air.

Increase the concentration of dissolved air can, by increasing the pressure in the saturator.

Experience in operating pressure flotation suggests that an increase in pressure in the saturator more 0,3-0,4 MPa reduces the efficiency of removal of petroleum products. This can be explained by the fact that along with increasing gas content of the flotation volume with increasing degree of supersaturation of the liquid is formed and the decrease of dispersion of air bubbles. In order to increase the gas content of the flotation volume was requested to obtain a stable emulsion by dispersing fine bubbles in the water-air mixture formed after the ejector.

Dispersion of bubbles in the water-air mixture, is delivered in a vortex mixing unit (APU), a special design. Using new technology allowed a considerable increase effect of flotation for treating industrial wastewater.

Technology fine dispersion of water-air mixture introduced to: - Site flotation cleaning of polluted runoff CHP-1 Penza capacity of 1200 m^3/day. Average annual economic effect from implementation of the proposed technology has made 1,9 $m\ln$. in prices of 2011. On the local treatment plant OAO Penzdizelmash "Penza capacity of 500 m^3/day.

Confirmation of the annual economic impact of the introduction was more than 0.42 $m\ln$ in prices of 2011.

In 2009, the scientific development "Flotation oily waste water using vortex mixing devices, were awarded the diploma of the Moscow international salon of innovations and investments.

At the Department of Water Supply and Sewerage "was developed and implemented a combined system of air aeration, providing for joint use of fine-bubble aeration and mixing of vortex airlift devices (SEM). SEM can be considered as an analogue of a mechanical stirrer. SEM allows you to create rotating ascending-descending flow of liquid in the aeration basin, which leads to the emergence of a countercurrent gas and liquid phase and increases the efficiency of fine-bubble aeration system. The design of the vortex airlift devices (SEM) does not contain any rotating parts, which greatly simplifies the

process of their exploitation. Replacement of mechanical agitators airlift hydrodynamic vortex mixing devices can eliminate the shortcomings inherent in pneumo mechanical aeration system.

The main characteristics of the operating mode airlift device are: the , defined as the ratio φ coefficient of gas content of water-air mixture of airlift zone occupied by gas Wg, m^3, to the total airlift zone We, m^3, reduced velocity of gas, or the intensity of bubbling Je, m/s, determined as the ratio of consumption supplied to the airlift of air Ov, $m^3/$ s, the cross-sectional area airlift Fe area, m^2; relative time - the ratio of time spent in the airlift area gas T, C, residence time in the airlift zone fluid Tx, c; relative expenditure - the ratio of volumetric flow passing through the airlift gas Og, $m^3/\sec$, the flow of pumped fluid through the airlift Ozh, $m^3/\sec$.

Experimental studies of the process of mixing airlift device it was found that the reduced fluid velocity and the coefficient of gas content V_g water-air can be determined from empirical equations:

$$V_g = 0,622 J_E^{0,4}; \qquad \varphi = 1,258\, J_E^{0,846}, \qquad (1)$$

Experimental Study of mixing and aerating the water using wind, carried on the apparatus comprising: a compressor, rotameter, valves, pipe aerator "Akva-layn", SEM, a water tank.

Tangentially attached to the trunk of a wind turbine intake pipes to ensure the creation of the rotational motiontion liquid. Circumferential velocity of the liquid in the bottom layers at the reduced rate of flow of the gas phase into the trunk of airlift $Je = 0,16$ $m/$ s, had values $v_{od} = 0,05\text{-}0,11$ $m/$ s, the speed of the downward flow of fluid in the wall regions reaching a value of $v_{нn} = 0,14 \, m^3/\sec$.

Determination of the dependence of the volumetric oxygen mass transfer coefficient K_{la} on the intensity of aeration was carried out by the standard method of variable oxygen deficiency in water.

Deoxygenation produced water with a consequent increase of dissolved oxygen concentration in the aeration process with a given intensity of aeration J, $m^3/ (m^2 \cdot$s$)$. For deoxygenation of water use enjoyed sodium sulfate with the addition of a catalyst - cobalt chloride. The concentration of oxygen dissolved in

water, dissolved oxygen was determined using a brand-AZHA 101.1 M . The share of air incoming at windmills, controlled by a rotameter and was defined as the ratio of air flow supplied to the wind, Qve to the total flow rate of air supplied to the tubular aerator «Aqua- line» and wind Qvo .

The results of experimental studies of mass transfer of oxygen, are presented in the form of graphs in Fig. 2.
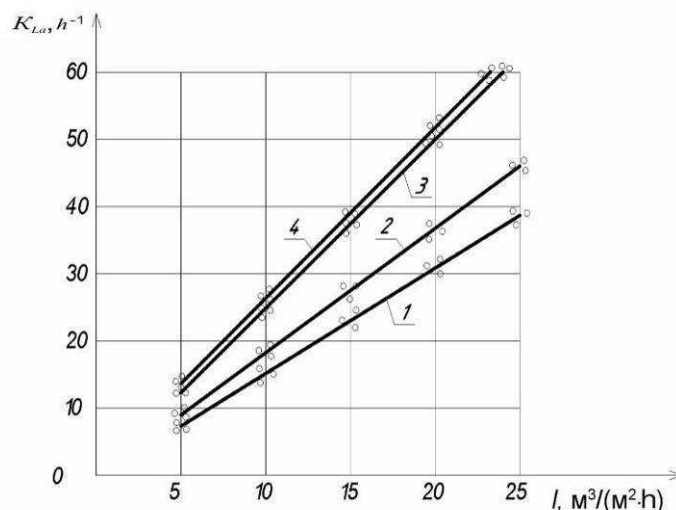
Fig. 3. The dependence of the bulk mass transfer coefficient K_{La} oxygen from the aeration intensity J and the proportion of air supplied to the rotational airlift device $\overline{Q} = Q_{вэ}/Q_{во}$: 1 – $\overline{Q}_а = 0$; 2 – $\overline{Q}_а = 0,05$; 3 – $\overline{Q}_а = 0,10$; 4 – $\overline{Q}_а = 0,2$

Studies have shown that wind power is an effective mixing device that allows a backflow effect and increase the degree of mixing of the aeration basin. Optimum operation of the combined system of aeration was observed in the proportion of air supplied to the multiplier, = 0,1. When applying 10% of the total consumption of compressed air wind turbine and 90% of total spending - for fine-bubble aeration system, aerator efficiency increases by 1.6 times.

Combined technology of aeration sludge mixture aeration tanks was implemented at sewage treatment plants .Kamenka - town of the Penza region, capacity $87,000 \, m^3/day$. Average annual economic effect of the introduction amounted to $0.22 \, m\ln$ .in prices of 2011. Andreev SY was proposed and tested in industrial wastewater treatment plants the technology of the provisional municipal wastewater in the vortex hydrodynamic devices (VGDU).

The proposed technology provides for the disposal of excess energy energy flow of wastewater pumped into urban wastewater treatment plants by feeding them at a residual pressure in VGDU, installed over the chamber quench pressure. Technology of the pretreatment of wastewater can implement the following methods to disperse the impact of wastewater systems:

1. Impact on waste water of high turbulence, leading to ortokinetical coagulation of fine particles and washing chalk FIR mineral particles adhere to them from organic pollution.

2. Saturation of the wastewater oxygen and increasing the Eh potential.

3. Bio coagulation   wastewater treatment using excess accurately activated sludge.

Washing of fines from the sand to adhere to these organic contaminants can intensify the work of Grit, significantly increase the efficiency of the detention of fine fractions of sand, to reduce the sol sion of sediment sand traps, fix it rot.

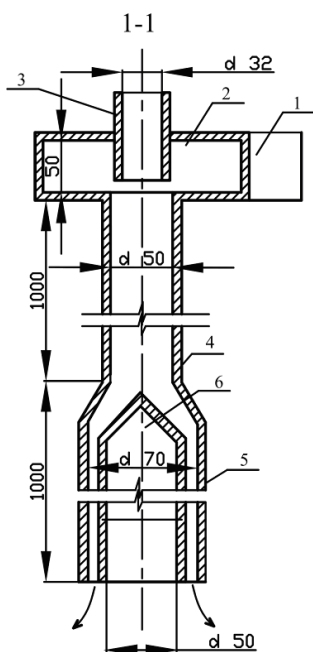
Fig. 4. Scheme of vortex hydrodynamic devices: 1 - tube entrance; 2 - Camera Input, 3 - air tube, 4 - vortex chamber; 5 - mixing chamber; 6 - body wrap
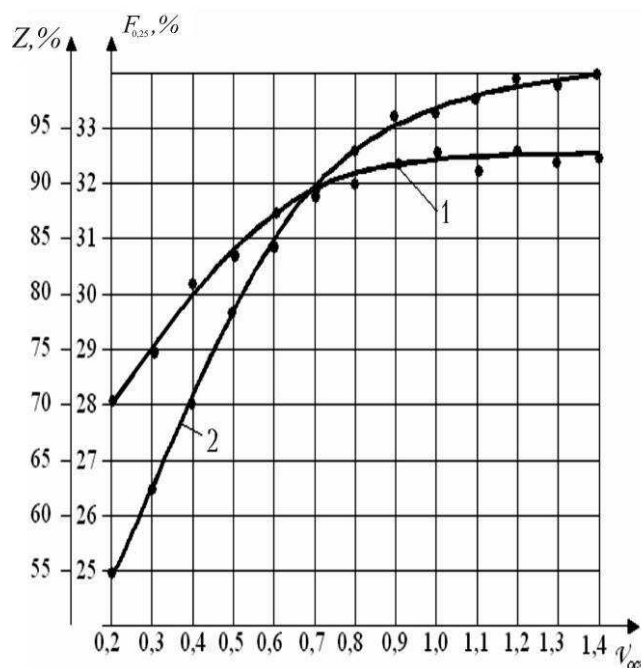
Fig. 5. Depending on changes in ash content of sludge B, the detainee in a model sand catcher (1), and the percentage content of sand fractions of less than 0.25 mm (2) the average axial velocity of the fluid vos in the vortex chamber VGDU

Reducing the concentration of suspended particles of mineral composition in waters entering the aeration tank, leads to a significant edge with reduction increase of silt, as the mineral particles almost completely passing a lot of excess sludge. The reduction rate of activated sludge by allows us to not only reduce costs associated with its disposal, but also increases age sludge. Increased age sludge to deter dividing the value (usually 5-7 days) causes a significant intensification process of biochemical oxidation of ammonium nitrogen.

Studies were conducted on the pilot plant, which consisted of: VGDU with a diameter of vortex chamber $dvk = 50\,mm$, a tank-flow divider model sand catcher and a model of sump. VGDU scheme shown in Fig. 4.

VGDU includes a cylindrical chamber with tangential entry attached to her nipple input 1, the vortex chamber 4 and chamber displacement 5. Due to tangential fluid under residual pressure through a pipe 1 in the chamber entrance 2 is created flow with vortex motion. In the transition from the chamber entrance, having a diameter D_{kv} in coaxially attached to it swirl chamber having a diameter d_{bk}, the angular velocity of the flow increases. In the axial zone VGDU creates a region with a pony wives pressure, where the air nozzle 3 is sucked into the air and fed excess activated sludge.

Depending on changes in ash content of sludge because of the delays in a model sand trap, and the percentage content of sand fractions of less than 0.25 *mm* from the average axial velocity of the fluid in the vortex chamber v_{oc} VGDU before becoming are shown in Fig. 4.

Depending on the effect of changes in wastewater (BOD_5) in clarifier model EBPK and soil organic matter (BOD_5) at the output of the model tank SBPK on the value of the average axial velocity in the vortex chamber v_{oc} VGDU and the concentration of activated sludge mixed with sewage at an average speed of the Force $v_{\text{oc}} = 0.7$ *m* / s are shown in Fig. 6 .

Treatment of experimental data allowed us to obtain the following empirical equation describing the change in the efficiency of BOD_5 reduction in pro primary sedimentation process of municipal wastewater after VGDU:

$$E_{po} = K_V K_c E\,; \quad K_V = 1 + 0{,}83 v_{\text{oc}}^{0,709}\,; \quad K_c = 1 + 0{,}023 C_{\text{ил}}^{0,622}, \qquad (2)$$

where the EPO - the effect of removing BOD_5 during primary sedimentation of wastewater pre-treatment in the past VGDU,% E - effect of UDD le of BOD_5 during primary sedimentation of sewage that have not undergone pre-treatment,% K_v - coefficient taking into account influence among her axial velocity of fluid in the barrel VGDU; K_C - coefficient taking into cache effect of the concentration added to sewage sludge excess; v_{oc} - average thrust velocity of the fluid in the barrel VGDU, m/s;

C_{il} - concentration of activated sludge mixed with sewage mg / l.

At the second stage of the research was conducted to study the process biologists cally municipal wastewater, the formation of pre processing in VGDU. The composition of the experimental setup consisted of control and experienced aeration tanks with a capacity of 0.12 m^3.

In the aeration tank were fed experimental pre-processed in VGDU waste water Mechanically treated in a model sand catcher and sucks sump in control - wastewater after sedimentation and sand catchers are not transmitted pretreatment in VGDU. The total duration of treatment in the modeling and control aeration tanks corresponded ne periods of aeration in the aeration tank aeration propellant. Analyses of the quality of wastewater were filtered in from samples taken from aeration tanks every hour.

Depending on changes in the concentration of organic pollution (BOD_5) in the process of biological treatment in experimental and control aeration tanks aeration in Fig. 8.

Our studies show that preliminary wastewater treatment in VGDU can improve the efficiency of primary clarifiers, resulting in a load on the aeration tank is reduced in 1,5 times. The concentration of pollutants at the outlet of the aeration tank decreases indicators BOD_5 – in 2 times; COD - in 1,7 times ; NH_4^+ - in 1,4 times ; PO_4^{3-} - in 1.14 times. Increase in activated sludge is reduced by 2 times.
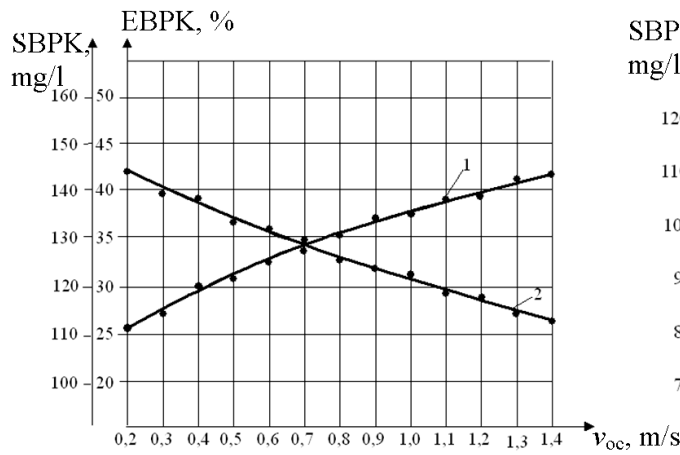
Fig. 6. Depending on the effect of changes in wastewater BOD_5 **in clarifier model EBPK (1) and the concentration of organic matter** (BOD_5) **at the exit of the settler SBPK (2) of the average axial velocity of fluid in the vortex chamber** v_{oc} **VGDU**
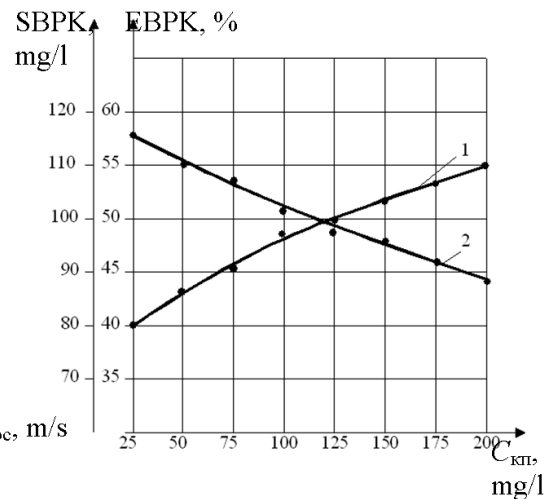
Fig. 7. Depending on the effect of changes in wastewater BOD_5 **in clarifier model EBPK (1) and the concentration of organic matter** (BOD_5)

Output from the decanter $C_{БПК}$ **(2) at an average axial velocity of fluid in the vortex chamber VGDU** $v_{oc} = 0,7$ m/s **the concentration of sludge mixed with sewage Force**
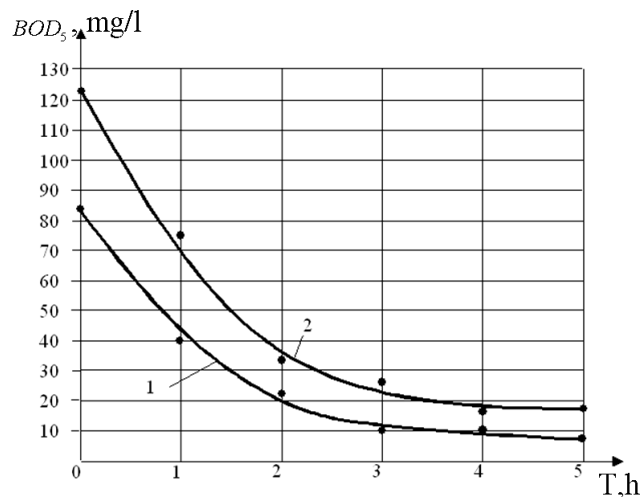
Fig.8. Depending on changes in the concentration of organic pollution (BOD_5) **in the process of biological treatment in an experimental (1) and control (2) aeration tank**

Technology of pre-treatment of urban wastewater in vihr6evyh hydrodynamic devices with the addition of excess activated sludge introduced to

the sewage treatment plant .Serdobsk-city of the Penza region, capacity $17,000 \, m^3 / day$. Average annual economic effect of the introduction amounted to 0.5 mln rub RU. in prices of 2011.

1.7 OPTIMIZATION OF INFORMATIVE POTENTIAL OF MODERN ENTERPRISE
Gonchar O.[1]

The modern stage of economic development, globalization of all public processes, is characterized by becoming of informative economy, when composition of traditional resources of public production (material, financial and labour) is implicitly filled up by an informative constituent. Information becomes important means and article of all productive and unproductive processes.

Information can be determined Globally, as fundamental fundamental principle, that assumes that, is generalized, going across from one state in other, she is recreated and appears all мікро- and by macrodynamic processes, phenomena, events, organic and inorganic objects to the universe.

The most common determination of information underlines that information - it fundamental only of energy of motion, mass and antimass on the basis of materialization and where materializations in мікро - and macrostructures [1, p. 148].

It is possible to assert in the conditions of modern development of scientific knowledge status, that information answers one of three evolutional stages depending on aims and pattern of her use.

On the first stage maintenance of information was determined as information, reports, new knowledge. It was foreseen that information caused the increase of probability of offensive of certain event. However in such understanding of the use of information maybe only in the conditions of anthropocentric approach (when a man comes forward as a consumer of information).

[1] Khmelnickiy State University, Khmelnickiy, Ukraine

On the second stage information began to be interpreted as a form of beating back. If one object represents some properties other, then this object becomes the transmitter of information. Similar approach means, that information is always secondary.

On the third stage, in connection with development of cybernetics, information began to be determined as a category of differences. Information passes the specific differences of natural objects in space and time.

For the use of information and, accordingly, informative resources in an economy, most acceptable is determination, in accordance with that information shows by itself natural essence, that carries in itself the characteristic signs of objects and phenomena of nature, that show up in space and time.

Simultaneously, taking into account high dynamism of public processes, in modern terms it is not enough to talk only about resources, it follows to investigate potentials of different levels, including is informative potential of separate managing subjects.

There are many determinations and contradictions in relation to determination of essence, composition of informative potential of enterprise, determination of priorities and correlations of different economic categories in the process of his forming. In particular, in relation to correlation of informative and intellectual constituent.

Question of informative economy is investigated in works of foreign and home scientists, among them works: Beltykowa E.A, Woronkowoi A.I., Melnik L.G. and other. However, the unsolved are remained by the problems of determination of constituents, optimization of processes of forming and management informative potential at the level of enterprise as one of motive forces of his development. An absent base and criteria of evaluation that complicates a management realization and development of economic potential of enterprise result in the choice of inadequate to the modern economic terms of strategies of development, especially innovative, efficiency reduces validity, accordingly administrative decisions.

Decision of these questions will give an opportunity purposefully to form and develop informative potential of enterprise, optimize control system by an enterprise and him by economic potential, to bring down the degree of

commercial risk and promote validity and operationability of the administrative decisions sent to providing of the protracted steady development.

To our opinion, informative potential of enterprise, as a constituent of him economic potential is an aggregate not only of informative resources, facilities of their accumulation, but also capacities for their realization, optimization and on this basis - perfection and development and not only informative potential but also combined economic potential on the whole, that, in turn, provides development of enterprise.

Id est to informative potential of enterprise it follows to include informative, intellectual and other non-material assets that is present in a presence or can be formed. And, from the point of view of forming of the combined potential of enterprise, informative, labour and intellectual potentials it follows to examine as independent elements, that, at successful combination, is able to bring sinergistical effect.

Thus, to informative potential of enterprise it follows to include informative, intellectual and other non-material assets that contain : first of all is knowledge and experience of workers (intellectual constituent of potential); economic information (marketing, information about the economic contractors of enterprise, technically – economic descriptions of equipment, technologies and others like that); adjusted connections with economic contractors (by consumers, suppliers, mediators et cetera), and also representatives of pin audiences (by mass medias, credit-financial establishments, political motions, by the organs of power and others like that), adjusted and a sale network is tested sometimes; facilities of communication and connection, informative systems and management (mainly computer) technologies; technical documentation; programmatic, informative and other providing of the computer informative systems (IC); highly scientific wares and services, technologies of their production; accordance witnessed by certificates enterprise and his products to the international standards; ownership rights are on the products of intellectual labour (now-how, patents, registered trade marks, "untwisted" brands, industrial prototypes and others like that); corporate culture and socialpsychological climate on an enterprise and in his subdivisions; image and business reputation and other.

Such structure of informative potential of enterprise (table. 1) can be offered.

From the brought list over of basic elements, informative potential of enterprise is not identical intellectual. Yes, the last is component part of informative potential. Him also it does not follow to equate and only with the non-material assets of enterprise, because informative potential contains both non-material and material part.

Table 1 - The Basic elements of informative potential of modern enterprise

Elements	Component
Knowledge and experience	knowledge and experience of personnel (intellectual potential)
	socialpsychological climate
	corporate culture
	image of enterprise
Documentations and rights	economic documentation
	technical, technological and others like that documentation
	ownership rights on patents, trade marks, industrial prototypes, now-how, trademarks
	certificates of accordance to the standards of quality, to the requirements of ecological safety and others like that
The highly scientific products	technologies
	wares
	favour
Informative systems and technologies, informative copulas	different types of information
	informative systems and technologies
	facilities of communication and connection
	informative, programmatic, technical and other providing of the informative systems
	connections with economic contractors, pin audiences, reputation of enterprise different types of information

The estimation of informative potential of enterprise is needed for adjusting of income tax and volume of depreciation decrees, increase of market value of enterprise and others like that. However in a greater degree it is needed for determination of prospects of development and optimization of choice of his concrete directions.

From these positions informative potential (his constituents) it follows to examine from the point of view of informative resources and capacities for their realization and development. Thus, consider appropriate to distinguish the resource constituent of informative potential, that would characterize the state of the informative rigging (informative resources) of development of enterprise, him quality and quantitative. And also the second part, that characterizes a capacity for realization of possibilities of development, that swim out from the present informative rigging (informative resources) (ability to take away and apply front-rank technologies, make highly scientific wares and render services, provide effective and productive copulas with economic contractors and pin audiences, provide the high level of corporate culture and favourable social psychological climate in a collective, to form a positive image and business reputation.

In the process of forming and management as by the combined potential of enterprise so him by informative potential important place to the it belong processes of evaluation. Complex estimation of informative potential of enterprise it is possible, to our opinion, to execute by means of widespread in mathematics method of distances. Thus the quantitative estimations of indexes it follows to compare directly, and quality estimations it is expedient to transfer in a ball.

Calculation formula looks like

$$l = \sum_{i=1}^{n} (1 - \delta_i) B_i, \tag{1}$$

where n – is an amount of indexes; B_i – is specific gravity of i index; δ_i – is a relative estimation of i index (comparatively with a standard).

Thus if desirable is a maximal value of index:

$$\delta_i = \frac{O_i}{O_{max}},$$

if desirable is a minimum value of index:

$$\delta_i = \frac{O_{min}}{O_i},$$

It follows to determine ponderability of indexes an expert method. According to a formula (1) more desirable is a less value of i-го of integral index, it testifies to the higher level of informative potential of enterprise (ideal situation subject to condition when I = 0).

At existent terms, the basic problem of evaluation is a choice of standard (bases) for comparison. Such there can be the best value of index from all enterprises that work at the market (in industry) and about activity of that it is possible to get reliable information. Interesting in this context, to our opinion, there can be an evaluation also of dynamics of development of informative potential of enterprise. In this case for the base of comparison it follows to choose indexes that characterize the state of constituents of potential, but previous periods (of accepted after basis).

In addition, after a formula (1) it is expedient to estimate a resource and здатнісну constituents of informative potential. It will allow separately to define both resource equipped of enterprise and capacity for her use, and to ground on results calculations concrete measures in relation to development of potential.

Questions of optimization of processes of forming, increase of efficiency of the use and providing of development of informative potential of enterprise certain services of enterprise must occupy in modern terms. Conception of becoming and perfection of management of enterprise potential must foresee continuous intercommunication with the process of perfection of control system by a production. Therefore a management potential can come true both within the framework of general tasks of control system by an enterprise on the whole and special control system by potential, that has all necessary attributes (own element composition, principles of functioning, structure, informative, economic, skilled, legal but orgware).

Task must be structured after levels:

- top management, human department of resources and department of technical studies, provide the increase of level of knowledge and qualification of personnel, and also form the level of corporate culture and social psychological climate;

- designer and technological departments are accountable for a completeness and quality of technical documentation;

- patent-licensed department and bureau of technical information, and also legal service of enterprise is accountable for providing of legal rights on patents, trade marks et cetera, their registration in corresponding establishments. They must control an order and terms of the use of the marked rights for an enterprise also;

- top management, leaders of structural subdivisions of enterprise, department of technical control, is accountable for the certification of products, technologies and production on the whole;

- department of the computer informative systems and technologies must be responsible for introduction, use, maintenance of capacity, modernisation of the informative systems and technologies, facilities of communication and connection. He (his subdivisions) responsible for informative, programmatic, technical and other providing of informative systems;

- department of marketing is accountable for plenitude and quality of economic information that characterizes the environment of menage and economic contractors of enterprise. Economic and financial subdivisions - for information that characterizes internal productive relations and efficiency of activity of enterprise;

- department of marketing is also responsible for adjusting and communicating with the economic contractors of enterprise and pin audiences. He answers and for forming and maintenance on a due levels of image and business reputations.

Chart of management of enterprise potential, including informative, as one of his constituents, can be presented, as a system of intercommunications and mutual dependence (Fig. 1).
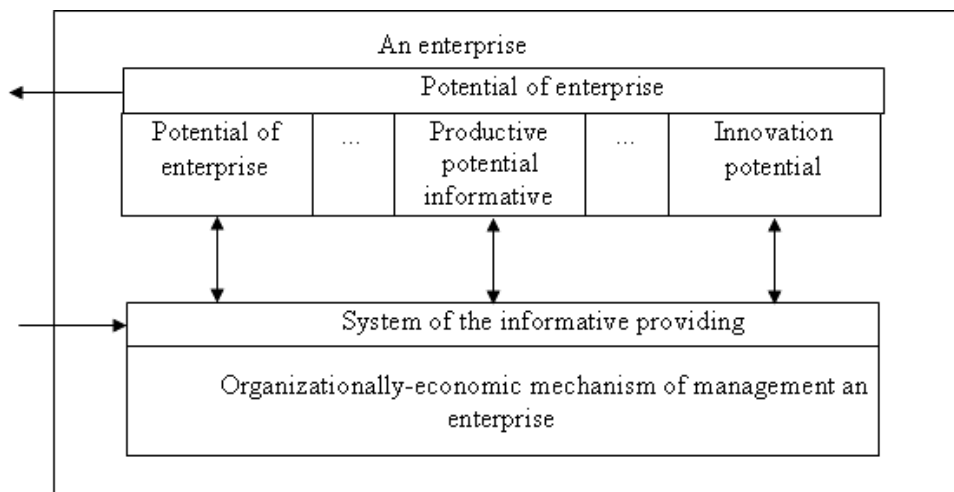
Fig. 1. Is Control system by potential of enterprise

Summarizing, it should be noted that in existent economic terms the state of informative potential determines the level of other constituents of potential of enterprise largely, especially innovative and intellectual. At a management potential within the limits of general control system of copula between the separate subsystems involved in a management an enterprise weak, or are fully absent, it determines subzero efficiency of results. To Tom, to overcome the indicated defects maybe by creation of the special mechanism of management of enterprise potential. And further researches must be sent exactly to development of organizationally-economic mechanism of management informative potential modern enterprises.

Research and decision of these questions will give an opportunity purposefully to form and develop informative potential of enterprise, optimize control system by an enterprise and him by economic potential, to bring down the degree of commercial risk and promote validity and operation ability of the administrative decisions sent to providing of the protracted steady development.

References

1.Ілляшенко С. М. Management innovative development. are Sumy: ВТД the "University book", К.: Kind. a house is "Princess Olga", 2005. – 324p.

2. Шарко М. In. Управление of развитием инноваций in промышленном производстве. it is Kherson: Олди-плюс, 2010.- 448p.

3. Яковлев Ю.П. Kontroling on the base of information technologies. - К.: Center of навч. years., 2006.- 318p.

2. MATHEMATICAL MODELING OF PROCESSES

2.1 INTELLIGENCE METHOD OF SOFTWARE QUALITY EVALUATION AND PREDICTION

Pomorova O.[1], Hovorushchenko T.[1]

Introduction

Safety Case methodology (Safety computer-aided software engineering) is developed over 20 years [1], [2]. The primary object of Safety Case methodology is to minimize software security and commercial risks by constructing a report, which should provide evidences, reasons and arguments that software is safe, and all requirements for the software is properly implemented. Currently, this methodology is generally accepted, but the level of its automation is still low.

The process of software developing for the Safety Case methodology depends on a large number of documents, source code, software evaluation methods and analysis of their results and software testing results. The main task of Safety Case methodology [3] is the automating of the creation of:

1) software requirements profile (including standards for software development, subject domain standards and customer requirements) - functional, inverse and non-functional requirements for software systems are analyzed; requirements for software safety and security are researched and completeness of all kinds of requirements is estimated;

2) software analysis results profile - metric analysis results, source code and software test results are studied and analyzed;

3) evaluation of results profile accordance to requirements profile - obtained software accordance to its requirements is evaluated.

One of the main tools of software quality analysis and evaluation is metric analysis. The metric is defined as a measure of degree of possessing property that has a numerical value [4]. Generally, software metric is a measure, which provides obtaining of numerical values of some software properties or its specifications. The modern software industry has accumulated a large number of

---

[1] Khmelnitsky National University, Ukraine

metrics, which evaluate some industrial and exploitation software characteristics. But aspirations of its universality, ignoring of type and application domain of design software, ignoring of software life cycle stages and its groundless using in industrial decisions making procedures significantly undermined the developers and users confidence to metrics. These circumstances require the careful selection of metrics for design software certain type and application domain, considering their restrictions at different software life cycle stages, establishing order for their common use, storage and integration of heterogeneous metric information to make timely industrial decisions.

Currently, only collection, registration and calculation of metric information are automated. The technique of metric analysis results processing [4] has the following unsolved tasks: 1) absence of unified standards for metrics, which leads to subjective selection of quality evaluation methods; 2) difficulty of interpretation the metrics values, which is caused by individual projects features and absence of metrics standard values; 3) absence of criterion to compared essentially new and previous projects, which leads to the impossibility of interpretation of obtained metrics for new project; 4) basic parameters in the selection of software realization versions are the design cost and time and software company reputation, but the decisions, taken on the basis of these parameters, not guarantee software quality.

On the basis of the above the need and actuality of scientific research in development of new effective methods of software quality evaluation and prediction arises. The intelligent methods, in particular artificial neural net's method of software quality evaluation and prediction (NMEP) [4], [5], are perspective today.

1. Software Design Results Evaluation and Quality Characteristics Prediction

Today, software is a defining component of many systems, including systems for critical applications, integrated (embedded) and specialized systems for various purposes. For such systems software bugs presence and low quality threaten the catastrophes that result to human victims, ecological cataclysms, and economic losses.

The problem of bugs exposure and removal is aggravated as increasing software complexity. Development of modern software design technologies requires the dynamic development of software quality evaluation tools, especially at the stage design (from the viewpoint of financial and time expedience).

The modern software industry is characterized by high competition. For success in this market the software company must to develop, to implement and to accompany the software considering the lead-times and providing the satisfactory quality. Therefore, many software companies are investing in software development technologies upgrading, on the basis that such facilities investment is necessarily covered a cost.

Nine stage design metrics with the exact values and 15 stage design metrics with the predicted values were selected as the basic metrics to development of intelligence method of design results evaluation and software quality characteristics prediction. The basic software design stage metrics and algorithms to measure were described in [4]-[6].
To determine the used design stage metrics ranges, we introduce some assumptions and impose certain limits on software and projects [7], that will be analyzed using artificial neural net's method of design results evaluation and software quality prediction (NMEP): 1) maximum 100 variables to calculate and output, 100 modified or created in the module variables, 100 managing variables and 100 unused in the module ("parasitic") variables for each software module; 2) software consists of maximum 50 modules; 3) maximum quantity of intermodals relations is 2450; 4) maximum 50 procedures for the data structure updating, 50 procedures for reading of information from the data structure and 50 procedures for the data structure reading and updating contain in each module, 5) each module actually gets access to a global variable as many times as it can get such access; 6) software contains maximum 50000 lines of source code; 7) the problem statement takes 10% of the time, the design - 35% of the time, the programming - 35% of the time and software testing, debugging and quality audit - 20% of the time; 8) models creation and modification take about

Table 1 - Software Design Stage Metrics Values Ranges

№	Design Stage Metrics with the Exact Values	Design Stage Metrics with the Predicted Values
1	Chepin's metric: -1, 0..32500	Expected Lines Of Code (LOC): -1, 0..50000
2	Jilb's metric (absolute modular complexity): -1, 0..2450	Halstead's metric: -1, 0..1562500
3	McClure's metric: -1, 0..120050	McCabe's metric: -1, 0..2402
4	Kafur's metric: -1, 0..497500	Jilb's metric (relative logical complexity): -1, 0..1
5	Cohesion metric: -1, 0..10	Expected quantity of program statements: -1, 0..50000
6	Coupling metric: -1, 0..9	Expected estimate of interfaces complexity: -1, 0..1
7	Metric of the global variables calling: -1, 0..1	Software design total time: -1, 0..520 (working days)
8	Time of models modification: -1, 0..46	Design stage time: -1, 0..182 (working days)
9	Quantity of found bugs during the models and prototype inspection: -1, 0..5000	Software design expected cost: -1, 0..25000 (usd)
10		Software quality audit expected cost: - 1, 0..2500 (usd)
11		Software realization productivity: -1, 0..5 (minutes for 1 line of code)
12		Program code realization expected cost: -1, 0..8750 (usd)
13		Expected functional points (FP): -1, 0..2945
14		Effort applied by Boehm's model: -1, 0..394 (man-months)
15		Expected development time by Boehm's model: -1, 0..520 (working days)

25% of the design stage time; 9) maximum quantity of models and prototypes errors for the one module should not exceed 100 errors; 10) quantity of software unique operators along with the subprogram names does not exceed 25000, the total quantity of software operands does not exceed 50000, the quantity of software unique operands does not exceed 400; 11) quantity of logical or cycle

operators does not exceed 50000; 12) quantity of software operators does not exceed 50000; 13) each variable of software module is passed on its interface; 14) the quantity of source code lines, divided into two, is the maximum software design expected cost in U.S. dollars; 15) software quality audit takes 50% of the time of testing, debugging and quality audit stage; 16) quantity of external inputs of each module is 49, quantity of external output of each module is 49, quantity of external requests to each module is 49, 17) each module has maximum 50 internal logical files and uses maximum 50 external logical files.

The ranges of software design stage metrics values are determined in Table 1.

The design results evaluation and software complexity and quality characteristics prediction are the results of processing of metrics from Table 1 using artificial neural network.

2. Artificial Neural Net's Method of Software Quality Evaluation and Prediction

NMEP provides an evaluation of the project and prediction designed software complexity and quality on the basis of exact and predicted values of complexity and quality metrics of the design stage. NMEP uses artificial neural network (ANN), which provides metrics processing and approximation.

Input data for ANN are the set of the design stage metrics with the exact values and the set of the design stage metrics with the predicted values.

The results of ANN functioning are 4 characteristics: 1) project complexity estimate; 2) project quality evaluation; 3) designed software complexity prediction; 4) designed software quality prediction (Fig.1)
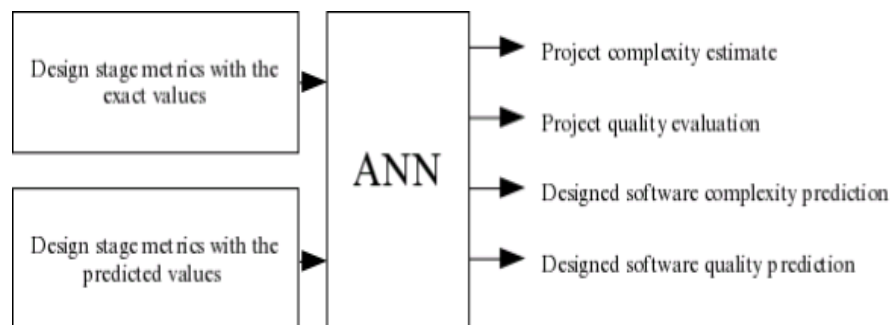

Fig. 1. NMEP concept

ANN has 9 one type inputs for the quantitative values of design stage exact metrics and 15 another type inputs for the quantitative values of design stage predicted metrics. If a certain metric is not determined, then -1 is given on the proper ANN input.

Project complexity estimate is value in the range [0, 1], where 0 - design stage complexity metrics with the exact values were not determined, approximately 0 - the project is complicated to realization and 1 - the project is simple to realization; project quality evaluation is value in the range [0, 1], where 0 - design stage quality metrics with the exact values were not determined, approximately 0 - is a low quality project and 1 - the project satisfies the customer requirements in quality; software complexity prediction is value in the range [0, 1], where 0 - design stage complexity metrics with the predicted values were not determined, approximately 0 - designed software will has significant complexity and 1 - designed software is expected simple; software quality prediction is value in the range [0, 1], where 0 - design stage quality metrics with the predicted values were not determined, approximately 0 - designed software will has low quality and 1 - high quality software is expected. The complexity characteristics include not only the simplicity or complexity of designed software from the viewpoint of its size, cost and design time, but also the maintenance difficulty or simplicity, usability and the effectiveness of the methods chosen to solve the task.

The conclusion about the project quality and complexity and the expected quality and complexity of designed software is based on an analysis of 4-th obtained results.

3. ANN Realization

Analysis of the artificial neural network's architecture was conducted [6] to select the architecture for the design stage software metrics analysis and software quality characteristics prediction. General regression neural networks (GRNN) are radial basis function (RBF) networks. GRNN are used to analyze the numerical series. Probabilistic neural networks (PNN) are radial basis function networks. PNN are intended for solving probability tasks, in particular, for the classification tasks. Kohonen self-organizing network (map) is designed for data clustering. Learning vector quantization networks (LVQN) are used for

clustering and classification. Elman and Hopfield networks are networks with dynamic feedback, focuses on processing of dynamic models that considering processes pre-history.

Because the task of metrics analysis and prediction of software quality characteristics doesn't have the properties of the numerical series, the feedbacks and the necessary for data classification and clustering, multilayer perceptron is chosen to solve this task. Using another type of neural network to solve this task will artificially distort its nature, and the ANN results are inadequate.

Multilayer perceptron (Fig. 2) is ANN for metrics analysis and software quality characteristics prediction.

ANN from Fig.2 is realized in the Matlab. To creation of ANN template the function *network* is used. Number of input vectors (*net.numInputs = 4*), layers (*net.numLayers = 4*), elements of each ANN input vector (*net.inputs {1}. size = 4; net.inputs {2}. size = 5; net. inputs {3}. size = 6; net.inputs {4}. size = 9*) were determined.

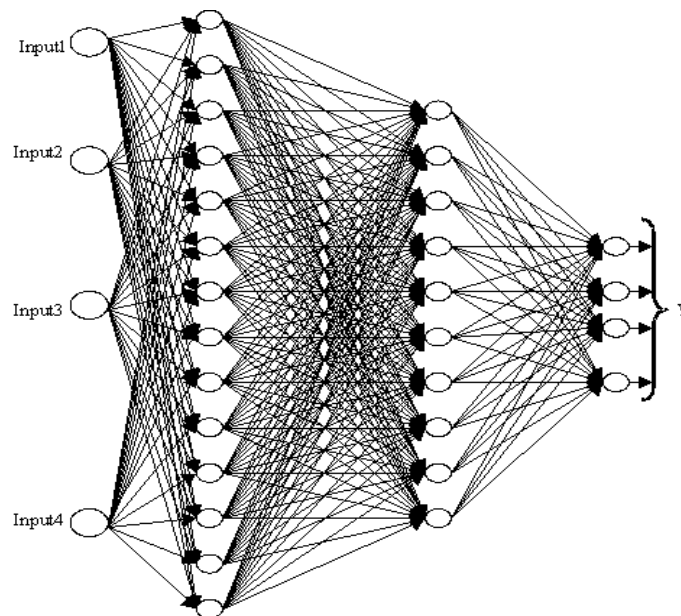Bias connection matrix: *net.biasConnect=[1;1;1;1].*

Fig. 2. ANN architecture for metrics analysis and software quality characteristics prediction

Input connection matrix, layer connection matrix, output connection matrix and target connection matrix are defined as follows: *net.inputConnect =*

[1 1 1 1; 0 0 0 0; 0 0 0 0; 0 0 0 0]; net.layerConnect = [0 0 0 0; 1 0 0 0; 0 1 0 0; 0 0 1 0]; net.outputConnect = [0 0 0 1]; net.targetConnect = [0 0 0 1].

Ranges of input vectors values: *net.inputs{1}.range = [0 32500; 0 2450; 0 120050; 0 497500]; net.inputs{2}.range = [0 10; 0 9; 0 1; 0 46; 0 5000]; net.inputs{3}.range = [0 50000; 0 1562500; 0 2402; 0 1; 0 50000; 0 1]; net.inputs{4}.range = [0 520; 0 182; 0 200000; 0 20000; 0 5; 0 70000; 0 2945; 0 394; 0 24].*

Number of neurons in ANN layers: *net.layers{1}.size=24; net.layers{2}.size=14; net.layers{3}.size=8; net.layers{4}.size=4.*

Nguyen-Widrow function (*initnw*) is an initialization function for each ANN layer. Hyperbolic tangent is the activation (transfer) function of 1-st, 2-nd and 3-rd layers, linear function is activation (transfer) function of 4-th layers.

ANN is represented in the Simulink (Fig. 3, Fig.4).
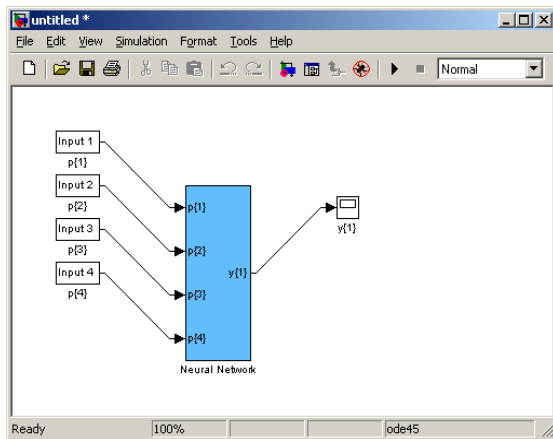
Fig. 3. ANN architecture in Simulink　　　**Fig. 4. Structural scheme of ANN layers**
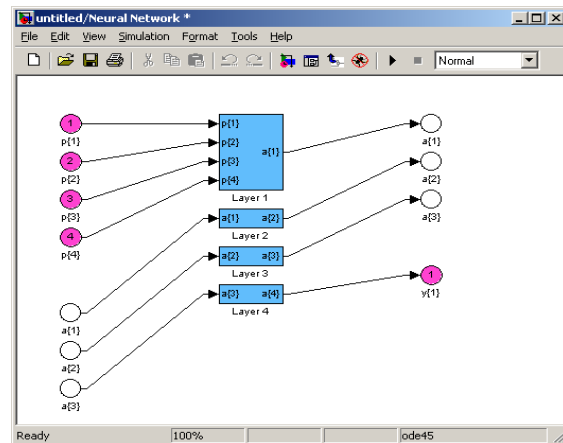
Analysis of The ANN Training Results

The sequence of training vectors (training sample) for obtained ANN training is defined as:

c={[32500;0;0;0] [30875;0;0;0] [...]; - training vectors for Input1;

[0;0;0.15;0;0] [0;0;0.2;0;0] [...]; - training vectors for Input2;

[3450;0;0;0;0;0] [5900;0;0;0;0;0] [...]; - training vectors for Input3;

[0;0;0;0;1.7;0;0;0;0] [0;0;0;0;1.8;0;0;0;0] [...]}; - training vectors for Input4.

Target vector is defined as:

m={[0.05;0.02;0.01;0.01] [0.1;0.04;0.02;0.02] [...]}.

ANN training method was selected on the basis of ANN training results with the training sample of 1935 vectors by different training methods: GDA - gradient descent with adaptive learning rule backpropagation method, LM - Levenberg-Marquardt backpropagation method, OSS - One step secant backpropagation method, RP - Resilient backpropagation (Rprop) method.

The research demonstrates that training performance did not differ significantly for different training methods (approximately 0,102197), therefore the select of training method was influenced by "the number of epochs" and "the training time". As best training method OSS was selected.

ANN testing was performed on the basis of testing sample of 324 vectors.

The process of ANN training and testing by GDA method is shown on Fig.5, by OSS method - on Fig.6, by LM method - on Fig.7, by RP method - on Fig.8. The bottom line shows the ANN training and the top line - ANN testing.

ANN training and testing charts show that the network is trained with the performance that is caused by insufficient quantity of training sample vectors.

Combinatory formula for the calculating of number of combinations (selections) is used to calculate the training sample maximum size: *C(24,4)=(24!)/(4!*(24-4)!)=10626*.

So, if more than 10 thousand training vectors are, then statistical methods can be applied to the task of design results evaluation and software quality characteristics prediction.

ANN is used at input information incomplete. According to the formula of ANN training sample size [8] we get that training sample of *N>(24*24)/(10^{-1})=5760* vectors is required for ANN training, which consists of 24-th input neurons, 24-th hidden layers neurons (14-th neurons - the first hidden layer (approximating) and 10-th neurons - the second hidden layer (adjustment)), with accuracy 10^{-1}.

ANN results analysis was performed on the basis of projects developed by software company "STU-Electronics", Khmelnitsky (Ukraine). Examples of results for 5 projects are shown in Table 2.

According to the results: 1-st project is evaluated as rather simple and high-quality; the designed software will have the same characteristics; 2-nd project - complicated and low quality; the designed software will have the same
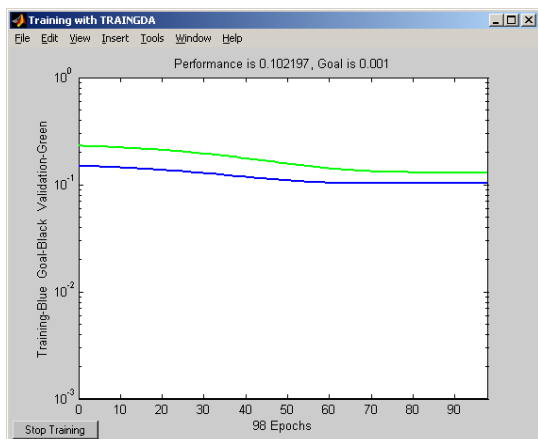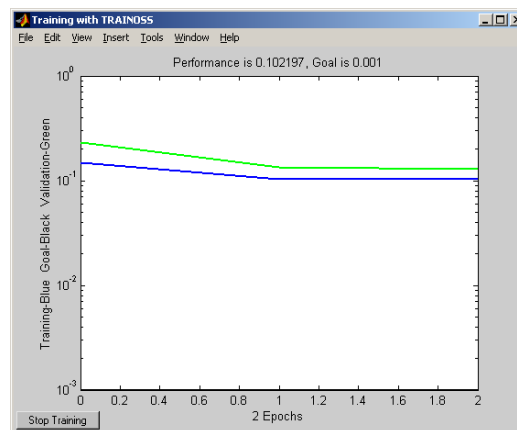
Fig. 5. ANN training and testing by GDA method

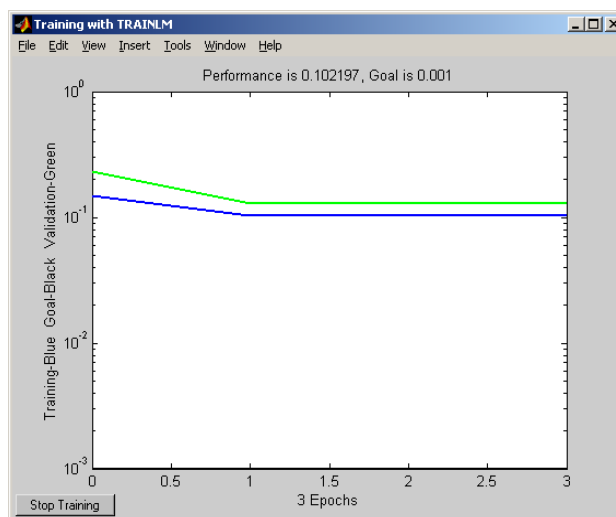**Fig. 6. ANN training and testing by OSS method**
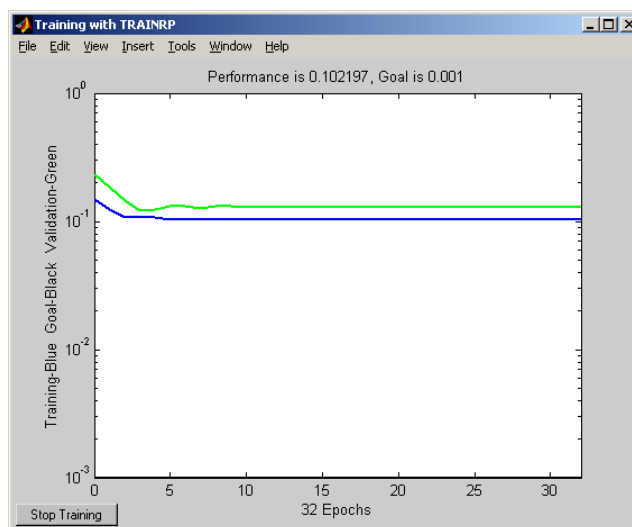

Fig. 7. ANN training and testing by LM method

Fig. 8. ANN training and testing by RP method

101

Table 2 - Processing Of Stage Design Metrics Using ANN

Project №	Stage Design Metrics	ANN Result
1	2	3
1	Chepin's metric - 1700 Cohesion metric -10 Coupling metric - 1 Expected Lines Of Code (LOC) - 3300 Halstead's metric - 73400 Software design total time - 27 working days Software design expected cost - 975 usd Expected functional points (FP) - 120	$Y_1=0{,}95$ $Y_2=1$ $Y_3=0{,}95$ $Y_4=0{,}96$
2	McClure's metric – 90000, Kafur's metric - 376900 Chepin's metric – 24530, Cohesion metric – 3, Coupling metric - 7 Expected Lines Of Code (LOC) - 40135 Halstead's metric – 124928, McCabe's metric - 1903 Software design total time - 396 working days Software design expected cost -19000 usd Expected functional points (FP) - 2220	$Y_1=0{,}25$ $Y_2=0{,}3$ $Y_3=0{,}2$ $Y_4=0{,}26$
3	Chepin's metric - 14538 , Cohesion metric - 7 Coupling metric - 4 Expected Lines Of Code (LOC) - 25530 Halstead's metric - 781232 Software design total time - 218 working days Software design expected cost - 10762 usd Expected functional points (FP) - 1210 Software quality audit expected cost - 1100 usd	$Y_1=0{,}55$ $Y_2=0{,}6$ $Y_3=0{,}51$ $Y_4=0{,}57$
4	McClure's metric – 12000, Kafur's metric - 64238 Chepin's metric – 3241, Cohesion metric - 9 Coupling metric - 3 Metric of the global variables calling - 0,089 Expected Lines Of Code (LOC) - 6240 Halstead's metric - 162251 Jilb's metric (relative logical complexity)- 0,12 McCabe's metric - 298 Software design total time - 69 working days Software design expected cost - 3660 usd Effort applied by Boehm- 60 man-month	$Y_1=0{,}9$ $Y_2=0{,}92$ $Y_3=0{,}89$ $Y_4=0{,}86$
5	Chepin's metric - 27625 Jilb's metric (absolute modular complexity) - 2090 Cohesion metric – 1, Coupling metric - 9 Quantity of found bugs during the models and prototype inspection - 4321 Expected Lines Of Code (LOC) - 47550 Halstead's metric - 1484376 Jilb's metric (relative logical complexity)- 0,95 Software design total time - 488 working days Software design expected cost - 23375 usd Effort applied by Boehm- 377 man-month	$Y_1=0{,}15$ $Y_2=0{,}11$ $Y_3=0{,}05$ $Y_4=0{,}06$

On the basis of ANN results, design cost and time (Table 3) the choice of project version was performed.

Table 3 The Criterions of Choice of Project Version

Version	Values Y_1, Y_2	Values Y_3, Y_4	Design cost	Design time
1	$Y_1=0,51$ $Y_2=0,56$	$Y_3=0,60$ $Y_4=0,57$	10875 usd	200 working days
2	$Y_1=0,32$ $Y_2=0,35$	$Y_3=0,38$ $Y_4=0,37$	11125 usd	210 working days

The characteristics of project versions from Table 3 evidence that both versions have approximately the same design cost and time, but significantly different estimates of project complexity and quality and prediction of designed software complexity and quality. On the basis of only cost and time software company can make a false conclusion about selection of the project version. ANN evaluations help to make the right selection.

Acknowledgment

The necessity and actuality of scientific research in software quality evaluation and prediction comes from the results of the software metric evaluation methods analysis.

The main parameters in the selection of software project version are the design cost and time and designing company reputation, but decisions on the basis of these parameters are not always guarantee the proper software quality. Predicted evaluations of designed software complexity and quality give the prediction about complexity and quality of concrete project version realization and allow comparing the different project versions, when the cost and time is approximately equal. The proposed approach provides the motivated and grounded decision about selection of the project version on the basis not only cost and time, but also considering quality characteristics.

Research showed that in future attention should be paid to the solution of: 1) the problem of metric information lack to increasing of the training and testing samples size; 2) the development of designed software complexity evaluation metrics from the viewpoint of the maintenance difficulty or simplicity, usability and the effectiveness of the methods chosen to solve the

task; 3) ANN architecture optimization and ANN performance function selection.

References

1. Bishop P. A Methodology for Safety Case Development / P. Bishop. - 1998

2. Kelly T. Arguing Safety – A Systematic Approach to Managing Safety Cases / T. Kelly. - 1998

3. A. Gordeyev, V. Kharchenko, A. Andrashov, B. Konorev, V. Sklyar, A. Boyarchuk. Case-Based Software Reliability Assessment by Fault Injection Unified Procedures // Proceedings of the 2008 International Workshop on Software Engineering in East and South Europe – Germany, Leipzig, 2008. – pp. 1-8

4. Pomorova O.V., Hovorushchenko T.O. Analysis of Methods and Tools of Software Systems Quality Evaluation // Radioelectronic and Computer Systems – Kharkiv: KhAI, 2009 – № 6, pp.148-158

5. Pomorova O.V., Hovorushchenko T.O. Intelligence Method of Design Results Evaluation and Software Quality Characteristics Prediction // Radioelectronic and Computer Systems – Kharkiv: KhAI, 2010 – № 6, pp.211-218

6. Pomorova O.V., Hovorushchenko T.O., Tarasek S.Y. Analysis and Processing of Software Quality Metrics on the Design Stage // Transactions of Khmelnitsky National University – Khmelnitsky: KhNU, 2010. - № 1, pp.54-63

7. Eric J. Braude. Software Engineering: An Objected-Oriented Perspective - New York: Wiley Computer Publishing, 2004. -655 p.

8. F. Wasserman, Neurocomputer Techniques: Theory and Practice [Russian translation]. Moscow: Mir, 1992. - 240 p.

2.2 MATEMATICAL MODELING AND INTENSIFICATION TECHNOLOGIES IN THE BUILDING INDASTRY
Kamburg V.[1], Malkyna N.[1]

The creation of any modern technology usually requires knowledge at the junction of a large number of related areas of science and technology, and structural complexity and multifactor implemented in practice, technological systems leads to the application of systems analysis and mathematical modeling, the classical scheme [1], which basically boils down to this .

---

[1] Penza State University of Architecture and Construction

In the first phase - to identify the main parameters and connections, reflecting the main features of the object, to investigate the resulting model is qualitatively and quantitatively, to develop, if necessary, algorithms and applications, an analytical and numerical modeling for the test cases and data specific to the studied processes and systems. The adequacy of the proposed models.

In the second stage - just like the first, based on fundamental laws, the known laws, empirical relations and the previously obtained results, refine the model, in the event of proven need, the introduction of additional parameters and relationships.

In the third stage - to investigate the whole system, to formulate new laws obtained and used as a further development of the theory and for practical purposes - the creation of new technologies and their target optimization.

This article focuses on two examples of our work with such an approach to address the building industry, based on the fundamental laws of heat and mass transfer, hydrodynamics and regularities of specific technologies and modern methods of mathematical modeling. The main results obtained in the Khmelnitsky National University (Ukraine, 1995-2007) and in the Penza State University of Architecture and Building (Russia, 2007-2011) under the leadership and personal involvement of the author and are protected by three PhD and one D. Sc. in Engineering dissertations (in the Ukraine and Russia), with implants in the burn center of Kiev (1996) and the Penza region (2008).

EXAMPLE 1. MATEMATICAL MODELUNG AND INTENSIFICATION WORK CONDENSATION GRAVITY FILTER THIN AIR PURIFICATION

One of the promising trends in technology development of thin clearing of air or other gas-vapor flows from aerosols and harmful compounds powder particles are condensation-gravity filters (FCT), with the main working element in the form of flow thermal diffusion chamber (LST) [1] - [4]. Such devices, by creating them in the fields of supersaturation, temperature controlled, concentration-E and in-line mode allows you to transfer contaminants from the gas in the liquid state without some classification of particle size, and easy to regenerate themselves with water or an appropriate solution . Direct

measurements are difficult to supersaturation fields, so their condition is made to assess methods of physical and mathematical modeling. The authors of [5] - [6] were able to explore the most interesting from the standpoint of practice, but complex in terms of solutions of the simulation system (1) - (3) TDK modes with values of thermal diffusion of Fe and Fe ratios Pe close to 1. However, the practical applications of these under-the results to date, in full, not be considered.

In this paper we solve the problem of mathematical modeling and intensify the process of TDK in the FCT, as a highly effective filter.

1. Strainer.

2. Cleaning filter to mol / L of impurities

3. Ventilation system with speed regulators and temperature of the flow.

4 Speed of flow.

5. Flow temperature controller.

6. Capacity to collect sediment.

7. Heating system hot plate with the regulator.

8. Slit channel (LST).

9. Humidification system surfaces.

10. Water flow regulator.

11. Temperature controller cold surface.

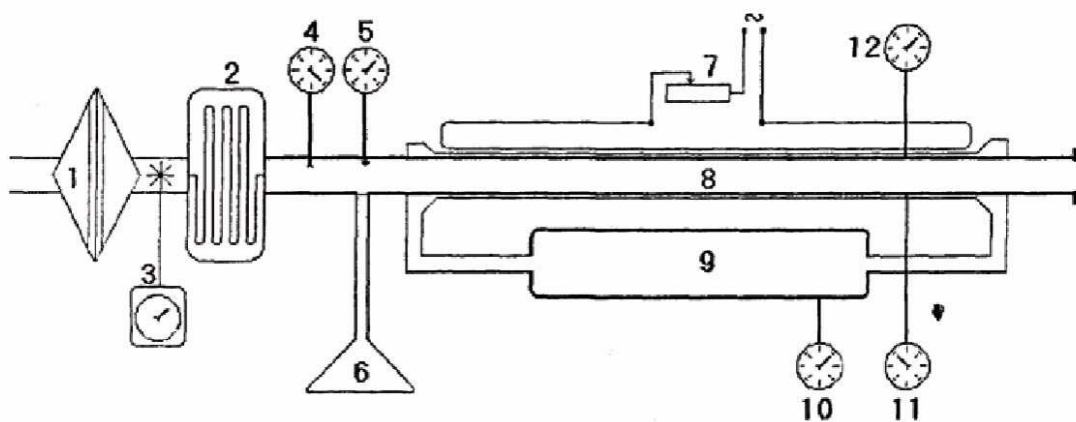12. Temperature controller with hot surfaces.

Fig. 1. The scheme of gravitational condensation-filter

The basic working element of the FCT, which is the LST, is modeled by [1] - [6] in the form of a flat slotted channel, wet the walls of which have temperatures T_1 and T_2 (Fig. 2).) Vapor concentration near the wall is saturated. The height of the channel d very large compared with less than its length L and width w. At the entrance to the channel has a steam-gas mixture with an average speed $<V>$temperature T_0 and vapor concentration C_0. The position of the inside LST given by the coordinates: $0 \leq x \leq d$, $0 \leq y \leq L$, and for the dimensionless coordinates:

$$\xi = \frac{x}{d}, \quad \eta = \frac{y}{L}, \quad 0 \leq \xi \leq 1, 0 \leq \eta \leq 1, \tag{1}$$
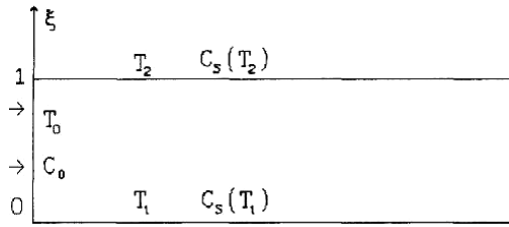
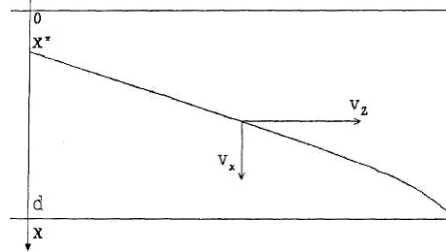**Fig. 2 a) Schematic of slotted channel**   **Fig. 2 b) The trajectory of a particle in a slot channel TDK**

Field distribution of temperature and supersaturation of vapor concentration inside the LST is described by the following system of equations, algorithms for the numerical solution of which the examples of calculations are given in [5] , [6], [9]:

$$6Pe\left(\xi - \xi^2\right)\frac{\partial T(\xi,\eta)}{\partial \eta} = \frac{\partial^2 T(\xi,\eta)}{\partial \xi^2} + \frac{\partial^2 T(\xi,\eta)}{\partial \eta^2}, \tag{2}$$

$$6\overline{Pe}\left(\xi - \xi^2\right)\frac{\partial C(\xi,\eta)}{\partial \eta} = \frac{\partial^2 C(\xi,\eta)}{\partial \xi^2} + \frac{\partial^2 C(\xi,\eta)}{\partial \eta^2},$$

$$Pe = \frac{\langle V \rangle d}{a_1}, \quad \overline{Pe} = \frac{\langle V \rangle d}{D_{12}} \text{ – thermal diffusion coefficients and the Peclet.}$$

a_1 - the thermal diffusivity of the mixture;

D_{12} - diffusion coefficient of vapor gas.

Boundary conditions:

$$T(\xi,\eta)|_{\eta \leq 0} = T, \qquad T(0,\eta) = T_1, \quad T(1,\eta) = T_2, \quad T(\xi,l) = T_1 + \left(T_2 - T_1\right)\xi = T_L$$

$$C(\xi,\eta)|_{\eta\leq0}= C_0, \qquad C(0,\eta)= C_s(T_1)= C_1$$

$$C(1,\eta)= C_s(T_2)= C_2 \ C(\xi,L)= C_1 +(C_2 - C_1)\xi = C_L, \tag{3}$$

The problem of the trajectories of different particles is solved for a horizontal slit ka-signal (Fig. 2b) under the following assumptions:

At the entrance to the canal and the entire length of the gas flow is laminar and the velocity distribution is described by the following formula [4], [7]:

$$v_z(x) = v_0\left[\frac{4x}{d} -\left(\frac{2x}{d}\right)^2\right], \tag{4}$$

- At the channel inlet concentration of aerosol particles is constant over the entire cross-section;

- The condition of a dilute solution ($\leq10^{-2}$ *mol / L* for impurities) - the interaction between particles is absent, that is, each particle moves independently of others and their trajectories do not intersect;

- The case of large aerosol particles, up to 25 microns with a low concentration, the rate is equal to the speed of a moving gas;

- The motion of particles affect the force of gravity.

Assuming that the quasi-particle motion, the trajectory of a particle in a plane slit channel can be written as follows [7]:

$$\frac{dx}{dt} = v_x(t) \ \frac{dz}{dt} = v_z[x(t)], \tag{5}$$

with initial conditions:

$$t_0 = 0; \quad x_0 = x^*; \ z_0 = 0, \tag{6}$$

With the above assumptions, the expressions for the vertical and horizontal components velocity can be written as

$$v_x(t) = k_1(k[x(t)]\cdot t + R_0^2), \qquad v_z[x(t)]= v_0\left[\frac{4x(t)}{d} -\left(\frac{2x(t)}{d}\right)^2\right], \tag{7}$$

$$k_1 = \frac{2\rho_i g}{9\mu_1} \qquad k(x) = \frac{\dfrac{D_{12}\mu_1 p_{l\infty}}{RT_{l\infty}\rho_i}\delta(x)}{1+\left(\dfrac{\mu_1 L}{R}\right)^2 \dfrac{D_{12} p_{l\infty}}{\lambda_l(T_{l\infty})^3}C_{1s}(T_{l\infty})}, \tag{8}$$

ρ_i – density drops;

$p_{l\infty}$ - the pressure away from the droplet;

R - universal gas constant;

$T_{l\infty}$ - The temperature drops away from;

L - latent heat of vaporization;

λe - thermal conductivity of gas;

μ_1 - molecular weight of the pair.

$\delta(x,z) = \dfrac{C(x,z)}{C_s[T(x,z)]} - 1$ - Supersaturation at a given point of the channel;

$C(x,z)$ – the vapor concentration at a given point;

$C_s[T(x,z)]$ – Concentration of saturated vapor at a given point, the temperature dependence of which is designed by well-known formula Clausius-Clapeyron: $C_s[T(x,z)] = \exp[A_0 - B_0/T(x,z)]$ where A_0 and B_0- constants depending on the physical properties of matter.

Under the above assumptions, the equations for calculating the condensation growth of the particle takes the form;

$$R(x,t) = \sqrt{R_0^2 + 2C_{1s}(T_{l\infty})k(x)t} \,, \tag{9}$$

Algorithm for the numerical simulation. . Let us introduce the following notation:

$$x_i = x(t_i), \qquad \Delta t = t_{i+1} - t_i \,, \tag{10}$$

Using simple numerical methods for solving problem (5) - (6), we can come to the following computational scheme:

$$z_{i+1} = v_0\left[\frac{4x_i}{d} - \left(\frac{2x_i}{d}\right)^2\right]\Delta t + z_i \qquad x_{i+1} = k_1\left[k(x_i)t_i + R_0^2\right]\Delta t + x_i, \tag{11}$$

$$x_0 = x^*, \qquad\qquad z_0 = 0 \tag{12}$$

Calculation of the scheme (11) - (12) lasts as long as one of the following conditions:

1. $x_i = d$ - the particle has fallen to the bottom wall of the channel.

2. $z_i > l$ - a piece flew out of the channel.

In practice, the filtering problems these two cases are characterized by removal filtration of particles and rum slippage, so the ratio of these cases is a measure of the effectiveness of the filter. To quantify the effectiveness of the filter coefficient is considered breakthrough.

We introduce the function as a breakthrough quantify the effectiveness of the filter as the ratio of the number of particles at the inlet and outlet of the channel:

$$K = \frac{N}{N_0} \qquad N_0 \mid_{z=0} = l \int_0^d n_0 v(x) dx \qquad N \mid_{z=l} = l \int_0^d n(x) v(x) dx, \qquad (13)$$

N_0 - a stream of particles entering the channel.

N - particle flow at the outlet of the channel.

According to assumption 3 the particle trajectories do not intersect, so there is the initial coordinate x^*, in which all particles with initial coordinates $x > x^*$ reach the bottom of the wall and settle on it, and all particles with initial coordinates $x < x^*$ will take off from the channel. Because we can write:

$$N(z) = b \int_0^d n(x) v_z(x) dx = n_0 b \int_0^{x^*} v_z(x) dx \mid_{z=0}, \qquad (14)$$

Consequently, the coefficient of breakthrough can be written as:

$$K(z) = \frac{\int_0^{x^*} v_z(x) dx}{\int_0^d v_z(x) dx} = \frac{3}{2} \left[2\left(\frac{x^*}{d}\right)^2 - \frac{4}{3}\left(\frac{x^*}{d}\right)^3 \right], \qquad (15)$$

But the sight of the function (4) and the results of numerical experiments show that there exists a coordinate $0 \le x^{**} \le x^*$ at which all particles with initial coordinates $x < x^{**}$ will fall to the bottom wall before a particle with initial coordinates $x^{**} < x < x^*$. This effect is explained by the fact that the particles reach a maximum speed of the center channel, and on approaching the wall velocity gradually decreases. Thus, the ratio of vertical and horizontal components of the velocity of the particles, which move-rye near a wall, is larger than the particles that move in the price-friction channel, whereby they quickly reach the bottom

of the wall. Consequently, a more accurate form of entries for the breakthrough coefficient is as follows:

$$K(z) = \frac{\int_{\frac{x^{**}}{d}}^{x^*} v_z(x)dx}{\int_0^1 v_z(x)dx} = \frac{4}{d}\left[\frac{(x^*)^2 - (x^{**})^2}{2} - \frac{(x^*)^3 - (x^{**})^3}{3d}\right], \quad (16)$$

Formula (15) is a special case of (16) at $x^{**} = 0$. Note that the trajectories of the particles will not overlap only if their initial coordinates $x > x^{**}$.

The written form factor breakthrough as a function of z allows to calculate coefficient of breakthrough K for each section of the channel, as well as consider the problem of optimizing the channel length and other parameters.

Fig. 3 a) - b) are characteristic results calculated trajectory of a particle at different values of the operating parameters specified in relative coordinates ξ and η.

Fig. 3 a): P_e=1.00; T_1=28°C; T_2=32.0; dt=0.01; r_0=0.1

Fig. 3 b): P_e=1.00; T_1=25°C; T_2=35.0; dt=0.01; r_0=0.1

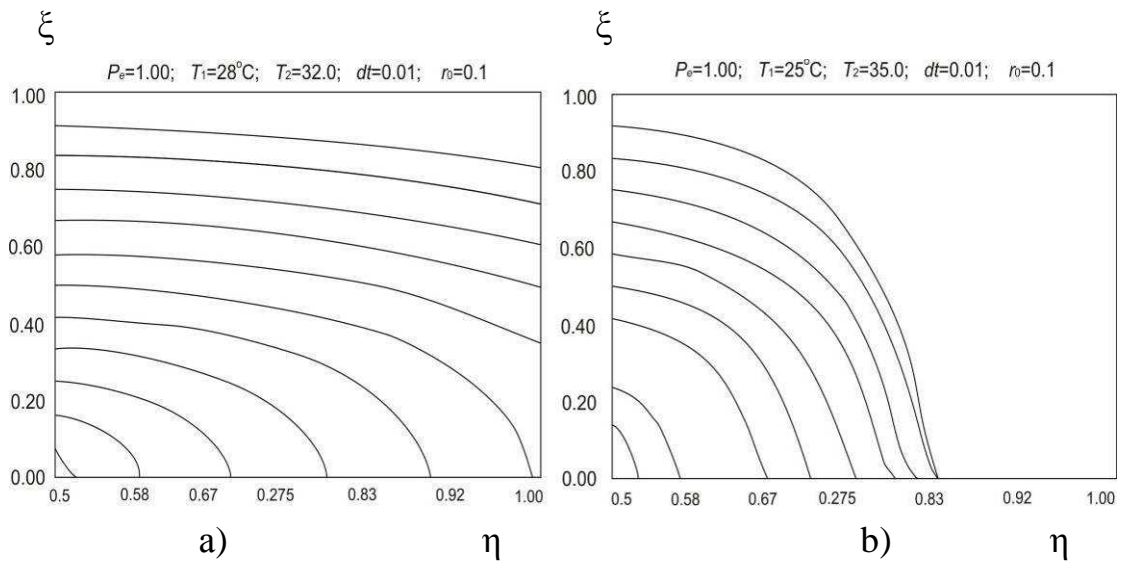**Fig. 3. The trajectory of *Z(x)***

In the examples above calculation shows the trajectories and the dynamics of particle growth from the initial radius of TDK particles and fields of supersaturation. The trajectories of the show, as a function whose values are the z coordinate of the particle as a function of the current coordinate x for different initial coordinates x (in units of 0,1 d).

For clarity, the *OX*, chosen so that the upper wall is , while the lower one. (This must be considered in the calculation of the breakthrough). The growth of the particles is shown as a function whose value is the particle radius (in mm) depending on the current coordinate *z*. The coefficient of P_e is equal to 1 everywhere.

In the first stage (Figure 2-3), the influence of the field of supersaturation at the initial radius of the particle $R_o = 0.1$ mm. Observed trajectory and growth of particles in the super-saturation that occurs when the temperature gradients 4, 10 and 20 degrees respectively.

It was found that for small temperature gradients the particles do not have time to you-grow, and most of them flew out of the channel (Figure 2).

But, by increasing the gradient rate overshoot decreases sharply (Fig. 3). Since at *z.* = 2:

$$dT = 4: \qquad x^* = 0.7 \quad x^{**} = 0.0 \quad K = 0.523$$
$$dT = 10: \qquad x^* = 0.4 \quad x^{**} = 0.0 \quad K = 0.235$$
$$dT = 20: \qquad x^* = 0.0 \quad x^{**} = 0.0 \quad K = 0.000$$

In the third case $K=0$, с $z=1.2$, therefore, it is possible to optimizing the temperature, so that $K=0$ for the coordinate z, is not less than specified. Thus, due to the proposed approach, the algorithms and the package of programs can be in practice to solve the problem of minimizing the temperature gradient to 100% of precipitation, depending on the length of the channel in a condensation-gravity filters.

In the second stage was considered a similar case, but the initial particle radius equal to 2 microns. Found that at $z = 1.1$:

$$R_o = 1: \qquad\qquad x^* = 0.1 \quad x^{**} = 0.3 \quad K = 0.125.$$

Summing up the results of these model-numerical simulations, we note that: quantitative stvo particles trapped by TDK can be characterized by the flow that enters the channel in the range of the initial coordinates from 0 к x^{**} and x^* к *d* and can be quantitatively estimated by (16) x^{**} tends to 0 while increasing the initial radius and decreasing the value of the field of supersaturation, x^* tends to 0 with increasing values of the field of supersaturation or by increasing the initial radius of the particle, the effect of supersaturation field is much larger, x^{**} x^* tends to increase the value in the field or supersaturation with decreasing

initial radius of the particle, the particle growth in a channel depends only slightly on its initial radius.

The simulation results are in good agreement with experimental data, the average difference at 4-12%. With the largest deviations correspond to high velocities and smaller differences in temperature of the chamber walls and the stream.

The simulation results are in good agreement with experimental data, the average difference at 4-15%. With the largest deviations correspond to high velocities and smaller differences in temperature of the chamber walls and the stream.

Typical resulting data on the dynamics of intensification of work, you TDK to extract the particles by the proposed method show that the temperature gradient is one of the parameters of intensifying the process of TDK, a key element of the working high-filter. Based on these models, numerical simulations and experiments necessary in each concrete case (geometry of the channel, the flow of the working environment, the size of the particles, their concentration, etc.) can be solved the problem of capturing the FCT as individual particles and their flow in whole.

Installation is displayed in operating mode by setting the temperature of the hot surface as a function of flow rate, its temperature, the temperature of cold wall of length of the channel. Based on these parameters are calculated and the limiting trajectory coefficient breakthrough. Temperature of the hot surface is defined so that the coefficient is zero overshoot.

Our proposed approach can solve the problem of intensification of the process of FCT for steam and gas flows with known geometric and hydrodynamic parameters of the PDO, as well as the properties of aerosol particles retrieved, optimized synthesized these parameters in the development of the FCT and choose the mode of its work to meet your specific ventilation and clean the air.

EXAMPLE 2. MATEMATICAL MODELUNG TECHNOLOGY MADE MACROPOROUS KERAMSIT

The main tasks in creating advanced technologies in the building of enclosures with the filling of permanent formwork keramsit coarsely. Most of

them are as follows.A process needs to prepare macroporous keramsit and its placement in permanent form in a way that ensured at minimum cost a number of preset desired properties and, in the first place - the minimum: the design strength , the consumption of cement glue thermal conductivity and bulk density. These tasks include a range of physical, mechanical, physicochemical, hydrodynamic, and technological parameters. Informed decision of these problems must be based on experimental data and their theoretical description, as well as comply with existing regulatory requirements.
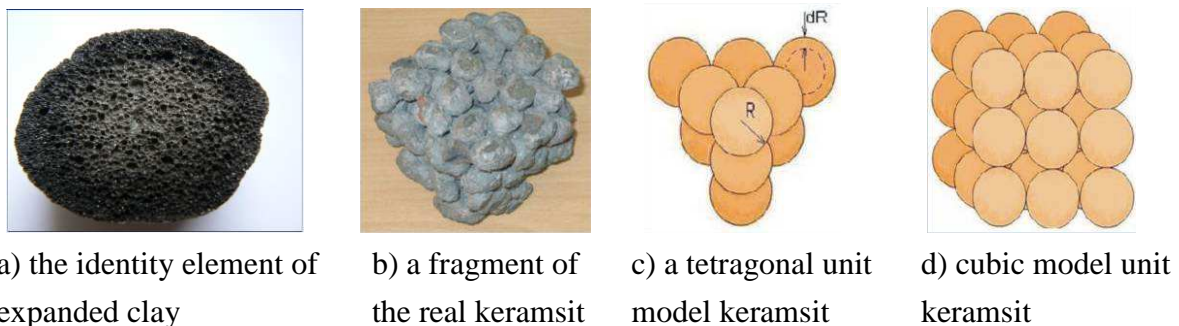

| a) the identity element of expanded clay | b) a fragment of the real keramsit | c) a tetragonal unit model keramsit | d) cubic model unit keramsit |

Fig. 4. Scheme of modeling the process of saturation keramsit and grout

In [10] - [13] developed the elements of mathematical models of processes of preparation and installation of macroporous keramsit (MPK), which are the aggregate grains in the form of solid porous expanded clay balls approximately the same size of radius *R* (Fig. 4 a) - d)).

For the development and refinement of the model representations of the cooking process KPKB need to solve the problem, which is an acceptable approximation, substantially reflects the physico-chemical, hydrodynamic and mechanical properties of materials involved, as well as the process of saturation In this formulation of such a task, a well-known authors of the References was not considered.

In this paper the mathematical model of saturated porous grout keramzite separate elements (PE) and its interpretation for the most common technological situations. Consider the equation of the forced diffusion of the solution in the form of one-dimensional problem from the outside heat and mass transfer, that is the solution, filling the space between the grains of keramzit, the ball inside in the radial direction in spherical coordinate system [10]:

$$E_K \frac{\partial W}{\partial t} = \frac{D_K}{r^2} \frac{\partial}{\partial r}(r^2 \frac{\partial W}{\partial r}) + \frac{k}{\eta} \frac{\partial W}{\partial r} \frac{\partial P}{\partial r} - cW, \qquad (17)$$

with boundary conditions:

$r = R - dR$: $W = 0$ (Glue penetrates deeper than the surface of PE dR) either:

$D_K \frac{\partial W}{\partial r} = 0$ (glue penetrates to the center with constant composition, ranging from Level dR)

$$r = R \; : D_K \frac{\partial W}{\partial r} = \beta_K (W - W_0) \qquad (18)$$

and initial conditions:

$$W \mid_{t=0} = W_0 \text{ , where} \qquad (19)$$

Eκ=Eκ(t) - specific effective porosity of grain *Eκ=Eκ(t)*, characterizing the fraction of time open to the diffusion of adhesive into the grain, which varies, in general, over time, in the process of mixing and laying.

$W = W(r,t)$ – volume fraction of liquid phase (degree of saturation has PE) PE at a distance r from the center of the sphere to its surface ($0 \leq r \leq R$) in a two-phase heterogeneous system "liquid - air" at time *t*;

Dκ - the diffusion coefficient in a grain of PE;

Wo - is the initial concentration of the solution grains;

k - permeability of expanded clay;

η - viscosity of the slurry;

β_K - Mass transfer coefficient between the solution and the outer surface of the grain;

P -folding vnutrizhidkostnoe pressure, mainly from the following four components:

$$P = P_{part} + P_{grav} + P_{rot} + P_{dist} \qquad (20)$$

where: P_{part} partial pressure of air (or the medium filling the pores of PE), which includes the pressure created by filling the pores with cement mortar and the surface tension forces in the pores;

P_{grav} - component of the pressure from the force of gravity;

P_{rot} - pressure due to forced convection of the solution from the mixer rotor due to centrifugal force;

P_{dist} - pressure, artificially created by external sources of disturbance of concrete mixture (eg, vibrators), to accelerate the saturation of the body PE cement mortar, as well as to create a more uniform impregnation zone *dR* on the ball and sealing the mixture;

c - with - efficient characterization of the total rate of chemical reactions in the process of mixing cement with water and then affecting the saturation of the solution.

Here we assume fairness PE surface and grout with a water cement ratio of the mass W/C is not changing during the process.

The system (17) - (20) is a generalized time-dependent model, containing the basic parameters of the process of saturation of PE. Investigation of the effect on the decision of the members of the expressions on the right side, describes and suggests ways to organize the mixing of appropriate technologies.

Quantify the impact of these factors on the overall saturation due to their numerous as difficult as all process steps. The solution to this problem is a subject for further research of the authors.

However, in the first stage, it is useful to conduct a qualitative analysis of the impact of each of the terms on the right side of the equation describing the basic physical and chemical, hydrodynamic and mechanical parameters of the process of saturation of PE, occurring in terms of (17) - (20).

Consider the basic technologically important situations.

1. PE ceramsite get wet in a stationary solution.

This is consistent with the terms of $P_{rot} = 0$, $P_{dist} = 0$.

Equation (2.13) takes the form

$$E_K \frac{\partial W}{\partial t} = \frac{D_K}{r^2} \frac{\partial}{\partial r}(r^2 \frac{\partial W}{\partial r}) + \frac{k}{\eta} \frac{\partial W}{\partial r} \frac{\partial (P_{part} + P_{grav})}{\partial r} - cW \qquad (21)$$

It reflects the processes of diffusion in a porous medium, taking into account the physical and chemical reactions occurring on grain.

If, moreover, to set *c=0*, we arrive at the case when significant physical and chemical transformations not. And the model equation to the form.

$$E_K \frac{\partial W}{\partial t} = \frac{D_K}{r^2} \frac{\partial}{\partial r} (r^2 \frac{\partial W}{\partial r}) + \frac{k}{\eta} \frac{\partial W}{\partial r} \frac{\partial (P_{part} + P_{grav})}{\partial r} \tag{22}$$

If we further assume that the pressure inside the pores of the depth of the grain does not change,

$$E_K \frac{\partial W}{\partial t} = \frac{D_K}{r^2} \frac{\partial}{\partial r} (r^2 \frac{\partial W}{\partial r}) \tag{23}$$

Together with the boundary and initial conditions (18) - (19), (23) is a classical problem of free diffusion in porous media.

2. The usual mixing in mixer.

Then $P_{vozm} = 0$ and arrive at the problem

$$E_K \frac{\partial W}{\partial t} = \frac{D_K}{r^2} \frac{\partial}{\partial r} (r^2 \frac{\partial W}{\partial r}) + \frac{k}{\eta} \frac{\partial W}{\partial r} \frac{\partial (P_{part} + P_{grav} + P_{vot})}{\partial r} - cW \tag{24}$$

The equations in the previous paragraph, for the cases of lack of physical - chemical interactions with *c=0* and constant pressure in a radial direction. In this case, you can also argue that P_{rot} will contribute more than the other two components of the change in radial pressure.

3. Mixing in the mixer with an external perturbation:

$$E_K \frac{\partial W}{\partial t} = \frac{D_K}{r^2} \frac{\partial}{\partial r} (r^2 \frac{\partial W}{\partial r}) + \frac{k}{\eta} \frac{\partial W}{\partial r} \frac{\partial (P_{part} + P_{grav} + P_{vot} + P_{dist})}{\partial r} - cW \tag{25}$$

The model reflects the situation when the mixing process is applied external influence such as a vibrator. In this case, the processes of diffusion induced grain into the solution significantly intensified, and this should lead to a significant reduction in time required impregnation with cement mortar. This explains the earlier assumption in the References.

The main practical conclusion - to save cement by reducing the mixing time is necessary in the mixing process to enable the vibration. dispersed to the effects of vibration at the time of preparation of expanded clay granules are dispersed and further activated, and sealed with cement mortar on the surface. Much intensity vibration exposure gives a concrete mixture with high viscosity at low water consumption and consumption of cement.

It is obvious that for macroporous claydite major influence on the solution of this problem would be to make members of the P_{dist} and cW, so when studying the process of saturation and its simulation is they need special attention.

In addition, the ratio shows that this term increases in absolute value, k/η more influence on the decision, and hence the rate of saturation, if the denominator - the strength - is reduced (in fact, W/C increases) or the numerator - the permeability of PE increases ($E\kappa$ effective porosity increases). Problem (17) - (25) can only be solved numerically because of the nonlinearity. To do this, develop a software package with an analysis of the specific values of physical, chemical and mechanical constants characterizing the properties of cement, additives, water-cement ratio and mode of preparation technology MPK. In addition, it is necessary to know all the constants and parameters in the model (17) - (20). This will require analysis of the known References, and special experiments.
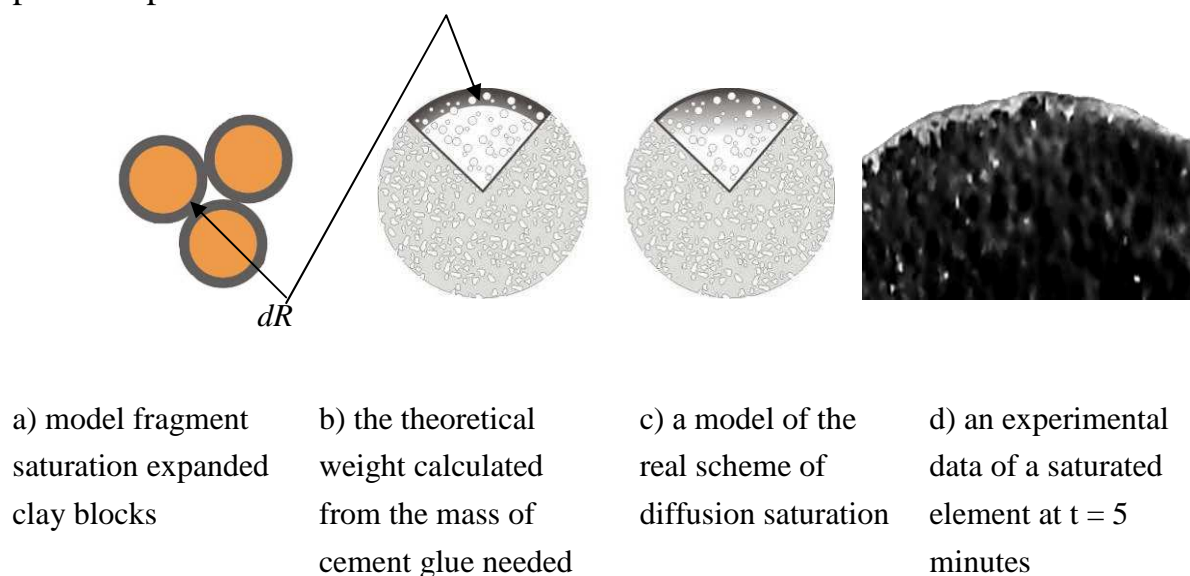

| a) model fragment saturation expanded clay blocks | b) the theoretical weight calculated from the mass of cement glue needed | c) a model of the real scheme of diffusion saturation | d) an experimental data of a saturated element at t = 5 minutes |

Fig. 5. - Schematic representation of the layer of depending on the reduced radiusimpregnating *dR* model representation (a ,c) and in the real (c)

Solving Problems (17) - (25) will provide an opportunity to estimate the true thickness of the diffusion layer *dR* PE-saturated cement solution in time *t*, and hence the total amount of glue to lay the formwork MPK volume formwork with filler volume PE, which will help to obtain an approximate solution of the basic technological challenges of organizing the process of preparing and laying MPK in permanent form at minimal cost, and providing the necessary number of

defined properties, in the first place, its design strength, flow, cement glue, heat and volume weight.

Established, which estimate the relative depth of the saturation of the regulatory requirements, the minimum strength MPK for common types of brands of cement, and expanded clay is used $0,02 \leq dR/R \leq 0,1$.

We consider the numerical solution of one-dimensional diffusion equation forced water-cement mortar, filling the space between the grains of polyethylene, the ball inside in the radial direction in spherical coordinate system(18)-(25).

The difficulty of solving such problems is a nonlinear function P, so well-known methods of solution, as a rule, are inoperative, and for each of its kind requires a special approach which takes into account the physical content of the process and the development of special algorithms and programs.

At each time step was solved by an ordinary nonlinear differential equation of order two (11) with boundary conditions (12) - (13). The numerical solution of this equation was among *Mathematica 7.0.* [7], based on recommendations from the References and comparisons with the performance RFP *MathCAD* and *MatLab* to solve similar problems. The figure shows the graphs of the calculations for t = 5 seconds for different values of the degree of saturation W depending on the reduced radius r/R.
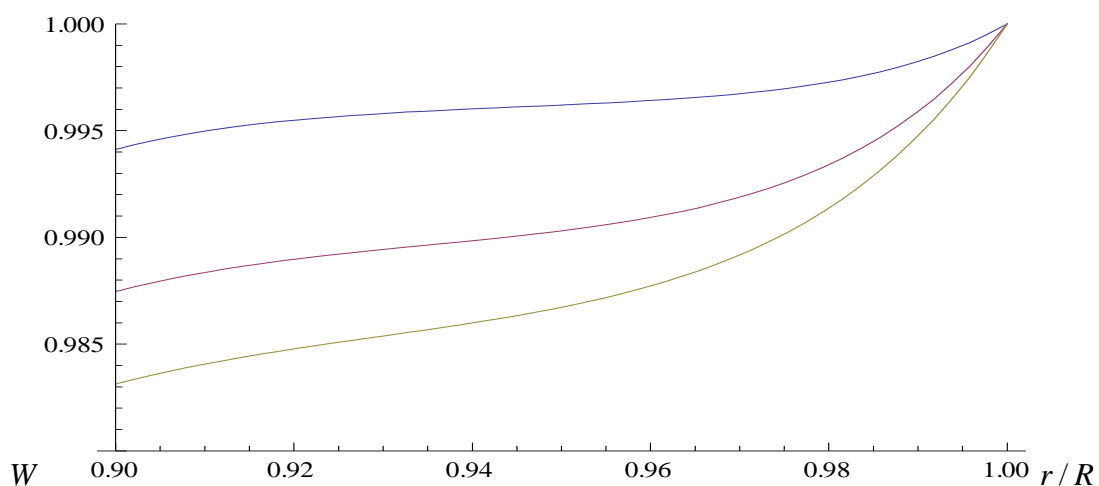

Fig. 6. A typical example of calculating the degree of saturation of the grout for t=5 seconds

Considered approximations of the external forces $P = \gamma \cdot e^{-\mu \cdot r}$ or $P = \gamma \cdot r + \mu$, γ – Linear velocity of flow of the solution by diffusion induced by external mechanical effects and chemical transformations.

Comparative solution is being implemented mathematical model in three ways:

1) With different values of the rate γ: 1-γ_1=0,8 (upper), 2-γ_2=1 (middle), 3-γ_3=1,3 (bottom). Asked parameters are: the diffusion coefficient D and the effective porosity of grain E_k.

2) With different values of E_k: E_{k1}=0.4; E_{k2}=0.5; E_{k3}=0.55. Asked parameters are: D and γ.

3) With different values of the coefficient D: D_1=0.2; D_2=0.25; D_3=0.35. Asked parameters are: γ, E_k.

Note that a rigorous proof of the countable stability of the algorithm in this paper is not, although carried out numerical simulations to model real physical model of constant values that point to the convergence. In addition, (18) - (20) the implicit time difference scheme that based on their general theory of stability of difference schemes, lets hope for the stability of the proposed numerical method. The issue is the subject of further research.

The problem of modeling non-stationary process of saturation of the water-cement mortar element of artificial porous aggregates for example, expanded clay. In a medium *Mathematica* 7.0 is implemented algorithm for the numerical solution of the corresponding nonstationary problem. By the developed program numerous calculations for model problems and real processes show performance of the proposed method.

A database in the medium *MCAccess*, select queries are implemented by the type of expanded clay and characterize its input parameters. Produced by filling out the information base for three types of expanded clay aggregates produced from alumina Penza region, and thereby laid the foundations of information modeling system of non-stationary process of saturation keramsit macroporous cement mortar.

References

1. Samarskii A.A., Mikhailov A.P. Mathematical Modeling: Ideas. Methods. Examples Publishing house Fizmatlit M. 2002.-320.

2. Fitzgerald G.V. Transient supersaturation in the thermal diffusion cells / Fitzgerald GV - Tr. with English. E.L. Aleksandrova. - Obninsk: Institute of Experimental Meteorology, 1970. - 90 pp.

3. Lipatov G.N. Experimental study termodiffuzioforeza large volatile aerosol particles / G.N. Lipatov. // Physics of the aerosol systems. - Kiev-Odessa.: High School, 1979. - Vyp.19 - C.19-22.

4. Yalamov Y.I. Theory of the Termal diffusional motion moderately large volatile aerosol particles. / Y.I.Yalamov., M.N Gaidukov M.N., E.R. Shchukin, J. of Ph. Chemistry. - 1975.-T. 49 .- № 2 .- P. 505-507.

5. Kamburg V.G. Generalized model for calculating the fields of supersaturation in the channels of different configurations / V.G. Kamburg, N.V. Sheptalin NV // Collection of scientific works "Integral transforms for boundary value problems" - Kiev: Institute of Mathematics, National Academy of Sciences of Ukraine .- 1996. - P.21-26.

6. Kamburg V.G. Study of the regularities of formation of satiety in the fields of dynamic flow thermal diffusion chambers by mathematical modeling / V.G. Kamburg, I.V.Zimbalistaja, M.V. Sheptalin et al Scientific journal "Journal of Technology University of Podolia (Khmelnitsky)" .- 2002. - V. 2, № 4. -P.14-18.

7. Yalamov Y.I. Theory of the Termal diffusional motion moderately large volatile aerosol particles. / Y.I. Yalamov , M.N.Gaidukov, E.R. Shchukin, J. of Ph. Chemistry.-1975.-T. 49.- № 2 .- P. 505-507.

8. Shulimanova Z.L. / Z.L. Shulimanova, E.R. Shchukin ER Termal diffusional eposition of aerosol particles from laminar gas flow to the cooling surface. - Moscow, 1984.-Dep. in VINITI № 2879.

9. Kamburg V.G. Mathematical modeling of heterogeneous equilibria of binary systems from data on vapor pressure and assessment of thermodynamic parameters. Publishing house "Poltava writer" in Poltava., 1998 - 154 sec.

10. Ryazanova, G.N. Kamburg V.G. Improved technology in the construction of walling permanent formwork. Publishing house Penza State University of Architecture and Construction– 2010.-168 sec.

11. Ryazanova, G.N. Kamburg, V.G. Tkachenko, A.N. Model view of the construction technology walling / / Scientific Bulletin VGASU. and Architecture - 2008 .- № 2 - p.78-84.

12. Ryazanova, G.N. Kamburg V.G., Baranova T.I., Tkachenko A.N. Technology and simulation of the construction of frame structures of macroporous concrete at concrete panel. / / RAASN, ACADEMIA. Architecture and Construction. - 2008 .- № 2 - p.71-76.

13. Ryazanova, G.N., Kamburg V.G., Baranova T.I., Tkachenko A.N. Process simulation problem of the construction of walling macroporous concrete at concrete panel. / / XXVIII Russian School on Science and Technology. Science and technology. Inter-regional Council for Science and Technology - Ekaterinburg, Ural Division, June 24-26, 2008, p.72-75.

14. G.N. Ryazanova, V.G. Kamburg, T. I. Baranova, A.N. Tkachenko. Technological Tasks of Erection Process Modelling of Enclosing Structures Made of High Porous Haydite Concrete in Monolithic Sheathing. / / The third international forum on strategic technologies-Novosibirsk, June 23-29, 2008.-s. 117-118.

15. Ivanov I.A. Lightweight concrete for artificial porous aggregates / I.A. Ivanov / Stroyizdat - M., 1993 - 182 sec.

16. Bazhenov, Y.M. Technology Concrete / Y.M. Bazhenov / / High School - Moscow, 1987 - 415 sec.

2.3 MATHEMATICAL MODELS OF THE ELECTROCHEMICAL PROCESSES IN VOLUMETRIC POROUS FLOW ELECTRODES

Koshev A.[1], Kosheva N.[1]

Electrochemical mechanism of the reactions occurring in electrochemical reactors designed for metal electrodeposition is, obviously, a unifying principle of their operation. The electrode potential and potential jump at the interface in the electrochemical system are crucial characteristics controlling both the transformation rate and nature of the end product. For many types of electrochemical systems, in particular, for threedimensional flow electrodes (TFEs), the problem arises of assuring uniform potential distribution in different electrode areas and, as a consequence, limitation of the useful electrode size and thickness. The potential distribution is determined by the following main factors: kinetics of electrode process, conductivities of the solid and liquid phases of the electrochemical system, and electrolysis regime (voltage, stirring, temperature). Evidently, to improve operation of the electrochemical reactors, irrespective of their destination and principles of organization of the electrochemical reactions, it is, essential, first, to develop scientific notions of the nature of electrochemical reaction and the influence of the current,

[1] Penza State University of Architecture and Construction, Penza, Russia

hydrodynamic, diffusional, and other characteristics of the electrochemical process on its efficiency and, second, to construct and develop the appropriate mathematical models and computational methods for the most favorable deposition regimes with allowance for the energetic and hydrodynamic possibilities of the reactors and their elements and construction. Among the promising three-dimensional flow electrodes intensifying electrochemical processes, especially in diluted solutions, fiber carbon electrodes have found practical use [1–4]. Because of a variety of factors influencing the operation efficiency of TFEs, the optimal operating conditions can be determined only through the mathematical modeling, optimization, and optimal control of the electrochemical processes occurring in the pores of volumetric porous electrodes, in conjunction with the experimental study of the nonstationary processes and properties of carbographite fiber materials. Although the general problems of the mathematical modeling of electrochemical processes are well-documented in the works of electrochemists and mathematicians, e.g., in [5–35], we did not find any publications devoted to the mathematical modeling of the processes occurring on three-dimensional porous flow electrodes in the nonstationary electrolysis regimes. The purpose of this work was to develop model representations for the nonstationary electrochemical TFEs in the nonstationary electrolysis regimes. In doing so, a change in the electrode and electrolyte parameters was taken into account as in [21–23]. As an illustration of the efficiency of a model of two-dimensional electrochemical system, the current and flow directions were chosen to be mutually perpendicular, without discussing advantages and disadvantages of such an organization of the process. This issue will be the subject of our further publications.

1. Basic equations

The basic equations used for constructing and studying the mathematical model of electrodeposition in various electrochemical systems are presented below. We assume that the flow N_i ($i=1,\ldots,n$) of charged particles of the sort *i* in the electrolyte volume is determined by the migrative and convective components, as is the case in the majority of electrochemical systems,

$$N_i = z_i\, u_i\, FC_i\, \nabla E + C_i\, V. \tag{1}$$

Here, z_i, C_i, u_i, are, respectively, the charge, concentration, and mobility of the *i*-th electroactive species in a pseudohomogeneous medium; ∇E is the gradient of electric potential; and *V* is the velocity vector of the convective solution transfer. The current in the electrode/electrolyte volume is expressed by the formula

$$J = F \nabla z_i N_I, \tag{2}$$

The material balance in the absence of a homogeneous electrochemical reaction is expressed as

$$\partial C_i / \partial t = - \nabla \cdot N_i, \tag{3}$$

where $\nabla \bullet N_i$ is the divergence of the *Ni* flow. For the stationary system, one has

$$\nabla \cdot N_i = 0. \tag{4}$$

From Eqs. (1) and (2) it follows that

$$J = F^2 \sum_i^n z_i^2 u_i C_i \nabla E + F V \sum_i^n z_i C_i, \tag{5}$$

or

$$J = \chi \nabla E + F V \sum_i^n z C, \tag{6}$$

where $\chi = F^2 \sum_i^n z_i^2 u_i C_i$ is the conductivity of the pseudohomogeneous medium. The conductivity can be considered constant if a change in the concentrations of electroactive species has only little effect on it (e.g., in the presence of a base electrolyte).

By multiplying each term in Eq. (4) by $z_i F$, summing over *i*, one obtains, in combination with Eq. (2),

$$\nabla \cdot J = 0, \tag{7}$$

or

$$\nabla \cdot [\chi \nabla E + F V \sum_i^n z_i C_i] = 0, \tag{8}$$

2. Generalized mathematical models

Further transformation of Eq. (8) depends on whether the electroneutrality condition $\sum z_i C_i = 0$ is fulfilled in the system or not. It is commonly supposed that this condition is fulfilled over all volume of the electrolyte solution, except for the electric double layer near the electrodes and other interfaces [34, p. 261].

However, the condition $\sum z_i C_i = 0$ does not hold in the case of metal electrodeposition in the pseudohomogeneous systems, e.g., in volumetric porous electrodes, where, from the macrokinetic standpoint, one can assume the presence of a potential jump at the solid electrode/electrolyte boundary in each elementary volume of the electrode space.

In the mathematical modeling and calculation of the electrochemical systems with volumetric porous flow electrodes designed for metal extraction, one can arbitrarily recognize two approaches: with (1) mutually parallel electric-field and electrolyte-flow lines in reactor and (2) mutually perpendicular or angular arrangement of the current and flow directions. The electrolysis regime is either galvano- or potentiostatic (dynamic).

In this work, an attempt was undertaken to describe the electrolysis process on a TFE for an arbitrary arrangement of the current- and electrolyte-supply boundaries, i.e., for both galvanostatic and galvanodynamic regimes in a three-dimensional electrochemical system.

Breaking of electroneutrality at any point indicates, generally, that either a positive or negative source of charged particles is situated at this point. As mentioned above, we consider the case of a pseudohomogeneous electrochemical system, e.g., of a volumetric porous electrode filled with a homogeneous electrolyte with the averaged effective characteristics. Such an approach was originally proposed by Ya.B. Zel'dovich and today is successively used for modeling pseudohomogeneous systems [8].

It would appear natural that the potential in such a model medium suffers jump at the solid electrode/electrolyte boundary in each elementary volume of the electrode space, where electrode reactions can proceed, thereby breaking the $\sum z_i C_i = 0$ condition. By transforming Eq. (3) with allowance for this fact, one gets

$$\partial C_i / \partial t = - \nabla \cdot (z_i \, u \, FC_i \, \nabla E + C_i \, V), \qquad (1)$$

or

$$Fz_i \, \partial C_i / \partial t = - \nabla \cdot (z_i^2 \, F^2 u_i C_i \, \nabla E + Fz_i C_i \, V), \qquad (2)$$

The summation over $i = 1, \ldots, n$ in Eq. (11) gives

$$\sum Fz_i \, \partial C_i / \partial t = \nabla \cdot [-\text{æ} \nabla E - FV \sum z_i C_i], \qquad (3)$$

or

$$F\partial\Sigma\ z_iC_i\,/\partial t = \nabla\cdot[-\text{æ}\nabla E] - F\nabla\cdot\ [V\Sigma\ z_iC_i] \qquad (4)$$

After removing from Eq. (4) the terms *zici* corresponding to the electrolyte components not involved in the electrochemical reactions, one arrives at the relation similar to Eq. (4), however, with the summation only over the electroactive species (indexed *k*) that are involved in the reactions:

$$F\partial\Sigma\ z_{\text{к}}C_{\text{к}}/\partial t = \nabla\cdot[-\text{æ}\nabla E] - F\nabla\cdot\ [V\Sigma\ z_{\text{к}}C_{\text{к}}], \qquad (5)$$

The second sum on the right-hand side of Eq. (14) has the form

$$\sum\frac{\partial C_k}{\partial x}V_X+\frac{\partial C_k}{\partial y}V_Y+\frac{\partial C_k}{\partial z}V_Z)=\sum|V|\left(\frac{\partial C_k}{\partial x}\cos\alpha+\frac{\partial C_k}{\partial y}\cos\beta+\frac{\partial C_k}{\partial z}\cos\gamma\right)=\sum|V|\frac{\partial C_k}{\partial r}, \quad (6)$$

where *r* is directed along the solution flow.

As in [25], one can readily obtain the following relation:

$$\frac{\partial C_{\text{к}}}{\partial r} = -\frac{S_V}{|V|z_K\,F}\,J_{Sk}, \qquad (7)$$

where S_V is the reaction surface and J_{si} is the density of polarizing current for the *i*th species.

Substitution of Eqs. (6) and (7) into Eq. (5) gives

$$F\partial\Sigma\ z_{\text{к}}C_{\text{к}}/\partial t =\ \nabla\cdot[-\chi\ \nabla E]+S_V\Sigma J_{Sk}$$

The conducting properties in each elementary volume of the pseudohomogeneous medium considered can naturally be modeled by two series-connected conductors [2] characterizing the solid and liquid phases of the system; $\rho=\rho_{\text{Ж}}+\rho_{\text{Т}}$. Considering that $\rho_{\text{т}}=1/\,\chi_{\text{г}}$; $\rho_{\text{Ж}}=1/\,\chi_{\text{ж}}$ и $\chi=1/\rho=1/(\rho_{\text{Т}}+\rho_{\text{Ж}})$, one gets

$$F\partial\Sigma\ z_{\text{к}}C_{\text{к}}/\partial t = \nabla\cdot[-(\,\text{æ}_T\,\text{æ}_{\text{Ж}}\,/(\text{æ}_T\,+\text{æ}_{\text{Ж}}))\nabla E]+S_V J_{Sk}, \qquad (8)$$

The set of Eqs. (17), in conjunction with Eqs. (16) and kinetic equations relating J_{Sk} with E_ξ,

$$J_{Sk}\left(x\right)= j_{0k}\,\frac{\exp\left(\alpha_k z_k F\left((E-\varphi_{Rk})/RT\right)-\exp\left((\alpha_k-1)z_k F\left(E-\varphi_{Rk}\right)/RT\right)\right.}{1+j_{0k}\exp\left(\alpha_k z_k F\left(E-\varphi_{Rk}\right)/RT\right)/z_k FK_m C_k}, (9)$$

can be used to calculate the potential, current density, and concentration distributions for the electroactive species in the volume of a porous electrode.

This set of equations should be supplemented by the natural boundary conditions

$$\frac{\partial E}{\partial n}(t)\Big|_{\sigma_K} = J(t)\rho_T \,;\; \frac{\partial E}{\partial n}(t)\Big|_{\sigma_A} = -J(t)\rho_{\text{ж}}\,;\; \frac{\partial E}{\partial n}(t)\Big|_{\sigma_И} = 0;\; C(t)\Big|_{\sigma_П} = C_0\,, \quad (10)$$

where n is directed along the normal to the boundary $\sigma=\sigma_K+\sigma_A+\sigma_И+\sigma_П$ of the reaction region. The terms in the latter sum stand for the outer boundaries of electrode, which are generally characterized by, respectively, the following components: current feed, current removal, insulator, and electrode surface through which electrolyte flows in.

One variant of the spatial orientation of a threedimensional TFE is schematically shown in Fig. 1.
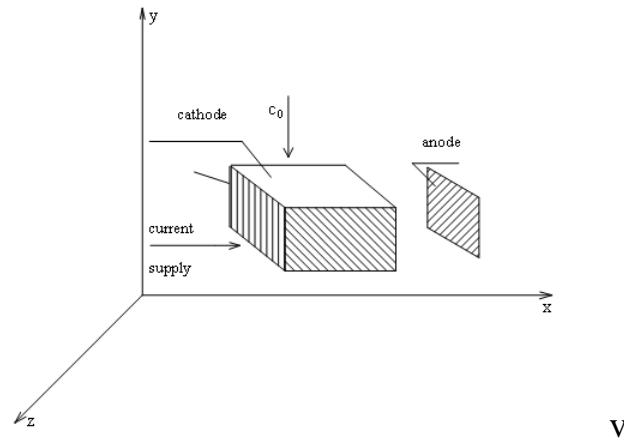
Fig. 1. Scheme of a volumetric porous flow electrode.

3. Mathematical models for calculations

In the case where only one electroactive component is present in the electrolyte solution and the electrolyte flow is directed along the current, the set of Eqs. (16)–(19) takes the form

$$zF\frac{\partial C}{\partial t} = -\frac{\partial^2 (1/\rho)E}{\partial x^2} + S_V J_S, \quad (1)$$

$$|V| zF\frac{\partial C}{\partial x} = -S_V J_S\,, \quad (2)$$

$$J_S(x) = j_0 \frac{\exp\left(\alpha zF\left((E - \varphi_R)/RT\right) - \exp\left((\alpha - 1)zF(E - \varphi_R)/RT\right)\right)}{1 + j_0 \exp\left(\alpha zF(E - \varphi_R)/RT\right)/zFK_m C}, \quad (3)$$

$$C(0,\tau)=C_0,\ C(x,0)=C_0,\ \frac{\partial E}{\partial x}(0,t)=\rho_T I(t),\ \frac{\partial E}{\partial x}(L,t)=\rho_{\textit{Ж}} I(t),\ E(x,0)=\varphi_R, \quad (4)$$

Note that the resistivity ≀ of a pseudohomogeneous medium in Eq. (1) is generally not constant across the whole width of the electrode and can change during the electrolysis because of the inclusion of a metal sediment into the conductance of the carbographite material. These variations can be included into the mathematical model as shown in [21]. In this case, Eq. (1) can be written in the expanded form,

$$zF\frac{\partial C}{\partial t}=-\frac{\partial^2 E}{\partial x^2}-\frac{\partial E}{\partial x}\frac{\rho_T\rho_{\textit{Ж}}}{(\partial\rho_T/\partial x)(\rho_T+\rho_{\textit{Ж}})}+\frac{\rho_T\rho_{\textit{Ж}}}{(\rho_T+\rho_{\textit{Ж}})}S_V J_S, \quad (5)$$

By introducing time grid for $0 \le t \le T$: $\Omega_t = \{t_i : t_0 = 0;\ t_i = i\Delta t,\ i=1,\ldots,m;\ t_m = T\}$ and spatial grid for $0 \le x \le L$: $\Omega_x = \{x_j : x_0 = 0;\ x_j = j\Delta x,\ j=1,\ldots,q;\ t_q = L\}$ and replacing partial derivatives by their discrete analogs, one obtains, at each grid point, the set of equations whose solution enables one to determine all electrochemical functions of interest.

4. Working in limiting current mode with parallel current and solution flow

In formulation of the given problem, there is an important condition of problem openness or closeness with respect to the initial conditions. The problem is closed when it is required to calculate the overall current density I and electrode thickness L providing, first, whole electrode working in the limiting diffusion current mode and, second, given metal extraction degree $R = 1 - cL/c_0$, where c_0 and c_L are, respectively, the deposited metal concentrations in the TFE input and output. Unless achievement of the given extraction degree is required, it is necessary to give another condition, for example, maximum extraction degree; otherwise, this problem seems insufficiently defined. We can solve the problem of the overall current density providing the electrode working in the limiting diffusion current mode with the given TFE thickness or calculate the electrode thickness for the given overall current density, but then this problem cannot be solved in some probable situations. Assume the given electrode thickness and some overall current density not providing the limiting diffusion current for the whole electrode. In order to observe the limiting

diffusion current in each point of TFE, it is necessary to increase the overall current density. However, as was demonstrated in [37], beginning from some level, such increase in *I* may produce the inverse effect, i. e., lower electrode polarization, for example, in its minimum point. A different situation arises, when for the given extraction degree *R* we calculate the overall current density *I* and electrode thickness *L* providing the whole TFE bulk working in the limiting diffusion current mode. In this case, in the first electrode surface element, beginning from the lead wire, only a part of current is spent to the electrochemical reaction, which is limited by the rate of metal ion transfer to the electrode surface. The balance current on the following surface element is also partially spent by the same mechanism, and so on, until achievement of the given decrease in the electrolyte concentration. Thus the TFE thickness and overall current density should provide the concentration decreasing to the given level and total current consumption in the limiting diffu sion current mode. Because in the limiting diffusion current conditions the conductivity solid and liquid phases in the system does not affect the electrochemical reaction, then we can logically expect that the con ductivity of the electrode material and solution should not be involved in solution of the given problem. We solve this problem by considering the stationary model for distribution of polarization *E*, current density j_S, and electroactive component concentration *c* in a three_dimensional flow electrode with rear or front electrolyte flow to the electrode [38]:

$$\frac{d^2 E}{dx^2} = \left(\frac{1}{\chi_T} + \frac{1}{\chi_G} \right) S_v j_s, \qquad (1)$$

$$\frac{dE}{dx}(0) = -\frac{I}{\chi_T} \; ; \quad \frac{dE}{dx}(L) = \frac{I}{\chi_G}; \qquad (2)$$

$$\frac{\partial c}{\partial \vec{n}}(x) = -\frac{S_v}{vZF} j_s(x). \qquad (3)$$

Here *x* is the coordinate of a point in the electrode $(0 \leq x \leq L)$, is the solution flow direction, v is the linear solution flow rate, χ_T and χ_G are the conductivities of electrode and electrolyte, espectively, *S*V is the specific reaction surface area, *z* is the discharged ion valency, and *F* is the Faraday constant. In the case of rear or front solution flow, is *x* or –*x*, respectively. If the

electrode is working in the limiting diffusion current mode in point x, then for rear solution flow wecalculate the limiting current density jpr:

$$j_S(x) = j_{pr}(x) = zFk_m c(x), \qquad (4)$$

$$\frac{dc}{dx} = -\frac{S_v}{vzF} j_S, \quad c(0) = c_0, \qquad (5)$$

Here km is the mass transfer coefficient. Integrating equation (1) from 0 to L, with respect to conditions (2), we have:

$$\frac{I}{\chi_G} = -\frac{I}{\chi_T} + \left(\frac{1}{\chi_T} + \frac{1}{\chi_G}\right) S_v z F k_m c_0 \frac{v}{S_v k_m}\left(1 - \exp\left(-\frac{S_v k_m L}{v}\right)\right), \qquad (6)$$

Because $j_{pr}(L) = zFK_m c_0 \exp(-\frac{S_v k_m L}{v})$, then

$$\frac{I}{\chi_G} = -\frac{I}{\chi_T} + \left(\frac{1}{\chi_T} + \frac{1}{\chi_G}\right) zFc_0 v\left(1 - \frac{j_{pr}(L)}{zFK_m c_0}\right)$$

Here we can estimate the overall current density I^* providing the limiting diffusion current in electrode point $x = L$ and, therefore, whole TFE work in the limiting diffusion current mode with rear solution flow to the electrode:

$$I_T^* = zFc_0 v\left(1 - \frac{j_{pr}(L)}{zFk_m c_0}\right), \qquad (7)$$

Taking into account that $jpr(L) = zFkmc(L)$, we have $IT^* = zFc_0v(1 - c_L/c_0)$ or finally:

$$I_T^* = zFc_0 vR, \qquad (8)$$

where $R = 1 - c_L/c_0$ is the given degree of metal extraction. As follows from formula (7), $IT^* = zFc_0v \times$, then $LT = v \times \ln /(SVkm)$. With respect to (8), we derive:

$$L_T = -\frac{v \ln(1 - R)}{S_v k_m}, \qquad (9)$$

Reasoning quite similarly for the process of electrolysis with front electrolyte flow, we will derive absolutely the same formulas for calculation of

the overall current density and thickness of the electrode working in the limiting diffusion current mode by the electro active component.

5. Results od calculations and experimental studies

For illustration, we represent the parameters of metal extraction on TFE calculated by formulas (8) and (9) with the bundled software corresponding to the model assumptions described in [36-38,21-23]. The calculations were carried out for the case of copper electrodeposition of sulfate electrolyte with the parameters: $c_0 = 10^{-4}$ M, $D = D = 0.75 \times 10^{-5}$ cm^2/s, copper ion reduction exchange current density $j0 = 2 \times 10^{-5}$ A/cm^2, equilibrium copper deposition potential $E_{Cu} = 0.333$ V, v = 1 cm/s, $\chi_T = 0.1$ S/cm, $\chi_G = 0.1$ S/cm, $S_V = 200$ cm^2/cm^3 [39].

Table 1 specifies overall currents IF and IP and metal extraction degrees RF and RP calculated by formula (8) and selected by the program, respectively, providing discharge of copper ions all over electrode thickness L in the limiting diffusion current mode for extraction degree R. The calculated data was compared with the results of experimental studies. We studied the copper deposit distribution by the electrode thickness for L of 1.4 and 2.0 cm. The electrodes of required thickness were assembled from graphite coal material VNG-30. As we know, if metal is electrodeposited all over the electrode

Table 1 - Overall current densities and metal extraction degrees providing TFE operation in the limiting diffusion current mode as calculated by omitting side electrochemical reactions

Extraction degree, RF	Extraction degree, R_P	Electrode thickness, L, cm	Overall current density, IF, A/ cm^2	Overall current density, P, A/ cm^2
0.99	0.96	1.564	0.02	0.03
0.9	0.92	0.782	0.018	0.024
0.7	0.8	0.409	0.014	0.07
0.5	0. 235	0.235	0.01	0.084

thickness at the limiting diffusion current, then weight distribution of the metal deposited on the electrode is logarithmic. As follows from the data in Fig. 2, on the electrode of 1.4 cm thick, copper ions are discharged at the limiting diffusion current. This is not the case of electrode of 2.0 cm thick: a deviation from the logarithmic curve is observed in the central part of the electrode, while copper

ions are discharged on the edges of the electrodes at the limiting diffusion current. The maximum copper extraction degree (0.99%) is achieved at the current density of 0.48 to 0.50 A/cm2 due to discharge of copper ions at the limiting diffusion current. A higher current density over 0.50 A/cm2 reduces the copper extraction degree. A significant difference between the calculated (Table 1) and experimental overall current densities is due to the fact that the calculations omitted probable parallel reactions: reduction of dissolved oxygen and hydrogen ions. The first reaction precedes reduction of copper ions, the second one is possible in the range of potentials corresponding to the limiting diffusion current of copper ion reduction. The results from the overall current density calculations with respect to these reactions (Table 2) evidence a good consistence of the calculated and experimental data. Here we used the following
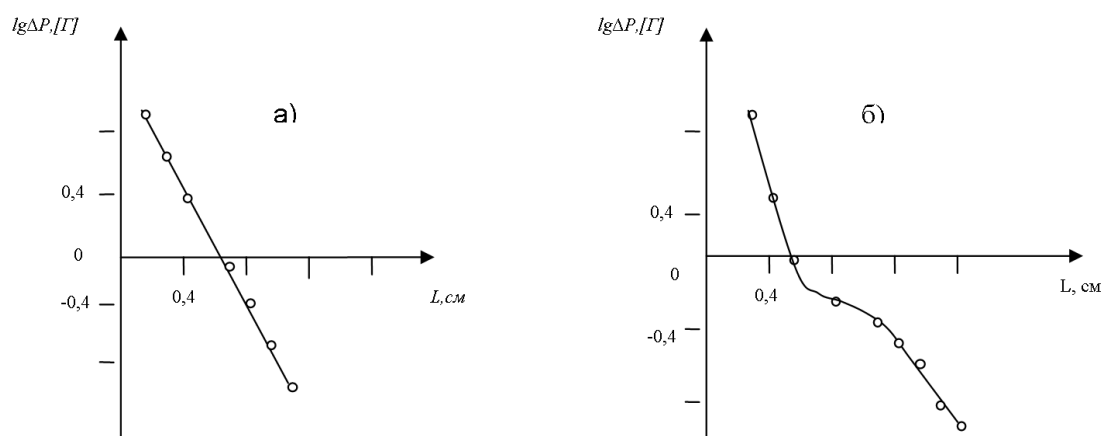
Fig. 2. Metal distribution by electrode thickness for *L*, cm: (a) 1.4, (b) 2. Overall current density 0.48 A/cm^2.

parameters of electrochemical reactions: equilibrium hydrogen release potential EH = 0, equilibrium oxygen reduction potential EO2= 1.23 V, hydrogen ion reduction exchange current density j0, H = 10^{-8} A/cm^2, dissolved oxygen reduction exchange current density j0 O2= 10^{-10} A/cm^2, α_{O2}=0.5, $c_{0\ O2}$= 2 × 10^{-7} mol/cm^3 [39]. Figures 2 and 3 represent the distribution of some electrochemical functions by the TFE thickness as calculated for TFE with L = 1.4 cm with rear solution feed and overall current density of 0.45 A/cm^2.

Table 2 - Overall current densities, electrode thicknesses, and metal extraction degrees providing TFE operation in the limiting diffusion current mode as calculated with respect to parallel electrochemical reactions

Extraction degree R_F	Extraction degree RP	Electrode thickness L, cm	Overall current density IP, A/cm^2
0.99	0.96	1.564	0. 5
0.985	0.98	1.42	0.45
0.9	0.92	0.782	0.3
0.7	0.8	0.409	0.07

Figure 3 shows the partial current profiles evidencing three above reactions simultaneously taking place on the electrode: reduction of molecular oxygen, copper ions, and hydrogen ions (hydrogen gas evolution). The distribution of the partial copper ion current is logarithmic, also evidencing discharge of copper ions in the limiting diffusion current mode.

Electrode point number
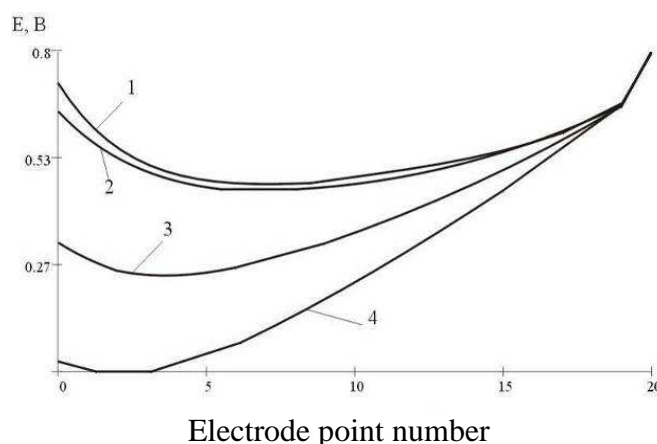
Fig. 3. Potential distribution by electrode thickness for time of electrolysis, s: (1) 600, (2) 1200, (3) 1800, (4) 2000. Electrode thickness 1.4 cm, overall current density 0.45 A/cm^2.

Figure 4 represents the potential distribution curves by TFE thickness as calculated for the process of copper extraction on the electrode with conductivity of 0.2 and 0.07 S/cm. Here we assume in both cases that copper ions are discharged all over the electrode thick ness at the limiting diffusion current. Figure 4 evidences, in particular, that operation of an electrode of low conductivity in the limiting diffusion current mode should be provided with significantly higher polarization of the electrode as compared to the same

processes with significantly higher conductivity of the solid phase in the electrode – electrolyte system.

a)

Electrode point number

b)

Electrode point number
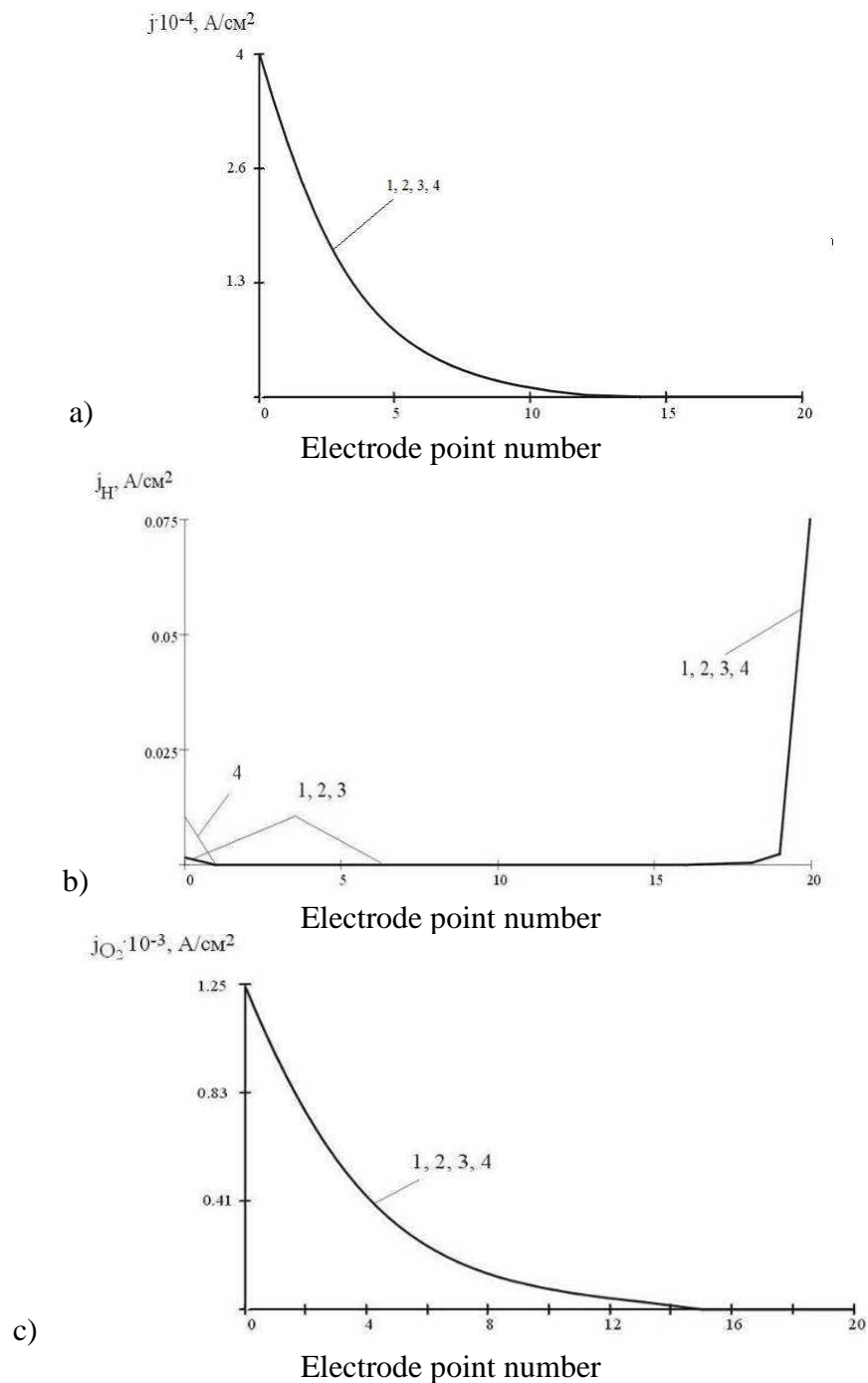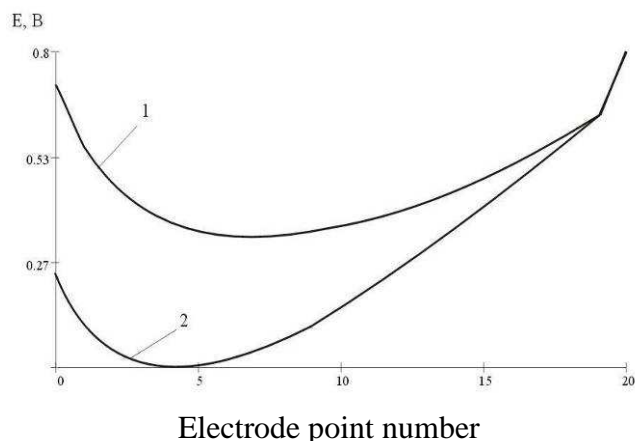
c)

Electrode point number

Fig. 4. Partial current distribution profile of copper electrodeposition (a), hydrogen evolution (b), and electrode reaction with oxygen gas (c) by electrode thickness for time of electrolysis, s: (*1*) 600, (*2*) 1200, (*3*) 1800, (*4*) 2000. Electrode thickness 1.4 cm, overall current density 0.45 A/cm2.

Electrode point number

Fig. 5. Potential distribution by electrode thickness at beginning electrolysis for copper electrodeposition on TFE in limiting diffusion current mode. Electrode conductivity, S/cm: (*1*) 0.2, (*2*) 0.07. Electrode thickness 1.4 cm, overall current density 0.45 A/cm^2.

References

1. Varentsov, V.K., Khimiya v Interesakh Ustoichevogo Razvitiya (Chemistry in the Interests of Permanent Progress), 1997, vol. 5, p. 147.

2. Varentsov, V.K., Intensifikatsiya Elektrokhimicheskikh Protsessov (Intensification of Electrochemical Processes), Moscow: Nauka, 1988, pp. 94–118.

3. Varentsov, V.K. Izv. Sib. Otd. Akad. Nauk SSSR, Ser. Khim. Nauk, 1984, no. 17, (6), p. 106.

4. Varentsov, V.K. and Varentsova, V.I., Gal'vanotekhnika Obrabotka Poverkhnosti, 2005, vol. 13, no. 3, p.26.

5. Daniel'-Bek, V.S., Zh. Fiz. Khim., 1948, vol. 22, p. 697.

6. Daniel'-Bek, V.S., Elektrokhimiya, vol. 2, p. 672.

7. Frumkin, A.N., Zh. Fiz. Khim., 1949, vol. 23, p. 1477.

8. Zel'dovich, Ya.B., Zh. Fiz. Khim., 1939, vol. 13, p. 163.

9. Ksenzhek, O.S. and Stender, V.V., Dokl. Akad. Nauk. SSSR,1956,vol.107,p. 280.

10. Gurevich, N.G. and Bagotskii, V.S., Rabota Zhidkostnykh Poristykh Elektrodov v Rezhime Vynuzhdennoi Podachi Reagentov. Toplivnye Elementy (Operation of Liquid Porous Electrodes in the Regime of Forced Reagent Supply. Fuel Elements) Moscow, 1964, pp. 75–85.

11. Chizmadzhiev, Yu.A., Makrokinetika Protsessov v Poristykh Sredakh (Macrokinetics of the Processes in Porous Media), Moscow: Nauka, 1971, 365 p.

12. Sioda, R.E., Electrochim. Acta, 1971, vol. 16, p. 1569.

13. Kreysa, G. and Linzbach, N., DECHEMA-Monogr., 1983, vol. 93, p. 177.

14. Kreysa, G., Chem.-Ing.-Tech., 1983, vol. 1, p. 23.

15. Coeuret, F. and Oltveria, V.F., Entropie, 1996, vol. 195, p. 21.

16. Newman, J.S. and Tobias, C.W., J. Electrochem. Soc., 1962, vol. 109, p. 1183.

17. Pollar, R. and Trainham, J., J. Electrochem. Soc., 1985, vol. 130, p. 1531.

18. Bek, R.Yu., Izv. Sib. Otd. Akad. Nauk SSSR, Ser. Khim. Nauk, 1977, no. 6, p. 11.

19. Doherty, T., Sunderland, J.G., Roberts, P.L., et al., Electrochim. Acta, 1996, vol. 41, p. 519.

20. Koshev A.N., Kamburg V.G., and Varentsov, V.K., Elektrokhimiya, 1991, vol.27, p.1189.

21. Koshev, A.N., Varentsov, V.K., and Gleizer, G.N., Elektrokhimiya, 1992, vol. 28, p.1170.

22. Koshev, A.N., Gleizer, G.N., and Varentsov, V.K., Elektrokhimiya, 1992, vol.28, p.1160.

23. Koshev, A.N., Varentsov, V.K., and Gleizer, G.N., Elektrokhimiya, 1992, vol.28, p.1265.

24. Koshev, A.N., Gvozdeva, I.G., and Varentsov, V.K., Elektrokhimiya, 1999, vol. 35, p. 784.

25. Maslii, A.I. and Poddubnyi, N.P., Elektrokhimiya, 1999, vol. 35, p. 373.

26. Maslii, A.I. and Poddubnyi, N.P., Elektrokhimiya, 2001, vol. 37, p. 359.

27. Maslii, A.I., Poddubnyi, N.P., and Medvedev, A.Zh., Elektrokhimiya, 2005, vol. 41, p. 1335.

28. Maslii, A.I., Poddubnyi, N.P., and Medvedev, A.Zh., Elektrokhimiya, 2005, vol. 41, p. 452.

29. Chizmadzhev, Yu.A., Markin, V.S., Tarasevich, M.R. and Chirkov, Yu.G., Makrokinetika Protsessov v Poristykh Sredakh (Macrokinetics of the Processes in Porous Media), Moscow: Nauka, 1971, 365 p.

30. Gurevich, I.G., and Vol'fkovich, Yu.M., Zhidkostnye Poristye Elektrody (Liquid Porous Electrodes), Minsk:Nauka i Tekhnika, 1974, 248 p.

31. Bek, R.Yu., Zamyatin, A.P., Koshev, A.N., et al., Izv. Sib. Otd. Akad. Nauk SSSR, Ser. Khim. Nauk, 1980, no. 2, p. 110.

32. Koshev, A.N., Varentsov, V.K., and Kamburg, V.G., Izv. Sib. Otd. Akad. Nauk SSSR, Ser. Khim. Nauk, 1984, no. 17, p. 120.

33. Varentsov, V.K. and Koshev, A.N., Izv. Sib. Otd. Akad. Nauk SSSR, Ser. Khim. Nauk, 1988, no. 17, p. 117.

34. Zherebilov, A.F., Koshev, A.N., and Varentsov, V.K., Izv. Sib. Otd. Akad. Nauk SSSR, Ser. Khim. Nauk, 1984, p. 43.

35. Newman, J., Elektrokhimicheskie Sistemy (Electrochemical Systems), Moscow: mir, 1977, 464 p.

36. 36 Koshev, A.N. and Varentsov, V.K., Elektrokhimiya, 1997, vol. 33, no. 8, p. 903 [Russ. J. Electrochem. (Engl. Transl.)], vol. 33, no. 8, p.903.

37. Koshev, A.N., Varentsov, V.K., and Chirkina, M.A., Fizikokhimiya Poverkhnosti I Zashchita Materialov,2009, vol. 45, p. 441.

38. Koshev, A.N., Chirkina, M.A., and Varentsov, V.K., Elektrokhimiya, 2007, vol. 43, p. 1372 [Russ. J. Electro chem. (Engl. Transl.), vol. 43, p.].

39. Spravochnik po elektrokhimii (Handbook of Electrochemistry), Sukhotin, A.M., Ed., Leningrad: Khimiya, 1981, p. 488.

2.4 MODELING OF PIEZOELECTRIC ACTUATOR HYSTERESIS

Sibielak M.[1], Konieczny J.[1], Rączka W.[1]

Introduction

Piezoelectric materials have been known for years, now they are widely applied as actuating elements in high-precision positioning systems in electron microscopes, in mirror positioning systems and in driving systems for pneumatic or hydraulic valves [1,2,4,5]. The properties of piezoelectric materials ensure the high-resolution of piezoelectric actuators, yet the required precision and repeatability of results is hard to obtain due to the occurrence of an inherent control voltage / strain hysteresis. The effect of hysteresis inhibits the implementation of high-precision positioning systems and necessitates the use of very costly displacement transducers. If this nonlinearity were compensated, no displacement measurements would be required in the control systems, making them more cost-effective. Linearization of piezoelectric actuator characteristics through compensation would ensure more favourable static and dynamic properties of the implemented systems.

The quality of compensation is the controlling factor of the positioning system precision: the better quality, the higher the positioning precision. The quality of compensation depends in the first place on the hysteresis model. In order to construct the optimal model, the stand was designed for testing the static and dynamic behaviours of piezoelectric actuators. It is the main goal to find features, but stand must enable other experiments. It must enable tests of devices which will include piezoelectric materials or not and will be generators, dumpers or measurement devices.

---

[1] AGH University of Science and Technology, Krakow, Poland

Piezoelectric materials have disadvantages too. They are nonlinear and they have hysteresis. In the last section of the paper mathematical model of the hysteresis was shown. This model was verificated by experiment.

1. Mechanical structure

The stand is designed to test the behaviour of piezoelectric elements under the action of applied force or voltage in various loading conditions and for a wide spectrum of applied excitations.

The following conditions are assumed:

- The motion is induced by a low-voltage piezoelectric pile,

- The displacement amplifier system utilises a lever mechanism,

- Amplification, stiffness, mass and damping factor must be changeable,

- The maximal applied force 5000 N,

- Piezoelectric actuator control via a high-voltage amplifier might be implemented for any source of the voltage signal 0-10 V (generator, PLC controller, PC)

Key of the experimental stand is a widely- applied lever configuration. The key advantage is that the displacement of an end section can be multiplied considerably, which is of primary importance here since the displacements generated by piezoelectric actuators are small as a rule. Accordingly, a structure is built in that way which enables changing of gain, beam mass and beam stiffness. It is possible by changing particular elements of stand. Piezoelectric actuators might be applied either in the form of single elements or piles of variable length (up to 600 mm) and up to 200 mm in diameter. The whole structure is made from general –purpose aluminium profiles, so the required sensors and transducers can be easily fixed both at the piezoelectric end and at the lever end.

Sensors can be also mounted in series with the piezoelectric element (for example the force sensor). Thanks to the presence of a rigid beam in the lever and the high gain, the employed displacement sensors might be simple and cheap. The slider bearing in the axis of rotation offers an obvious advantage as no vibrations are generated, while they might occur in ball bearings. All those

features supported by easy and quick replacement of piezoelectric elements offer excellent potentials for testing.

The stand performs really well in static tests. It is prepared for dynamic testing of piezoelectric actuators, though the beam mass presents a certain problem. The beam mass has to be large, though, to ensure the required stiffness. The stand might be also used for testing vibrating systems [3,5,6,7], i.e. vibration reduction and vibration generation and shaping systems.
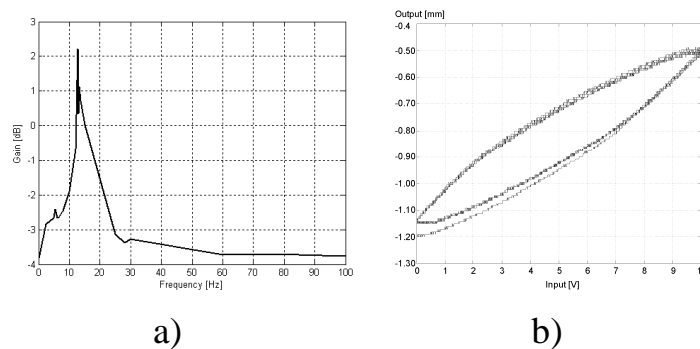
a)   b)

Fig 1. Displacement transmissibility characteristics vs. frequency of a piezoelectric actuator (no extra load) (a) and Static characteristic of a piezoelectric actuator under the loading 5 kg (b)

The stand comprises a set of discs varying in mass (from 50g to 1000 g), a set of springs of variable stiffness (from 4 to 30 N/mm) and a damper with a controllable damping force.

2.   Measurement and control

The basic measurement and control system consists of a displacement sensor, a high-voltage amplifier, a control card and a PC. The control circuit utilises a high voltage amplifier which provides the control of piezoelectric actuators throughout the range of control voltages from –20 to 120 V in the feedback or open- loop configuration. The measurement circuit comprises an induction displacement transducer. Both circuits are connected to the A/D and D/A converter card in the PC. Several types of displacement, acceleration and force sensors are available for these applications.

The PC and the measurement and control card supported by commercially available software enable the testing of static and dynamic characteristics of piezoelectric actuators and sensors and of position or force control systems. One

has to bear in mind that as systems with several DOFs can be designed, the testing of vibration reduction (Jang 1999) or generation algorithms is also possible.

Selected results of static and dynamic tests of a piezoelectric actuator are compiled in Fig 1.

3. Model of piezoelectric actuator

Assumed that model of hysteresis for piezoelectric actuator made of stack will be based on hyperbolic tangent. Operator of hysteresis defined as:

$$H(u)(t) = \int_0^t h(t) \cdot \dot{u}(t) dt + \tanh(-a \cdot k / 2 + xa) dt \qquad (1)$$

where:

$$h(t) = 0.5 \cdot (1 + sign\,(\dot{u}(t))) \cdot \tanh'(k \cdot (u(t) - xa) - k \cdot a / 2) +$$
$$+ 0.5 \cdot (1 - sign\,(\dot{u}(t))) \cdot \tanh'(k \cdot (u(t) - xa) + k \cdot a / 2)$$

$$\tanh(x) = \frac{e^x - e^{-x}}{e^x + e^{-x}}$$

$$\tanh'(x) = \frac{4}{(e^x + e^{-x})^2}$$

a,k,xa – parameters of hysteresis.
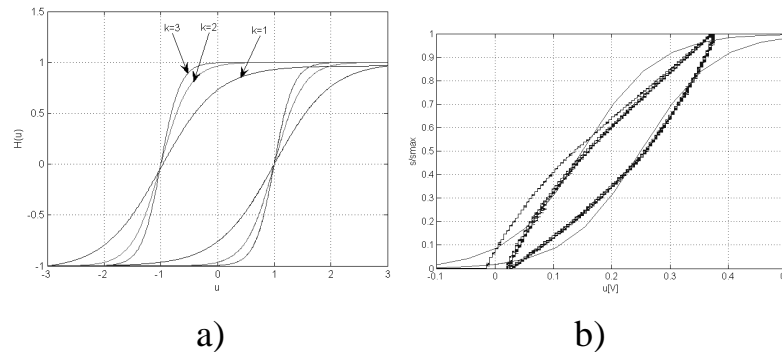
Fig. 2. Hysteresis for different parameters (a), experimental verification (b)

Verification of hysteresis model was done using experimental data. Parameters of the model calculate by use least-squares method. Calculated characteristics of hysteresis is shown on figure above.

Summary

The stand is intended for testing of piezoelectric actuators and sensors operating with small displacements. Piezoelectric sensors generate very small displacements as a rule; hence, mechanical amplifiers are often incorporated.

The impacts of the presence of an amplifier on static and dynamic parameters of the actuating element can be investigated, too.

The application of a PC to the system control enables the testing of positioning algorithms as well as vibration reduction and generation algorithms. These tests can be automatic and semi-automatic to support extended experimental programmes.

Some imperfections of the stand, which was found during first tests such as too small resolution, not good enough power supplier and others less important, will improve.

Mathematical model proposed in this paper is useful for designing control systems. This model quite good approximate features of the piezoelectric actuator and SMA actuator [6] as well.

Acknowledgement

References:

1. Janocha H., Kuhnem K. 2000. Real-time compensation of hysteresis and creep in piezoelectric actuators. Sensors and Actuators A: Physical Vol. 79, Issue: 2, February 1, 2000, pp. (83-89) ISSN: 0924-4247

2. Schafer J., Janocha H. 1995. Compensation of hysteresis in solid state actuators. Sensors and Actuators A: Physical Vol. 49, Issue: 1-2 June, pp. (97–102) ISSN: 0924-4247.

3. Konieczny J., Rączka W., Sibielak M.: Experimental investigation of the semi-active vibration isolation system // proceedings of 9th Conference on Active noise and vibration control methods Krakow–Zakopane, Poland, May 24–27, 2009

4. Sibielak M.: Identification of hysteresis operator for a controllable damper with piezoelectric actuator, proceedings 7th Conference on Active noise and vibration control methods : Wigry, Poland, (2005).

5. Sibielak M.: Model of hysteresis of piezoelectric actuator proceedings of 9th International Carpathian Control Conference Romania, May 25–28, (2008) pp. 611–614

6. Rączka W., Konieczny J., Sibielak M.: Mathematical Model of a Shape Memory Alloy Spring Intended for Vibration Reduction Systems // Solid State Phenomena Vol. 177 (2011) pp 65-75

7. Rączka W., Sibielak M., Konieczny J.: Smart vibration isolation systems with shape memory alloy proceedings of 7th International Carpathian Control Conference Czech Republic (2006)

2.5 FUZZY MODEL OF SMA ACTUATOR

Konieczny J.[1], Rączka W.[1], Sibielak M.[1]

Introduction

The paper consider laboratory tests of SMA wire used as a linear actuator and its fuzzy logic model. This actuator wires contract much like little muscles a distance of approximately 4-5% when they are heated and relax when they are cooled. The list of applications of SMA wires is very long, examples of them are in [1,2,]. We can say that we could use it in all applications where is required physical movement in a small space with low to moderate cycling speeds. SMA wires as actuators are much smaller for the work they do from classical solutions which employ motors or solenoids. But such actuators have disadvantages like e.g. strong nonlinearity and histeresis. These are main problems in designing linear actuator [4,5,6,7,8]. Therefore SMA wires are used very often as two-state actuators which work like „ON-OFF" actuators. Problems with SMA wires as actuators are: static and dynamic properties [3], sensitivity on environmental condition, repeatability, nonlinearity and hysteresis.

1. Testing SMA wires

Tested wire is made of Nickel and Titanium. It is an alloy specially made to be used as an actuator. The high repeatability of such applications requires a very repeatable material.

Tested SMA wires are made of NiTi alloy which features are:

- M_f=57 °C, M_s=67 °C, A_s=72 °C, A_f=90 °C

- Diameters of tested specimen - 0,0254mm $\div$0,508 mm

- Maximum pull force – 930g

- Approximate current at room temperature - 1000 mA

- Average contraction time – 1 s

- Off time 90°C wire 3,5 s

- Density   - 6,45 g/cm^3

- Specific heat - 6-8 cal/(mol ºC)

- Melting point - 1250 ºC

- Thermal expansion coefficient martensite - 6,6 x 10-6/ ºC

[1] AGH University of Science and Technology, Krakow, Poland

- Thermal expansion coefficient austenite - 11,0 x 10-6/ ℃

- Electrical resistivity martensite - 421 ohms/Cir Mil Ft

- Electrical resistivity austenite - 511 ohms/Cir Mil Ft

- Flexinol® is a trade name for shape memory alloy actuator wires,

- One-way shape memory effect,

- Approx. contraction 3% (normal bias spring)

- Approx. contraction 4% (dead weight bias)

- Motion repetition even 10 millions cycles, but in higher stresses it decreases to few thousands of cycles or less.

Laboratory tests of SMA wire was made with laboratory test stand. Position , load/force, wire temperature, environment temperature, current flow in wire and applied voltage to the wire was measured. Amplitude of excitation was change from 0% to 100% with steps 10%. Three different mass loads was used. It was 112g, 515g, 890g it is 12%, 55%, 95% of theoretical max load

Static tests was made using triangle signal excitation which was raised very slowly and linearly from 0 up to Umax and next falling down similarly from Umax to 0. Tests was done for wires 0,15mm, 0,20mm, 0,25mm and 0,30mm.

Selected characteristics are shown in Fig. 1a and 1b.

a)   b)
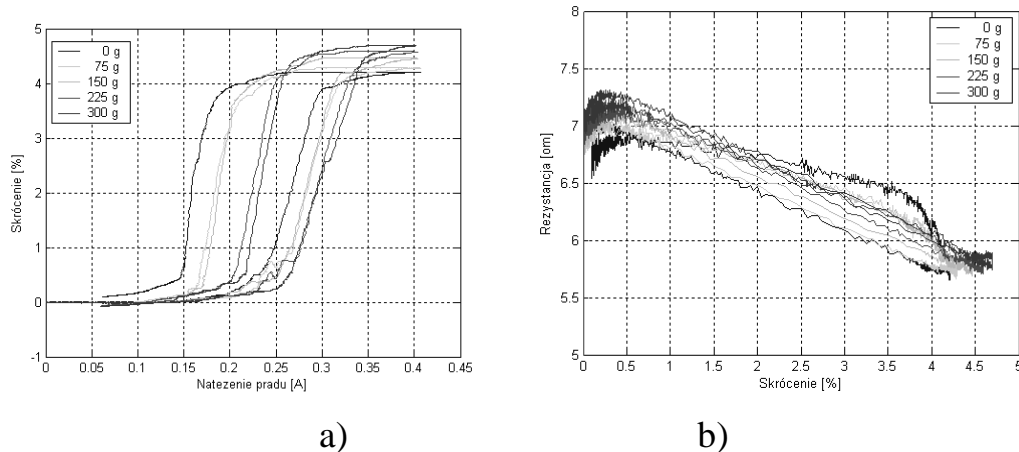
Fig. 1. Static characteristic: strain vs. current (a) resistance vs. strain (b) for fiber 0,15mm

These test show that it is real problem with controlling of strain of SMA wires in positioning systems because of nonlinearity of SMA wires. Therefore in

control systems we must use transducers to measure position and temperature of wire as second feedback loop for controlling temperature of the wire. It complicates the control system and we can say that all advantages of SMA (they are small, simple etc.) are shatter by needs of using of theses transducers when we want to use it as a good linear actuator.

In Figure 1b we can observe interesting dependence of resistance vs. strain. It suggests that it is possible to measure strain of a wire by measuring its resistance. Authors of the paper [2] tested SMA wires as a strain or stress sensors. Their conclusion is, that it is possible to use SMA as a strain sensor although it is difficult. Having in mind disadvantages with all that transducers in control system, we built fuzzy logic model of SMA. By using it we can estimate strain of wire. Strain of the wire is estimated on measuring resistance of the wire.

2. Fuzzy model

The model of SMA is made as a fuzzy model which is a mathematical model useful in designing control systems.

Fig. 2. Block schema of an idea of fuzzy model

Features of fuzzy model
- Fuzzy model - Takagi-Sugeno-Kang,
- Membership function - generalized bell curve,
- And method - product
- Or method - maximum
- Defuzzification method - weighted average
- Rules – 2 or 5 or 10 or 15

Figures 3 to 5 show responses of real wire and its fuzzy model for respectively 2, 5, 10 and 15 rules.

a)   b)
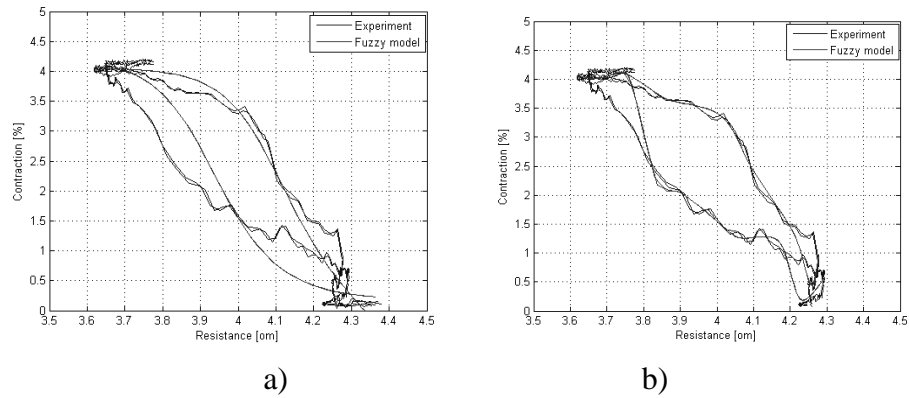
Fig. 3. Static characteristic: contraction % vs. resistance of wire for lab. test (blue), fuzzy model (red). Mass Load 515g. Current excitation amplitude 0,8 [A]. 2 rules (a), 5 rules (b).
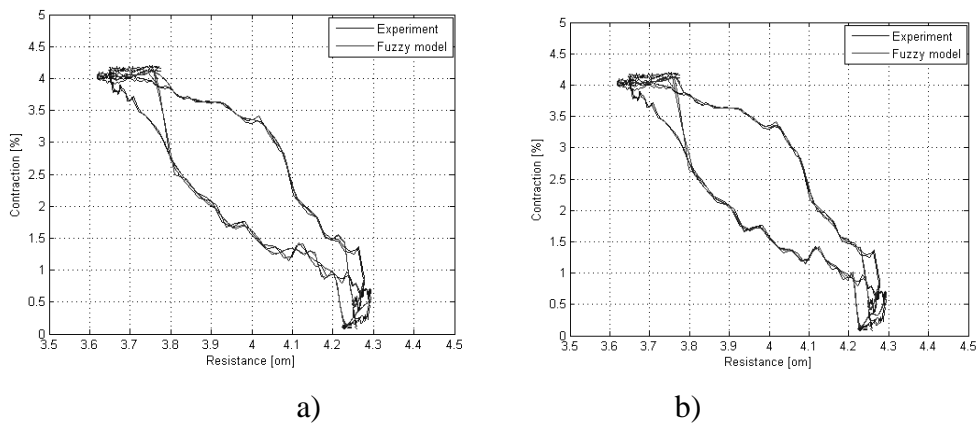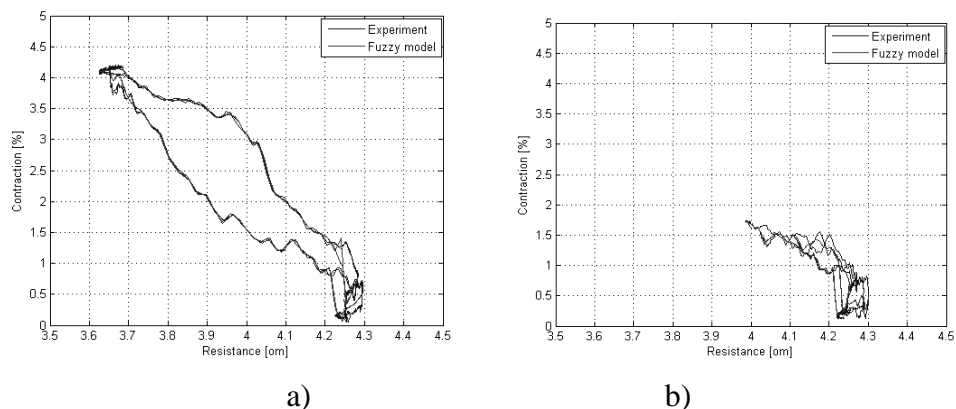

a)   b)

Fig. 4. Static characteristic: contraction % vs. resistance of wire for lab. test (blue), fuzzy model (red). Mass Load 515g. Current excitation amplitude 0,8 [A]. 10 rules (a), 15 rules (b).

a)   b)

Fig. 5. Static characteristic: contraction % vs. resistance of wire for lab. test (blue), fuzzy model (red). Mass Load 515g. 15 rules. Current excitation amplitude 0,64 [A] (a); 0,4 [A] (b).

Summary

Mathematical model proposed in this paper is useful for designing control systems for controlling contraction of an SMA wire. LVDs and others such position transducers are too expensive compare to cost of SMA actuator. Therefore they will not useful for positioning system with SMA. Measuring temperature and using mathematical model to calculate contraction of an actuator is better but still not precise. Measuring resistance and using mathematical model to calculate contraction of an actuator will be the best solution if presision will be better.

References:

1. Bojarski Z., Morawiec H. 1989. Metale z pamięcią kształtu. Warszawa, PWN 1989.

2. Wayman C. M., Otsuka K. 2002. Shape Memory Materials, Cambridge University Press, UK.

3. Konieczny J., Rączka W., Sibielak M.: Experimental investigation of the semi-active vibration isolation system // proceedings of 9th Conference on Active noise and vibration control methods Krakow–Zakopane, Poland, May 24–27, 2009

4. Sibielak M.: Identification of hysteresis operator for a controllable damper with piezoelectric actuator // proceedings 7th Conference on Active noise and vibration control methods : Wigry, Poland, (2005).

5. Sibielak M.: Model of hysteresis of piezoelectric actuator // proceedings of 9th International Carpathian Control Conference Romania, May 25–28, (2008) pp. 611–614

6. Rączka W., Konieczny J., Sibielak M.: Mathematical Model of a Shape Memory Alloy Spring Intended for Vibration Reduction Systems // Solid State Phenomena Vol. 177 (2011) pp 65-75

7. Rączka W., Sibielak M., Konieczny J.: Smart vibration isolation systems with shape memory alloy // proceedings of 7th International Carpathian Control Conference Czech Republic (2006)

8. Rączka W. 2003. Controlled SMA Spring in Frahm's Vibration Absorber. // Mechanika, t.22, z.3, 2003, pp. 389-394.

2.6 COMPUTER MODELING OF WHEEL STEEL INGOTS FORMATION

Bilousov V.[1], Bondarenko V.[1]

Nowadays the overwhelming majority of developments is carried out by means of mathematical modeling technique.

In this respect computer technologies that have made a giant leap are of great help to enterprises. End-to-end designing, robotized lines, machine tools with NPC, systems of volumetric modeling and many other things allow operators to create scientifically proved master schedules which consider manufacturing conditions most efficiently and are directed at cost saving and productivity increase of the equipment.

Recent years have seen the development of new progressive master schedules of smelting, shaping into ingots and refrigeration of wheel steel of various brands. In particular, there has been introduced in mass production a technology of casting wheel ingots into round steel molds, manufacturing six and eight blank ingots, cast into round pig-iron and steel molds.

So far, however, the following problems have not been cleared up: the choice of optimal parameters of casting steel into round molds and durations of their refrigeration in casting molds with the reduction of number of rejects, caused by shrinking defects and cracks, as well as the casting cycle duration decrease, refrigeration of wheel steel ingots, both in pig-iron and steel molds. The solution of these problems will allow to save, on the one hand, power resources for steelmaking, and, on the other hand, increase equipment productivity.

Now the general rules of the effects of temperature and time of pouring steel into pig-iron and steel molds, duration of refrigeration of an ingot in a steel mold on ingot quality are known. These processes are closely interrelated, and establishing their optimal parameters is a complicated scientific and technical problem.

Identifying the effect of temperature and time of shaping steel into round ingots, ingot solidifications in both, pig-iron and steel molds, as well as the

---

[1] Donetsk National University, Ukraine

choice of optimal parameters of casts manufacturing is a long, expensive and labour-comsuming process. Taking into account the fact that settling some manufacturing matters by purely experimental methods is money-losing and (inefficient), now the overwhelming developments and solutions even of the most complicated questions in all areas of engineering are carried out by means of computer technologies and mathematical modeling of master schedules.

The purpose of this paper is to use the method of mathematical modeling for solving some problems of manufacturing high-quality ingots of wheel steel of some brands.

For this purpose, the mathematical model of crystallizing eight blank ingots of wheel steel of KP-2 brand, as well as of KP-T, R-7, R-8 brands was developed. The numerical experiment was carried out to find out the effect of temperature of metal and duration of steel casting (casting rate) on the formation of shrinking defects, to estimate the propensity of steel to fire cracking, warming of the piped end of 8 eight blank ingots, cast into pig-iron and steel molds. The optimal parameters of the casting technology and refrigeration of round ingots of wheel steel in a steel mold were formulated.

The pattern of calculating an open and closed shrink hole was chosen on the basis of assayed hydrodynamic, thermal and kinetic processes of steel ingot formation. The pattern was grounded on A.A.Bochvar and J.A.Nekhendzy's [1] assumptions, that linear shrinkage does not start from the solidus temperature, but a little bit earlier, during the period, when a solid enough skeleton of semi-solidified dendrites is formed, i.e. from the effective crystallization interval line, above the solidus temperature. It used to be considered, that shrinkage begins at 75 % of a solid phase, however the latest explorations show, that this figure can vary within a wide range, depending on steel composition. It has forced to put into the basis of solidification kinetics the theory of quasi-equilibrium biphase zone, offered by Borisov [2] and written down as follows:

$$\xi = 1 - \left(1 + \frac{c_{\text{ж}}}{L}(T_l - T_s)\right)\left[1 - \left(\frac{T_l - T}{T_l - T_s}\right)^{2/3}\right] + \frac{c_{\text{ж}}}{L}(T_l - T_s). \tag{1}$$

where T - current temperature, ^{0}C;

c - thermal capacity, Joule/K;

ξ - fraction of the solid phase;

L - latent heat of crystallization, Joule;

Tl, Ts - liquidus and solidus temperatures , K.

The index ж corresponds to the liquid metal phase

The processes running in the melt and in the walls of a steel mold, are described by the system of equations in cylindrical coordinates and the edge conditions consisting of [3]:

Navier-Stokes equation:

$$\frac{\partial \vec{V}}{\partial t} + \left(\vec{V}\nabla\vec{V}\right) = -\frac{1}{\rho}\nabla P + \nabla\nu\nabla\vec{V} + \vec{g}\beta T \; ; \qquad (2)$$

The equation of heat transfer:

$$c\rho\left[\frac{\partial T}{\partial t} + \left(\vec{V}\nabla T\right)\right] = \nabla\lambda\nabla T \; ; \qquad (3)$$

The equation of indissolubility:

$$\frac{\partial\left(rV_r\right)}{\partial r} + \frac{\partial\left(rV_z\right)}{\partial z} = 0 \; ; \qquad (4)$$

where: $\vec{V}$ - vector of speed, km/s;

t - dimensional time, s;

ρ- density, kg/m^3;

P - pressure, н/м2;

ν - kinematic factor of viscosity, m^2/s;

$\vec{g}$ - free fall acceleration, m/s^2;

β - factor of volumetric expansion 1/К;

r, z - current coordinates, m;

c - factor of thermal capacity with constant pressure, Joule /kg K;

λ - factor of heat conductivity Watt/mК.

In view of these assumptions edge conditions are formed as follows:

Entry conditions

$$t = 0: \qquad V_r = V_z = 0; \quad T\Big|_{\substack{0 \le r \le l_r \\ 0 \le z \le l_z}} = T; \quad T\Big|_{\substack{l_r \le r \le l_r' \\ l_z \le z \le l_z'}} = T_{изл}, \qquad (5)$$

where: V_r иV$_z$ - horizontal and vertical components of speed;

l_r and l_z - left and bottom ingot borders;

l'_r And l'_z - left and bottom steel mold borders.

Boundary conditions for speed and temperature at the steels casting period are written down as follows:

$$r = 0: \qquad V_r=0 \qquad \frac{\partial V_z}{\partial r}=0 \qquad\qquad \frac{\partial T}{\partial r}=0 \qquad\qquad (6)$$

$$z= H: \qquad V_r=0 \qquad V_z=0 \qquad\qquad \frac{\partial T}{\partial r}=0 \qquad\qquad (7)$$

$$r = L_r: \qquad V_r=0 \qquad V_z=0 \qquad \lambda_{\textit{ж}}\frac{\partial T}{\partial r}_{\textit{ж}}=\lambda_{\textit{ш}}\frac{\partial T}{\partial r}\Big|_{\textit{из}} ; \quad T_{\textit{ж}}=T_{\textit{из}} \qquad (8)$$

$$z = L_z: \quad V_r=0 \quad V_z = \begin{cases} V_m, & 0 \le r < R \\ 0, & R \le r \le L_z \end{cases} \quad T = \begin{cases} T_0, & 0 \le r < R \\ \lambda_{\textit{ж}}\dfrac{\partial T}{\partial r}_{\textit{ж}} = \lambda_{\textit{из}}\dfrac{\partial T}{\partial r}\Big|_{\textit{из}} ; T_{\textit{ж}}=T_{\textit{из}}, R \le r \le L_z \end{cases} \qquad (9)$$

Indexes *m, ж, из* correspond to the parameters referred to the solid and liquid metal phases and to the steel mold.

On its border the steel mold there is environment, so the following boundary conditions are true for both, the casting period and the solidification period, :

on the external wall of the steel mold:

$$\lambda_{\textit{из}}\frac{\partial T}{\partial r}\Big|_{\textit{из}} = -\alpha_{\textit{в}}(T - T_{\textit{ср}}); \qquad\qquad (10)$$

on the plate stand

$$\frac{\partial T}{\partial z}\Big|_{\textit{из}} = 0. \qquad\qquad (11)$$

$\alpha_{\textit{в}}$ - factor of heat interchange with the ambient.

R- nozzleradius, m;

$\lambda_{\textit{ж}}$ and $\lambda_{\textit{из}}$ -heat conductivity of a solution phase and a steel mold, Wt/m K;

$T_{\textit{ср}}$ - ambient temperature.

During the solidification the boundary conditions (6) - (9) do not change, and the boundary conditions (9) will be transformed to the following kind:

$$z = L_z: \quad V_r=0 \qquad V_z = 0 \qquad T = \lambda_{\textit{ж}}\frac{\partial T}{\partial r}\Big|_{\textit{ж}} = \lambda_{\textit{из}}\frac{\partial T}{\partial r}\Big|_{\textit{из}} ; T_{\textit{ж}}=T_{\textit{из}} \qquad (12)$$

On the basis of the formulated mathematical pattern of forming eight blank ingots of wheel brands of steel, a bunch of applied programs for calculating hydrodynamic and heart transfer processes in the system of 'an ingot – a steel mold – environment' was developed. The mathematical model is grounded on the finite-difference approximation of nonlinear equations in particular derivatives of energy pulse transfer, indissolubility and conditions of unambiguity [4]. The bunch was developed in integrated DELPHI 2006 environment.

The calculation was executed by means of the applied program, developed with the help of the software designing method for modeling the transfer processes of metallurgical product manufacture, proposed by the authors.

The fig.1 represents the scheme of program modules interaction.
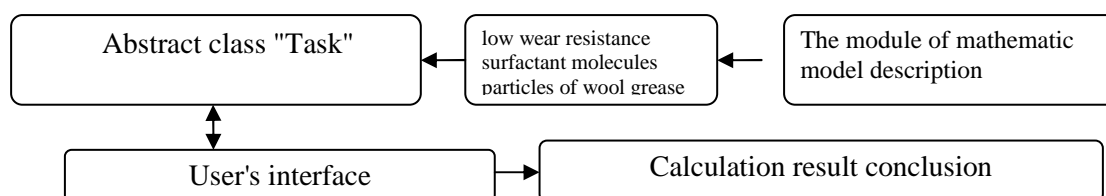
Fig. 1.

The abstract class "Task" includes properties in the form of the variable functional types, describing blanket parameters of transfer and solidification problems (such as a file of temperatures, speeds), solid phase fractions, etc.) and the methods for blanket stages of calculation. Here the properties of a class represent "empty" functions which are filled in and used in the subsequent process of calculation.

Fig. 2.

151
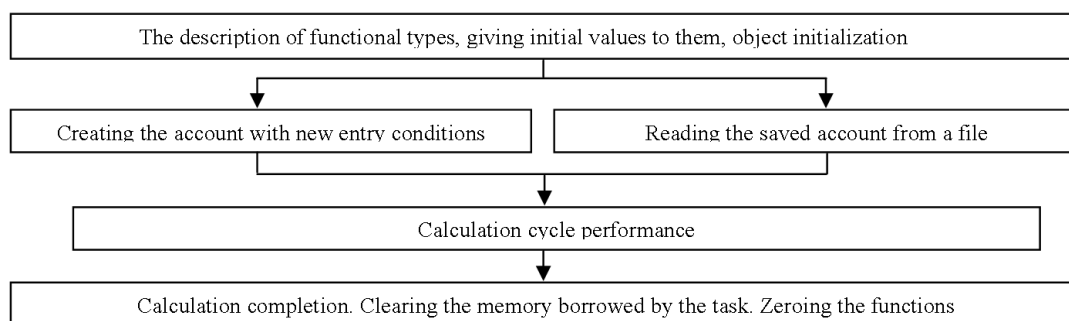
The sample of an abstract class "Task" represents a stream to OS Windows which is carried out within the basic applied calculation program (fig.2):

The program module of interface contains functions which will convert variables and files from the module of the mathematical pattern into variables of functional types of the common task module. This process is illustrated on fig.3 on the example of the individual value

Calculation and interface part are carried out in various streams of OS Windows that allows to use effectively modern multinuclear and multiprocessing computer systems.

The interface module serves for user's running of the program, data inputting and outputting.

Assaying theoretical and experimental research works of ingot formation, hydrodynamics, heat transfer; explorations of the pipe depth, change of the liquid phase in axial section of the ingot, temperatures of surface eight blank ingot and steel mold, carried out in the conditions the working manufacture of JSC «Interpipe-NTZ», as well as the numerical experiment, have shown the adequacy of the mathematical pattern, computing algorithm and satisfactory coordination of the received results. A calculating error of modeling within the limits of 6 to 22 %.
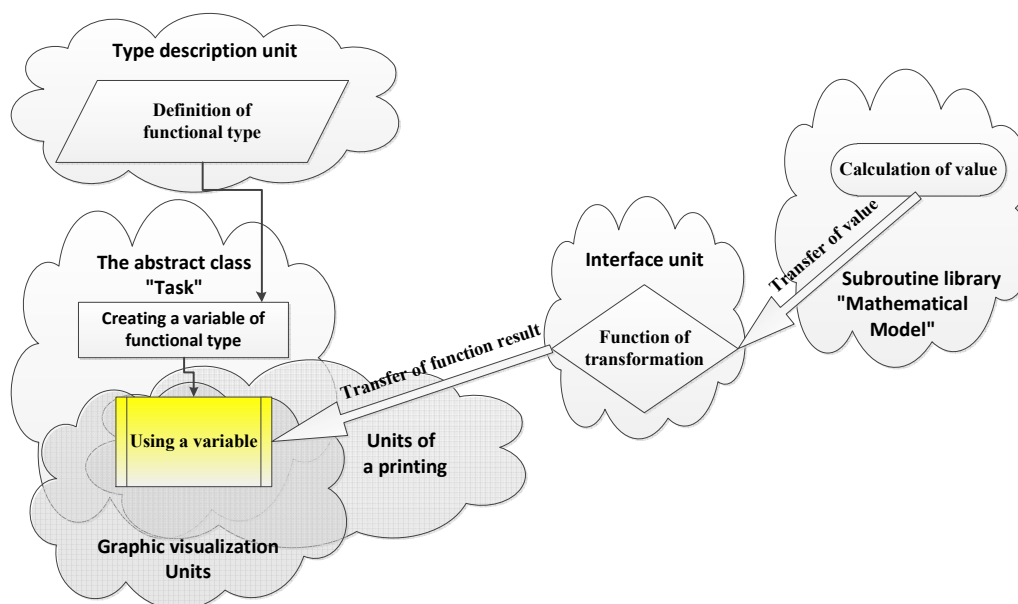
Fig. 3.

The current lines and the direction of vertical component of the speed vector at various moments of casting and ingot solidification are shown.

The results of numerical experiment have shown that with the speech increase of casting the wheel steel of KP-2, KP-T, R 7, R 8 brands into pig-iron and steel eight blank steel mold the pipe increases. The same tendency is observed with the increase in cast metal overheating.

It was found out that the height of the insulating liner within the limits of 200 to 250 mm does not make considerable effect upon the depth of the pipe with the ingot solidification both in pig-iron and steel molds.

The open pipe is formed within 90 minutes. During this period the crystalline corset of the ingot is formed. The active hydrodynamic phase lasts not less than 50 minutes. The filtration processes last about 1.5 hours. During this period the ingot is actually formed.

The distribution of temperature by section and height of wheel eight blank ingot, cast in pig-iron and steel molds was stated and demonstrated. In a steel mold the ingot solidifies more quickly, than in pig-iron.

The values of temperature, gradient of temperature on height and section of the ingots after their refrigeration within 3.5 and 4 hours differ approximately for 10 - 50 ^{0}C and for 20 - 40 ^{0}C accordingly.

The steel overheating reduction by 5 ^{0}C within the interval from 79 to 69 ^{0}C leads to the 5 ^{0}C temperature reduction of the surface of the ingot in the middle of its height, cast in the cast-iron mold and by 10 ^{0}C in steel mold. The ingot surface temperature, cast in a steel mold is 15 - 25 ^{0}C less than that, cast in pig-iron. The steel overheating temperature before casting hardly influences the change of the gradient of temperature of the ingot surface .

Modeling of formation of the ingot and experimental researches establish a casting time in eight blank pig-iron and steel molds of the ingot of the wheel steel during 14 - 16 min and duration of their refrigeration up to strip within 3 hours of 30 minutes.

References

1.   Нехендзи Ю.А. Стальное литье. -М., Металлургиздат, 1948. –787с.

2.   Борисов Г.П. Давление в управлении литейными процессами. -К., Наукова думка, 1988.-272 с.

3.   Повх И.Л., Белоусов В.В., Недопекин Ф.В. Тепломассоперенос в затвердевающем бинарном расплаве в условиях смешанной конвекции с учетом турбулентности. Инженерно-физический журнал, 1994,т.67,№3-4,с.203-208

4.   Затвердевание металлических композиций: производство и моделирование// Недопекин Ф.В., Белоусов В.В., Кондратенко В.М. и др. Донецк ООО «Юго-восток», ЛТД, 2005.- 231с.

2.7 MODELLING OF SELECTED PHENOMENA WHICH OCCUR IN OFFSET PRINTING PRESSES

Jurkiewicz A.[1], Piętak Z.[1], Krzyżkowski J.[1], Pyryev Y.[1]

Introduction

Offset printing is a indirect lithographic printing technique. It means that printing elements of the printing plate lie almost on the same height as non-printing ones. Difference between those two types of elements is in their physical and chemical properties, especially in their ink affinity [1].

The most important unit of every printing press is the printing unit, which consists of inking system, dampening system and three printing cylinders (plate, blanket and impression cylinder). Generally, printing unit, especially of the
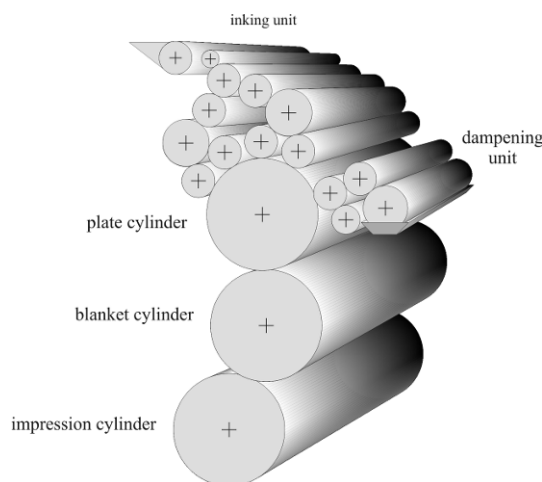
Fig. 1. Scheme of the printing unit

offset printing press, is mainly made up of rollers and cylinders of different size, materials and construction (Fig. 1). All the features of those cylinders and rollers

[1] Politechnika Warszawska, Warsaw, Poland

as well their adequate adjustment have great influence on proper work of printing machine and quality of the printouts.

Printing process in offset technique goes in the following way: Dampening unit moistens printing plate with dampening solution. After that, inking unit covers plate with the ink, which is affiliated only by the printing elements.

Inked picture is transferred from the plate to the offset blanket (spread on the blanket cylinder) and than to the printing substrate, for instance, paper.

Our research team deals with problems and phenomena, which take place in printing presses. We especially take up contact problems between rollers and cylinders, vibrations of printing units and thermodynamical phenomena of inking systems.

Unfortunately in a Polish and a worldwide References is missing the science information on these subjects. It sometimes happens, that there appear equations, which nobody knows, where they are from and who developed those equations. For this reason, they can not be used in further studies, because we do not know if they are reliable.

On the other hand, in science References, there are a lot of issues described and studied. They are not directly related to printing technology, but their results may be used during analysis of phenomena in printing machines, e.g.: such contact issues as Hertz issues, vibrations of two degree-of-freedom systems, heat transfer in layered systems and the others.

1. Problem regarding contact between rollers and cylinder in the printing unit

Setting an adequate contact stress between cylinders and rollers in the offset printing machine is of great importance. It has impact on quality of printouts, wear of exploiting materials, wear of various parts of the printing press and time of preparing it to operate.

The stress between ink rollers is a set involving the measurement of the contact area width. The width is measured on the ink stripe transferred to the paper. Next, a distance between the rollers is reduced using a trial and error method, up to having the ink stripe width corresponding with that stipulated in the technical instruction. A clamp between the cylinders in the printing unit is

calculated as well. As regards cylinders which bearer rings (also called cylinder bearers, which are made of hardened metal fixed at the ends of the cylinders) contact each other during the printing, the clamp is calculated by adding a height of the plate over the plate cylinder's bearer rings and a height of the blanket over the blanket cylinders' bearer rings. As regards cylinders whose bearer rings do not contact each other during the printing, the obtained result is diminished by a distance between the plate cylinder's bearer rings and the blanket cylinder's bearer rings [2].

It is important to make the contact area width dependent on reduction of the distance between axes of the rollers, and not dependent on stress, because in fact this is displacement (not the stress) which is applied to the axes of the rollers. Therefore, the equation of theory of elasticity for displacements (Lame) [3], assuming the Hertz's conditions, as well as homogeneous and isotropic nature of bodies, was used. Additionally, the Fourier transform [4] was involved. Another parallel assumptions were made according to which if the cylinder radii and roller radii are much bigger than the contact area width, each of the bodies may be regarded as an elastic half-space in accordance with Hertz theory.

The equation for reduction of the distance between axes of the two rollers, where such reduction depends on the contact area width, the rollers' radii, Poisson's ratios and Young modulus of the rollers, with simultaneous involvement of Hertz assumptions, shall be as follows [5]:

$$d = \frac{a^2 E_*}{4R} \sum_{l=1}^{2} \eta_l \ln\left(e^{m_l} \frac{4R_l^2}{a^2} \right)$$ (1.1)

where: $a-$ half of the contact area width, R_l for $l = 1, 2$ – radius accordingly of lower roller and upper roller, v_l for $l = 1, 2$ – Poisson's ratio accordingly of lower and the upper roller, E_l for $l = 1, 2$ – Young's modulus accordingly of lower and the upper rollers and:

$$m_l = -\frac{v_l}{1-v_l} + \frac{1}{1-v_l} \frac{a^2}{4R_l^2} , \quad \eta_l = \frac{1-v_l^2}{E_l} , \quad l = 1, 2 , \quad \frac{1}{E_*} = \eta_1 + \eta_2 , \quad \frac{1}{R} = \frac{1}{R_1} + \frac{1}{R_2} .$$
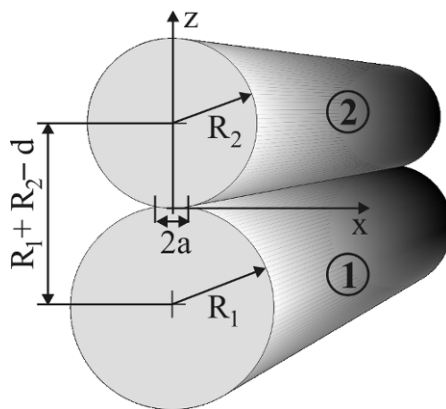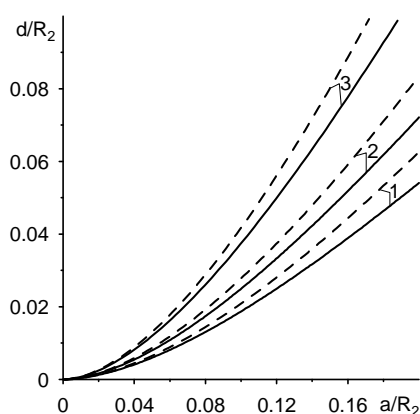
Fig. 2 Scheme of two rollers contact

Fig. 3. Correlation between dimensionless reduction in of the distance between axes of the rollers d/R_2 **and dimensionless contact area width** a/R_2 **for different values** R_2/R_1 **and for different Poisson's ratios** v_2; **curves 1 –** R_2/R_1=0.5; **2 –** R_2/R_1=1; **3 –** R_2/R_1=2; **continuous curves** v_2=0.5, **dashed curves** v_2=0.3

In the ink unit of the offset machine there is a contact between the rigid surface and the elastic surface, the latter one is usually made of rubber. This is likewise in the printing unit, because there is a contact between the metal printing plate or the steel impression cylinder and the elastic blanket. In case of the blanket this is of great importance, because contact is provided not only by a rubber top layer but also by a compression inner layer as well. The structure of the compression layer is similar to that of a sponge or a foam. Young modulus for steel is much bigger than Young modulus for materials such as rubber – blanket top layer or blanket inner layer – compression layer. According to that assumptions, the top body 1 is to be regarded as an elastic body, and the bottom body – i.e. body 2 – as the rigid one. Therefore, while plotting the graph of dimensionless reduction of the distance between axes of the rollers and

dimensionless contact area (Fig. 3), based on equation (1.1), Young modulus $E_1 = \infty$ [6, 7] was used.

2. Vibrations analysis of printing unit cylinders of offset printing press

One of the most important sources of vibrations in printing units of offset presses are gaps (canals) in the plate and blanket cylinders (Fig. 4) [8, 9, 10].

Inside those gaps, locks for fixing plate and blanket are mounted. While rolling the gaps each other comes to sudden fall of stiffness of the system. It excites vertical vibrations of the cylinders. Another reason of vibrations of this type is cylinders' unbalance [8].
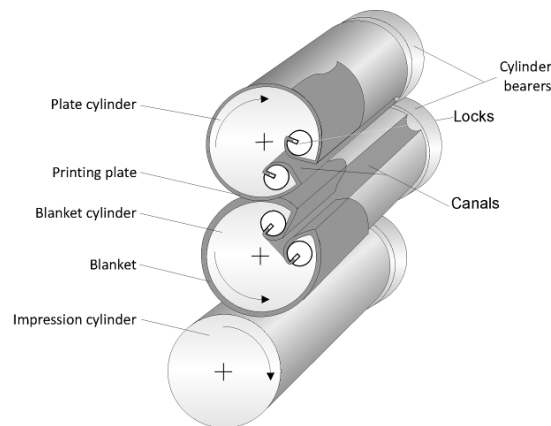
Fig. 4. Cross section of plate and blanket cylinders
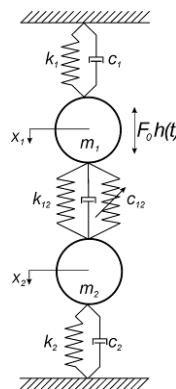
Fig. 5. Model of offset printing unit

Vertical vibrations of the cylinders, caused by mentioned above reasons, may be modeled by the two degree-of-freedom model presented in Fig. 5.

It should be emphasized, that in this model only two masses, which represent plate and blanket cylinders, are taken under consideration. We

resigned of the third one – impression cylinder. This attitude comes from construction of the printing unit, where between plate and blanket cylinders only takes place an initial tension. The impression cylinder is separated from them.

Model presented in the Fig. 5 is described by the following system of equations:

$$
\begin{cases}
m_1\ddot{x}_1 + (c_1 + c_{12} + c(t))\dot{x}_1 + (k_1 + k_{12} + k(t))x_1 - (c_{12} + c(t))\dot{x}_2 - (k_{12} + k(t))x_2 = F_0 h(t) \\
m_2\ddot{x}_2 + (c_2 + c_{12} + c(t))\dot{x}_2 + (k_2 + k_{12} + k(t))x_2 - (c_{12} + c(t))\dot{x}_1 - (k_{12} + k(t))x_1 = 0
\end{cases}, \quad (2.1)
$$

where: m_1, m_2 – masses of the plate and blanket cylinder, respectively; c_{12}, c_1, c_2,– viscous damping coefficients of cylinder bearers and the press frame, respectively; k_{12}, k_1, k_2,– stiffness coefficients of cylinder bearers and the press frame, respectively; $k(t)$ – non-dimensional force which represents in time changing stiffness of the blanket; $c(t)$ – non-dimensional force which represents changing in time viscosity of the blanket, $h(t)$ – non-dimensional vibrations exciting force, F_0 – maximal value of vibrations exciting force, which occurs because of unbalance of the cylinders.

First of all, variations of ink film thickness caused by vibrations of unbalanced plate cylinder were analyzed. In this case we considered situation where $k(t)=0$, $c(t)=0$.

Solving system (2.1) we calculated amplitude of cylinders' displacement [11]:

$$
\max[x_1(t) - x_2(t)] = \max Z(t) = a = \frac{F_0}{m_1 \omega_{01}^2} \sqrt{\frac{4\eta_2^2 \gamma^2 + (\gamma^2 - \lambda^2)^2}{A^2(\gamma) + 4\gamma^2 B^2(\gamma)}}, \quad (2.2)
$$

where:

$$
A(\gamma) = (\gamma^2 - 1)(\gamma^2 - \delta^2 - \lambda^2) - \delta^2 \beta(\gamma^2 - \lambda^2) - 4\gamma^2(\eta_2\mu_2\beta + \eta_1\eta_2 + \eta_1\mu_2),
$$

$$
B(\gamma) = \mu_2 + (\eta_1 + \mu_2\beta)\lambda^2 + \eta_2(1 + \delta^2\beta) + \eta_1\delta - (\eta_1 + \eta_2 + \mu_2\beta + \mu_2)\gamma^2,
$$

$$
\delta = \omega_{20}/\omega_{01}, \quad \gamma = \omega/\omega_{01}, \quad \beta = m_2/m_1, \quad \lambda = \omega_{02}/\omega_{01},
$$

$$
\mu_2 = h_{20}/\omega_{01}, \quad \mu_1 = \mu_2\beta, \quad \eta_1 = h_{01}/\omega_{01}, \quad \eta_2 = h_{02}/\omega_{01}
$$

$$
\omega_{01}^2 = k_1/m_1, \quad \omega_{02}^2 = k_2/m_2, \quad \omega_{10}^2 = k_{12}/m_1, \quad \omega_{20}^2 = k_{12}/m_2,
$$

$$
2h_{01} = c_1/m_1, \quad 2h_{02} = c_2/m_2, \quad 2h_{10} = c_{12}/m_1, \quad 2h_{20} = c_{12}/m_2
$$

We made an assumption, that displacement of the cylinders is equal to the fluctuations of the ink film thickness transferred to the paper. For exciting forces $h(t)=\sin(\omega t)$ and $h(t)=\cos(\omega t)$ we yield curves presented in the Fig. 6 [11].

For our calculations we used following parameters: $m_1=190$ kg, $m_2=210$ kg, $k_1=k_2=200{\cdot}10^6 \text{Nm}^{-1}$, $k_{12}=7,5{\cdot}10^4 \text{ Nm}^{-1}$, $c_1=c_2=1,9{\cdot}10^4 \text{ Ns}^2\text{m}^{-1}$, $c_{12}=7,5{\cdot}10^4 \text{ Ns}^2\text{m}^{-1}$, $F_0=129,5$ kg m s^{-2}, $\omega=78,5$ s^{-1}.

We considered also fluctuations of the ink film thickness for another type of exciter. In this case $F_0=0$.

As it was mentioned above, when cylinders gaps roll over each other, sudden shift of the system stiffness occurs. Force excited in this way can be modeled as a change of stiffness and viscosity of the offset blanket. It may be described by the equation:

$$F(t) = k(t)(x_1 - x_2) + c(t)(\dot{x}_1 - \dot{x}_2), \; k(t) = kf(t), \; c(t) = cf(t). \tag{2.3}$$

Periodical function $f(t)$ is shown in Fig 7.
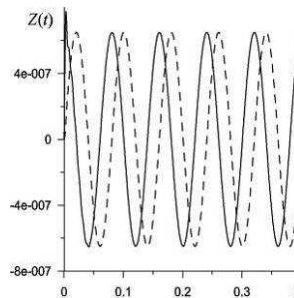
Fig. 6. Fluctuations of the ink film thickness caused by cylinder vibrations for $h(t)=\sin(\omega t)$ **(dashed line) and** $h(t)=\cos(\omega t)$ **(solid line) exciting forces**
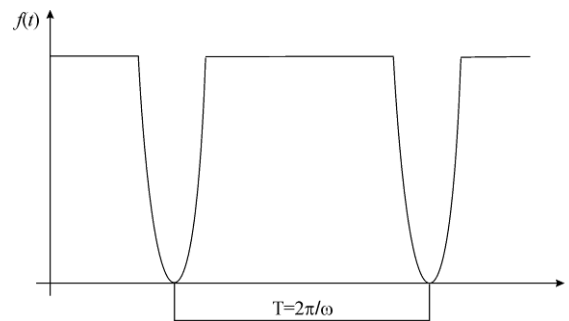
Fig. 7. Force modelling periodical change of stiffness and viscosity of the offset blanket

System of equations (2.1) was solved numerically for two cases. The first one doesn't take under consideration cylinder bearers ($k_{12}=0$) and the second one does ($k_{12}>0$).

We looked for parameters of the press work, which may cause parametric vibrations, i.e. when condition (2.4) will be accomplished:

$$\omega = \frac{2\Omega_i}{n}, \; n=1, 2, 3,\dots, \tag{2.4}$$

where Ω_i – eigenfrequencies of the system.

In figures 8 and 9 results of carried out simulations are presented. Calculations were made for the following parameters:

$m_1=190 \text{ kg}$, $m_2=210 \text{ kg}$, $k_1=k_2=10,0\cdot 10^6 \text{ Nm}^{-1}$, $c_1=c_2=1,9 \text{ Ns}^2\text{m}^{-1}$, $k=7,5\cdot 10^6 \text{ Nm}^{-1}$, $c_{12}=0$, $c=7,5\cdot 10^4 \text{ Ns}^2\text{m}^{-1}$ and different values of parameter k_{12}, eigenfrequencies of the system Ω_1, Ω_2, frequencies of printing press work ω and factor n. The following initial conditions were used: $z_1(0)=0,1 \text{ mm}$, $z_2(0)=0$, $\dot{z}_1(0)=0$, $\dot{z}_2(0)=0$.
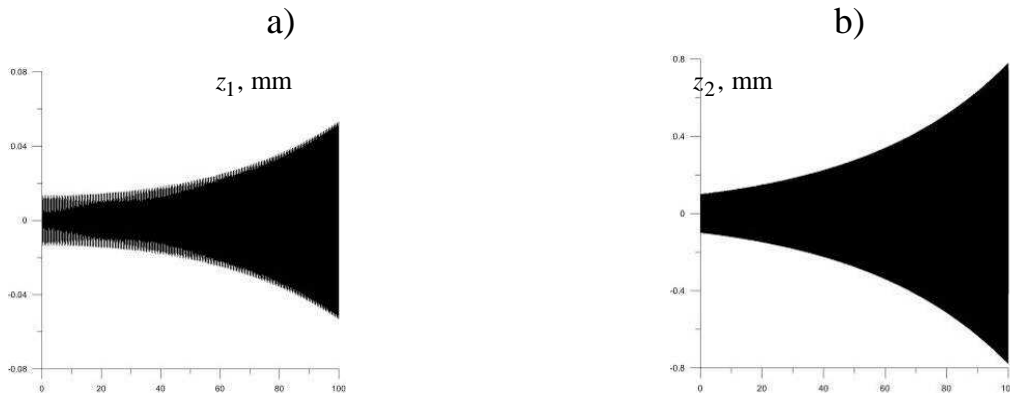
Fig. 8 Displacement of a plate cylinder $z_1(t)$ (a) and a blanket cylinder $z_2(t)$ (b) for $k_{12}=0$, $\Omega_1 = 218,928 \text{s}^{-1}$, $\Omega_2 = 230,274 \text{s}^{-1}$, $n = 5$, $\omega = (2\times 230,274/5)\text{s}^{-1} = 92,1096 \text{s}^{-1}$

In the Fig. 8 we can see, if maximal eigenfrequency of the system is multiplicity of the machine's work frequency and there are not cylinder bearers ($k_{12}=0$), parametric resonance occurs. We also noticed, if lower eigenfrequency is multiplicity of the printing press work, parametric resonance almost never takes place. Moreover, when cylinder bearers are introduced to the system ($k_{12}>0$) parametric resonance never occurs (Fig. 9).

Fig. 9 Displacement of a plate cylinder $z_1(t)$ (a)) and a blankiet cylinder $z_2(t)$ (b) for $k_{12}=10 \cdot 10^6$ Nm^{-1}, $\Omega_1=233,468$ s^{-1}, $\Omega_2=388,932$ s^{-1}, $n=5$, $\omega=(2 \times 388,932/5)$ s$^{-1}=86,4923$ s^{-1}

3. Modelling of the temperature phenomena in the inking unit

An inking unit of offset printing press consists of three sections: the ink feeding section, rubbing section and forming section [8]. Each of them mainly contains stiff and elastic rollers situated alternately. Function of the inking unit is to provide a uniform ink film to the printing plate. High viscous and indicating tixotropic properties of offset ink while transport among inking rollers gains appropriate rheological properties

Temperature variations affect the measurable indicators of quality printouts. Thus it seems reasonable to accurately know the issues of inking unit heating up.

The aim of the study is to build and solve a mathematical model of temperature changes in the inking unit occurring due to friction. Considered issue boils down to solving the heat conduction equations for appropriate boundary conditions. These conditions require mathematical modeling and description of friction phenomena.

3.1. Problem description

In offset printing process, temperature of inking rollers in the inking unit and its close surrounding gradually increases. This phenomenon is largely due to pressure between rotating steel and rubber coated rollers and influence of the reciprocating motion along their axes. The main cause of temperature increase is the friction between the flexible and stiff axially oscillating rollers. Researches [12, 13, 14] indicate that temperature increases with speed of the press, pressure between the rollers and the contact zone. The temperature rise is also precisely defined by the type of material, which rollers are made of, and their diameters.

162

As a result of friction on the contact surface of the rollers the heat is generated. It is generally accepted [15] that the work of friction is converted into thermal energy. Practically, this means that heat creates two streams of the same direction and opposite senses directed inside the bodies (rollers) which are in contact and between which occurs the friction.

The temperature increase in the inking unit causes the heating of the whole printing unit. Heat is discharged from the printing unit through evaporation of dampening solution, ink transfer to the paper, radiation and convection.

3.2. Mathematical formulation and solution of the problem

Due to the high real speed of the rotating rollers Ω and the fact, that we assumed the surface of the flexible roller is thermally isolated, the problem of rollers' pair is simplified and reduced to the problem of the roller with liquid coolant inside and roller surrounding. The roller on the border with its surrounding reaches the temperature equal to the ambient temperature, Fig. 10.
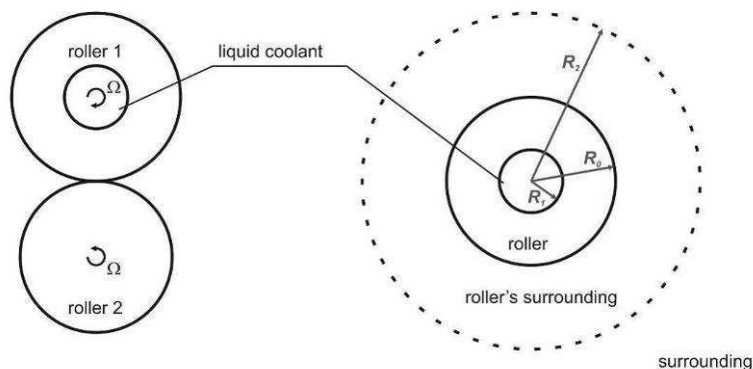
Fig. 10 Transition from the real issue to the model [13]

Trials of the solving this problem are presented in [16].

3.2.1. Mathematical model

In the case of axially symmetrical state of the cylinder temperature T_1 and the cylinder surrounding temperature T_2, the heat conduction equation for isotropic bodies in cooperation with cylindrical coordinates (R, φ, z) given in [4, 16] will take the form as follows:

$$\frac{\partial^2 T_1(R,t)}{\partial R^2} + \frac{1}{R}\frac{\partial T_1(R,t)}{\partial R} = \frac{1}{k_1}\frac{\partial T_1(R,t)}{\partial t}, \quad R_1 < R < R_0 \qquad (3.1)$$

$$\frac{\partial^2 T_2(R,t)}{\partial R^2} + \frac{1}{R}\frac{\partial T_2(R,t)}{\partial R} = \frac{1}{k_2}\frac{\partial T_2(R,t)}{\partial t}, \ R_0 < R < R_2 \quad (3.2)$$

with the following boundary conditions:

$$\lambda_1 \frac{\partial T_1(R_1,t)}{\partial R} = \alpha_1^T \left[T_1(R_1,t) - \theta_1^0 h_1(t) \right] \quad (3.3)$$

$$\lambda_1 \frac{\partial T_1(R_0,t)}{\partial R} - \lambda_2 \frac{\partial T_2(R_0,t)}{\partial R} = (1-\eta_1)\eta_2 f(V_r)V_r P \quad (3.4)$$

$$T_1(R_0,t) = T_2(R_0,t) \quad (3.5)$$

$$T_2(R_2,t) = \theta_2^0 h_2(t) \quad (3.6)$$

and boundary conditions:

$$T_1(R,0) = 0, \ R_1 < R < R_0 \quad (3.7)$$

$$T_2(R,0) = 0, \ R_0 < R < R_2 \quad (3.8)$$

Above, the following indications are used: T_1, T_2 – temperature increase of the roller and the roller's surrounding, respectively, t – time, P – contact pressure, V_r – relative velocity of rollers in contact, $f(V_r)=f_0\mathrm{sgn}(V_r)$ – kinetic friction coefficient, k_1, k_2 – thermal diffusivity of roller and roller's surrounding, α_1^T – coefficient of heat transfer between the coolant and the material, which the roller is made of, λ_1, λ_2 – thermal conductivity of the roller and roller's surrounding, respectively, η_1 – part of power which is lost, e.g. because of material consumption, h_n – dimensionless increase of internal ($n = 1$) and external ($n = 2$) temperature, $T_1^0(t) = \theta_1^0 h_1(t)$, $T_2^0(t) = \theta_2^0 h_2(t)$ – temperature increase of coolant and roller's surrounding, respectively, $Q(t) = \theta_0^0 h_0(t) = (1-\eta_1)\eta_2 f(V_r)V_r P$ – density of friction power, which equals the sum of heat flows directed respectively to the inside of the first and second roller (3.4). Heat flux density was calculated using the formula:

$$Q(t) = (1-\eta_1)\eta_2 f_0 |V_r| P. \quad (3.9)$$

The construction and operation of the inking unit (rotary and reciprocating motion of rollers) result in the periodical character of relative displacement of

the rollers being in contact along the axis. The fact, that the heat generated by friction takes place in the changing contact area:

$$S(t) = 2a\big(L - |Z(t)|\big) \tag{3.10}$$

where: S – contact area between rollers, a – contact area width, L – roller length, $Z(t)$ – relative roller displacement, is taken into account by introducing into heat flux formula (3.9) a depending on time factor $\eta_2 = S(t)/S_1$, where: S_1 – roller lateral surface area $S_1 = 2\pi R_0 L$.

Change of heat flux can now be written as:

$$Q(t) = \theta_0^0 h_0(t) \tag{3.11}$$

where: $\quad \theta_0^0 = (1 - \eta_1)\dfrac{af_0 \omega Z_0 P}{\pi R_0}, \quad h_0(t) = \big(1 - z_0 |\sin \omega t|\big)|\cos \omega t|, \quad z_0 = \dfrac{Z_0}{L}, \quad Z_0$ –

maximum relative displacement of rollers, ω – frequency of relative rollers displacement.

3.2.2. Model solved by Laplace transform

Using the Laplace transform and Borel convolution theorem [17] we found the ultimate solution, and wrote it in the form:

$$\big(T_1(R,t), T_2(R,t)\big) = \sum_{n=0}^{2}\left[\frac{\big(\overline{\theta}_{1n}(R,0), \overline{\theta}_{2n}(R,0)\big)}{\Delta(0)} + \sum_{k=0}^{\infty}\frac{\big(\overline{\theta}_{1n}(R,s_k), \overline{\theta}_{2n}(R,s_k)\big)}{s_k \Delta'(s_k)}\exp(s_k t)\right] *$$
$$* \frac{d}{dt}\big(\theta_n^0 h_n(t)\big) \tag{3.12}$$

where:

$$\Delta(s) = \lambda_1 Q_1^{(1)}(R_0, R_1, s) Z_{00}^{(2)}(R_2, R_0, s) + \lambda_2 Q_2^{(1)}(R_0, R_1, s) Z_{10}^{(2)}(R_2, R_0, s) \tag{3.13}$$

$$\overline{\theta}_{10}(R,s) = R_0 Q_2^{(1)}(R, R_1, s) Z_{00}^{(2)}(R_2, R_0, s) \tag{3.14}$$

$$\overline{\theta}_{11}(R,s) = Bi_1\big(\lambda_1 Z_{00}^{(2)}(R_2, R_0, s) Z_{10}^{(1)}(R_0, R, s) + \lambda_2 Z_{00}^{(1)}(R_0, R, s) Z_{10}^{(2)}(R_2, R_0, s)\big) \tag{3.15}$$

$$\overline{\theta}_{12}(R,s) = \lambda_2 Q_2^{(1)}(R, R_1, s) \tag{3.16}$$

$$\overline{\theta}_{20}(R,s) = R_0 Q_2^{(1)}(R_0, R_1, s) Z_{00}^{(2)}(R_2, R, s) \tag{3.17}$$

$$\overline{\theta}_{21}(R,s) = Bi_1 \lambda_1 Z_{10}^{(1)}(R_0, R_0, s) Z_{00}^{(2)}(R_2, R, s) \tag{3.18}$$

$$\overline{\theta}_{22}(R,s) = \big(\lambda_1 Q_1^{(1)}(R_0, R_1, s) Z_{00}^{(2)}(R, R_0, s) + \lambda_2 Q_2^{(1)}(R_0, R_1, s) Z_{10}^{(2)}(R, R_0, s)\big) \tag{3.19}$$

$$Q_2^{(1)}(x, y, s) = Bi_1 Z_{00}^{(1)}(x, y, s) + Z_{10}^{(1)}(y, x, s) \tag{3.20}$$

$$Q_1^{(1)}(x,y,s) = Bi_1 Z_{10}^{(1)}(x,y,s) + s_1^2 xy Z_{11}^{(1)}(y,x,s) \tag{3.21}$$

$$Z_{00}^{(1)}(x,y,s) = I_0(q_1 x)K_0(q_1 y) - I_0(q_1 y)K_0(q_1 x) \tag{3.22}$$

$$Z_{11}^{(1)}(x,y,s) = I_1(q_1 x)K_1(q_1 y) - I_1(q_1 y)K_1(q_1 x) \tag{3.23}$$

$$Z_{10}^{(1)}(x,y,s) = q_1 x\left(I_1(q_1 x)K_0(q_1 y) + I_0(q_1 y)K_1(q_1 x)\right) \tag{3.24}$$

$$Z_{10}^{(2)}(x,y,s) = q_2 y\left(I_1(q_2 y)K_0(q_2 x) + I_0(q_2 x)K_1(q_2 y)\right) \tag{3.25}$$

$$Z_{00}^{(2)}(x,y,s) = I_0(q_2 x)K_0(q_2 y) - I_0(q_2 y)K_0(q_2 x) \tag{3.26}$$

$$\Delta'(s_k) = d\Delta(s)/ds\big|_{s=s_k}. \tag{3.27}$$

Where the following indications are used: $I_m(z)$, $K_m(z)$ – modified mth-order Bessel functions, of the first and second kind respectively [18], $q_n = \sqrt{s/k_n}$, $Bi_1 = R_1\alpha_1^T/\lambda_1$ – Biot's number [17].

Roots s_k of the characteristic equation $\Delta(s) = 0$ lie on the negative part of the real axis of complex plane of Laplace transform parameter, i.e. $s_k = -\mu_k^2$.

It is worth noting, that the first term in equation (3.12) corresponds to the stationary solutions of this problem, and received in the earlier work [10]. The following stationary solution was obtained from the non-stationary solution for a function satisfying the condition $h_n(t) \to 1$, $t \to \infty$:

$$\left(T_1(R), T_2(R)\right) = \left(T_1(R,t), T_2(R,t)\right)\big|_{t\to\infty} = \sum_{n=0}^{2}\left[\frac{\left(\overline{\theta}_{1n}(R,0), \overline{\theta}_{2n}(R,0)\right)}{\Delta(0)}\theta_n^0\right] \tag{3.28}$$

A preliminary numerical simulation was conducted.

Conclusions

The aforementioned considerations regarding phenomena observed with respect to the printing unit of the offset printing machine lead to the following conclusions:

1.   The problem of contact between the rollers and the cylinder is of great importance. It is crucial to provide for setting an adequate contact area width. Apart from that, it is possible to conclude from the graph (Fig. 3) that bigger reduction of the distance between axes of the rollers results in increasing the contact area width. An increase of radius R_1 of the rigid body causes an increase of the contact area width and in bigger summary indentation of the

rollers concerned. Additionally, an increase of Poisson's ratios involves an increase of the contact area width as well as an increase of the indentation of rollers. A crucial conclusion is also that if any of the bodies is a rigid one, then their indentation does not depend on Young's modulus, because wherever $E_1 = \infty$, the element of the equation involving E_2 becomes reduced.

2.   Numerical analysis of the printing unit's model shows that unbalance of the plate cylinder or wear of bearings may excite vibrations, which have influence on ink film thickness transferred to the paper. Amplitude of this vibrations may be as high as 0,6 μm. If we consider offset printing technique, where standard ink film thickness is equal about 1,5-2,0 μm, it may be noticeable for human eye. Quality of printouts produced in such conditions will be disqualifying impaired.

Moreover, analyses show that cylinder bearers prevent printing unit from excitation of parametric resonance. Lack of cylinder bearers causes that parametric resonance may occur in printing unit, but only when maximal eigenfrequency of the system is multiplicity of its work frequency.

3.   The article presented analytical solutions for the proposed model of the heating up phenomenon of the inking rollers. The first term of the non-stationary solution covers the stationary case of this problem. We expect that the results obtained in the future will give the possibility of efficient cooling control, in fact temperature control, of the inking unit. Keeping the inking unit temperature at a constant level is a necessary condition to stabilize the properties of ink. Stable characteristics of the ink during the printing process will allow to reach higher repeatability of printouts' quality within the circulation. Work on the proposed model in [16] and in this article are still ongoing. As part of further work is planned to verify the model by measurements.

References

1. Czichon H., Technologia form offsetowych, Oficyna Wydawnicza Politechniki Warszawskiej, Warszawa 2002

2. Dejidas L. P., Jr., T. M. Destree, Technologia offsetowego drukowania arkuszowego, COBRPP, Warszawa 2007

3. Timoshenko S., Goodier J. N., Teoria sprężystości, Arkady, Warszawa 1962

4. Nowacki W. (1970), Teoria sprężystości, PWN, Warszawa 1970

5. Jurkiewicz A., Pyr'yev Y., Analiza nacisków pomiędzy walkami arkuszowej offsetowej maszynie drukującej, Opakowanie, no 3/2011, p. 75-79

6. Чехман Я.I., Сенкусь В.Т., Дідич В.П., Босак В.О., Друкарське устаткування. Підручник. Українська академія друкарства, Львів 2005

7. Тюрин А.А., Печатные машины – автоматы, Книга, Москва 1980

8. Kipphan H., Handbook of print media. Technologies and production methods, Springer-Verlag, Heidelberg 2001

9. Kulikov G.B., Diagnosing Causes of Increased Vibration of Printing Units of Tower Rotary Printing Machines, Journal of Machinery Manufacture and Reliability, 37(4), 2008, p. 391-396

10. Ciuplaski S., Maszyny offsetowe zwojowe, OWPW, 2001

11. Krzyżkowski J., Pyryev Y., Analysis of vibrations of printing units of offset printing presses, VI Międzynarodowe Sympozjum Mechaniki Materiałów i Konstrukcji Augustów, Conference proceedings, 2011, p. 190-192

12. Chober D., Petriaszwili J.: Badania warunków temperaturowych zespołów farbowych arkuszowej maszyny offsetowej, Świat Druku, 12/97, 1997, p. 42-44

13. Chou S.M., Bain L.J, Durand R., Sanderson E.: Novel printing press for waterless lithography, TAPPI Proceedings International Printing & Graphic Arts Conference, Atlanta, TAPPI Press, 1996, p. 165-174

14. Tołstoj G.D.: Ekspriementalnoje issliedowanije nagrewa elasticznych krasocznych walikow, Naucznyje Zapiski UPI XVI, 1961

15. Ling F.F.: Surface mechanics, New York, Wiley 1973

16. Piętak Z.M., Pyryev Y.: Mathematical modelling and description of friction and temperature phenomena in inking unit, Challenges of Modern Technology, 2, 1(2011), p. 41-44

17. Carslaw H.S., Jaeger J.C: Conduction of heat in solids, Oxford, Clarendon Pres 1959

18. Handbook of mathematical functions: with formulas, graphs, and mathematical tables, red. Abramowitz M, Stegun I.: Dover Publications Inc., New York 1965

19. Osiński Z., Teoria drgań, PWN, Warszawa, 1980

20. Hayashi C., Nonlinear oscillations in physical systems, WNT, Warsaw 1968

21. V. V. Bolotin, The dynamic stability of elastic systems, Holden-Day, San Francisco 1964

2.8 UNCERTAINTY ANALYSIS IN THE ROAD TRAFFIC NOISE MODELLING

Batko W.[1], Pawlik P.[1]

Introduction. According to the Directive 2002/49/EC [3] of the European Parliament dedicated to the environment protection (introduced into the legal system of the member countries) the basis for the assessment of noise hazards constitutes the knowledge of the equivalent sound level calculated for the period of: 12 hours of the day (6:00 – 18:00) $L_{Aeq\ day} = L_{Aeq\ 12}$, 4 hours of the evening (18:00 – 22:00) $L_{Aeq\ evening} = L_{Aeq4}$ and 8 hours of the night (22:00 – 6:00) $L_{Aeq\ night} = L_{Aeq\ 8}$.

Their knowledge is the basis for the calculation of long-term sound levels in the whole calendar year:

$$L_{Aeq,day} = 10\log\left(\frac{1}{365}\sum_{k=1}^{365}10^{0.1L_{Aeq,day,k}}\right) \tag{1}$$

$$L_{Aeq,evening} = 10\log\left(\frac{1}{365}\sum_{k=1}^{365}10^{0.1L_{Aeq,evening,k}}\right) \tag{2}$$

$$L_{Aeq,night} = 10\log\left(\frac{1}{365}\sum_{k=1}^{365}10^{0.1L_{Aeq,night,k}}\right) \tag{3}$$

These data are used for the estimation of the whole year noise annoyance, which is represented by the day-evening-night noise level given by the dependence:

$$L_{A,den} = 10\log(\frac{12}{24}10^{0.1LAeq,day} + \frac{4}{24}10^{0.1(LAeq,evening+5)} + \\ +\frac{8}{24}10^{0.1(LAeq,night+10)}) \tag{4}$$

[1] AGH University of Science and Technology, Cracow, Poland

Knowledge of the value estimated in such way, constitutes the grounds for the preparation of the necessary programs of the environment acoustic protection. It is obtained from the model noise computations and has a visual representation of data in a form of strategic acoustic maps. Such acoustic maps are being developed by computational methods recommended by the European Directive [3], using the input data obtained as the result of measurements and calculations and also performing necessary verifications and validations. In the light of the modern approach to estimations of the environment acoustic hazards the acoustic map realisation is a measurement, which requires the uncertainty estimation. The uncertainty assessment reflects the lack of the accurate knowledge of the value being estimated. The accurate knowledge of the year-average day-evening-night noise indicator L_{Aden} requires infinite number of input information, which in practice are inaccessible. Therefore it is necessary to consider the input data for model calculations not as individual values but as intervals of their possible variability. Such treatment of input data for the models can be related to the impossibility of the accurate estimation of: noise propagation conditions, parameters of the noise generating source, or not fully representative measurements which are necessary in noise hazard calculations. Therefore, it is necessary to develop formal tools of the noise modelling uncertainty analysis in the decision process, related to the acoustic environment management.

The paper presented hereby is a continuation of the previous investigations of the authors [1,2]. It is aimed at showing the possibility of the quality assessment of the acoustic map as a function of uncertain computational input data, at the application of the interval arithmetic mathematical formalism [6,7]. The considerations are focused on the uncertainty analysis of modelling the equivalent sound level L_{AeqT} (related to a road traffic noise) in the time period T.

The main noise source in the municipal environment - in Poland and in other European Union countries - is a communication noise, which in towns is dominated by a road traffic noise (in app. 80%). Development of acoustic maps for this noise requires knowing the traffic structure on roads and in the vicinity of the analysed zone. Especially it is necessary to know how many light n_1 and

heavy vehicles n_2 are passing in the time period T and to know their characteristic exposure noise levels L_{AE1} and L_{AE1}, which constitute the potential uncertainty source concerning the equivalent noise level assessment L_{AeqT}, (calculated for the time period T). They form the basis for calculations of the long-term noise indicators.

1. Measuring-computational model of the estimation of the equivalent sound level LAeqT around the arterial road

The equivalent sound level L_{AeqT} around the arterial road, through which in the time period T n_1 light vehicles (passenger and delivery cars) and n_2 heavy vehicles (trucks and busses) passed and related to them characteristic exposure noise levels L_{AE1} and L_{AE2}, is calculated from the following equation [5]:

$$L_{AeqT} = 10\log\left[\frac{1}{T}\left(n_1 \cdot 10^{0.1L_{AE1}} + n_2 \cdot 10^{0.1L_{AE2}}\right)\right] \qquad (5)$$

Values L_{AE1} and L_{AE2} are noise measures of individual light and heavy vehicle, respectively, and the average noise value – proper for these types of vehicles - can be attributed to them. Occurring in Equation (5) value n_1/T determine the average intensity of light vehicles and n_2/T determine the average intensity of heavy vehicles in the time period T.

Taking into account the fact, that in the time period T :

$$n_1(T) = p \cdot n(T) \qquad (6)$$

light vehicles and

$$n_2(T) = (1-p) \cdot n(T) \qquad (7)$$

heavy vehicles are recorded, at the total number:

$$n(T) = n_1(T) + n_2(T) \qquad (8)$$

of vehicles passing during the time period T. Values p and $(1-p)$ determine the percentage of light and heavy vehicles, which during the reference period is not changing. These notions can be equated with the probability of passing of the defined vehicle type during the base time period constituting the grounds for modelling the equivalent noise level around roads.

It is obvious, that values estimated in such way, can be corrected for the effects related to noises caused by: atmospheric phenomena, acoustic waves reflection from the earth surface and building walls, or diffraction on buildings and screens as it is in the noise calculation programs: CADNA, SoundPLAN, IMMI, NITHRA, or others.

2. Model formalism of the interval arithmetic

For the uncertainty determination of the acoustic parameters being modelled the authors propose to use the formalism of the Moore's [6,7] interval arithmetic, which performs mathematical operations on intervals (interval numbers) and not on numbers. Interval numbers can represent variability ranges of the modelled parameters determining their measuring or computational uncertainty.

Intervals are determined as closed, limited sets of real numbers, e.g.:

$$\mathbf{x} = [\underline{x}, \overline{x}] = \{x \in R : \underline{x} \leq x \leq \overline{x}\} \tag{9}$$

where $\underline{x}$ is the lower limit of the interval – infimum, while $\overline{x}$ denotes the upper limit – supremum, and x is an arbitrary number belonging to the interval.

The basic arithmetic operations are defined on the interval set:

$$\mathbf{x} \Diamond \mathbf{y} = \{z = x \Diamond y \quad : \quad x \in \mathbf{x} \quad y \in \mathbf{y}\} \tag{10}$$

where $\Diamond$ is one of the operators of: addition, subtraction, multiplication or division. These operators, apart from division, are defined for arbitrary intervals. For division it should be assumed that: $0 \notin \mathbf{y}$.

Applying the formalism of the interval arithmetic it is possible to determine the result variability range at each stage of calculations, taking into account the uncertainty of measurements, calculations and the one related to the machine word length.

3. Application of the interval arithmetic for the uncertainty determination

The uncertainty analysis of the determination of the equivalent sound level L_{AeqT} of three selected localisations of the road artery for the measuring data obtained during the environment acoustic control, was carried out. The formalism of the interval arithmetic was used for this purpose. The uncertainty

of input parameters of the model (5) and of the modelling result was determined in a form of interval numbers.

The Figure below (Fig. 1) presents the variability intervals of the sound levels in dependence on the percentage uncertainty of n_1, n_2, L_{AE1} and L_{AE2} parameters. For each localisation two line of the same colour were assigned, where one was the lower and another the upper limit of the variability intervals of the equivalent sound level in dependence of the input parameters. The interval numbers describing the variability of input parameters were written in the following form:

$$\boldsymbol{n_1} = [n_1 - n_1 \cdot k/100 \ , \ n_1 + n_1 \cdot k/100 \ ], \tag{11}$$

$$\boldsymbol{n_2} = [n_2 - n_2 \cdot k/100 \ , \ n_2 + n_2 \cdot k/100 \ ], \tag{12}$$

$$\boldsymbol{L_{AE1}} = [L_{AE1} - L_{AE1} \cdot k/100 \ , \ L_{AE1} + L_{AE1} \cdot k/100 \ ], \tag{13}$$

$$\boldsymbol{L_{AE2}} = [L_{AE2} - L_{AE2} \cdot k/100 \ , \ L_{AE2} + L_{AE2} \cdot k/100 \ ], \tag{14}$$

where: $k \in \ <0,5>$, by bold type are marked interval numbers, values of n_1, n_2, L_{AE1} and L_{AE2} are values measured by the Certified Acoustic Laboratory.
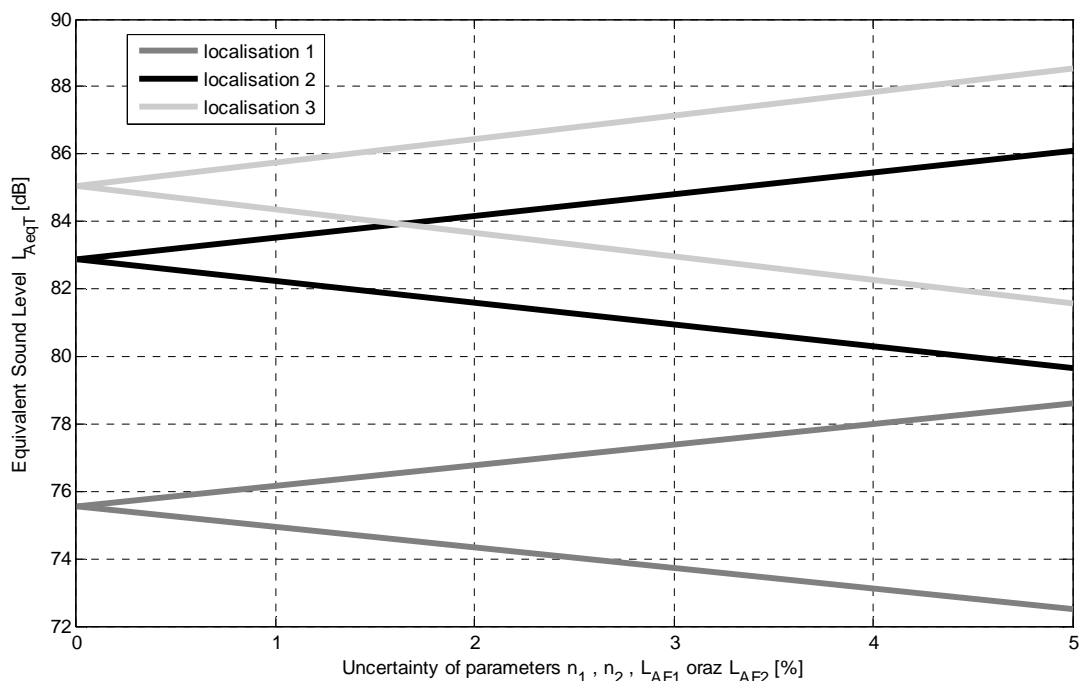
Fig.1. Uncertainty of the equivalent sound level in dependence of the percentage uncertainty of n_1, n_2, L_{AE1} and L_{AE2} parameters.

Uncertainty of the estimated equivalent sound level determined by means of the interval arithmetic, equal app. ±3 dB at 5% uncertainty of the input parameters.

Conclusions

The presented paper is a trial of inducing discussion on the basic problem of several research tasks concerning the development and utilisation of the digital noise maps, in the environment acoustic state assessment and the related decision making processes in the environment management. It especially concerns investigations related to the analysis of the possible errors of the road traffic noise modelling and the corresponding verification of its accuracy.

The cognitive approach proposed in the paper, indicates sources of possible digital errors which can appear in the estimation of the environment road noise hazard.

The contents of the paper is aimed at discussion and logical analysis of the current methods of solving problems of the uncertainty assessment in environmental acoustic hazards. The possible way of searching for better solution was indicated. The attention was directed towards the possibility of the estimation of the road traffic noise modelling uncertainty by means of the interval arithmetic formalism. This formalism can be treated as a generalization of the current computational methods. Uncertain variables occurring in models are, in some ways, similar to random variables which constitute the bases of the traditional uncertainty analysis (on the grounds of the international document [4] issued by seven most important metrological organisations). However, they do not generate problems related to the necessity of the difficult estimation of their probabilistic characteristics and corresponding problems of statistical verification of the assumptions essence. The range of allowable changes, determined by an expert on the basis of his knowledge of approximate values of the assumed parameters of the effect being under modelling, can be attributed to them.

Acknowledgments

References

1. Batko W. Pawlik P., Application of the interval arithmetic in the reverberation time uncertainty assessment, DAGA 2011- 'Sounds good' - The 37th Annual Conference for Acoustics in Düsseldorf, 21-24 March 2011.

2. Batko W. Pawlik P., New approach to uncertainty assessment of acoustic effects in the environment [abstract], Archives of Acoustics; ISSN 0137-5075. — 2010 vol. 35 no. 2 p. 278, [XV International Conference Noise Control 2010 : 6–9 June 2010 Książ, Wałbrzych].

3. Directive 2002/49/WE of the European Parliament and of the Council of 25 June 2002, relating to the assessment and management of environmental noise, Official Journal of the European Communities 18 July 2002.

4. Guide to the Expression of Uncertainty Measurement. International Organization for Standardization, ISBN 92-67-10188-9,1995

5. Makarewicz R. : Hałas w środowisku, Ośrodek Wydawnictw Naukowych, Poznań 1996.

6. Moore R. E., Interval Arithmetic and Automatic Error Analysis in Digital Computing, Ph.D. Thesis, Stanford University, October 1962.

7. Moore R. E., Interval Analysis, Prentice-Hall, Englewood Cliffs, NJ, USA, 1966.

2.9 ANALYSIS OF CENTRING POSSIBILITY OF A CONVEYOR BELT WITH A BICONICAL IDLER

Furmanik K.[1], Pytko S.[1]

Introduction

Centring idlers, which have to assure driving of a belt along a route axis with possibly low motion resistances have an essential function in a belt conveyor. It is an important principle for a proper conveyor exploitation, because the belt convergence is always connected with defined losses [1-7]. The idlers and their systems, which automatically react in direction and value of forces decentring of belt route and other solutions are used for centring of the belt [5].

The force which centres the belt is friction force obtained due to a proper bevelling of idler, by which one can understand its deflection of axis from perpendicular position to belt longitudinal axis. The belt and idler durability depends in a great range on correctness of their friction cooperation. Too much

[1] AGH University of Science and Technology Cracow, Poland

values of bevelled angle of idlers are a cause of excessive wear of idlers and belt and also increasing of belt motion resistances (Fig.1a).

The centring idlers ought to cooperate with a belt in a range of elastic slips, in the aim to limit their friction wear, though the knowledge of their friction characteristics is essential (Fig.2)

In the solution like in Fig.1b side centring idlers are considerably less loaded by the belt than the central idler, and in a case of small supplying of output their centring operation is rather small. Hence utilization of more loaded
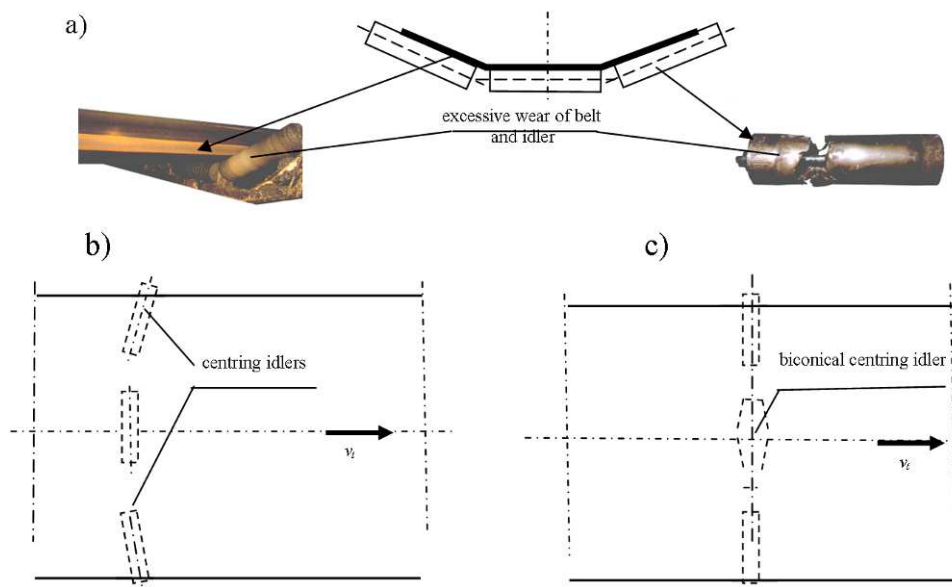
Fig.1. Examples of cooperation of centring idlers with a belt: a) results of excessive bevelling of side centring idlers; b) support with two side centring idlers; c) support with biconical centring idler
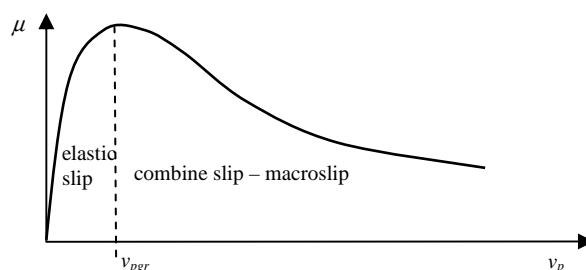
Fig.2. Characteristics of friction pair: centring idler – belt

central biconical idler (Fig.1c) can be more effective to this centring. The friction cooperation of cylindrical centring idler with a belt was given in the paper [2], but in this paper the possibilities of centring of belt with a biconical idler for getting possibly great centring force with small additional resistances

and velocity of belt slid has been analyzed. The obtained dependences enable the analysis of influence of geometry and tribology (materials) of friction pair, i.e. the biconical idler and belt for its effective centring over the supports with this type of idlers. The results of experimental verification will decide about the possibilities of their implementation in design practice and exploitation of belt conveyors.

Analysis of friction cooperation of a conical idler with a belt

In the case of rectilinear motion of a belt held with a conical idler of linear contact, except the resistances resulting from their deflection into the zone of contact as well as resistances of idler bearing they are occurring some additional friction resistances caused by slips from a difference of circumferential velocities over idler side surface (Fig.3a). To simplify the
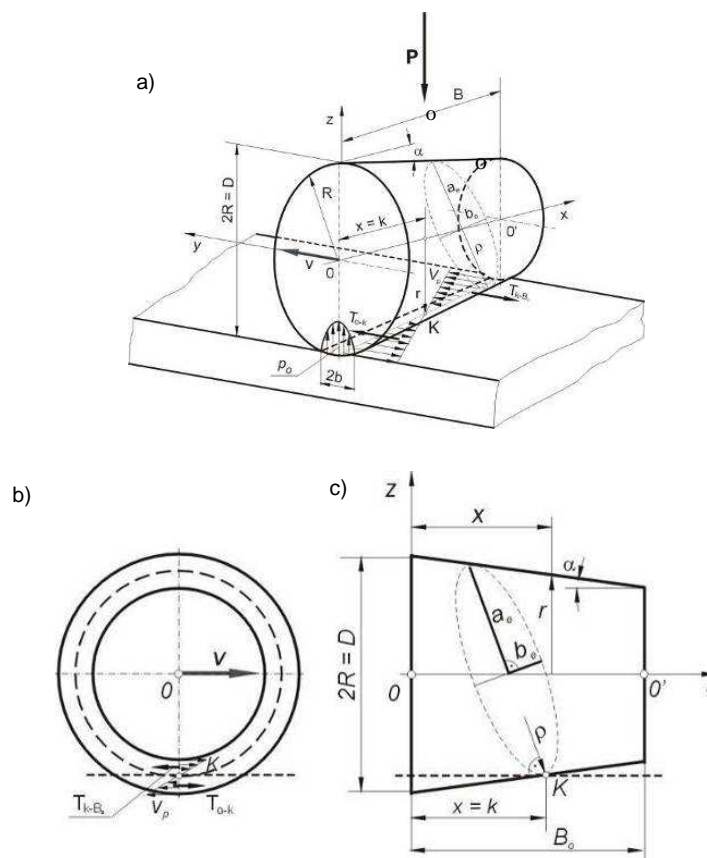
Fig.3. Schemes: a) – c) presenting friction cooperation of a conical idler with a belt

analysis the system of idler – belt has been taken into consideration as in Fig.3a and assumed that a "pure rolling" occurred only in one contact point *K*, but the slips took place in other line contact points. Actually only in certain

surrounding of K point there were no slips due to the deflection of belt; thus for a simplifying of further considerations the phenomenon have been eliminated. In the zone of contact of an idler and a belt there are slips with friction forces creating additional resistance and the moment of friction forces, which could be used for the belt centring. Along the contact line radius contacts of idler side surface with a belt has been changing and in a result of this have also changed elementary surface thrusts, in spite of saving the constant linear thrust.

On the basis of Fig.3c one has assigned the r cone radius and ellipse semi-axes a and b emerged from crossing of cone by perpendicular plane to a line of its contact with a belt and then one could write the dependences:

$$r = R - xtg\alpha , \tag{1}$$

$$a_e = \frac{\cos\alpha}{\cos 2\alpha}(R - xtg\alpha) , \tag{2}$$

$$b_e = \frac{1}{\sqrt{\cos 2\alpha}}(R - xtg\alpha) , \tag{3}$$

In the aim to denote a radius of ellipse curvature on perpendicular plane towards a contact line (Fig.3c) more advantageous is to describe it by parametric equations:

$$x_t = a_e \cos t$$

$$y_t = b_e \sin t , \tag{4}$$

when: $0 \le t \le 2\pi$.

For $t = 0$, so in the point of cone contact with a belt a curvature radius will be equal to:

$$\rho = \frac{(1 + y'_{t=0})^{\frac{3}{2}}}{\left|y''_{t=0}\right|} = \frac{b_e^2}{a_e} = \frac{1}{\cos\alpha}(R - xtg\alpha) , \tag{5}$$

Assuming that the P force (Fig.3a) causes a constant loading along a contact line an elementary normal loading will be:

$$q_n = \frac{P}{B_o} , \tag{6}$$

Assuming as the basis the Hertz solutions one can assign stress values and their distribution in a contact surface and deflection of cooperating bodies. For

the discussed case the maximum stress in a zone of contact one can define by a formula:

$$p_o = 0,59\sqrt{\frac{PE_1E_2}{B_o(E_1+E_2)(R-xtg\alpha)}} \ , \tag{7}$$

while breadth of conical idler contact with a belt (Fig.3a):

$$2b = 8,11\sqrt{\frac{P(E_1+E_2)(R-xtg\alpha)}{E_1E_2B_o}} \ , \tag{8}$$

where: E, E – modules of casing elasticity of idler and belt.

A distribution of thrusts in contact breadth for defined x abscissa one can express by a formula:

$$p(y) = \frac{P}{\pi b^2}\sqrt{b^2-y^2} \ , \tag{9}$$

when: $|y| < b.$

Beneath two cases have been discussed, when in dependence of $T = \mu P$ friction force from thrust force the friction coefficient:

$$1) \ \mu(v_p) = A = \ const, \tag{10}$$

$$2) \ \mu(v_p) = A - Bv_p, \tag{11}$$

where A, B – constants; v_p – slid velocity.

In the first case when $\mu(v_p) = A = \mu$ the dT elementary friction force in a contact with a belt one can calculate from a formula:

$$dT = \int_{y=-b}^{y=b} \mu p(y)Pdydx = \frac{\mu P}{B_o}dx = tdx \ , \tag{12}$$

hence the t elementary friction force in a contact line is constant (Fig.4). After an integration the friction forces

over idler breadth (from $0 - B_0$) one can express by dependences:

$$T_{0-k} = \int_0^k dT = \frac{\mu P}{B_o}k \ , \tag{13}$$

$$T_{k-B0} = \int_k^{B0} dT = \frac{\mu P}{B_o}(B_o-k) \ , \tag{14}$$

Theoretically at the *K* contact point of abscissa $x = k$ one can find the "pure rolling" on a rolling circle of *r* radius at $v_p = 0$, but in other contact points have occurred slips of velocity:

$$v_p = \frac{v}{r}(R-r) \,, \tag{15}$$

when:

$$r = R - ktg\alpha \,, \tag{16}$$

In the case when $\mu = const$ and thrust along side surface of idler in contact with a belt is constant, the elementary friction force is also constant, and at *K* point of abscissa $x = k$ this force is equal to 0, because there is no slip. The friction forces T_{0-k} and T_{k-Bo} induced by slips settle an equilibrium where their moments against the idler axis are equal and than we have as following:

$$M_{0-k} = M_{k-B0} \,, \tag{17}$$

Considering that:

$$dM = rdT = (R - xtg\alpha)\frac{\mu P}{B_0}dx \,, \tag{18}$$

thus:

$$M_{0-k} = \int_0^k dM = \frac{\mu P}{B_0}(Rk - \frac{k^2}{2}tg\alpha) \,, \tag{19}$$

$$M_{k-B_0} = \int_k^{B_0} dM = \frac{\mu P}{B_0}(RB_0 - \frac{B_0^2}{2}tg\alpha - Rk + \frac{k^2}{2}tg\alpha) \,, \tag{20}$$

hence after considering their dependences (17) and transformations one has obtained an equation:

$$k^2 tg\alpha - 2Rk + RB_0 - \frac{B_0^2}{2}tg\alpha = 0 \,, \tag{21}$$

with a following solution:

$$k = \frac{R - \sqrt{R^2 - tg\alpha(RB_0 - \frac{B_0^2}{2}tg\alpha)}}{tg\alpha} \,, \tag{22}$$

In Fig.4 it was shown a scheme of forces operating in contact of idler and belt, when a coefficient of friction $\mu = const.$
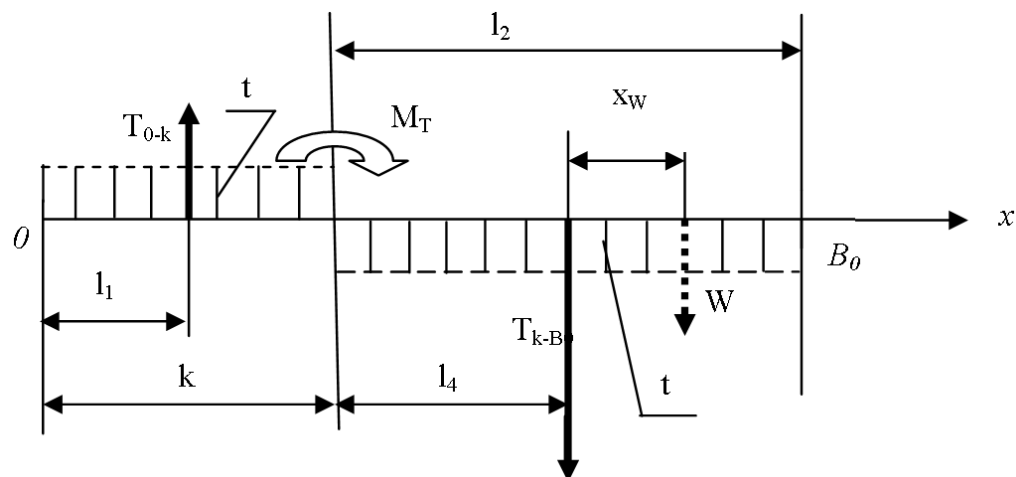
$$k = 0\vec{K} \; ; \quad l_1 = 0.5 \, 0\overline{K} \; ; \quad l_2 = K\overline{B}_0 \; ; \quad l_4 = 0.5 l_2$$

Fig.4. Scheme of forces operating in contact of idler and belt when $\mu = const$

A supplementary resistance W (Fig.4) caused by the slips describes a formula:

$$W = T_{k-B_0} - T_{0-k} = \frac{\mu P}{B_0}(B_0 - 2k) , \qquad (23)$$

elementary resistance:

$$w = \frac{W}{P} = \frac{\mu}{B_0}(B_0 - 2k) , \qquad (24)$$

As a result of reduction of force system operating in contact (Fig.4) one has obtained a resultant resistance W applying in the point x and the moment of M_T friction forces, which value one can calculate from a formula:

$$M_T = \frac{\mu P k}{2} , \qquad (25)$$

The W resistance calculated from the formula (23) additionally increases belt motion resistances.

In the second case, i.e. with $\mu(v_p) = A - Bv_p$, after assuming of dependence (15) the slip velocity is equal to:

$$v_p = v - \frac{v}{r_{x=k}}r = v(1 - \frac{r}{r_{x=k}}) = v(1 - \frac{R - xtg\alpha}{R - ktg\alpha}) , \qquad (26)$$

and the elementary friction force in contact of idler with belt:

$$dT = \frac{\mu(v_p)P}{B_o \cos\alpha}dx = \frac{P}{B_o}[A - Bv_p(1 - \frac{R - xtg\alpha}{R - ktg\alpha})]dx = \frac{P}{B_o \cos\alpha}[A - Bv_p \frac{(x-k)tg\alpha}{R - ktg\alpha}]dx , \qquad (27)$$

181

It results from the dependence (27), that on the breadth contact of idler with belt beginning from the point K the absolute value of elementary friction force t decreases in linear way, but velocity of slip v_p increases, what has been given in Fig.5.
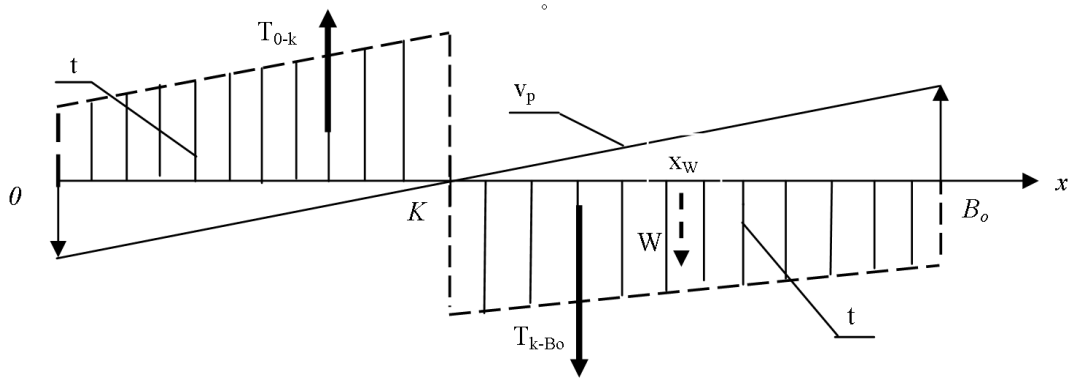
Fig.5. System of forces operating in contact of idler and belt with $\mu(v_p) = A - Bv_p$

After the integration of equation (27) and transformations one have obtained the values of friction forces for the both zone of contact:

$$T_{0-k} = \int_0^k dT = \frac{P}{B_0}[(A + \frac{Bv_p tg\alpha}{R - ktg\alpha})k - \frac{Bv_p tg\alpha}{2(R - ktg\alpha)} \cdot k^2], \qquad (28)$$

$$T_{k-B_0} = \int_k^{B_0} dT = \frac{P}{B_0}[A(B_o - k) - \frac{Bv_p tg\alpha}{R - ktg\alpha} \cdot (\frac{B_o^2}{2} - 2B_o k + \frac{3k^2}{2})], \qquad (29)$$

In the results of force reduction T_{0-k} and T_{k-B0} operating in contact one has obtained the W resultant resistance and moment of M_T friction forces; this additional resistance was expressed by the formula:

$$W = T_{k-B_0} - T_{0-k} = \frac{P}{B_0}\left\{A(B_0 - 2k) - \frac{Bv_p tg\alpha}{(R - ktg\alpha)} \cdot [\frac{B_0^2}{2} - k(2B_0 - 1) + k^2]\right\}, \qquad (30)$$

with elementary resistance:

$$w = \frac{W}{P} = \frac{1}{B_0}\left\{A(B_0 - 2k) - \frac{Bv_p tg\alpha}{(R - ktg\alpha)} \cdot [\frac{B_0^2}{2} - k(2B_0 - 1) + k^2]\right\}, \qquad (31)$$

The M_T moment of friction forces in contact one can define from then dependence:

$$M_T = W \cdot x_W = T_{0-k}(x_{0-k} + x_{k-B0}), \tag{32}$$

where x_W – abscissa of W resultant of friction force (Fig.5) expressing by the following dependence:

$$x_W = \frac{T_{0-k}(x_{0-k} + x_{k-B0})}{W}, \tag{33}$$

The abscissae x_{0-k}, x_{k-B0} forces of T_{0-k}, T_{k-B0} have been assigned as the abscissae of a centre of gravity of figure assigned by friction force distributions on the intervals 0-k and k-B_0 after earlier value determination of friction forces as following with $x = 0$; $x = k$ and $x = B_0$. After carrying out of necessary calculations and transformations these abscissae have been obtained as the following dependences:

$$x_{0-k} = \frac{b_1(3a_1 + c_1)}{6(a_1 + 0.5c_1)} \; ; \qquad x_{k-B0} = \frac{b_2(3a_2 + c_2)}{6(a_2 + 0.5c_2)}, \tag{34}$$

where:

$$a_1 = \frac{P}{B_0}(A - Bv_p \frac{ktg\alpha}{R - ktg\alpha}) \; ; \qquad b_1 = k \; ; \quad c_1 = \frac{PBv_p ktg\alpha}{B_0(R - ktg\alpha)}, \tag{35}$$

$$a_2 = \frac{P}{B_0}[A - Bv_p \frac{(B_0 - k)tg\alpha}{R - ktg\alpha}] \; ; \quad b_2 = B_0 - k \; ; \quad c_2 = \frac{PBv_p(B_0 - k)tg\alpha}{B_0(R - ktg\alpha)}, \tag{36}$$

Taking into consideration these above mentioned dependences in the formula (32) one has got:

$$M_T = \frac{P}{B_0}[Ak + \frac{k^2 Bv_p tg\alpha}{2(R - ktg\alpha)}] \cdot \left\{ \frac{k\left[A - \frac{2}{3} \cdot \frac{Bv_p ktg\alpha}{R - ktg\alpha}\right]}{2A - \frac{Bv_p ktg\alpha}{R - ktg\varepsilon}} + \frac{(B_0 - k) \cdot [A - \frac{2}{3} \cdot \frac{Bv_p(B_0 - k)tg\alpha}{R - ktg\alpha}]}{2A - \frac{Bv_p(B_0 - k)tg\alpha}{R - ktg\alpha}} \right\}, \tag{37}$$

Taking the value of M_T friction force moment operating on the belt one can determinate the value of φ angle of its deflection onto horizontal plane, tangential to the conical surface of idler. Treating a belt as a beam of *EI* rigidity based on slidable supports according to the Mohr graph analytical method the deflection angle of beam longitudinal axis in the middle of its length has been determined, what was presented in Fig.6.

A value of φ angle one can calculate of the formula:

$$\varphi = \frac{M_T l}{12EI}, \tag{38}$$
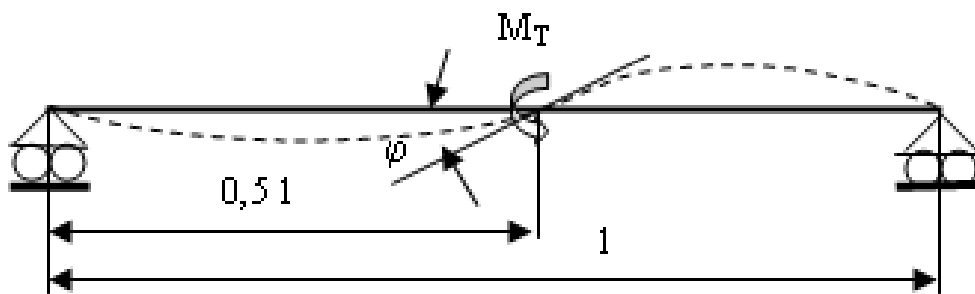
Fig.6. Scheme of a belt loading with centring moment

For the first case, when $\mu(v_p) = const$, after taking the dependence (25) in (38) one have obtained :

$$\varphi = \frac{\mu P k l}{24EI}, \tag{39}$$

And for the second case when $\mu(v_p) = A - Bv_p$, one have obtained:

$$\varphi = \frac{Pl}{12EIB_0}[Ak + \frac{k^2 Bv_p tg\alpha}{2(R - ktg\alpha)}] \cdot \left\{ \frac{k\left[A - \frac{2}{3}\cdot\frac{Bv_p ktg\alpha}{R - ktg\alpha}\right]}{2A - \frac{Bv_p ktg\alpha}{R - ktg\varepsilon}} + \frac{(B_0 - k)\cdot[A - \frac{2}{3}\cdot\frac{Bv_p(B_0 - k)tg\alpha}{R - ktg\alpha}]}{2A - \frac{Bv_p(B_0 - k)tg\alpha}{R - ktg\alpha}} \right\}, \tag{40}$$

It would be easy to check that the obtained dependences for the first case, i.e. $\mu(v_p) = A = const$, were the particular case in $\mu(v_p) = A - Bv_p$ and $B = 0$.

As the result of belt deflection of φ angle (Fig.6) on a centring idler operating under M_T friction force moment its centring velocity will be:

$$v_c = v_t \sin\varphi, \tag{41}$$

where: v_t – belt velocity.

The above considerations were connected with the conical idler, nevertheless in the case of biconical idler a convergence of belt would cause an asymmetry of its loading and then the centring resultant moment will be the difference of M_T friction force moments occurred on the both halves of this idler, and the additional resultant friction resistance – sum of W resistances over these halves. To avoid an edge influence of idler onto a belt one ought to round a coupling of profiles of its halves. The real effectiveness of belt centring

with biconical idler will depend on its stretching, i.e. of a place of casing of this idler into belt conveyor.

Final conclusions

The condition of effective centring of a belt is a possibility of taking the great part of belt thrust on idler unit by the centring idler, and due to their geometry and positioning save the friction cooperation in a range of elastic slips ($v_p \leq v_{pgr}$ – Fig.2). The analysis carried out in the paper allowed for formulation of the following conclusions:

1. effective and energy saving centring of a belt can be ensured by its cooperation in a range of elastic slips with biconical idlers, in such a case the wear of cooperating friction pair will be low; the dependences obtained in the paper allow determinate for conclusive characteristics friction the geometric parameters of biconical idler ensuring such a cooperation;

2. biconical centring idlers ought to take the possibly great part of belt thrust onto the idler unit and their surfaces would ensure the great and stable values of friction coefficient , also in the case of occurring some belt pollution;

3. one could be verified the practical usability of a biconical centring idler on the way of experimental investigations; learning and applying reasons would suggest for the continuation of further theoretical and experimental works of this subject.

References

1. Antoniak J.: Equipment and Systems of Underground Haulage in Mines.[in Polish], 1979 Katowice.

2. Furmanik K.: Problem of Friction Cooperation of a Conveyor Belt With a Centring Idler.[in Polish], Zagadnienia Eksploatacji Maszyn 2000, issue 4 (124), p. 9-21.

3. Gladysiewicz L.: Belt Conveyors. Theory and Calculations. 2003 Wroclaw.

4. Grimmer K.J.: Zwei ausgewahlteProbleme der Bandfordertechnik. Forschritt Berichte VDI Zeitchrift R.13 Nr 10.

5. Kulesza A.: Stations of Centring Belt Driving into Belt Conveyors of Unstable Route [in Polish] Transport Przemyslowy i Maszyny Robocze 2011, issue 2(12), p. 15-20.

6. Пытко С. Фурманик К.: *Трибологические аспекты взаимодействия центрирующего ролика с транспортёрной лентой.*"СЛАВЯНТРИБ–7а".Материалы международной научно-практической школы-конференции. Том 3, с. 68-76, Рыбинск-Санкт-Петербург-Пушкин, 2006.

7. Zur T., Hardygora M,: Belt Conveyors In Mining [in Polish], 1979 Katowice.

2.10 SMART VIBRATION ISOLATION SYSTEMS

Rączka W.[1], Sibielak M.[1], Konieczny J.[1]

Introduction

Vibration isolations systems are used for minimisation of force or displacements of protected mass. It can be achieved in several different ways using elastic elements such as springs or pieces of elastic materials are incorporated in structures. Springs in vibration isolation system are used to shape the frequency characteristics of the plant, therefore various spring constructions are available wherein various spring properties are utilised. Spring stiffness together with the mass of the plant, which is usually beyond our control, determines the natural frequencies of vibrations. Since it is sometimes necessary to change the characteristics of the whole plant or its selected part (such as vibration absorber), the coefficient of stiffness has to be controlled. Such springs allow for construction of vibration isolation systems, which afford controlled variations of plant characteristics. The stiffness coefficient can be controlled through the incorporation of a unit of subsequently including elastic elements, pneumatic springs, springs made of materials with controllable properties (for example Shape Memory Alloy) . In the case of spring units, when new springs are added the changes in the stiffness coefficient are discrete; in the case of pneumatic or SMA springs the stiffness coefficient can be varied continuously. It is way SMA spring was developed in Department of Process Control.

1. Smart spring

Shape Memory Alloys (SMA) are metals which are capable of storing their original shape in memory and regaining it when subjected to external conditions, such as magnetic field or temperature fluctuations. Well known shape memory alloys are: Ni-Ti, Cu-Zn, Au-Cd, Ag-Cd, Cu-Al. Specific properties of these alloys are related to the inverse martensite transition. The best known shape memory alloy is that of titanium and nickel (mass concentration of nickel 53-57%) also known as Nitinol. The phase transition,

---

[1] AGH University of Science and Technology, Poland

which affects the shape memory in NiTi alloy, involves the transition from martensite to austenite. Two processes occurring in SMA materials are distinguished: shape memory as one- and two- directional shape memory effect and superelastic behaviour named pseudoelastic behaviour too [2,3,4]. The superelastic behaviour is used in vibration systems. In this paper changing of value of Young modulus through changing temperature of SMA is used as the basis of conception smart spring. Effect of changing mechanical and physical properties are connected with phase transformations. For used alloy (NTC01) the average temperatures at which phase transitions take place are: Mf=30 °C, Ms=45 °C, As=50 °C, Af=70 °C and E-modulus for Martensite equals 15 GPa

a)   b)
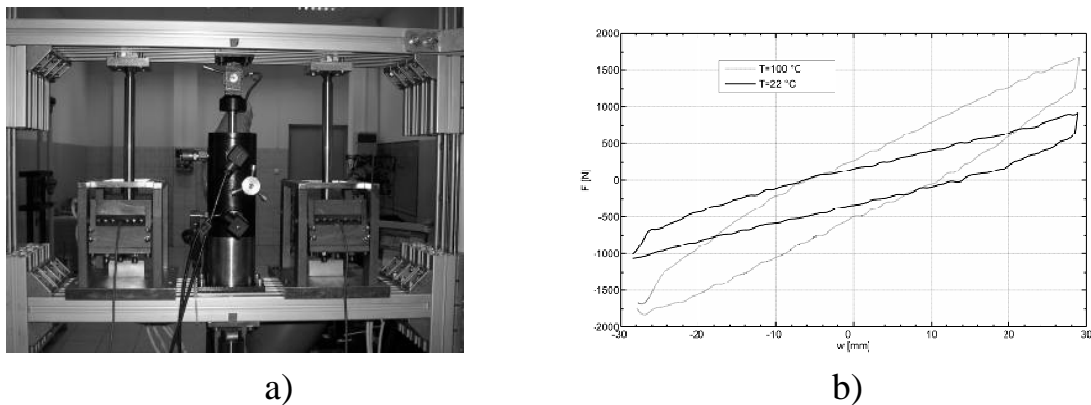
Fig. 1. General view of vibration isolation system with SMA springs (a) and characteristics of the springs (b) for chosen temperatures.

and for Austenite 30 GPa. The developed springs are shown on the Figure 1a in vibration isolation system. This smart spring was used in some vibration isolation systems with arbitrary chosen structures. On Figure 1b are shown chosen characteristics of the springs.

2. SDOF vibration isolation system

The smart springs are used in vibration system SDOF. Smart springs are used between mass m of the plant to be vibroisolated and the vibration exciter.

For reduction the vibrations of the mass, the vibration isolator could be tuned to changing excitations [1,5,6], in other words the resonant frequency could be changed by special controller. Thus the vibration isolation system changes dynamic characteristic. Vibration of the mass m in resonance might be reduced by changing resonant frequency of the system by changing stiffness of

the spring. It is very effective method in case of mono-harmonic excitations. By changing dynamic characteristics of vibration isolation system by changing its parameters we could tune features of the system. A spring with a controlled stiffness coefficient allows for alternating the natural frequency of the system. In case of a SMA spring with a controlled stiffness, we make use of the fact that the Young modulus for austenite is twice as big as for martensite. When spring temperature is changed (for instant due to current flow through spring), the stiffness coefficient can be easily controlled.

Vibration isolation system was built in laboratory and was tested. General view of this system is shown on Fig. 1a. Chosen frequency characteristics are presented on Fig. 2a and 2b. These are characteristics of vibration propagation from excitation to protected mass.
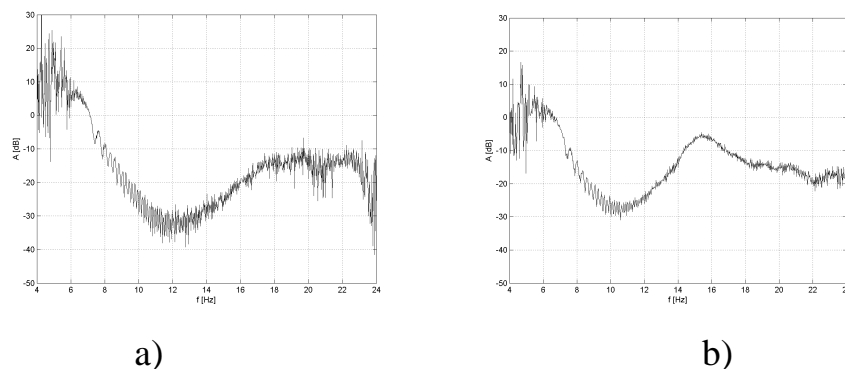
It is readily apparent that the characteristic frequencies of the system are changing through changing of temperature of the smart spring. Resonant frequency change form 11.8 Hz at temp. 60°C to 13.5 Hz at temp. 90°C. System has change displacement transmissibility characteristic and -10dB system has at 19.5 Hz at temp. 60°C and at temp. 90°C at 21.5 Hz of excitation. Changing value of top of gain on characteristic is probably due to changing of material dissipation in smart spring, but it not be tested very precise.

a)   b)
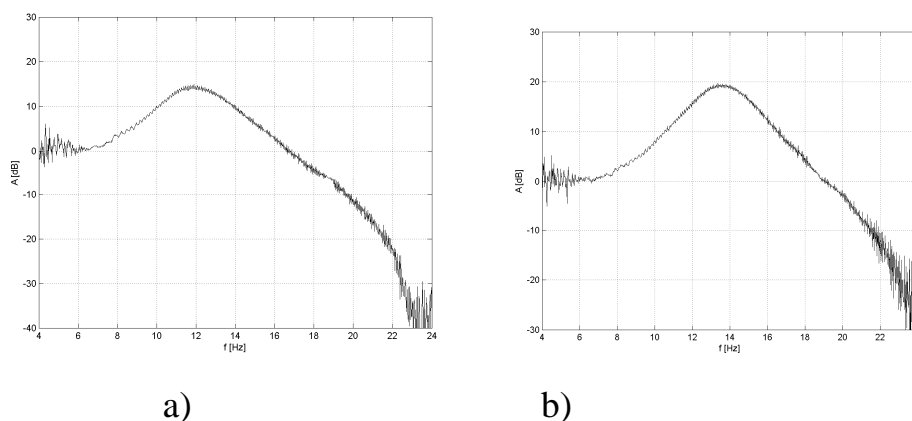
Fig. 2. Displacement transmissibility characteristics vs. frequency for the springs at temperature 60°C (a) and 90°C (b).

3. Dynamic Vibration Absorber

This vibration absorber was first invented in 1909. The smart springs are used in vibration absorber. Smart springs are used between protected mass m_1

and m_2 mass of the vibration absorber. For reduction the vibrations of the main mass, the vibration absorber has to be tuned to the frequency of excitations [3], in other words the natural frequency (ω_o) of the absorber must be same with frequency of excitations ω. Thus the vibration absorber suppresses the mono-harmonic excitations. Vibration of the mass m_1 might be reduced even to zero as long as there is only one disturbance frequency to which the Frahm's absorber theoretically might be tuned (ω_o) and the frequency of excitations is near ω_o. At frequencies vastly differing from ω_o, the reduction performance will be decidedly lower. It is worthwhile to mention that the frequency of excitations must not change since the classical vibration absorber is not capable of tuning to variable frequency. Vibration reduction is most effective when the absorber is tuned to the frequency of excitations, nevertheless in practical applications this frequency is often varied. In case of a SMA spring with a controlled stiffness, we make use of the fact that the Young modulus for austenite is twice as big as for martensite. When spring temperature is changed (for instant due to current flow thru spring), the stiffness coefficient can be easily controlled.

Vibration absorber was built in laboratory and was tested. Chosen frequency characteristics are presented on Fig. 4a and 4b. This are characteristics of vibration propagation from excitation to protected mass.

a)   b)

Fig. 4. Displacement transmissibility characteristics vs. frequency of smart absorber for springs temperature 70°C (a) 90°C (b)

It is readily apparent that the vibrations which are reduced the best are changing thru changing of temperature of the smart spring. System has not bad displacement transmissibility characteristics (-30dB). This is caused by dissipation of vibration energy too. It is probably due to substantial friction in

material of smart spring, but it not be tested very precise.

Summary

The paper is concerned with application of SMA materials in SDOF vibration isolation system and vibration absorber. Such laboratory systems in which a smart spring were occupied were build and tested. These vibration isolation systems could change the range of effective damping through changing their properties. The systems are capable of changing their dynamic characteristics, so it is possible to tune them to properties of excitation. Thus modified vibration isolation system will increase the range of effective reduction through extending the frequency range to which they can be tuned.

References:

1. Rączka W., Sibielak M., Konieczny J.: Smart vibration isolation systems with shape memory alloy // proceedings of 7th International Carpathian Control Conference Czech Republic (2006)

2. Konieczny J., Rączka W., Sibielak M.: Experimental investigation of the semi-active vibration isolation system // proceedings of 9th Conference on Active noise and vibration control methods Krakow–Zakopane, Poland, May 24–27, 2009

3. Rączka W.: Testing of a spring with controllable stiffness. // proceedings of 9th International Carpathian Control Conference Romania, May 25–28, (2008) pp. 543–546

4. Otsuka K., Wayman C.M.: Shape Memory Materials, Cambridge, 1998.

5. Rączka W.: Controlled SMA spring in Frahm's vibration absorber. // Mechanics 22 AGH University of Science and Technology (2003)

6. Rączka W., Konieczny J., Sibielak M.: Mathematical Model of a Shape Memory Alloy Spring Intended for Vibration Reduction Systems // Solid State Phenomena Vol. 177 (2011) pp 65-75

3. TECHNOLOGY MANAGEMENT OF QUALITY AND STRENGTH OF ENGINEERING STRUCTURES

3.1 QUALITY OF THE SURFACE AFTER MECHANICAL PROCESSING

3.1.1 TOPOGRAPHIC PARAMETERS OF SURFACE AFTER EDM AND THEIR INFLUENCE ON WEAR PROCESS

Matuszewski M.[1]

Introduction

A lot of conducted investigations, e.g. [7, 9] indicate that from features of surface layer (SL), generated as effect of realization of assumed technological process, depend the course of wear process - its mechanism, intensity and results.

In References sources it is possible to find the numerous definitions of surface layer. Though, sometimes they are differ, the essence of surface layer is always the same. According to fundamental work [2], as the surface layer is understood the material points set which are placed between the external surface and the conventional one, being the border of feature values changes of subsurface zone, caused as the result of the external extortion such as: pressure, temperature, chemical and electric factors, bombardment of the charged particles and electrically indifferent ones. The other part of the object's material beyond the surface layer is the matrix. In Polish Standard [6] the definition of surface layer is nearing and following: "The surface layer is the layer of material limited by real surface of object, including this surface, as well as the part of material deep from real surface, which shows the altered physical features and sometimes chemical ones, in relation to features of this material up-object".

Because the external part of SL is the surface of elements, described among other by parameters of surface geometrical structure (SGS), thus on above mentioned wear process influence has also its topography [5]. This structure is formed by the unevenness of the surface the eminences and the

---

[1] University of Technology and Life Sciences, Bydgoszcz, Poland

depressions as the results of either realized machining and the wear process. As far as, the placement of characteristic elements of geometric structure of the surface is concerned, the surface have the anisotropic or isotropic character.

Elements' surface layer, generated from the beginning of their manufacturing process of machine elements to its end is called technologic surface layer (TSL), however, the surface layer elements of machine kinematical pairs during operational process, under external loads, is called service generated layer (SGL).

1. Structural elements of surface

To basic quantities which describe SGS one ranks: set of roughness parameters, texture direction, waviness, shape errors and possible defects on surface. The influence of individual quantities on the wear process is diverse. The greatest influence on tribologic characteristics of co-operating surfaces of machine elements have two first above mentioned parameters. The influence of remaining parameters is not so essential for course and description of process of operating, additionally, meaning of these quantities in every working conditions is not the same. Different is also level of acquaintance of these problems. On the ground of References study it was affirmed that the best known, and in References reports the most extensively described, are different parameters of roughness and relation between state of surface layer described by them and intensity of wear process. Doubtlessly they are essential for both, conformal and non-conformal contact areas of co-operating surfaces. Comparatively least are the information relating dependences of course of SGL transformation on parameters which are the measure of texture direction of SGS.

Knowledge of mechanisms and regularity of wear process of friction pair makes possible to control of processes: technological and operational, so the changes in surface layer would minimum and ensure the longest time of work with unchanged, constructively assumed the features of kinematical pairs.

The satisfying machining accuracy and roughness are obtained in the case of erosive machining with assumed tribologic criteria. Roughness, obtained in electroerosive machining depend on many factors, e.g.: current intensity, impulse time, propriety of material of electrodes and workpiece, as well as kind of used dielectric liquids and others.

In consideration of minimization of frictions, and the same - resistances to motion, one of possible way is obtaining the smallest value of roughness parameters. By means of the erosive machining it is possible to get the roughness parameters of machined surfaces in the range of several micrometers, even to several decimal parts of micrometer [1, 4, 8].

Second factor which significantly influences on usable features of erosive machined surface of machine elements, i.e. texture direction of structure, exists only in principle in the case of hybrid machining. Machining tracks are visible on each machined surfaces. Obtained surface have character anisotropic or isotropic character – Figs. 1 and 2. The anisotropy of surface is visible particularly for connection of erosive with mechanical machining, see Fig. 1.

The clearest texture direction of structure one obtained by means of mechanical machining – abrasive honing (Fig. 1b), but after electrochemical-abrasive honing visible machining traces are obtained too. The surface texture direction is in close relation to kinematics of tool. In one-way honing case surfaces with orthotropic structure which have got perpendicular or horizontal scratch, in dependence on kind of honing, suitably: longitudinal or transverse. In the case of two-way honing structure with intersecting machining traces are obtained. Angle of their intersecting is contained in the range from 0° to 180° and it depends on kinematics of tool.

The surface structure after contactless machining processes sometimes has also texture direction which is consequential to previous machining operation, e.g.: electrochemical polished surface have machining traces after proceeded grinding [4].
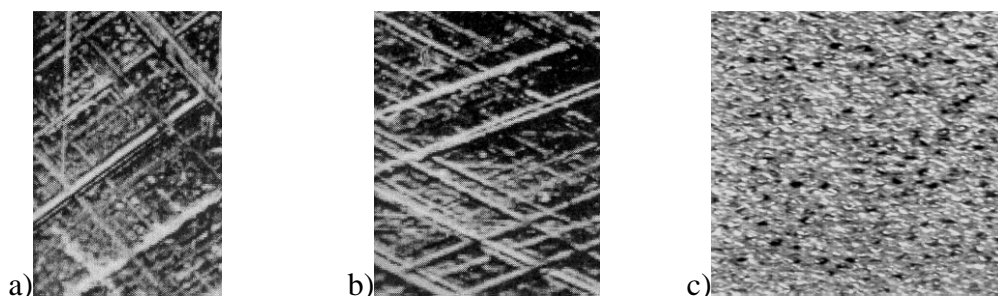
Fig.1. Geometric structure of surfaces machined by means of: a) electrochemical – abrasive honing, b) abrasive honing, c) EDM

In the case of „clean" erosive processes, surfaces in principle have got isotropic character, thus they have not clear texture direction – see Fig. 1c. It is result of stochastic character of process.

The parameters of the same kind of process influenced also SGS. In Fig. 2 surfaces machined of EDM with different parameters of erosive process are shown. They also confirm last observation.

a) b)
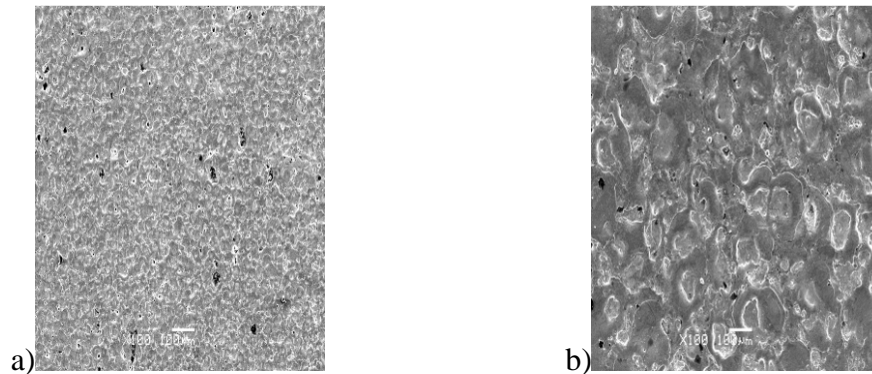
Fig. 2. Geometric structure of surfaces machined by means of EDM with different parameters: a) current intensity $I = 1$ A, impulse time $t_i = 3,2$ μs, break-time $t_p = 6,4$ μs; b) current intensity $I = 6$ A, impulse time $t_i = 100$ μs, break-time $t_p = 50$ μs

On above pictures is clearly visible, that the assumed technology has the essential influence on received SGS. It is possible to notice, that the change of basic parameters, such above mentioned, causes the change of shape and distribution of machining traces on surface.

2. Influence of sgs character on wear process

The surface layer, correctly generate in manufacturing processes of machine elements, assures maximum resistance to results of wear process. The same, it is the factor which ensures long operational durability of co-operating elements of friction pairs. As earlier mentioned, for wear process the essential element of SGS is its texture direction, particularly for conformal contact of co-operating surfaces of kinematical pair elements.

2.1. Aim and methodology of experimental investigations

Assumption of experimental investigations was to qualify the influence of distribution and the orientation of the machining traces after erosive processing, which next depend on kind of machining process, as well as the assumed its

parameters, on intensity of wear process of examined surfaces. They were conducted in two-ways, i.e. the first part of studied surfaces had anisotropic character, obtained as result of electro-erosive-abrasive honing, however second part – isotropic – after EDM. These surfaces co-operated with counter sample which structure had anisotropic character - oriented machining traces were visible.

In order to realization of the aim of investigations special test stand was design and made – Fig.3.

In the case when structure of samples surfaces had anisotropic character, relative movement of counter sample was reciprocating (Fig. 3a), however, in the case of isotropic structures of surface relative movement was oscillative (Fig. 3b).

In variant I (Fig. 3a) tested sample (1) is motionless and is connected to the base, however counter-sample (2) – reciprocating motion received by means of slider crank mechanism (3). Association (fit) of sample regard counter-sample is H7/f6. In variant II (Fig. 3b) in locating bush (3) three samples (2) are fixed motionlessly, which co-operated with oscillating counter-sample (1). The load of samples is realized by spring tension. This way pressure of counter-sample to tested samples is realized by tension force 450 N, which fulfils the theoretical pressures 1,5 MPa in contact area.
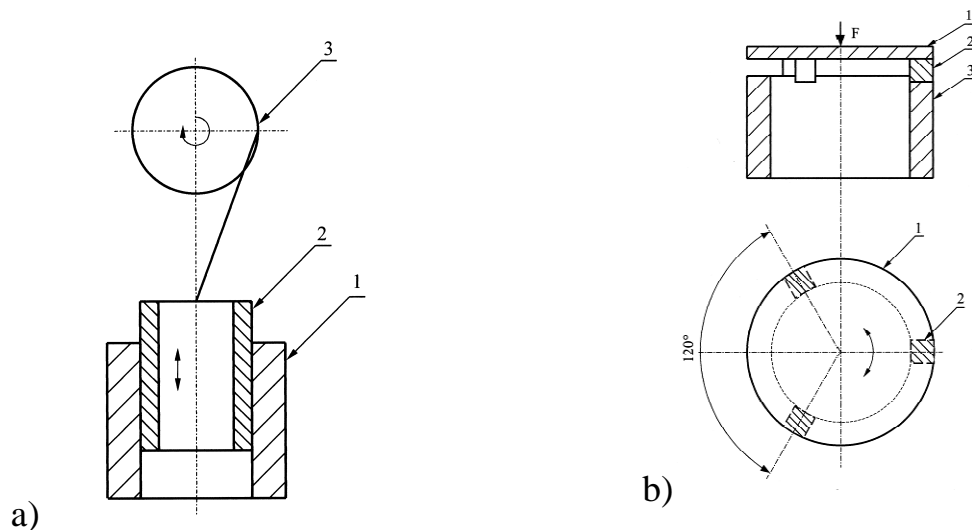
Fig. 3. Idea of co-operation of frictional surfaces during experiments; movement of counter--sample is given: a) reciprocating, b) oscillative

The changes of state of surface geometrical structure for anisotropic structures were observed for three values of angles (α) of machining traces intersection (the angle of honing): $\alpha = 0°$ – one-way transverse honing, $\alpha = 45°$ – two-way honing, and $\alpha = 180°$ – one-way longitudinal honing. For isotropic structures observation of this wear process was conducted for two different structures which were characterized by different values of initial roughness.

The samples for first variant were made of steel C45 and characterized by hardness 30 HRC, the counter sample – of steel 41Cr4, hardness 60 HRC. For second variant material of samples is the also steel C45, and counter sample – the steel 102Cr6, Their hardness were respectively: 40 and 60 HRC. In both variants hardness of counter samples were decidedly greater than hardness of samples. It is in order the changes of state of surface geometrical structure will happen first of all in surface layer of samples.

In both cases the samples co-operated with counter-samples in lubricant – the machine oil. The velocity of relative movement during investigations for first case was 0,017 m·s^{-1}, and for second – it was 0,05 m·s^{-1}.

2.2. Results of experimental investigations

In Figs. 4 and 5 the results of preliminary investigations in form of graphs were presented. The change of SGS state is described by value of the change of roughness parameter *Ra* in function of friction way.
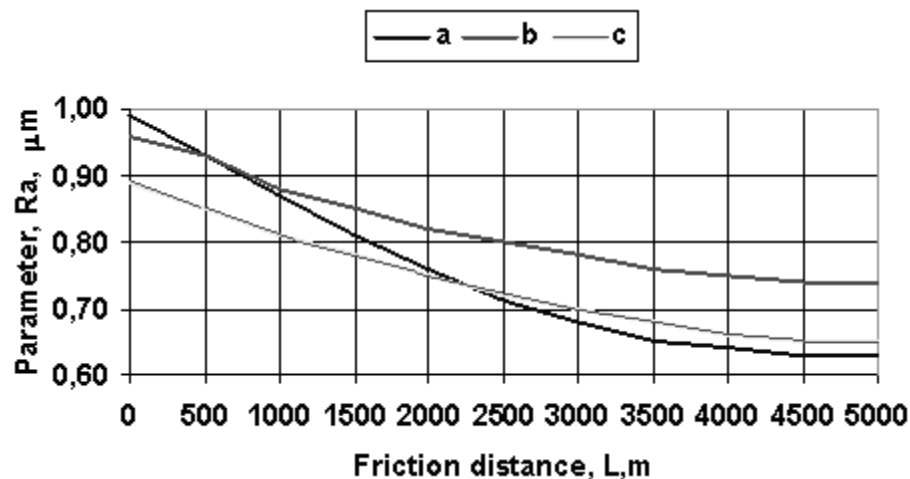
Fig. 4. The values of roughness parameter *Ra* in function of the friction way for following intersection angles of the traces after processes: a) $\alpha = 0°$, b) $\alpha = 45°$, c) $\alpha = 180°$ (kind of machining process is described above)

From carried out investigations results, that the angles (*α*) of machining traces intersection influenced roughness parameter *Ra*. The greatest changes happen for angle 0°, however the smallest – for angle 180°. For all, three co-operation conditions it is possible to observe that the intensive changes of roughness parameter value happened in initial period, and in next periods follows decrease of intensity of these changes and stabilization was observed. This is comfortable with expected mechanism of wear process.

In this graph, similarly for introduced above, the intensive character of changes is visible at the beginning of co-operation, later – with growth of friction way – follows the decreasing of changes and, on the ending – stabilization of process. For structure with smaller value of initial roughness, stabilization follows more quickly, as well as the changes of parameter roughness values are smaller than for structure characterized by larger initial roughness.
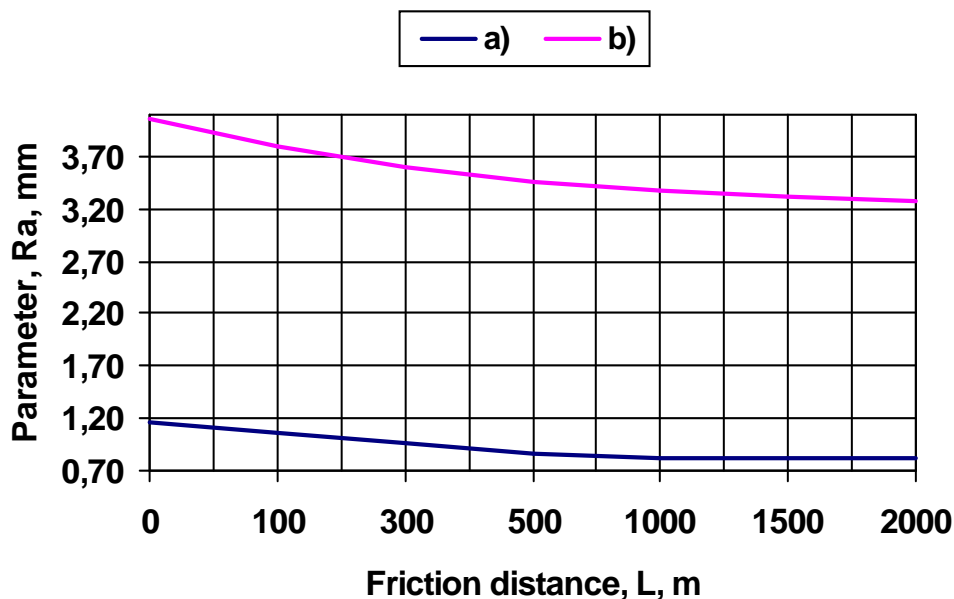
Fig. 5. The values of roughness parameter *Ra* in function of friction way of for isotropic structures with following values of initial roughness: a) *Ra* = 1,16 μm; b) *Ra* = 4,06 μm

In investigations mass decrement which accompanied to SGS changes were observed too. Relationships which describe gradient of roughness parameter changes is also worked out.

Conclusions

Conducted experimental investigations show that the intensity of wear process depends on features of geometrical structure of surface which are generate at a stage of production.

The results of investigations extended the knowledge about mechanisms of wear process of surfaces of kinematical pairs elements.

Studying mechanisms and relations which occur during destruction of friction pairs, it will be possible to choose optimum (for tribologic criteria) machining process in consideration of traces distribution after machining.

The obtained features of surface layer should assure during operation the minimum changes in surface layer, and also the longest period of work with unchanged, constructively assumed features of frictional pairs.

References

1. Budzyński A.F., Zakościelny St.: Research Concern Abrasiveness and Grindability of ECH Honing Surfaces. Proceedings of EM'82. Bydgoszcz 1982, pp. 16÷21 (in Polish).

2. Burakowski T., Wierzchoń T.: Engineering of Surface of Metals. WNT, Warszawa 1995 (in Polish).

3. Matuszewski M., Styp-Rekowski M.: Significance Meaning of Texture Direction of Surfaces' Geometric Structure for Course of Wear Process. International Journal of Applied Mechanics and Engineering, vol. 9/2004, pp. 111÷116.

4. Oczoś K.E., Lubimov V.: Geometrical Structure of Surfaces. Rzeszów Technical University Publishers, Rzeszów 2003 (in Polish).

5. Pawlus P.: Surface topography, measurement, analysis, influence. Rzeszów Technical University Publishers, Rzeszów 2006 (in Polish).

6. Standard PN-87/M-04250: The surface layer. Terminology (in Polish).

7. Styp-Rekowski M.: Significance of Constructional Features for Angular Ball Bearings Life. Scientific Number of Technical and Agricultural University, series Dissertations, No. 103, Bydgoszcz 2001 (in Polish).

8. Tomczak J.: Dielectric Fluids for EDM. Proceedings of EM'90. Bydgoszcz 1990, pp. 239÷248 (in Polish).

9. Tomczak J.: Electrolytical Polishing. Proceedings of EM'90. Bydgoszcz 1990, pp. 249÷258 (in Polish).

10. Żurowski W., Sadowski J.: Research on Maximal Resistance of Metallic Body Systems to Tribological Wear. Inżynieria Powierzchni nr 1/2001, pp. 41÷55 (in Polish).

3.1.2 GEOMETRICAL MICROSTRUCTURE OF SURFACE MILLED WITH A BALL-END CUTTER AT A CNC MILLING MACHINE

Miko E.[1]

Introduction

Higher and higher accuracy of metal cutting, especially by turning and milling, causes that machined surfaces often do not require further finishing, which indirectly affects the operating properties of a product. Recently, a number of producers have replaced polishing of certain elements with first casting or forging and then turning or milling them to obtain the final dimensions and surface finishing by means of tools with ceramic and CBN wedges [1]. The constitution of the geometrical structure and the properties of the superficial layer generated by chip milling are important problems and, therefore, require further theoretical and experimental investigations. An important feature of the superficial layer quality is its roughness [2,3].

High speed tracer milling (HSM) and contour milling performed by means of numerically controlled (CNC) milling machines are commonly used in the manufacturing of elements with complex shapes, such as casting and injection moulds, matrixes, blanking and press-forming dies, turbine blades, screw propellers and others [4, 5]. One of the most popular methods of milling is machining with a ball-end cutter, which enables, for example, full form contouring on a CNC or tracer machine. No replacement of the tool is necessary, so the set-up and machining time is much shorter. In the case of a 3-axis milling machine, it is desirable to use ball-end cutters, which permit quite different tool orientation in relation to the workpiece and, accordingly, machining a surface with complex 3D shapes [6]. Moreover, it would be essential to plan an effective (optimal) tool path for cutting, especially during 3-axis milling of a 3D curvilinear surface. Milling with a ball-end cutter allows obtaining high geometrical surface quality. Also, this type of milling can be applied to tasks once performed by EDMs (milling of hardened materials or indenting). Therefore, machining with ball-end cutters has become the scope of interest of

---

[1] Kielce university of Technology, Poland

many researchers and production engineers [7-10]. A ball-end cutter is indispensable in machining of surfaces inclined at a large angle [11].

At present, it is required that form and dimensional accuracy should be higher and surface roughness smaller, therefore face milling is being more and more frequently applied as a final treatment [3]. Milling with a ball-end cutter can be used as finishing of machine parts, if the requirements concerning surface quality are lower. Of significance are also the geometrical structure and the size of irregularities when a machined surface is subjected to further treatment. The above factors will affect the machining time and related costs. In order to reduce high labour consumption of finishing (usually manual polishing) [4], it is advisable to reduce as much as possible surface irregularities after milling.

For these reasons, the investigations often focused on the evaluation of the influence of machining factors on roughness of surfaces machined with a ball-end cutter. Due to the fact that the surface geometrical structure obtained after machining was non-homogeneous, the surfaces had to be evaluated using a scanning microscope. Measurements of longitudinal and lateral roughness were also useful. Besides, the frequency of longitudinal and lateral profiles of milled surfaces was analysed.

1. The research subject, range and methodology

The aim of the research is to analyse the influence of selected machining factors on the roughness of surfaces milled with ball-end cutters on a CNC milling machine.

The samples were machined applying the parameters given in Table 1. The machining was performed by changing one of the milling conditions, i.e. feed f_z, tool path interval f_w or rotational speed n and, accordingly, cutting speed v_c, and by milling with an adequate part of the curvilinear edge of the insert.

The samples used in the experiments were made of C45 carbon steel and MO58 brass. Their construction allowed measurement of the longitudinal and lateral roughness.

As soon as the cutting tests were completed and the specimens removed off the machine tool, longitudinal and lateral profiles of the roughness of the machined surface were registered and analysed. In-cut and out-cut milling was performed on a CNC TRIAC 200 milling machine using the Castrol Syntilo

RHS coolant. The applied CNC TRIAC 200 milling machine made by DENFORD was equipped with a 3-axis HEIDENHAIN 360 controller. The machining programs were generated with the MASTERCAM MILL system. Since the machine tool head cannot be turned, the samples were fitted in a specially designed machining holder. This enabled surfacing at 0° and 60° angles, which corresponded to the application of two different parts of the curvilinear edge of the cutter. A Heliball CM D120 ball-end cutter with a CR D12−QF−(IC328) double-edged insert 12 mm in diameter made by ISCAR was used for the machining.

The complex analysis of the geometrical surface structure [3, 9] involved registration and study of the morphology of samples by means of a JEM-540 electron scanning microscope made by the Japanese company JEOL.

Table 1 - Cutting conditions for the studied samples

Cutting conditions	Tool - *Heliball* ball-end cutter made by ISCAR	
	CM D12 CR D120−QF−(IC328) insert	
Sample setting angle	0°	60°
Feed per tooth f_z [mm/tooth]	0.04; 0.08; 0.12; 0.16; 0.20; 0.24	0.02; 0.04; 0.08; 0.12; 0.16; 0.20
Types of milling	In-cut, out-cut	In-cut, out-cut
Workpiece material	45 carbon steel, MO58 brass	
Tool rotational speed n [rpm]	500; 1000; 1750; 2500; 3750; 4000	
Tool path interval f_w [mm]	0.1; 0.3; 0.5; 0.7; 0.9; 1.1	

The research divided into four stages was conducted at the laboratories of the University of Technology in Kielce.

❑ The first part of investigations concerning machining was carried out at the Laboratory of Numerically Controlled Machine Tools, where by means of the MASTERCAM program the geometries of specimens were prepared and CNC machining programs were developed. The programs were transmitted to a CNC TRIAC 200 milling machine, on which most tests, i.e. machining, were performed. Two materials, 45 steel and MO58 brass, were used for machining and other tests.

❑ The next step was to measure the roughness *Ra* using a PM-03 profilometer in a room which satisfied the requirements given in the specifications of the device. Values of the lateral (perpendicular to the feed direction) and longitudinal (parallel to the feed direction) roughness were measured.

❑ At the third stage, the obtained surfaces were observed, evaluated and analysed with respect to the microstereometry achieved by means of an electron scanning microscope. The observed surfaces of brass and steel specimens were registered in the graphical file format that was attached to the investigation results.

❑ Finally, a PM-03 profilographometer was used to register and measure lateral and longitudinal profiles. The POM–16 software was applied to determine the standardised unilateral functions of spectral power density (FSPD) of these profiles.

2. Analysis of results

Figures 1 − 4 show the influence of the studied factors on the lateral and longitudinal roughness *Ra* of 45 carbon steel samples after machining with a ball-end cutter with a diameter of $D_c = 12$ mm.
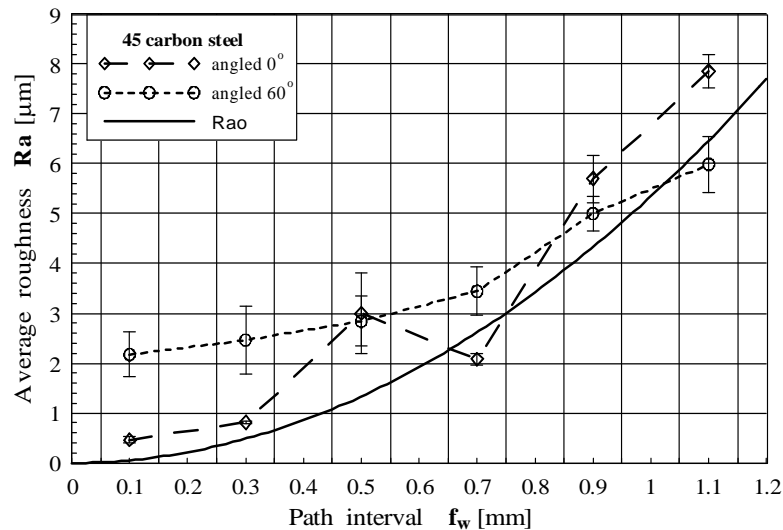
Fig. 1. Influence of the tool path interval f_w on the lateral surface roughness *Ra*. The cutting conditions used were: $a_p = 0.25$ mm, n = 2500 rpm, $f_z = 0.08$ mm/tooth, $D_c = 12$ mm, in-cut milling

An increase in the tool path interval f_w causes an increase in the lateral roughness *Ra* (Fig.1). This figure shows the theoretical values of the parameter Ra_o determined from Eq. (2). One can see that the values measured on surfaces machined at 0° and 60° angles are greater than the theoretical ones. Particularly great discrepancies occur for small tool path intervals f_w. This confirms that other factors, except for the cutter wedge representation, have considerable influence on the roughness of a machined surface. The factors include relative vibrations of the tool and the workpiece, the run-out of the cutter wedge and the plastic strain of the material.
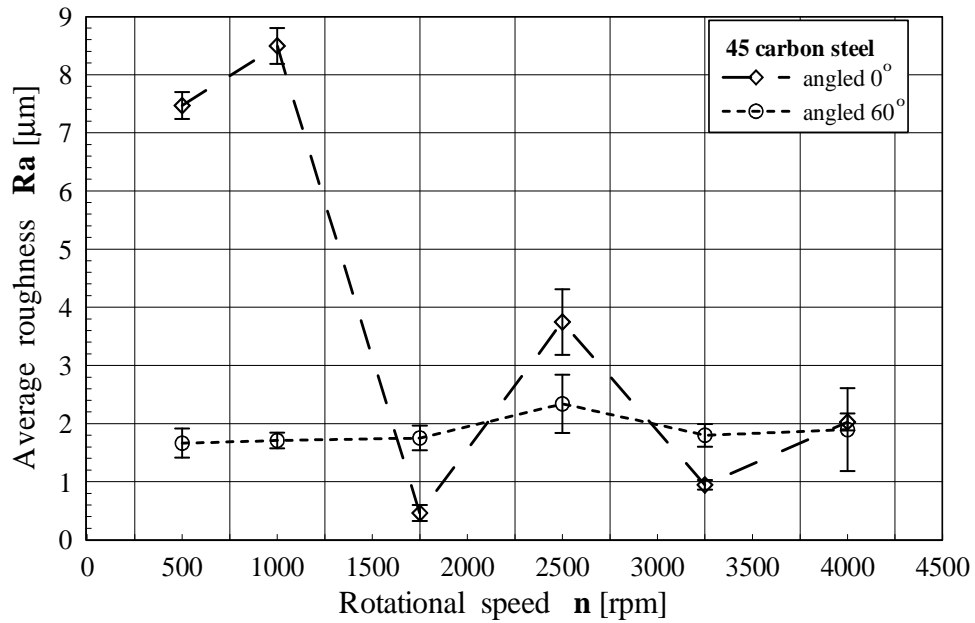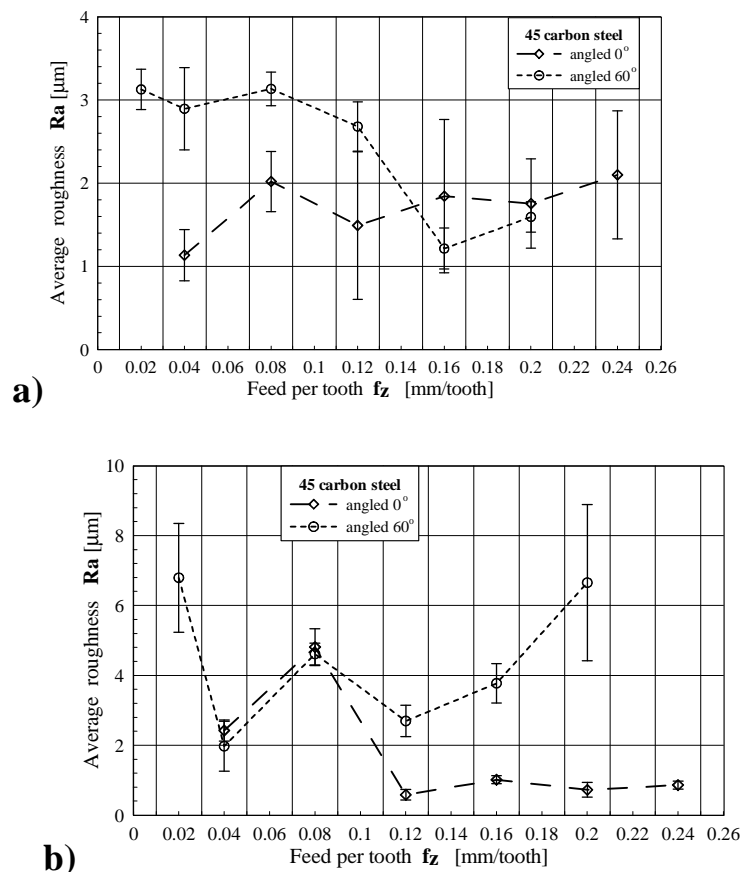
a)

b)
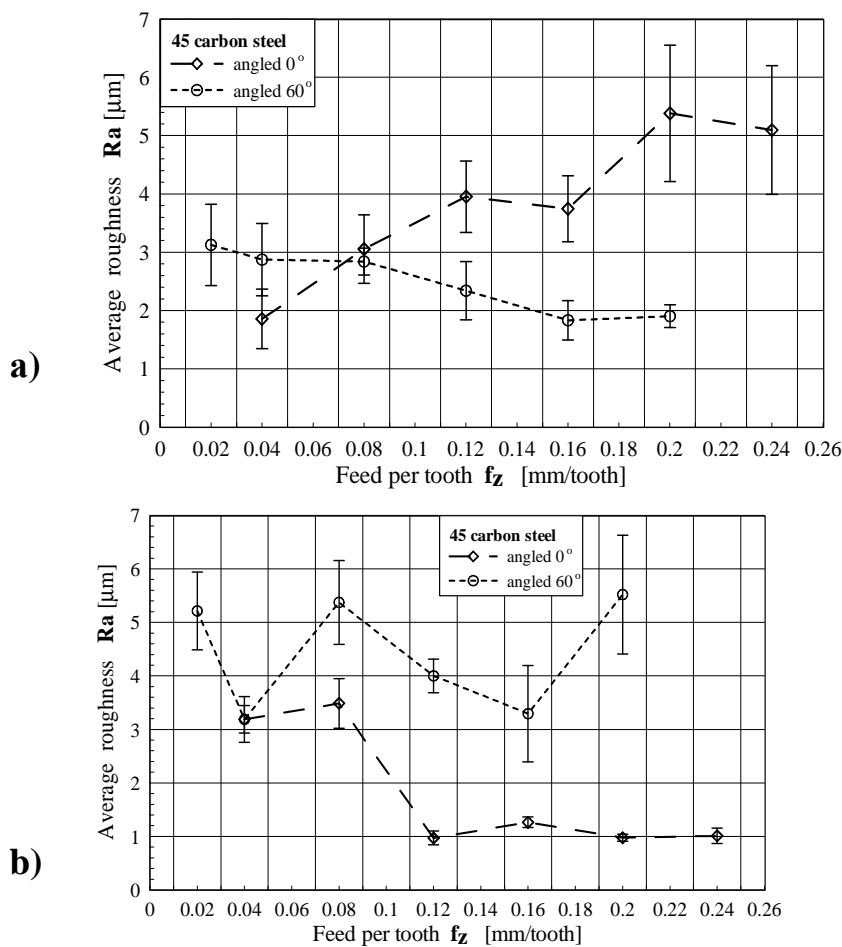
Fig. 2. Influence of the feed f_z on the lateral surface roughness *Ra*. The cutting conditions used were: $f_w = 0.5$ mm, $a_p = 0.25$ mm, n = 2500 rpm, $D_c = 12$ mm; a) in-cut milling; b) out-cut milling

During the in-cut milling of 45 steel, an increase in f_z causes an increase in the lateral roughness *Ra* when the sample is set at $0°$ angle and its decrease at $60°$ (Fig. 2a). During out-cut milling, an increase in f_z results in a decrease in the value of the parameter *Ra* at $0°$ angle; yet no clear influence of f_z is observed at $60°$ angle (Fig. 2b).

The cutter rotational speed *n* has no particular effect on the value of the parameter *Ra* when the angle of setting is $60°$. However, the influence is not clear at the downward trend and $0°$ angle (Fig. 3).

The effect of the feed f_z on the longitudinal roughness *Ra* is not clear during in-cut or out-cut milling (Fig. 4). In most cases, the roughness *Ra* was smaller after milling at $0°$ angle than after milling at $60°$ angle. A completely different situation was observed during milling with a single wedge cutter with a diameter of $D_c = 8$ mm [12]. During milling at $0°$ angle with a double-wedge cutter 12 mm in diameter for a given depth $a_p = 0.25$ mm, only one wedge was used. At $60°$ angle, however, two wedges were used. We can speculate that the increase in the roughness *Ra* was caused by the run-out of the cutter wedges. Despite the fact that at $0°$ angle we have the effect of small cutting speed and its unfavourable influence on the roughness, confirmed during machining with a cutter 8 mm in diameter [12], the increase in roughness was smaller than at machining with a cutter 12 mm in diameter. The roughness was greater only when 45 steel was milled at small values of rotational speed, n = 500 and n = 1000 rpm (Fig. 3), and great feeds at $0°$ angle rather than at $60°$ (Fig. 2b). This was probably due to a build-up edge, which is observed at small cutting speed, and such occurred for those revolutions and the $0°$ setting angle.

Figure 5 shows a photograph of surface morphology of a 45 carbon steel specimen machined with a ball-end cutter with a diameter of $D_c = 12$ mm. The lateral and longitudinal profiles of surface roughness can be seen on the left and at the top respectively.

The presented out-cut milled surface has clear marks resulting from tool paths.

Fig. 3. Influence of the rotational speed *n* on the lateral surface roughness *Ra*. The cutting conditions used were: $f_w = 0.5$ mm, $a_p = 0.25$ mm, $f_z = 0.08$ mm/tooth, $D_c = 12$ mm, in-cut milling

Fig. 4. Influence of the feed *f_z* on the longitudinal surface roughness *Ra*. The cutting conditions used were: $f_w = 0.5$ mm, $a_p = 0.25$ mm, n = 2500 rpm, $D_c = 12$ mm; a) in-cut milling; b) out-cut milling
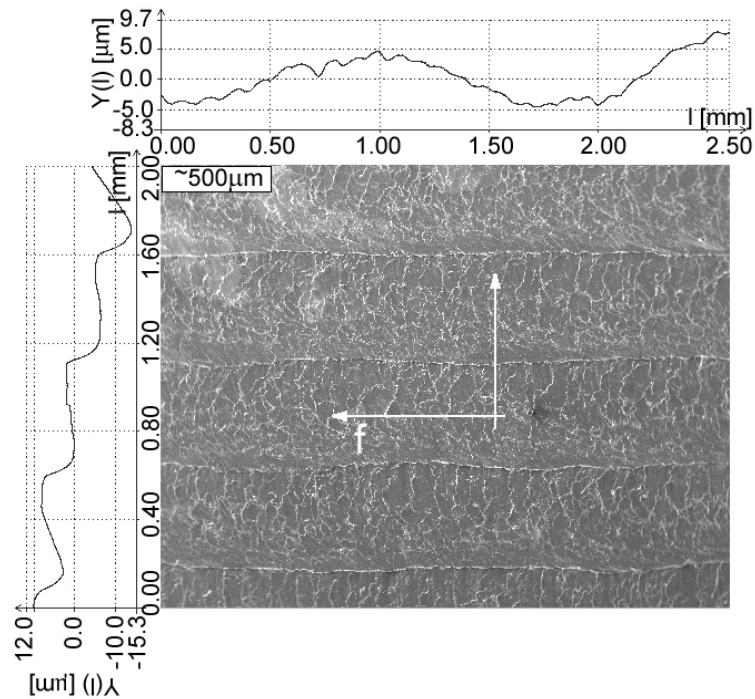
Fig. 5. Morphology and longitudinal and lateral profilograms of a surface machined with a ball-end cutter. The cutting conditions used were: $f_z = 0.04$ mm/tooth, $a_p = 0.25$ mm, $f_w = 0.5$ mm, $D_c = 12$ mm, n = 2500 rpm, 45 steel workpiece material, 0° angle, out-cut milling. Magnification of 50
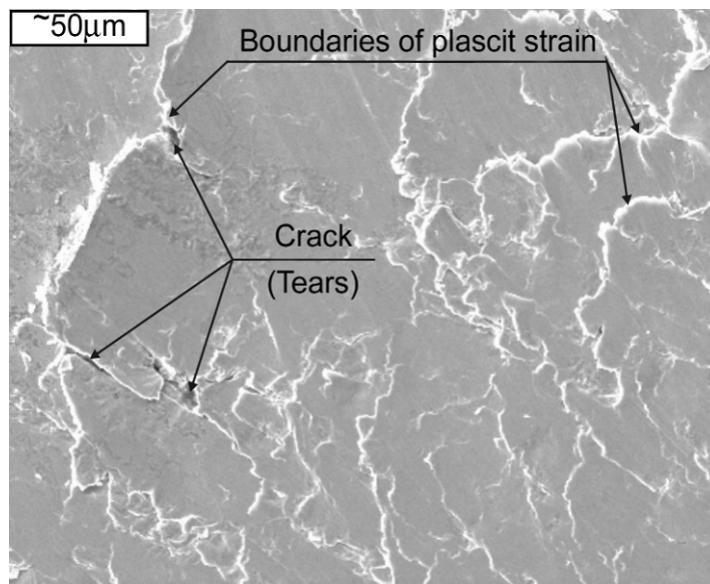
Fig. 6. Surface morphology. The cutting conditions used were: $f_z = 0.2$ mm/tooth, $a_p = 0.25$ mm, $f_w = 0.5$ mm, $D_c = 12$ mm, n = 2500 rpm, 45 steel workpiece material, 0° angle, out-cut milling; magnification of 300

In a lateral profilogram the predominant frequency results from the tool path interval f_w. The value of roughness for this profile is Ra = 3.19 ± 0.26 μm (Fig. 2b). Tool paths and tool marks are also seen and the intervals between them are equal to f_z. In a longitudinal profilogram the predominant frequency corresponds to feed per tooth f_z. The value of the parameter *Ra* for this profile is Ra = 2.42 ± 0.30 μm (Fig. 4b). The frequency analysis of these profiles is shown in Figs. 7 and 8. Also, in Fig. 6, where magnification of 300 was applied, there are tool marks and boundaries of the material flow. Cracks and tears of the workpiece material are also observed.
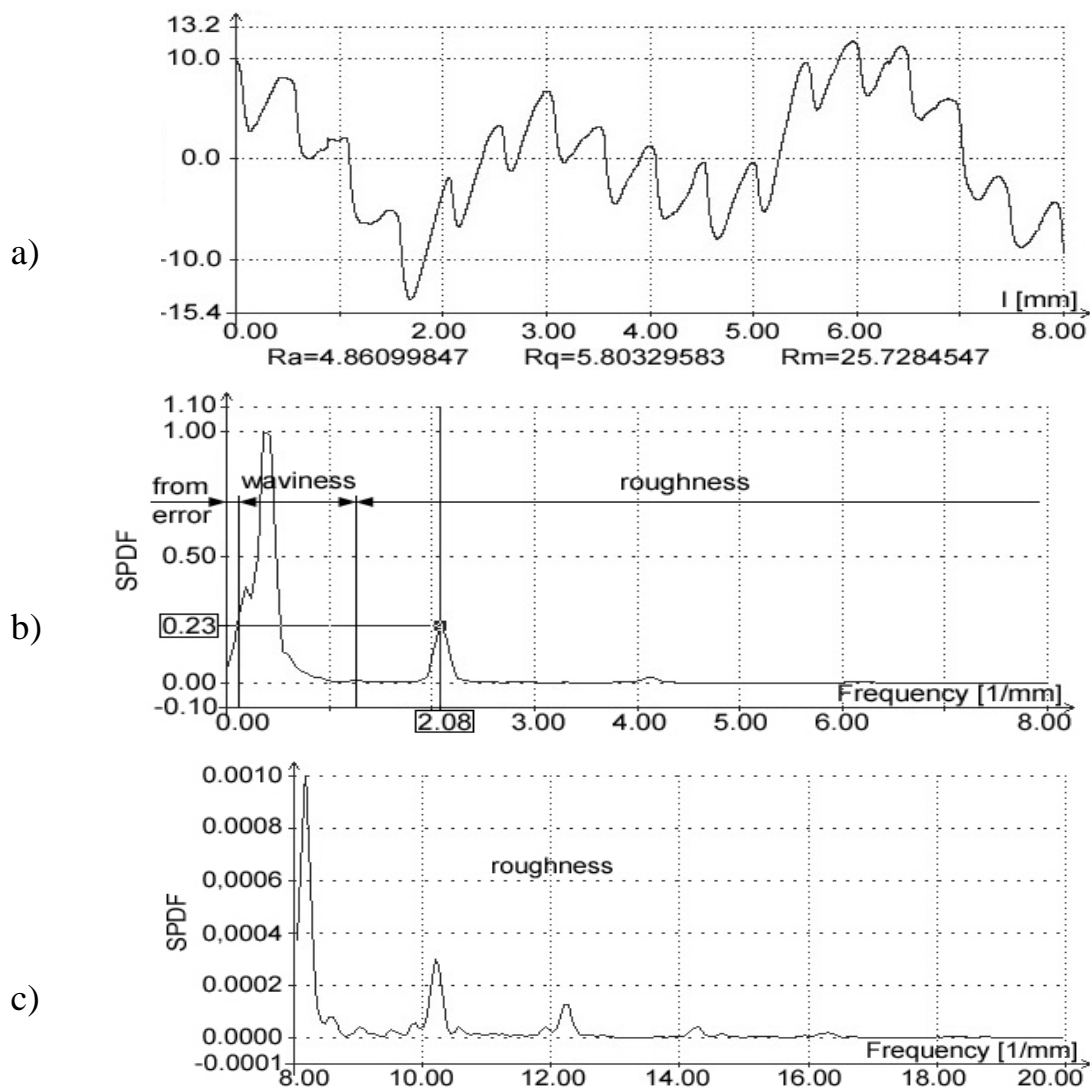
Fig. 7. Lateral profilogram (a) and the corresponding diagram of a standardized unilateral function of spectral power density of a profile (b, c). The cutting conditions used were: f_z = 0,04 mm/ tooth, a_p = 0.25 mm, f_w = 0.5 mm, D_c = 12 mm, n = 2500 rpm, 45 steel workpiece material, 0° angle, out-cut milling
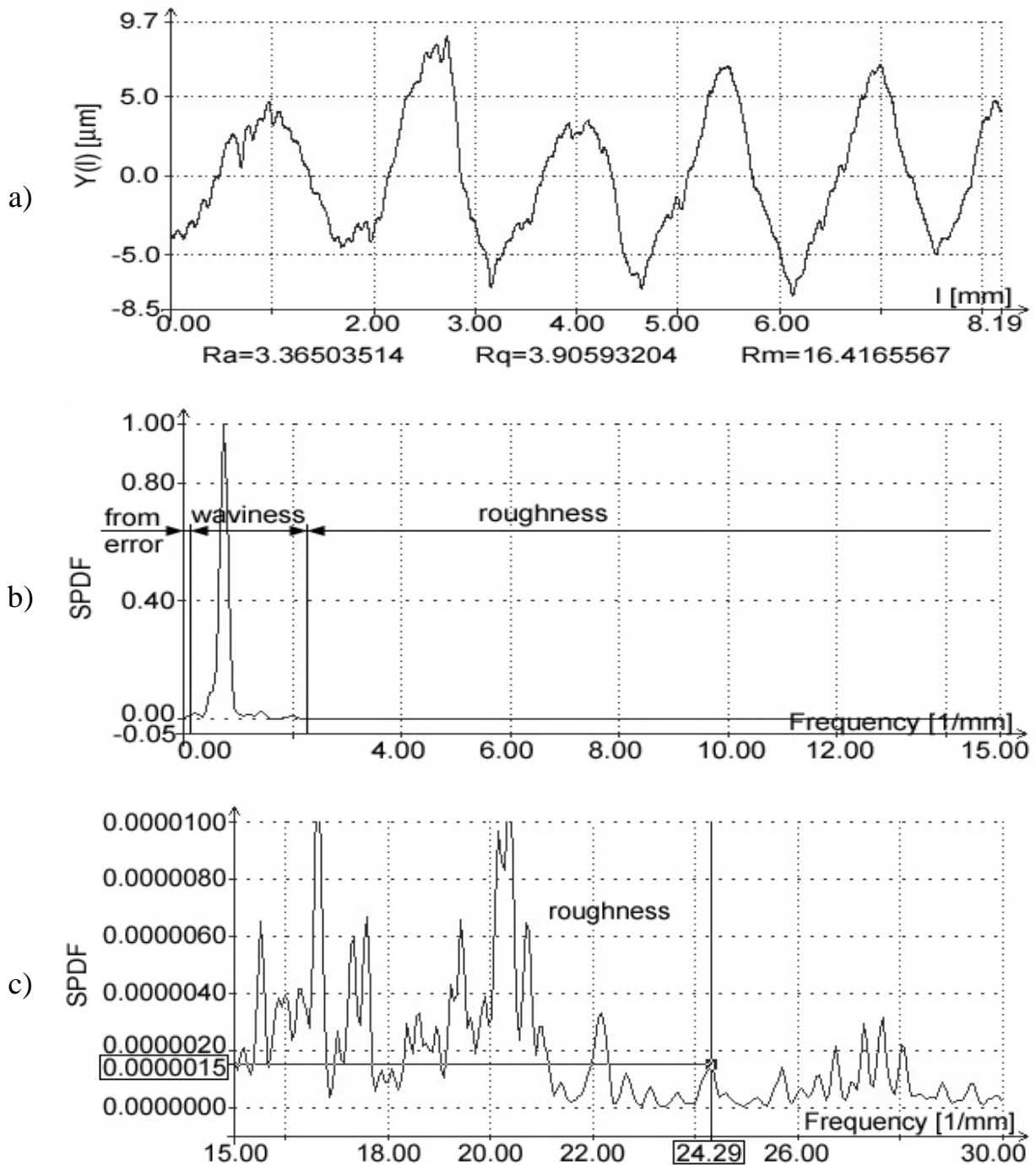
Fig. 8. Longitudinal profilogram (a) and the corresponding diagram of a standardized unilateral function of spectral power density of a profile (b, c). The cutting conditions used were: $f_z = 0.04$ mm/ tooth, $a_p = 0.25$ mm, $f_w = 0.5$ mm, $D_c = 12$ mm, $n = 2500$ rpm, 45 steel workpiece material, 0° angle, out-cut milling

The registered longitudinal and lateral profiles of the microroughness of surfaces milled according to the sampling plan (Table 1) were analysed by determining a standardised unilateral function of spectral power density (FSPD). The investigation results are presented in the form of profilograms and the

corresponding FSPDs (periodograms), which define the profile frequency structure. Besides, in the FSPD diagrams, the ranges corresponding to: form and surface waviness and roughness errors are marked.

Bands corresponding to the tool path interval f_w were identified in the analysed lateral periodograms, whereas bands corresponding to feed per tooth f_z in the longitudinal ones.

Selected investigation results are presented in Figs. 7 and 8. Figure 7 shows a band with a frequency of 2.08 1/mm corresponding to $f_w = 0.5$ mm, which is within the range of roughness. This means that, for the cutting conditions given in Fig. 7, this value of f_w will cause irregularities that are roughness. In Figs. 7b and c subsequent harmonics of this band are seen. The influence of the tool path interval is predominant here.

Figure 8 presents a longitudinal profilogram and its frequency analysis. In Fig. 8b a band with a frequency of 0.8 1/mm situated within the range of waviness can be seen. The surface roughness, as the band indicates, is probably a result of errors of the machine tool table shift caused by the waviness of the shears of a Triac 200 milling machine. In Fig. 8c a band with a frequency of 24.29 1/mm was identified, which corresponds to feed per tooth of $f_z = 0.04$ mm/tooth. This figure shows a random character of the spectrum.

Conclusions

The comparative studies of the in-cut and out-cut ball-end milling using a cutter with a diameter of Dc = 12 mm revealed that surface irregularities were smaller after in-cut milling.

Actually, when the diameter of the cutter is $D_c = 12$ mm, smaller irregularities *Ra* are observed at 0° angle (milling with the cutter tip) than at 60° angle (milling with the cutter sides). We can speculate that the increase in roughness during milling with the cutter sides is probably caused by the run-out of the cutter wedges, which does not occur during milling with the cutter tip because, for such a setting and depth of cut $a_p = 0.5$ mm, only one wedge is used. During milling with the cutter tip the effect of small cutting speed is observed. It has unfavourable influence on the surface roughness. In most cases, the effect of the run-out of the cutter wedges predominated over the effect of

small cutting speed, hence the irregularities of surfaces milled with the cutter sides were usually greater than of those milled with the cutter tip.

In the diagrams of the function of spectral power density of lateral profiles there are bands with a frequency corresponding to the value of the tool path interval and their subsequent harmonics. In the diagrams of the function of spectral power density of longitudinal profiles there are bands with a frequency corresponding to the value of feed per tooth. In the diagrams we can also see a spectrum of a random character representing the influence of other factors of the machining system and the tool.

The photographs of the machined surface present results of morphological investigations, i.e. influence of a change of particular parameters (f_z, f_w, n) on the character of the machined surface.

The photographs, where the feed was the key parameter include, except for the evaluated surface, longitudinal and lateral profiles testifying to difficult cutting conditions. In the photographs showing milling with the cutter tip (0° angle) there are clear grooves (i.e. tool marks with unremoved material fragments and tears along the edges. This is caused by unfavourable cutting conditions near the tip, where the cutting speed is close to zero.

References

1. Jang D. Y., Choi Y. G., Kim H. G., Hsiao, A.: Study of the correlation between surface roughness and cutting vibrations to develop an on-line roughness measuring technique in hard turning. International Journal of Machine Tools and Manufacture, vol. 36, Nr 4, 1996, s. 453 – 464.

2. Aronson R. B.: Surface Finish is the Key to Quality, Manufacturing Engineering, August 2001.

3. Nowicki B.: Struktura geometryczna – chropowatość i falistość powierzchni. WNT Warszawa, 1991.

4. Nowicki B: Automatyzacja obróbki wykańczającej powierzchni krzywoliniowych. Mechanik, nr 1, 1995, s. 5 – 9.

5. Altintas Y., Lee P.: Mechanics and dynamics of ball end milling. Transactions of ASME, Journal of Manufacturing Science and Engineering, vol. 120, 1998, s. 684 – 692.

6. Altintas Y., Lee P: A general mechanics and dynamics model for helical end mills. Annals of the CIRP, vol. 45/1, 1996, s. 59 – 64.

7. Lim E. M., Menq CH. H.: The prediction of dimensional error for sculptured surface productions using the Ball- end milling process. Part 2: Surface generation model and experimental verification. International Journal of Machine Tools & Manufakture, vol. 35, nr 8, 1995, s. 1171 − 1185.

8. Lin R., Koren Y.: Efficient tool − path planning for machining free − form surfaces. Transactions of the ASME, Journal of Manufacturing Science and Engineering, vol. 118, 1996, s. 20 − 28.

9. Naito K., Ogo K., Konaga T., Abe T., Kanda K., Matsuoka K.: Development of ball end milling for fine, high-efficiency finishing. International Journal of the Japan Society for Precisioning Engineering, vol. 28, nr 2, 1994, s. 105 − 110.

10. Olejarczyk K.: Frezowanie łopatek narzędziami z ostrzami cermetalowymi i z regularnego azotku boru. Mat. konf. I Forum prac badawczych „Kształtowanie części maszyn przez usuwanie materiału" Koszalin 1994, s. 168 − 174.

11. Chu C. N., Kim S. Y., Lee J. M., Kim B. H.: Feed – rate optimization of ball end milling considering local shape features. Annals of the CIRP, vol. 46/1, 1997.

12. Miko E: Investigation into the surface finish in milling using a ball nose end mill. Advances in manufacturing science and technology, 25(2001)3, s. 71 − 86.

3.2 HARDNESS OF SURFACE

3.2.1 SELECTED TRIBOLOGICAL PROPERTIES OF NANOSTRUCTURED HVOF SPRAYED COMPOSITE COATINGS

Żórawski W[1]

Introduction

Nowadays nanostructured materials are of particular scientific interest because of their physical and mechanical properties, which are superior to those of conventional materials. They are more widely used in various industrial applications [1,2] mainly due to decreasing production costs. The most common processes applied to fabricate nanostructured materials involve atomic or molecular layer deposition, e.g. Physical Vapour Deposition (PVD), Chemical Vapour Deposition (CVD) or sol-gel techniques. An advantage of the process is that the coatings possess very good properties. Disadvantages include small efficiency and high cost [3, 4]. The study of nanostructured materials has been

[1] Kielce University of Technology, Poland

extended to coatings processed using the thermal spray technique. The possibility of making coatings with superior properties (e.g. wear resistance) when compared to the conventional thermal spray coatings currently available opens a wide range of research opportunities for different materials. In thermal spray processes, materials in wire or powder form are fed into a flame, arc or plasma spray gun, where they are fully or partially melted and accelerated in a gas stream toward a substrate to be coated. Nanostructured materials cannot be fed directly into the spray guns. They are deposited in the form of suspension or powders, whose grains are agglomerated nanocrystals [5-8]. Although the coatings produced by thermal spraying posses numerous defects such as pores and microcracs, the process efficiency is much higher and the costs are considerably lower, compared to those of the other processes. It is thus possible to use this technique on an industrial scale. Tungsten carbide, characterized by high hardness and toughness, is a material commonly applied in industry. It is particularly suitable for cutting tools and machine parts, which need to be highly resistant to wear. The use of tungsten carbide, as a material with excellent properties, increased with the introduction of the process of detonation spraying in the 1950s, despite the fact that the method did not become widespread for commercial reasons. Coatings deposited by plasma spraying have properties inferior to sintered materials. This is due to the high temperature of the plasma stream and the presence of oxygen, which leads to phase transitions in the sprayed powder. A rapid development of coating processes took place in the early 80s, when Browning Engineering introduced the high-velocity oxyfuel (HVOF) process [9,10]. Therefore nanostructured WC-Co coatings are of particular scientific interest because of their physical and mechanical properties, which are superior to those of conventional materials. Tungsten carbide coatings were deposited by using the atmospheric plasma spray (APS) or D-gun process or the high velocity oxy-fuel (HVOF) process. The high temperature of the APS process caused decarburization of tungsten monocarbide to W_2C and occurrence of metallic tungsten. The phenomena can be described by the following reactions [11]:

$$2WC \rightarrow W_2C + C$$
$$W_2C \rightarrow 2W + C$$
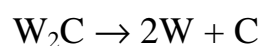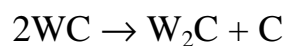
There was a considerable decrease in the amount of carbon due to the coating oxidation in the flame, which can be described by the following reaction:

$$2C + O_2 \rightarrow 2CO \text{ (gas)}$$
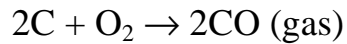
All these processes are dependent on the thermal spray parameters; they have a significant influence on the coating wear resistance. The D-gun process is a method that yields coatings with excellent properties; however, it is expensive to operate. The high velocity oxy-fuel (HVOF) process is one of the most popular thermal spray technologies. The HVOF process possesses advantages over APS such as high particle velocities and lower temperature of spraying stream, producing more densely coating with reduced formation of detrimental reaction products. HVOF differs from conventional flame spraying as it applies considerably higher velocities of the combustion gases. The acceleration of the powder particles fed into a HVOF gun is also higher, roughly 650 m/s for modern equipment. The very high kinetic energy of particles striking the substrate surface does not require the particles to be fully molten to form high quality HVOF coatings. This is certainly an advantage for the carbide cermet type coatings and is where this process really excels. The High Velocity Oxy-Liquid Fuel (HVOFL) spraying systems are a new generation of hypersonic spraying systems, where velocity and temperature of the sprayed particles are better controlled (Fig. 1).
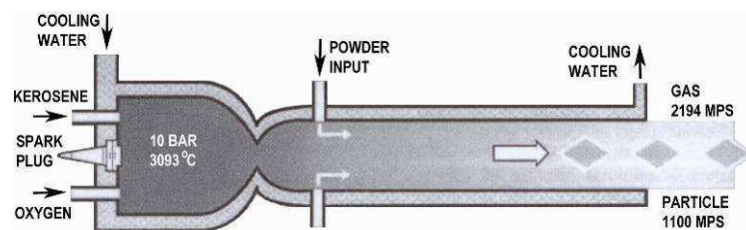
Fig. 1. Schematic diagram of the HVOLF process

Fuel and oxygen mix and atomize after passing through orifices into the combustion chamber creating stable and uniform combustion. The exit nozzle of the combustion chamber is sized and shaped to create a hypersonic overextended jet and maintain a low-pressure region where the powder is

introduced. HVOLF sprayed coatings are widely used to improve the service life of machine components. Numerous applications of HVOF process due to its flexibility and superior quality of coatings are present in different branches of industry. Investigations carried out in this paper involve properties of nanostructured and conventional WC-12Co cermet coatings deposited by the HVOLF method and include their microhardness, microstructure, phase composition coefficient of friction and wear resistance.

1. Experiment

The powder and sprayed coating structure was analyzed using tungsten carbide, WC12Co. The nanostructured tungsten carbide powder (Infralloy S7412) and sprayed coating was denoted as WC12Co-N, while that with a conventional powder (Amperit 519.074) and sprayed structure as WC12Co-A. In both cases, the grain size ranged from 15 to 45 μm. The grain sizes, cross-sections and morphology of grain surfaces for the two powders are shown in Fig. 2 and 3 respectively. The materials are designed to be used in thermal spraying. They are produced by agglomeration and sintering of fine powder grains. They contain a very large amount of spheroid-shaped grains, which
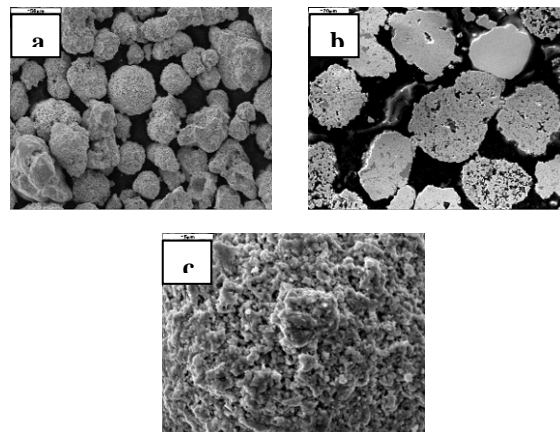
Fig. 2. WC12Co-N powder, morphology of; a) grains, b) cross-section of grains, c) grain surface

causes that the powder grains are loose, compared to those with irregularly shaped grains. As can be seen in metallographic images, the porosity of the conventional powder grains is more visible (Figs. 2b and 3b). Morphology of grains surface (Fig. 2c and 3c) show distinct difference of grains surfaces morphology. It is result of different dimension of material applied to produce

powder. Grains of nanostructured powder consist of nanometric and submicron WC crystals in the range of 50-500 nm (Fig. 4). In the case of conventional powder WC12Co-A, 1 µm grains were applied.
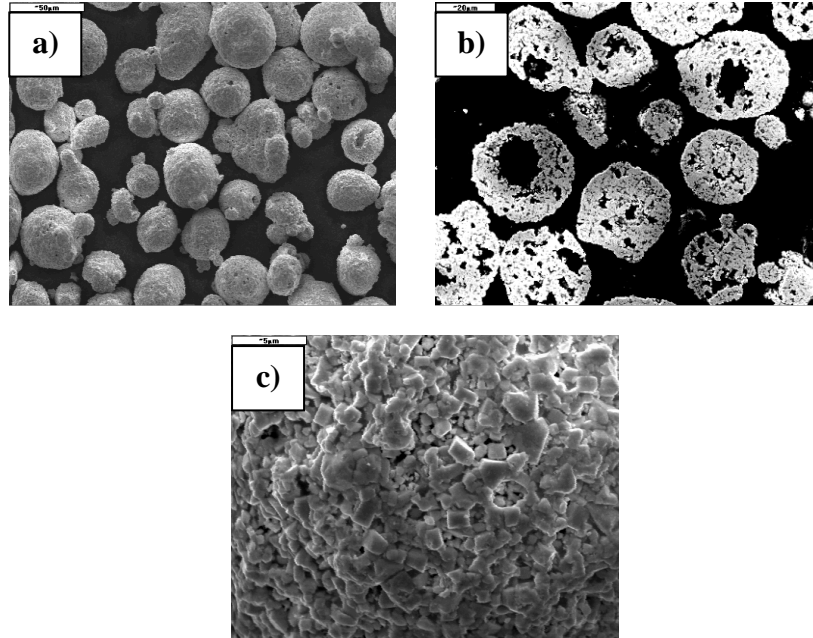
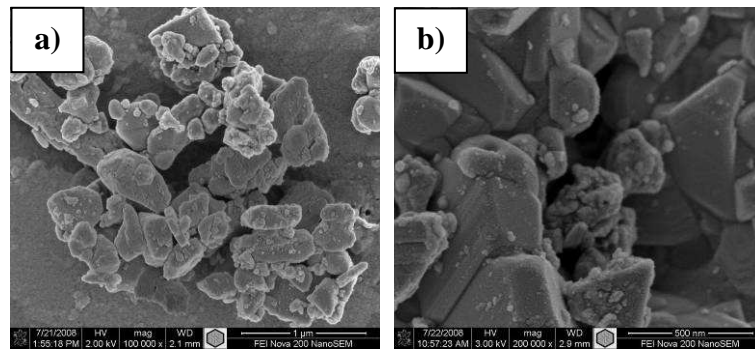**Fig. 3. WC12Co-A powder, morphology of; a) grains, b) cross-section of grains, c) grain surface**

Fig. 4. Nanometer and submicron WC12Co-N powder particles on; a) the powder grain surface, b) the cross-section of powder grain

Figures 5a and b show the grain size distribution and relative density distribution measured using a Sympatec Gmbh Helos laser diffraction system. Both powders have a very narrow grain size distribution, which is characteristic of the materials to be used in spraying. The WC12Co-N powder contains more grains with a greater diameter. In this case, $d_{90} = 61.28$ µm, whereas for

WC12Co-A, the coefficient coincides with the declared grain size distribution and is $d_{90} = 43.37$ μm.
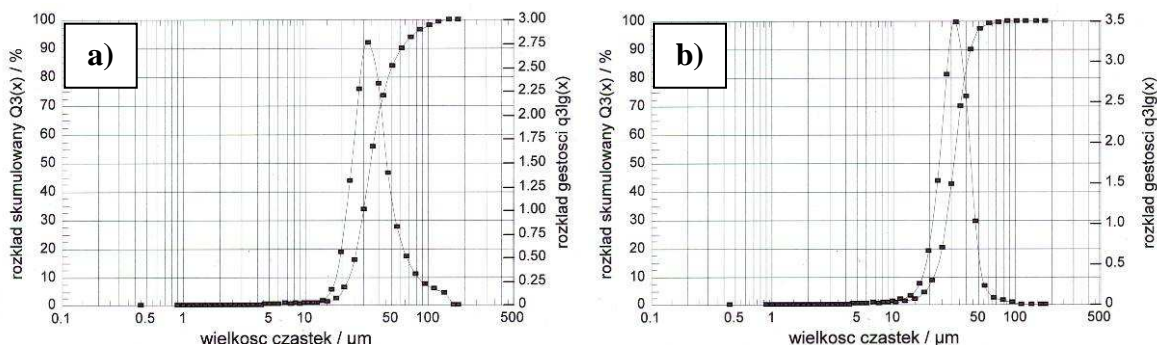
Fig. 5. Powder granulometric distribution a) WC12Co-N, b) WC12Co-A

The coatings were deposited using a kerosene-fuelled HVOLF thermal spray gun, TAFA–JP-5000 (Tab. 1).

Table 1 - HVOLF spray parameters

Spray parameters	WC12Co-N, WC12Co-A,
Barrel length, mm	150
Oxygen pressure, kPa	890
Kerosene mass flow, l/h	22,7
Powder feed rate, g/min	330
Feeder gas	argon
Spray distance, mm	380

The metallographic examination involved depositing coatings on low-carbon steel sheets with dimensions of 50mm x 25mm x 5 mm. In the tribological test, however, the coatings were deposited on low-carbon steel disc samples with dimensions of ϕ30 mm x 6 mm. Before spraying, the substrate had to be degreased and grit blasted with electrocorundum EB-12 at a pressure of 0.5 MPa. The thickness of the coatings after grinding was 0.3 mm. The structure and chemical composition of the powders and the coatings were analyzed using the following scanning microscopes: JSM–5400 with an ISIS 300 Oxford (EDS) microprobe and FEI COMPANY Nova™ NanoSEM 200. Their phase composition was studied by means of a Bruker D8 Advance diffractometer and the analysis involved Co-Kα radiation with the wavelength of X-rays λ = 1.78897 Å.

Dry abrasive rubber wheel tester (T-07) with alumina (grain size 0,5 mm) as abradant was applied to estimate abrasive resistance of sprayed coatings. A CSM Instrument ball-on-disc type tribotester was used to determine the coefficient of friction under unlubricated conditions for the sprayed carbide coatings. The ball made of bearing steel 100Cr6 had a diameter of 6 mm. The testing involved applying a computer to aid in registering and controlling the action of the friction force in the function of time. The parameters for the tribotester were as follows: radius - 10 mm, load - 1 N, linear velocity v = 0,063 m/s, number of laps – 10000, total distance – 754m. The coatings of disc samples were ground and polished for one hour. The roughness of the WC12Co-N coating was $R_a = 0.043$ μm, and that of the coating WC12Co-A was $R_a = 0.015$ μm. Their microhardness measured with a Vickers indenter with a load 5 N was 1159 HV and 966 HV respectively as the average of 10 measurements carried out by CSM Micro Identation Tester.

2. Results and discussion

The microstructures of the HVOLF-sprayed coatings are shown in Fig. 6.
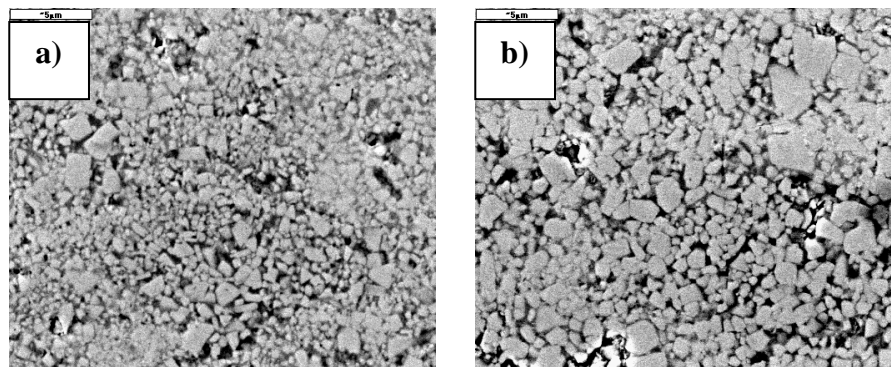
Fig.6. Cross-section of supersonic sprayed coating: a) WC12Co-N, b) WC12Co-A

The metallographic images of the two WC12Co coatings showed that there were some small undeformed tungsten carbide grains embedded in the cobalt matrix. From the EDS microanalysis it was clear that the coating content was different in each zone. The light-coloured grains in the WC12Co coatings testified to a high amount of tungsten, whereas the dark-coloured matrix was an area with a high content of cobalt and a low content of tungsten. The different sizes of tungsten carbide grains were visible in both coatings. The coating deposited using the nanostructured powder had a more fine-grained structure

with unmodified nanocrystals. It exhibited lower porosity despite the fact that the nanostructured powder contained bigger grains. The coating produced from the conventional powder, on the other hand, had higher porosity resulting from the higher porosity of the grains, which can be seen in the metallographic images. Microstructure of two WC grains in sprayed coating and connected electron diffractions in bright field (BF) is shown at Fig. 7. Grains are surrounded by amorphous cobalt matrix. The dimensions of WC crystals are the range of 50-500 nm. Electron diffractions (SADP) corresponds with hexagonal structure of WC and orientation [102] .
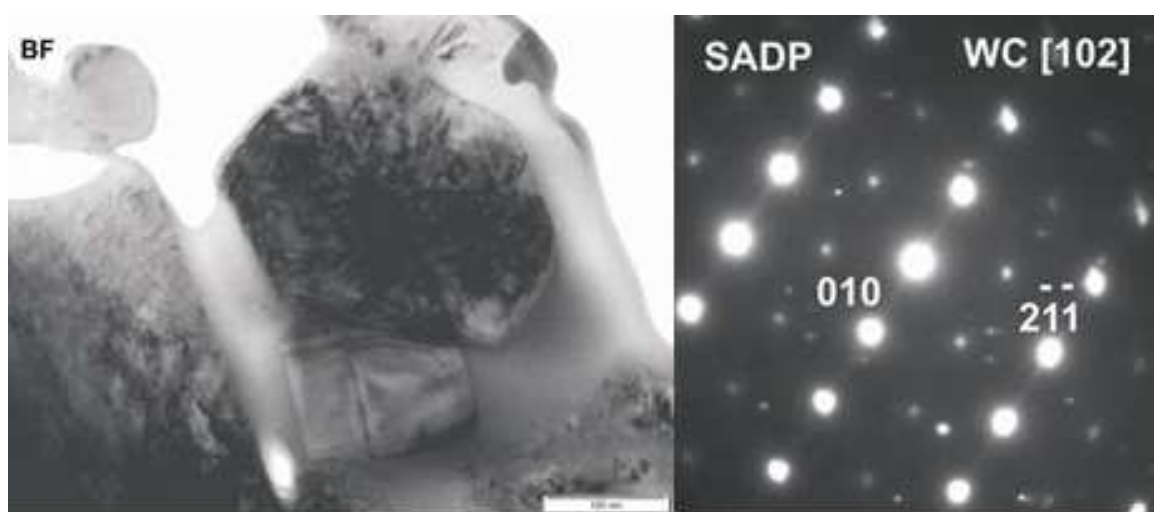
Fig. 7. WC grains in WC12Co-N coating

Microstructure of WC12Co-N coating in bright field and corresponding HAADF picture from chosen part of the coating is shown at Fig. 8. Example of EDS analysis spectra (Fig. 8b, point 1,2,3,4) confirmed presence of WC grains and different contents of Co (Fig. 8c). Table 2 presents results of chemical analysis of sprayed coating with different grains composition.

Table 2 - Results of chemical analysis of WC12Co-N coating

Point	% at.		
	W	C	Co
1	31,3	13,2	55,5
2	52,6	47,1	0,3
3	50,1	48,9	1,0
4	48,6	40,3	11,1
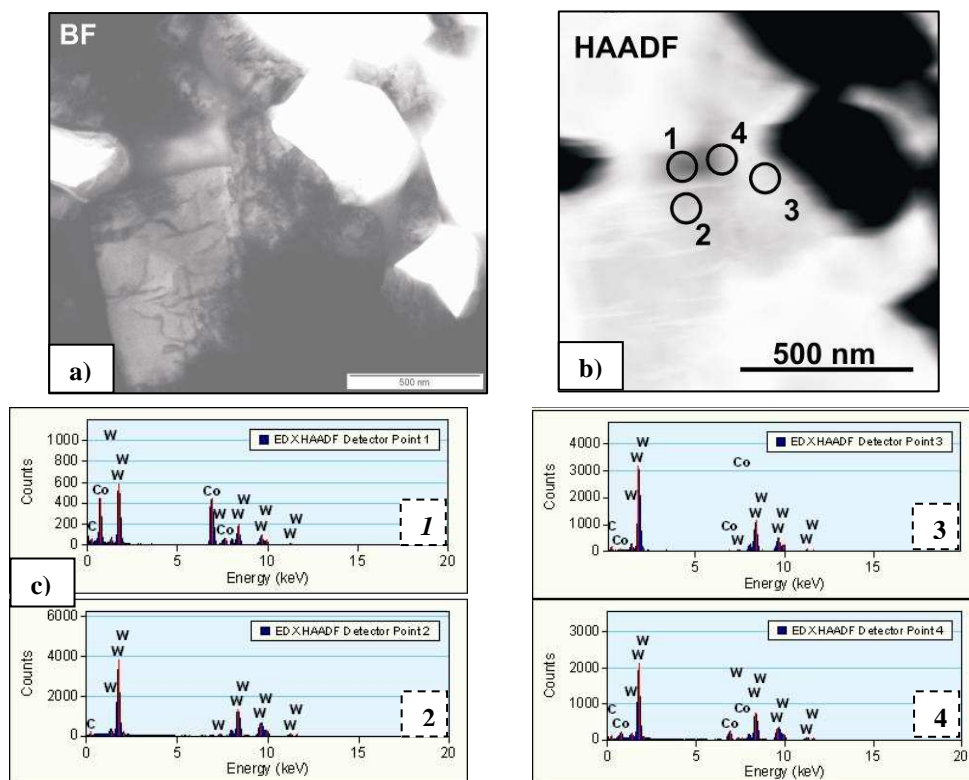
Fig. 8. WC12Co-N coating; a) microstructure in bright field, b) HAADF picture of microstructure, c) results of EDS analysis

On the base of analysis of microstructure of WC12Co-N sprayed coating (Fig. 7,8), it can be concluded that nanocrystal grains present in powder are also present in sprayed coating. It confirm that process of hypersonic spraying with relatively low temperature of spraying stream and short dwell time of particles in this stream, do not cause decomposition of WC nanocrystals despite their very small dimensions. Significant changes in phase composition of WC which occur particularly during plasma spraying substantially decrease properties of coatings [8,9]. Influence of heat on sprayed WC12Co-N powder is well seen In the case of cobalt, which in many places create amorphous structure surrounding nanocrystal grains of WC.

The analysis of the powder diffraction patterns showed that the WC grains in the nanostructured powder were twofold smaller than those in the conventional powder. The diffraction patterns (Fig. 9) revealed the presence of WC and Co both in the WC-Co powder and the deposited coating. The new phases that appeared in both coatings, i.e. W_2C, WC_{1-x} and W, were attributable to the previous disintegration of WC in the spray stream. The diffraction lines of

the phases after the spray were considerably wider. They testified to a significant degree of elastic and plastic deformation, i.e. a high level of energy stored in the form of network defects. That particularly referred to the Co phase.
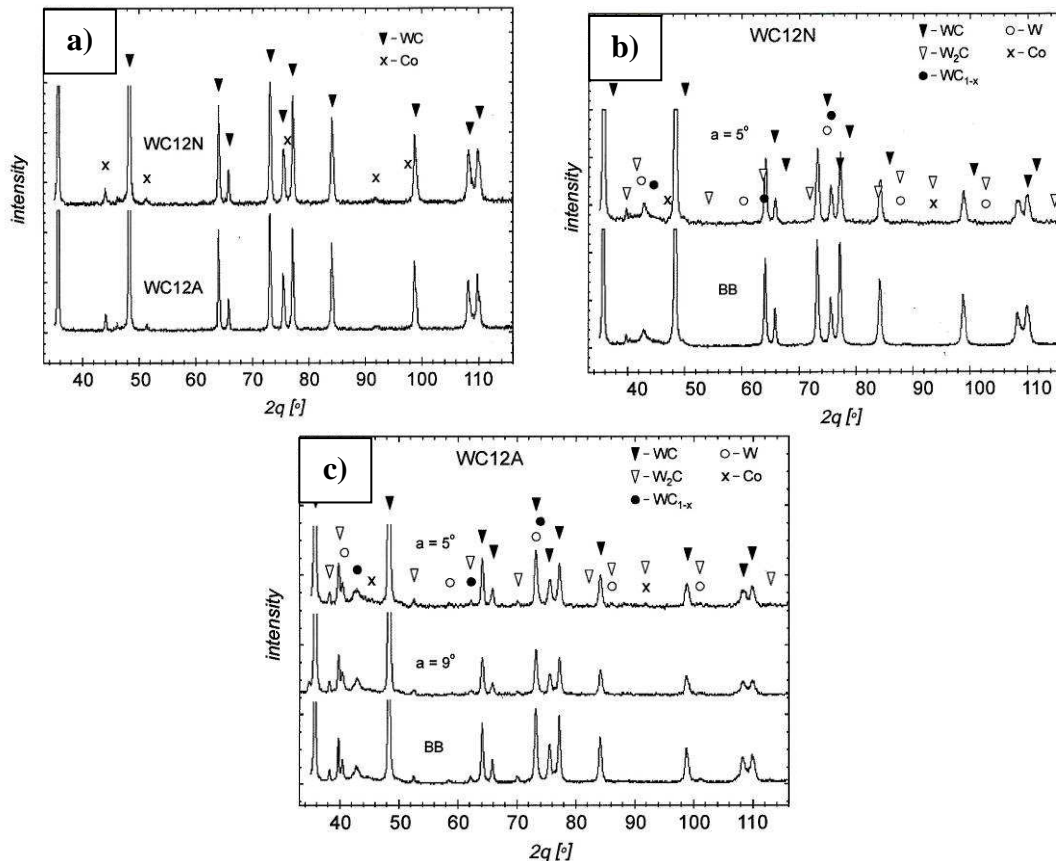

Fig. 9. Diffractogram of: a) powders WC12Co-N and WC12Co-A, b) coating WC12Co-N, c) coating WC12Co-A

Figure 10 shows time-dependent changes in the coefficient of friction for both coatings. As can be seen in the two diagrams, the coefficient of friction for the sprayed WC12Co-N stabilized after the first 50 m, with a slight growth tendency. The changes in the coefficient of friction for the WC12Co-A coating revealed much higher level and significant oscillations.

The results of abrasive wear test are presented in the Fig. 11. Before the test, all the specimens were cleaned with acetone and then weighed on an electronic balance with an accuracy ±0.1 mg. The tests show that WC12Co-N coatings posses higher abrasion resistance than coatings sprayed with application of conventional powder.
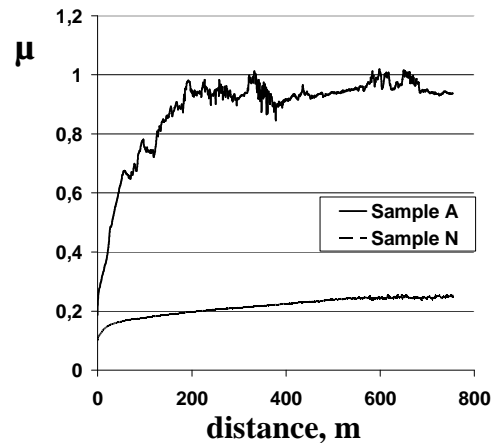
Fig. 10. Coefficient of friction for hypersonic sprayed coating: a) WC12Co-N coating, b) WC12Co-A coating
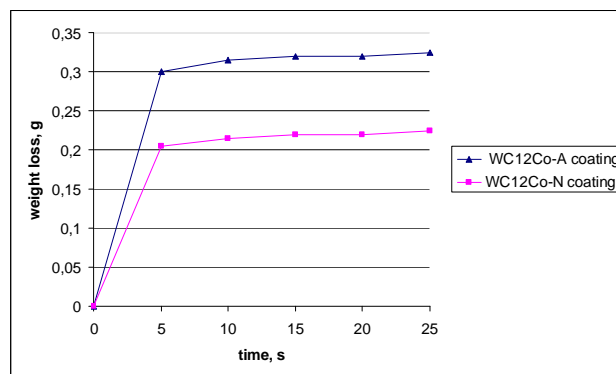
Fig. 11. Abrasive wear of HVOLF sprayed WC12Co-N i WC12Co-A coatings

Conclusions

1. The nanostructured WC-12Co coating possessed nanocrystal grains which have been presented in sprayed powder.

2. Influence of heat on sprayed WC12Co-N powder create amorphous structure of Co which surround nanocrystal grains of WC.

3. The microhardness of the nanostructured WC-12Co coating was higher than that of the conventional WC-12Co coating; the average microhardness exceeded 1159 HV, which was 20% more than that of the conventional coating.

4. The coefficient of friction for the HVOLF-sprayed WC-12Co nanostructured coating was relatively steady and four times lower than for the conventionally sprayed WC-12Co coating.

5. The highest abrasion resistance reveal nanostructured WC12Co coating after ESD process.

Acknowledgements

References

1.   He, Jianhong; Schoenung, Julie M.; Nanostructured coatings. Materials Science and Engineering: A Volume: 336, Issue: 1-2, October 25, pp. 274 – 319 (2002.

2.   Dahotre N.B., Nayak S.: Nanocoatings for engine applications. Surface and Coating

Technology 194 58-67 (2005).

3.   Lima, R.S.; Khor, K.A.; Li, H.; Cheang, P.; Marple, B.R.; HVOF spraying of nanostructured hydroxyapatite for biomedical applications. Materials Science & Engineering A Volume: 396, Issue: 1-2, April 15, pp. 181-187 (2005).

4.   Ji, Gang; Elkedim, Omar; Grosdidier, T.; Deposition and corrosion resistance of HVOF sprayed nanocrystalline iron aluminide coatings. Surface and Coatings Technology Volume: 190, Issue: 2-3, January 21, pp. 406-416 (2005).

5.   Fauchais, P., Montavon, G., Bertrand, G.: From powders to thermally sprayed coatings. Journal of Thermal Spray Technology 2010, 19 (1-2), pp. 56-80.

6.   Lima, R.S.; Khor, K.A.; Li, H.; Cheang, P.; Marple, B.R.; HVOF spraying of nanostructured hydroxyapatite for biomedical applications. Materials Science & Engineering A Volume: 396, Issue: 1-2, April 15, pp. 181-187 (2005).

7.   Bolelli, G.; Cannillo, V.; Gadow, R.; Killinger, A.; Lusvarghi, L.; Rauch, J.; Romagnoli, M.; Effect of the suspension composition on the microstructural properties of high velocity suspension flame sprayed (HVSFS) Al2O3 coatings. Surface & Coatings Technology Volume: 204, Issue: 8, January 15, 2010, pp. 1163-1179.

8.   Fang, Z. Zak; Wang, Xu; Ryu, Taegong; Hwang, Kyu Sup; Sohn, H.Y. Synthesis, sintering, and mechanical properties of nanocrystalline cemented tungsten carbide – A review. International Journal of Refractory Metals and Hard Materials Volume: 27, Issue: 2, March, 2009, pp. 288-299.

9.   Żórawski W.: HVOF spraying as an alternative to chromium plating. International Conference „Modern Wear and Corrosion Resistant Coatings Obtained by Thermal Spraying" Warszawa 2003.

10.   Krommer P., HeinrichP.,Kreye H.: High velocity oxy-fuel flame spraying: past-present-future. 8. Kolloquium HVOF Spraying, Erding 2009, pp.9-16.

11.   Liao H., Normand B., Coddet C.; Influence of coating microstructure on the abrasive wear resistance of WC/Co cermet coatings. Surface & Coatings Technology 124 (2000), pp. 235-242.

3.2.2 POMIARY IMPULSÓW ELEKTRYCZNYCH I WŁAŚCIWOŚCI EKSPLOATACYJNE POWŁOK WĘGLIKOWYCH NANOSZONYCH OBRÓBKĄ ELEKTROISKROWĄ

Radek N.[1], Wrzałka Zdz.[1], Shalapko Y.[2]

Wstęp

Od opatentowania przez B. R. Łazarenko i N. I. Łazarenko elektroiskrowego sposobu obróbki materiałów w latach 1946 [1] badania nad fizyką procesu elektrycznej erozji materiałów w obróbce ubytkowej (EDM - Electro Discharge Machining) i przyrostowej (ESA - Electro Spark Alloying) prowadzone są przez zespoły badawcze na całym świecie.

Według danych literaturowych [2÷3] w procesie erozji w wyniku wyładowania elektrycznego charakterystyczne jest występowanie trzech obszarów:

- obszar przyanodowy,
- kanał wyładowania (obecnie określany mianem kanału plazmowego),
- obszar przykatodowy.

B. N. Zolotych [3] uważa, że aby poznać proces erozji elektrycznej należy określić mechanizm przekazywania energii dostarczonej w impulsie obszarom bezpośrednio uczestniczącym w procesie wyładowania (elektrodom, cieczy dielektrycznej lub gazom). Energia ta powoduje erozję elektrod. Charakter przekazywania energii anodzie i katodzie jest różny i zależy głównie od nośników prądu. Na anodzie cały prąd jest przenoszony przez elektrony, podczas gdy na katodzie przez jony i elektrony. W efekcie przyjętego przez B. N. Zolotycha modelu wyładowania elektrycznego, procesy na anodzie i na katodzie są rozpatrywane oddzielnie.

Energię impulsu można wyrazić w następujący sposób [3]:

$$W_i = \int_0^{t_i} U(t)I(t)dt \, , \tag{1}$$

---

[1] Politechnika Świętokrzyska, Starosta Powiatu Kieleckiego, Polska
[2] Khmelnitckij Narodowy Uniwersytet, Ukraina

gdzie:

W_i - energia impulsu,

U(t) - napięcie w impulsie,

I(t) - natężenie prądu w impulsie,

t_i - czas trwania impulsu.

Energię impulsu w uproszczeniu oblicza się z zależności [3]:

$$W_i = U_r \cdot I_r \cdot t_i \text{,} \qquad (2)$$

gdzie:

W_i - energia impulsu,

U_r - amplituda napięcia roboczego,

I_r - amplituda natężenia prądu roboczego,

t_i - czas trwania impulsu.

Energia dostarczana do powierzchni elektrod (anody i katody) podczas obróbki elektroiskrowej B. N. Zolotych [3] zapisuje jako sumę:

$$W_E = W_A + W_K \text{,} \qquad (3)$$

gdzie:

W_E - energia przekazywana elektrodom,

W_A - energia przekazywana anodzie,

W_K - energia przekazywana katodzie.

Natomiast energię impulsu [3] można przedstawić w następujący sposób:

$$W_i = W_E + W_W \text{,} \qquad (4)$$

gdzie:

W_i - energia impulsu,

W_E - energia przekazywana elektrodom,

W_W - energia działająca w kanale wyładowania.

Przekazywanie energii elektrodom może być realizowane za pośrednictwem następujących procesów [3÷5]:

• bombardowanie katody jonami pod działaniem pola elektrycznego w strefach przyelektrodowych i bombardowanie anody elektronami,

• promieniowanie kanału wyładowania,

● termicznego (gazokinetycznego) bombardowania cząstkami znajdującymi się w kanale wyładowania,

● przy małych grubościach szczeliny międzyelektrodowej może mieć miejsce wymiana energii pomiędzy elektrodami w rezultacie oddziaływania strumieni pary powstających na anodzie i na katodzie.

Proces obróbki elektroiskrowej jest możliwy dla wszystkich materiałów, które są przewodnikami prądu, bez względu na ich twardość, kształt lub wytrzymałość [6].

Współcześnie stosowane są różne odmiany obróbki elektroiskrowej spełniające standardy wytwarzania powłok, a także kształtowania mikrogeometrii powierzchni [7÷14].

Cechą charakterystyczną powłok nanoszonych elektroiskrowo jest to, że mają one specyficzną, nie trawiącą się strukturę - pozostają białe. Warstwa wierzchnia kształtowana jest w warunkach lokalnego oddziaływania wysokiej temperatury i dużych nacisków. Wartości podstawowych parametrów obróbki elektroiskrowej są następujące [4]:

● ciśnienie fali uderzeniowej od iskry elektrycznej wynosi $(2÷7)*10^3$ GPa,

● temperatura osiąga wartości rzędu $(5÷40)*10^3$ °C.

Współczesne zastosowania przemysłowe obróbki elektroiskrowej obejmują następujące dziedziny: przemysł motoryzacyjny, przemysł kosmiczny, przemysł lotniczy, przemysł okrętowy, przemysł zbrojeniowy, przemysł energetyczny, mechanika precyzyjna, produkcja narzędzi oraz medycyna.

1. Materiały i urządzenia

Przedmiotem badań był pomiar i analiza impulsów elektrycznych podczas obróbki elektroiskrowej oraz ocena właściwości eksploatacyjnych naniesionych powłok elektrodą węglikową. Do badań została użyta elektroda WC-Co (anoda) o przekroju 3 x 4 mm, natomiast materiałem podłoża była stal C45 (katoda). Do badań wykorzystano urządzenie EIL-8A (o ręcznym posuwie elektrody). Ogólny widok urządzenia wraz z elektrodą WC-Co umieszczoną w uchwycie przedstawiono na rysunku 1. Opierając się na doświadczeniach własnych oraz zaleceniach producenta urządzenia przyjęto następujące parametry nanoszenia powłok elektroiskrowych: napięcie U = 230 V, pojemność kondensatorów C = 300 μF, natężenie prądu I = 2,4 A.

**Rys. 1. Widok urządzenia EIL-8A**

2. Wyniki badań

2.1. Pomiary i analiza impulsów elektrycznych

Badanie procesu obróbki elektroiskrowej wymaga pomiarów natężenia prądu i mocy stosowanych impulsów elektrycznych. Tranzystorowy układ formowania impulsów jest zasilany ze źródła zasilania, jakim jest kondensator mocy. Sposób realizacji pomiarów przedstawiono na rysunku 2.

Do pomiaru prądu wykorzystano cęgową sondę cyfrową typu CM-05 firmy Prova Instruments Inc., będącej przetwornikiem prąd/napięcie zbudowanym na bazie czujnika Halla. Pozwala ona na pomiar płynącego w pręcie prądu, zarówno stałego jak i przemiennego, z zapewnieniem separacji galwanicznej układu pomiarowego od układu silnoprądowego. Napięciowy sygnał wyjściowy sondy jest podawany bezpośrednio na oscyloskop cyfrowy TDS 210 (Tektronix). Na drugim kanale oscyloskopu mierzone jest napięcie pomiędzy elektrodą, a obrabianym elementem. Poprzez moduł komunikacyjny TDSCM dane pomiarowe przesyłane są do komputera. Wielkości pomiarowe są dostępne także w postaci pliku w kodzie ASCII.

Do wyznaczania przebiegów prądu i napięcia wyładowania elektrycznego podczas procesu ESA wykorzystano stanowisko pomiarowe zbudowane z oscyloskopu cyfrowego Hewlett - Packard typ: HP 54602A, sondy prądowej i komputera IBM PC. Na stanowisku możliwa jest rejestracja wartości chwilowych prądu i napięcia wyładowania iskrowego. Użycie oscyloskopu

cyfrowego zapewnia jednoczesność pomiaru napięcia i prądu. Bufor pamięci pozwala na zapamiętanie 500 próbek, co zapewnia zarejestrowanie kilku okresów wyładowania (przy odpowiednio dobranej podstawie czasu). 8-bitowa rozdzielczość pomiaru amplitudy wydać może się zbyt mała, jednak otrzymane wyniki są zadowalające. Pewną niedogodnością jest możliwość rejestracji tylko dwóch przebiegów. Parametry procesu obróbki elektroiskrowej zostały dobrane doświadczalnie.
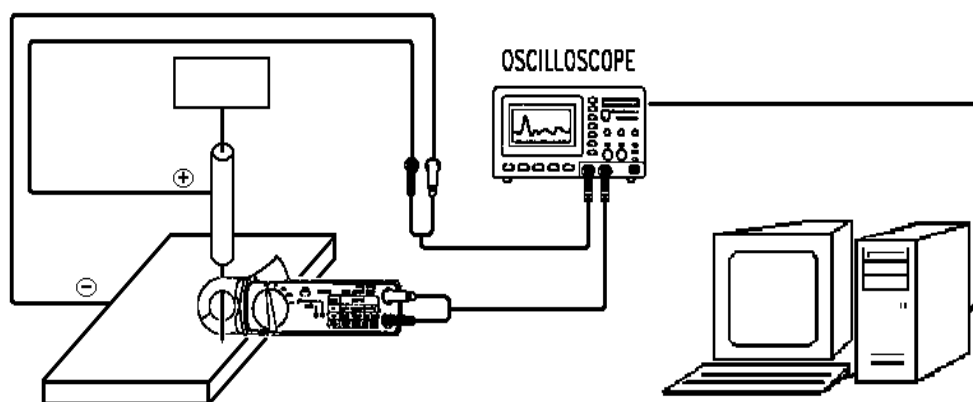

Rys. 2. Schemat układu pomiarowego

Przykładowy przebieg prądu wyładowania elektrycznego zarejestrowany podczas obróbki elektroiskrowej przedstawiono na wykresie (Rys. 3). Natomiast wykres (Rys. 4) przedstawia pojedynczy impuls wyładowania elektrycznego podczas ESA.

Z otrzymanych wykresów możemy odczytać podstawowe wielkości elektryczne podczas wyładowania, tzn. prąd $i(t)$ i napięcie $u(t)$ impulsu elektrycznego. Po cyfrowej obróbce tych wielkości, możemy obliczyć np. moc chwilową impulsu elektrycznego wyrażoną wzorem $p(t) = u(t) \cdot i(t)$. Ponadto możemy odczytać czas trwania impulsu wyładowania iskrowego. Mając dane prąd, napięcie oraz czas trwania impulsu wyładowania iskrowego możemy obliczyć chwilową energię impulsu elektrycznego. Z literatury wiadomo, że na grubość naniesionej warstwy i na jej własności eksploatacyjne największy wpływa ma energia impulsu. Na wyznaczonych przebiegach możemy zaobserwować „ujemne" wartości natężenia prądu i napięcia, co świadczy że następuje również proces erozji materiału podłoża (stal C45). Jest to sprzeczne z

227

teoretycznymi podstawami obróbki elektroiskrowej, według której proces erozji powinien zachodzić tylko na elektrodzie roboczej (anodzie). Jednak wyjaśnienie tego zjawiska będzie tematem dalszych badań.

Otrzymane charakterystyki prądu i napięcia wyładowania elektrycznego mogą posłużyć do optymalizacji procesu ESA, co pozwoli na kształtowanie warstw o określonych własnościach użytkowych.
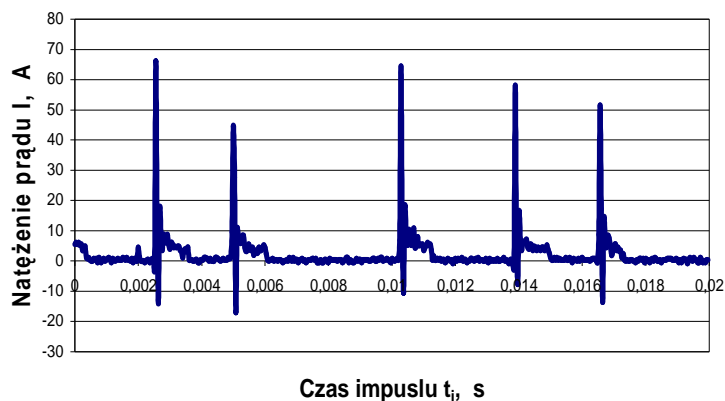
**Rys. 3. Przebieg zmian parametrów prądowych (I = 0, 4 A; C = 150 μF)**

Rys. 4. Pojedynczy impuls wyładowania elektrycznego (I = 3 A; C = 300 μF)

2.2. Analiza mikrostruktury i pomiary mikrotwardości

Pomiary mikrotwardości wykonano na prostopadłych zgładach w trzech strefach: w powłoce, w strefie wpływu ciepła jak również w materiale rodzimym. Rysunek 5 przedstawia fotografię mikrostruktury powłoki WC-Co z odciskami penetratora. W oparciu o uzyskane wyniki stwierdzono, że grubość uzyskanych warstw wyniosła od 20÷30 μm, natomiast zasięg strefy wpływu

ciepła (SWC) w głąb materiału podłoża ok. 15÷20 μm. Na przedstawionej fotografii mikrostruktury widoczna jest wyraźna granica pomiędzy powłoką, a podłożem. Ponadto na fotografii (rys. 5) można zaobserwować pory i mikropęknięcia w naniesionej elektroiskrowo powłoce.

Na wykresie (rys. 6) przedstawiono uzyskane wyniki pomiarów mikrotwardości. Obróbka elektroiskrowa spowodowała zmianę mikrotwardości w próbce. Powłoka WC-Co miała średnio mikrotwardość 621 $HV_{0,04}$ nastąpił wzrost mikrotwardości o 350% względem podłoża. Wzrosła też mikrotwardość SWC, 194% względem podłoża. Mikrotwardość podłoża nie zmieniła się, przed i po obróbce elektroiskrowej wynosiła średnio 135 $HV_{0,04}$.
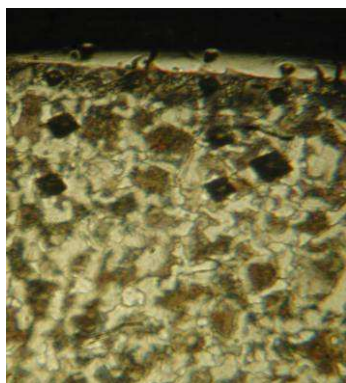
Rys. 5. Mikrostruktura powłoki WC-Co z odciskami penetratora
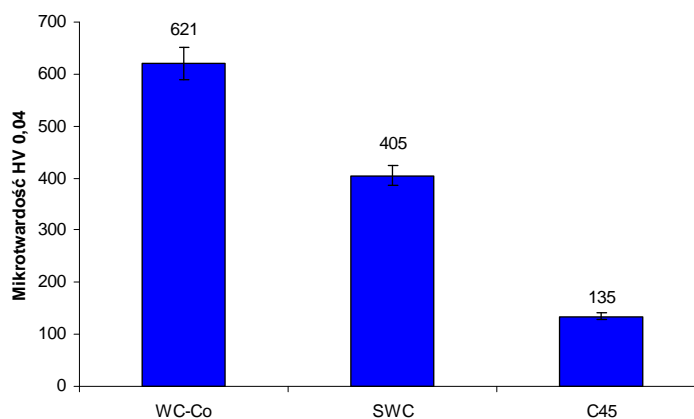
Rys. 6. Wyniki pomiarów mikrotwardości

2.3. Badania odporności korozyjnej

Badania odporności korozyjnej zostały przeprowadzone za pomocą skomputeryzowanego zestawu do badań elektrochemicznych Atlas'99 firmy Atlas-Sollich. Pomiary przeprowadzono dla powłoki WC-Co oraz materiału podłoża metodą potencjodynamiczną. Metoda ta należy do najbardziej rozpowszechnionych i nowoczesnych badań elektrochemicznych.

Krzywe polaryzacji katodowej i anodowej wykonano polaryzując próbki z szybkością zmian potencjału wynoszącą 0,2 mV/s (w obszarze ±200 mV od potencjału korozyjnego) oraz 0,4 mV/s w obszarze wyższych potencjałów. Próbki z wyodrębnionym obszarem o średnicy 10 mm polaryzowano do

potencjału 500 mV. Krzywe polaryzacji wykonano po 24 godzinach ekspozycji w testowanym roztworze (3,5% NaCl) w celu ustalenia się potencjału korozyjnego. Badania wykonano w temperaturze pokojowej - 21°C ±1°C.

Przykładowy wykres krzywej polaryzacji dla powłoki WC-Co przedstawiono na rysunku 7. Charakterystyczne wartości elektrochemiczne badanych materiałów przedstawiono w tabeli 1.
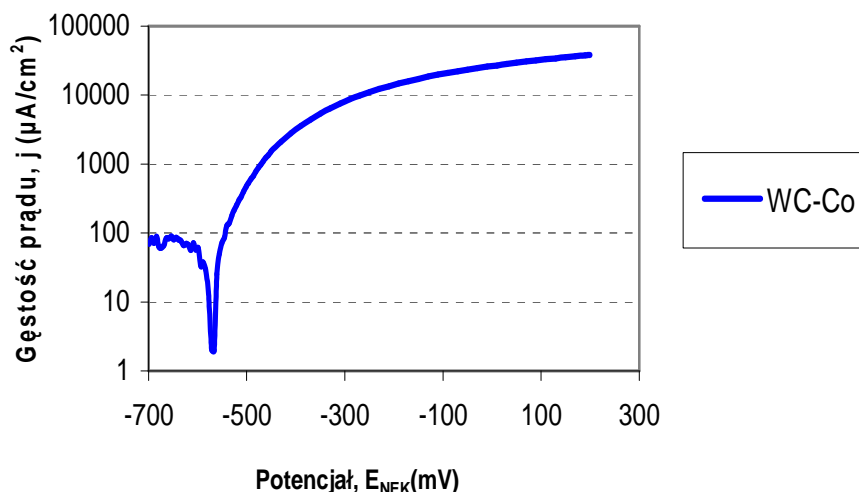
Rys. 7. Krzywa polaryzacji powłoki WC-Co

Tabela 1 - Wartości gęstości prądu i potencjału korozyjnego badanych próbek

Badany materiał	Gęstość prądu korozyjnego I_k [μA/cm^2]	Potencjał korozyjny E_{KOR} [mV]
C45	112	-458
WC-Co	68,3	-570

Powłoka WC-Co nałożona elektroiskrowo, której gęstość prądu korozyjnego wyniosła 68,3 μA/cm^2 charakteryzuje się prawie dwukrotnie większą odpornością korozyjną w odniesieniu do materiału podłoża (stal C45) 112 μA/cm^2.

2.4. Badania tribologiczne

Badania oporów tarcia zostały przeprowadzone przy użyciu testera tribologicznego T-01M tupu kulka-pierścień, którego zasadę działania przedstawia rysunek 8. Jako próbki stosowano pierścienie ze stali węglowej

wyższej jakości C45, na które naniesiono elektroiskrowo powłoki WC-Co. Przeciwpróbką była kulka o średnicy φ6,3 mm wykonana ze stali 100Cr6.

Badania przeprowadzono przy następujących parametrach tarcia:

- prędkość obrotowa n = 341 obr/min,
- ilość obrotów i = 3410,
- czas próby t = 600s,
- wartości obciążenia Q = 4,9 N; 9,8 N; 14,7 N.
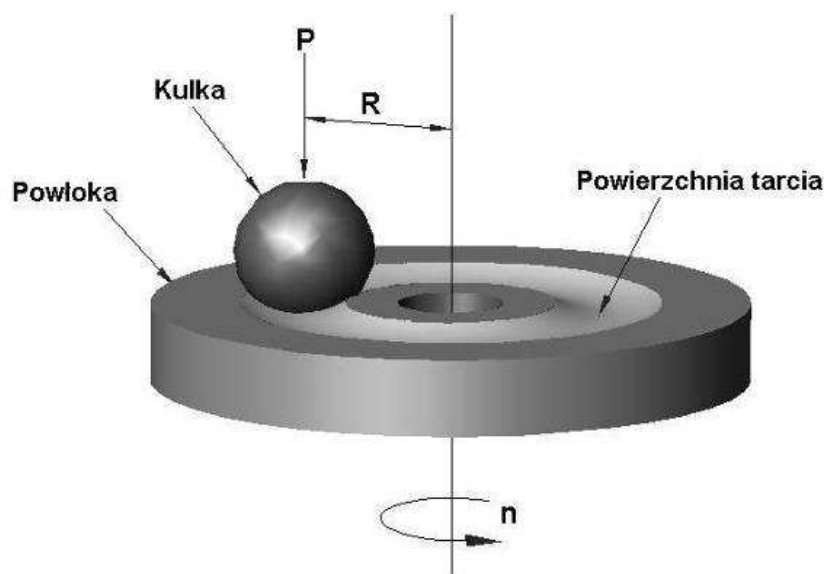
**Rys. 8. Zasada działania testera T-01M**

Na przykładowych wykresach (rys. 9÷11) przedstawiono przebiegi współczynników tarcia w funkcji tarcia przy obciążeniu: 4,9 N; 9,8 N; 14,7 N.

Podczas tarcia technicznie suchego badanych powłok nastąpiło przekształcenie technologicznej warstwy powierzchniowej w eksploatacyjną warstwę powierzchniową. Efekt ten nastąpił pod wpływem obciążenia i prędkości ślizgania oraz oddziaływania atmosfery otoczenia z badaną powierzchnią.

Na wykresie (rys. 9) można zaobserwować, że stabilizacja współczynnika tarcia nastąpiła po upływie 150 sekund i oscyluje na poziomie 0,55÷0,6. Przy obciążeniu 9,8 N (rys. 10) stabilizacja współczynnika tarcia nastąpiła po upływie 120 sekund, wartość jego oscylowała na poziomie 0,45÷0,52. Na wykresie (rys.11) można zaobserwować, że po upływie 140 sekund wartość współczynnika tarcia wzrasta liniowo.
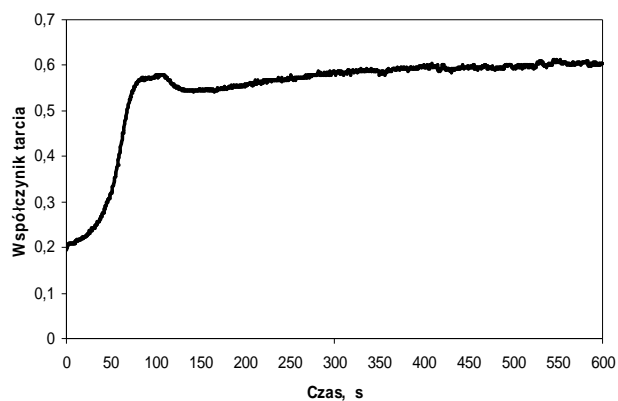
Rys. 9. Zależność współczynnika tarcia od czasu (obciążenie 4,9 N)
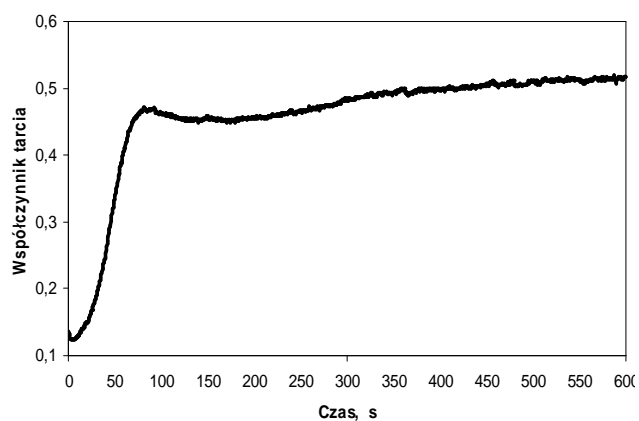
**Rys. 10. Zależność współczynnika tarcia od czasu (obciążenie 9,8 N)**
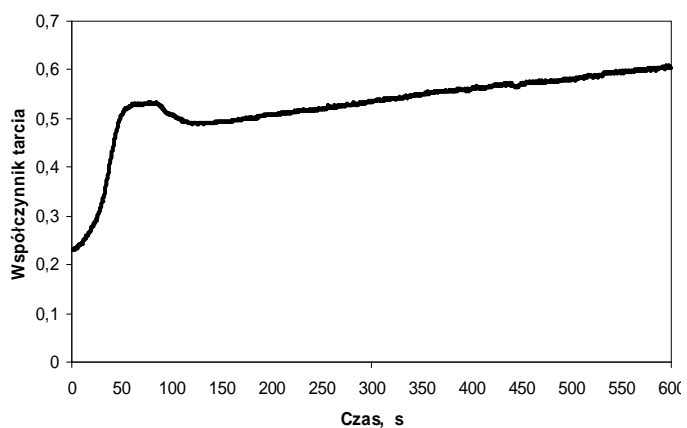
Rys. 11. Zależność współczynnika tarcia od czasu (obciążenie 14,7 N)

2.5. Pomiary chropowatości

Jedną z głównych wad powłok naniesionych obróbką elektroiskrową, jest ich duża chropowatość końcowa. Dotychczas przeprowadzone badania oraz analiza literatury wykazują, że kształtowanie powierzchni zachodzi w wyniku nakładania się na siebie kraterów będących wynikiem erozji podłoża jak również grzbietów utworzonych z przemieszczających się na powierzchnię cząstek materiału powlekającego elektrody. Tak powstała powierzchnia, posiada szereg następujących cech: regularność, brak kierunkowości, duże promienie zaokrągleń wierzchołków mikronierówności. W wielu opracowaniach naukowych analizuje się wpływ parametrów procesu na chropowatość powierzchni. Sterując tymi parametrami można uzyskać zakładane zmiany mikrogeometrii powierzchni. Jest to zatem sposób na wytwarzanie powierzchni o zadanej rozwiniętej powierzchni chropowatej, zwanej relifem powierzchniowym.

Pomiary chropowatości powłok WC-Co, wykonano w dwóch prostopadłych do siebie kierunkach. Pierwszy pomiar, był wykonany zgodnie z ruchem przemieszczania się elektrody, natomiast drugi pomiar, był prostopadły do ściegów skanujących. Z dwóch pomiarów, obliczono wartość średnią parametru Ra, dla danej powłoki. Powłoki WC-Co, posiadały chropowatość Ra = 1,55÷2,07 μm. Próbki ze stali C45, na które nanoszono powłoki, miały chropowatość Ra = 0,42÷0,58 μm. Przykładowy protokół pomiarów parametrów mikrogeometrii badanych próbek, przedstawiono na rysunku 12.
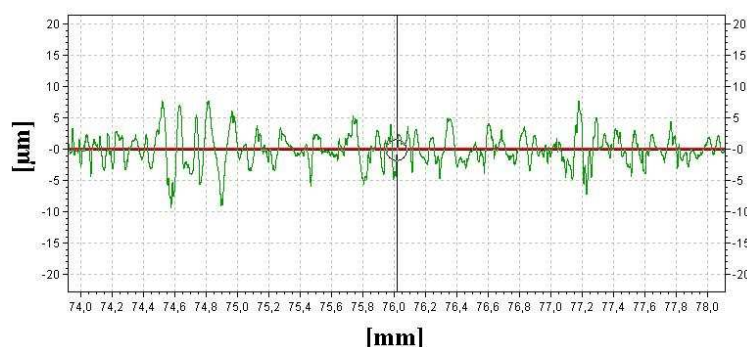
Rys. 12. Przykładowy protokół pomiarów chropowatości dla powłoki WC-Co

Wnioski

1. Podsumowując uzyskane wyniki badań należy zaznaczyć, że zbudowano układ pomiarowy, który składa się: z urządzenia EIL-8A, oscyloskopu cyfrowego TDS 210 (Tektronix) oraz sondy cyfrowej typu CM-05. Układ zapewnia pomiary podstawowych wielkości elektrycznych, tzn. prądu i napięcia impulsu elektrycznego. Układ umożliwia również cyfrową obróbkę tych wielkości, w tym wyznaczenie dodatkowych wielkości elektrycznych, np. mocy chwilowej impulsu elektrycznego.

2. Wadą zastosowanego układu jest możliwość rejestracji tylko dwóch przebiegów oraz stosunkowo wolny proces przesyłania danych z oscyloskopu do komputera. Poza tym zastosowany w badaniach cyfrowy oscyloskop pomiarowy zbudowany jest na bazie 8-bitowych kart przetwornikowych, co zmniejsza dokładność pomiaru.

3. Alternatywnym rozwiązaniem jest użycie w miejsce oscyloskopu wielokanałowej 14-bitowej karty kontrolno-pomiarowej, zapewniającej dużą szybkość i dokładność przetwarzania A/C przy wykorzystaniu bufora FIFO lub kanału DMA.

4. Otrzymane charakterystyki prądu i napięcia wyładowania elektrycznego mogą posłużyć do optymalizacji procesu ESA, co pozwoli na kształtowanie warstw o określonych własnościach użytkowych.

5. Powłoki WC-Co naniesione elektroiskrowo charakteryzowały się znacznym wzrostem chropowatości Ra, w stosunku do chropowatości materiału podłoża. Wzrost chropowatości nie zawsze jest wadą, w pewnych przypadkach chropowata powierzchnia może być wykorzystana jako zasobnik smaru, do intensyfikacji wymiany ciepła oraz katalizy.

6. Analiza mikrostruktury powłoki naniesionej elektroiskrowo wykazała, że w powłoce znajdują się mikropęknięcia i pory.

7. W wyniku obróbki elektroiskrowej otrzymano powłokę WC-Co o średniej mikrotwardościwardości 621 $HV_{0,04}$, podczas gdy mikrotwardość materiału podłoża (stali C45) wynosiła 135 $HV_{0,04}$.

8. Badania oporów tarcia wykazały, że najniższe wartości współczynnika tarcia uzyskano przy obciążeniu 9,8 N, którego wartość oscylowała na poziomie 0,45÷0,52.

9. Badania odporności korozyjnej dowiodły, że powłoka WC-Co nałożona elektroiskrowo charakteryzuje się prawie dwukrotnie większą odpornością korozyjną w odniesieniu do stali C45.

Literatura

1. G.B. Patent No. 637793 „A metod of working Metals" - 1946.

2. DiBitonto D. D., Eubank P. T., Patel M. R., Barrufet M. A.: Theoretical models of the electrical discharge machining process. I-A simple cathode erosion model. Journal of Applied Physics 66/9 (1989), 123-131.

3. Zolotych B. N.: Osnovnyje voprosy kaciestviennoj teorii elektroiskrovoj obrabotki v zidkoj dielektricieskoj srede. Problemy elektrićeskoj obrabotki metallov, Moskwa 1962.

4. Miernikiewicz A.: Doświadczalno-teoretyczne podstawy obróbki elektroerozyjnej (EDM). Politechnika Krakowska - Rozprawy - nr 274 - Kraków 2000.

5. Praca zbiorowa pod redakcją Petrowa J.: Elektroiskrowoje legirowanie metallićieskich powierchnostoj. Kisziniew, 1985.

6. Abu Zeid O.A.: On the effect of electrodischarge machining parameters on the fatigue life of AISI D6 tool steel. Journal of Materials Processing Technology, 68, 1(1997), 27-32.

7. Radek N.: Tworzenie powłok o zróżnicowanych własnościach wybranymi technologiami: elektroiskrową i laserową. Politechnika Świętokrzyska, Praca doktorska, Kielce 2006.

8. Radek N.*: Determining the operational properties of steel beaters after electrospark deposition. Eksploatacja i Niezawodność - Maintenance and Reliability, 4(2009), 10-16.

9. Radek N., Antoszewski B., Kamiński J.: Badania eksperymentalne powłok stellitowych nanoszonych elektroiskrowo. Inżynieria Maszyn, 12, 2-3(2009), 92-97.

10. Radek N., Wrzałka Z., Szalapko Y., Bronček J.:. rozdział monografii pt. „Struktura geometryczna powierzchni i własności tribologiczne przeciwzużyciowych powłok elektroiskrowych. Rozdział 3.3 w monografii: Inżynieria powierzchni wybrane zagadnienia", Wydawnictwo Politechniki Świętokrzyskiej w Kielcach, 132-139, 2011.

11. Radek N.: Własności przeciwzużyciowych warstw powierzchniowych wytworzonych technologią elektroiskrową. Tribologia, 5(2010), 191-200.

12. Depczyński W., Radek N.: Sposób wytwarzania powłok cynkowych i napraw powłok cynkowych, Patent RP nr 380946, 2009.

13. Chen Z., Zhou Y.: Surface modification of resistance welding electrode by electro-spark deposited composite coatings: Part I. Coating characterization. Surface and Coatings Technology, 201 (2006), 1503-1510.

14. Ruijun W., Yiyu Q., Jun L.: Interface behavior study of WC92-Co8 coating produced by electrospark deposition. Applied Surface Science, 240(2005), 42-47.

3.2.3 PRELIMINARY DATA OF BOILING HEAT TRANSFER OF LASER TREATED HEAT EXCHANGER SURFACES

Radek N.[1], Łukasz J.[1]

Introduction

Phase change heat exchangers used in many technical applications need to be more and more efficient. They should dissipate significant heat fluxes, so more advanced solutions are necessary. One of the methods of boiling heat transfer augmentation is the surface treatment. Many different techniques are used – for example rough surfaces or the application of microstructures. In the latter case it is possible to considerably increase the heat flux. For example Wondra and Stephan [1] experimentally analysed boiling of FC – 72 on tubular surfaces covered with micro pin fins bonded on a plain copper surface through galvanisation. The pore diameters were 3.5 µm and 3.9 µm, while the microstructure height was 45 µm and 32 µm, respectively. It was found that the heat flux dissipated from the treated surface was even 7.1 times higher than for the smooth surface without such coating. Similarly, other forms of surface treatment – such as oxidation – can enhance boiling. Hong et al. [2] found out that oxidised surfaces increased heat transfer coefficient by 1.5 – 1.75 times for water boiling and up to 1.5 times for R – 11 boiling in comparison with the reference surface (without oxidation). Chang and You [3] tested FC-72 boiling heat transfer on surfaces covered with porous layers composed of solid particles bonded with epoxy. Aluminum, copper, diamond and silver powder particles were used of diameters ranging from 1 µm to 50 µm. The application of such structures resulted in increased heat flux even by ca. 330 % in relation to the smooth surface. These techniques are very common and involve the application of an additional coating on the surface, however, sometimes the exchanger is subject to different treatment. Nimkar et al. [4, 5] investigated boiling of FC – 72 dielectric liquid on a surface with pyramidal shaped cavities of the size 40 µm square mouth and 240 µm square base etched in silicon. The authors analysed the effect of cavity spacing on the heater – the cavities were located 0.5mm, 0.75 mm and 1,0 mm apart from the centre of one another. The most

---

[1] Kielce University of Technology, Poland

significant augmentation was observed for the spacing of 0.75 mm, while the surface of 0.5 mm spacing underperformed comparing with the smooth surface due to repulsive interactions between the nucleation cavities and difficult boundary layer mixing. Recent paper by Forrest et al. [6] gives data on the enhancement of the critical heat flux and nucleate boiling heat transfer coefficient (over 100 %) in case of water boiling on silica nanoparticle thin – film coatings applied on nickel wires. Here, the application of such coatings changes the surface wettability, but causes almost no change in surface roughness.

Because of a shortage of experimental data in this area the present paper deals with surfaces with cavities produced with laser treatment – it is a new concept and similar research data are hard to find in References. The aim of the project is to determine how such treatment can effect boiling heat transfer (heat flux) comparing with the smooth reference surface. The preliminary data are obtained for surfaces of different surface finish to check if such a treatment method is advantages for phase change heat exchangers and, if it is, which parameters might affect this process (e.g. surface morphology, the kind of boiling liquid, etc).

1. Fundamentals of augmented boiling heat transfer

Boiling heat transfer is described with a boiling curve – a function of heat transfer coefficient or heat flux on wall superheat. The superheat is defined as a difference between saturation temperature of the liquid and surface temperature.

If the temperature of the heating surface is increased over the boiling temperature, at first no vapour bubbles are present and heat is transferred in the natural convection mode. Then, when the liquid is slightly superheated and superheat is high enough – about 2 to 6 ^{o}C for water [7], boiling begins and vapour bubbles are created on the surface. It is a nucleate boiling regime. Here, a sudden increase in dissipated heat is observed and heat transfer is more and more intense as the temperature of the surface is further increased. With a rise in heat flux more vapour is produced and, consequently, neighbouring bubbles join together to finally create a vapour blanket which insulates the surface from the liquid. It leads to a decrease in heat flux. A new unfavourable mode of heat transfer is observed – film boiling. Further increase is heat flux is attributed

mainly to radiation heat transfer [8]. The most important mode of heat transfer is nucleate boiling, since it offers high heat dissipation rate at small temperature differences.

Boiling on treated surfaces is different than on the smooth surface – there are other phenomena involved and the analysis should consider surface morphology as well. Afgan et al. [9] investigated water, ethanol and R123 boiling heat transfer on horizontal tubes whose diameters were 3, 4, 16 and 18 mm. These surfaces were covered with sintered powder layers of grain sizes ranging from 63 to 100 μm. Porosity of the produced structure was 30 – 70 %, while their thickness 0,45 – 2,20 mm. It was observed that boiling begins at lower superheats than for the smooth surface – at 1 – 1,5 K. There are a few boiling modes on the boiling curve as presented in Fig. 1. They are typical for the porous layer. The first one covers small superheat values and here the increase in heat flux results from more nucleation sites becoming active as temperature rises.

At higher superheats the boiling curve is in mode II. A significant increase in superheat between I and II is linked to the creation of a vapour blanket inside the porous layer. A constant value of the exponent n in this mode proves that the vapour thickness is almost contant, since the vapour layer of a given thermal resistance causes a rise in heat flux which is propoportional to superheat.

A high amount of vapour in mode I at increasing superheat and limited possibility of its removal from the microstructure leads to vapour retention in the porous structure and, consequently, to the creation of a stable vapour film – mode II. The transition between I and II can take place in various forms (mode III, IV, V and VI) depending on heat flux, at which the increase of surface temperature occurs.

The authors explain this phenomenon by describing the vapour and liquid flow in the boiling process. The stable liquid circulation in the porous structure occurs when the capillary pumping is at least equal to the total pressure drop of vapour and liquid flows. As heat flux rises vapour flow increases and, as a consequence, water flow is also higher. Total pressure drop rises, which might be bigger than the capillary pumping. At this point vapour film occurs at the base of the microstructure.
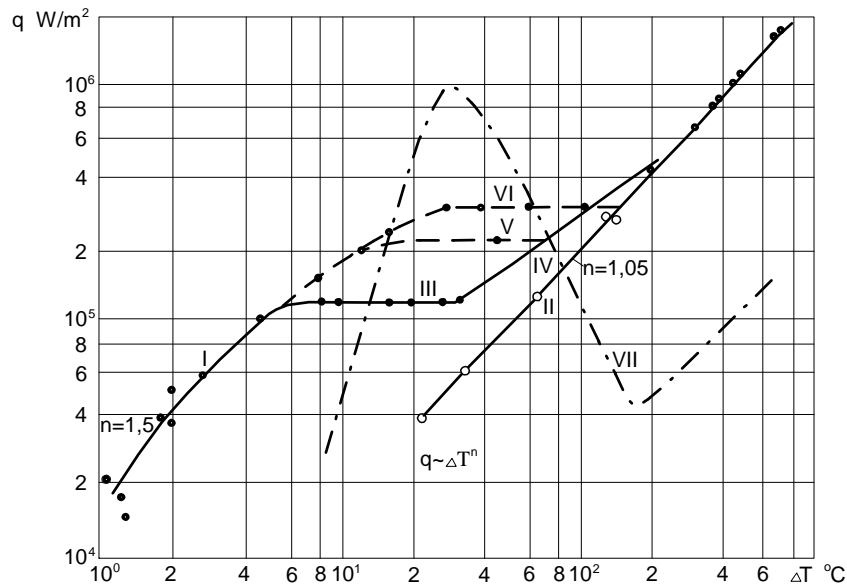
Fig. 1. Boiling curve for water: tube of 16 mm diameter, porosity of the layer 70%, thickness of the layer 2,2 mm. Dashed line – smooth reference surface [9].

The augmentation of heat transfer due to the application of porous microstructures might be significant. Figure 2 presents test results for distilled water boiling heat transfer at ambient pressure on the surface covered with porous layer of 0,6 mm height and porosity ca. 60 % [10]. It was concluded that it might be possible to dissipate over 10 times more heat – for lowest superheats – if porous layers are used, as compared to the smooth reference surface.
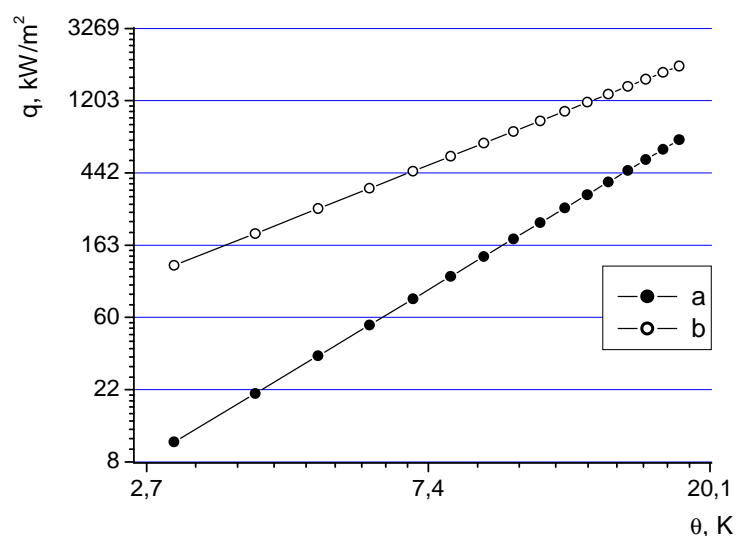
**Fig. 2. Boiling curves for distilled water: a – smooth surface [11],
b – microstructural coating [10].**

However, porous layers have disadvantages and new methods of heat transfer augmentation are constantly looked for. One of very new concepts is the use of laser treatment. If such a technology proves to be useful, it might be easier to produce heat exchanger surfaces. Besides, vapour produced in the porous layer might block the fluid transport and lead to lower heat fluxes at high superheats. The design of new efficient surfaces for heat exchangers should be focused on limiting this is unfavourable phenomenon. Laser treatment might be an option to verify.

2. Experimental procedure

The tests have been performed on a resistance ribbon whose dimensions are ca. 40 mm x 4 mm x 0.5 mm (length x width x thickness) for two working liquids: distilled water and ethyl alcohol (purity of 99.8 %). The ribbon itself served as a heater surface since electricity was supplied to it with copper wires connected to a transformer. The subsequent laser treatment was performed with the aid of a BLS 720 laser system employing the Nd:YAG type laser operating in the pulse mode. The erosion was performed with the point pulsed-laser technique using the Nd: YAG type of laser under the following conditions:

- laser spot diameter, $d = 0.7$ mm,
- laser power, $P = 20W; 30$ W,
- beam shift rate, $V = 1200$ mm/min,
- nozzle-sample distance, $h = 6$ mm,
- pulse duration, $t_1 = 0.45$ ms,
- frequency, $f = 50$ Hz.

The rounded geometrical parameters of the samples have been presented in Table 1 with the focus on the produced cavities since a lot of data on boiling heat transfer suggests that surface microgeometry has a significant impact on the heat fluxed dissipated during boiling. Figure 3 presents surface topography of the four surfaces, while Figure 4 microgeometry profiles of the selected samples. The smooth surface (described as number 0 in the table) without any laser induced cavities has been considered as reference.
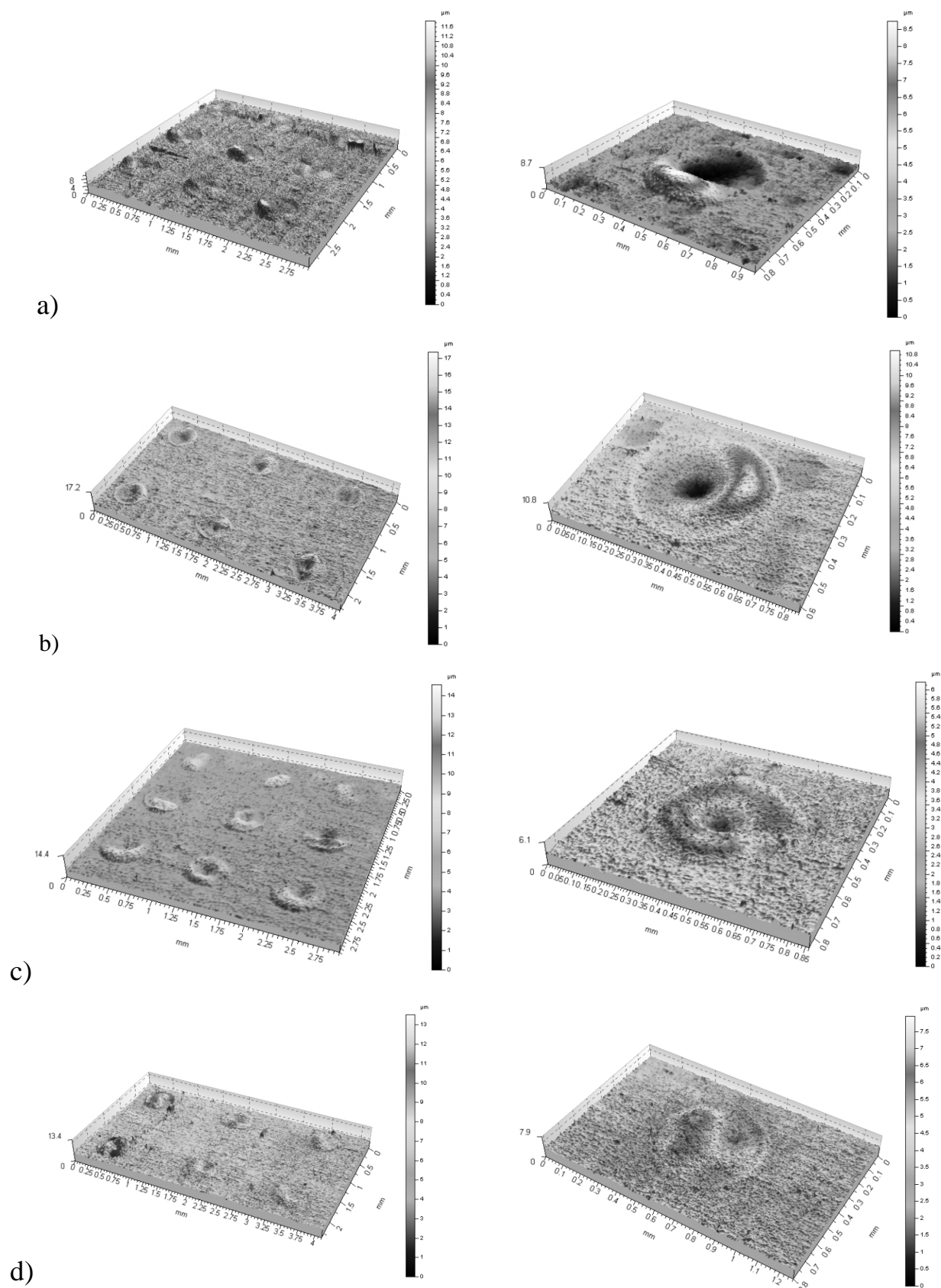
Fig. 3, b, c, d. Surface topography of samples no 1 (a), 2 (b), 3 (c) and 4 (d). On the left: the whole surface; on the right: a single cavity.

Table 1 - Geometrical parameters of the samples.

Surface number	Cavity depth, μm	Cavity diameter , mm
0	-	-
1	1.9	0.22
2	4.0	0.21
3	2.6	0.17
4	2.0	0.20

a)

b)
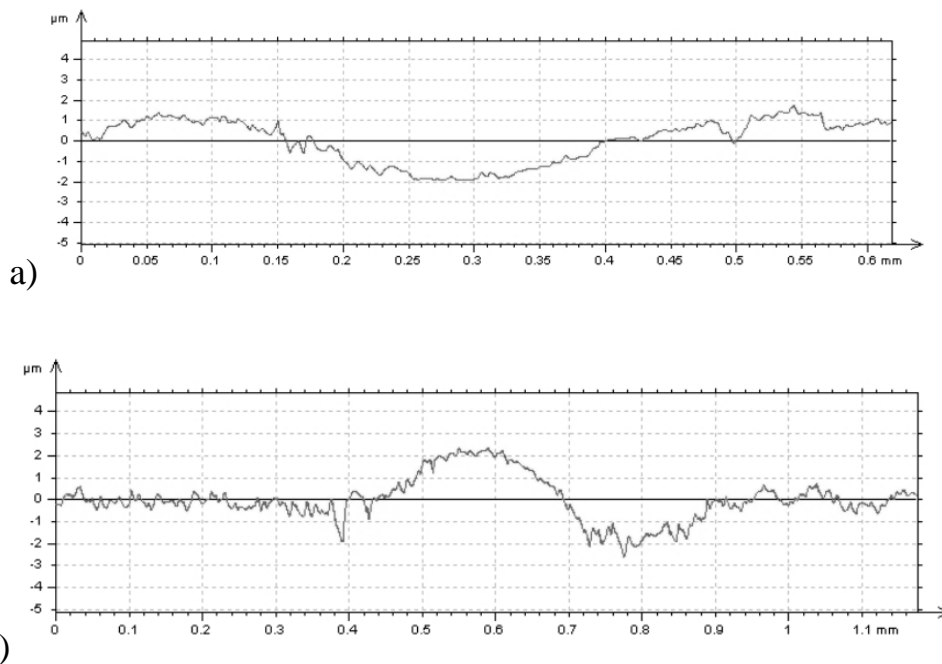
Fig. 4a, b. Microgeometry profiles for samples no 1 (a) and 4 (b).

The experimental set – up consists of a vessel, in which water and ethyl alcohol are boiled. The heater unit is immersed in it and is heated by the flow of the electric current supplied through the transformer. The liquid level is maintained at ca. 5 mm above the sample. The power supplied to the heater can be calculated basing on the known electrical resistance and voltage measured with a multimeter. The temperature of the surface is taken as the reading from a K type thermocouple combined with a measuring unit. The thermocouple is located just below the heater surface. The heater is attached to a bakelite plate with silicone. This minimises heat losses and only the surface open to the liquid pool is considered. Fig. 5 presents the schematic of the heater unit with the main elements.
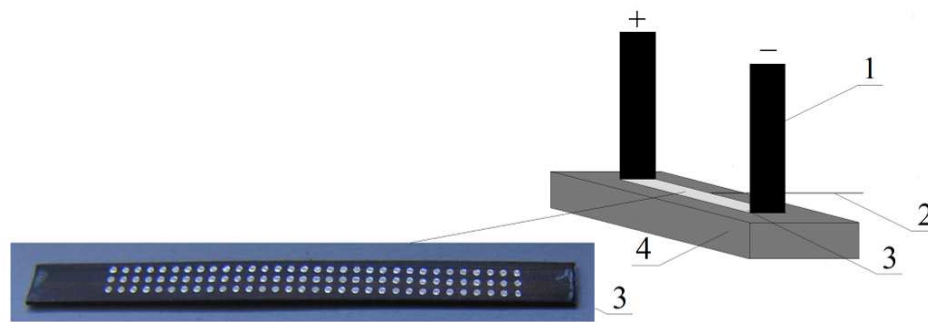
Fig. 5. Heater unit: 1 – electrical connections, 2 – thermocouple, 3 – sample (heater surface), 4 – bakelite insulation plate.

3. Test results

The experiments have been performed under atmospheric pressure on the smooth and laser treated samples with water and ethyl alcohol as working liquids. Due to limitations of the experimental stand, the tests for distilled water have been conducted at the subcooling level of ca. 30 ^{o}C (subcooling is defined as the difference between the saturation temperature and the actual liquid temperature). While the results for ethyl alcohol have been obtained under pool boiling conditions.

Table 2 presents the results for distilled water as the ratio of the heat flux for the considered laser treated sample to the heat flux from the smooth surface (q_{laser}/q_{smooth}) all for the same surface temperature of the samples 105 ^{o}C. It is apparent that sample 1 is most efficient in dissipating heat. Heat flux can be almost twice as much as for the smooth surface, which means that a heat exchanger produced with such a modified surface can have smaller heat transfer area in comparison to the smooth surface and, thus, can be smaller and lighter. The other laser treated samples actually decreased heat flux.

Table 2 - Distilled water test results.

Sample 1	Sample 2	Sample 3	Sample 4
1,91	0,58	0,66	0,44

In order to verify this phenomenon ethyl alcohol has been used in the experiment. In this case it has been observed that at the surface wall superheat of ca. 13,6 ^{o}C (which is an elevation of the sample surface temperature over the saturation temperature of the liquid) sample no 4 performed best. The ratio of

the heat fluxes for samples 1 – 4 are given as: $q_1:q_2:q_3:q_4 = 1:2,25:1,27:5,06$. The opposite effect was recorded for the tests with distilled water.

This phenomenon can be explained by different surface tension of water and ethyl alcohol. The alcohol can wet the surface more easily and, thus, it actives smaller cavities easier so that they could produce vapour bubbles and improve heat transfer conditions. The cavity in Fig. 4 b has more irregular surface with many small cracks where vapour can be sustained after bubble detachment – this gives way to new bubbles being produced in case of ethanol.

With regard to water test results, the analysis of the surface morphology indicates that sample no 1 had the biggest cavity diameter and small distance between the cavities. This proves to be advantageous for transport properties of water into the cavities. Bubbles after detachment from neighbouring cavities can join together which might improve heat transport. Exactly the opposite is true for ethyl alcohol, which might be the result of different surface tension of both liquids (the diameter of water vapour bubbles is larger than ethanol vapour bubbles). Besides, the test results presented in the paper indicate that with regard to laser treated surfaces not only surface finish needs to be considered but also the kind of the working fluid. It could be linked to relatively small depths of the cavities, which in boiling heat transfer enhancement tests for other surface modification techniques often reach 1 – 2 mm.

It is, however, clear that the use of laser treatment produces more efficient heat exchanging surfaces. The heat flux for the same superheat of sample no 1 modified with laser is almost two times higher in comparison with the smooth surface for water.

Conclusions

The application of laser treatment increased heat flux for boiling heat transfer. Consequently, heat exchangers with such a modified surface can be smaller or operate at smaller temperature differences to dissipate the same amount of heat. However, more research is needed in this area to determine, for example, the impact of other working liquids and to obtain an insight into the enhancement mechanism, which might produce the surface with optimal cavity dimensions. With more experimental data it might also be possible to propose design standards for such heat exchangers in the industrial scale.

References

1. Wondra F., Stephan P., Pool boiling heat transfer from tubular microstructured surfaces in saturated FC-72, ECI Int. Conf. on Boiling Heat Transfer, Spoleto, 2006.

2. Hong K.T., Imadojemu H.E., Webb R.L., Pool boiling of R-11 refrigerant and water on oxidized enhanced tubes, Fundamentals of Phase Change: Boiling and Condensation, ASME-HTD, vol. 273, p. 1 – 9, 1994.

3. Chang J.Y., You S.M., Enhanced boiling heat transfer from microporous surfaces: effects of a coating composition and method, Int J. Heat Mass Transfer, vol. 40, 18, p. 4449 – 4460, 1997.

4. Nimkar N.D., Bhavnani S.H., Jaeger R.C., Nucleation char. of a structured surface in a dielectric coolant in the absence of spreading effects, p. 82 – 89, Inter Society Conference on Thermal Phenomena, 2004.

5. Nimkar N.D., Bhavnani S.H., Jaeger R.C., Effect of nucleation site spacing on the pool boiling characteristics of a structured surface, Int. J. of Heat and Mass Transfer, vol. 49, p. 2829 – 2839, 2006.

6. Forrest E., Williamson E., Buongiorno J., Hu L.-W., Augmentation of nucleate boiling heat transfer and critical heat flux using nanoparticle thin – film coatings, International Journal of Heat and Mass Transfer, 53, p. 58 – 67, 2010.

7. Cengel Y.A., Heat Transfer: a practical approach, McGraw-Hill, 2003.

8. Carey V.P., Liquid – vapor phase – change phenomena. An introduction to the thermophysics of vaporization and condensation in heat transfer equipment, Hemisphere, 1992.

9. Afgan N.H., Jovic L.A., Kovalev S.A., Lenykov V.A., Boiling heat transfer from surfaces with porous layers, Int. J. Heat Mass Transfer, vol. 28, 2, p. 415 – 422, 1985.

10. Orman Ł.J., Possibility of the application of microstructures in heating and ventilation systems, Structure and Environment, Kielce University of Technology, 1, vol. 2, p. 41 – 45, 2010.

11. Orman Ł.J., Nucleate boiling heat transfer on a smooth surface of a fin, Proc of XII Int. Symposium „Heat Transfer and Renewable Sources of Energy", Szczecin, p. 363-369, 2008.

3.2.4 DETONATION-SPRAYED WC-12%CO AND WC-17%CO COATINGS ON DIAMOND-IMPREGNATED SEGMENTS
Borowiecka-Jamrozek J.[1]

Introduction

Metallic-diamond composites are tool materials in which diamond particles are embedded in a metallic matrix. Such materials can only be produced using the powder metallurgy technology [1].

Figure 1 illustrates a typical fracture of a diamond-impregnated segment.

Diamond-impregnated segments are produced from metallic and diamond powders by mixing and hot pressing or mixing, die pressing and sintering.

The segments soldered to a steel disc constitute the cutting elements of circular saws for cutting natural stone and other construction materials. The segments uniformly distributed around the disc are made by sintering cobalt and diamond powders [2].
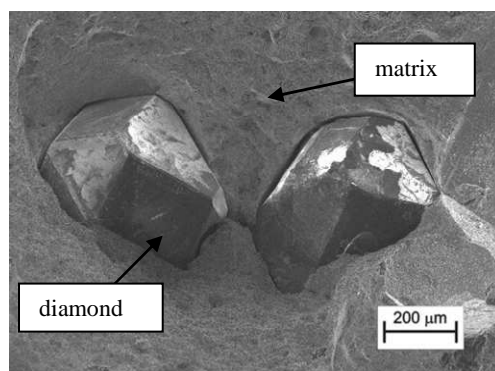
Fig. 1. Cross-section of the metallic-diamond composite

In certain applications of diamond-impregnated tools, when the quality of cut is important, sandwich-type three-layer segments are used. The layers differ in abrasion resistance. The abrasion resistance of inner layers needs to be lower than that of the outer layers to ensure saddle-shaped wear of the working surfaces, which prevents deviation of the saw blades.

In the case of homogeneous segments, the worn edges make the cutting action of the saw in the kerf difficult.

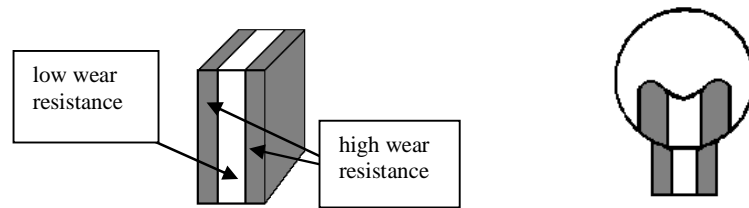---

[1] Kielce University of Technology

Fig. 2. Structure of a sandwich-type segment and saddle-shaped wear of the working surface

Sandwich-type segments are shaped by cold pressing. This process is technologically complex, especially if the narrow segments are to be suitable for saws with diameters less than 500mm. It is necessary to use a hydraulic press equipped with a volumetric feeder to assure uniform filling of the die cavity with a mixture of metallic and diamond powders. The powders are then subjected to initial granulation, which increases the production costs [3].

Sandwich-type segments are relatively difficult to produce. This paper proposes an alternative method, which involves applying WC-12%Co and WC-17%Co coatings on homogeneous substrates using the gas-detonation method [4].

1. Experiment

The tests were conducted on specimens prepared by sintering Cobalt SMS powder (Umicore, Belgium) with an average particle size of 1 μm (Fig. 3)
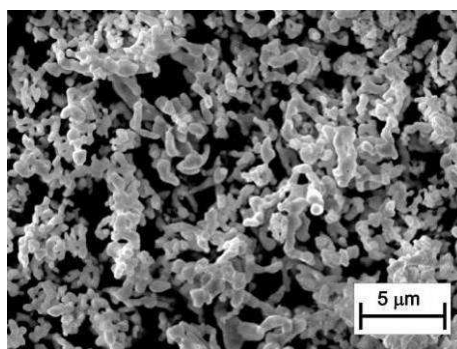

Fig. 3. Cobalt SMS powder

The particle size was determined using a Fisher sub-sieve sizer. The specimens were produced by hot pressing in a graphite die. The process of sintering was conducted for 2 minutes at a temperature of 850 °C and a pressure of 35MPa.

The coatings were produced using a Perun-S valveless dispenser at the Surface Advanced Technology in Warsaw. Prior to coating, the surfaces were degreased with acetone and grit-blasted with electrocorundum *EB 14*.

The properties of the coatings were established by performing the following tests: a microstructure analysis, a point analysis, a linear analysis using a Joel JSM 5400 scanning microscope equipped with an ISIS 300 energy dispersive X-ray spectrometer (EDS), a phase composition analysis using a Bruker D-8 Advance X-ray diffractometer, a microhardness test, and abrasion resistance test using a T-07 tester.

2. Results

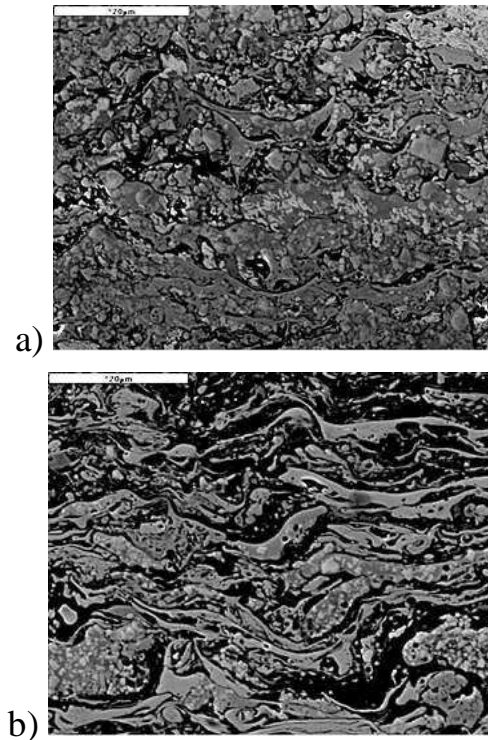The microstructure of the coatings obtained by detonation spraying are shown in Fig. 4.

Fig. 4. Microstructure of the coatings: (a) WC-12%Co, (b) WC-17%Co

The multi-layer microstructure of the coatings results from the strong deformation of the powder particles, which occurs during the deposition process. The layers vary considerably in the oxygen content, as shown by the point and linear analyses.
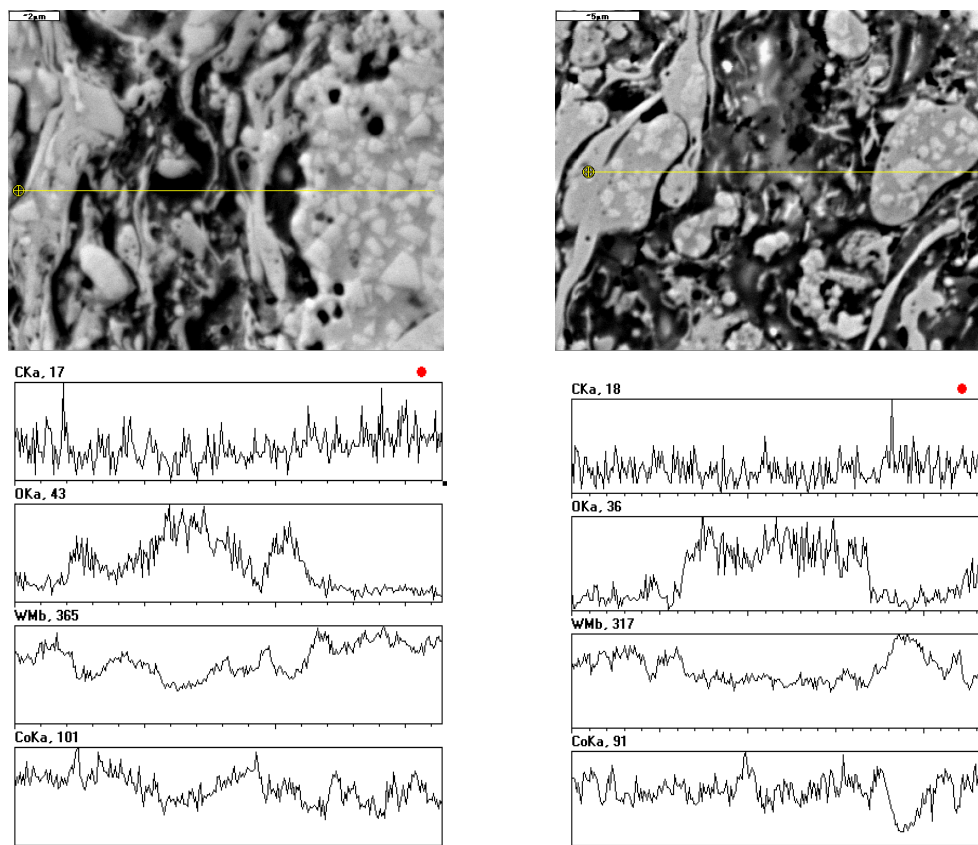
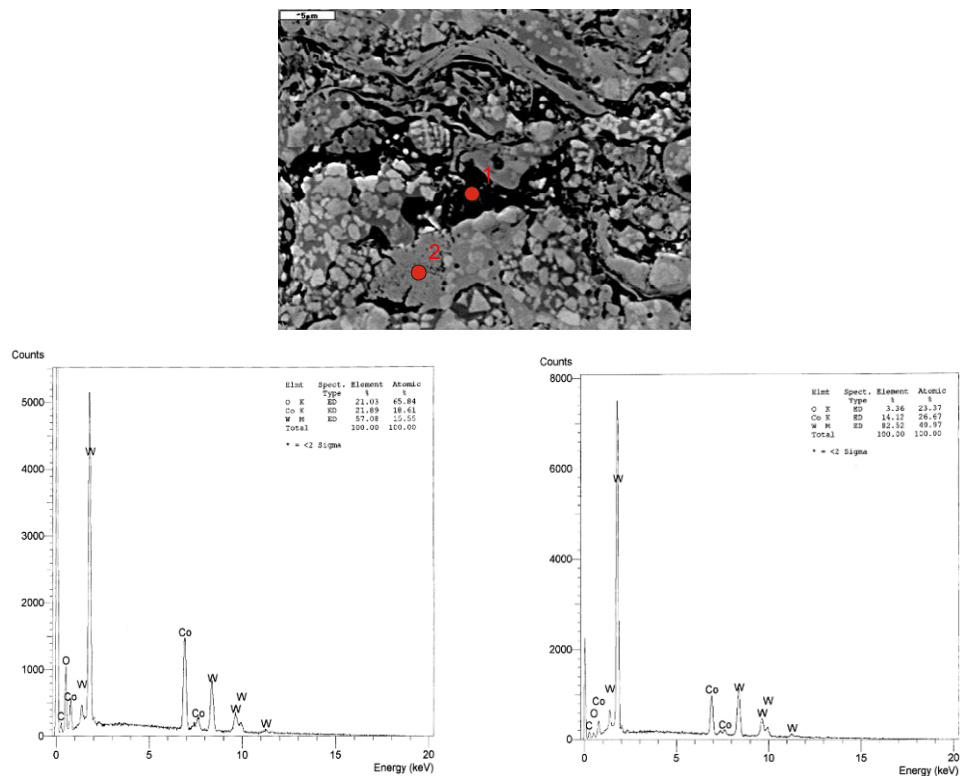**Fig. 5. Linear analysis of the coatings: (a) WC-12%Co, (b) WC-17%Co**

Fig. 6. Point analysis of the WC-12%Co coating: the dark-coloured component (1), the light-coloured component (2)
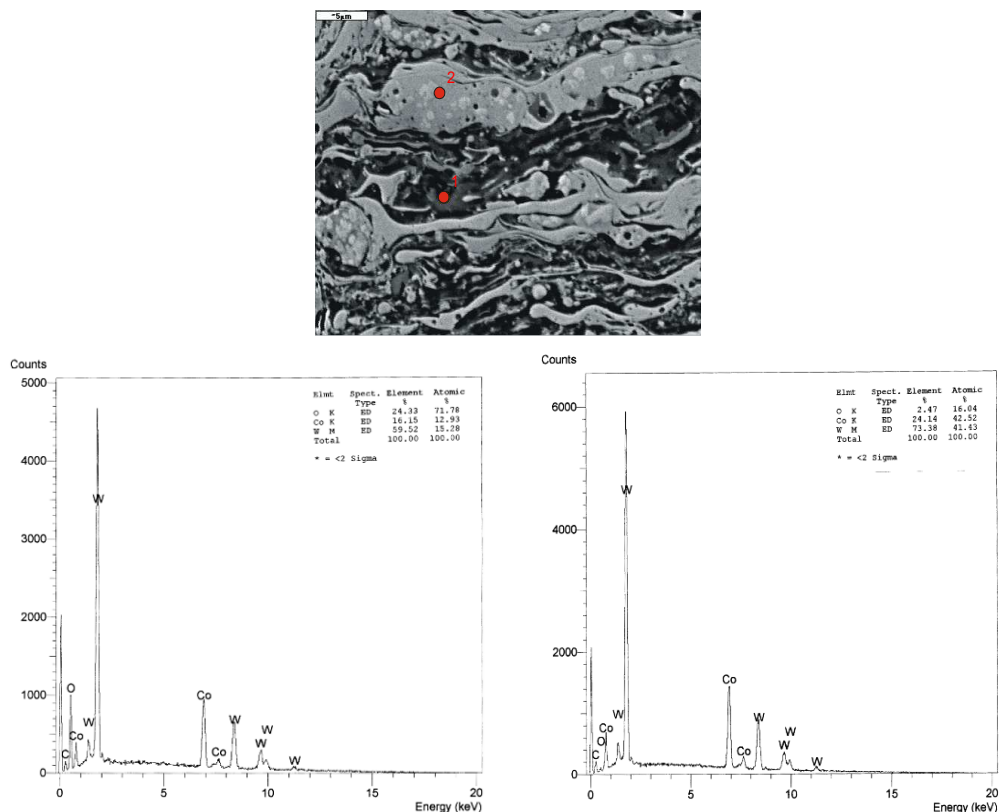
Fig. 7. Point analysis of the WC-17%Co coating: dark-coloured component (1), light-coloured component (2)

Phase identification using the X-ray diffraction technique revealed considerable differences in the composition of the carbide phase in the coatings. The WC-12%Co coating contained WC and a small amount of W_2C.
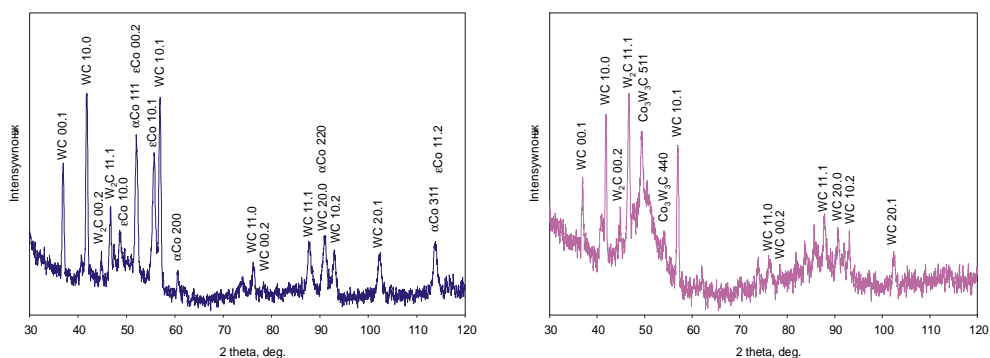

Fig. 8. Diffractograms of the coatings (a) WC-12%Co and (b) WC-17%Co

The content of WC and W_2C carbides in the WC-17%Co coating increased significantly. The analysis revealed also the presence of another carbide - $(W,Co)_6C$.

A change in the composition of the carbide phase was probably due to the partial combustion of carbon during the detonation spraying of the coating. The porous structure of the *Diamalloy 04152* powder particles was also of significance; it allowed diffusion of the oxidizing gases.

The formation of complex M_6C-type carbides is regarded to be an unfavourable phenomenon. A decrease in the content of the binding cobalt phase may lead to a considerable decrease in the strength and plastic properties of the coating material.

The hardness of the WC-12%Co coating was much higher than that of the WC-17%Co coating. After a Vicker's hardness test, there were no cracks around the indentation corners, which indicates that the coatings have appropriate plastic properties. No cracking or delamination around the indentations at the interface between the coating and the substrate confirms good adherence of the coating to the substrate. The strength of the substrate surface layer was improved by cold working, which involves collisions of the WC-Co powder particles with the sinter surface.
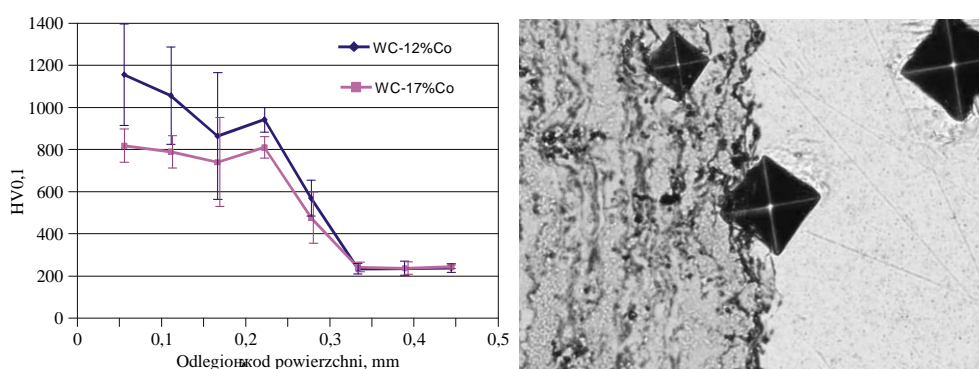

Fig. 9. Relationship between the microhardness and the distance from the surface

The abrasion resistance of the coatings was measured using a T-07 tester. The tests reveal that the wear resistance of the WC-12%Co coating is high, higher than that of the WC-17%Co coating. It is supposed that the high rate of wear of the WC-17%Co coating, which is twice as high as that of the WC-

12%Co coating, is attributable to a decrease in the content of WC at the expense of W_2C and $(W,Co)_6C$.
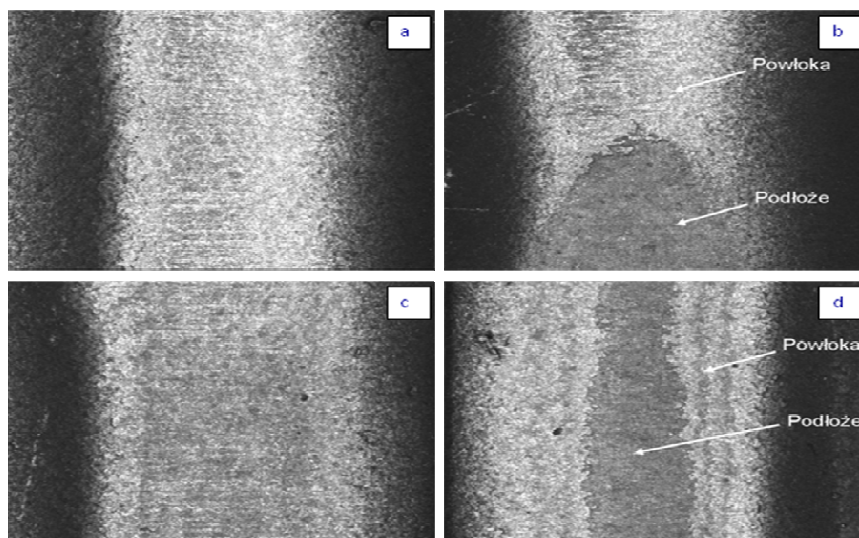

Fig.10 Traces of wear after abrasion resistance tests: WC-12%Co coating (a), WC-12%Co coating (measurement results not taken into account) (b), WC-17%Co coating (c), WC-17%Co coating (test results not taken into consideration) (d)

Conclusion

The experimental results confirm that the gas detonation method is well-suited for depositing WC-Co coatings with high hardness and different chemical and phase composition. The coatings produced from WC-12%Co powder possessed higher hardness and nearly twice as high abrasion resistance as the WC-17%Co coatings. Both coatings were well adhered to the cobalt substrate. As a result, the strength of the substrate surface layer, several dozen micrometers in thickness, was improved significantly by cold working.

During coating deposition, the temperature of the substrate material did not exceed 150°C; it had virtually no effect on the properties of the diamond crystals. It can be concluded that the method is suitable for increasing the abrasion resistance of the segment side surfaces. Thin WC-Co coatings applied to the side surfaces of the homogeneous metallic-diamond segments ensure uniform lateral wear of the saw. This can be an alternative to *sandwich*-type segments. The analysis described in this paper was qualitative in nature. No tests were conducted to estimate the efficiency of the tool.

Reliable tests to assess the durability of metallic-diamond tools are static in nature, time-consuming and very costly. This paper deals with qualitative analysis only; the wear rate was typical of saws used for cutting sandstone slabs.

References

1 Tönshoff H.K., Hillmann-Apmann H., Asche J., Diamond tools in stone and civil engineering industry: cutting principles, wear and applications, Diamond and Related Materials 11/2002, pp. 736-741

2 Konstanty J., The materials science of stone sawing, Industrial Diamond Review, 1/91, pp. 27-31.

3 Konstanty J., Cobalt as a Matrix in Diamond Impregnated Tools for Stone Sawing Applications (Rozprawy, Monografie), AGH. Uczelniane Wydawnictwa Naukowo-Techniczne, Kraków 2002.

4 Borowiecka-Jamrozek J., Rozprawa Doktorska, PŚK, 2008

3.2.5 PROBLEM OF DEFORMATIONS OF VACUUM QUENCHED COMPONENTS

Brezničan M.[1], Fabian P.[1], Meško J.[1]

Introduction

Requirements for tools and for components in energy industry are very high at present. The most required properties of quenched components are lifetime, dimensional precision and stability. That is the reason why is the vacuum heat treatment focused on achieving homogeneous martensitic microstructure with minimum content of residual austenite.

Vacuum quenching or quenching in special furnace atmosphere is the only way to quench steels without scalings production on the surface of quenched components. At components with pure surface we may relevantly compare dimensions and geometry before and after quenching.

Vacuum quenching is especially significant in order to quench stainless and tool steels which often need high austenitizing temperature before quenching. The higher austenitizing temperature is, the higher increase of

---

[1] University of Žilina

decarburization layer is. The vacuum does not allow production and increase of decarburization layer on the surface.

1. Materials and Experimental Methods

As experimental materials there were selected stainless steel with low carbon content and tool steel with higher carbon content (Tab. 1 and Tab. 2). Both are special steels, but X12Cr13 is steel which contains chromium low-carbon martensite after quenching.

X12Cr13 is the basic martensitic steel which will attain high mechanical properties after heat treatment. It has good impact strength, corrosion and scaling resistance up to 649 °C. The applications are cutlery, stream and gas turbine blades and buckets, bushings, valve components, fasteners, screens and kitchen untensils. Structural parts are using in water or steam, components for paper, textile and food industry. The recommended austenitizing temperatures belongs to 950 – 1000 °C (up to 1050 °C, when the tempering will be not necessary or when the component will be only low-temperature tempered), followed by oil, gas or air cooling. [7]

Table 1 - Chemical composition of X12Cr13 steel

(Weight %)		C	Cr	Mn	Si	Ni
X12Cr13	min.	0.08	11.50	–	–	–
	max.	0.15	13.50	1.50	1.00	0.75

90MnCrV8 is the medium alloyed cold work steel with nearly 1% carbon, high hardening capacity, limited through hardenability, dimensionally stable and good compressive strength. The applications are guide strips, ejector pins, cutting, punching and stamping tools, thread cutting tools, measuring tools, broaches and box grooves. The recommended austenitizing temperature belongs to 780 – 820 °C, followed by oil or hot salt bath cooling. The temperature of salt bath belongs to 220 – 180 °C. [1]

Table 2 - Chemical composition of 90MnCrV8 steel

(Weight %)		C	Mn	Cr	V	Si
90MnCrV8	min.	0.85	1.80	0.20	0.05	0.10
	max.	0.95	2.20	0.50	0.20	0.40

As a measure content there was selected a shaft. Drawing is on Fig. 3. Experimental heat treatment was realized in a bicameral vacuum furnace with use of standard heat treatment parameters for following steels. Steel X12Cr13 was heated by 3 steps with austenitizing temperature 1030°C and quenching medium was a high pressure gas (argon). The temperature regime is on Fig. 1.
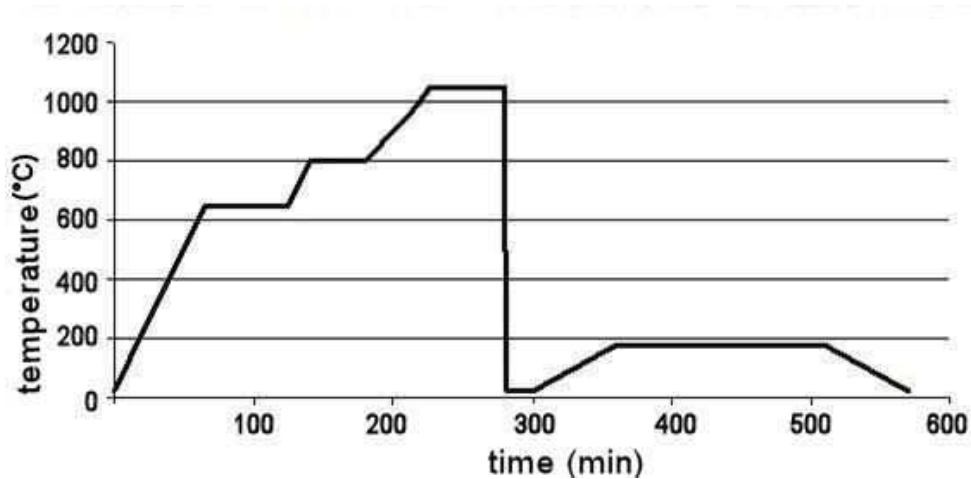

Fig. 1 Heat treatment temperature regime of steel X12Cr13

Steel 90MnCrV8 was heated by 2 steps with austenitizing temperature 800°C and quenching medium was special oil for vacuum quenching. The temperature regime is on Fig. 2. Both steels were low-temperature tempered after quenching.
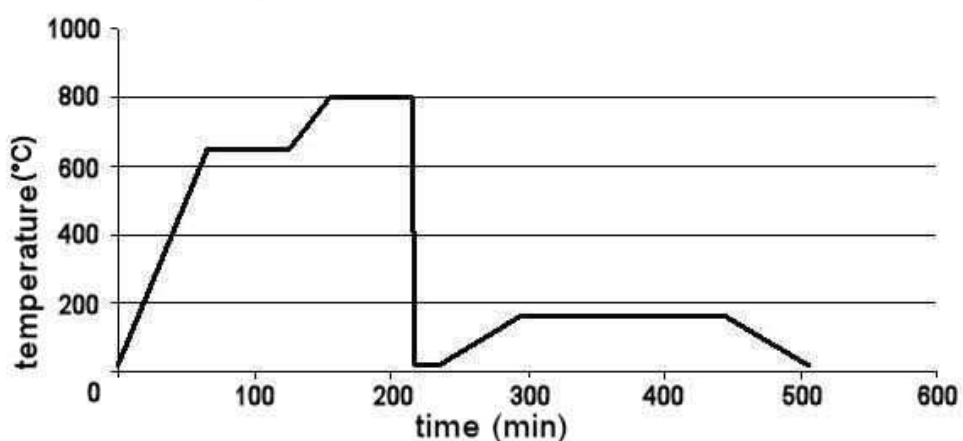

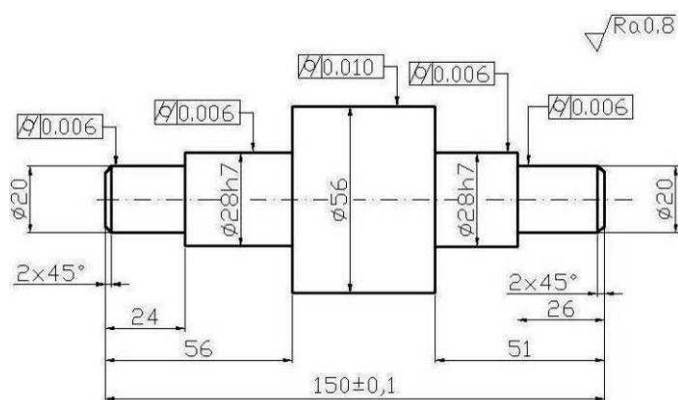**Fig. 2 Heat treatment temperature regime of steel 90MnCrV8**

Fig. 3 Drawing of quenched sample

In the case of microstructure samples heat treatment regime was corrected for dimensions of these samples.

2. Results and Discussion

The Microstructure and hardness correspond with used temperature regime. The microstructure consists of δ-ferrite with chromium martensite (Fig. 4) in the case of X12Cr13 steel and tempered martensite with carbides (Fig. 5) in the case of 90MnCrV8 steel (correspond with CCT diagrams for these steels).

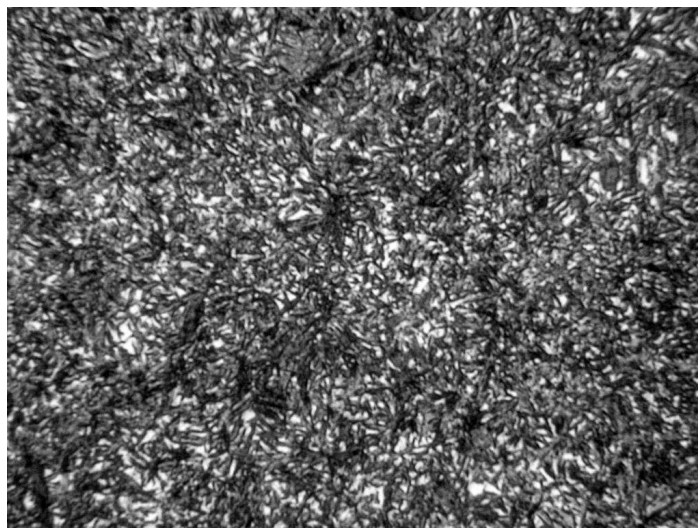**Fig. 4 The microstructure after quenching of X12Cr13 steel (500x)**

Fig. 5 The microstructure after quenching of 90MnCrV8 steel (500x)

Big clearly bounded grains on Fig. 4 are δ-ferrite. Needles inside the grains are martensite. Dark field on Fig. 5 represents tempered martensite. White field represents carbides.

Average hardness of quenched X12Cr13 steel is 54 HRC and of quenched 90MnCrV steel is 60 HRC (Tab. 3). Both are normally achieved hardness in these steels after quenching.

Table 3 - Hardness of quenched components (HRC)

X12Cr13		90MnCrV8	
54.55	54.75	59.15	59.50
54.30	54.12	59.45	60.01
54.15	54.04	59.95	59.88
Average: 54		Average: 60	

Change of dimension was measured by 3D measuring device. Volume change dependency on the dimensions is on Fig. 6. On the x-axis are dimensions (diameters) of every one step of the shaft. Geometry change dependency on the dimension is on Fig. 7. On the x-axis are diameters and length of every one step of the shaft as a ratio of diameter to length.
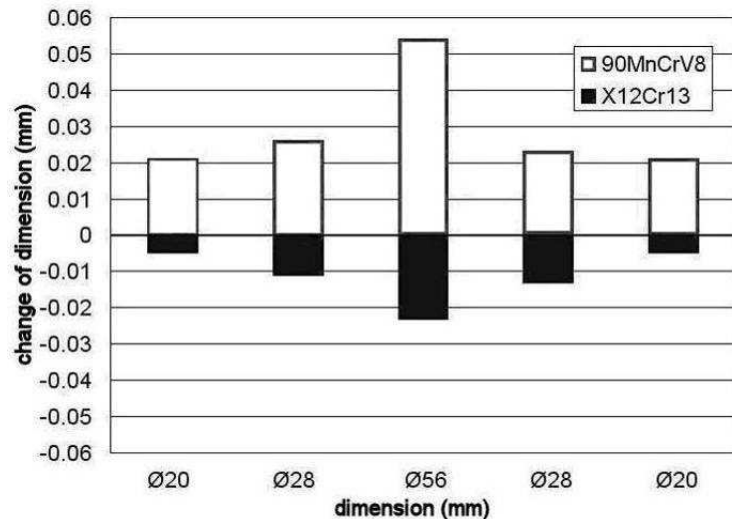
Fig. 6 Change of dimensions

The results show that low-carbon (chromium) martensite reduces volume of content after quenching by 0.1%. Standard high-carbon martensite increases volume of content after quenching by 0.2%. It is clear, that type of martensite affects not only on the mechanical properties of steels, but on the character of deformations too.

Graphic display of volume changes on Fig. 6 shows that the change in the case of steel 90MnCrV8 is double higher than change in the case of steel X12Cr13 and is reverse directed. The higher the dimension is the higher the change of dimension is.
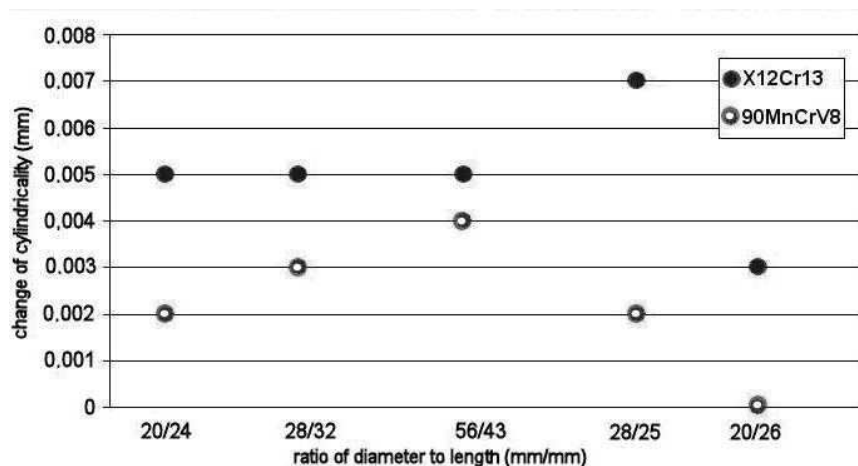

Fig. 7 Change of cylindricality dependency on the dimensions of component

Geometry change depends not only on the type of martensite, but on the full chemical composition of steel. Higher geometric stability as X12Cr13 steel

has 90MnCrV8 steel (Fig.7). It is known, steel 90MnCrV8 is very geometrically stable steel.

Conclusion

Vacuum quenching is energy intensive technology, but the best results in quenching of stainless and tool steels are achieved with this. This is also the deformations that are the lowest with use of vacuum quenching. The results in this document are initial only. The results showed that the character of volume change depend mainly on chemical composition of martensite. Quantity of volume change is not exact parameter and depends on the temperature regime, type of quenching medium and other technological parametres, but especially on the chemical composition of material.

What's important is a different impact of standard carbon martensite and low-carbon chromium martensite on the character of volume change. Reduce of volume after quenching means the need to choose the higher allowance for grinding.

Based on these results we can conclude that they behave like steel and related chemical composition. Interface between positive and negative change in volume is primarily dependent not only on carbon content, but also the chemical composition of martensite on what are a significant proportion of chemical elements such as chromium, nickel and manganese. It is, however, that dimensional change is given based on the particular type of heat treatment at the same time respecting all principles of quenching. Failure to comply with principles such as the imposition of charge there is further influence of geometry, so that is no longer dependent only on the volume change caused by changes in microstructure and thus it can't be applied to the result of a change geometry in this work.

Acknowledgement

References

1. Doerrenberg. Doerrenberg Edelstahl GmbH products catalog. 2006. [online]. Doerrenberg. de. [cit. 15. 10. 2010]. Available on: http:// www. doerrenberg. de/ fileadmin/template/doerrenberg/stahl/DatenblaetterEng/ 1.2842_en.pdf.

2. Durand-Charre, Madeleine. Microstructure of Steels and Cast Irons. Berlín: Springer-Verlag Berlin Heidelberg New York, 2004. 399 p. ISBN 978-3-540-20963-8.

3. Hanas, P; Vodičková V. Vliv tepelného zpracování a deformace na fázové složení slitin na bázi Fe3Al. Strojírenská technologie, 2010, roč. XV., č. 4, s. 13-18. ISSN 1211-4162.

4. Koutský, Jaroslav. Slitinové oceli pro energetické strojírenství. Praha: SNTL, 1981. 340 s.

5. Martienssen, Werner; Warlimont, Hans. Springer Handbook of Condensed Matter and Materials Data. Berlín: Springer-Verlag Berlin Heidelberg, New York, 2005. 1120 p. ISBN 978-3-540-44376-6.

6. Morávek, O; Baborovský, V. Nástrojové materiály a tepelné zpracování nástrojů. Praha: SNTL, 1972. 508 s.

7. Bronček J., Vidiečan J.,, Dzimko M.:Comparison of roughness measurement methods [Porovnanie metód merania drsnosti] /.In: Zeszyty naukowe : nauki techniczne - budowa i eksploatacja maszyn. - ISSN 1897-2683. - Nr. 16 (2011), s. 19-25.

3.2.6 SURFACE LAYER TRANSFORMATION INFLUENCED BY SOME OPERATIONAL FACTORS

Musiał Ja.[1]

Introduction

The features of surface layer of the kinematical pair elements there are the factors, which greatly influenced operational possibilities of the pairs. Thereby, they are also the factors which determine usable features of whole machine, e.g.: its durability, reliability, rate of production and others.

The surface layer (SL) is constituted during whole manufacturing process and its features depend in the largest degree from kind and parameters of operations which technological process consists. However, the features of SL do not make up durable set of factors. Under the external loads (force, thermal or chemical extortions) they undergo the changes accelerating or delay elementary

---

[1] University of Technology and Life Sciences, Bydgoszcz, Poland

processes of destruction of SL of elements and thus of wear process of kinematical pair.

From above mentioned short considerations one can formulate conclusion that possibilities of machine are determined not only by decisions undertaken in stage of design and construction, as well as production, but also in the phase of its operation. However, for correct decisions, one should know influence of individual operational features (extortions) on the changes of SL state during operational process. The main aim of presented investigations is determination of mentioned above relationships.

1. Object and conditions of experiments

The state of surface layer is described by the features set which contain parameters: physic-chemical, stereometric physic-chemical, and first of all – stereometric [2].The decisive meaning about properties and characteristics of surface layer, indirectly influencing also on remaining earlier introduced groups of factors, have describing the stereometric structure of surface parameters (called more often *Surface Geometrical Structure*).

The surface geometrical structure (SGS) is one of characteristic element of surface layer, which determines the course of wear process [3]. During kinematical pairs operating, the clear changes in structure of geometrical surface are visible. They have relations with operational factors in destruction process, caused in this case mainly by the rolling friction [4]. Whole spectrum of changes creates view of transformation of service generated layer (SGL). The acquaintance of changes course in structure of geometrical surface is the indispensable element of design processes of operating machines and their modeling [11].

According to processes setting during kinematical pairs operation, the course of changes of surface geometrical structure can be differ. In order to determine the course of transformation and relations the test in following range were undertaken:

- delimitation of operational factors set that have essential influence for transformation process,

- determination of relation between above mentioned factors and changes of describing surface geometrical structure (SGS) quantities,

- description of registered changes by means the mathematical models.

As object of investigations the angular ball bearings were accepted. This type of bearing was chosen, because the intensity of phenomena during transformations of SGS is great with regard on constructional features and connected with them – kinematics of its elements [4]. Mentioned features create the good conditions for transformation's monitoring.

With regard on: character of loading, the kinematics of bearing elements and operating matter in real conditions, the greater changes are happen on inner rings and therefore the changes thereon these rings were observed in presented investigations.

1.1. Set of operational factors

The influence of external loading on the changes in surface layer is the complex operational problem. Therefore, the choice of essential factors for given operational process is difficult task. Taking into account the matter of process the following set of independent variables will be analyze [12]:

- the amplitude of variables pressures in zone of contact of balls and raceway in different places on its circuit, σ_ψ:0; 621; 887; 1381; 1520 MPa,

- the frequency of load variations, f : 75; 95 Hz.

The monitored changes were recorded in real-time and observations was made:

- on the start of investigations: 0 s, (with index 1),

- in period of settled intensity of changes: 2,1 s, (with index 2),

- in final period of fitness of bearing: 3,9 s , (with index 3).

Mentioned above data were assumed on the ground of complex investigations of angular rolling bearings described in [10].

1.2. Set of measured quantities

As the measures of changes occurring in SGS, the values of roughness parameters were accepted. With regard on fact, that surface with curvilinear contour (concavo-convex) was investigated, theoretical surface of its curvature was determine, and then – it was subjected to filtration, this way receiving the image mapping on plane surface. In Fig. 1a the real picture of measured surface

is introduced. The same surface but after filtration of the curvilinear contour of theoretical surface is shown in Fig. 1b.
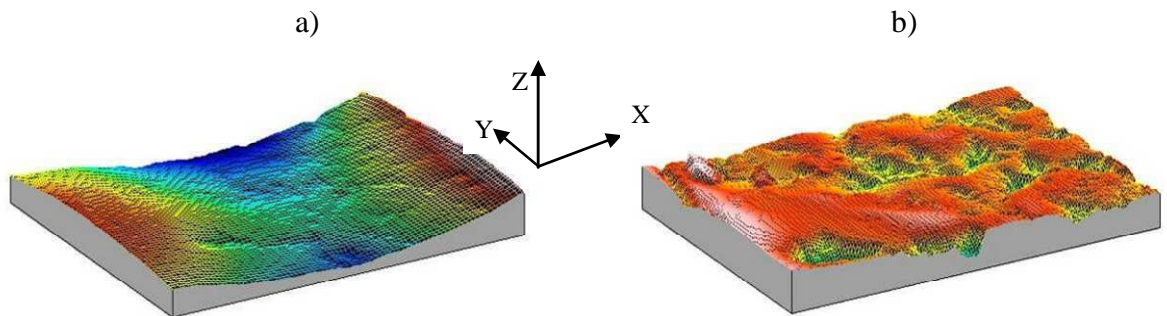

Fig. 1. Microgeometry of investigated surface: a) real measured surface, b) roughness of measured surface after filtration of theoretical, nominal curvilinear surface

On the ground of numerous References's information, eg. [8, 9] one affirm, that to assessment of SGP using all known parameters not always is needed. On this base, in presented investigations the elements of measured parameters set was chosen. One of them is the basic parameter of roughness – mean arithmetical deviation, *Sa*. Considering that the investigated rolling bearings are subjected to changing load, in experiments parameter *Sv* – denominative the maximum value of depression, was accepted to analysis. The choice of this parameter motivating is following. One should affirm the depressions of roughness profile as discreteness of structure and as such, they can to compose the places of initiation of fatigue cracks. However, from second side superficial depressions can compose volumes in which grease is accumulate – so their influence can be positive.

In the aim of comparison of earlier introduced the amplitudinal parameters, in analysis the parameter *St* – the total height the micro roughness, was also used.

In arrangement of stereometric measurements, the important parameter is the spatial roughness parameter *Sds* – the thickness of tops on the area of 1 square millimeters.

In order to assessment of surface roughness will be complete, besides introduced above parameters, to investigations was also accepted parameter *Sdq* – average square inclination, describing the shape of unevenness.

This way, in result of conducted analysis and parameters' selection, to following considerations there is receive the set of roughness parameters contains following components: *Sa*, *Sv*, *St*, *Sds*, *Sdq*.

The measurements were conducted in spatial arrangement (3D), in spite that valid standard captures it on plane (2D). It was made because observing unquestionable trends one was found that the spatial describer in near future the geometrical structure of surface arrangement will valid.

Additionally, the characteristic of surface roughness was replenished by functions of autocorrelation for individual times.

2. Results of investigations

The results of measurements for full range of effective load of tested type of bearing and for some time were taken down in Table 1.

Table 1 - Exemplary values of roughness parameters, for time $\tau_3 = 3,9 \cdot 10^5$ s

Pressure / Parameter	The amplitude of pressures $\sigma_\square$, *MPa*				
	0	621	887	1381	1520
Amplitude parameters					
Sa, μm	0,19	5,87	7,00	8,50	9,09
Sv, μm	2,97	43,21	42,21	39,45	36,81
St, μm	3,44	71,45	70,86	68,93	63,87
Spatial parameter					
Sds, pks/mm^2	476	402	371	159	48
Hybrid parameter					
Sdq, $\mu m/\mu m$	0,044	0,053	0,052	0,054	0,053

The relations of roughness parameters in form of 2D graphs was introduced in following figures: in Fig. 2 – against value of pressure σ_ψ and in Fig. 3 – against time τ, – factors having the essential influence on the state of the geometrical structure during bearings operation.
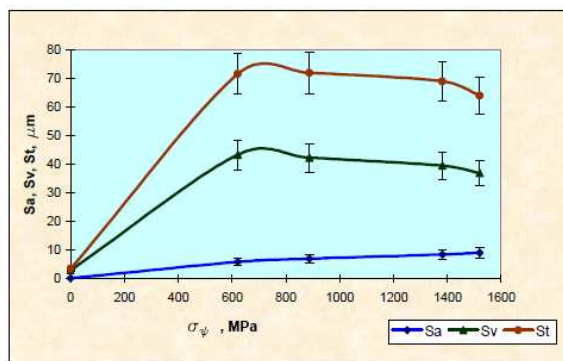
Fig. 2. Graphs of dependences of some roughness parameters on values of contact pressure for $\tau_3 = 3{,}9{\cdot}10^5$ s

On the ground of recorded dependences of values of parameters: *Sa*, *Sv* and *St* on contact pressure one can affirm that the changes of value of parameters roughness in large degree depend on the pressure amplitude. Particularly, initial growth of contact pressure σ_ψ in the range $\langle 0; 621 \rangle$ MPa causes the large increase of parameters value. For further growth – these changes are quite small. The influence of pressures on parameter *Sa* is smaller than on *Sv* and *St*. This due to averaging character of parameter *Sa*. On individual changes in SGP they react in considerably smaller degree than parameters *Sv* and *St*, which are measured between extreme points.

In Fig 3 were introduced the graphs, on the ground which is possible to estimate how the studied parameters of roughness change in whole time of transformation. The measuring points were connected, because on the ground of random investigations with great probability, it is possible to accept that changes will be like on introduced graphs.
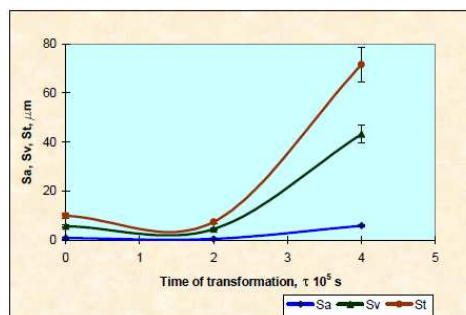

Fig. 3. Graphs of dependences of roughness parameters on values of time for $\square_\square$ = 621MPa
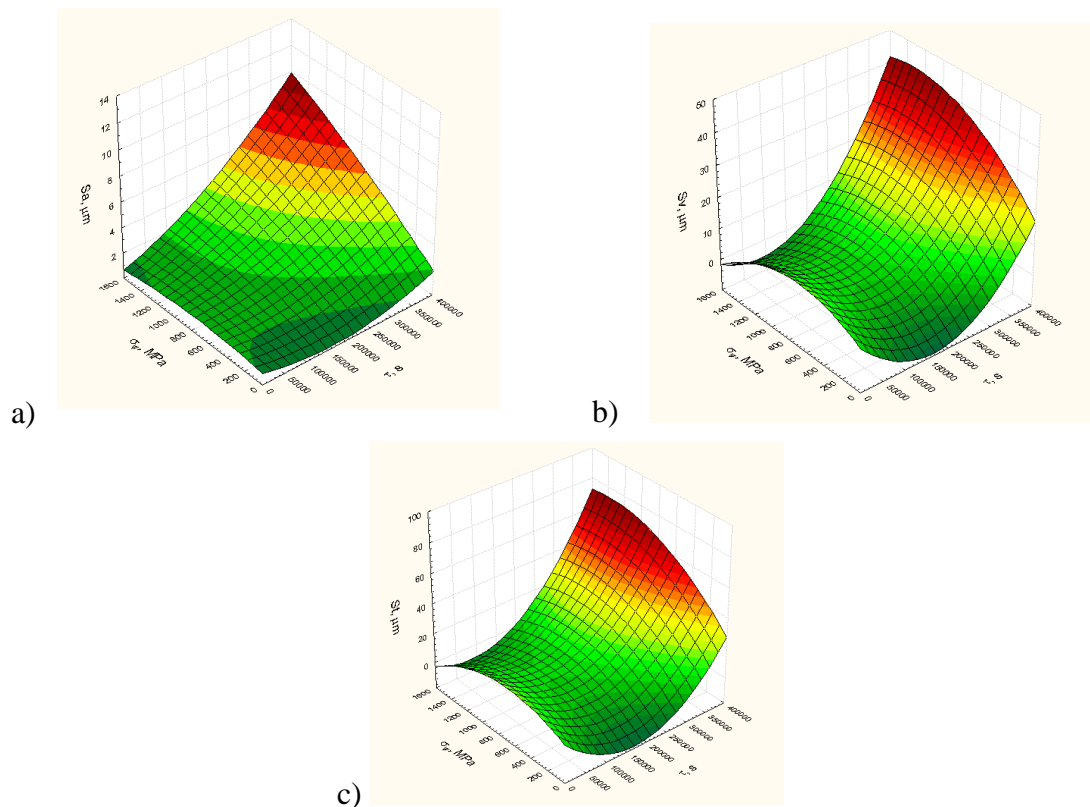
a)

b)

c)

Fig. 4. Spatial (3D) graphs of relations between some roughness parameters:
Sa **(a),** *Sv* **(b),** *St* **(c), and operating conditions:** σ_ψ **and** τ

For all studied parameters decrease of their value was affirmed in time from τ_1 to τ_2. However diverse growth happened in following operating – larger for parameters: *Sv* and *St* (more susceptible on extreme's) than for *Sa*, which are averaging valueṣ.

Spatial graphs of assumed relations in whole ranges of investigated parameters were presented in Fig. 4.

Second of studied factors were the frequency of load variations. In Table 1 the set of the same (like above) roughness parameters was introduced, for two values of frequency and for amplitudes of contact pressure $\sigma_\psi = 621$ MPa.

Table 1.1 - The values of roughness parameters for different frequency of load f

Frequency Parameters	75 Hz	95 Hz
Amplitude parameters		
Sa, μm	7.00	6.92
Sv, μm	42.21	43.79
St, μm	70.86	71.04

On the base of above presented results is possible to affirm that essential changes in studied range of changeability of this factor is not observe in SGS. One can to accept that the absolute changes of roughness parameters comprise in the range of statistical deviations.

3. Mathematical models

In the aim of determinations the relationships between roughness parameters of raceways on the inner ring and amplitude of contact pressure $\square_\square$, as well as time of transformation τ, the regress equations in assumed form were estimated. The detailed forms of models for individual parameters were introduced in Table 2.

Statistical quantities: R – the coefficient of correlation, as well as coefficient F/F_{tab}, which is the measure of significance and adequacy of mathematical model, were introduced too.

The calculated values of coefficients of correlation R are near 1.0, and the values of coefficient $F/F_{tab.}$ are very great, so it seems that determined models for all observed parameters are significance and adequate.

Table 2 - Models of relations between some roughness parameters and operating factors

Mathematical models	R	$F/F_{tab.}$
$Sa = 0{,}9257 - 9{,}0739 \cdot 10^{-6} \cdot \tau + 0{,}0009 \cdot \sigma_\psi + 2{,}8829 \cdot 10^{-11} \cdot \tau^2 + 1{,}2928 \cdot 10^{-8} \cdot \tau \cdot \sigma_\psi - 6{,}9507 \cdot 10^{-7} \cdot \sigma_\psi^2$	0,881	182,309
$Sv = 3{,}9473 - 0{,}0002 \cdot \tau + 0{,}0195 \cdot \sigma_\psi + 4{,}8195 \cdot 10^{-10} \cdot \tau^2 + 4{,}7165 \cdot 10^{-8} \cdot \tau \cdot \sigma_\psi - 1{,}4435 \cdot 10^{-5} \cdot \sigma_\psi^2$	0,789	150,154
$St = 7{,}4697 - 0{,}0003 \cdot \tau + 0{,}0323 \cdot \sigma_\psi + 8{,}3217 \cdot 10^{-10} \cdot \tau^2 + 8{,}6077 \cdot 10^{-8} \cdot \tau \cdot \sigma_\psi - 2{,}4202 \cdot 10^{-5} \cdot \sigma_\psi^2$	0,787	126,829

Conclusions

Conducted considerations, as well as investigations, both theoretical and experi- mental, permitted on expression several conclusions. The most essential, in the author's mind are following:

1. Verification of choice of factors determining the changes in structure geometrical surface proved significance two of them: amplitude of pressure in contact area and time of transformation. Third tested quantity – the

frequency of load variations – in studied range of values turned out with unimportant factor.

2.   Pressure in contact area of elements of kinematical pair in essential degree determines the course of changes in SGS. For this kind of load (extortion), in studied range of changes was observed the extreme of function (the maximum) describing the dependence of value of parameters roughness on the pressures and therefrom indirectly – on external load.

3.   Defined position in relation to external force of motionless bearing ring makes possible the determining of changes in SGS of raceway in function of load using one bearing only, in whole range of internal load inside the bearing. It significantly shortens these long-lasting investigations

The results of presented above investigations compose in some degree further enlargement of knowledge of process of rolling friction as system of elementary phenomena depended on constructional, technological and operational factors.

References

1.   Burakowski T., Marczak R.: Selected Processes of Service Generated Layer Constitution (in Polish). Tribologia, v. 30, No. 6/1999, pp. 757□765.

2.   Burakowski T., Wierzchoń T.: Engineering of Surface of Metals (in Polish). WNT Warszawa 1995.

3.   Lubimov V., Musiał J., Styp-Rekowski M.: Diagnostics of Surface Geometric Structure State with Developed Sculpture. Diagnostics vol. 33/2005 (in Polish).

4.   Musiał J.: Influence of Transformation Course of Technological Surface Layer into Service Generated One on Functional Features of Rolling Bearings (in Polish). Proceedings of IX Congress of Maintenance of Technical Devices. Krynica 2001, pp. 109-115.

5.   Musiał J.: Investigations of Influence of Some External Loading in Relation to Geometry of Functional Surfaces of Rolling Bearings (in Polish). Doctor's dissertation, Technical and Agricultural University, Bydgoszcz2003.

6.   Musiał J., Styp-Rekowski M.: Modeling of Changes of Surface Geometrical Structure of Kinematical Pairs with Friction Rolling. Problems of Operating, No.1(60). Radom 2006 (in Polish).

7.   Musiał J., Styp-Rekowski M.: Optimization of Mathematical Model of Changes in Surfaces' Geometric Structure of Rolling Bearings' Elements. Proceedings of XXIInd Symposium PKM, vol. III. Gdynia – Jurata 2005 (in Polish).

8.   Nowicki B.: Advances in Texture of Surface Metrology. Proceedings of IIIrd

International Conference SL'96. Gorzów Wlkp. – Lubniewice 1996 (in Polish).

9.   Oczoś K.E., Lubimov V.: Geometrical Structure of Surfaces. Rzeszów Technical University Publishers, Rzeszów 2003 (in Polish).

10.   Styp-Rekowski M.: Significance of Constructional Features for Angular Ball Bearings Life. Scientific Number of Technical and Agricultural University, series Dissertations, No. 103, Bydgoszcz 2001 (in Polish).

11.   Styp-Rekowski, M., Musiał J.: Forming of Tribological Features in Following Stages of Engineers Activity. Tribologia nr 5-6/1997 (in Polish).

12.   Styp-Rekowski M., Musiał J.: Transformation of Technological Surface Layer into Service Generated Layer in Kinematic Pair with Rolling Friction (in Polish). Problems of Terotechnology, v. 11, No. 3/2000, pp. 241÷248.

3.2.7 MODIFICATION OF STEEL SURFACES IN CYCLIC SWITCHED DISCHARGE

Lukyanyuk M.[1], Pastuh I.[1]

Introduction and problem statement

Metal technology is always based on two-way improvements, which contradict each other. On the one hand to ensure maximum durability, which in most cases due to the increased hardness, and with another increase in metal cutting technology, which in most cases requires a reduction of hardness. Thus technology metal practically based on a compromise of two contradictions: wear on one side, adaptability on the other. Currently successfully used in the production of more than hundreds of different technological processes metal to ensure the most optimal balance performance parts and technology for their manufacture. At the present stage of engineering a compromise between operational requirements for machine parts, manufacturability of their production and economic indicators led to the transition from bulk methods of modification of properties of metal products to the surface, as in the wear resistance is mainly involved is surface detail, and it is subject matter of priority modification [1].

There are many different methods of modification of metal surfaces and none of them can not be considered universal. Recently, the most promising

[1] Khmelnitsky National University

methods are implemented in the gas at low pressure of the electric field on it. Electrical discharge that occurs while between the anode and cathode may be different in nature (in our case - the smoldering) provides sufficient intensification of the process [2, 3].

1. Main terms of modification process

Total ordering processes modifying surfaces using glow discharge qualifies them as a vacuum-gas-diffusion [3-6]. Most theoretical studies of the process relates to its possible options, where power is continuously loaded in the discharge chamber, i.e. the equipment of continuous power discharge. Option of continuous power discharge can not always achieve the desired results, especially in the presence of surfaces modified areas of irregular shape (sharp peaks, or face, narrow cracks, deep holes, etc.). In addition nitriding at a constant feeding has a significant drawback technology plan. He is the difficulty of forming gardens. This on-one before due to the fact that in all places where the cracks more than 0.5 mm, there is a local burning discharge, but not using the glow and the arc mode. This leads to local overheating of parts, and in some cases impossible to expedite the process, because when trying to increase tension in places such an electric arc, which leads to local melting and destruction of parts. The need for consideration of this circumstance greatly complicates the same training process associated with the construction of special suspensions, tables, which would exclude the presence of local stress concentrators, narrow cracks, holes, etc. Areas of complex configuration substantially complicate the process modifications using continuous power discharge. Sharp peaks, sometimes faces can serve as stress concentrators and provoke the emergence of corona and arc discharges. Narrow cracks, deep holes block the penetration of glow discharge at considerable depth. The effect of blocking the process of discharge of a significant penetration depth of narrow slits and holes due to shape trajectories of particles incident flow. The trajectory of incident particles flow in narrow cracks and deep holes is a parabolic curve, directed from the entrance aperture (slit) to the walls, this is due to the presence of constant electric field discharge. One way to change the flight path of particles incident flow is off the electric field at a certain time, for the flight by

inertia particles tangentially to their parabolic trajectory. This will facilitate the penetration of particles at much greater depth.

The development of technology modification of surfaces using the glow discharge gradually took certain steps. In the initial period of installation nitriding in glow discharge were designed to direct the polarity diagram (symbolic name), in which detail is a cathode with a constant power. This method of power has certain advantages:

- power system is simple;

- this method delivers a large amount of energy incident flux, and consequently the surface of parts being processed;

- greater intensity of the process with less duration;

- very high stability of discharge;

- the ability to control discharge stability by introducing filters to smooth pulsations.

However, as a drawback should be allocated, the presence of ripple filters, which is somewhat complicated scheme of power supplies, increase their cost, power consumption.

The main drawback of the same DC power supply is the complexity of processing holes and cracks.

Schematic diagram of the device for nitriding in glow discharge with a constant power supply is presented in Fig. 1. One way to improve the quality of processing of steel surfaces in a glow discharge is to establish dial-discharge cycles (ЦКР). Introduction ЦКР does not require the creation of fundamentally new equipment, just modifications of existing facilities.

One way of modifying equipment for nitriding in glow discharge (the simplest) is a disabling capacitive-inductive filters are designed for smoothing pulsations aligned current. The impact of such modifications bring changes in the nature of the process, but not as substantial as in this case is not observed a complete disconnect voltage discharge, but its ripples. Besides, is not expected ways of regulating the process within one cycle. The cycle is regulated at the same frequency of the power supply. The second direction is the introduction of modifications in the scheme of the power switch, discharge, which would have

formed the necessary configuration signal. The most promising option for construction of the switch is an electronic version of it (КР).

In the diagram of the device (Fig. 1), supply chain between discharge after unit 4.5 - sensor control system discharge, discharge switch is introduced in the guideline, while there is a chance the mobile switching installation, its conversion to work in one of two modes: 1 - Switch to the presence of cyclic switching level (КР), and 2 – no one.

Use to modify the surfaces of equipment with cyclically-switched discharge opening new opportunities, because it has significant advantages over conventional, with a constant power level:

- increasing the possibility of nitriding of parts of complex shape (presence of deep and narrow grooves, holes of small diameter and large depth, etc.);
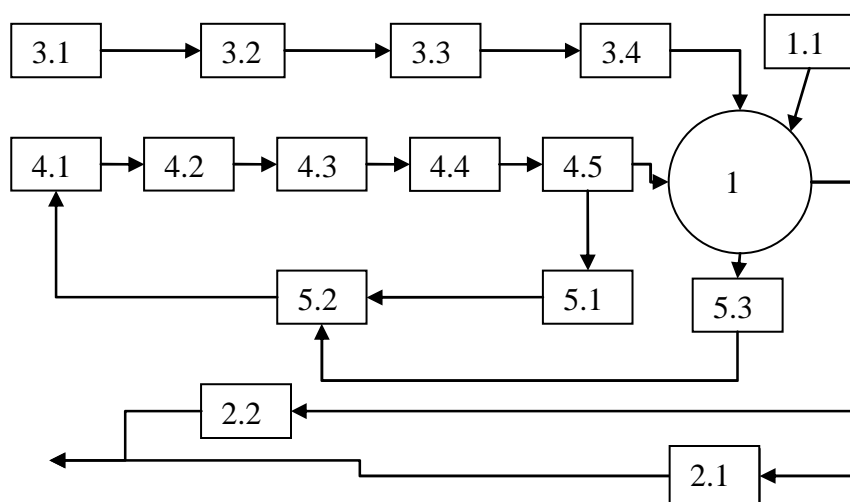

Fig. 1. Block diagram of setup for nitriding in glow discharge: 1 - discharge chamber; 1.1 - means of mechanization of cameras; 2.1 - vacuum pump prior to pumping air discharge chamber, 2.2 - deep vacuum pump, 3.1 – gas holding compartment; 3.2 - training system gas mixture; 3.3 - gas cleaning system, 3.4 - gas supply system in the discharge chamber; 4.1 - voltage regulator; 4.2 - transformer, 4.3 - rectifier; 4.4 capacitive-inductive filters, 4.5 - sensor control system discharge; 5.1 - glow discharge control system ; 5.2 - discharge control system, temperature control system 5.3.

- reduces the risk of local damage surfaces modified by reducing the probability of arc discharges;

- expanding the range of permissible regulation of such important in terms of optimizing the process parameters such as pressure in the discharge chamber and the surface temperature of parts;

- option for autonomous heating system components greatly simplifies the control surface to prevent overheating caused by an additional energy discharge [7].

During the work on research opportunities to improve existing and create new equipment for the process of modification of metal surfaces using circularly dial glow discharge we have developed an experimental model for the implementation of cyclically switched discharge.

2. The main provisions of the development of equipment for cyclic switching discharge

Development of an experimental prototype of a device for cyclic switching gas discharge based on the following premises:

- maximum compatibility with existing electrical and electronic equipment;

- using available element base;

- the ability to provide a broad range of parameters switching to further optimization and comparative analysis;

- reliable protection of equipment against overload and abnormal situations.

Justification of switching parameters is based primarily on these requirements pulsed current:

- pulse shape must be rectangular, which provides a jump from zero to the desired area of abnormal glow discharge;

- pulse duration must be less than the time of arc (approximately 100 ms), thus forming an arc is broken (if necessary interrupt current can be carried in any pulse);

- pause, which followed after each pulse must be so short that provide easy ignition discharge under the action of the next pulse, i.e., be less than a few milliseconds;

- the ratio of pulse duration and pause should vary widely for the effective management of process heating units.

Typical values of pulse duration, recommended [8] are in the range 20 - 100 microseconds, while a pause as the duration can vary between 20 - 200 microseconds. It should be at the same time noting that the processes of ignition and extinguishing discharge observed a significant lag, and this imposes certain restrictions on the choice of switching time parameters. Moreover, the inertia of gas discharge processes may depend on the geometry of the discharge space and its size, which in real terms may be changed in a fairly wide range. Thus we can conclude that it would be rash to unconditionally transfer guidelines [8, 9], which are derived based on experiments conducted on an experimental installation of the camera with a diameter of 400 mm and height 600 mm, in case of much larger size and the discharge chamber. The same applies to the results obtained during physical examinations of miniature gas discharge devices (so-called laboratory grade). As a result it was decided at this stage of research and development of construction equipment to provide a broad range of switching options to its current specification after a series of preliminary experiments. So ask the range of variation accepted repetition rate f of one to ten kilohertz ($f = 1...10$ kHz), fill factor of a period of zero to one,

$$\eta = t_n / T = 0...1,$$

where T - period of repetition, $T = 1/f$;

t_n - pulse duration (duration of active period).

3. The choice of the secondary power source structure

As mentioned above, the totally new equipment for the process of nitriding in cyclically switched discharge does not appropriate enough to modernize existing equipment previously created for processes with constant power discharge chamber. We decided as a base to use existing power supply facilities for nitriding in glow discharge, including - the relevant control units (КПА - nitriding process controller), and current sensor and voltage discharge. To implement the pulse mode power supply installation additionally equipped with T-shaped RC - smoothing filter and a specially designed controller intermittent mode (КПР), which includes a power electronic device with key ЕК control and protection.

To construct the power switch set to powerful transistor structure MOSFET, which is celebrated the following benefits in the first place - in comparison with bipolar transistors:

- low power consumption in the circles of government;

- good performance when run in parallel, allowing relatively easy to increase the power key (up to certain limits).

At the same time as using bipolar transistors, in this case the actual problem of overload protection for shock, which dramatically reduces the reliability of a key. Functional diagram of the intermittent mode controller is shown in Fig. 2. There appear to ease some of the significant from the viewpoint of explanation of the principle elements of the system settings: three-phase rectifier 1 (includes T-shaped RC-smoothing filter), discharge chamber 2, current sensor R_i - 3, nitriding process controller 4.
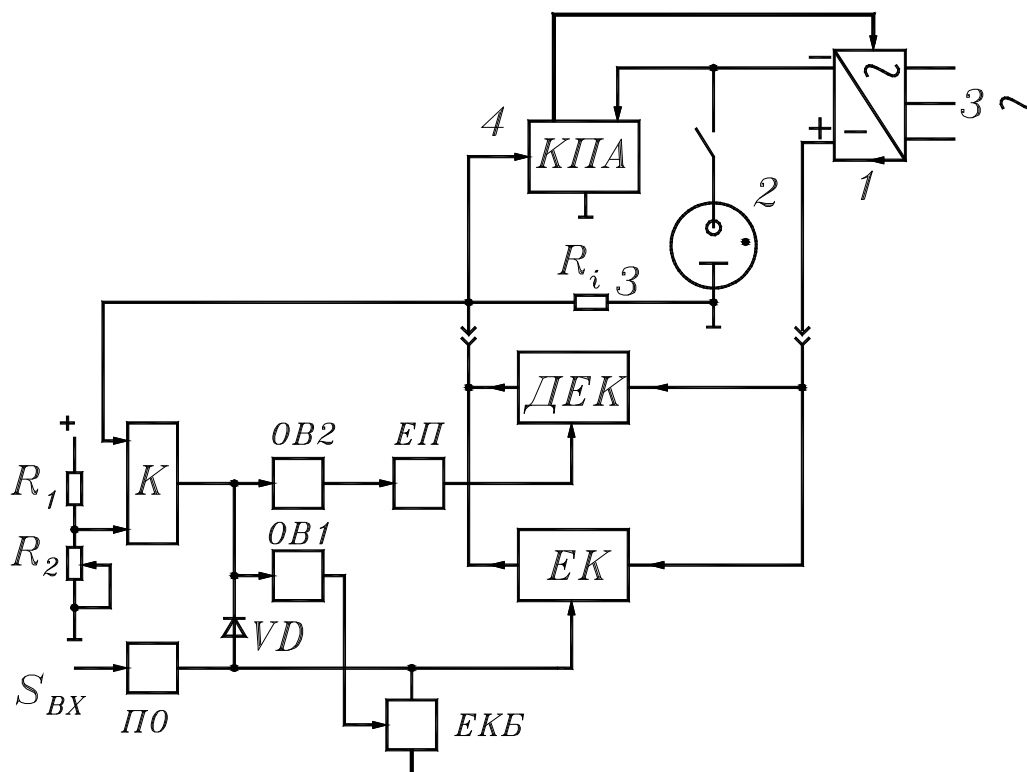

Fig. 2 Functional diagram of the controller intermittent mode: 1 - three-phase rectifier, 2 - discharge chamber, 3 - current sensor, 4 - nitriding process controller; R_i - current sensor; R_1, R_2 – threshold setters; K - comparator; S_{BX} - input control signal; ПО - amplifier-limiter; ОВ1, ОВ2 - vibrators; ЕК - electronic key; ДЕК - Auxiliary electronic key; ЕП - emitter follower, ЕКБ - electronic key lock; VD - blocking diode

As an electronic key uses two parallel included in an output transistors, each of which is characterized by boundary values of voltage and current, respectively - 900 V and 8 A.

Before proceeding to the statement of the principle of protection of electronic key for the current, we note the following. First, protection should operate in excess of any impulse discharge current pre-set safety value. Second, after the operation and protection of the reasons that caused this activation (e.g., short-term accidental increase supply voltage) protection system must return to the starting position and camera - to continue working in normal pulse mode. Thirdly, a special role to play defense system during the initial installation and turn ignition discharge, as in this case the location of the operating point of current-voltage characteristics of gas discharge virtually uncontrolled, and therefore the probability of overload for a considerable shock.

Based on the foregoing, it is advisable to build a defense so that:

- signal handling by installing shock translated from pulse mode to continuous support by electronic key (ДЕК), a tolerant respect for current overload;

- in continuous mode protection system in the block КПР monitored current values of current and cutoff curves performed under control of the КПА bloc;

- failure by the current overload alarm system automatically returning in restoring pulse by switching electronic key EK and close the auxiliary electronic key ДЕК.

Control pulses are used to cycle through the main circuit electronic key EK, formed from the input S_{BX} or harmonic pulse shapes using the amplifier-limiter *ПО*. Normal mode of installation is that using the key EC cyclically current generated source 1, in terms of power the camera 2. This is ensured by periodic alternation of intervals of existence in the cell of abnormal glow discharge intervals extinguishing discharge. Instant values of discharge current is continuously monitored by the comparison in comparator K signal from current sensor R_i and threshold voltage, which is set divider R_1, R_2. In the case of excess discharge current critical voltage at the comparator output goes from the output of "log.1" in state "log.0", which in turn leads to run vibrators *OB1*

and *OB2*. The positive momentum from the output of vibrator *OB1* opens parallel electronic key lock control impulses *ЕКБ*, resulting in basic electronic key EK closed. Simultaneously, the positive momentum from the output of vibrator *OB2*, amplified by the power emitter follower *ЕП* opens auxiliary thyristor electronic key *ДЕК*, tolerant in respect of significant congestion at current. As a result, the camera moves from cyclical mode dial to the mode of continuous discharge. This is achieved not only the protection of key *ЕК* overload by a current, but also protection for the voltage, which is important in the closed position of power transistors *ЕК*. Cycle protection continues after the initial impulse of vibrator *OB1* in the case when the output of comparator K is stored status "log. 1 ", indicating that under current overload, but in this case, control impulses EC blocked by opening diode VD.

Manage the installation work on the range of protection, including the cutoff curves, performed nitriding process controller KPA staff which is part of the equipment installation nitriding.

Once the overload persists for shock, and accordingly - blocking of the key factors EK, setting automatically returns to the cyclic mode switching. This occurs after the receipt of the first positive pulse control signal that opens the power transistors EC. As a result, bypass key EK thyristor *ДЕК* last closed, which provides a way out of cycle security. For ease of initial startup and adjustment works when using manual modes.

Power is provided from the *КПР* block stabilized source with output voltage of 15 V.

When used for surface modification ЦКР possible partial or complete replacement of function block control and management of discharge, but to abandon the latter is inappropriate. Switch can provide stability only in case of discharge of forming a signal configuration when playing it in less time transition in glow discharge arc, the duration of the pause - at least since the extinction of arc discharge.

The presence in the circuit installation unit cyclic switching discharge does not preclude the use of equipment in a continuous discharge, providing the possibility of mobile variation modes: direct and dial-up.

In the power supply with variable current cutoff options fully or partially one of the phases (usually positive when using the process of direct polarity). The absence of such a cutoff increases heating anode, which reduces the intensity of the process. However, this phenomenon may lead to softening of the nitriding process, receiving respectively - better plasticity of the modified layer. A reduction of the negative impact of a positive phase of the process of nitriding can achieve a form of voltage asymmetry by shifting its mean value in the negative zone. In principle a form of voltage may be sinusoidal, rectangular or arbitrary programmable up to its changes. Obviously, the use of rectangular voltage with other parameters constant gives greater saturation by power incident flux, respectively - more rigid regime, with less duration of treatment. The simplest option is to use a transformed industrial frequency voltage to a certain extent similar in principle (excluding the effect of positive phase) to the nitriding of intermittent power.

Nitration at constant power is also a significant drawback technology plan. He is the increased complexity of forming gardens. This is primarily due to the fact that in all places where the cracks are more than 0.5 mm, there is a local burning discharge, but already in the mode of arc. This leads to local overheating of parts, and in some cases - simply impossible to expedite the process, because when you try to increase the tension in those places there is an arc. The need for consideration of this circumstance complicates the design of suspension or tables, which would ensure the deployment of dense detail on them. However, even with the conditions of a dense deployment of components on the table the presence of chamfers on bearing surface also causes a problem because they, along with the supporting surface of the table form a wedge crack. Another disadvantage, especially compared to nitriding oven, is the low efficiency of modification of the holes - especially small diameter, with their relatively large length (the theory of the hollow cathode discharge is known that the field strength in the hole is almost zero at a depth of more than two millimeters) which once again shows the relevance of technology nitriding in glow discharge with intermittent power supply - switched cyclically discharge. The use of cyclically switched discharge power discharge chamber, which is

energized in the form of intermittent signal, introduces a number of significant advantages:

- the possibility of forming such ЦКР in which the duration of the signal in the cycle does not exceed the time of transition in glow discharge arc, the duration of the pause - at least since the extinction of arc discharge, in his appearance that rejects the need for automatic cut-off arc, or they can be used under the scheme with an extremely simplified algorithm;

- greatly simplifies the process of forming gardens, as virtually eliminating the need for compliance with cracks and deep holes;

- an opportunity nitrogenize small diameter holes with relatively large depth of;
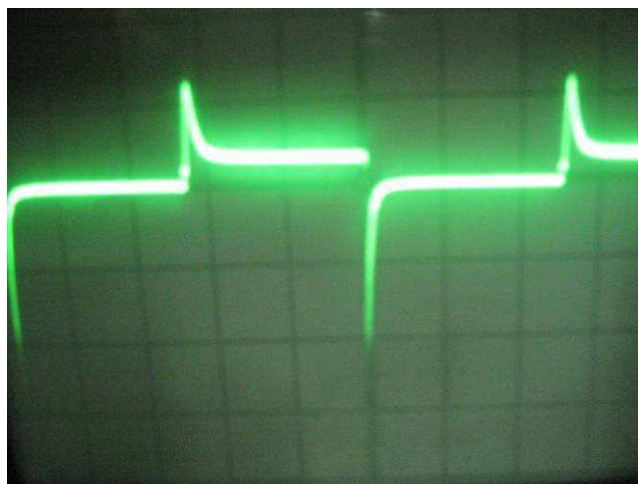
Fig. 3. Forms at the discharge current changes cyclically switched discharge rectangular shape with a coefficient of filling period $\eta = 0,5$ **.**

As a drawback when using ЦКР should be noted that the transfer of incident energy flux is only so much of the cycle, where there is an alarm, and effectiveness of the lower and in some cases phase nitration of two or more times longer than with a continuous discharge.

But on the whole process of surface modification in cyclically switched discharge opening up new opportunities associated with variants of the ЦКР characterized: frequency, timing and pulse shape. The implementation process for frequency switching, the ratio of cycle period to signal duration and shape of the signal a great opportunity to significantly influence the results of surface treatment.
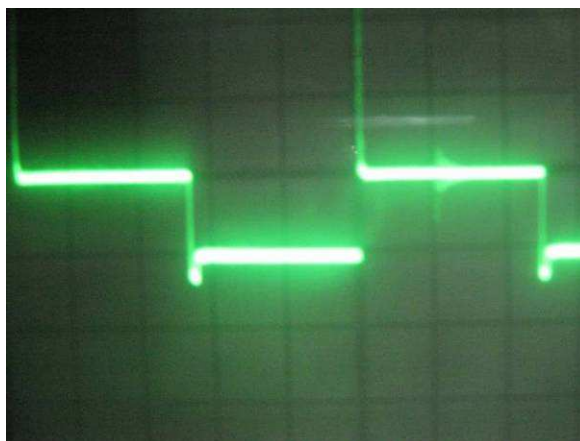
Fig. 4. Forms of change in discharge voltage discharge cyclically switched rectangular shape with a coefficient of filling period.

Conclusions

Practical implementation of the device described above КПР at the facility nitriding in glow discharge cyclically-switched confirmed its performance in terms of real processes. It achieved all planned premise that paves the way for experimental use cyclically-switched discharge for surface modification of metal alloys on a fundamentally new basis. Application of definite method allows to solve a number of problems of technological procedures, foremost among them - changed parts of complex shape, with holes and indentations of small and large transverse dimensions for length. Similar details nitrogenize managed effectively only using furnace nitriding in ammonia gas environments, i.e. a process that is unacceptable in modern terms, not only because of its economic performance, but primarily from the standpoint of environmental safety. Also significantly decreases the likelihood of surface damage caused by a random transition in glow discharge arc, which is often observed in the application of continuous power discharge chamber.

Influence of waveform power discharge on the kinetics of nitriding process and its results are a great opportunity for the study of the process.

Using technology in nitriding in glow discharge cycles digit dial allows you to get regulated, and even predictive process surface modification of metals and alloys, the formation of surface layers with desired properties, especially for parts of complex configuration.

References

1.   Термическая обработка в машиностроении: Справочник/ Под ред. Ю.М. Лахтына, А.Г. Рихтарда. М.: Машиностроение, 1980, 783 с.

2.   Б.Н. Арзамасов, А.Г. Братухын, Ю.С. Елисеев, Т. А. Панайоти. Ионная химико-термическая обработка сплавов. М.: Изд-во МГТУ им Баумана, 1999, 400 с.

3.   И.М. Пастух Теория и практика безводородного азотирования в тлеющем разряде. – Харьков: ННЦ ХФТИ, 2006. – 364 с.

4.   Пастух И. М. Модификация металлов с применением азотирования в тлеющем разряде: состояние и перспективы. – Хмельницкий: Проблеми трибології; 2004, - №-4, С. 42-55.

5.   Пастух И. М., Андреева А. А., Шулаев В. М. Вакуумно-диффузионная обработка поверхности металлов с применением тлеющего и дугового разрядов в газах // Новые процессы термической обработки. Библиотека ОТТОМ. – Харьков, ННЦ ХФТИ. – 2004. – С. 5-57.

6.   Пастух І. М., Лук'янюк М. В. Азотування в циклічно комутованому тліючому розряді: початкові положення. Вісник ХНУ. – 2008. - №6. – С. 38-41.

7.   Давидов А. М., Лук'янюк М. В., Пастух І. М. Апарат реалізації режиму азотування в циклічно комутованому тліючому розряді. Вісник ХНУ. – 2010. - №1. – С. 50-53.

8.   Grum R. Pause plasma treatment the innovation for ion nitriding // 1st International conference of ion nitriding. – Cleveland, Ohio. – 1986. – P. 143-168.

9.   Grum R. Industrial advances for plasma nitriding // Ion nitriding and ion carburizing: 2nd International cjnference of ion nitriding/carburizing – Cleveland, Ohio. – P. 157-163.

10.   Попович М. Г., Ковальчук О. В. Теорія автоматичного керування: Підручник. – К. :Либідь, 1997. – 544с.

3.2.8 ADVANCED TECHNOLOGY TO INCREASE DURABILITY OF THE SURFACES FOR PRECISION MECHANICS

Pisarenko V.[1]

Introduction

Swingeing majority of construction details of modern mashinbuilding make from alloys on the basis of iron, which have low corrosive firmness even in the conditions of the atmospheric influencing. In addition still it is necessary

[1] KNVO "FORT", Vinnitsa, Ukraine

to take into account that also, that most details of fine mechanics work in the conditions of the partial greasing, or at complete his absence and are found at the same time under act of corrosion and wear.

Traditionally, in mashinbuilding of providing of requirements of corrosive firmness of details which work in the conditions of the partial greasing, or at complete his absence decides mainly due to the use of too dear firm to corrosion materials (steel, bronze, composition-metal and other), but the high wearproof and heatproof of surface is not here guaranteed.

Application of metallic coverage (chrome-platings, nickelages and etc.) in the case of corrosion protection the details which are made from alloys on the basis of iron does not provide simultaneously the enough protracted defence from a wear and corrosion. It is known in addition, that metallic coverages which inflict by electrochemical methods lower durability from a fatigue. Also it is too problematic and expensive to inflict metallic coverages on the surface of opening at making of high-fidelity details.

Thus, an actual task is development of such technologies of finish chemic-thermal treatment of surfaces of details, which foresee the complex providing simultaneously of high indexes of durability, wearproof, heatproof and corrosive firmness.

The search ecologically of clean technology of receipt of superficial layers with high properties of wearproof and corrosive firmness which does not need the use of scarce technological materials on comparison with the methods of galvanic coverage became the important task in the period of mastering of production of details of fine mechanics in Ukraine.

To the details of fine mechanics on to the external environments the requirements of receipt of not only the proper mechanical properties and necessary resistance of corrosion and tearing down, but also insignificant roughness of surface of knots of friction and low permanent to the coefficient friction are produced.

The analysis of foreign sources shows that in connection with that the requirements to phyisc-mechanical and chemical properties of construction materials become more hard and exact, the all more of attention are spared to the improvement of the known methods of chemic-thermal treatment CTT.

A long ago the known process of gas satiation by nitrogen with the use of ammoniac gaz mixtures is continuously perfected. Addition to the ammonia of carbon mixtures improves wearproof of superficial layer [1].

Following after satiation by nitrogen oxidization of superficial layer is also instrumental in the rise of wearproof and corrosive firmness [2, 3]. Satiation by nitrogen in salt bath (teniofer-process) with oxidization of diffusive superficial layer in the process of his forming began to be used by industry of Germany from in 1981. A firm "Degussa" registered a commodity sign and this technology under the name "Tafftride". Also some similar technological processes offered Great Britain (firm "Lucas Electrical Ltd") – "Nitrotec", the USA (firm "Kolene") – "QPQ".

Summarizing developments of row of firms in this direction, it is possible to select such three variants of technological process CTT:

- nitrocarbonation with oxidization at cooling at the end of process (the proprietary name "Tafftride Q");

- nitrocarbonation with oxidization at cooling at the end of process and tooling (by the polish) of superficial layer (the proprietary name "Tafftride QP");

- nitrocarbonation with oxidization at cooling at the end of process and tooling after which oxidization of superficial layer is conducted still one time (the proprietary name "Tafftride QPQ").

Below the resulted application domains of these three variants of technological process.

A process "Tafftride Q" is used for the improvement of wearproof, corrosive firmness, heatproof, durability from a fatigue, increase of resistance to the adgesion grasping, rise of term of service.

A process "Tafftride QP" is used, when next to high properties of wearproof and corrosive firmness it is necessary reduction of roughness of surface.

A process "Tafftride QP" is used, when it is necessary to provide the insignificant roughness of surface, low coefficient of friction, extraordinarily high corrosive firmness, attractive original appearance and low reflection of light.

As a rule, all these three variants of chemic-thermal treatment are conducted in cyanide - tsianat fusions.

Education on the surface of composition layer which is folded with is the feature of nitrogenization in fusions ε- nitrid and contains a carbon and oxygen, that stipulates high properties of plasticity and wearproof.

The superficial layers got at treatment on technology "Tafftride" have considerably more low coefficient of friction, especially in the conditions of absence of greasing (dry and half-dry friction), than the layers got on technology of temper on martensit, or chrome-plating.

Ohsawa [4] considers that unlike the layers of chrome, coefficient of friction of the surface treated by means the processes "Tafftride QP" and "Tafftride QPQ" remains stable even at different speeds of friction.

From data of "France and Haaze" [5] the coefficient of friction after loading of 7 MPa during 40 acquires hours the balanced state and is found in scopes: $0{,}03< f <0{,}004$.

In accordance with electrochemical researches of Eberthbah and other [1] at nitrogenization in a gas environment there is tenfold reduction of speed of corrosion in solution of chlorous sodium by concentration of 0,9 M. After additional oxidization of nitrogenization layer speed of corrosion slows down on two orders.

Next to considerable reduction of speed of corrosion firmness rises to through corrosion in the ten and hundred one times.

The comparative industrial tests show that superficial chrome-plate layers 20-30 μm, usually place in salt fog during 70 hours to appearance of tracks of corrosion, and the layers got after treatment by a method "Tafftride QP" – 120 hours and more than 200 hours after treatment by method of "Tafftride QPQ".

The formed oxide-nitrid areas anymore plastic, than tapes oxides Fe2O3, and at the same time own near to the last preadgsion properties. Researches, implementation Mittemeir and Collin [4], showed that a next oxidization of nitrogenization surface also caused filling of crack α– phases by oxygen. During conducting of the combined chemic-termal treatment possible sharp rise of corrosive firmness.

The as a result conducted analysis of previous researches and developments basic directions of conducting of works on the improvement of technology of chemic-termal treatment on the base of process of nitrogenization with the purpose of improvement of properties of wearproof and corrosive firmness were determined. Applied by some foreign firms process of liquid nitrogenization in salt bath with a next oxidization also in fusion of salts of the little use for the terms of home production in communication with the necessity of application of salts.

Unlike the simple systems there is iron-nitrogen, iron-carbon (cementation), iron-oxygen (oxidizing), which it is enough trained, the system the iron- nitrogen -carbon-oxygen is too difficult and on today is not almost explored. In communication with that at creation of a new technology CTT, which is based on compatible diffusion of nitrogen, carbon and oxygen in iron, conducting of researches on determination of optimum parameters became a necessity: temperature condition, composition of gas mixture, duration of process of diffusion.

The complex providing by a method CCTT is the basic feature of the developed technology simultaneously high descriptions of wearproof, heatproof, corrosive firmness and black of surface. The developed technology suitable for strengthening of surface of wares of made from alloys on the basis of iron (steel, cast-iron).

1. Research of structural structure of superficial layer after CCTT.

From standards, that were processed on different modes, polishing-standarts prepared. For preparation of polishing-standarts from standards the layer of surface not less than 3 was taken off mm, and then polishing for metal-graphic researches was conducted. Digestion of micro polishing-standarts was conducted in a 4% solution of aquafortis in an ethyl alcohol.

On prepared polishing-standarts hardness was measured and explored microstructure of the fixed layer.

After the got results of values of hardness for standards with equivalent terms for the identical brands of steels and modes CTT the averages of results of measuring were determined.

The structure of the fixed superficial layer was estimated and taken pictures for the help to the microscope МИМ– 8. The got foto of structure of superficial layers are presented on fig. 1–4.

Fig. 1. Microstructure of the superficial layer on steel 20, x 200

Fig. 2. Microstructure of the superficial layer on steel 3. Mode CTT: 580 ^{o}; 3 hours, x 200

On the pictures of microstructure expressly it is visible white area. The white area presents by itself ε- carbonitrid. Oxycarbonitrid appears at the presence of oxygen.

Fig. 3. Microstructure of the superficial layer on steel 3. Mode CTT: 570°; 10 hours, x 200

Fig. 4. Microstructure of the superficial layer on steel 40X, x 200

Analyzing the microstructure of the surface layers (Fig. 1-4), obtained at different duration of CTT can be concluded that the surface layer of white carbon-nitride can form also at the small duration of the CTT. When the duration of the CTT hours white layer is rough and porous (Fig. 3). Also formed a white porous layer with cracks in the CTT in ammonia without additives carbon containing gas (Fig.4).

286

By changing the composition of the gas mixture the number of additives, propane butane and maintaining a certain degree of dissociation of ammonia can form the surface layers of different thickness

Diffusion layer under the surface white layer under the microscope is almost undetectable. In some cases it differs from the core of a few more mordant and sometimes are white streaks in a layer of nitride.

So visible, in some cases diffusion zone in reality is only part of the depth of diffusion impregnation.

2. Research of properties of diffusive layer.

Diffusion layer thickness and hardness distribution of its depth investigated by measuring the microhardness instrument PMT-3 at a load of 50 g. Injections carried out every 0,02 mm in the perpendicular from the edge of the deep.

With a total thickness of diffusion layer made the distance from the edge of the sample to the first injection of core hardness. Microhardness measurements conducted at various locations on the Fig. 9 clearly shows traces of measuring microhardness.

The hardness was measured on a flat surface of the sample using the PMT-3 device at a load of 100 g after a light cleaning of the surface.

In Table. 1 shows the average values of hardness of the surface at different locations mixture of gases which is fed into the furnace.

Table 1 - Mean values of hardness of surface after CTT.

Type of the steel	Size of hardness of surface for different modes CTT, H_{100}			
	520°C, 48 h, 100% ammonia	560°C, 5 h, 94% ammonia, 6% propan-boutanou	560°C, 5 h, 90% ammonia, 10% propan-boutanou	570°C, 6 h, 53% ammonia, 47% natural gas
Steel 45	644	658	644	794
40X	734	877	824	897
38X2MЮA	1200	934	897	970

Analyzing the data in Table 1 for steels 45 and 40X should be emphasized that the joint diffusion of nitrogen and carbon values observed increase of hardness in comparison with the process of nitriding in the same ammonia.
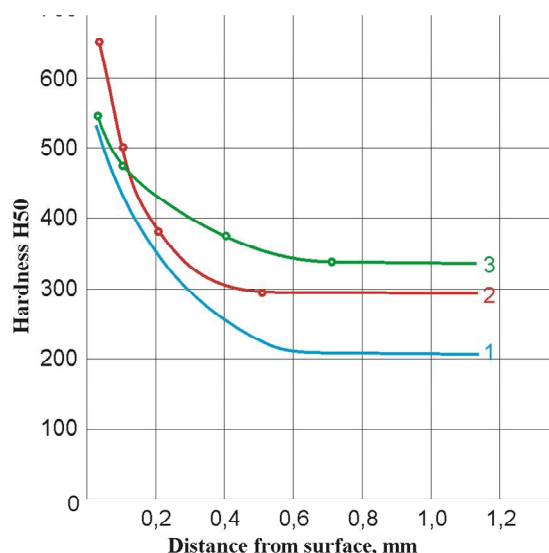
Fig. 5. The values of hardness distribution on the thickness of diffusion layer.
1 – steel 20Х, 2 – steel 30ХН2ВФА 3 – steel 38Х2МЮА.

A higher value of hardness in the surface alloy steel 38H2MYUA associated with the formation of nitrides of alloy elements.
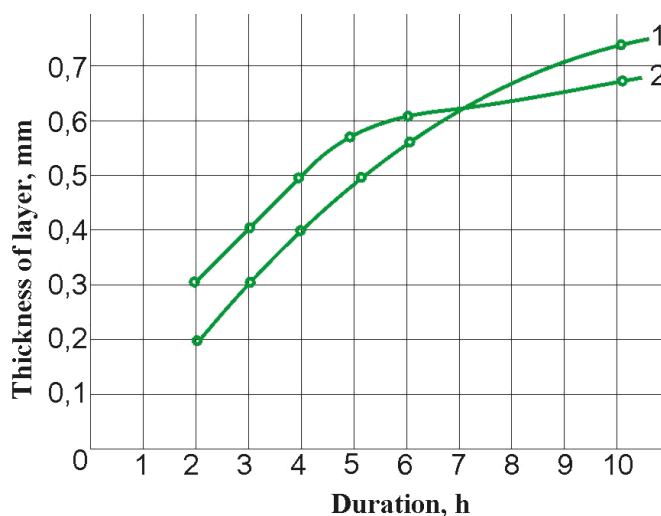

Fig. 6. Dependence of the thickness of diffusion layer on the duration of the CTT.
1 – material of the sample – steel 3; 2 – steel 40Х.

In the presence of nitride steel elements (Al, Ti, Cr) obtained by CTT diffusion layer has a higher hardness. Distribution of hardness in the depth of diffusion layer for steel 40X and 45 at different modes of CTT shown in Fig.5-6.

Analyzing the distribution of hardness on the thickness of diffusion layer of steel 38Х2МЮА for different ways of strengthening can be concluded that

the process studied CTT as a result of the distribution of hardness close to the gas nitriding process and has a 10 times shorter duration

3. Tests of corrosion resistance

Corrosion resistance was studied in comparison with other methods of coating on samples made of steel 45, in a cell salt fog of 5% aqueous solution of sodium chloride. Test results are shown in Fig. 7. When conducting research it was found that the highest corrosion resistance is provided by the presence on the surface of solid oxycarbonitride layer. Control availability oxycarbonitride layer implemented by dipping the sample for 10 - 20 seconds in 17% aqueous solution of copper sulfate
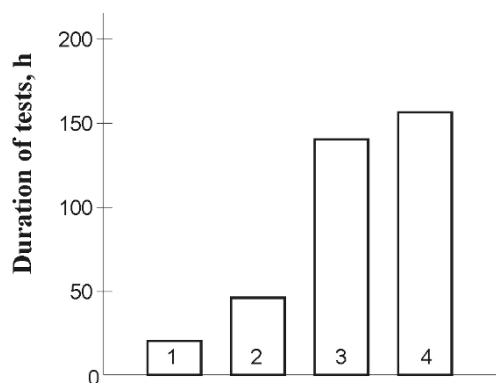
Fig. 7. Corrosion resistance of specimens of steel 45 in salt fog of 5% aqueous solution of NaCl: 1 – without treatment, 2 – steam thermal oxidation; 3 – solid chrome 18 ... 20 microns; 4 – CCTT.

In the presence of solid oxycarbonitride layer deposition of copper on the controlled surface is observed. In the absence oxycarbonitride copper layer deposited on the controlled surface.

4. Investigation of wear resistance and sliding friction

The survey was conducted on a machine for testing materials on friction and wear model 2070 CMT-1.

Investigation of wear resistance of samples was carried out under the scheme "ring - the ring".

Since the surface diffusion layer is homogeneous properties (hardness, chemical composition, structure) in thickness, to define the nature of the

deterioration in its various areas, one of the samples as a benchmark, was made of steel ШХ15 with homogeneous properties (HRCэ 59) around volume.

Rotations of samples was determined on the basis of the relative velocity of sample slip oksykarbonitrydnym layer relative to the sample tempered steel ШХ15 – 0,65 m / sec.

Tests were conducted at an industrial lubrication oil.

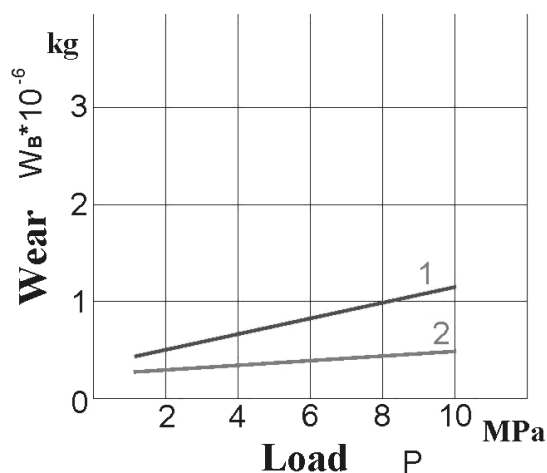Test results on size of wear patterns depending on the average specific pressure are shown in Fig. 2 - 3.

Fig. 8. Wear WB samples depending of the average specific pressure, P: 1 – sample after CTT; 2 – sample - standard

Results of tests for determining the coefficient of friction depending on the average specific pressure are shown in Fig. 9.
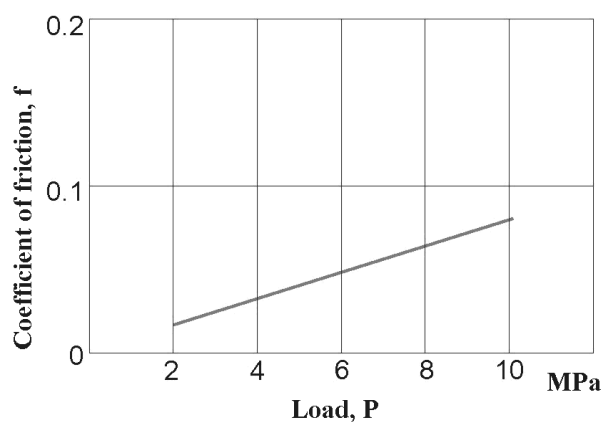
Fig. 9. Coefficient of sliding friction depending on the load, P

Test results showed high wear resistance and low coefficient of friction surface and the sample after KCTP that do not yield results obtained with known methods of treatment: volumetric hardening, nitriding in a salt melt, high gas nitride carburizing (Fig. 9).

References

1. Spies, H. -J; Winkler, H. –R;Langenhan, B: Zum Korrosions – und Verschleiβverhalten von E-Nitridschten auf Stahlen. Harterei – Tech. Mitt. 44 (1989) 2, s. 75-82.

2. Pakrasi, S: NiOX-ein modifiziertes Nitrocarborieververfahren mit anschliebender oxidation. Harterei – Tech. Mitt. 43 (1988) 6, s. 365-373.

3. Wahl, G: Verbesserung der Bauterleingenschften durch Nitrocarburieren im Salzbad, Zwichenbearbeiten und Oxidieren. Harterei – Tech. Mitt. 42 (1987) 3, s. 161-168.

4. Ohsawa, M: Der heutige Stand des Nitriens im Fahrzeugbau in Japan. Harterei – Tech. Mitt. 34 (1979) 2, s. 3-10.

5. Franke, R; Haase, J: Gleitreibungs – und Verschleiβ – untersuhungen an nitrocarburierten Randschichten mit unterschiedlichen Nachbechanlungen. Harterei – Tech. Mitt. 46 (1991) 5, s. 294-300.

6. Ebersbach, U; Friedrich, S; Nighia, T; Spies, H: Electrochemische Korrosionsuntersuchungen an gasoxinitriertem und salzbadnitrocarburiertem stahl in Abhangigkeit vom Aufbau der Nitrierschicht. Harterei – Tech. Mitt. 46 (1991) 6, s. 339-349.

7. VDJ-Z, ноябрь 1984, т. 126, n 21, с. 811-818. Материалы фирмы Degussa.

8. The combined chemic-thermal processing as a way of increase of durability of details of exact mechanics / V.G. Pisarenko // Problems of Tribology. – 2011. – № 2.

3.2.9 MICROSTRUCTURE AND RESIDUAL STRESSES OF COLD SPRAYED COPPER COATINGS

Żórawski W.[1], Skrzypek S.[2], Shalapko Y.[3]

1. Introduction

The cold gas technique was developed in the mid-1980s by prof. A. Papyrin's team in the Institute of Theoretical and Applied Mechanics in Nowosybirsk. The research, as the result of which they obtained coatings made

[1] Kielce University of Technology
[2] AGH University of Science and Technology
[3] Khmelnitsky State University

of different metals, alloys and composites, showed new possibilities of how this technique could be applied. The method was named "Cold Gas Dynamic Method"(CGDM). Currently, in accordance with EN 657:2005, the name "Cold Spraying" is used. Research centres in the USA, Russia, Germany and Japan conduct studies of this method. It is based on compression and heating the gas to the temperature of even 873 K and then its acceleration to supersonic velocity (2÷4 Ma) in the Laval nozzle. As during its flow through the divergent part of the nozzle the gas is decompressed, its temperature decreases significantly, even below the ambient temperature, and that is how the method acquired the name "cold gas spraying" [1,2,3]. The coating material is entered coaxially to the gas flux, and at the moment it strikes the surface its velocity reaches 300 to 1200 m/s (Fig. 1). In currently working cold spraying systems the gas is compressed to the pressure of 3.5 MPa with the expenditure of 90 m^3/h [4,5]. The used powders granulation ranges vary from 1 to 50 μm. Nitrogen, helium, air or their mixtures are used as working gases. Lower cost is the advantage of nitrogen, however, when higher velocities are needed, helium is used. As its costs is considerably high, it is combined with nitrogen to obtain the desirable velocity of gas fluxes. When helium is used separately, systems which make its recovery possible are installed.
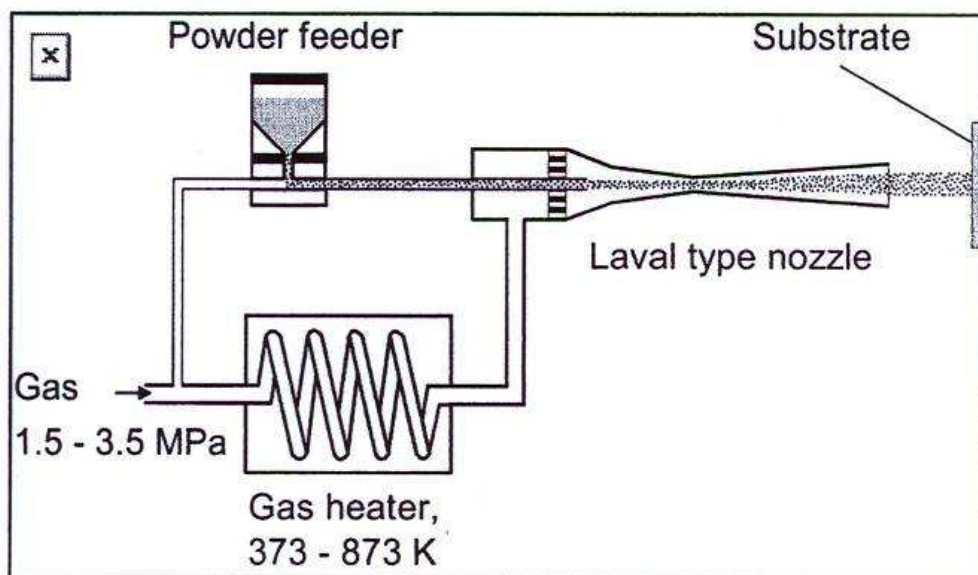

Fig. 1. Principle of cold spraying [2]

Basic issues connected with cold spraying include the determination of the critical velocity v_{kr}, for the defined unit: coating material – substrate. If the velocity of a particle is too low, it returns from the substrate and the coating is not formed. At higher velocity particles behave as in abrasive blasting, causing erosion of the substrate. It is only when the critical velocity v_{kr} is exceeded that particles are subject to plastic strain, adhere to the substrate and form the coating (Fig. 2).

2. Experimental details

The investigated coating was achieved by means of cold spray system in Dresel & Grasme GmbH, Bad Krozingen (Germany). The copper powder used for spraying had granulation of $5 \div 25$ μm. Spraying parameters are presented in Table 1.The studies of the sprayed coating, as well as its linear analysis were conducted by means of SEM Jeol JSM 5400 and ISIS 300 Oxford (EDS). Investigations of phase composition and residual stress were evaluated with Brucker D-8 Advance diffractometer.
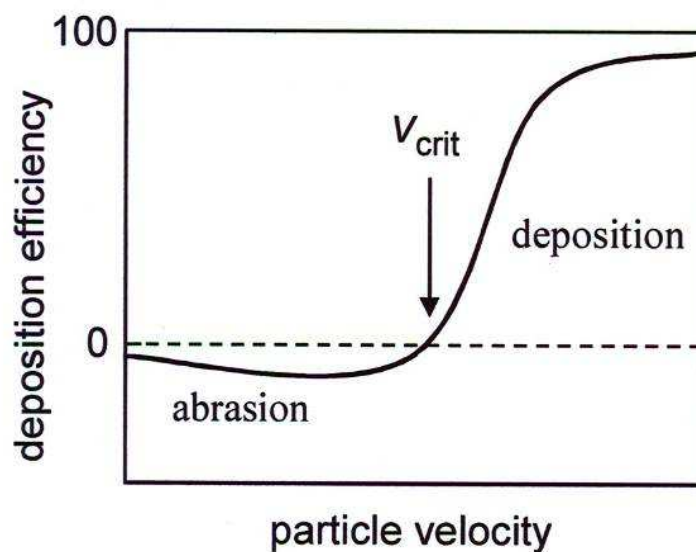
Fig. 2. The influence of the particle velocity on depositing efficiency [3]

Table 1 - Cold spray parameters.

Lp.	PARAMETER	VALUE
1.	Nitrogen flow rate, m^3/h	75
2.	Nitrogen pressure, MPa	3,0
3.	Nitrogen temperature, K	523÷573
4.	Powder expenditiure, kg/h	3
5.	Spraying efficiency, %	60÷70
6.	Spraying distance, mm	20÷50
7.	Particles velocity, m/s	> 570

3. Results and discussion

3.1. SEM/EDS analysis

The visible significant plastic strain of the cooper grains can be seen at the surface (Fig. 3a) and at the cross-section of cold sprayed coating (Fig. 3b). The grains when crushed cause elimination and considerable reduction of empty spaces in the coating, whose porosity declines on impact. Therefore, the surface of the cold sprayed coating contains visible poorly strained and insufficiently bonded to substrate grains of powder.
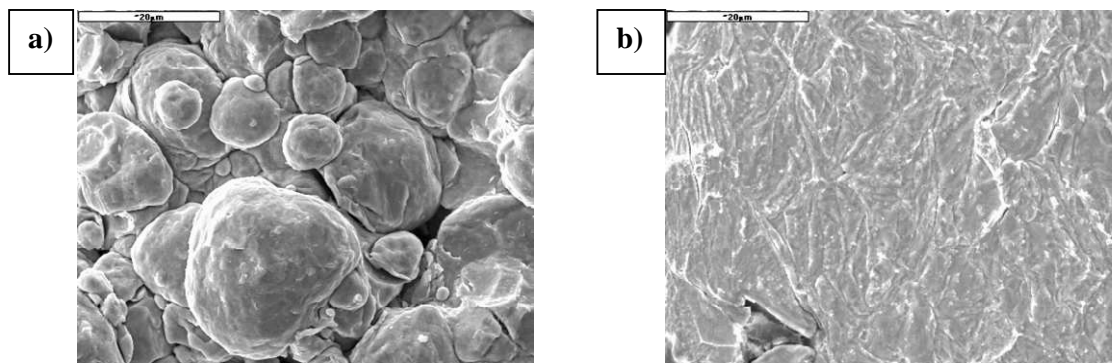
Fig. 3. Cold sprayed copper coating surface (a) and its cross-section after etching (b).

The issues of particles bonding to the substrate and forming of the coating has not been definitely investigated [1,3]. During spraying, the particles remain in solid state and have relatively low temperature that does not exceed the temperature in which plastic properties of the coating material can be raised. That is why it is assumed that the coating is formed as a result of local intensive plastic strain of a particle. Influenced by stresses produced by a very strong impact resulting from a particle and substrate interaction, thin oxide films are

disrupted [6], which makes contact between chemically clean surfaces possible at simultaneous intensive and local heat emission caused when kinetic energy turns into heat energy [1]. The mechanism of particle bonding created in this way is quite similar to the mechanism that takes place during explosive welding [7,8,9,10].

Figure 4 presents the cold sprayed copper coating microstructure and its local chemical analysis results (FDS). The sprayed copper grains form a coating of a very high density. Strained particles adhere closely to each other and the number of oxide bands is scanty (Fig. 4a). A small number of very little pores can be seen. Such a combination, little coating porosity and very low oxygen contents (Fig. 4b) enables cold sprayed copper coatings to obtain excellent electrical properties.
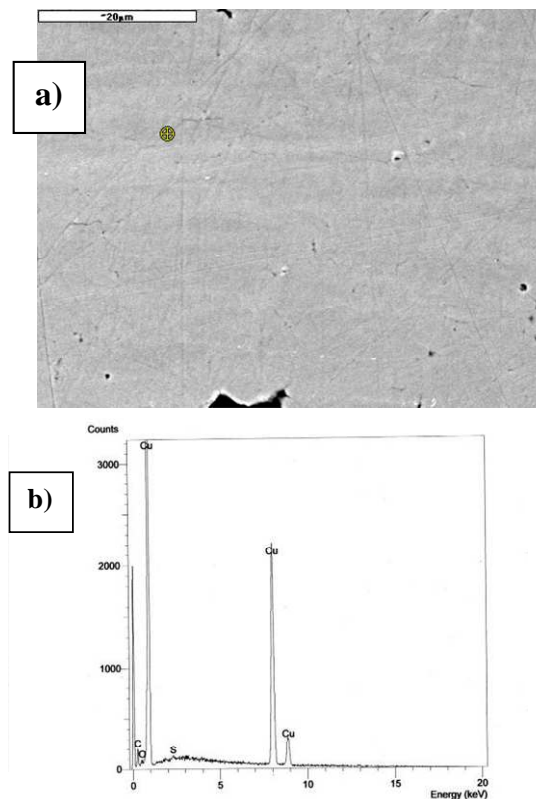
Fig. 4. Cold sprayed copper coating: a) microstructure, b) local chemical analysis

Figure 5 shows the results of the copper coating linear analysis. Diffusion bonding between the substrate and the coating (Fig. 5b)was not observed on the basis of the elements contents level change at the site where copper coating bonds to the substrate of aluminum alloy (Fig. 5a).
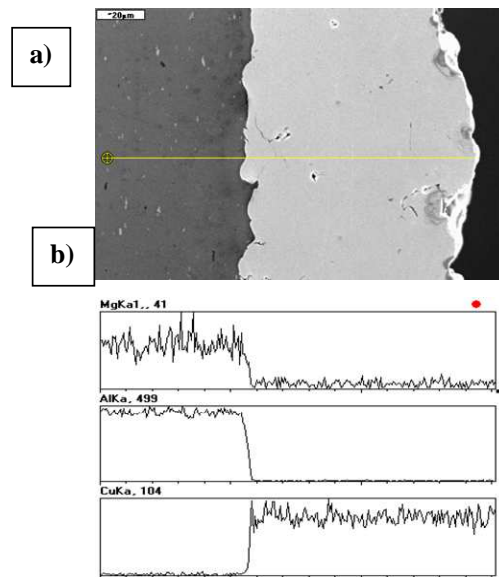
Figure 5. Cold sprayed copper coating: a) microstructure, b) linear analysis

3.2. XRD analysis

Figure 9 shows patterns of cooper cold sprayed coatings obtained with D8-Advance diffractometer. Investigations were carried out using λCuK_α wavelength, with GID geometry, with incidence angle of X-ray beam for $\alpha =3$, degree (Fig. 9a) and using λCoK_α , with BB geometry (Fig. 9b). In both cases of investigations the obtained cooper coating has not been changed due to chemical and phase composition. Moreover particles during deposition place to each other without special orientation (texture), however they are plastically deformed and they contain high density of crystal defects what is confirmed by diffraction line broadening.
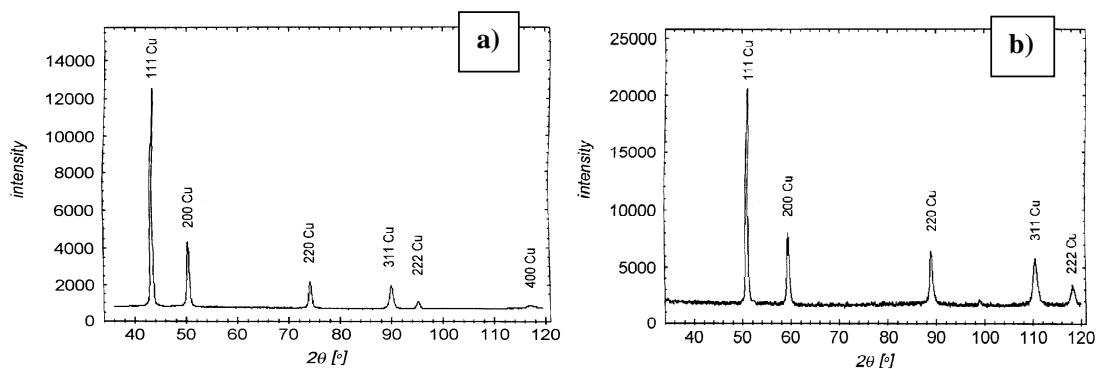
Fig.9. Diffraction patterns of cold sprayed cooper sample a) using λCuK_α wavelength and GID geometry, with incidence angle of X-ray beam for $\alpha =3$, degree, b) using λCoK_α and BB geometry .

3.3. Determination of residual stresses from diffraction measurements

A general description of stress measurnaments by X-ray diffraction $sin^2\psi$ and g-$sin^2\psi$ methods is based on References and on own elaborations [11,12,13].

The average lattice strain in L_3 direction is equal to ;

$$<\varepsilon'(\varphi,\psi)>_{(hkl)}= s_1(hkl)(\sigma^I_{11}+\sigma^I_{22}+\sigma^I_{33})+\frac{1}{2}s_2(hkl)(\sigma^I_{11}\cos^2\varphi+\sigma^I_{22}\sin^2\varphi+\sigma^I_{12}\sin2\varphi)\sin^2\psi$$

$$+\frac{1}{2}s_2(hkl)\sigma^I_{33}\cos^2\psi+\frac{1}{2}s_2(hkl)(\sigma^I_{13}\cos\varphi+\sigma^I_{23}\sin\varphi)\sin2\psi$$

where: $s_1(hkl)$ and $s_2(hkl)$ are diffraction elastic constants for quasi-isotropic polycrystalline and σ^I_{ij} macrostresses are defined with respect to the sample system.

If space components of stress tensor are neglected the simplification of above equation for plain stress field can be expressed:

$$\varepsilon_\phi,\psi = 1/2\,S_2\sigma_\varphi\sin^2\psi + S_1(\sigma_1+\sigma_2)=\frac{d_\psi-d_o}{d_o}$$

$$\sigma_\varphi = \sigma_2\sin^2\varphi + \sigma_1\cos^2\varphi$$

where: σ_φ is measured stress which is composed by σ_1 and σ_2 as principal stresses of plain state of stress according to last equation $1/2S_2=(1+\nu)/E=12.1$ $x10^{-6}$ MPa^{-1} and $S_1= -3.1 \times 10^{-6}$ MPa^{-1}.

The level of residual macro-stress was measured by new. g-$sin^2\psi$ method according to above procedure and was calculated under flat stress state ($\sigma_1 = \sigma_2 = -53$ MPa.)

5. CONCLUSIONS

The process of cold spraying results in significant plastic strain of copper grains, which when crushed cause elimination and considerable reduction of empty spaces in the coating. The achieved coating has a very high density and scanty number of oxide bands. Based on the change of elements contents levels at the contact site of the cooper coating and the substrate made of aluminum alloy, the diffusion substrate-to-coating bond was not observed. The phase

composition during deposition process stayed unchanged. Residual stresses of cold sprayed cooper coating after applied process are compressive ($\sigma_1 = \sigma_2 = -53$ MPa.). Grains of deposited cooper are not textured and they are strongly plastically deformed after deposition.

References

1. Van Steenkiste H., Smith J.R., Teets R.E., Moleski J.J. Gorkiewicz D.W., Tison R.P., Mararantz T.W., Kowalsky K.A., Rigss W.L., Zajchowski P.H., Pilsner B., Mccune R.C., Barnett K.J.: Surf. Coat. Tech. 111(1999), p. 62.

2. Stoltenhoff T., Voyer M., Kreye H.: Proc. ITSC 2002, Essen., p. 366.

3. Gärtner F., Stoltenhoff T., Schmidt T., Kreye H.: Proc. ITSC 2005 Basel, p.158.

4. Richer P., Krömmer W., Heinrich P.: Proc. ITSC 2002, Essen., p. 375.

5. Cheng O.: Proc. Itsc 2004, Osaka, p. 309.

6. Schmidt T., Gärtner F., Stoltenhoff T., Kreye H., Assadi H.: Proc.Itsc 2005 Basel, p. 232.

7. Papyrin A.N., Kosarev V.F., Klinkov S.V.,.Alkhimov A.P.: Proc. ITSC 2002, Essen, 380.

8. Assadi H., Gärtner F., T. Stoltenhoff, Kreye H.: Acta Mater., 51/2003, Issue 15 , p. 4379.

9. Richer P., Jodoin B., Taylor K., Sansoucy E., Johnson M., Ajdelsztajn L.: Proc. ITSC 2005, Basel, p. 193.

10. Lima R.S., Karthikeyan J.,.Kay C.M, Lindemann J., Berndt C.C.: Thin Solid Films 416 (2002), p.129.

11. Skrzypek S.J.: Surface Engineering (in polish) (2001), no 2 p.47.

12. Skrzypek S.J., Baczmański A., Ratuszek W.,Kusior E.: Journal of Applied Crystallography 34 (2001), p.427.

13. Skrzypek S.J.: Thesis and monographs, no108 (in polish), AGH University of Science and Technology Publishing House, Kraków 2002.

4. PRACTICAL EXPERIENCE IN SOLVING PROBLEMS OF TRIBOLOGY

4.1 WORKING CAPACITY OF CONTACT SURFACES

4.1.1 EXPERIMENTAL ACCESS TO INVESTIGATION OF TRIBOCORROSIVE PROPERTIES OF MECHANICAL PARTS SURFACES

Kunda J.[1], Bronček J.[1], Hadzima B.[1]

Introduction

The need to select or design new surfaces for future equipment as well as minimize the operating costs and extend the life of existing machinery has led to demands for a much better understanding of surface degradation processes particularly when tribological components are operating in corrosive environments. This has given rise to the active research area of tribocorrosion which seeks to address the concerns above and understand the surface degradation mechanisms when mechanical wear and chemical or electrochemical processes interact with each other.

1. Definition of corrosion

Corrosion is the physicochemical interaction between metal and environment. Corrosion resulted in permanent chemical changes of metal and therefore metal changes his chemical, physical and mechanical properties [1, 2]. Corrosion of the most technical metals is spontaneously because of metals tendency to achieve the thermodynamically stable state. Most of the technical metals (except copper, silver, gold and platinum) are no-noble and therefore it is presumption of interaction with environment in common conditions. It is very important to know the corrosion rate of the metal in specific media. The corrosion rate is the rate of the changing the metal to its corrosion product and it is determining by the rate of chemical reactions or by the rate of the transport of active components near metal surface. If the corrosion products are simply or complex ions and they are soluble in corrosion media then the metal is in active state. Some metals in some specific media during interaction between metal and

---

[1] University of Žilina

environment create the insoluble corrosion products with low porosity and with good adhesion to metal surface. The metals with natural passivation ability are stable in common media [3]. Existence and/or rebuilding rate of the passivation layer after its damage determine the corrosion resistant of the metal surface during tribocorrosion processes. Rebuilding of the layer is described by electrochemical conditions in the corrosion system. The full range current density – potential corrosion diagram describes the metal-environment processes. The typical corrosion diagram for the metal with ability for passivation in media is in Figure. 1.

At the potentials lower than Ecorr the cathodic partially reaction accelerates and anodic partially reaction decelerates. Metal is in immune state. The part of the polarization curve at potentials over Ecorr corresponds to active state of the metal surface (metal is dissolving). The conditions for creation of insoluble corrosion products (with good adhesion to metal surface) arise at the maximum of the current density (icp, Ep) at the interface of active and passive state. The surface is full passivized at the full passivation potential and corrosion density decreases to very low, technical acceptable value [1, 4].
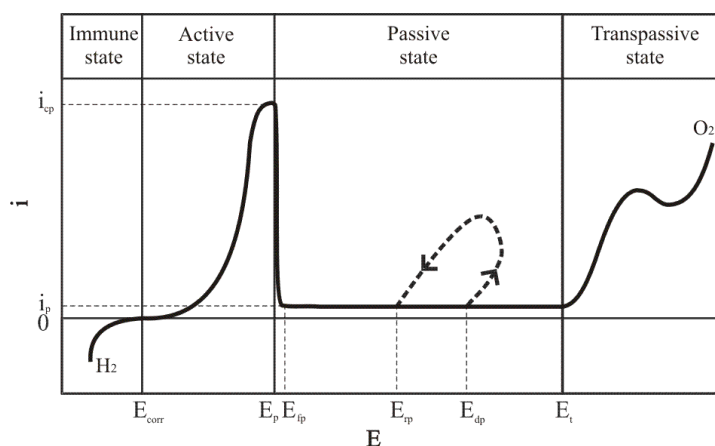

Fig. 1. Full range corrosion diagram [4, 5]

Transition of the metal surface to the passive state depends on ability to overcome of critical passivation current density icp. Creation of the passive layer is easier with lower value of the icp. On the other hand, metal can be passivized in operation media with high oxidative capacity for this metal. E.g. common steel corrodes in the distilled water or in the diluted nitric acid but same steel can be passivized in concentrated nitric acid. Some metals like Al, Ti,

Zr, Cr or stainless steels (with Cr content above 12 wt.%) have critical current density value lower than oxidative capacity of common atmosphere or common water [4, 5].

2. Definition of tribocorrosion

Tribocorrosion has evolved into a new and emerging area of research with many applications going beyond the conventional. It is basically an integration of two major areas of significance and application in mechanical systems namely Tribology and Corrosion [6, 7]. Tribology is the science of friction, wear, and lubrication, whereas corrosion relates to chemical aspects of the material degradation in mechanical systems [8, 15, 16].

Tribocorrosion can be defined as a degradation phenomenon of material surfaces (wear, cracking, corrosion, etc.) subjected to the combined action of mechanical loading (friction, abrasion, erosion, etc.) and corrosion attack caused by the environment (chemical and/or electrochemical interaction) [10], as highlighted in Figure 2.
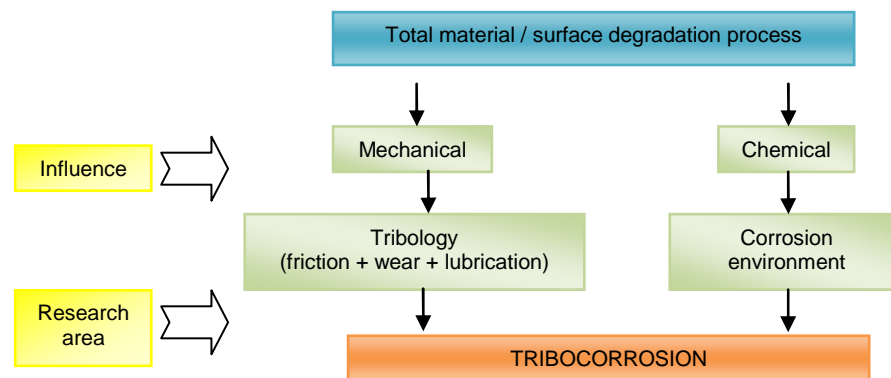

Fig. 2. Basic concept and definition of tribocorrosion

Tribocorrosion involves the interaction between mechanical wear processes and electrochemical and/or chemical corrosion processes and leads to a material loss rate that is a summation of these effects.

3. Factors affecting tribocorrosion process

Tribocorrosion behavior depends on the properties of the contacting materials, the mechanics of the tribological contact, and the physicochemical properties of the environment. These aspects are strongly interrelated-either synergistic or antagonistic, which can have beneficial or deleterious influence

over the performance of the tribological system. Therefore, the need is to study tribocorrosion from a systems perspective as it involves an integration of several subsystems. Figure 3 shows the important parameters affecting the tribocorrosion behavior in case of a sliding contact under electrochemical control [8, 10].
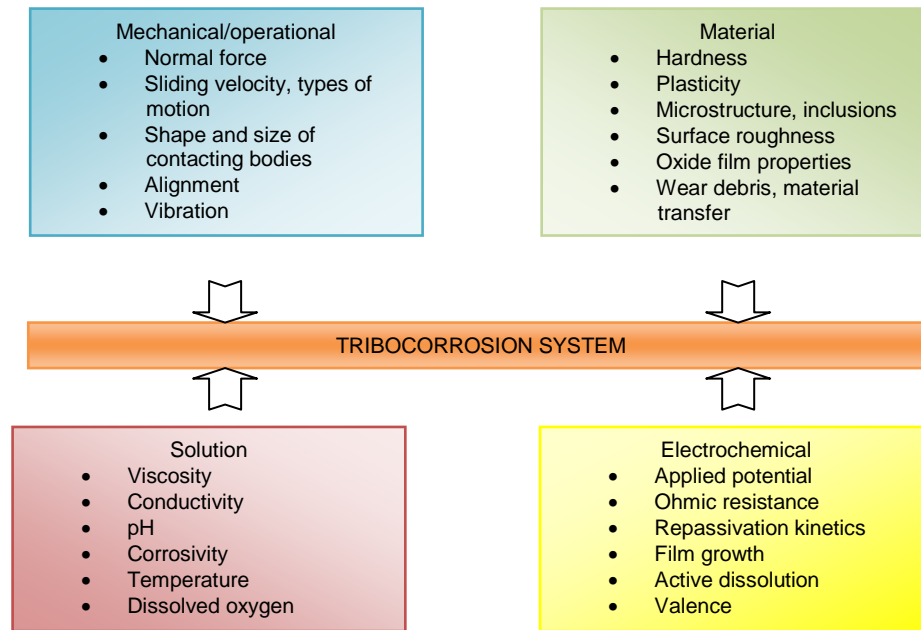
Mechanical/operational	Material
• Normal force • Sliding velocity, types of motion • Shape and size of contacting bodies • Alignment • Vibration	• Hardness • Plasticity • Microstructure, inclusions • Surface roughness • Oxide film properties • Wear debris, material transfer

TRIBOCORROSION SYSTEM

Solution	Electrochemical
• Viscosity • Conductivity • pH • Corrosivity • Temperature • Dissolved oxygen	• Applied potential • Ohmic resistance • Repassivation kinetics • Film growth • Active dissolution • Valence

Fig. 3. Factors influencing the tribocorrosion

Materials

The properties of all the materials involved in the tribological contact including those of the reaction products formed on the rubbing surface are of importance. In the absence of corrosion, wear resistance of a material depends on properties such as hardness, rigidity, ductility, and yield strength. The relationship between these properties on tribocorrosion rate is not very clear. Published research has tried to study the synergistic effects between wear and corrosion processes which result in accelerated material loss and in some cases actually decelerate material loss.

A wide range of corrosion resistant materials rely on a relatively thin surface oxide film to provide a barrier to charge transfer between the relatively active bulk material and the corrosive environment. This film renders the surface passive, but within the tribological contacts, the passive film can be removed by mechanical wear or impingement processes. Wherever the film is mechanically

damaged and removed, the charge transfer can take place at the interface without any resistance from the barrier film. This interaction between tribological and electrochemical corrosive effects increases loss of materials significantly. It will be much higher than the summation of material loss under pure corrosion (without tribological movements) and pure wear conditions (preventing corrosion under cathodic conditions) [11, 12].

Mechanical/operational parameters

The rate of tribocorrosion for a given metal-environment combination depends on the applied forces and the type of contact - sliding, fretting, rolling, or impact. The other factors include sliding velocity, type of motion, shape and size of contacting bodies, alignment, vibration, and so forth. For example, in the case of fretting corrosion, there are small amplitude oscillations occurring in a corrosive environment. Contact geometry involving shape and size of contacting surfaces is another important parameter in tribocorrosion, as it determines the size of the contact zone and the alignment of the rubbing surfaces. Different mechanical processes have different parameters affecting the process, like in case of erosion, the energy and the angle of incidence of the impacting particles and their shape are critical variables.

Solution/environment

For a given contact conditions (metal pair or nonmetal pair), environmental effects/variables play a major role in tribocorrosion. Its influence is in the form of the medium at the interface, that is, solid, liquid, or gaseous and its corresponding properties like viscosity, conductivity, pH, corrosivity, temperature, and so forth. For example, when the metals are exposed to air, the relative humidity will determine whether a thin liquid electrolyte film may form at the surface changing the corrosion mechanism. In case of aqueous systems, concentration of oxygen, pH and concentration of certain anions like chloride ions influences corrosivity. In case of high-temperature applications, the physical nature of the scales formed is critical. Certain corrosion products containing sulfur have a relatively low melting point, which can lead to the formation of highly corrosive molten salts on the surface.

Electrochemical parameters

In tribocorrosion, electrochemical aspects are very important, as the corrosion monitoring is being done by using basic electrochemistry. Basic parameters are applied potential, ohmic resistance, passive film growth, active dissolution, and so forth, as shown in Figure 3. The electrochemical aspect is considered mainly because tribocorrosion phenomena have been studied for many years by electrochemists and tribologists. Electrochemists have concentrated their attention on the study of the kinetics of repassivation of metal surfaces activated by scratching, whereas tribologists have been interested as to how surface oxidation during rubbing affects the rate of mechanical wear [7, 10].

4. Basic methodology of tribocorrosion properties measuring

As mentioned earlier, in order to study the tribocorrosion behaviour, mechanical and corrosion responses from the tribocorrosion test system are required to be collected and monitored. Generally, tribometer has facility to measure the evolution of frictional forces and electrochemical technique is used to monitor the corrosion response from the test system. A schematic diagram of the basic methodology of a tribocorrosion test system is shown in Figure 4. Electrochemical interfacing consists of a potentiostat and three electrode attachments, such as reference electrode (RE, either SCE (standard calomel electrode) or SHE (standard hydrogen electrode)) and counter electrode (CE, platinum wire or graphite rod). The sample is acting as the working electrode (WE) [13].
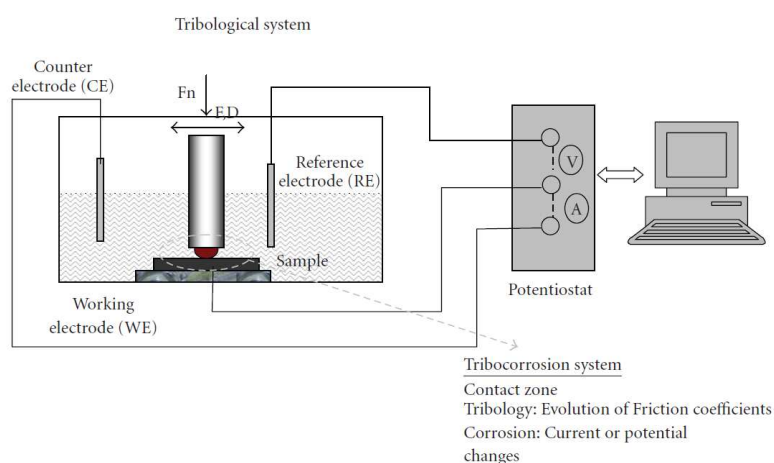

Fig. 4. Basic methodology in a tribocorrosion study [13]

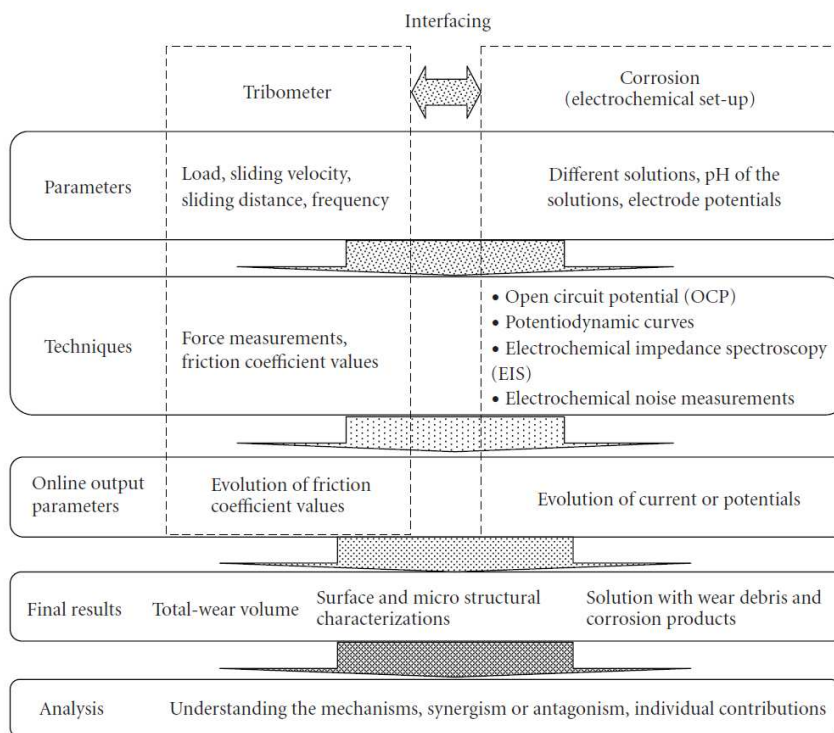Basic steps in a tribocorrosion tests are explained in a schematic diagram in Figure 5.

Fig. 5. Basic steps in a typical tribocorrosion study [13]

The selection of parameters depends on the application and research interest. For example, in case of an orthopedic application, the influence of load or cycles might be the parameter of interest. In dental application, the pH of the solution could play a role and might be investigated. The technique to be used varies with the nature of the test system. Generally, open circuit potential (OCP) measurements provide the evolution of potential and potential changes in the system with respect to standard electrodes (e.g., standard calomel electrode, SCE). Further, the corrosion current evolution can be studied at a constant potential from the system. Likewise electrochemical impedance spectroscopy (EIS) can be used to understand the properties or characteristics of films formed at the contact zone. Usually such measurements are taken before and after the sliding or tribotest.

The online measurements of friction coefficient and corrosion parameter (either current or potential) can be very useful in analysis. An example from a

previous tribocorrosion study of TiCxOy film (Titanium carboxide film for decorative applications, electrolyte: artificial sweat solution) is shown in Figure 6 [13].
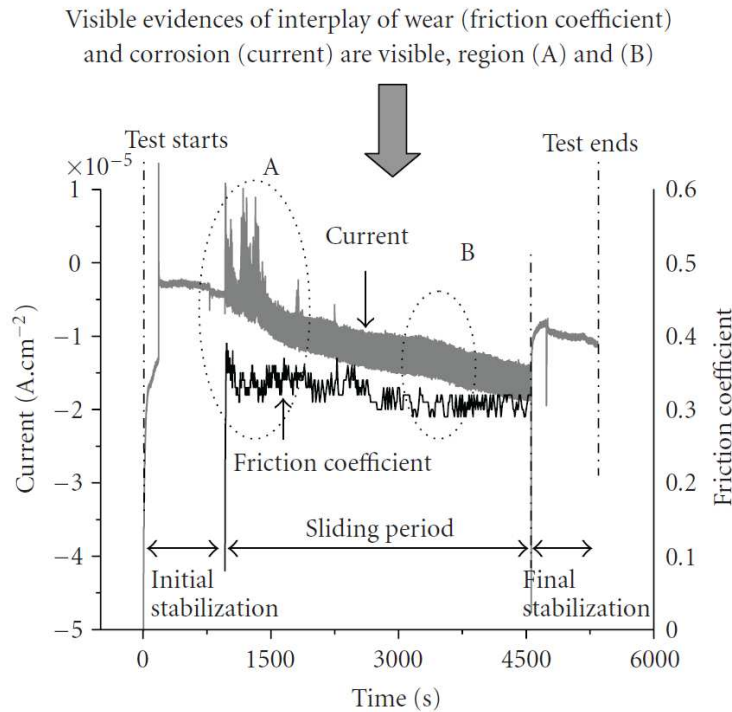

Fig. 6 An example of tribocorrosion study evolution of friction coefficient, and current, as a function of sliding time [13]

5. Practical limitations in the tribocorrosion studies

One of the major difficulties in tribocorrosion studies is the interlaboratory comparability of the results of a standard test apparatus. One of such modified systems, a pin-on disk tribometer used for tribocorrosion studies of thin films, is shown in Figure 7. In fact, such test systems have an advantage of distinct methods in collecting and processing the tribological responses. However, several practical and technical problems may arise in employing such systems for carrying out the experimental studies on tribocorrosion and analysis of the results. Some of the limitations of a modified system can be listed as follow; geometry and construction of a corrosion cell, proper locations of electrode possible leakage of the electrolyte, and collection and synchronization of the data from the tribometer and potentiostat.
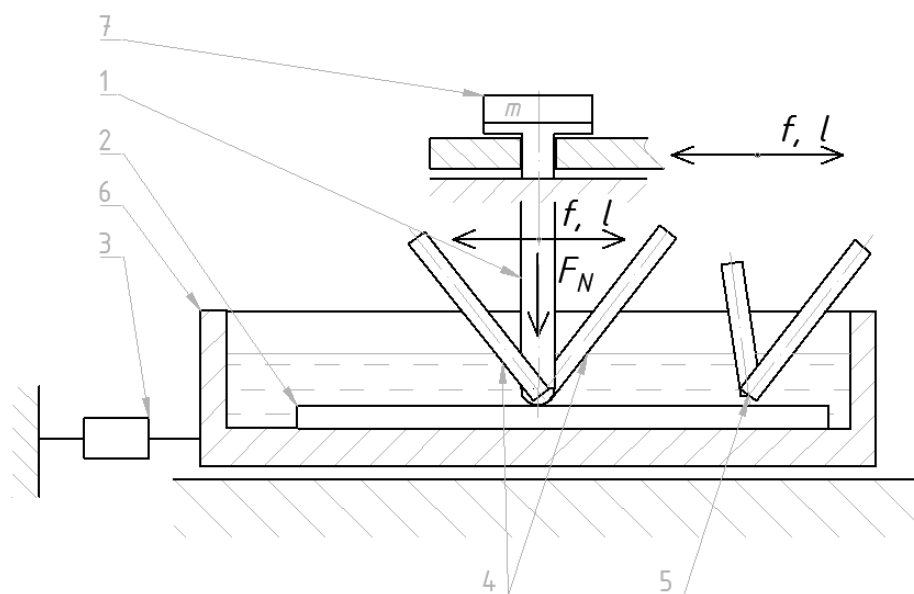
Fig. 7. Scheme of modified tribocorrosion experimental set-up with a reciprocating sliding tester (1 – pin; 2 – sample; 3 – load cell; 4 – electrode WE; 5 – electrode RE; 6 – container)

6. Dynamic tribocorrosion test system and understanding the synergism

It is also important to note that corrosion test favors a stabilized system and indicates the changes in the surface chemistry under the influence of solution or environments. It is also important to note that corrosion testing systems favor a stabilized system and monitor the changes in the surface chemistry under the influence of environmental factors. However, it is impossible to have a tribological system (where the contacting bodies are in motion), under stable conditions. Hence, it is a challenge in understanding and/or interpreting the corrosion results from the tribological/dynamic conditions. At the same time, this is the novelty of the tribocorrosion studies. Better knowledge about the interaction of both tribology and corrosion will help in understanding the impact on the system. For example, in the tribocorrosion studies in a reciprocating sliding tribometer (Figure 7), the current evolution is associated with sliding movement and velocity evolutions. Such effects are visible in the evolution of current and friction coefficient values as a function of time. For example, the marked regions "A and B" in Figure 6 demonstrate that the sudden variation in the evolution of current is linked with changes in the

friction coefficient, indicating the interplay of tribology and corrosion in the tribocorrosion process .

Conclusion

Tribocorrosion as a phenomenon, which occurs in loaded technical and biological systems, needs a systematic theoretical and practical study too. According to the tribological definition tribocorrosion belongs to the wear, when the main role is represented by tribological processes characterized by basic wear kinds - abrasive, erosive and adhesive strengthened by tribochemical and chemical reactions, which are running in contact of tribological surfaces. The main basis of this analysis is a subject of an intensive examination and it appears, that for the right understanding an experimental research supplemented with the analytic analysis of load, environment and material properties influence is needed [9]. The miscellaneousness of the experimental devices and testing stands affords different results and their interpretation. Many researchers were attempting to create the mathematical or software model because of the right understanding of tribocorrosion processes [5]. These models have a limited usability, while the number of influencing parameters makes this phenomenon more difficult. These methods are limited according to ensure the right testing conditions. Their extension and generalization to the real conditions is disputable at all. In the interest of the systematical solution of tribocorrosion problem is also needed to think about the fact, that its existence can be modified by deposited and modified coatings and layers [14].

Acknowledgement

References

1. Liptáková, T. – Šestina, I.: Fundamentals of corrosion and protection against corrosion of metals in gas industry. EDIS – ŽU v Žiline, Žilina 1997

2. Bakhvalov, G.T. – Turkovskaya, A.V.: Corrosion and protection of metals. Pergamon Press, Oxford 1965.

3. Černý, M. a i.: Corrosion properties of metals structural materials. SNTL Praha, Praha 1984

4. Škublová, L.: Corrosion resistence of Mg-3Al-1Zn alloy in simulated body fuids. [PhD Thesis], ŽU v Žiline, Žilina 2010.

5. Hadzima, B. – Liuptáková, T.: Fundamentals of the electrochemical corrosion of metals. EDIS ŽU v Žiline, Žilina 2008.

6. Celis, J. –P., Ponthiaux, P.: Tribocorrosion, Wear, vol. 261 937–8, 2006.

7. Landolt, D.: Electrochemical and materials aspects of tribocorrosionsystems, Journal of Physics D, vol. 39, no. 15, pp. 3121–3127, 2006.

8. Celis, J. – P., Ponthiaux, P. – Wenger, F.: Tribo-corrosion of materials: interplay between chemical, electrochemical, and mechanical reactivity of surfaces, Wear, vol. 261, no. 9, pp. 939–946, 2006.

9. Fischer, A. – Mischler, S.: Tribocorrosion: fundamentals, materials and applications - editorial, J. Phys. D: Appl. Phys. 39 issue 15, 2006.

10. Mischler, S.: Triboelectrochemical techniques and interpretation methods in tribocorrosion: a comparative evaluation. Tribology International, vol. 41, no. 7, pp. 573–583, 2008.

11. Wood, R. J. K.: Tribo-corrosion of coatings: a review, Journal of Physics D, vol. 40, no. 18, pp. 5502–5521, 2007.

12. Ponthiaux, P. – Wenger, F.– Drees, D.– Celis, J. P.: Electrochemical techniques for studying tribocorrosion processes, Wear, vol. 256, no. 5, pp. 459–468, 2004.

13. Mathew, M. T. – Ariza, E. – Rocha, L. A. – Fernandes, A. C.– Vaz, F.: TiC_xO_y thin films for decorative applications: tribocorrosion mechanisms and synergism, Tribology International, vol. 41, no. 7, pp. 603–615, 2008.

14. Kunda, J.: Experimentálny prístup k určovaniu tribokoróznych vlastností tenkých povlakov - písomná práca k dizertačnej skúške, Žilina, 2011.

15. Moravec, J. – Stroka, R.: Magnetic Forming. Terotechnologia 2009 – Zeszyty naukowe 13. PL ISSN 1897 – 2683, 2009, p. 295 -301.

16. Zimneová, M., Fabian, P.: *Hodnotenie tribologických skúšok*. DOKSEM 2009. Medzinárodná doktorandská konferencia „Nekonvenčné technológie 2009". Žilina – Strečno 2008, ISBN 978-80-554-0062-4.

4.1.2 VIBRATING SLIDE IN MECHANICS OF NOMINAL FRICTIONAL FIXED CONTACT
Kostogryz S.[1]

Introduction

For study the resonance phenomena in the nominally-stationary frictional contact with vibrational friction of extraordinary significance becomes experimental determination of the amplitude-frequency characteristics of the nominal tangential stresses in the contact.

Such a problem in terms of its implementation is problematic because it can not be solved in the known theory of automatic control by direct methods, because for that at a given external sinusoidal shifting power to measure peak value of nominal tangential stresses in the contact and each fixed frequency. This can not be practically implemented because with its familiar controls mechanical processes "climb" in the contact impossible.

To this end, we proposed a technique based on the laws of descent vibrations through nominally-fixed frictional contact with a close to linear properties. One element of this contact is a pattern still attached to the sloping area that is exposed to vibrations in the plane of inclination, and the second element is freely available on the sample counter specimen. This area of contact is parallel to an inclined plane.
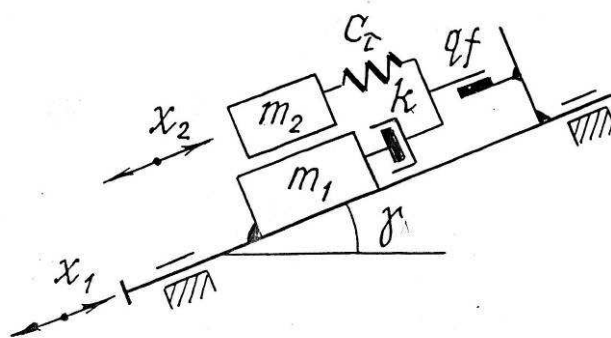

Fig. 1. - Schematic diagram of interaction elements of nominally real frictional contact on the vibrating inclined plane

[1] National university of Khmelnitsky

The design of dynamical model of the system linearized and presented in Fig. 1. In this model, elastic properties are modeled by tangential stiffness C_τ and damping properties by coefficient of viscous damping k. This friction properties included specific force of friction qf. If the mass m_1 (Fig. 1) set the tangential motion of the vibration level $x_1(t)$, then vibration, passing through the contact will cause a vibration moving $x_2(t)$ for counter specimen of mass m_2. Moreover, the relative vibration specimen and movement of the counter specimen $x(t) = x_1(t) - x_2(t)$ under certain conditions will occur in full prior displacement contact elements can not pass in relative slip. The condition, which occurs when "the failure of contact" has the form:

$$qf - \frac{Q_2}{A}\sin\gamma \le \tau_{kx},$$
(1)

where qf - specific (nominal) friction in contact;

Q_2 - weight of counter specimen;

A - nominal contact area;

τ_{kx} - amplitude of nominal tangential stresses in the contact that caused vibro displacement its elements under the action of the kinematic excitation $x_1(t)$.

Differential equations of motion of mass m_2 of counter specimen across the whole of the previous offset kinematic excitation $x_1(t)$ has the form:

$$\ddot{x}_2 + \frac{\delta}{\pi}\Omega_\tau\dot{x}_2 + \Omega_\tau^2 x_2 = \frac{\delta}{\pi}\Omega_\tau\dot{x}_1 + \Omega_\tau^2 x_1$$
(2)

where $\Omega_\tau = (AC_\tau/m)^{\frac{1}{2}}$ - own frequency of oscillations mass m_2 at fixed m_1;

δ - logarithmic decrement of oscillations, for the coefficient of viscous resistance k.

The Laplace Image of coordinates x_2 to find from differential equation (2) with zero initial conditions :

$$x_2(S) = \frac{\dfrac{\delta}{\pi}\Omega_\tau S + \Omega_\tau^2}{S^2 + \dfrac{\delta}{\pi}\Omega_\tau S + \Omega_\tau^2}\, x_1(S)$$
(3)

where $x_1(S)$ - Laplace Image of forced function $x_1(t)$;

S - Laplace operator.

Tangential stress into contact with kinematic excitation of vibrations $x_1(t)$ as the sum of elastic and dissipative component was find:

$$\tau_{kx} = [x_1(t) - x_2(t)]C_\tau + \frac{1}{A}[\dot{x}_1(t) - \dot{x}_2(t)] \cdot k \qquad (4)$$

Using the expression (4) for direct Laplace transform with zero initial conditions, we obtain the expression for Laplace Image of nominally tangentional stress into contact by kinematic excitation of vibrations in it:

$$\tau_{kx}(S) = \left[\frac{\delta}{\pi}\Omega_\tau S + \Omega_\tau^2\right] \cdot [x_1(S) - x_2(S)] \qquad (5)$$

Substituting in (5) formula (3), we are obtain:

$$\tau_{ks}(S) = \frac{S^2 m_2}{A}\left(\frac{\dfrac{\delta}{\pi}\Omega_\tau S + \Omega_\tau^2}{S^2 + \dfrac{\delta}{\pi}\Omega_\tau S + \Omega_\tau^2}\right)x_1(S) \qquad (6)$$

Divide the expression (6) on $x_1(S)$ and to obtain an expression for the transfer function of the nominally tangential stresses into the contact:

$$W_{\tau_{ks}}(S) = \frac{S^2 m_2}{A}\left(\frac{\dfrac{\delta}{\pi}\Omega_\tau S + \Omega_\tau^2}{S^2 + \dfrac{\delta}{\pi}\Omega_\tau S + \Omega_\tau^2}\right), \qquad (7)$$

where $W_{\tau_{kx}}(S) = \dfrac{\tau_{kx}(S)}{x_1(S)}$ transfer function from coordinates x_1 to the nominally tangential stresses in the contact..

Substituting in formula (7) $S = i\omega$ - circular of frequency of forced oscillations come from the transfer function to the amplitude-phase frequency response of the nominally tangential stresses in the contact. The expression for its modules, ie amplitude-frequency response will look like:

$$\left| W_{\tau_{kx}}(i\omega) \right| = \frac{\omega^2 m^2}{A} \sqrt{\frac{1 + \left(\frac{\delta}{\pi}\right)^2 \left(\frac{\omega}{\Omega_\tau}\right)^2}{\left(1 - \frac{\omega^2}{\Omega_\tau^2}\right)^2 - \left(\frac{\delta}{\pi}\right)^2 \cdot \left(\frac{\omega}{\Omega_\tau}\right)^2}} \,, \tag{8}$$

It is easy to show that the multiplier of the radical in expression (8) is module of the amplitude-phase frequency response of the nominally tangential stress for contact with the driving by specific shear strength [1] - $\left| W_{\tau_k}(i\omega) \right|$.

Given this ratio $\left| W_{\tau_{kx}}(i\omega) \right|$ and $\left| W_{\tau_k}(i\omega) \right|$ obtained:

$$\left| W_{\tau_{kx}}(i\omega) \right| = \frac{\omega^2 m_2}{A} \left| W_{\tau_k}(i\omega) \right|, \tag{9}$$

It should be noted that $\left| W_{\tau_{kx}}(i\omega) \right|$ is dimension N/mm^2·m^{-6} , and $\left| W_{\tau_k}(i\omega) \right|$ is dimensionless quantity.

The amplitude of shear stresses in the nominally-fixed frictional contact for the scheme of interaction of its elements, shown in Fig. 1 and for harmonic vibrations of an inclined plane with an amplitude $x_1(\omega)$ can be represented by the expression:

$$\tau_{kx}(\omega) = \frac{\omega^2 m_2}{A} \left| W_{\tau_{kx}}(i\omega) \right| \cdot x_1(\omega), \tag{10}$$

Substituting expression (10) in (1) and introducing the notation $q = Q_2 \cos\gamma / A$ and $Q_2 = m_2 g$, after certain transformations we obtain the condition of "breakdown" of contact:

$$f - \frac{x_1(\omega)\omega^2}{g} \left| W_{\tau_k}(i\omega) \right| = tg\,\gamma(\omega). \tag{11}$$

With this condition we obtain the formula for the experimental determination of the amplitude-frequency response of the nominal tangent in contact with power supply interaction of its elements placed on vibrating inclined plane:

$$\left| W_{\tau_k}(i\omega) \right| = \frac{[tg\,\gamma_0 - tg\,\gamma(\omega)]g \cdot \cos\gamma(\omega)}{x_1(\omega)\omega^2} \,, \tag{12}$$

where γ_0 - angle of friction into contact

$$\gamma_0 = arctgf \qquad (13)$$

$\gamma(\omega)$ - the angle of inclined plane at a given frequency of forced oscillations ω.

Formula (12) underlies the method of experimental determination of the amplitude-frequency response of the nominally - fixed frictional contact to we applied of amplitude and frequency dependence of the nominal tangential stresses in the contact on the outside of the specific force of shear of vibrational friction.

For its practical implementation we developed a special plant, built under the scheme of interaction of its basic elements, corresponding to Fig. 1. Working with plant to build in some points at fixed magnitude ω of graphs amplitude frequency response of the nominal tangential stresses in the contact occurs on the method developed by us in that order.

First, determine the method of inclined-plane angle of static friction γ_0 in the contact, which occurs when "failure". Then for each fixed frequency of vibrations ω for inclined plane specimen and counter specimen and at given amplitude $x_1(\omega)$ of longitudinal vibrations inclined plane, gradually increasing the angle of the plane γ, determines the smallest angle $\gamma(\omega)$ at which there is a "failure" to counter specimen at given frequency vibrations of plane was determined. Substitute the values of these variables in the formula (12) and take into account the modulus of the amplitude-frequency characteristics $\left|W_{\tau_k}(i\omega)\right|$. This is results of the experimental studies to construct the amplitude-frequency response for the nominal tangential stresses in the contact.

It is also possible a different approach to the definition $\left|W_{\tau_k}(i\omega)\right|$ by the formula (12). At the same time determine the angle of static friction γ_0 and inclined plane is set on $\gamma(\omega) < \gamma_0$, which take constant for all frequencies of forced oscillations. Then, changing for each fixed frequency amplitude of motion $x_1(\omega)$, determine the lowest level of the amplitude at which a given frequency there is a "failure" of contact. When you do this γ_0, $\gamma(\omega)$, ω, $x(\omega)$

substituted in the formula (12) and determine $\left|W_{\tau_k}(i\omega)\right|$. As shown for such experiments, this approach was more convenient to use than the first.
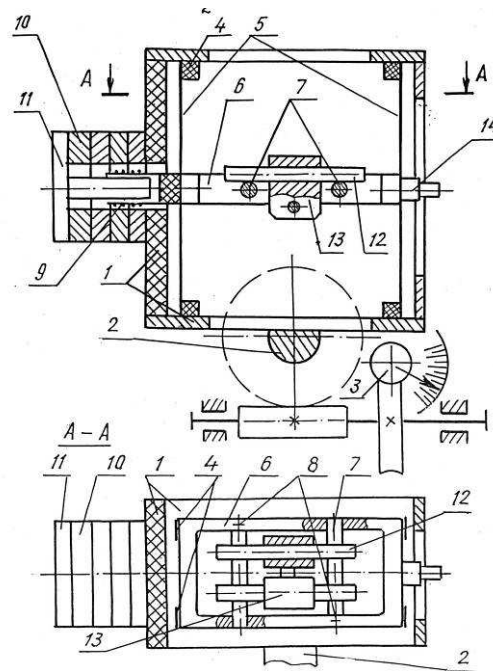

Fig. 2. The constructive scheme of the plant for determines the static and dynamic characteristics of nominally fixed frictional contact on vibrating inclined plane.

The Fig. 2 illustrates a constructive scheme and interaction the basic elements of installation. On Fig. 3 shows its general view. The frame 1 from light alloy fixed on the output shaft 2 precision worm gears with a total gear ratio $U = 3600$. One complete turn the shaft of the worm 3 corresponds to $6'$ establish angle of rotation shaft 2 of frame 1, making it more accurate before $1'$ and define the angles γ_0 and $\gamma(\omega)$.

In frame 1 symmetrical on four pillars 4 installed in pairs along the left and right of plate spring 5, which serve as the suspension system, which forms an inclined plane that made as a frame 6, which is fixed between the springs 5. The frame 6 holds two identical cylindrical sample 7, which are installed in the tower frame holes and fixed with screws 8, which provides the possibility of quick change.

At one of the ends of frame 6 is installed coil 9 of electromagnetic vibrator. Cylindrical counter specimen 12 has the same dimensions as the samples. They are installed in pairs in the carriage 13, which consists of two

identical parts, each of which can freely rotate relative to one second, the need for self orientation of all four points of contact samples of counter specimen. Mass of counter specimen and carriage is m_2.
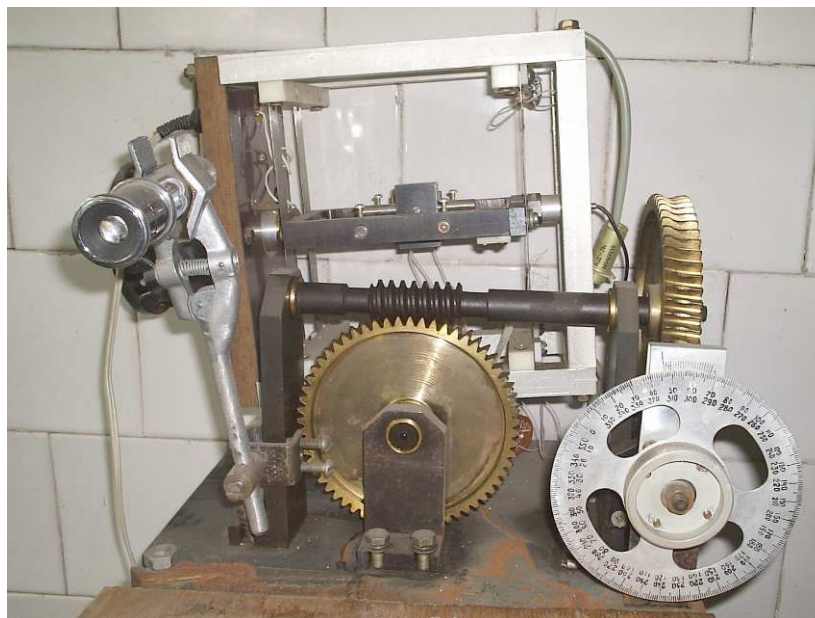

Fig. 3. General view of the plant made for a constructive scheme, shown in Fig. 2.

The plant can operate in static and dynamic modes. In static mode, measure of angle of friction γ_0 and through it determines the static coefficient of friction. With rotation of the crank shaft of the worm 3 frame 6 of the specimens set in a horizontal position and strictly symmetrical with respect to counter-specimen 7 placed on them block of the counter-specimens 12 with carriage 13. Then, gradually turning the crank angle increases beyond 6 to until will not "failure" of counter-specimens and together with the carriages will not slip on the specimens. Angle frame in this state will be equal to the angle of static friction in the frictional contact and determine by the indications digital counter which connected to shaft 3 and limb.

On this installation in static mode can be obtain diagram «tangential stress - strain" for frictional contact. To this end, set on the frame 6 inductive proximity sensor of motion. The frame 6 is set in a horizontal position. On specimen 7 freely put a counter-specimen 12. Output of sensor connected with measurable instrumentation. Turning the crank shaft of the worm 3 is gradually increased the angle of frame 6 and register the change of gap between core of

inductive sensor and face of counter-specimen 12, which is contact tangential strain caused by the action of tangential component of gravity for counter-specimen. The increasing of angle of frame 6 leads to an increase of tangential component of gravity and to the growth of strain. For magnitude of the angle frame 6 is calculated the tangential tension in contact and have the values of tangential displacement in contact, build a diagram "tangential stress - strain".

In operate of plant in a dynamic mode, the frame 6 with the counter-specimen set at an angle much smaller than γ_0. Then, using of generator of frequency, en electric signal of minimum level give on vibrator. At the same time the frame 6 will perform harmonic oscillations in an inclined plane that passes through all four points of contact of counter-specimen with specimen. Smoothly increasing amplitude of electric signal, from testimony of accelerometer 14 determined the acceleration of frame 6, which will "failure" of counter-specimen - $x_1(\omega)\omega^2$. Substituting the acceleration for frame 6 in formula (12) with the known γ_0 and $\gamma(\omega)$ we can calculated, for each of the fixed frequency of forced oscillations ω, a numerical magnitude of the amplitude-frequency response $\left| W_{\tau_k}(i\omega) \right|$ and thus the total response build an appropriate of amplitude-frequency characteristics.

For experimental studies of cylindrical specimens and identical to them counter-specimens from drawings that depicted in Fig. 2 were used. The materials of specimens were structural steel and alloys: steel 45 (normalized and treatment), steel 0,4% Cr (HRC $42 \div 45$), aluminum alloy D16 and brass L60.

By method of vibrating inclined plane of the experimental data that are used in constructing the amplitude-frequency characteristics of the nominal tangential stresses for the conditions of contact with the higher pair. Experimental data are a set of values of the module return amplitude-frequency response for a fixed frequency of oscillation. This set of points in a coordinate system $\left| W_{\tau_k}(i\omega) \right|^{-1} - \omega$ obtained for each material of the specimens. Examples of experimental data sets for determining inverse amplitude-frequency response of the nominal tangential stresses in the contact are shown in Fig. 4. This figure shows a clear dependence $\left| W_{\tau_k}(i\omega) \right|$ from the oscillation frequency of a pronounced resonance minimum. This minimum is manifested in all the

experiments on those or other frequencies. Its physical meaning is that the resonant frequency corresponds to the minimum amplitude of the specific force shear in the contact. If we consider the effect of reducing the coefficient of friction at resonance, the resonant frequency corresponds to the minimum magnitude of the effective coefficient of friction in contact, compared with a static coefficient of friction. This recognizes the work we set [2] the frequency dependence of the ratio of the effective coefficient of friction in contact f_e from static coefficient of friction f_0, which has a resonant nature:

$$f_e / f_0 = \left| W_{\tau_k} \left(i\omega \right)^{-1} \right| \tag{14}$$
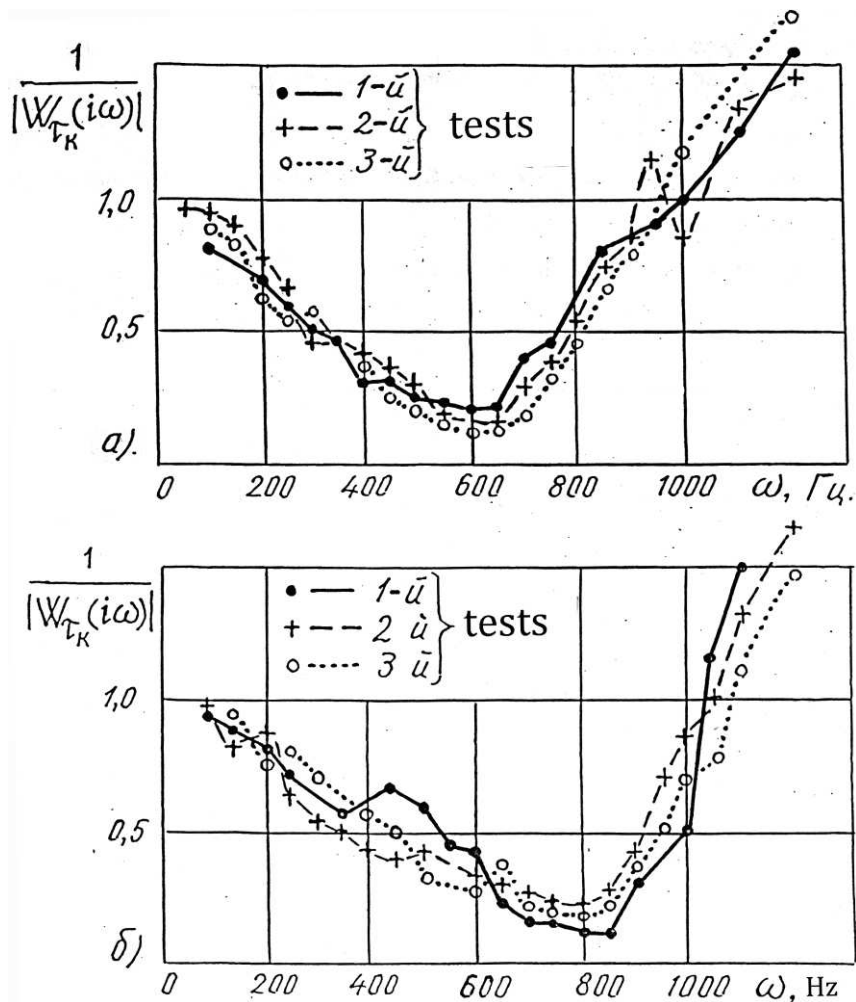
Fig. 4. Inverse amplitude-frequency responses of nominally fixed frictional contact that obtained by method of vibrating inclined plane for different materials of contact pairs: brass L60 (a), steel 0,4% Cr (b).

Having accomplished the processing of experimental data presented in Fig. 4, by method of least squares, you can get an experimental graphical dependence module of the amplitude-frequency response of the nominal tangential stresses in the contact. These allow determine the initial tangential contact rigidity and logarithmic decrement of oscillations, as well as solve other related matters.

Reference

1. Kostogryz S.G Mechanics of vibration friction for nominally-fixed frictional contact: Abstract dis .. Dr. techn. Sciences: 05.02.04 , 1995. - 36

2. Kostogryz S., Kovalevsky V., Shalapko Y. Resonance effects of friction in the nominally - fixed mechanical contact with low-amplitude fretting. / / Friction and wear. Volume 2. - № 3. - 1991. - pp. 459-464.

4.1.3 MODELING OF DYNAMICAL BEHAVIOR OF NOMINAL-FIXED JOINTS

Kurskoy V.[1], Shalapko Y.[1], Radek N.[2]

Introduction

The method, which assess the impact of surface modification by creating a regular relief on the surfaces in long-term ability to maintain the integrity of contact under vibration loads

Reliability and durability of equipment connect with the need to ensure adequate quality of individual units and elements of their interface that, in the case of nominally-fixed joints (NFJ), often achieved by applying coatings and change the properties of the surface layer.

Among the large number of currently applied of methods for modifying surfaces remains unclear what impact the issue have of processing macrogeometry of surface for long-term ability to maintain the integrity of contact. Macrogeometrical characteristics are especially important for the initial

[1] National university of Khmelnitsky
[2] Centrum Laserowych Technologii Metali, Politechnika Świętokrzyska, Kielce, Polska

conditions of the contact as significantly affect the elastic characteristics of contact and, consequently, tribological characteristics of the joints.

Surface profile formed in the processing of the surface layer by high-energy methods of such as laser processing, electric-sparks, has the character of regular micro and macro irregularities[1,2].

Therefore, for quantitative and qualitative assessment of the working surface from a position of long-term conservation of the nominal contact of joints parts, in the design stage, it is expedient to apply the methods of mathematical analysis for the definition of the geometry of the surface. In the study of the integrity of nominally-stationary friction joints under cyclic loads were applied surface modification techniques that alter the geometry of the surface layer in a wide range of values - from changes of roughness to a regular macro geometry of surface (Fig. 1). It is reasonable to define the criteria that will compare the geometry of surfaces at different ways of surface modification.

a)

b)
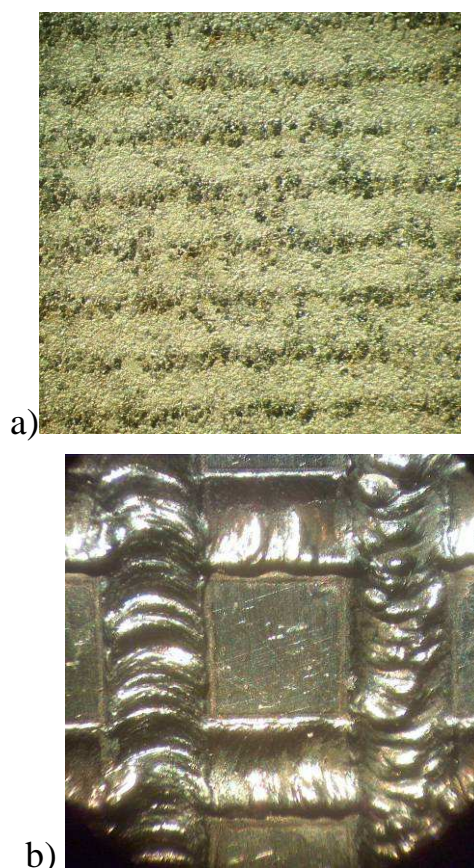
Fig. 1. The metallic surface after electric-spark alloying (a) and laser irradiation (b) (x 100)

2. Criteria of surface modification

The surface profile parts after surface modification has a significant deviation from the nominal form of the surface. Since the investigated coatings are applied with a certain frequency (step), the surface profile after treatment, with certain assumptions, can be considered as periodical and use for approximation of profile surface by using discrete microelements (DME). For the mathematical description of the surface was elected element in the form of elliptic paraboloid. The affordability model is based on micro elements in the form of elliptic paraboloid and demonstrated in Fig. 2 (material prepared on the device surfaces of three-dimensional study by laser scanning Talyscan firm Rang Taylor Hobson.
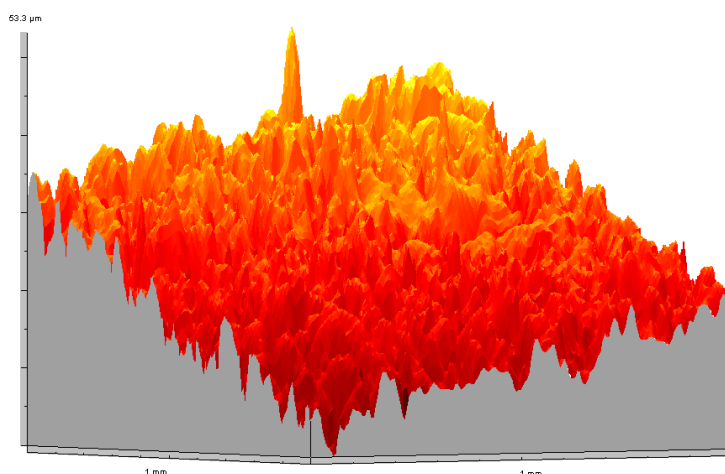
Fig. 2. General view of the surface field size 1x1 mm

Using as a prototype elliptic parabolic surface DME opens the opportunity for consistency of mathematical description of shape as the basis of the supposed put of the elliptic parabolic (EP). Preliminary application of the principles EP set out in [3, 4]. Design model of a contact pair shown in Fig. 3.

To assess the ability of method of surface modification of parts nominally-fixed friction joints ensure the minimization of relative displacement, and, correspondingly, increase the term of operation of machine parts

Determine of properties of the contact zone is outstanding in terms of the integrity of the contact. These properties, in a dynamic perturbation, is en elastic properties of zones of deformation and their parameters of mass . In this case, the loading is perceived contact on the level of each elliptic paraboloid. It is

necessary to determine the resultant characteristics of contact that will enable to assess the elastic properties of elements in accordance with the terms of the load.
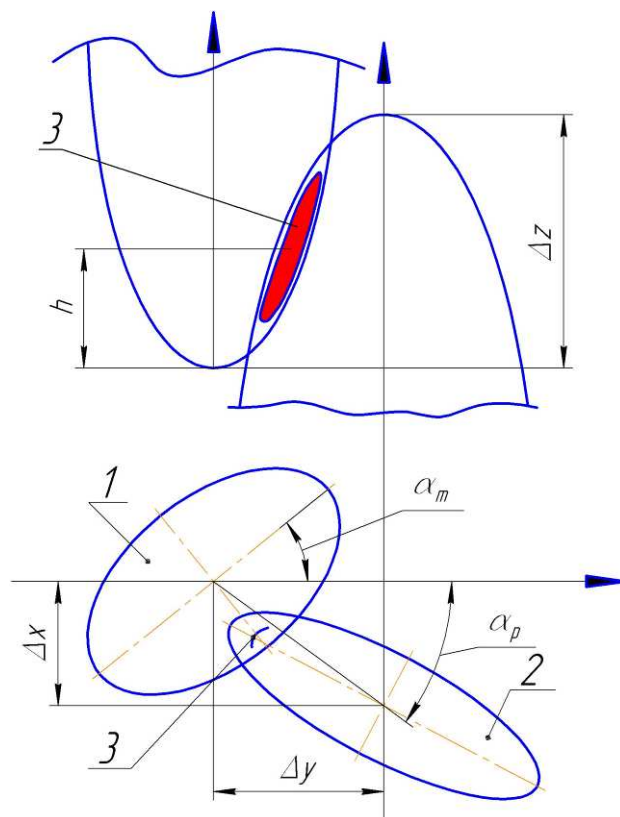

Fig. 3. Contact microelements 1 i 2, 3 - contact spot

A line of mutual penetration of two elliptic paraboloid define by solution of system equations that describe a pair of DME:

$$\begin{cases} z = \dfrac{(x)^2}{a} + \dfrac{(y)^2}{b} \\ z = -\dfrac{(x_\alpha - \Delta x)^2}{c} - \dfrac{(y_\alpha - \Delta y)^2}{d} + \Delta z \end{cases},$$

where a, b - eccentricity ratios of the body 1;

c, d - eccentricity ratios of the body 2;

Δx, Δy, Δz - displacement of body 2 relatively body 1 for axes x, y and z respectively,

$x_\alpha = x{\cdot}\cos\alpha_p - y\cdot\sin\alpha_p$, $y_\alpha = x{\cdot}\sin\alpha_p + y{\cdot}\cos\alpha_p$ - coordinates x and y body 1 in the new system, taking into account the angle of rotation.

General view of the obtained surfaces is presented in Fig.4.

322
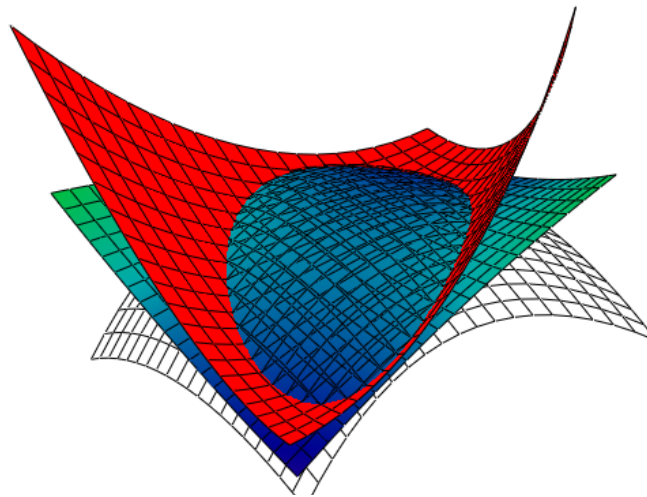
Fig. 4. Deformed surface of section for contact

To determine the resulting vector will consider two paraboloid contact, presenting it as a sum of discrete contacts. The resulting vector interaction at DME has the form:

$$\vec{F}_r = |F| \cdot \vec{N},$$

where $|F|$ - module force elastic interaction, which is determined from geometric and elastic characteristics of the material;

$\vec{N}$ - normal unit vector for a given point.

Factor definition of discrete unit vector is angles of relative axes of coordinates. Determination of the angle of the resulting vector of relatively coordinate system performed by definition of the normal resulting vector and angles between the axes and coordinates. The resulting vector can be represented in the form:

$$\vec{N} = \begin{pmatrix} \displaystyle\int_{y\min}^{y\max}\int_{x\min}^{x\max} (\frac{d}{dx} f_R(x,y)) dxdy \\ \displaystyle\int_{y\min}^{y\max}\int_{x\min}^{x\max} (\frac{d}{dy} f_R(x,y)) dxdy \\ \displaystyle\int_{y\min}^{y\max}\int_{x\min}^{x\max} dxdy \end{pmatrix}$$

Corresponding angles can be found at the following formulas:

$$\alpha = \arccos\left(\frac{\displaystyle\int_{y\min}^{y\max}\int_{x\min}^{x\max}(\frac{d}{dx}f_R(x,y))dxdy}{\sqrt{\left(\displaystyle\int_{y\min}^{y\max}\int_{x\min}^{x\max}(\frac{d}{dx}f_R(x,y))dxdy\right)^2+\left(\displaystyle\int_{y\min}^{y\max}\int_{x\min}^{x\max}(\frac{d}{dy}f_R(x,y))dxdy\right)^2+\left(\displaystyle\int_{y\min}^{y\max}\int_{x\min}^{x\max}dxdy\right)^2}}\right)$$

$$\beta = \arccos\left(\frac{\displaystyle\int_{y\min}^{y\max}\int_{x\min}^{x\max}(\frac{d}{dy}f_R(x,y))dxdy}{\sqrt{\left(\displaystyle\int_{y\min}^{y\max}\int_{x\min}^{x\max}(\frac{d}{dx}f_R(x,y))dxdy\right)^2+\left(\displaystyle\int_{y\min}^{y\max}\int_{x\min}^{x\max}(\frac{d}{dy}f_R(x,y))dxdy\right)^2+\left(\displaystyle\int_{y\min}^{y\max}\int_{x\min}^{x\max}dxdy\right)^2}}\right)$$

$$\gamma = \arccos\left(\frac{\displaystyle\int_{y\min}^{y\max}\int_{x\min}^{x\max}dxdy}{\sqrt{\left(\displaystyle\int_{y\min}^{y\max}\int_{x\min}^{x\max}(\frac{d}{dx}f_R(x,y))dxdy\right)^2+\left(\displaystyle\int_{y\min}^{y\max}\int_{x\min}^{x\max}(\frac{d}{dy}f_R(x,y))dxdy\right)^2+\left(\displaystyle\int_{y\min}^{y\max}\int_{x\min}^{x\max}dxdy\right)^2}}\right)$$

The resulting solution regarding the determination of the resultant force in each case determines the ratio between normal and tangential components of reaction . In the case to the nominally-fixed frictional joints crucial to ensure the integrity of contact is the value tangential force. Accordingly, depending on the applied load and degree of deformation of model elements will change the value of the tangential loading to the surface of contact .

3. Integrated characteristics of a contact zone

Given the proposed method of surface modification importantly determine the extent of influence of technological aspects on coatings, in particular, step and width of the modified zone. On fig. 5 presents the dependence of tangential stiffness of contact surfaces subjected to laser treatment and electric-sparks from the step of processing.

For correct modeling of behavior of contact under conditions of alternating tangential loading, mass characteristics of the contact zone is defined as the sum of the masses of individual elements of the model, which at load involved in contacting:

$$M = \sum_{i=1}^{N}V_i\cdot\rho = \rho\sum_{i=1}^{N}\iint_{D}F(x,y)dxdy,$$

where N - number of micro contacts;

ρ - density of the material surface;

$F(x, y)$ - function describing the surface mode of elliptic paraboloid;

D - domain of elements that is limited in height.
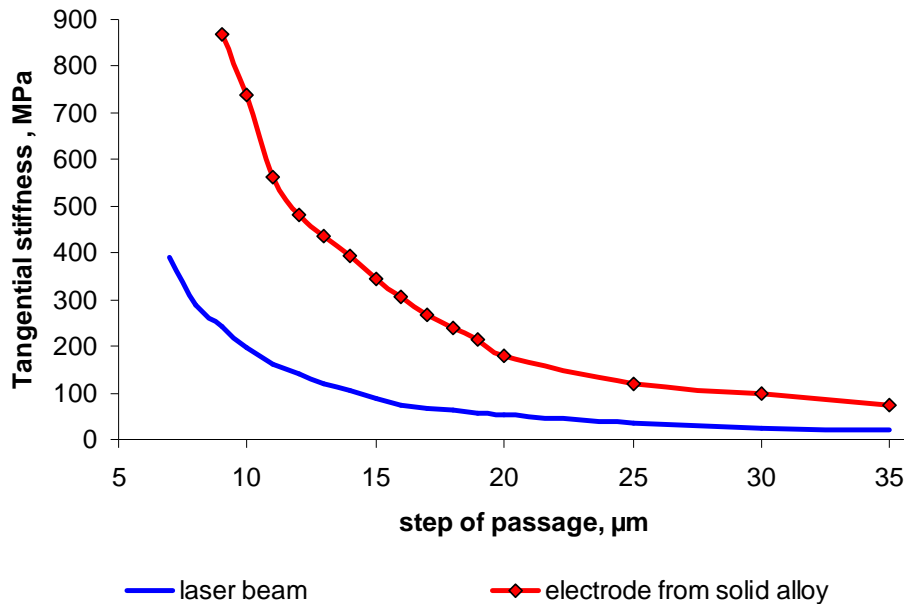

Fig.5. Dependence of tangential stiffness of contact surfaces from the step of passage of laser beam and electrode from solid alloy

Results of mathematical modelling of contact by results of the offered method of the analysis of the modified surface are resulted in table 1.

Table 1 - Integrated characteristics of a contact zone for a steel 30HGSA

Type of processing	specific value tangential stiffness, $\dfrac{H}{\textit{мкм}} \Big/ \textit{мм}^2$		specific value mass of modified layer, µg/µm²
	10 MPa	20 MPa	
electrode from solid alloy	230,52	251,489	0,19

4. Modeling of behavior of a contact zone

Given the complexity of terrain surfaces, which have been modified and given the fact that the elastic characteristics of the resulting of modification is largely different from the characteristics of the basic material, then contact of

surface into a dynamic loading need consider as a separate element of dynamic system (Fig.6).
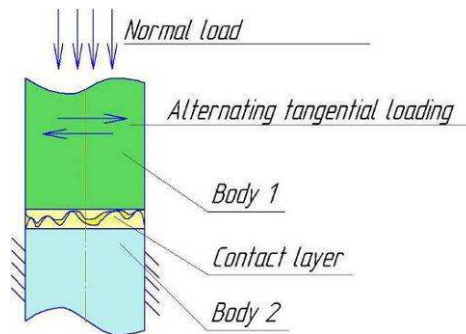

Fig.6. Representation of contact as three-component dynamical system

In this case, the mutual displacement of body 1 and body 2 $\Delta\Sigma$ can be represented as the sum of slip ΔK and deformation of the surface layer $\Delta\Pi$ (Fig.7).
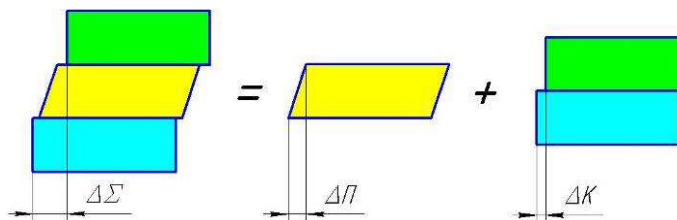

Fig 7. Scheme of distribution of the relative displacement of parts of contact

The elasto-deformated contact layer is a contact area, for which motion is different from the law motion of bodies indicated in Fig. 7. The reason is that subjects in the methods of surface treatment of parts significantly alter the mechanical properties of the surface layers compared to the basic material. Thus hardness for steel 30HGSA crude is $HV_{100} = 510$, while for laser treatment of the same material $HV100 = 700$, and at electric-sparks coating $HV_{100} = 1130$. An important feature of the present contact zone is that area is selected layer, composition and specificity of any changes in the process of exploitation. In the initial moments at vibration of contact consist from it up micro roughness of contacting bodies. With further development of fretting-wear, accumulation of wear products, area changes its structure by increasing the size of the metal layer that is drawn to the dynamic motion and replaces it with a layer of wear products that finally shows the destruction of the contact. This process is quite

complex, because despite the low amplitude of reciprocal displacement, some formed by wear products derived from the contact that alters the characteristics of the layer. In general, the mass of elastically deformed layer can be represented as:

$$M = M_0 - M_{\det},$$

where M_0 - initial mass of elastically-deformable surface layer that irregularities are formed by modification of surface;

$M_{\det}$ - mass of material surfaces, which was removed from the surface due to wear or brought out of contact.

Assessment of fracture process of contact , based on the concept of "third body" is given in [5-8]. In condition of nominal-fixed joints, regardless of the layer products of wear , a crucial factor for ensuring the integrity of joint is share from the total area of "third body" which is indestructible machined surface irregularities. Therefore, the integrity of the contact can be evaluated in terms of structure contact zone - for contact in a state of coupling the vast majority of the masses "third body" of the mass inequalities, while in a slip of his products are wear. To estimate the effective mass of a "third body" was used method of estimation of intensity of formation of elements of a "third body" in the form of wear products [8]:

$$M_{\det} = M_{stab} + \left(M_{start} - M_{stab}\right) \cdot e^{-(C_S - C_W)\cdot\left(\frac{N}{2\cdot\pi\cdot v}\right)},$$

where M_{stab} - weight of products of wear when equilibrDMEm processes of their formation and excretion from the contact;

C_S, C_W - factors that determine the intensity of the flow of destructive processes in the contact zone and depend on the geometrical characteristics of surface and speed of relative motion, respectively;

$M_{\max}$ - maximum amount of wear products in the absence of removing them from the contact;

M_{start} - mass of the surface layer to the flow of destructive processes;

v - frequency of oscillation.

In Fig. 8 show the relationship between the mass of elastically-deformable layer from the number of loading cycles.

Then, in view of the selected area can be represented by a zone of contact as the following scheme.

The dynamic state of the system described by the following equations system:

$$\begin{cases} \ddot{x}_1 \cdot m_1 = -c(x_1 - x_2) + F_{mp} \\ \ddot{x}_2 \cdot m_2 = c(x_1 - x_2) - c_K x_2 \end{cases},$$

where x_1, x_2 - coordinates of the bodies 3 and 2 respectively;

$\ddot{x}_1, \ddot{x}_2$ - acceleration of bodies 3 and 2 respectively;
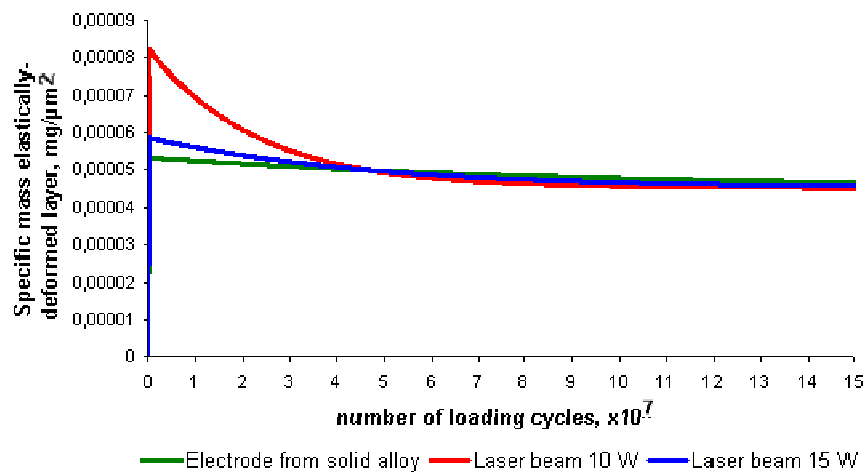
Fig. 8. Dependence of mass elastically-deformed layer on the number of loading cycles
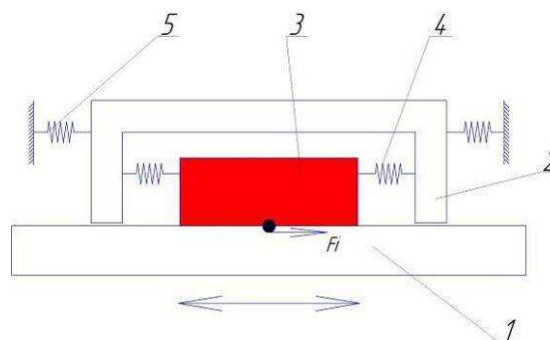
Fig.9. Schematic diagram of the contact model:
1 - body 1, 2 - body 2, 3 - stressed-deformed surface layer, subjected to treatment, 4 - stiffness of elastic-deformed surface layer, 5 - stiffness of construction

c - elastic characteristics of the contact zone;

c_K - elastic characteristics of the basic material;

F_{mp} - force of friction;

Modeling of work for NFJ with using the proposed method involves introducing into the model as initial values of integral characteristics of the mass and tangentional stiffness. Based on the dependence of mass elastically deformed layer on the number of loading cycles are changing the dynamic properties of the contact zone, and therefore the system's ability to resist of tangentional displacement. Simulation results for the investigated materials are shown in Fig. 10. Charts slip coefficient depends on the number of loading cycles for surfaces subjected to laser exposure by capacity of 10 and 15W.
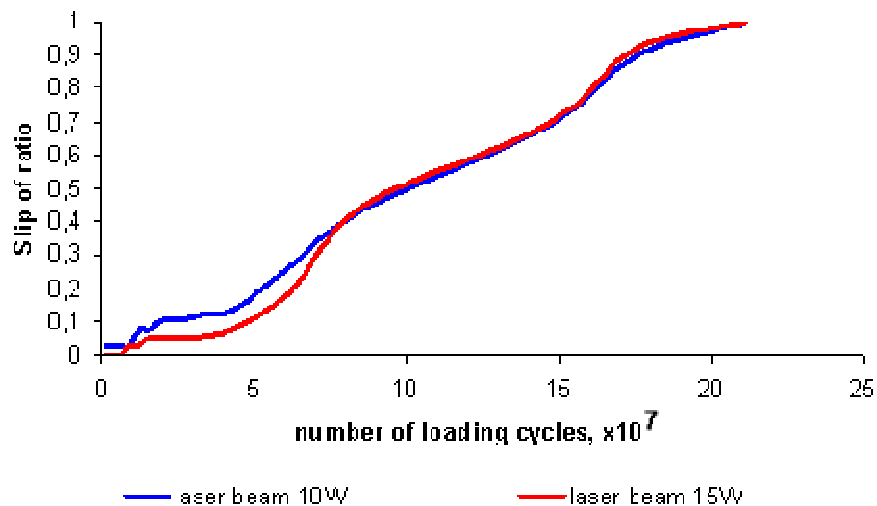

Fig. 10. Simulation of dependence of the coefficient of slip from number of loading cycles for surfaces subjected to laser processing by capacity of 10 and 15W

5. Comparison of results of numerical modeling with experimental data.

Adequacy by adopted mathematical model and experimental results is shown in Fig. 11-18. Contact behavior under oscillation load for steel 30HGSA after electrosparks alloying (material electrode - WC-8 and diameter - 1 mm, speed rotation of electrode - 600 min^{-1}, capacity of condensing units - 1 μF, pulse duration - 12μs, current intensity - 12.8 A rate of pass - 0.8 mm / s, circuit application - grid).
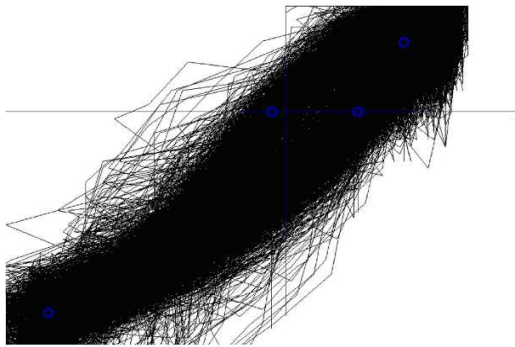
Fig. 11. Results of experimental studies (number of loading cycles $N = 1,5 \cdot 10^7$**, amplitude of excitation** $A = 71,4\ \mu m$**, normal load 45N)**
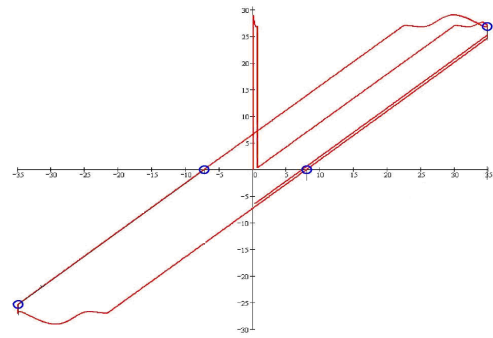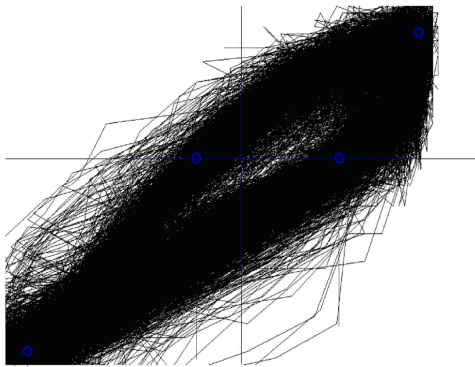

Fig. 12. Results of mathematical modeling (a moving mass layer $m = 8,3562\ \mu$ **mg, stiffness system** $c = 230\ N/\mu m$**, the amplitude of excitation** $A = 70\mu m$**, normal load 45N)**

Fig. 13. Results of experimental studies (number of loading cycles $N = 5 \cdot 10^7$**, amplitude of excitation** $A = 73,5\ \mu m$**, normal load 45N),**
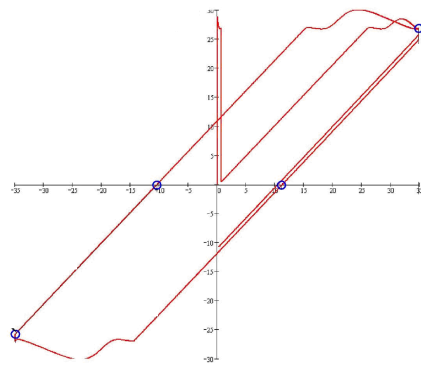

Fig. 14. Results of mathematical modeling (a moving mass layer $m = 1,3895\ \mu$ **mg, stiffness system** $c = 230\ N/\mu m$**, the amplitude of excitation** $A = 70\mu m$**, normal load 45N)**
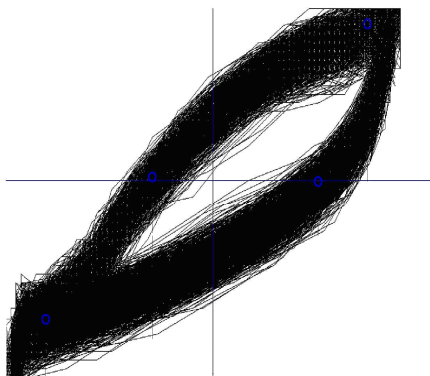

Fig. 15. Results of experimental studies (number of loading cycles $N = 10^8$**, amplitude of excitation** $A = 74,6\ \mu м$**, normal load 45N)**
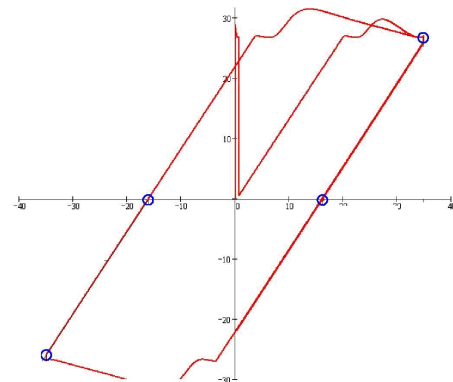

Fig. 16. Results of mathematical modeling (a moving mass layer $m = 0,425\ \mu$ **mg, stiffness system** $c = 230\ N/\mu m$**, the amplitude of excitation** $A = 75\mu m$**, normal load 45N)**
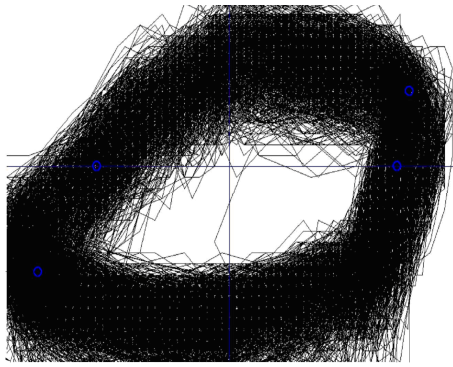
Fig. 17. Results of experimental studies (number of loading cycles $N = 1,5 \cdot 10^8$ **, amplitude of excitation** $A = 75,21\ \mu\text{м}$ **, normal load 45N),**
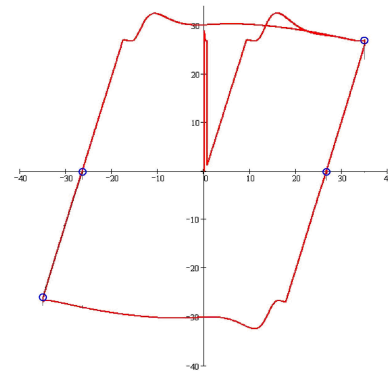
Fig. 16. Results of mathematical modeling (a moving mass layer $m = 0,273\ \mu$ **mg, stiffness system** $c = 230\ N/\mu m$ **, the amplitude of excitation** $A = 75\mu m$ **, normal load 45N)**

CONCLUSIONS

Fig. 19 shows the graph of slip ratio of the number of loading cycles for the experimental determination and mathematical modeling.

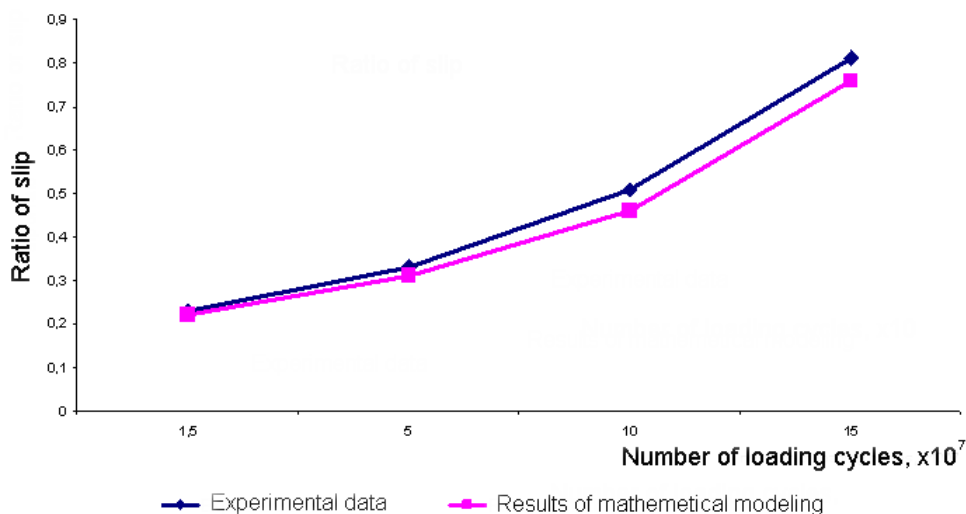**Fig. 19. The growth of slip for nominally-fixed contact at treatment by electrosparks alloying. Comparison for experimental and mathematical modeling**

Thus the proposed method to evaluate the influence of surface modification methods by creating a regular relief on the surfaces of nominally-fixed friction joints in long-term ability to maintain the integrity of contact under vibration loads.

References

1. Norbert Radek, Jurij Szalapko. Manufacture of heterogeneous surfaces by electro-spark deposition and laser beam//Вісник двигунобудування-2006.-№ 2 – с.208-210

2. Norbert Radek, DarDMEsz Zasada, Jurij Szalapko. Mikrostruktura a wlasciwosci powlok elektroiskrowych modyfikowanych wiazka laserowa//Obrobka erozyjna(Electromachining), Bydgoszcz-Wiktorowo – 2006. – s. 252-259

3. Пастух І. М., Курской В. С. Методика ідентифікації поверхонь фретинг-контакту // Вісник Хмельницького національного університету. – 2010, № 1. – С. 47-50.

4. Пастух І. М., Курской В. С. " Формування моделі поверхні контакту та її характеристик" // Вісник Хмельницького національного університету." – 2010, № 3. – С. 11-15

5. M. Godet, Third-bodies in tribology, Wear 136 (1990) 29–45.

6. Y. Berthier, Maurice Godet's third body, in: D. Dowson (Ed.), Proc. Of the 22nd Leeds-Lyon SymposDMEm on Tribology: The Third Body Concept, Tribology Series, vol. 31,Lyon, 5–8 September 1995,Elsevier,Amsterdam, 1996, pp. 21–30.

7. M. Godet, The third body approach: a mechanical view of wear, Wear 100 (1984) 437–452.

8. Юрій Шалапко, Віталій Гончар Поведінка „третього тіла" в умовах середньоамплітудного фретингу. //Машинознавство-2004.-№6(84).-С.39-42.

9. Wear modeling and the third body concept, N. Fillot, I. Iordanoff, Y. Berthier Wear 262 (2007) 949–957

4.1.4 THE CHEMICAL STRUCTURAL MECHANISMS FOR FRICTION OF JOINTS WHICH PROVIDE WEAR-RESISTANCE

Shevelya V.[1], Oleksandrenko V.[1], Kalda H.[1]

In the decision of problem of machines reliability and longevity increase the question of knots of friction wearproofness occupies an important place. The analysis of tribotechnical researches shows that one-sided attempts to find accordance between wearproofness, physical and mechanical material characteristics, properties of secondary structures which appear during friction

[1] Khmelnitsky National University, Ukraine

did not give satisfactory results. The most perspective from this point of view is the research of mechanical –physical- chemical nature of friction and wear taking into account its dynamic character [1].

A friction is conditioned by continuous mechanical co-operation of contacting bodies, which causes the development of the scalene physical phenomena of rheological nature in the conjugating superficial skims of material and its simultaneous chemical co-operating with the active components of environment. Thus physical and chemical processes are indivisible, take place simultaneously, bound by at least one source of flowing – mechanical energy brought during a friction, can have both mutually strengthening and competitive character and in turn form tribojoint resistance to wear in the terms of dynamic contact of surfaces. Id est the wearproofness is not property of material, but is determined by character and intensity of processes that take place in the friction contact zone.

A dissipative process is the basis of external friction nature. The dynamic contact of solids is accompanied by continuous withdrawal of mechanical energy to tribosystems, its dispersion and absorption. Mechanical energy transformation can take place after different mechanisms as a result of dissipative phenomena display. Comparatively small amount of energy is spent on the material wear. According to the first beginning of thermodynamics the friction work (without the account of the mechano-emissive phenomena) equals:

$$A_{frc} = Q + U, \tag{1}$$

where Q is a thermal effect; U is a change of tribosystem internal energy.

The friction work A_{frc} numeral equals mechanical energy W_{mech}, which is withdrawn to tribosystems. Heat generation is conditioned by flowing of tribochemical reactions and dynamic phenomena that have rheological nature (relaxation, hysteretic, microplastic internal friction). Thus, in general the total power balance of friction process can be expressed as the following:

$$W_{mech} = W_{chm} + W_{rh} + W_{stc}, \tag{2}$$

where W_{chm} is energy that is spent on tribochemical reactions; W_{rh} is energy that is dissipated due to the rheological phenomena; W_{stc} is resilient energy that is stocked (accumulated) by material of superficial layer.

The more the amount of dispersed energy is, and the less is the level of accumulated energy, which is gone to destruction, the higher is capacity and wearproofness of friction pair. In other words, the wearproofness of material is determined by flowing intensity in the friction zone of protective relaxation processes, which hinder to the accumulation of critical destruction energy.

Mechanical energy dissipation takes place mainly in accordance to rheological mechanisms, related to the display of materials unresiliency (the viscoelasticity) and in accordance to tribochemical mechanisms, which stipulate the formation of chemical co-operation products. Mechano-emissive phenomena: luminescence, electrons emission, photoemission, acoustic emission, – are characterized by relatively subzero intensity of flowing at a friction and low power imputs.

Most knots of friction work in chemical active environment (gas, liquid) and are manufactured from metals or their alloys which are thermodynamically unsteady. Taking into account, that the mechanical loading assists the increase of surface chemical potential, it stipulates the flowing of tribochemical reactions, which are inalienable component of friction process of solids, have mainly exothermic character and relate to the powerful relaxation processes. Thus chemical reactions can flow both between the activated solid and components of its surrounding environment, and between solids which are in a dynamic contact – reaction in hard phases (grasping). From the point of view of tribotechnical descriptions increase of knots of friction undoubtedly the first type of tribochemical co-operation has advantages. The result of tribochemical dissipative processes is the forming on the friction surface passivating tapes as a result of active zones reaction of metal with a gas or liquid environment. These tapes protect basic material foremost from an adhesion wear, and also from the tired destruction. Flowing of mechano-chemical and, in particular, tribochemical reactions is connected with substance structure deserializing (by appearance of vacancies, internodal atoms, distributions which are the centers of chemical transformations development) and structure mobility (moving of point and linear

defects, intergranular limits and cracks). Thus, in the basis of tribochemical co-operation is a change of material substructure, which takes place under the influence of mechanical process of conjugating surfaces deformation.

On the other hand, substructural transformations, which take place in a skim adherent to the zone of actual surfaces contact, stipulate the display of internal friction mechanisms which is one of the basic rheological characteristics of metals behavior in the conditions of the dynamic loading. An internal friction arises up in the elements of friction pair due to the imperfect resiliency of contacting materials at distribution in them of deformation waves, generated in the zone of discrete friction contact and characterizes the ability of solid to disperse the mechanical energy withdrawn to it during the cyclic (dynamic) loading, transferring it in a heat. For the last decades on the basis of internal friction research the microrheology of solids (metals, polymers) has got a considerable development which allows to go from the formalized phenomenological description of the rheological phenomena to description of concrete physical micromechanisms of such phenomena. Having regard to that fact that an internal friction has general physical nature with the relaxation phenomena in solids at the action of the dynamic loading, it became possible to talk about many types of tensions relaxation micromechanisms depending on the concrete speed-loading and temperature terms of tribojoint work and material properties.

Taking into account, that an internal friction (which represents the dynamic mechanisms of tensions relaxation) sharply reduces tension from impulses or shots that accompany an external friction, smoothes out dynamic tensions in the places of their concentration, the problem of wear minimization in a number of cases [2, 3] is taken to providing of high internal friction of contacting materials at the set speed-loading and temperature terms of contact co-operation. From here, in particular, turns out, that one secondary structure can not protect a metal from a wear, they can be effective only when they are formed on metal-lining with favourable properties.

Depending on metals nature and terms of external friction those or other mechanisms of mechanical energy dissipation will be realized, the most

effective from which are relaxation (amplitude-independent), hysteretic and microplastic (amplitude-independent) internal friction [4-6].

To the mechanisms of relaxation internal friction belongs: termoelastis, magnetoelastic and dislocation relaxation. These types of relaxation are conditioned by thermal, magnetic and atomic alteration at the action of relatively small deformation amplitudes, forming the so-called background of internal friction. On the background of internal friction at the certain temperature-frequency parameters of mechanical vibrations relaxation maximums of internal friction are laid on : the Snoek peak (diffusion of introduction atoms in the field of net tensions in metals with volume-centered cubic lattice), the Finkelstein-Rosin peak (diffusion of introduction atoms in volume-centered cubic lattice and close-packed hexagonal (space) lattice), the Zener peak (diffusion in the sosoloids of substitution), the Köster deformation peak (co-operating of distributions with the atoms of admixtures), grain boundary peak. The maximums of structural relaxation appear in the temperature ranges of phase transitions. The background of internal friction has the higher level, the more the general metastability of material state is. All relaxation processes which result in stabilizing of structure and lower the general level of the system free energy diminish the background of internal friction.

With the increase of deformation amplitude of hysteretic internal friction is realized. The reverse and irreversible phenomena of hysteretic are distinguished. At considerable deformation amplitudes a microplastic internal friction (with formation of new structural defects) appears, the level of which can reach a quite high values. To the sources of energy dissipation also the processes of formation and development of new surfaces devision (relaxation microfissures) belong.

Balance of internal dispersion of wave front energy due to rheological effects will be dynamic enough. Modern physical experimental methodologies give an opportunity to determine the parameters of material unresiliency and their change under the influence of temperature-power terms. In this case the prospect of estimation of energy dispersive properties of material is opened after the internal friction mechanisms and wearproofness prognostication.

Thus, essence of triboprocesses is in fact that they flow in the conditions of impulsive power co-operation of contacting surfaces and accompanied by the withdrawn mechanical energy dispersion. There are two basic ways of irreversible dissipation of mechanical energy during a friction: tribochemical and rheological, the display of which is conditioned by substructural changes that take place in material during the dynamic contact of surfaces, and thus they are simultaneously connected and competitive, predominating of which is determined by the row of factors: properties of environment, parameters of the external loading and material nature of friction pair. Correlation of the dissipated and accumulated energy by a superficial skim will determine kinetics of damages development and destruction.

For research of influence of mechano-chemical and rheological processes on wearproofness of the united pairs depending on the speed-loading and temperature modes of one-side friction of skidding and fretting taking into account influence of contact of environment surrounding a zone, the corresponding complex of options and methodical providing were worked out.

By authors first from united positions of dissipative nature of the phenomena initiated at the external loading mechano-chemical reactions and rheological processes of contact co-operation are considered in complex [1, 7, 8], quantitative data about their interconnection and influence on tribotechnical descriptions of the united surfaces are got and summarized. Theoretical positions of physical and chemical mechanics of materials – tribochemistry and triborheology of metals, are deepen.

It is confirmed, that the increase of material wearproofness (pic. 1) depending on the speed of skidding and temperature, which develop at this stage, is determined by the display of relaxation internal friction peaks (IF)[8, 9]. At small speeds of skidding a mionectic wear is predefined by the Snoek peak appearance, and a middle one – by the Köster peak. The diminishing of damping ability of material δ results in the wear increase of friction pair as a result of development of the destructive grasping phenomena. It is found out (pic. 1, a, b), that in the conditions of friction, when material is characterized by a low level of IF (in our case at V = a 1,15 m/sec and 4 m/sec) the increase of oxidizing activity of gas environment in the order: argon, air, oxygen assists the

increase of material resistance to the wear that testifies in this case about the positive role of intensification of tribochemical relaxation phenomena in the increase of contacting surfaces wearproofness. At the terms of temperature-speed contact, that assist the display of maximum IF by material (the Köster peak at V = a 2,42 m/sec), composition of environment insignificantly influences on its wear (fig.1, a), however in this case the wear ability of material grows with the increase of content in the environment of oxygen (fig.1, b).

The influence on the display of rheological of relaxation processes of the initial structural state of steel, determined by heat treatment, and structural transformations which take place in a superficial skim at the dynamic contact of surfaces, is shown. Forming at the certain temperature-speed terms of friction (200...300 °C) of minimum wear area, except the display of the Köster relaxation peak, predefined by the development of the dynamic deformation aging (DDA). Thermoplastic (substructural) strengthening of steel: increase of hardness, durability as a result of DDA at maintenance of diffusive mobility of admixtures atoms, that can be confronted at a speed of distributions motion, and
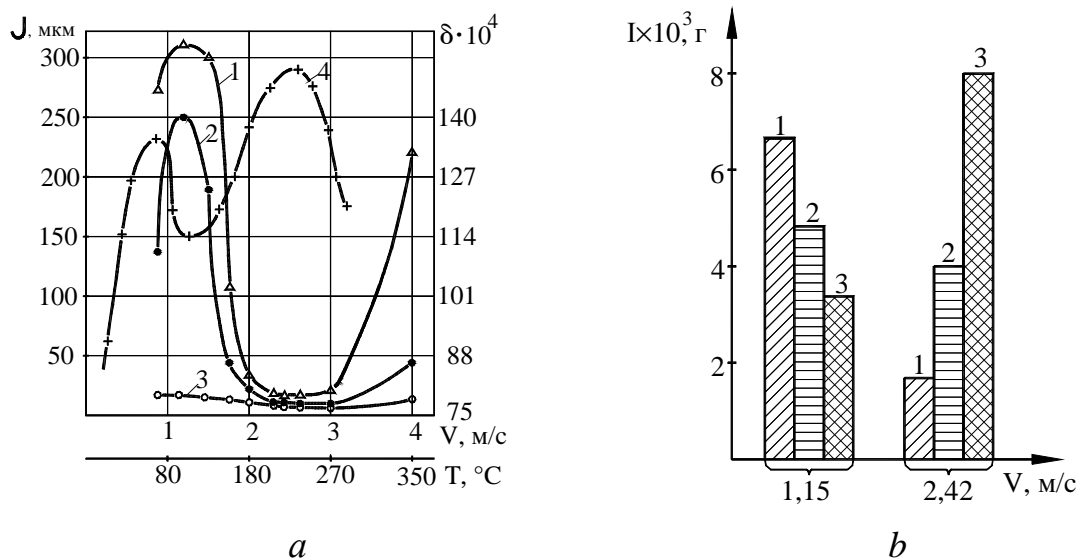

a   *b*

Fig. 1. Dependence of wear of disks Ст3 (a) and bullets ШХ15 (d) on speed skidding for the friction pair of bullet-space (P_{oc} = 60 H) in an environment: 1 – argon; 2 –air; 3 – oxygen; 4 – temperature dependence of internal friction, δ = f(T)

imposition of deformation maximum of internal friction (the Köster relaxations) at certain speed of friction assists effective dissipation of the withdrawn

mechanical energy due to the imperfect resiliency of contacting materials. In such state the metallic lining has the most favorable rheological characteristics for maintenance the oxidizing tapes on its surface. Increased metastability of tempering structures, which assists the display of IF mechanisms of structural-distributive nature, provides high wearproofness of hard-tempered steel at mionectic speeds of skidding. The increase of temperature-speed parameters of friction results in development at the hard-tempered steels the processes of the dynamic aging (to withdrawal under tension), which assist the stabilizing of structure, increase of resistance to microplastic deformations, decline of relaxation ability of material and sharp decrease of wearproofness.

The dependence (fig. 2) of fretting-proofness of the heat-treated carbon steel on a temperature and structure of withdrawal taking into account influence of peak-loading terms of friction is studied [10-12]. At the certain fretting modes (fig. 2, a) the unmonotonous change of local fretting-wear is set with the increase of temperature of hard-tempered steel withdrawal with a minimum of fretting-proofness for the structure of troostite ($t_{ann} = 400$ °C). It is discovered that the leading process of damage at the fretting corrosion of steel is an adhesion-tireless wear with imposition of locally-abrasive action of tribocorrosion products.
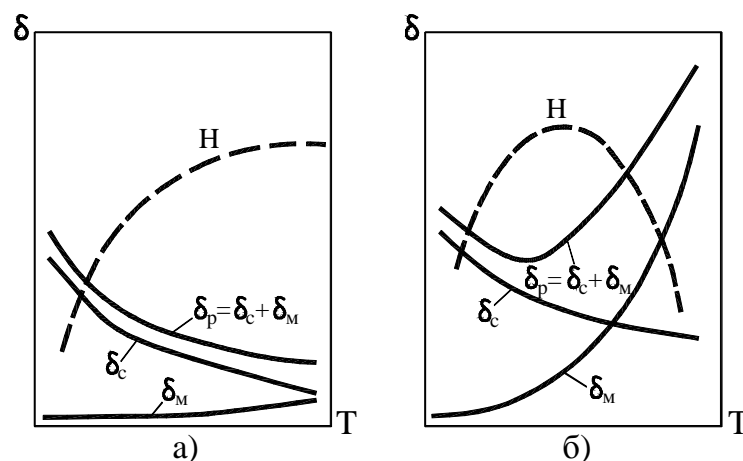

Fig. 2. Influence of temperature of steel withdrawal on structural-distributional δ_c **and magnetically-mechanical** δ_M **components of internal friction: a –** $\tau = 50$ **МПа; b –** $\tau = 140$ **МПа (***H* **– local fretting-wear)**

An universal parameter that characterizes relaxation properties of metal at the dynamic loading is an internal friction. It is shown that steel in hard-tempered and the low withdrawal states has increased fretting-proofness due to structural-distributional relaxation of tension (structural-distributional internal friction).Increased fretting-proofness of high-temper steel at the hard modes of fretting is conditioned by a magneto-mechanical internal friction (fig. 2). Influence of withdrawal temperature on the constituents of internal friction depends on the level of operating contact tension. The constituent of internal friction, related to the structural-distributional processes, plays a qualificatory role in hard-tempered and low withdrawal steels, when losses on magneto-mechanical hysteretic are very poorly expressed (fig. 2, a). After withdrawal at a high temperature 600 ºC the increase of internal friction is largely determined by magneto-chemical losses, and at the increased contact loading these losses become dominant (fig. 2, b). Therefore there is a change of character of dependence of total internal friction and, accordingly, size of fretting-wear from the temperature of withdrawal with the increase of contact tension.

The conducted research testify the connection with the internal friction not only wearproofness but also wear ability of steel, and depending on the structural state of the heat-treated steel and peak-loading mode of fretting the leading mechanism internal friction, which is accountable for relaxation of tension, changes.

Peak dependence of steel fretting-proofness in connection with the change of its relaxation ability is studied. It is set that extreme character of local wear change from amplitude of skidding is conditioned by development of processes that results in stabilizing of structure to the decline of distributions movable as a result of their blocking by atoms-admixtures. Obviously, that the most favorable terms for this purpose arise up at the certain temperature-speed terms of contact vibroskidding. The mechanism of dislocation change of relaxation prevails at small amplitudes and mionectic temperatures, and at the increased values of amplitude and temperature - diffusive. As summarizing (Fig. 3) rheological approach in forming of fretting-proofness extremums is offered.
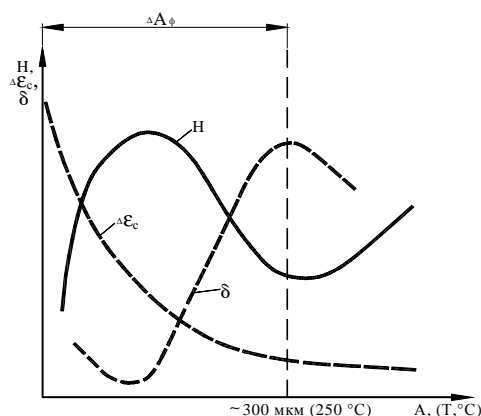
Fig. 3. Peak-temperature dependences of loss of relaxation ability as a result of DDA Δε$_c$,, relaxation internal friction δ and local wear H

Tribochemical processes are also the effective channel of dissipation of the mechanical energy withdrawal to the solid. As a rule, such processes are exothermic, and a thermal effect during a friction is proportional to the dispersed energy for time unit. In addition, co-operation of environment components and metal activated by a friction results in formation on the surfaces of compounds, which influence on knot of friction wearproofness.

It is shown [7, 13], that an external friction initiates in different environments: air, water solutions of electrolytes, hydrocarbon liquids of the same type chemical co-operations of material of the united pairs with active components, among which the most widespread are oxygen and water in the different states, that results in their expense and selection to hydrogen, methane, oxide and dioxide of carbon. Analogical processes are also observed at the cyclic bend of standards, id est is characteristic for mechanical influence on a metal. Power charges on realization of mechano-chemical processes assist dissipation of the energy withdrawal at a friction. Schematically chemical mechanism of mechanical co-operation can be presented as:

$$O_2$$
$$\downarrow$$
$$H_2O \rightarrow MeC \rightarrow CO_2 + CO + H_2 + CH_4$$
$$\downarrow$$
$$MeO(MeOH)$$
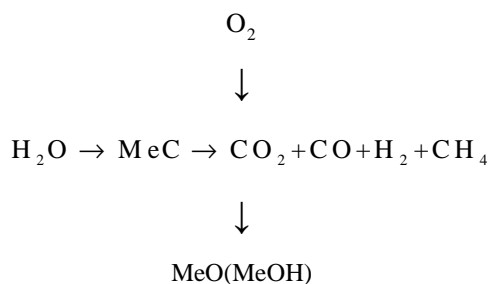
Oxygen both free (O2) and cut-in in liquids (for example, $O_2^{H_2O}$), and that which is in the constrained state in the molecules of water (H_2O), spent on oxidizing processes, the product of that is both gaseous substances CO and CO_2 and hard tapes of compounds are oxides (hydroxides) of metals, the intensity whose formation during contact co-operation influences on the wear of the united surfaces. Displacements in an expense and formation of certain components depend on terms that arise up at a friction.

One of the most powerful factors, that influence both on rheological behavior of solids and flowing of the chemical phenomena, is a temperature. The comparing [14] of temperature dependence of fretting-proofness of the row of construction metallic materials to temperature dependences of rheological parameters which characterize relaxation properties (relaxation ability, relaxation internal friction, creep) is conducted. Close cross-correlated connection is shown between tribotechnical and rheological descriptions. The account of change character of relaxation ability and concrete mechanisms of tension relaxation allows from united (rheological) positions to interpret the different types of fretting-proofness dependences on a temperature and amplitude of metallic materials fretting which was observed practically.

The influence [15] of heating of environment on wearproofness of conjugating pair at the one-directed friction-skidding midair, distilled water and hydrocarbon liquids: reactive fuel, hydraulic liquid, aerooil is studied. It is set (pic. 4) that in the environment of air with the increase of temperature the intensity of tribochemical reaction of decomposition of water molecules on the material activated by a friction, which is determined by the amount of hydrogen that was distinguished, grows very poorly, and oxide which is related to absorption of free oxygen not only does not increase, but decrease in twice. It specifies on uselessness in the conditions of dynamic contact of materials the Arrhenius equation, which is used when energy of activating which is needed for realization of reaction is taken away exceptionally due to tricking into of
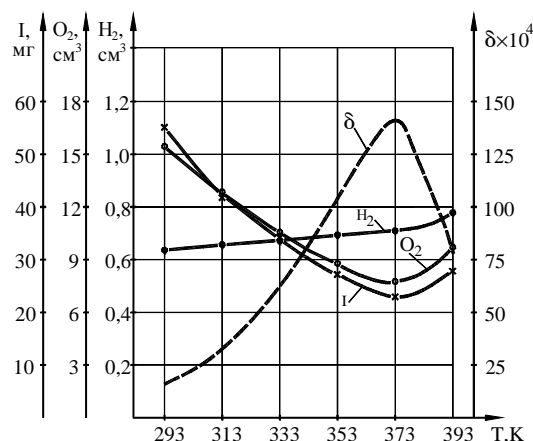
Fig. 4. Temperature dependences of amount of the hydrogen (H$_2$) distinguished during a friction, withdrawal oxygen (O$_2$), wear (I) and internal friction (δ) of steel ШХ15 ($f \approx 1$ Hertz) in air environment $V = 0,85$ м/sec; $P_{oc} = 60$ Н); a friction pair "bullet-space"

warmth from an environment. During a friction except thermal, tricking into of mechanical energy takes place the concentration of which in the superficial layer of contacting materials assists initiation and acceleration of chemical processes. But dispersion of the deformation energy accumulated by material is related also to the display of rheological (relaxation) processes. In this case time of relaxation of the tensions, caused by external periodic forces arising up in the zones of actual contact as a result of its discreteness, is related to resiliently-viscid properties of solid, with the display of peaks of internal friction at certain temperature-frequency terms [4-6].

Thus, flowing of tribochemical co-operations is conditioned by the display of thermal and mechanical factors. Intensity of tribochemical reaction will not depend on a temperature in case that the origin of the states accountable for realization of reaction does not depend or very poorly depends on a temperature. If with the increase of temperature relaxation of active centers appearance of which is caused by the accumulation in microvolumes of material of critical energy deformations is more accelerated, so that they become less accessible for a start and activating of chemical reactions, then intensity of tribochemical processes will decrease. And in case of weak display of mechanisms of internal friction and advantage of thermal influence on chemical behavior of material and environment components, with the increase of

temperature there will be an acceleration of tribochemical co-operations. In accordance with the indicated processes will change and size of wear of contacting pair which depends on the display of rheological and tribochemical dissipative processes.

Display in a district 373 K of internal friction relaxation peak (the Snoek peak) stipulates the decline of tensions concentration and considerable deceleration of tribooxide processes with participating of free oxygen in air environment. As a result the intensity of tapes appearance decrease, and thus wear of compounds tapes, which shows up in wear minimization of friction pair. At the further increase of temperature as a result of slump of the Snoek maximum the level of internal friction decrease, the concentration of loading in the microvolumes of surface increases and as a result, the accelerating action of temperature factor rises on tribochemical co-operating of environment components with material of friction pair, and a wear increases as a result of activating of appearance and wear of co-operation hard products.

The protective and destructive dynamic processes of relaxation, which characterize power balance at dissipation of energy, are investigated. It is set that the loss of relaxation ability is related to speed growth of irreversible rheological processes that results in stabilizing of structure and sharp increase of relaxation firmness of friction surfaces. For prevention of grasping and providing of stable wearproofness the necessary reverseness of relaxation processes is at minimum localization of contact loading. Therefore from the rheological point of view the contact phenomena at a friction can be interpreted as processes of self-organizing which is accompanied by loading relaxation.

The technology [16] of obtainingt of the combined coatings, that will realize principle of structural damping and will be based on general application of the electro-spark alloying of surface tightly-fusible metals (Ti, Zr) with the next nitriding of mouldable layers in plasma of glow-discharge is worked out. The marked coatings promote machine components wearproofness to 5 times.

Thus, in one cases the processes of relaxation assist the increase of wearproofness. To such protective processes, for example, the structural, distributional change, diffusive relaxations belong. At exhausting of the marked relaxation mechanisms of contact tensions in local volumes a metal acquires

critical relaxation firmness, the destructive processes of relaxation are included as a result formation of fragile fatigue cracks and tribochemical reactions in hard phases – grasping. On the basis of the marked approach classification of protective and destructive mechanisms of tension relaxation is presented. General structural requirements to steels, which provide their wearproofness, are set forth in the terms of internal friction.

References

1. Шевеля В.В., Олександренко В.П. Трибохимия и реология износостойкости. – Хмельницкий: ХНУ, 2006. – 278 с.

2. Шевеля В.В., Назаренко П.В., Гладченко А.Н., Шевеля И.В. Внутреннее трение как фактор износостойкости трибосистемы // Трение и износ. – 1990. – Т. 11, № 6. – С. 979–986.

3. Шевеля В.В. Реология износостойкости и совместимости пар трения // Трение и износ. – 1993. – Т. 14, № 1. – С. 48–62.

4. Постников В.С. Внутреннее трение. – М.: Металлургия, 1969. – 332 с.

5. Головин С.А., Пушкар А., Левин Д.М. Упругие и демпфирующие свойства конструкционных металлических материалов. – М.: Металлургия, 1987. – 200 с.

6. Гордиенко Л.К. Субструктурное упрочнение металлов и сплавов. – М.: Наука, 1973. – 224 с.

7. Шевеля В., Олександренко В., Калда Г. Процеси механічної і хімічної релаксації при динамічному навантаженні металів // Машинознавство. – 2003. – № 2 (68). – С. 21–26.

8. Шевеля В.В., Олександренко В.П., Калда Г.С. О роли релаксационных явлений и субструктурных превращений при трении металлов // Проблеми трибології. – 2003. – № 2. – С. 3–11.

9. Шевеля В.В., Джимала А., Калда Г.С., Олександренко В.П., Шевеля И.В. Трибохимия и реология износостойкости металлических и металлополимерных систем // Трибофатика: Пр. 4-го міжнар. симпозіуму з трибофатики (ISTF 4), 23–27 вересня 2002 р. – Тернопіль: Тернопільський державний технічний університет ім. І. Пулюя, 2002. – Т. 2. – С. 537–541.

10. Шевеля В.В., Калда Г.С. Амплітудна залежність фретингостійкості // Машинознавство. – 1998. – № 6. – С. 2–5.

11. Шевеля В.В., Калда Г.С. Вплив структурного стану і мікропластичності сталі на її фретингостійкість // Машинознавство. – Львів. – 1998. – № 11–12. – С. 24–29.

12. Шевеля В.В., Калда Г.С., Олександренко В.П., Шевеля И.В. Амплитудная зависимость фреттинг-износа в связи со структурным состоянием стали //

Вимірювальна та обчислювальна техніка в технологічних процесах. – 2001. – № 1. – С. 29–33.

13.   Олександренко В.П., Белянский В.П. Исследование закономерностей трибохимических реакций // Проблеми трибології. – 1996. – № 1. – С. 101–110.

14.   Шевеля В.В., Калда Г.С., Соколан Е.С. Температурная зависимость фреттингостойкости // Проблеми трибології. – 1998. – № 2. – С. 77–81.

15.   Олександренко В.П. Влияние температуры на физико-химические процессы контактного взаимодействия и износостойкость трибосопряжений // Вестник двигателестроения. – 2005. – № 3. – С. 164–169.

16.   Олександренко В.П. Износостойкость комбинированных покрытий // Вісник Хмельницького національного університету. – 2006. – № 1. – С. 10–14.

4.1.5 PROCESSES OF WEAR OF TRIBOJOINTS FROM HEAT-RESISTANT ALLOY ON COBALT-BASED AT NON-STATIONARY THERMO-MECHANICAL CONTACT

Ivschenko L.[1], Tsyganov V.[1], Shalapko Y.[2]

Greater part of tribojoints, in particular, aviation turbo-engine, works in the conditions of difficult dynamic loading. Thus there is the combined influence of high temperatures, properties of gas environment and mutual moving of details with the presence of vibrations, operating in different directions, including presence of the shock loading. Without the account of all of complex of factors of loading there is distortion of research results and creation of picture of process of wear little answering real.

Presently one of the most perspective materials for details which are exploited in extreme terms, there is an alloy of XTH-61. This alloy has a hypereutectic structure with primary grains of carbide (Ti, Nb) C and eutectic of Co+(Ti, Nb)C, two phases is characterized, one phase is a matrix, second – carbides. The high wear-resistances of this alloy is arrived at the even distributing of high durability matrix phase of nonsolid on the basis of cobalt, that allows, in particular, effectively to utilize him for solders on the bracer shelves of shoulder-blades of turbo-engine. Difficult chemical composition of

[1] Zaporizhia National Technical University, Ukraine
[2] Khmelnytskiy National University

alloy of XTH-61 is supposed by the comprehensive study of his wear-resistances in the conditions of most close by operating.

In general case physical and chemical co-operation of solids at a contact is characterized flowing of flowage of surfaces. The terms of loading determine the state of superficial layer and wear-resistances of contacting details in a greater degree, and high temperatures, being a factor, arousal diffuse processes in the area of friction, reduce the indexes of mechanical durability.

In addition, a temperature also influences on the degree of flowing of superficial reactions and, especially, on co-operation between crystals. For certain temperatures there can be homogenization of fragile excretions of the second phase, enlargement or dissolution of consolidating γ'-phase and layers carbide of metal to do fragile [1]. From other side, the increase of temperature is instrumental in intensification of oxidizing processes that tells on intensity of wear.

It is known that the wear of heatproof alloys [2, 3, 4] can take a place on a few different mechanisms. Different character of wear depending on a temperature takes a place both for heatproof alloys on the basis of Ni and Co and for soft steels on the basis of Fe. The change of one or another factor of loading and appearance of new factor causes the change of mechanism of wear, his physical picture.

In particular, an additional loading the single or periodic shock loading can result in contact motion, both in normal and in tangential directions. It, in same queue, can result in the decline of force of friction which was marked in a number of works [5, 6]. At a blow imposition of deformation of material can be carried out, both in a contact area and in a volume.

For researches of wear-resistances of similar of tribojoints the special devices and methods of tests which allow realizing the terms of different types of difficult loading at friction with the high temperatures of environment were developed [7]. Possibility to get and study functional dependences of friction-wear descriptions of materials of pair, carry out the comparative estimation of friction pair, make the physical design of processes in real of tribojoints appears thus.

As results of the conducted researches an area and distributing of wear on a contact surface at a friction depends on the partition of normal dynamic load. Difficult character of loading results in the tense state of superficial layers of material, that is accompanied an higher wear. The change of character of loading at a friction causes the change of the state of superficial layer and, as a result, changes wear-resistances of of tribojoints [8].

With the purpose of exposure of features of wear-resistances of alloy of XTH-61in the conditions of high temperatures and difficult loading tested on a stand [7] at temperatures 20, 500, 900 and 1000 ^{o}C in an air environment. Contact co-operation of two flat standards was designed in the mode of hitting with the subsequent slipping. The normal specific shock loading made from 0 to 0,6 N/mm^2, the mutual moving of standards took a place with amplitude 0,17 mm and by frequency 66 Hz, time of tests – 2 hours.

The graphs of intensity of wear depending on the temperature of tests are resulted on Fig.1.

Decline of wear at temperatures to 600…700^{0}C is explained formation of the shell like the hard greasing firmly coupled with a metal [3,4]. There is a friction an oxide on an oxide and increase of temperature is instrumental in more rapid formation of shell. The further increase of temperature is accompanied the increase of intensity of wear because of loss of bearing strength of superficial layer.

The got character of dependences, presumably, can testify to changing of mechanism of deformation in the superficial layers of materials which contact. At enhanceable temperatures (higher 0,4 – 0,5 temperature of melting) plasticity of the work-hardened nickeliferous alloys diminishes quickly, that in same queue is related to the transition of character of destruction as a result of increase of degree of the slipping on the scopes of grains [1]. The appendix of the dynamic loading at contact co-operation strengthens this process.

Oxidizing processes are also instrumental in appearance of transitional area. Thus more thick layer appears in the cavities of barrier of surface, because on tops an oxide layer under the action of the normal loading is constantly crushed and speeds away partly, promoting the same to the increase of actual

area of contact and decline of the specific loading in a contact, and, consequently, to the decline of intensity of wear.
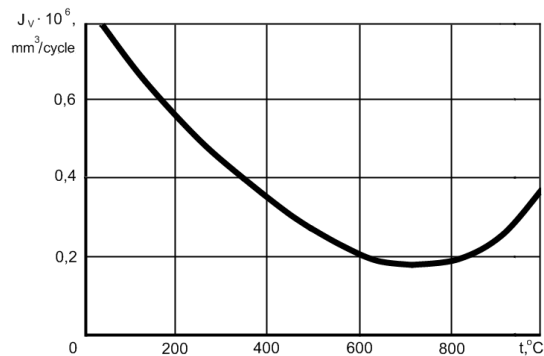

Fig. 1. Dependence of change intensity of wear of alloy of XHN-61on the temperature of tests

With the increase of temperature transition time diminishes from plastic to resilient deformation, to forming of final roughness and the period of the set wear comes quick.

And if at normal temperatures an anchorman is a tireless type of wear, there is his deceleration at enhanceable temperatures, because present on-the-spot micro crack are taken off in the process of wear, not enabling to develop them. At the same time formation of protective layer does not eliminate the processes of deformations metal, and only slows them. It is thus necessary for providing of high wear-resistances, that the relation of speeds of education and abrasion of protective layer aspired to unit. If this relation will be more units, at the increase of thickness layer durability of his tripping with a parent metal goes down, probability of his destruction and passing rises to the catastrophic wear.

General amount of cycles of contact, necessary for forming of protective layer will make:

$$P = \frac{1}{k}(P_{ox} + P_{def} + P_{disp}),$$

where P_{ox} – an amount of cycles, necessary for oxidization of surface;

P_{disp} – an amount of cycles, necessary for grinding down of products of wear;

P_{def} – an amount of cycles, necessary for the compression of appearing products of wear;

k – coefficient, taking into account simultaneity of flowing of processes of oxidization of surface, grinding down and compression of products of wear.

The size of P_{ox}, proper time of formation of shell, comports with equalization of Arrhenius for speed of oxidization, to describing flowing of reactions in a homogeneous environment:

$$A = A_o \exp(-Q/RT),$$

where A_o – Arrhenius constant;

Q – energy of activating;

R – universal gas constant;

T – temperature of oxidization.

The sizes of P_{disp} and P_{def} are proportional work of destruction of single volume of wearing out material. However, as a process of formation of protective layer goes continuously, the size of P must be less than.

Microhardness of superficial protective layer at the temperature of tests of 500…700 ^{o}C in 2,3...3,1 time higher as compared to material of basis. It is experimentally [9] set that the relation of hardness of appearing tape on-the-spot friction to hardness of basic material characterizes wear-resistances of materials at high temperatures. However at high hardness of superficial protective layer probability of embitterment and destruction last increased considerably, promoting the same to passing to other type of wear, for example, to the abrasive.

Thus, intensity of wear can be defined use dependence:

$$J_V = \frac{B_o A^{B_1} P_{sp}^2 \delta_o L V_o H}{2\rho n \sigma_d V_w H^{/}} KC,$$

where A – amplitude of the mutual motion of contact surfaces;

P_{sp} – specific pressure in a contact;

δ_o – a thickness of shell;

L – way of friction;

n – number of cycles of loading;

σ_d – durability of tripping of tape with a parent metal;

V_o – velocity of formation of shell;

V_w – velocity of wear of shell;

H – microhardness of surface;

$H^/$ – microhardness of base metal;

B_o, B_1, ρ – constants, temperature-dependent working environment;

K, C – constant, depending on velocity of slip of surfaces.

To check up the got positions were conducted research on determination of change of work of output of electron from the surface of standards. The state of the real surface of metals is related to forming on-the-spot of electric dipole moments and local electric charges which determine the size of electrostatic barrier in-process electron output. Because of the not homogeneous state of metallic surface there is the proper relief of electrostatic barrier, conditioned divergence of work of output of electron for the different areas of surface. Thus, for this surface of metal power relief, conditioned distributing of work of output of electron on a surface is characteristic. Comparing initial power relief (before tests on wear-resistances) to relief after tests it is possible to define areas surfaces which suffered the different degree of flowage.

As a method of measuring of work of output of electron the method of dynamic condenser of Kelvin, in which measuring is made on the contact difference of potentials, arising up between a measurable surface and surface of standard, was in-process utilized. Thus measurable and standard standards form a flat condenser and does not contact between it. Measuring of contact difference of potentials was in-process executed at atmospheric pressure. Frequency of vibrations of electrode-standard from gold made 500 Hz, a diameter 1,4 mm. Distributing of work of output of electron was determined a scan-out with a step 0,2 mm on one line in a center the working surface of standards within 5 μeV. Standards were maintained to establishment thermodynamics of the equilibrium state of surface. To measure distributing of work of output of electron of standard after tests at the temperature of 1000 ^{0}C not succeeded from bad indemnification of signal. The results of measuring of work of output of electron from the surface of the probed standards are presented on a Fig. 2.
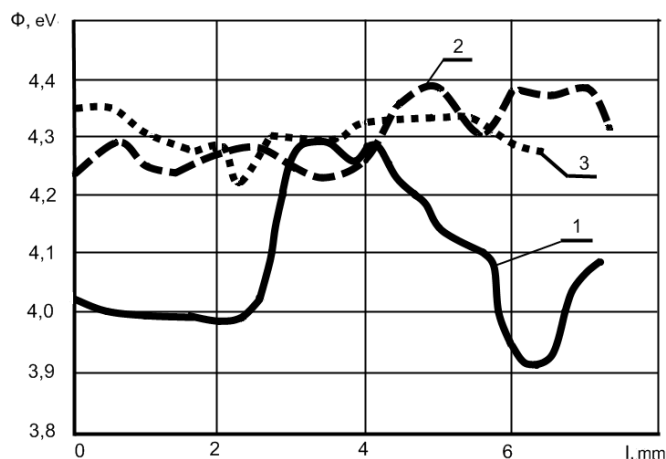
Fig. 2. Distributing of work of output of electron along the surface of standards from the alloy of XHN-61after a wear at a different temperature
$$1 - T = 20 \ ^{0}C^{;} \ \ 2 - T = 500 \ ^{0}C^{;} \ \ 3 - T = 900 \ ^{0}C^{;}$$

As follows from the presented results a high temperature at the friction of alloy of XHN-61 result in the receipt of surface with the large area and diminishing of variation of work of output of electron that confirms the change of the state of superficial layer.

Analogical information is got as a result of contact deformation of alloy of XHN-61 at friction with the different regime of loading: two-dimensional (blow with slipping in plane perpendicular direction of blow) and three-dimensional (blow with slipping in two mutually perpendicular directions) at the temperature of 20 ^{0}C [10]. Structural alteration of superficial layer is accompanied the change of power relief a surface. The increase of wear of standards is characterized diminishing of size of work of output of electron. A large value here has an increase of number of distributions and dislocation steps with growth of flowage. As is generally known, dislocation steps carry an electric charge, i.e. form electric dipoles [11].

The less value of size of work of output of lone electron at normal temperatures is caused growth of amount of the charged microscopic dislocation steps which are formed on-the-spot in the process of friction under influence of external removable tensions and diminish wear-resistances of the probed surfaces. Diminishing of variation in the values of work of output of electron at high temperatures specifies on an increase here of homogeneity of surface layer.

352

It is possible to assume that the non-linearity of dependence of by volume intensity of wear at different temperatures and increase of wear marked before at temperatures more 700 ^{o}C, related to the amount of distributions in a superficial layer. Their interaction increases at the high-slay of distributions, there is their fixing which hampers wedging out of metal of new distributions and concomitant defects in same queue. The amount of active centers on-the-spot stops to grow, attaining a satiation, that is accompanied the decline of wear at the increase of temperature to the maximum value and stabilizing of work of output of electron.

Thus, for the estimation of wear-resistances of tribojoints from the alloy of XHN-61at a difficult loading and high temperatures using of complex approach of determination of intercommunication of tribotechnical and structural properties of contacting materials is needed for the different types of loading. Thus the plastic-grinding down pattern of behavior of metal at a friction owes examined as physical and chemical, I.e. process which is accompanied the complex of structural, physical and physical and chemical changes of superficial layer of the deformed metal.

Difficult non-stationary character of loading results in the specific tense state of superficial layers of materials of tribojoints that affects his wear-resistances. Warming the areas of contact, the change of character of loading results in transformation of the state of superficial layer, power relief of surface and, as a result, to the change wear-resistances of tribojoints. Increase of wear-resistances of alloy of XHN-61 possibly at creation of optimum terms of loading by structurally-technological modification of tribogroup taking into account a temperature and composition of environment.

References

1. Симс, И. Жаропрочные сплавы/ И.Симс, В.Хагель. – М.: Металлургия, 1976. – 568 с.

2. Wang, Dao-Juan. Effect of microstructure and properties on the nigh temperature wear characteristics of 3Cr2W8V (H21) steel /Dao-Juan Wang, De-Lin Sku, Xin-Cheng Gua. – Wear. – 1987. – P. 101-117.

3. Stott, F.N. The influence of oxides on the friction and wear of alloys /F.N.Stott, G.C. Wood. – Tribology Inst. – 1978. – № 4. – P. 211-218.

4. Iwabuchi, A. Fretting wear of Inconel 625 at high temperature and high L vacuum /A. Iwabuchi. – Wear. – 1985. – № 1-3. – P. 163-175.

5. Aleksyeev, YU. N. K voprosu o vliyanii mgnovennogo izmeneniya normalnogo davleniya na velichinu sily kontaktnogo treniya / YU. N.Aleksyeev, G. V. Gonskiĭ D. L. Luchika // Samoletostroenie i tehnika vozdushnogo flota.- 1972 .- Vyp. 29.- S. 99—104.

6. Gaylord, E. W. Coefficient of static friction under static and dynamic applied loads / E. W. Gaylord., H. Shu // Wear.-1961, 4, N5.- P. 401— 412.

7. Ivshchenko, L.I. Uskorennye ispytaniya slozhnonagruzhennyh detalyej tribosopryazhenii L.I.Ivshchenko, V.V.Tsyganov, V.I.Chernyi //Vísnik dvigunobuduvannya. – 2009.- №1.- S.150-154.

8. Ivshchenko L.I. Osobennosti iznashivaniya tribosopryazhenii v usloviyah trehmernogo nagruzheniya /L.I. Ivshchenko, V.V.Tsyganov, I.M.Zakiev // Trenie i iznos. – 2011. – Tom 32, № 1. S. 500-509.

9. Chatynyan, L.A. Novye materialy i pokrytiya dlya raboty s treniem v vakuume pri vysokih temperaturah L.A. Chatynyan // Trenie i iznashivanie pri vysokih temperaturah. – M.: Nauka, 1973. – S. 44-48.

10. Ivshchenko, L.I. Stan poverhnevogo sharu detalyej triboz'jednan za ríznih shem kontaktuvannya / L.I. Ivshchenko, V.V Tsiganov, S.V. Loskutov, S.V. Sejdametov: sb. nauch. tr. //Problemi tertya ta znoshuvannya.- Kyiv: NAU, 2008.- Vip.49, tom 1.- S.72-83.

11. Alehin, V.P. Fizika prochnosti i plastichnosti poverhnostnyh sloev materialov / V.P. Alehin. – M.: Nauka, 1983. – 280 s.

4.1.6 ON INFLUENCE OF RAILWAY WHEELS MANUFACTURE TECHNOLOGY ON WHEEL/RAIL WEAR
Bogacz R.[1]

1. Introduction

Pressure poured cast wheels are used by all major North American railroads, in all climates from +40C to -40C, with axles loads of 32.5 metric

---

[1] Department of Civil Engineering, Kraków University of Technology, Poland

tons, and such wheels are known for their durability, dimensional consistency, superior rotundity, ability to resist severe thermal loads from tread braking, and excellent service performance. Much research work has taken place in Europe and North America and numerous scientific and technical papers have been written about wheel/rail systems. The majority of work done in Europe has been devoted to the hardness of wheels as an important factor of track damage. There are very popular, albeit inaccurate statements, stating that increased wheel hardness is responsible for increasing the magnitude of track damage.

2. Test stand EMS 60 and wheel/rail wear testing

Wear testing (unlubricated) was conducted on the EMS 60 test stand at IK in Warsaw. New 920 mm diameter wheels and new 60E1 rails were used for each wear test, and each wheel type was tested three times. Pressure poured cast wheels of ER7, AAR Class B, and AAR Class C steels and forged/rolled wheels manufactured by a leading European manufacturer, and also tyred wheels used in Poland, were gathered for testing. Two types of European rails were tested – Thyssen/Krupp UIC 60 E1 rails provided by Krakow University of Technology and Huta Katowice UIC 60 E1 rails provided by PKP PLK. All wheels and rails were hardness tested prior to wear testing and were found to be within specification. Hardness readings for the Thyssen Krupp rail were 280-283 BHN and the hardness readings for the rail provided by PKP PLK was 290-293 BHN. Wheel and rail profiles were taken at the start of testing, and after 25,000 cycles, 50,000 cycles, and 100,000 cycles of rig operation. Wheel profiles were taken with a wheel profile measurement gauge at four points around each wheel, every 90 degrees around the clock. We note that all wheels started the test with the same flange/tread profile, as machined in Poland. Rail profiles were taken with a rail profile measurement gauge at the center of the rails, and at points 200 mm to the left and right of center. Loading on the test stand was 55kN. In order to obtain simulated service flanging of the wheel against the rail, a 1.5 degree wheel angle of attack was applied vs. the longitudinal axis of the rail. This allowed for continuous flanging of the wheel against the rail. The test rig pulled the wheel along the rail under load, then allowed the wheel to roll back into position before another load cycle began. Figure 1 shows the EMS 60 test stand, while the picture on the right side shows the wheel/rail orientation. Results for

the wheel/rail wear testing were very favorable for the pressure poured cast wheels. For wheel wear and rail wear, the pressure poured cast wheel caused significantly less wear than the forged/rolled UIC monobloc wheel and the tyred wheel. Table 1 shows the average wear, for rails and wheels, as measured by IK staff, after 100,000 cycles of operation on the EMS 60 test stand. Rail wear, the primary focus of the study, was obtained from rail profiles. Wheel wear was determined on the basis of wheel weight loss from a formula/method used by the Railway Institute. From these results it is clear that the Class C pressure poured cast wheel is not having an adverse effect on rail wear. Test details and various profiles are contained in a report produced by IK [1] .
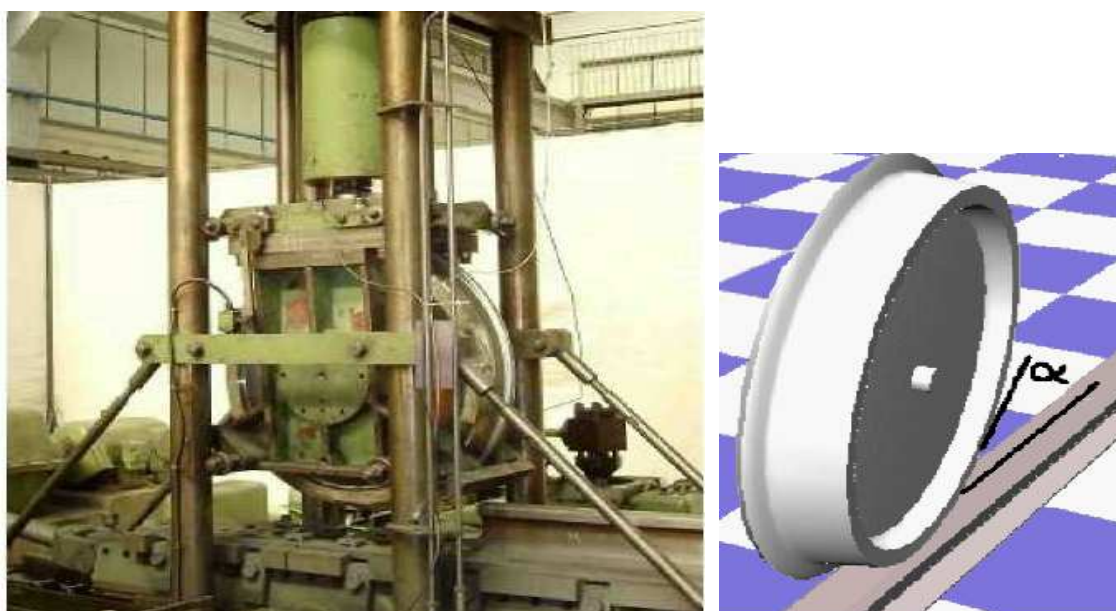
Fig.1. Test rig EMS 60 used for comparison of wear of forged/rolled monobloc UIC standard wheels with cast wheels manufactured by *Amsted Rail* and the wheel/rail orientation.

Table 1 - Average wear of rails and wheels after 100,000 cycles of operation.

Wheel Type	Average wear of rails, [mm]	Average wear of wheels, [g]
Forged/rolled UIC monoblock	3.86	898
Tyred	3.33	811
Cast ER7	1.46	350
Cast Class B	1.42	334
Cast Class C	1.26	292

3. Experimental measurement of wheel/rail contact stiffness and plate stiffness

The determination of the wheel/rail contact stiffness and the wheel plate stiffness is important to evaluation of the wheel/rail interaction, wear of rails and the influence of vehicle on track durability. The above mentioned two kinds of stiffness were measured on the EMS 60 test stand (at IK) using a classic mechanical method and laser method for displacement measurements Figure 2. Measurements were repeated and the average value was taken to obtain linear or nonlinear characteristics.

Fig. 2. Laser measurement of wheel plate and wheel/rail contact stiffness.

An example of the wheel plate measurement is shown in the left hand side of Figure 2, while the wheel/rail contact stiffness measurement is shown on the right side. Results of laser measurements of the contact stiffness and measurement of the plate stiffness as well as nonlinear and linear approximated characteristics are given in Figure 3 and Figure 4. The tests were conducted on a specially designed EMS 60 stand at Railway Institute in Warsaw, allowing simulation of rolling wheels on the rails in a curved track. Additionally computer simulation of the dynamic interaction of wheels with corrugated rails and simulation of wear was also conducted.
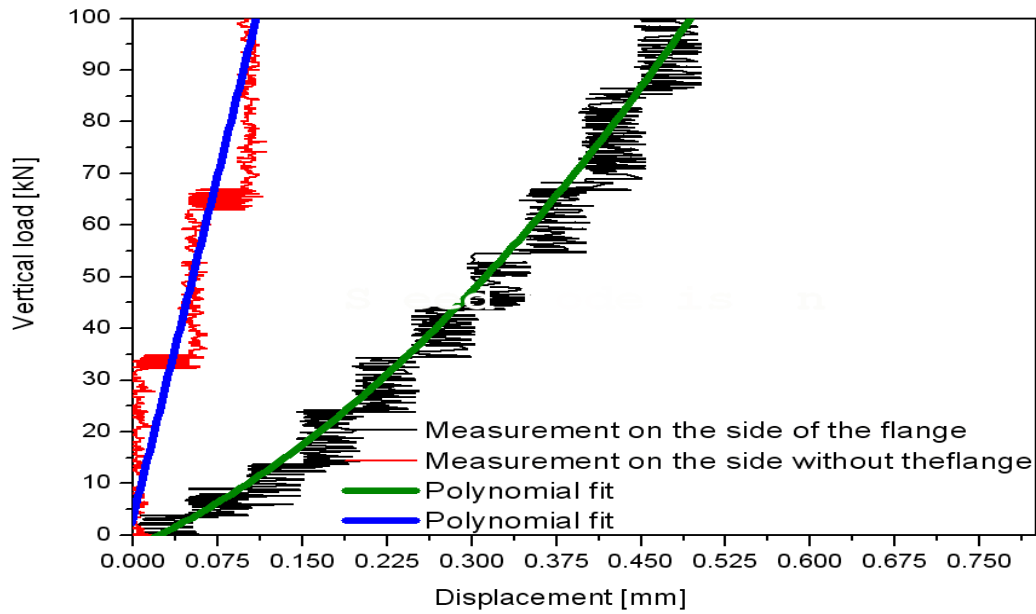
Fig. 3. Example of contact stiffness measurements and nonlinear approximated characteristics.
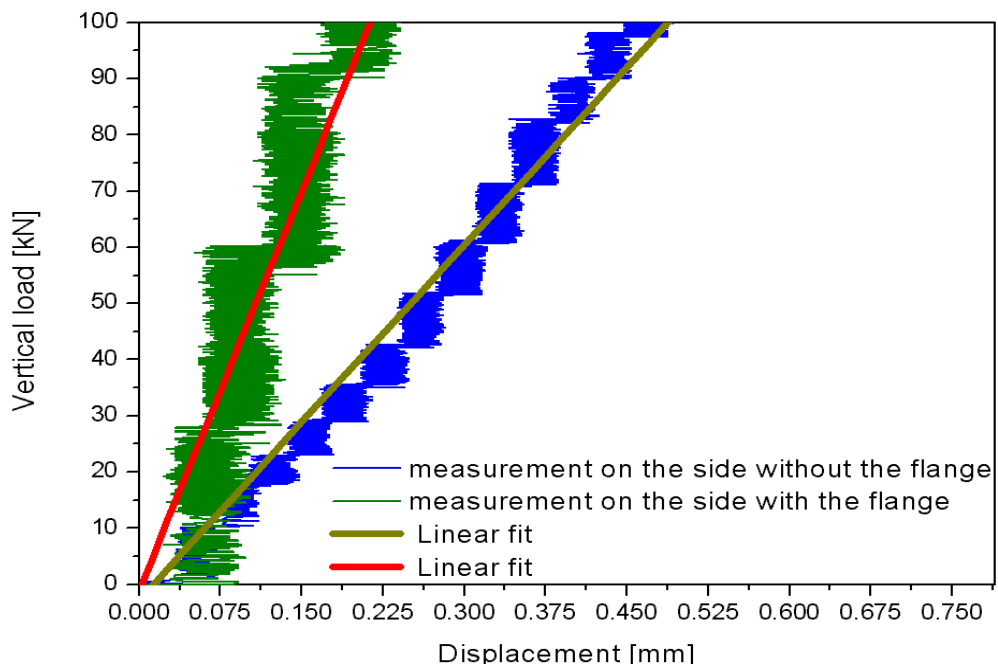

Fig. 4. Example of the plate stiffness measurements. Force versus displacement on left and right side of the wheel and linear approximated characteristics

Fig. 5 shows results of the average plate stiffness measurement (measured on both sides of the rim).
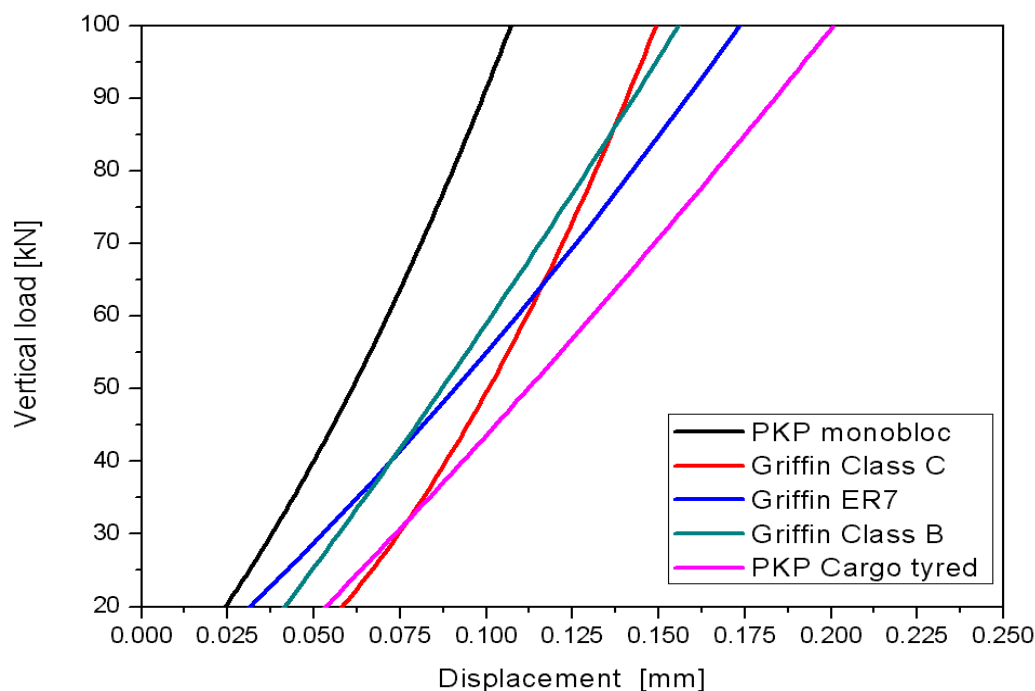
Fig 5. Results of the plate stiffness measurements (average from both sides of the rim)

The wheel/rail interaction depends on contact stiffness and on the stiffness of wheel plate, which are first of all function of the Young modulus of wheel material, shape of the wheel plate and shape of the rim (rolling surface). Also residual stresses in wheels and rails are important factors influencing quality of interaction and damage. It ought to be noticed that due to different structure of the rim material, differences in wheel plate design, forged and cast wheels present various quality of interaction. After determination of above parameters of the particular wheel, we can predict the dynamic behavior of the rail vehicle at given traveling speed and conduct the simulations.

4. Computer simulation of dynamic interaction of wheel with corrugated rail (cargo car interaction with track)

Let us consider a cargo car bogie which is moving along straight track having one corrugated rail. A pictorial of the bogie is shown in Fig. 6, while the shape of corrugated rail is shown in Fig. 7.
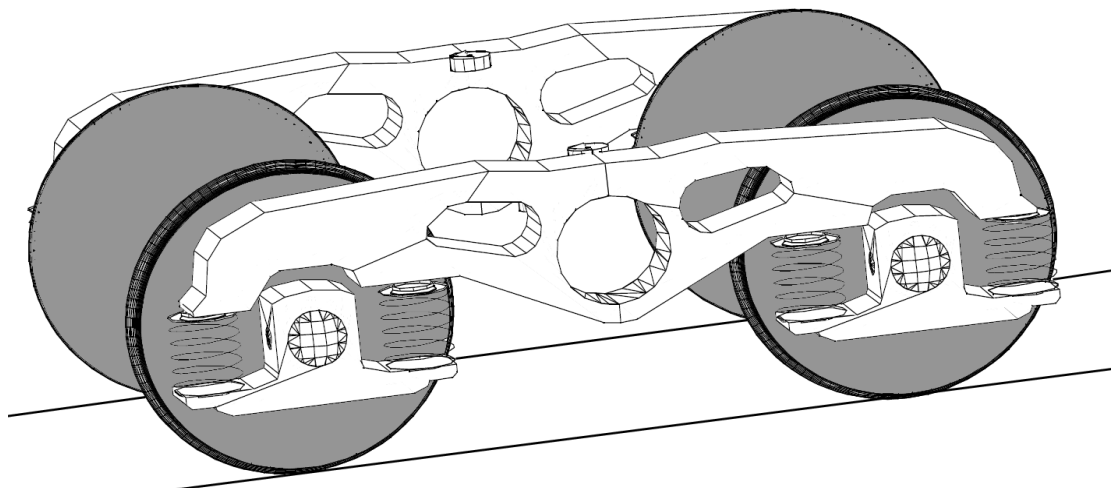
Fig. 6. Scheme of the bogie used in dynamic simulations.

For simulation typical European rail UIC 60 E1 is used. The shape of corrugated rail is assumed to be sinusoidal with amplitude of 10, 20, and 30 µm, wave length 100 mm and length of corrugated rolling surface equal to 1.000 mm. The traveling speed assumed using is a few values of the range (20 – 100 km/h). Evaluation of forces and power of wear is studied using modified "Simpack" program.
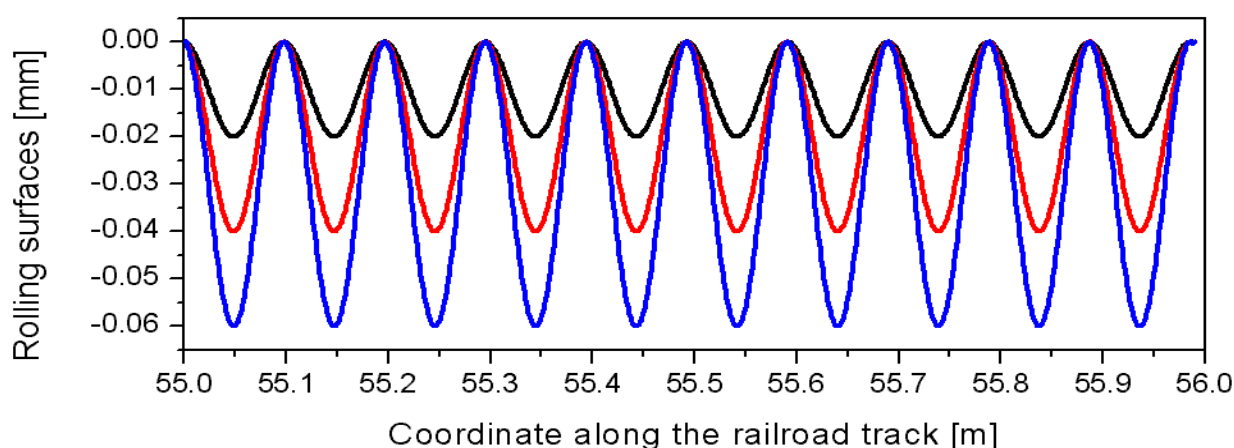
$$Z = A(1 - \cos kx) \tag{4.1}$$

Fig. 7. Shape of corrugated rolling surface of the rail with amplitude 10, 20, and 30 µm.

The classic expression used for calculation of intensity of wear is as follows:

$$I_w = |Cx*Tx| + |Cy*Ty| \, , \qquad\qquad (4.2)$$

where: Cx is longitudinal creepage, Cy is lateral creepage, Tx are longitudinal creep forces, Ty are lateral creep forces. Additionally the wear depends on material parameters.

It is very interesting to compare dynamic forces and wear in similar driving conditions with forged/rolled monobloc wheels and new pressure poured cast wheel design of ER7 material because material of both types of wheels are chemically identical, the difference is only in the manufacturing technology. One can see a great differences in dynamical interaction forces and in the wear, shown in Fig. 8 and in Fig. 9.
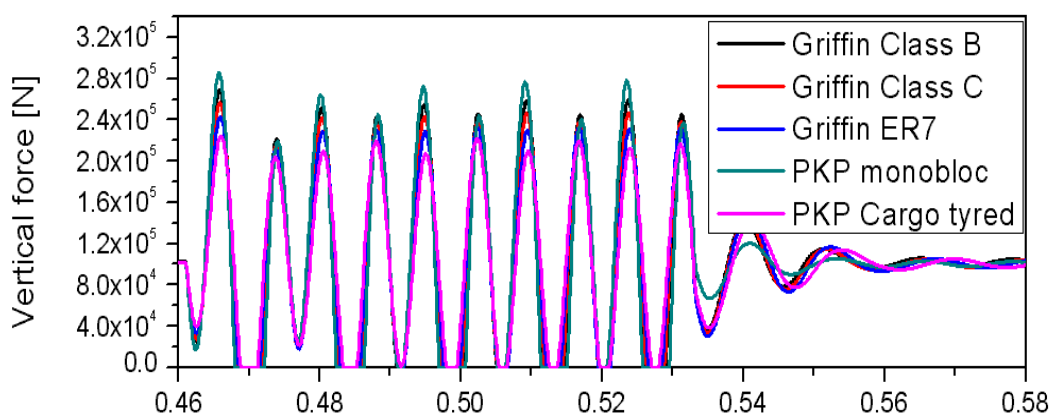

Fig. 8. Response of the wheel interacting with corrugated rail at speed 50 km/h (amplitude 30 μm, front wheel of the buggy, corrugated side)

Using the classic expression used for calculation of intensity of wear (4.2) when shape of the wheel is just the same one obtain similar values of wear intensity. This is evidently contradiction with comparative experimental investigation mentioned above. One of the important factors is grain dimensions, grain shapes and orientation. In the case of the pressure poured cast wheels we have other situation as in the case of forged/rolled monobloc wheels. The orientation of grains is shown on Fig. 10.
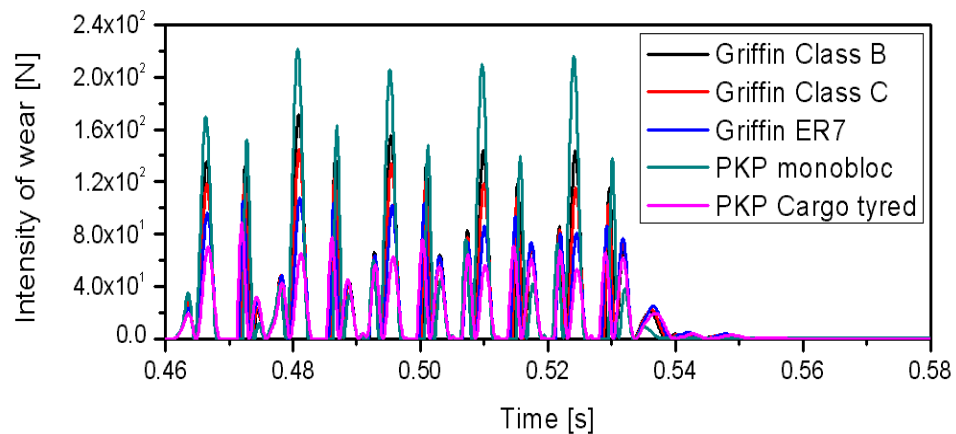
Fig. 9. Intensity of the wear during interaction with corrugated rail (speed 50 km/h, amplitude 30 μm, front wheel of the buggy, corrugated side)
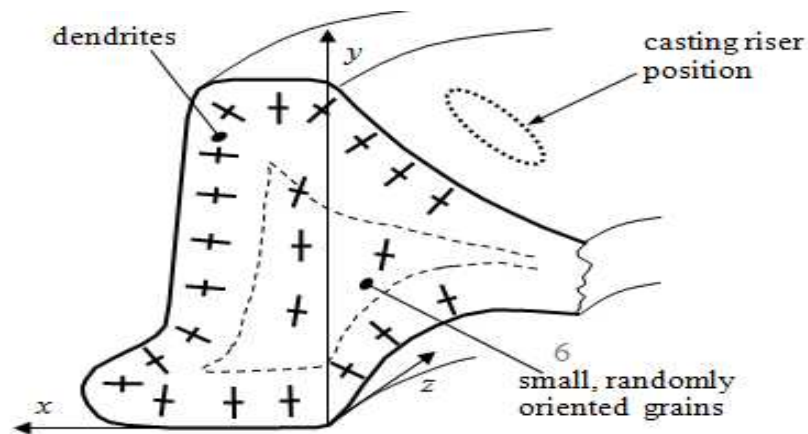

Fig.10. Regions of Dendrites and Small Grains in Power Pressure Cast Wheel

5. Conclusions

Wheel/rail wear testing and dynamic modeling simulations show that the Class C pressure poured cast wheel is not more likely to damage track and infrastructure than currently used forged/rolled and tyred wheels. Wheel wear and rail wear are less for the cast Class C wheel, and also for the cast ER7 and cast Class B wheels, than for ER7 forged/rolled and tyred wheels.

The results of the tests showed significant advantage of cast wheels over forged/rolled wheels for both wear of rail as well as wear of wheels. Details connected with wheel wear and rail wear for the cast Class C wheel, and also for the cast ER7 and cast Class B wheels, than for ER7 forged/rolled and tyred wheels are given in ref. [4].

References

1 IK Railway Institute, Materials and Structures Laboratory LK, "Wear Test of Rail Used in Europe vs. Cast and Forged/Rolled Wheels on Stand EMS60 – Project No. 2605/22," Warsaw, Poland, July, 2010.

2 Bogacz R., Kowalska Z. (2001), Computer simulation of the interaction between a wheel and a corrugated rail, Eur. J. Mech. A/Solids 20, 2001, pp. 673-684.

3 Schramm, R. E., Szelążek, J., and Clark, A. V.(1996), Ultrasonic Measurement of Residual Stress in the Rims of Inductively Heated Railroad Rims, Materials Evaluation, August 1996, pp. 929-934.

4 Lonsdale, C., Bogacz, R., Norton, M. (2011), Application of Pressure Poured Cast Wheel Technology for European Freight Service. Proc. of World Railway Congress, Lille France 20011.

5 Osuch, K., Stone, D.H. Orringer, O.(1995), European and American wheels and their resistance to thermal damage, , Proc. 11th International Wheelsets Congress, Paris 1995, Vol. 1, pp. 77-86.

4.1.7 HYDROGEN-DIFFUSION MACHINING OF CONSTRUCTIONAL MATERIALS

Gladky Y.[1], Makovkin O.[1]

In modern machine-building we strive for manufacturing major of articles by means of wasteless technology, but the share of machining by cutting still amounts up to 40%. Hard-to-machine constructional materials use (high-strength, heat-proof and heat-resistant steels and alloys) is connected with a chip removal (chip breaking) problem. These factors lead to premature tool collapse and productivity decrease. Improvement of the ways of cutting tool wear resistance increase, constructional materials processing, as well as cutting process productivity rise has been a vital problem for researchers and process men.

There are plenty ways and techniques, increasing cutting tool's serviceability, among which the one suggested by the authors is worth for attention. It's based on phisicomechemical situation change in the cutting zone at hydrogen presence – hydrogen-diffusion machining (HDM).

---

[1] Khmelnitsky National University of Ukraine

It's been known about influence of hydrogen, which is present at metal cutting zone, scince 20th century. Thus, prior blank or tool saturation with electrolytic hydrogen in certain conditions lightens chip formation process and increases tool's wear resistance, but runaway hydrogen penetration depth at saturation, as well as the need of extra powerful equipment use for huge blanks and short 'life span' of electrolytic hydrogen don't let us use such articles and tools. An attemp of hydrogen feed in the cutting zone from flasks and spesial facility had good results: temperature-powered cutting parameters, tool life both with chip formation character were changing considerably [1]. But, this technology has got several essential lacks: usage of flasks with liquefied hydrogen at production conditions is, practically, impossible in keeping with safety measures and economic standpoint.

Having analysed existing ways of hydrogen feed to the cutting zone and estimated their positive and negative aspects we suggested using so called 'accumulating tool' as atomic hydrogen sources, that is a tool with hydrogenous coating applied, and able to accumulate hydrogen at high temperatures as well as to recharge quickly [2]. Theoretic explaination of machining intensification and interpretation of the results recieved at experimental research have been made [3].

Hydrogen influence on mechanic properties of metals is one of the strongest in comparison with other gases. The unique hydrogen mobility is much determined by free nucleus' movement in metal crystal lattice, deprived of electron, i.e. proton. According to Archakov's data [4], hydrogen diffusion coefficient in the iron may vary from 1,5*10-5 upto 6,3*10-4 sm^2/s, depending on temperature increase from 20 to 900^{0}C accordingly.

1. Materials' machinability increase hypothesis.

The principle of materials' destruction mechanism in the cutting zone is put to the base of the materials' machinability increase by cutting hypothesis, as well as tool wear resistance hypothesis.

Chip formation can be considered as a destructive process from fracture machanics standpoint, which is connected with microcracks formation in largest shearing stress planes and their merging into the mainline (macrocrack) [3]. In

this case, destruction (chip formation) may take transcrystalline or intercrystalline type.

Establishing special conditions in the material or changing deflected mode in the cutting zone, it's possible to get a condition, in the result of which transition from power-intensive (intragranular) to intergranular – non-power-intensive destruction takes place. Hydrogen takes such a part in intergranular destruction and facilitates material's embrittlement in the cutting zone only. Difficulty of realization of the hypothesis suggested is found in ensuring local hydrogen influence in the cutting zone and, practically, absence of its influence on the machined detail's material. On the other hand, hydrogen, interracting with tool surface in the air, has to activate the creation of layers on its surfaces (third phase), which change friction and wear tribotechnical characteristics. Taking into account specific character of cutting tribology, tool's wear process may be regarded as a cyclic process of surface layers creation and destruction, i.e. mechano-chemical wear.

To achieve the increase of tool's wear resistance as well as materials' processing we propose to make hydrogen feed directly to the cutting zone. As a hydrogen source we can take high-capacity hydrogen accumulators – metal hydrides and intermetallic junction hydrides.

Both metal hydrides and intermetallic compounds ability to fulfill different functions, connected with hydrogen accumulation, sets conditions for their perspective usage. Chemically combined usage in hydrogen hydrides at their high sorption capasity, according to safety measures and economic standpoint, has its advantage over traditional ways.

There are many metal hydrides, as well as intermetallic junction hydrides, but not all of them satisfy demands set above. Detailed analysis of known material combinations with hydrogen showed, that BeH_2, MgH_2, ScH_2, $TiH_{n(n=1.63..2.00)}$, $ZrH_{n(n=1.54..2.0)}$ hydrides are of great interest. However, low hydrogen percentage in these combinations (upto 2%) restricts their usage.

Metal intermetallic junctions with hydrogen are of specific significance, as they are able to accumulate large amounts of hydrogen in comparison with usual metals. Besides, components that form intermetallic compounds sometimes cannot absorb enough hydrogen separately. Among major

intermetallic compounds are *Mg2Ni-H, TiFe-H,* compounds *(Mg2Ni+Mg)-H2, (Mg2Cu+Mg)-H, LaMg12-H.*

But hydrogen capacity of combinations mentioned above is not high yet (upto 6%). To increase hydrogen capacity and prevent intermetallic junctions disintegration into fine-dyspersated powders at usage, composite materials may be used for hydrogen sorption, which don't destroy at long-run exploitation and possess improved technical characteristics in comparison with pure intermetallic junctions. They are:

- Skeleton materials – working substance and filling agent form rigid framework. Components of the material must not interact. Pseudoalloys like *Ti2Ni-H, (Ti-Mg+additive)-H* refer to such materials.

- Laminates – metals or intermetallic compounds with loose oxides coating, applied on their surface, accelerating hydrogen sorption and desorption processes. Nickel, copper or infrequently iron coatings are applied. Coating can be applied vacuum-evaporated, electrolysed, spot-welded or other available ways.

- Several intermetallic compounds, each of which is fine accumulator. The major condition is the absence of interaction at exploitation. The most perspective compounds are *(TiFe+LaNi$_5$)-H* и *(Ti$_{0.8}$Zr$_{0.2}$Cr$_{0.8}$Mn$_{1.2}$)H.*

For hydrides fusion low-preassure equipment is used [5].

Several special technologies to get titanium hydride as a cutting tool coating have been developed at Technological University of Podillya (Khmelnitsky).

So called 'barrier layer' for protection from hydrogen penetration [6] is formed on the tool's surface, and titanium coating (Ti) formation is carried out by condensation method with ion bombardment and further hydrogenation (fig. 1,a). The coating, accumulating hydrogen on tool's surface serves as hydrogen source. But such a technology doesn't provide enough hydrogen reserve, which is used at the cutting tool operation for a long time.

Thus, special 'accumulating tool' that consists of usual tool and hydrogen accumulator (fig. 1,b) has been suggested for use as a hydrogen source. It's placed and pressed to the tool's surface with a special protective clip-casing.

2. Probation results.

'Tool-accumulators'' serviceability tests were carried out at constructional material turning cut at 1K62 lathe with stageless rotation frequency regulation.

Hydrogen influence on cutting process power characteristics (cutting force constituents P_Z, P_X, P_Y), as well as cutting temperature T, optimal cutting velocity level V_{OPT}, plastic deformation degree of the material being processed K_L, wear resistance have been determined.
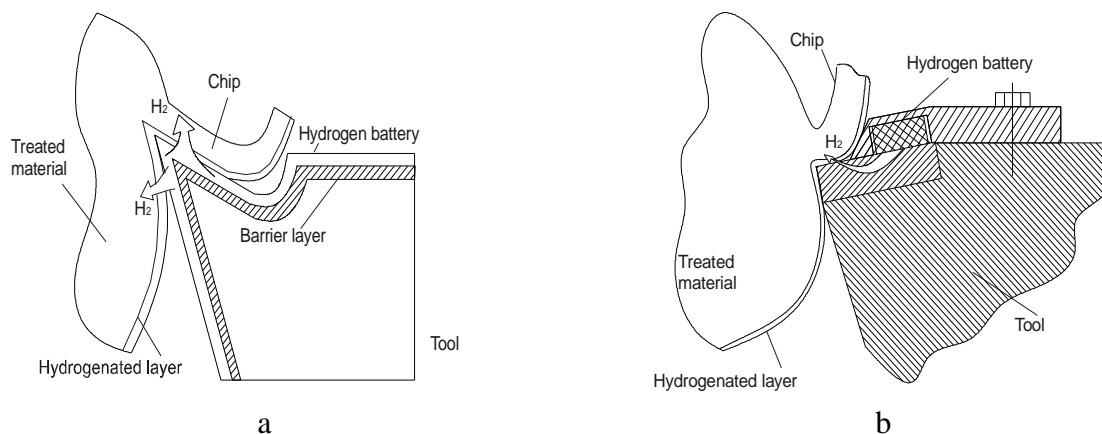

Fig. 1 Schemes of hydrogen feed to the cutting zone: a – form the hydride coating; b – from hydrogen accumulator.

The research was carried out on the materials, differing both with chemical compound and structure: Ст.3, 40X, 03X18H10T steel, XH35BTЮ high-temperature alloy. Turning was carried out with the tool made of P6M5 steel and BK6M hard alloy.

Thus, turning steels with P6M5 tool, according with work temperatures restricted by heat-resistance (upto 650^{0}C), Mg_2NiH_2, MgH_2, TiH_x, $Ti_2Ni(H_x)$ accumulators, having temperature interval of hydrogen dissosiation beginning at 200-300^{0}C, were used as hydrogen source.

At 'accumulating tool' serviceability probation on the basis of BK6M hard alloy Ti_2NiH_x, $(Ti-Mg)-H$, $TiFe$ accumulators, having temperature interval of hydrogen dissosiation beginning more than 300^{0}C, were used as hydrogen source.

The results of cutting research with 'accumulating tool' from P6M5 testify that in all cases hydrogen feed machining causes decreasing of cutting efforts and plastic deformation degree of the material being processed.

Temperature in pair contact zone, working in hydrogen medium decreases considerably, that causes optimal cutting velocity level V_{OPT} increase. Relative variation of some steel cutting process characteristics with 'accumulating tool' from P6M5 in comparison with usual tool is given in table 1.

Table 1

The material being processed	Relative variation of cutting process parameters in hydrogen-aerial medium				
	V_{OPT}, %	P_Z, %	P_X, %	P_Y, %	K_L, %
Ст3	+34	-42	-33	-22	-22
40Х	+43	-63	-50	-45	-57
03Х18Н10Т	+34	-60	-150	-88	-60

Wear of 'accumulating tool' made of P6M5 high-speed steel at turning at V_{OPT} is several times less in comparison with usual tool wear under the same conditions. Besides, chip removal process facilitation is observed at optimal cutting velocity due to chip formation process change – articulate chip, turning into element, is formed instead of typical for cutting with usual tool (fig.2).
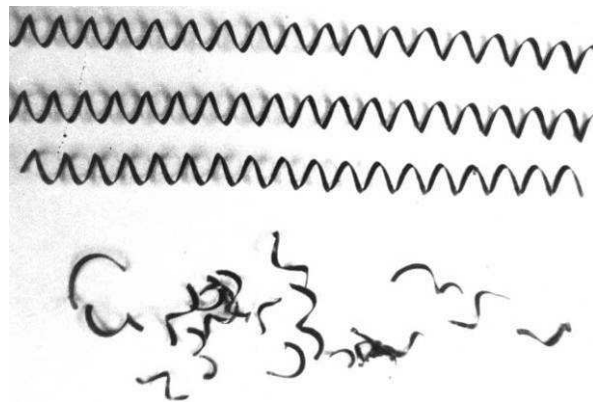

Fig. 2. The nature of chip formation in cutting.

At 'accumulating tool' serviceability probation on the basis of BK6M hard alloy an accelerated wear of tool, operating in hydrogen medium, for first 10 minutes of test has been registered. Thus, for cutting tool durability increase it has been suggested to use barrier layers, which protect tool material from hydrogen influence.
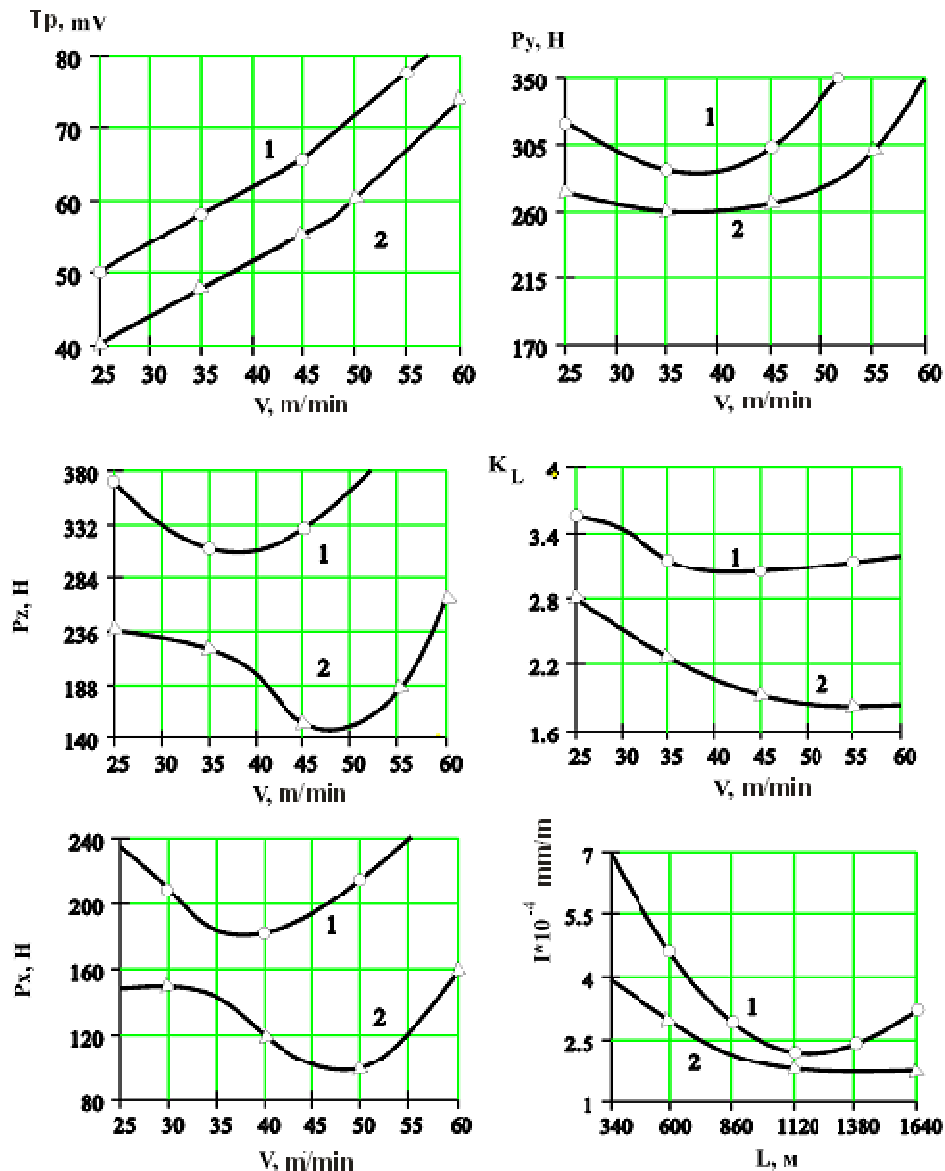
Fig. 3. Dependency of cutting process parameter of XH35BTЮ heat-resistant alloy with BK6M hardalloyed tool: 1 – usual tool, 2 - accumulating tool

The results of 'accumulating tool' research with barrier layer are given in fig. 3. They testify that machining with hydrogen feed causes cutting efforts, plastic deformation degree of the material being processed as well as temperature decrease, increasing optimal cutting velocity level V_{OPT} 'Accumulating tool' wear at turning at V_{OPT} is several times less in comparison with usual tool wear under the same conditions. Table 2 gives several cutting process parameters change in hydrogen medium in comparison with processing in the air.

Table 2

The material being processed	Relative variation of cutting process parameters in hydrogen medium				
	$V_{OПT}$, %	P_Z, %	P_X, %	P_Y, %	K_L, %
40X	+27	-20	-	-	-
03X18H10T	+33	-35	-32	-15	-50
XH35BTЮ	+36	-114	-100	-30	-63

3. Discussing the results.

Cutting is a complex process, which includes elasto-plastic deformations, friction, contact surfaces wear, material destruction. It's characterised by high contact tensions, temperautre, and high plastic deformation degree. Besides, new (juvenile) chip zones take part in wear process constantly. As shown above, condition change in 'friction-wear' zone at hydrogen presence considerably influences power consuming, qualitative and quantitative process components.

Destruction process of the material processed can be explained with the influence of tension and deformation regularities on hydrogenation. Thus, metal lattice deformation increases its energy level, influences on dislocation-vacancy structure that determines steel hydrogenation process to a great extent [7]. At the same time, one must define three hydrogenation cases: 1) hydrogenation of strainless lattice metal; 2) hydrogenation of distorted lattice metal; 3) hydrogenation within metal deformation process (the most important for our case).

Hydrogenation intensity is going up from the first to the third case. Little deformations, which are accompanied by negligible lattice distortions (in case of tool material), don't influence on hydrogen diffusion greatly, as well as on metal disposition to hydrogen fragility. Large deformations (in case of cut off metal, i.e. chip) cause both crystal lattice disruptions and defects formation in the form of microvoids in the entire material. Another one confirmation of hydrogen penetrating abilities into plastic deformation area is the research [8], the results of which testify that increasing deformations by 10% causes increasing of steel hydrogen penetration P_H by 100%.

Tables 1, 2 give us the results of relative changes of some cutting process parameters in hydroge medium in comparison with machining in the air. As

appears from the above, there is a bond between the effect caused by hydrogen-diffusion machining and constructional steels' properties.

Blank's chemistry has an influence on hydrogen diffusion in the steel, on its solubility in steel lattice and hydrogen absorption by collectors. Other elements presence also has an influence on each element's diffusion. Explanation of this lies, possibly, in the fact that some elements change iron crystal lattice, which other ones pass through. *Ni* presence in steel (in our case 03X18H10T steel cutting) provides alloy for high hydrogen penetration [9]. For instance, hydrogen diffusion activation energy into 35H3 nickel steel, containing 3,25% *Ni*, according to the work [10] is 75,6 kJ/mole, and into 40X steel, containing 0,89% *Cr* - -186,1 kJ/mole.

There is another regularity. Considerable cutting efforts fall isn't determined at low machining velocity. It can be explained by the fact that 'accumulating tool' warming-up temperature as well as deformation speed isn't yet enough for the beginning of intensive hydrogen dissosiation and considerable chip material embrittlement.

So why won't intensive wear of cutting tool made of high-speed steel in gaseous hydrogen take place and why do hard alloys wear out intensively?

In our opinion, the above mentioned phenomenon can be explained in the following way.

Firstly, creation of surface layer hydrophilic state is necessary for hydrogen wear realization (hydrophilic state is local increase of hydrogen concentration in surface layer owing to diffusion, exceeding concentration in the rest capacity). One of the major factors influencing this condition are metal structure and its change, which takes place at friction, and metal chemistry.

Changes, occurring in metal surface layer at friction, lead to complicated structural transformations and unsoundness increase that has an influence on hydrogen behaviour in the given zone. Hydrogen diffusion for different metal structural elements proceeds irregularly. In our opinion, hydrogen weakens crystal limits and reduces cohesion in cleavage face and may, mainly, migrate in these directions. This goes with K. Smithells' conclusions [9]. S.S. Nosireva in her work [11] showed the fact that hydrogen diffusion speed depends on steel

structure. She determined that metal with different structure and the same saturation conditions absorbs different quantity of hydrogen (table 3).

Hydrogen solubility being greater in austenit than in ferrite and considerably greater than in martensite, and hydrogen diffusion speed in ferrite exceeds diffusion speed in austenit, then we can suppose that hydrogen absorption by steel as well as machinability depend on structure, crystal lattice parameters and collectors presence there, where molecular hydrogen could be accumulated, which cousing lagre pressures facilitates steel embrittlement. Therefore, as table 3 shows, the largest optimal speed increase is observed in steels with ferrite structure and the less one – with austenite class (stainless steel)

Table 3

Structure	Hydrogen quantity, absorbed by 100g of metal, sm^3
Martensite	6
Troostite	15,9
Sorbite	46,5
Perlite-ferrite normalised	25,5

One of the most important factors, influencing on durability of steel to hydrogenous effect is carbon concentration in it, as alloys of *Fe-C* system have decreasing diffusion coefficient D_H with increasing carbon concentration. Thus, carbon concentration increase from 0.01 to 0.8% leads to D_H decrease in steels from $4 \cdot 10^{-3}$ to $1 \cdot 10^{-3}$ м^2/s [8].

Secondly, carbon concentration has an influence on hydrogen penetration of steels P_H. We can assume that carbon concentration increase by each 0.1% will cause P_H decrease by 4.1% [12]. Thirdly, hydrogen chemical affinity with carbon may cause steel carbide phase restoration according to reaction:

$$Fe_3C + 2H_2 = 3Fe + CH_4$$
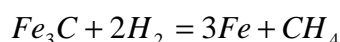
This process is following with decreasing of capacity that leads to additional tensions on grain boundaries. Thickness of the layer, which is subjected to decarbonization and considerably changes its properties, is going down with carbon increasing in steel [13].

Alloying elements, forming chemical compounds (hydrides), have an influence on ability of steel to absorb hydrogen [14]. For instance, hydride-forming admixtures of molybdenum, vanadium, chrome, and other elements keep atomic hydrogen in interstitial solid solution condition, slow down its desorption from metal as well as hydrogen transition to moleclular form, and hinder destruction.

Summing up above mentioned, we can make a conclusion – P6M5 high-speed steel, which consists of fine-dyspersated martensite alloyed with tungsten, molybdenum, vanadium, chrome, and has increased temper in comparison with constructional steels (upto 1%) hydrophilic state isn't formed during the interval before regrinding (durability period), and thus, disastrous hydorgen wear doesn't take place.

Secondly, working at accelerated cutting modes high temperatures occur in tool-blank contact zone, they lead to oxidizing process forcification on contact surfaces as well as tool overheating (heat-resistance loss). Hydrogen, being strong reducing agent and getting in that zone first of all reacts with air oxygen and protects tool from oxidizing wear.

Thirdly, hydrogen-phase hardening (HPH) phenomenon is observed at metal cutting in gaseous hydrogen medium in instrumental material. Material strengthening at HPH is caused by two physical reasons: 1) internal deformation – material phase hardening at hydrogen saturation and hydride transformations development, considering phase particiaption, which have different specific volume, 2) active interaction of occluded hydrogen and hydride phases that are formed with generated crystalline constitution defects [15]. Any metal may be exposed to HPH, being influenced from hydrogenous medium and appropriate parameters, for instance active gaseous hydrogen, hydrogenous gases, plasma, electrolytic hydrogen etc. In all cases at HPH crystalline defect density is considerably increased (by 2…4 units), which is accompanied by block structure desintegration and angular disorientation increasing. Another confirmation of the hypothesis is microhardness analisys of 'accumulating tool' cutting blade surface after operation in gaseous hydrogen medium. Tool surface microhardness is almost two times higher.

As it was noticed in trial experiments, during cutting with hard-alloy tool its accelerated wear in hydrogen medium takes place. It was taking place during first 10 minutes of research. So, the hypothesis that atomic hydrogen penetrates into defects like micricracks, pores and areas between tungsten and cobalt carbides has been framed. Hydrogen is mobilized there, and destroys tool, creating high pressures.

So, it has been suggested to cure all defects in sintered powder-alloy. Chrome is the most stable chemical element to hydrogen. Patent method of tool crack resistance rise, developed at Technological University of Podillya, was applied at work. We called chrome layer as 'barrier', it can increase tool destructive viscosity and protect it from hydrogen penetration. As our research shows (fig. 3, table 2), such additional processing favourably facilitates chip formig processes.

Conclusions.

The results of the research confirm relevance of the suggested hypothesis for constructional materials machinability in gaseous hydrogen medium, penetrating into the cutting zone under high temperatures, high contact tensions, high degree of plastic deformation; it facilitates chip forming process, embrittling predestruction zone. As a result of such interaction, cutting forces components, temperature in the cutting zone and wear itself decrease.

Accumulating tool on the basis of intermetallides and composite materials of industrial manufacture, which provide enough hydrogen quantity for a long use at hard-machinable materials processing and having high viscosity, durability and other special properties is suggested to be used as a hydrogen source.

A link between structure, chemistry, instrumental material thermotreatment, as well as load-temperature factor on the one hand and destruction resistivity under hydrogen on the other hand has been constituted.

References

1. А.с.1009715 А СССР, МКИ В 23 Q 11/10. Система подачи газа в зону резания. /Э.А.Станчук, А.П.Шумилов (СССР).- №3372853/25-08; Заявлено 23.12.81; Опубл. 07.04.83 //Бюл.№13.

2. Патент 23912 А Україна, МКИ В23Н3/00, С23С16/00. Спосіб підвищення стійкості ріжучого інструменту та оброблюваності конструкційних матеріалів /Р.І. Сілін, Я.М. Гладкий, А.А.Бурлаков, В.О. Остаф'єв, (Україна)- Заявл. 06.02.97. Одерж.31.08.98.

3. Гладкий Я.М. Науково–прикладні основи підвищення зносостійкості інструментальних матеріалів шляхом використання прогресивних технологій: Дис. доктора технічних наук: 05.02.04.- Хмельницький, 1998.- 300 с.

4. Арчаков Ю.И. Водородоустойчивость стали.- М.: Металлургия, 1978. - 150 с.

5. Sieverts A.- Z. Metallkde, 1929, 21, 37-44.

6. Патент 22093 А Україна, МКИ С23С16/00; С21D7/02 Спосіб підвищення тріщиностійкості інструмента /Я.М. Гладкий, Р.І. Сілін, В.І. Семенюк, (Україна)- Заявл. 13.02.96. Одерж.30.04.98.

7. Карпенко Г.В., Василенко И.И. Коррозионное растрескивание сталей.- Киев.: Техника, 1971.- 212 с.

8. Schwartz W., Zitter H. Loslichkeit und Diffusion von Wasserschtoff in Eisenlegirungen.- Arch.Eisen – hutten.- 1965.- Bd.36.- s.343.

9. Смителлс К. Газы и металлы: Пер с англ.- М.: Металлургиздат, 1940. - 228 с.

10. Гаркунов Д.И. Повышение износостойкости на основе избирательного переноса. - М.: Машиностроение, 1977. - 215 с.

11. Защита от водородного износа в узлах трения /А.А. Поляков, Д.Н.Гаркунов, Ю.С.Симаков. и др. /Под ред. А.А. Полякова. - М.: Машиностроение, 1980. - 135 с.

12. Андрейкив А.Е., Харин В.С. Распределение диффундирующего водорода в окрестностях вершины трещины в деформируемом металле //ФХММ. – 1982. - №3. – С.113 – 115.

13. Матюшенко В.Я. Износостойкость наводороженных металлов // Исследование водородного износа. - М.: Наука, 1977. - С. 24 - 27.

14. Потак Я.М. Хрупкое разрушение стали и стальных деталей. - М.: Оборонгиз, 1955. - 237 с.

15. Гольцов В.А. Явление управляемого водородофазового наклепа металлов и сплавов // Свойства конструкционных материалов при воздействии рабочих сред. - Киев: Наукова думка, 1980. - С. 151-165.

4.2. PROCESSES OF THE FRICTION IN THE CONDITIONS OF BOUNDARY LUBRICATION

4.2.1 WHAT WE KNOW ABOUT THE BOUNDARY LUBRICATION
Pytko S.[1], Pytko P.[1], Furmanik K.[1]

Introduction

In many publications and research works it has been used a term the "boundary lubrication". This physical and tribology term and connected with it a phenomenon has been treated by the scientists who gave the foundation of tribology. In the monograph "Granichnaja Smazka"[1] there were mentioned physicists and chemists as well as physical chemistry specialists concerning with this problem, there were about 300 items of science citations. Among others there are the papers of professor Kostecki. The Authors of this paper would like to present the learning information concluding from their own investigations and scientific discussions published on this subject.

Interesting is a fact that during a dry friction a friction coefficient increases with a decreasing of loading, particularly with a loading in a microscale of frictional elements. Results of these investigations were shown in Fig.1 [7].
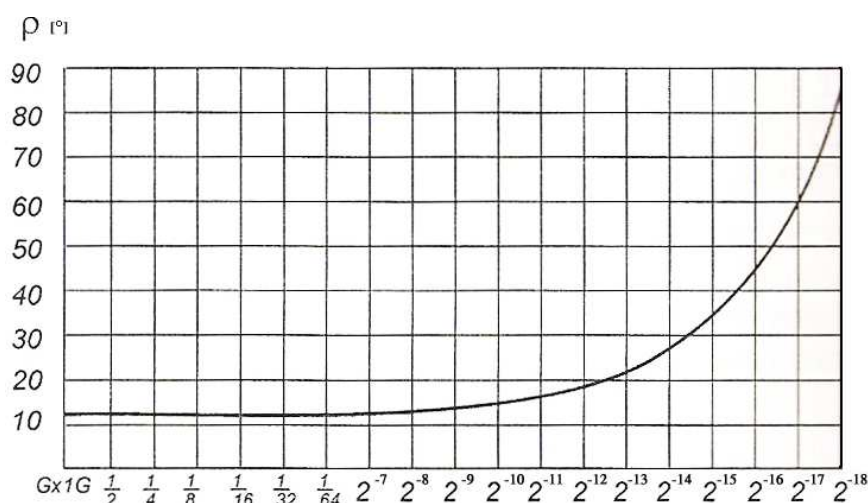
Fig.1. Diagram of friction angle change with a change of specimen thrust on a stand Fig. 2

---

[1] AGH University of Science and Technology, Cracow, Poland

Value G = 2N, ρ (rake of the inclined plane rake, tangent ρ, tan ρ = μ) [7]

In the aim to find out how changed a friction coefficient with rather small thrusts the investigations on the inclined plane which was presented in Fig.2 have been carried out. The equipment allowed to measure in easy way a friction angle ρ, of which a tangent was equal to a friction coefficient μ.

From the presented investigations one has resulted that for the friction coefficient except the thrust force some other phenomena has an influence then these which resulting from a dependence known in References. Thus from what will depend the friction coefficient μ given in textbooks on machine construction and formulated according to the formula (1) from physics learning?:

$$\mu = T/N, \qquad (1)$$

where: μ - friction coefficient; T - friction force; N- normal force resulting from a loading.
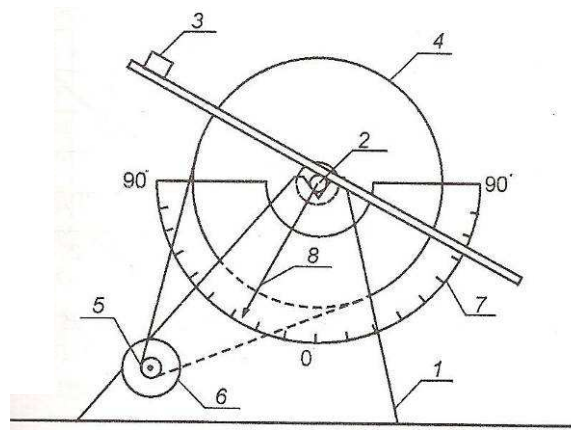
Fig.2. Testing stand (inclined plane): 1-bearing support; 2 - specimen of exchanging weight value; 3 - wheel for an angle inclined plane changing; 4 - drive of inclined plane changing; 5 and 6 [7]; 7- protractor, angle indicator

If one finds out that the most dangerous wear during element friction is when the element welding (seizing) occurs usually eliminating an element of equipment from further exploitation, one can denote that:

$$N = F_r \cdot p_q$$

$$T \; = \; F_r \cdot \sigma_t, \tag{2}$$

where: F_r - area of real contact surface,

p_q - unitary thrusts in contact,

σ_t - unitary stresses necessary for cutting of welded areas.

Substituting the formulae (2) into dependence (1) one will obtain the following formula of friction coefficient:

$$\mu \; = \sigma_t / p_q, \tag{3}$$

We remember these basic formulae of physics and tribology in the aim to understand the fact, that for decreasing of friction coefficient one ought to decrease to possible values an indicator value i.e. σ_t or possibly increase p_q.

It is generally known that the friction coefficient should always be little because of :

- motion resistances and connected with them energy losses,

- wear of machine elements.

So how to decrease the σ_t value in practice? It is possible to achieve it in two methods:

- by producing of layers (coating) on machine element surfaces of small σ_t, value with chemical or physical methods,

- or by implementation between friction elements the third body of little friction coefficient among their layers.

The bodies fulfilling these conditions are lubricating substances. Hence we can ascertain from the formula (3) that in the case of two elements of friction made from different materials the friction coefficient will be less when areas temporary welded, if lubrication fails ,they will be cut due to influence of small cutting stresses σ_t or if will be able the possibly great loading without any deflections, i.e. if p_q will be great. Materials fulfilling these conditions are among others a bearing alloy called " white metal" or babbitt. It is known that EP additives in oils produce in suitable temperatures special coating against a seizing. Their activity in suitable temperatures prevent an element seizing, what is presented in Fig. 7 [6].

We ought to take attention to the fact that in the case of friction elements in terrestrial atmosphere some layers occur as a result of oxygen influence which create any buffer on their surfaces against the cold welding of loaded elements. The friction with such elements in technology is called a dry friction. This layer on a surface of elements made of steel is graphically presented in Fig. 3.

Naturally in the case of uncovering of layers as a result of friction and wear of elements in the vacuum and also in the universe there is no such an oxide layer.

Concluding from Fig. 3 in the atmosphere onto made of steel elements have been emerged oxide layers with water absorbed from water steam existing in the atmosphere.

How will be presented the situation in the case when these elements will be lubricated? It is obvious that bedside other functions of lubricant agent good lubrication exists when between friction elements there is a layer of lubricant agent.
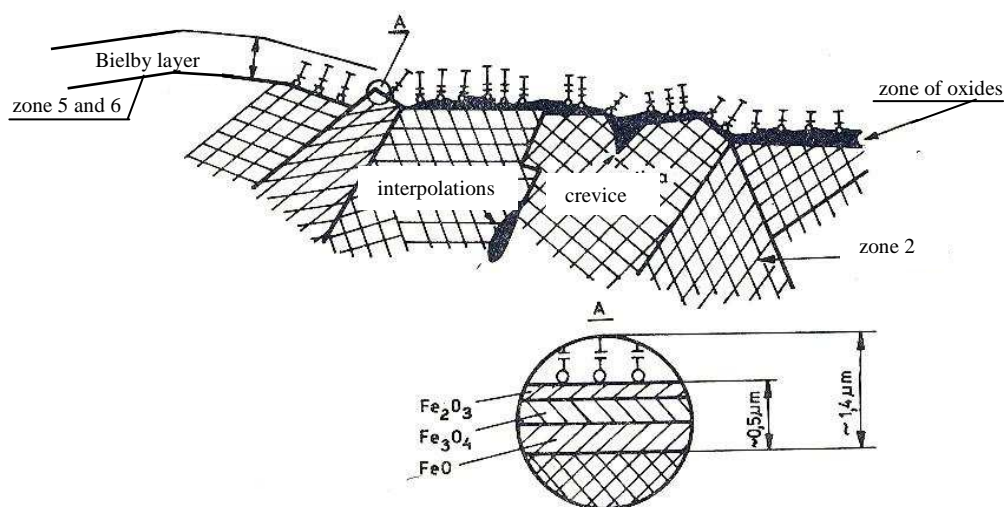
Fig. 3. Structure of steel layer in terrestrial atmosphere conditions [2]

It means that in such conditions one occurs an exchange: instead of friction between elements there is the friction between lubricant layer agent, which resistance is of many orders less than in the case of dry friction. For a creation of this friction some conditions and states of motion have to be fulfilled. In Fig. 4 the different shapes of cooperating elements enabling an occurring of

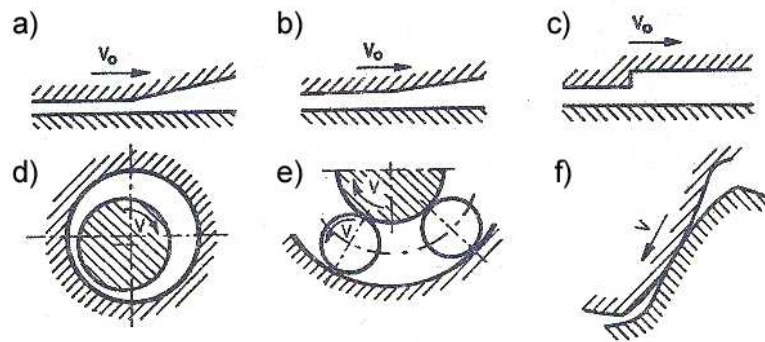lubricant layer between these layers so called lubricant wedge have been presented.

Fig. 4. Shapes of elements enabling an occurring of lubricant wedge [2]

In Fig. 5 there is the graphic presentation of an influence of motion element velocity on arising of liquid friction, hydrodynamic one. When the V motion velocity is small there is no wedge. It emerges in the case of sufficiently great velocity and its value depends on thrust between friction elements and viscous quality of lubricant agent.

Beneath some basic problems of tribology phenomena enabling an understanding of notion of boundary lubrication have been shown.
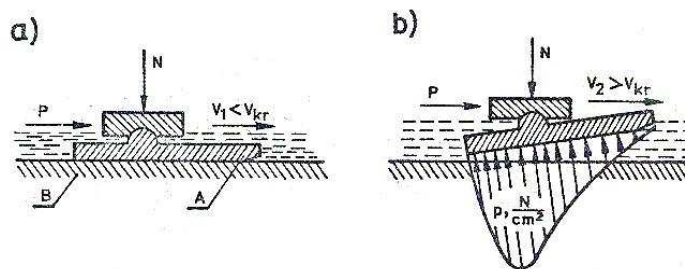
Fig. 5 Graphic presentation of a lubricant wedge arising [2]: a) in a rest state or when V shift is very little; b) with increasing V shift

1. Conception of boundary lubrication

1.1. Conception of boundary lubrication with oils

From the economic or durability point of view everybody who has exploited any machine or equipment would like to ensure an operation of cooperating elements with a liquid friction ensuring:

- small element motion resistances hence the little power consumption,

- small wear of elements, hence increased free of failure frequency and durability and due to these less costs of exploitation.

So far as we knew from the theory and industrial practice during the work of machine elements like slide and rolling bearings, toothed wheels, cams, engine sleeverings and other elements they have happened such situations when a lubricant film was broken and begun an unequal surface contact. Very often this situation was caused by overloading of system and also as a result of a deflection of shaft and other machine elements, which gave other thrusts than these calculated ones. At the time on contact surfaces have arisen a thin small layer of lubricant agent called boundary layer as it was presented in diagrammatic way in Fig. 6.
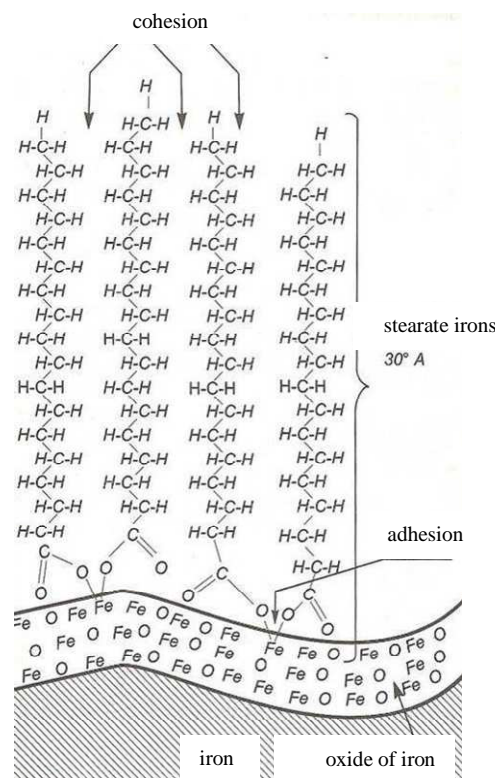
Fig. 6. Diagram presented a layer of hydrocarbons onto iron oxides one [1]

In some situations to avoid a seizing of machine elements into oils and plastic greases one has to add some special additives producing a special layer of small σ_t, values, decreasing a friction coefficient and preventing of element

seizing. These special additives into oils would be additives in lubrication technology called EP (extreme press) additives which during an overloading and temperature increase entered in reaction with metals into elements producing the new easy slipped layers on elements in this place, where would be arise the seizing. How and when would operate such additives into oils and greases one can see in Fig.7 [4].

As it results from Fig. 7 in a moment of beginning of friction element cooperation there is an increase of temperature in a zone of contact and simultaneously an increase of μ, friction coefficient which is stabilized in time (AB section in Fig. 7). If the good conditions for liquid lubrications have finished then it increased not only a friction coefficient towards the value [in diagram C point] but also T temperature to T_{kr} value. If the additives of EP type were not operating at that time it would arise the seizing of cooperating elements. In the case if these additives will react when the friction coefficient decreases and these elements will not seized. Such a temporary enduring gives a possibility of further operation of cooperating elements.
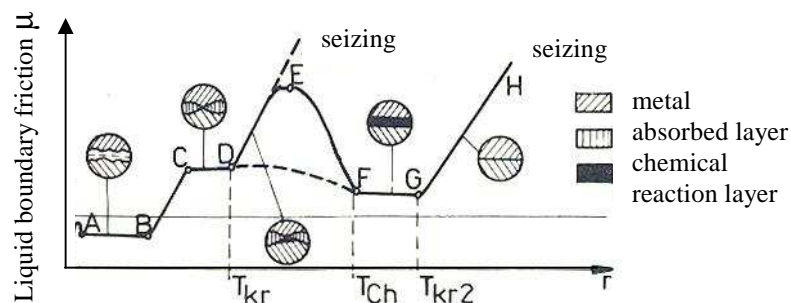

Fig. 7. Diagram of friction coefficient μ dependence upon temperature in contact of lubricated friction elements. T_{kr} - critical temperature in a moment of the first EP additive reaction; T_{ch} - temperature in a moment of special chemical reaction of EP additives, T_{kr2} - critical temperature 2 when the next reactions of EP additives proceeds [4]

A scheme of emerging of such a layer when additives are sulphur compounds has been presented in Fig. 8. It concludes from Fig.8 that onto an element made of steel iron sulfides, which give possibilities of easy shifting of elements and prevent against a seizing have olccured, it means that σ_t of this layer was small. The described above situation was an example of proceeding

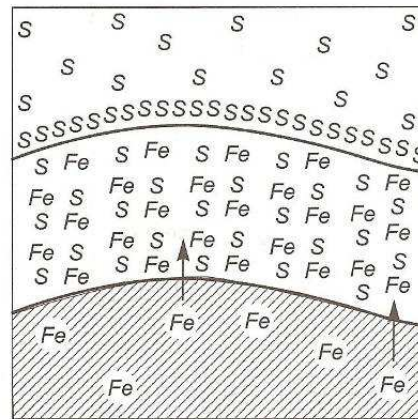of so called boundary friction at the lubrication of elements by oils with EP additives.

Fig. 8. Scheme of layer onto steel element surface after reaction of additive from oil [1, 3]

One can define a boundary lubrication on the basis of diagrams obtained at the time of testing of lubricant agents upon the four ball testing equipment, what the scheme is presented in Fig. 9a. In Fig. 10 [3] friction moment changes at the time of testing upon this equipment with a continuous loading of upper ball has been shown.
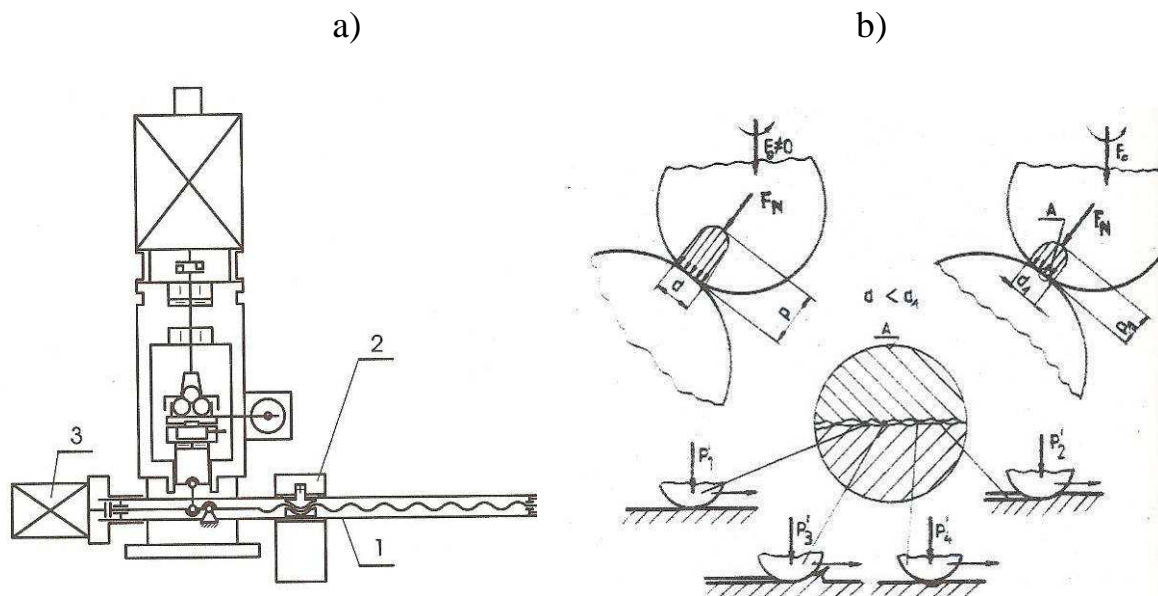
a)   b)

Fig. 9. Kinematic scheme of the T-02 four ball testing equipment made by the ITE: a) 1- lever; 2- weight; 3 - engine shifting a weight [8]; b) possible different states of wear onto contact surface of upper ball with lower one
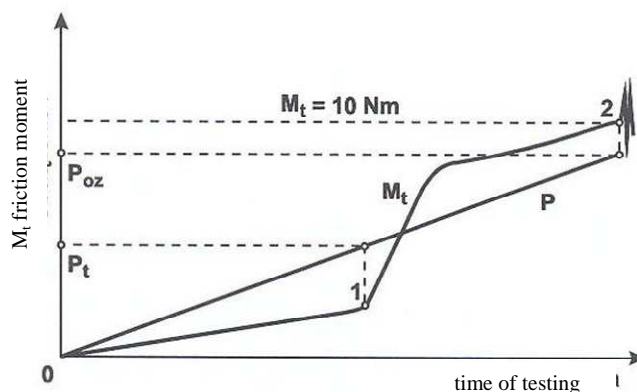
Fig. 10. Diagram of friction moment according to the dependence of upper ball on four ball testing equipment [8]

It is interesting that with increasing of loading and simultaneously emerging of wear traces the moment of friction increases proportionally to the loading of upper ball. In certain moment of loading increase of the upper ball, what produces the increase of thrust, arises a sudden increase of friction moment, what is shown in Fig.10, point 1. In such a moment arises the boundary friction emerging M increase to such a value, that produced heat and temperature perform operation of additives into oil. When formed layers on wear surfaces of σ_t friction values are not equal to friction forces at the time occurs the welding of balls i.e. seizing. In Fig. 10 point 2.

In Fig. 11a the trace of wear onto lower ball has been shown and at the point of this wear (in Fig. 11b) in B point occur small layers resulting from a reaction of the EP additives into oils presented above in Fig. 8.
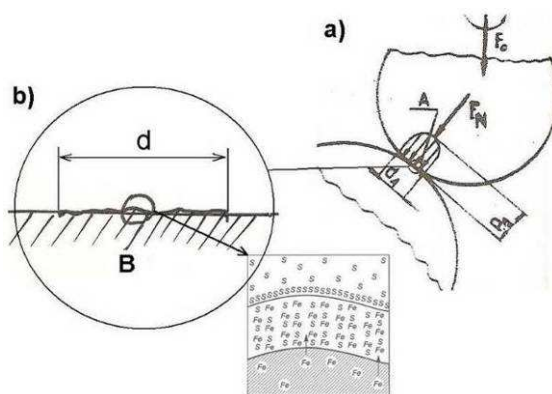

Fig. 11. Contact of upper and lower balls a) in a trace of wear in B point b) processing reactions from the EP additive on sulfur basis

The interesting investigations onto the four ball testing equipment have been carried out at the Academy of Berlin (BAM) for the different loading values of upper ball, but at the different rotations, what automatically changed a value of shifting velocity of upper ball on lower balls. The results of those testing was presented in Fig. 12 [6].
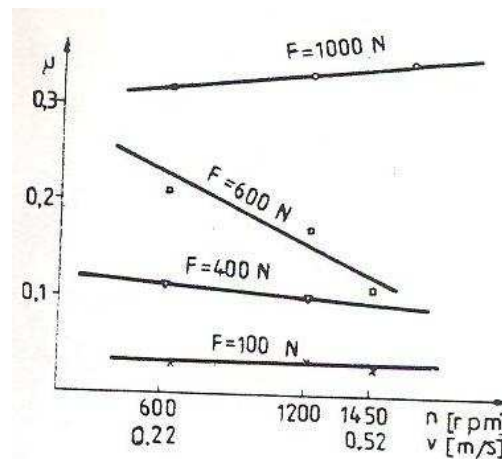

Fig.12. Diagrams of friction coefficient values at the different loadings and rotations of upper ball onto the four ball testing equipment [6]

As it has resulted from curves in Fig. 12 in the case of loading of upper ball by force of 1000 N with the increase of rotations slightly has increased the μ, friction coefficient, however at the loading of 600 N with the increase of rotations the μ coefficient of friction has decreased. This fact has been showed that an initial wear caused such sizes of wear (in contact of surfaces) onto balls that occurred the liquid friction.

At present there are treated dozens of technologies of new materials for bearing shell of slide bearings and skids. Treating the "Burana" space shuttle documentation in Kiev over 100 new technologies of upper layers of materials of σ_t small values have been tested. However in the aim to fulfill conditions of formula (3) under a thin layer the another layer of great p_q values has been given. Such a technology has been applied in a production of tapes for bearing shells destined for many machines in this number of combustion engines.

1.2. Conception of a boundary lubrication with plastic lubricants

Very often machine elements are lubricated by plastic lubricants with additives of graphite or molybdenum disulfide. Then a greasing layer has been shown as in Fig. 15. One also ought to know that in the case of lubrication by plastic lubricants making of quite thick lubricating layer is more difficult than in the case of oil lubrication. Thus in many situations we add into plastic lubricants, indifferently of their chemical structure, a substance which is a thickener. Crystal elements or formulae like a graphite (C) or disulfide of molybdenum (MoS_2) or more seldom of wolfram have produced the buffer layer preventing against the machine element seizing. It is also in conditions of great thrusts and small sliding velocities between machine elements these crystal elements or formulae cover a coarse element surface and form a layer of small value, i.e. decreasing the μ friction coefficient. In Fig. 16 and 17 a structure of these additives, of graphite (C) and molybdenum disulfide (MoS_2) have been shown.

The very large researches on 10 graphite modifications has been carried out by one of the Authors with B. Shcherski in 60[ties] years of twenty century and has proved how essential role in the denoting of graphite qualities has its genesis.
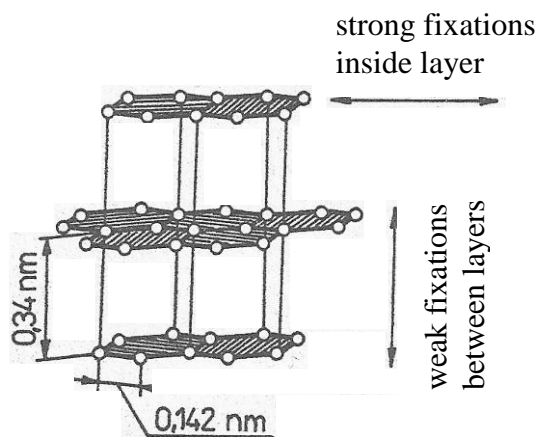

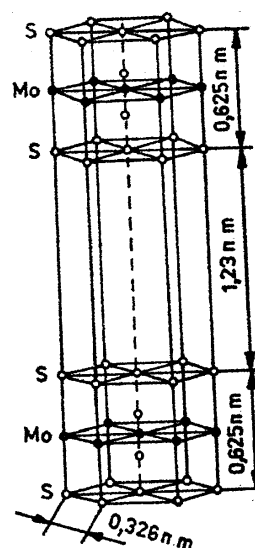**Fig.13. Graphite structure (2)**

Fig. 14. Structure of the disulfide of molybdenum MoS2 (2)

The disulfide of molybdenum as a lubricant substance was widely implemented and tested in 60ties years of 20ty century. Because of its structure presented in Fig.14. it has such like graphite such a quality, that produces the layer on lubricant element surface of σ_t small value and of the same decreases the friction coefficient μ.
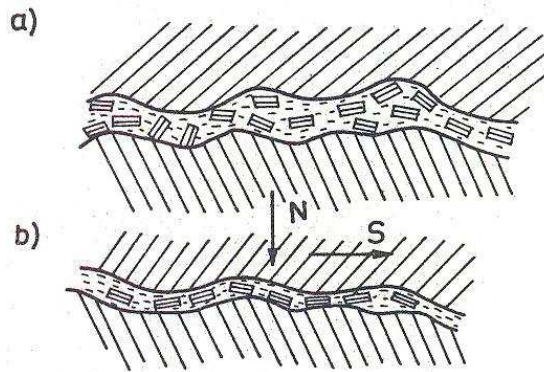

Fig. 15. Lubricant layers with additives of crystals a) with a sufficient lubricant layer; b) with a boundary lubricant layer [5]

One have to remember that these additives have their application limits according to the temperature, as it was presented in Fig. 16 next they lose their own qualities lowering the value of friction coefficient, and even this friction coefficient increases after their implementation.
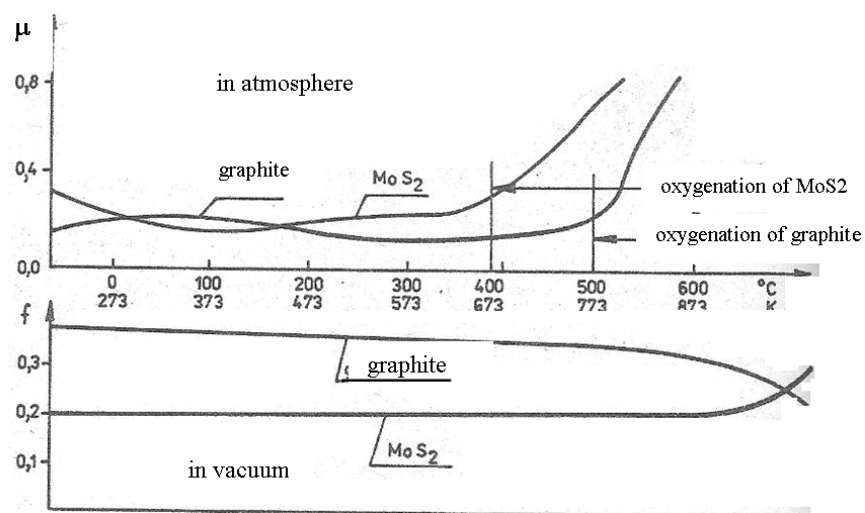

Fig. 16. Diagram of friction coefficient value according to temperature for graphite and disulfide of molybdenum [5]

1.3. Conception of boundary lubrication with solid lubricant

There are such cases in technology when a lubrication with oils and plastic lubricants is not possible. In these situations one can use for machine elements solid lubricants as it is given in Fig. 17. At that time one of setting elements is made of lubricant i.e. of graphite with binding agent and wearing off causes a coating by a very thin layer of lubricant agent of σ_t small value and it decreases μ friction coefficient.
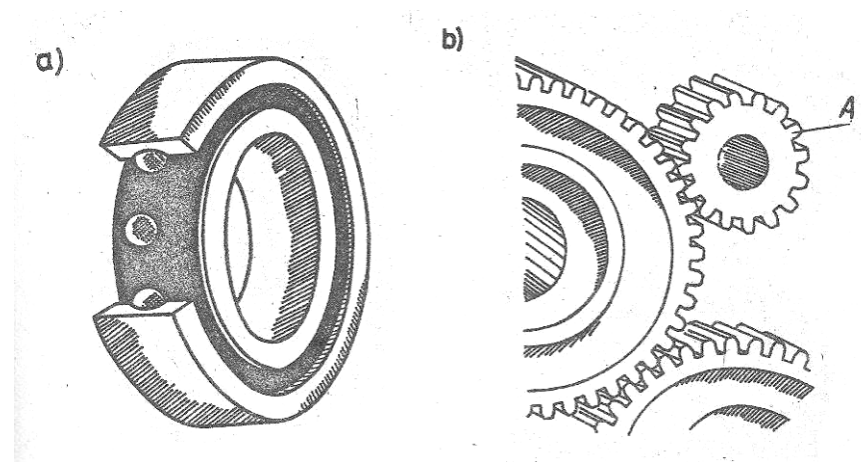

Fig. 17. Examples of machine element lubrication with solid lubricants a/ working layers of rolling bearing; b/ working layers of gear teeth [9]

Conclusions

As results from a description of boundary lubrication and mentioned above examples we meet very often the boundary lubrication in technology. If one cannot allow to machine element seizing what is a catastrophic failure, demanding the given element removal from a machine, we add to oils the special additives against seizing and wear, the effects of which we can test onto four balls testing equipment made by the ITE in Radom, of number T02.

In the case of lubrication with plastic lubricants the boundary friction similarly like with oils react when an approach of element surface is so great that the EP additives into oils of these lubricants produce some layers preventing the seizing. In the case of lubrication with plastic lubricants like graphite, disulfides of molybdenum or wolfram onto the surfaces occur from these additives layers of very small values of cutting forces preventing of seizing.

In the case of lubrication with solid lubricants as it has been shown in Fig. 17 in fact there all the time was a boundary lubrication. This type of lubrication gives us a protection before cooperating element seizing , because it is applied with little sliding velocities. One ought to know that at the time of element cooperation in contact a thickness of lubricating layer has a few micrometers. The most important thing during the lubrication is that does not come to contact the elements for the longer time and that between these elements emerges the layer preventing from welding of irregularities of surface of machine elements.

References

1. Bujanovski I.A., Fuks I.G., Shabalina T.N.: *Granichnaja Smazka*. Wyd. Neft i Gaz Moskva 2002.

2. Czichos H.: *Film Failure of sliping Hertzian Contacts.The influence of Contact Geometry*. Proc. of the JSLE -ASLE Intern. Lubricatiion Conference. Tokio, 1975.

3. Godfrey D.: *Boundary Lubrication*. Proc. Simp. "Intersciplinary apporoach to friction and wear." San Antonio 1967 s. 335-384.

4. Matvejevski R.M.,Bujanovski I.A.: *Protivo zadirnaja stoikost smazochnych sred pri trenii v rezhimie granichnoj smazki*. Wyd. Nauka Moskva 1978 r.

5. Pytko S.: *Podstawy tribologii i techniki smarowania.* Wyd. AGH, Kraków 1989

6. Pytko S.: *Methods of tests with application of four-ball machine*. Proc. "Trobotechnika v teorii a praxi" Karlowe Wary 1989 t.1 s. 35-44

7. Rymuza Z., Pytko S.: *Scaling in friction experiment*. Proc. First Intern. Brazilian Conference on Tribology. Rio de Janeiro 2010.

8. Szczerek M., Tuszyński W.: *Badania tribologiczne-zacieranie*. Wyd. Inst.Techn. Eksploatacji Radom. 2000 r.

9. Kragielski I.V.: *Trenije i iznos*. Moskva 1968 r.

4.2.2 THE CALCULATED - EXPERIMENTAL METHODOLOGY OF RESEARCH FRICTION CHARACTERISTICS UNDER BOUNDARY LUBRICATION

Dykha O.[1], Babak O.[1], Skrypnyk T.[1], Posonskiy S.[1]

Introduction

Among known test methods of of friction units with lubrication the most perfect are tests under the four-ball scheme. This is standard method and it is

[1] Khmelnitsky National University, Ukraine

widely applied all over the world [1] (in Russia - ГОСТ 9490-75; in USA - ASTMD 2596, ASTMD 2783; in Germany - DIN 51350; in Poland - PN - 76/C - 04147; in England - IP 300; in Bulgaria БДС 14150-77). The main defect of the test there is absence of the mathematical description of the wear process on this scheme. This brings only to qualitative description of the process. Besides four -ball test use only standard material from become 52100 steel balls. But scheme of the external contact two balls not adequately prototypes the contact of the real interfacing the of friction units of the machines.

In this connection in given work was put problem to give the quantitative description of the wear process samples for different schemes of the tests and materials. The base of the decision of the problem there is decisions direct and inverse war - conact tasks for contact and wear samples of the different form [2-4]. And as a result get the mathematical models of the wear process with using the accounting programs.

1. Technique of construction of models of wear process on an example of the four-ball scheme

The scheme of tests is considered at which top sphere rotates and bases with effort Q to three motionless bottom spheres (fig. 1). As a result of tests for the bottom spheres the circular platform of wear process of radius a is formed. By influence of elastic deformations of spheres on formation of a platform of contact it is neglected. The zone of contact top and the bottom spheres is filled by the lubricant material.
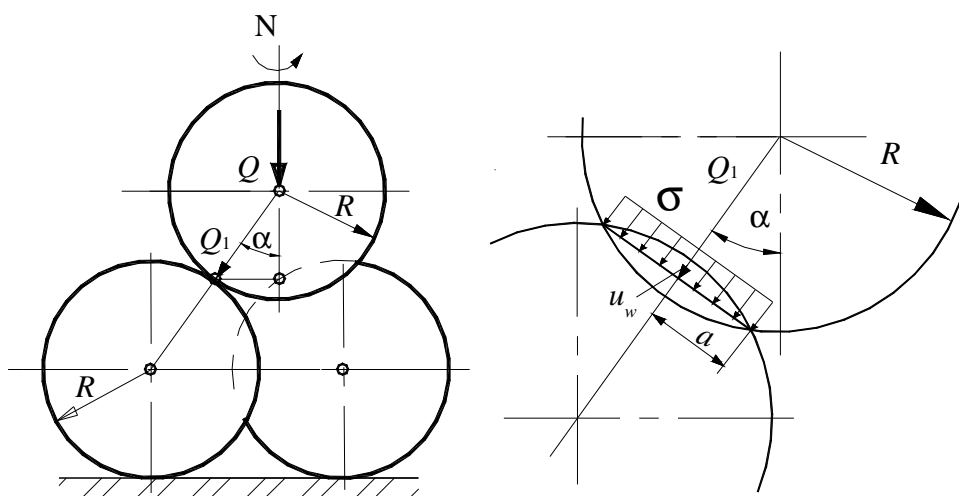

Fig. 1. Schem of four-ball wear test

For the description of the wear process of the bottom spheres under the accepted scheme of test the model in the form of dependence of intensity of wear process on two parameters is accepted: loadings and speeds of sliding:

$$I = \frac{du_w}{dS} = k_w \left(\frac{\sigma}{E^*} \right)^m \left(\frac{VR^*}{\nu} \right)^n, \qquad (1)$$

where σ – contact pressures;

E^* –the resulted module of elasticity of materials of contacting spheres;

V – the relative speed of sliding;

R^* – the resulted radius of contacting spheres;

ν – the kinematic viscosity of a lubricant (at 100 °C);

u_w – the linear wear of the bottom spheres;

S – the way of friction for the bottom spheres;

K_w, m, n – the parameters of model of wear process.

Dependence of linear deterioration u_w on radius of a platform of wear process a of the bottom spheres is defined from geometry of crossing of spherical surfaces (fig.1):

$$u_w(S) = \frac{a(S)^2}{2R}. \qquad (2)$$

From tests it is possible receive dependence of radius of a circular platform of wear process on a way of friction in the form of sedate approximation:

$$a(S) = cS^\beta, \qquad (3)$$

where c, β – the parameters of approximation.

At uniform distribution of contact pressure on a platform of contact from a condition of balance in contact of spheres it is had:

$$\sigma = \frac{0{,}4082Q}{\pi a^2}. \qquad (4)$$

After substitution (2-4) in (1) and integration, we shall receive:

$$\frac{c^2 S^{2\beta}}{2R} = K_W \left(\frac{0,4082Q}{c^2 \pi E^*} \right)^m \left(\frac{VR^*}{v} \right)^n \frac{S^{1-2\beta m}}{1-2\beta m}. \qquad (5)$$

Whence m from a condition of feasibility of the equation (5) at any s it will be determined:

$$m = \frac{1-2\beta}{2\beta}. \qquad (6)$$

For a finding of parameter n tests are spent at two values of speed of sliding V_1 and V_2 and two groups of data with parameters receive:

$$a = c_1 S^{\beta_1}; \quad a = c_2 S^{\beta_2}. \qquad (7)$$

At constant test specifications for the wear process is accepted $\beta_1 = \beta_2 \approx \beta$.

Substituting expressions (7) in (5), we shall receive system of two equations:

$$\left. \begin{array}{c} \dfrac{c_1^2 S^{2\beta}}{2R} = K_W \left(\dfrac{0,4082Q}{c_1^2 \pi E^*} \right)^m \left(\dfrac{V_1 R^*}{v} \right)^n \dfrac{S^{1-2\beta m}}{1-2\beta m} \\[4mm] \dfrac{c_2^2 S^{2\beta}}{2R} = K_W \left(\dfrac{0,4082Q}{c_2^2 \pi E^*} \right)^m \left(\dfrac{V_2 R^*}{v} \right)^n \dfrac{S^{1-2\beta m}}{1-2\beta m} \end{array} \right\}. \qquad (8)$$

For definition of parameter n we shall divide the first equation into the second and after transformations we shall receive:

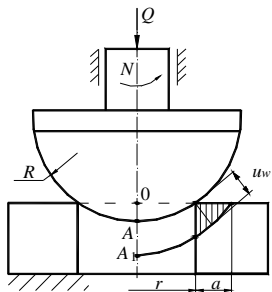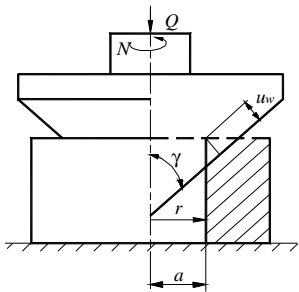$$n = (2m + 2) \frac{\lg(c_1/c_2)}{\lg(V_1/V_2)}. \qquad (9)$$

For a finding of factor K_w we shall take advantage of one of the equations (8):

$$K_w = \frac{\beta c_1^{2m+2}}{R} \left(\frac{2\pi E^*}{0,4082Q} \right)^m \left(\frac{v}{V_1 R^*} \right)^n. \qquad (10)$$

2. Results of modelling of wear process at tests under schemes: a sphere-ring, a cone-ring.

The scheme of contact of four spheres is used for test interfaces of not similar form from steel materials (gearings, cam mechanisms, bearings, etc.) For test materials of sliding bearings, including polymeric for interfaces of the similar form (sliding bearings, hinges, etc.) the sphere - a ring is offered to use for tests the scheme. For expansion of types of tests of constructional materials the third scheme of tests a cone - a ring is offered. Manufacturing of the conic sample more simple, than manufacturing of a sphere.

Table 1 - The schemes of tests and parameters of models of wear process

Parameters	Ball – ring	Cone – ring
m	$m = \dfrac{1-\beta}{\beta}$	$m = \dfrac{1-\beta}{\beta}$
n	$n = (m+1)\dfrac{\lg(c_1/c_2)}{\lg(V_1/V_2)}$	$n = (m+1)\dfrac{\lg(c_1/c_2)}{\lg(V_1/V_2)}$
K_W	$K_w = \dfrac{\beta c_1^{m+1} r^{m+1}}{R}\left(\dfrac{2\pi E^*}{Q}\right)^m\left(\dfrac{\nu}{V_1 R^*}\right)^n$	$K_w = \beta c_1^{m+1}\cos\gamma\left(\dfrac{2\pi r E^*}{Q}\right)^m\left(\dfrac{\nu}{V_1 R^*}\right)^n$

As the general form of model of wear process is used the form (1).

The schemes for calculation and results of definition of parameters of models of wear process are shown in table 1.

3. The device for tests

For quantitative definition of parameters of models of wear process by results of laboratory researches the device for tests on the basis of four - ball

machines of friction has been designed by means of program Solid Works (fig.2).

The top sphere 1 is based in an aperture of the end of a spindle. It does not suppose palpation of a sphere at rotation and increases rigidity of unit. The bottom three spheres in 2 diameter of 12,7 mm are installed on tempered surface of a support 4. The top plane of a nut 3 is used as measuring base for measurr size of wear. The wear is measured without disassembly of the device. For measurement of the sizes of spots of wear process on the bottom spheres microscope МПБ-2 with by division of 0,05 mm is used. After measurements of wear process of test proceed under the accepted program.
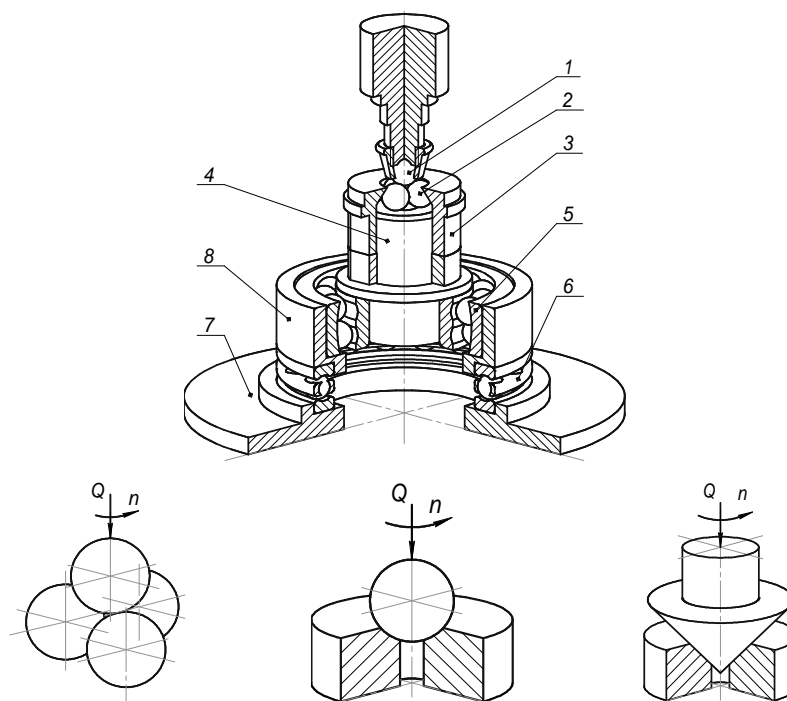

Fig. 2. The device for tests

Exception of skews and self-installation at contact of spheres is provided with spherical bearing 5.

For measurement of the moment of friction the persistent bearing 6 is used. The top sphere is loaded by means of the lever with the transfer attitude $k = 3,25$.

The thermometer of ЭТП-М is applied to the control of temperature to a zone of friction of spheres. A sensitive element of the thermometer (pos. 9, fig.

2) it is placed in a support under the bottom spheres. During tests the continuous control of temperature of greasing over a zone of friction is carried out.

4. Results of tests of lubricant and constructional materials

For research of influencing of speed of sliding two types of lubricating materials were explored:

1. M6/12 – Г1, $\nu = 12$ mm^2/s;

2. 15W-40, $\nu = 15$ mm^{2}s.

The tests were conducted on the four-ball test machine of friction at the following terms:

1. Diameters of overhead and lower spheres 12,7 mm.

2. Loading on an overhead sphere 65 N;

3. Frequencies of rotation of overhead sphere $N_1 = 200$ rev/min, $N_2 = 500$ rev/min ($V_1 = 0,077$ m/s, $V_2 = 0,192$ m/s).

The results of tests are presented in tabl. 2.

Table 2 - Middle sizes of radiuses of tearing down of lower balls, in mm

Lubricant	20 min	40 min	60 min	90 min	120 min
			$n = 200$ rev/min		
М6-12Г	0,55	0,73	0,79	0,80	0,80
			$n = 500$ rev/min		
М6-12Г	0,61	0,80	0,80	0,81	0,82
			$n = 200$ rev/min		
15W-40	0,50	0,65	0,66	0,69	0,71
			$n = 500$ rev/min		
15W-40	0,57	0,70	0,73	0,77	0,80

Graphic interpretation of results of tests is shown on fig.3.
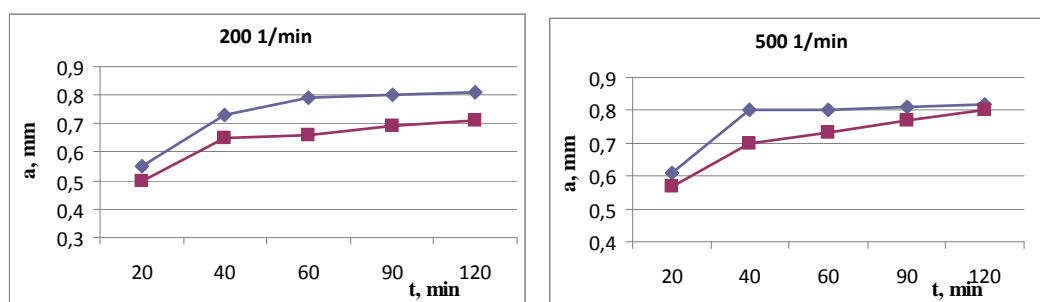

Fig. 3. Dependence of size of wear on time (♦ – M6-12Г; ■ –15W-40)

Options durability algorithm dependencies were calculated using MathCad.

Parameters of approximation of experimental features were determined using Excel.

Example of calculation for the first type for oil M6-12Г below.

Table 3 - Parametres of wear

Lubricant	M6-12Г	15W-40
β	0,272	0,266
c_1, mm$^{1-\beta}$ (200 rev/min)	0,0367	0,0353
c_2, mm$^{1-\beta}$ (500 rev/min)	0,0347	0,0339
m	1,674	1,759
n	-0,328	-0,232
K_W	0,026	0,018

After implementation of the current algorithm obtained the necessary parameters approximating function and parameters of the function of intensity of wear, presented in Table. 3.

The values obtained in dimensionless complex parameters of intensity of wear make it possible to quantify the impact factors of the contact pressure and sliding speed of wear.
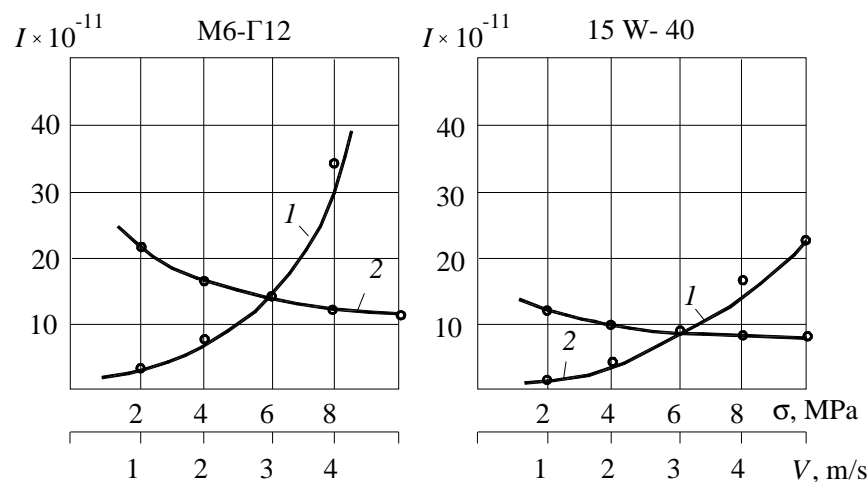

Fig. 4. Dependence of wear intensity of the contact pressure (1)
and sliding speed (2)

Fig. 4 presented graphic intensity of wear of contact pressure and sliding speed, built on the basis of the accepted models wear with the parameters obtained and calculated as a result of tests carried out two types of lubricants for two values of velocity slip. These options allow you to define models wear intensity values of wear of friction units, working with the specified lubricants for different load and speed conditions of sliding. General analysis of the results clearly indicates increasing wear resistance with increasing slip speed in the working range of settings in which trials were conducted for both types of lubricants.

Conclusion

Presented experimental research methodology estimated the impact speed sliding wear of friction units based on the results of laboratory tests for four-ball cheme under boundary lubrication

Refrences

1. Крагельский И. В. Трение и износ / И. В. Крагельский. – М.: Машгиз, 1962. – 383 с.

2. Справочник по триботехнике / под общ. ред. М. Хебды, А. В. Чичинадзе : в 3 т. – Т. 1. Теоретические основы. – М. : Машиностроение, 1989. – 400 с.

3. Кузьменко А. Г Контакт, трение и износ смазанных поверхностей. Монография / А.Г.Кузьменко, А.В. Дыха. – Хмельницкий: ХНУ, 2007. – 344 с.

5. NEW ASPECTS IN TECHNOLOGIES OF PROCESSING OF MATERIALS

5.1. PROCESSING OF METAL

5.1.1 RESEARCH THE PROPERTIES, STRUCTURE AND MACHNINING CAPABILITIES SINTERED CORUNDUM ABRASIVES
Niżankowski Cz.[1]

Introduction

For over thirty years we observe a very intensive development of production of alumin aabrasives sintered [1].

Impetus to this development has been the one hand, the need to reduce production costs electricalkorundum abrasives, on the other hand need to produce a finer abrasive characteristics of supplies. The first objective was achieved mainly by lowering the temperature of manufacture abrasives corundum by sintering, because of the abrasive classic noble elektrokorundu melted at ca 2650K as opposed to sintered alumina abrasives with which the synthesis takes place mainly at temperatures ranging from 1430K to 1970K. The second objective was achieved as by the possibility of producing abrasive grains oz up a given shape, and by utilizing the properties of the manufactured abrasives ultrafine structure. Structure of sintered alumina abrasives of the implementation process as it allows micromachining in a self-sharpening of abrasive particles, which improves not only to increase the sustainability of grinding wheels and abrasive belts, but also to improve the geometric structure and physico-chemical machined surface layer [1,2]. The first synthesis of abrasive grains on a normal sintered alumina was performed in late 1974 in a well-known American corporation 3M (Minnesota Minig and Manufacturing Corporation), but it was only in 1979 it was the abrasive used in wheels to be called. Highpressure grinding, which aims to remove the damaged layers deep from the surface of billets, slabs and plates of steel [3].

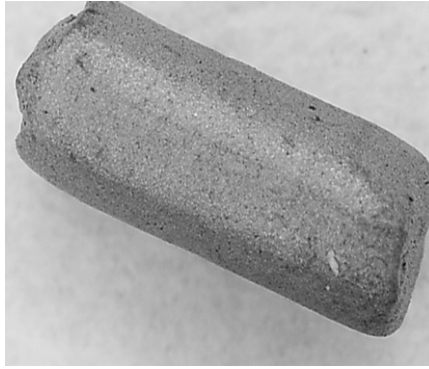[1] Instytut Technologii Maszyn i Automatyzacji Produkcji

Fig. 1. General view of abrasive grain 76A of ordinary sintered alumina [2]

In 1983, the same corporation conducted by sol-gel synthesis of the first alumina sintered submicrocrystalline, a trade name Cubitron (CB).

Fig.2. Exterior grit Cubitron (CB) with submicrocrystalline sintered alumina [1]

However, the abrasive tools of this appeared abrasive tool on the market until after 1990. Area of their application was really impressive, from coarse to fine grinding [1,3]. In 2006, Rappold Austrian company announced that it has synthesized 'nanocrystalline' sintered alumina. In fact, the abrasive is produced with the characteristic dimension of crystallites of a few hundredths of meters [4], layer by chemical deposition from the gas phase chemical reactions involving the activation of the atmosphere by means of glow discharge, or by PACVD (Plasma Assisted Chemical Vapour Deposition). It is estimated that currently as many as six countries of the world (U.S., PRC, FR, Japan, Germany and Austria) are manufactured in sintered alumina abrasive in a full range of structural and that the size crystalline few μ meters, just a few tenths of a few hundredths of μ meters [4].
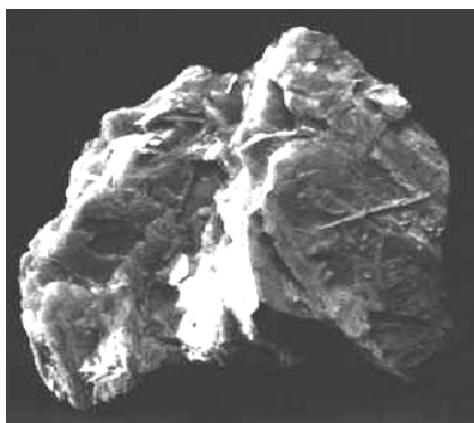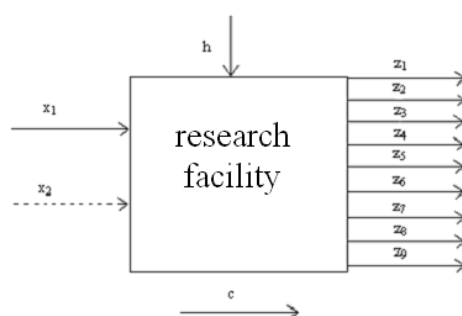
Fig. 3. Exterior grit NanoWin (NW) with nanocrystalline alumina sintered [4]

1. Overview of experimental studies

1.1. Diagram of research and description of the factors

X-size of the input:

x_1 - the size of crystallites in the sintered alumina abrasive grains (a species of grain);

x_2 - cutting speed (only for Z9);

Z – output;

z_1 - the shape of abrasive grains;

z_2 - abrasive grain structure;

z_3 - density abrasive;

z_4 - the content of magnetic fraction;

z_5 - abrasive ductility;

Z_6 - chemical composition of the abrasive;

z_7 – microhardness;

z_8 - compressive strength;

z_9 - the machining ability abrasive grains (the relative efficiency of grinding);

C - constant volume;

c_1 - sets of abrasive grains;

c_2 - used equipment for measuring and testing;

c_3 - the application of research methods and techniques;

H- size interfering;

(Eg, crystallite size dispersion).

1.2. Research Methodology

The study was conducted according to the elemental, the static, deterministic, complete plan experience (PSDK) without repetition of individual systems of the plan, due to the high cost of effort and research. Adopted the following levels of the input x1:

1) $x_1 = 0,02 \pm 0,01$ μm   (NW)

2) $x_1 = 0,2 \pm 0,1$ μm   (CB)

3) $x_1 = 2 \pm 1$ μm   (76A)

The ability of abrasive grains sliced determined by the relative performance micromachining.

$$Z = \frac{G_S}{G_M} \%, \tag{1}$$

where : G_m- Chip load;

G_s - weight loss grit.

1.3. Tech Research

The study used abrasive type 76A, and Cubitron NanoWin 24th seed numbers The shapes of abrasive grains have been determined by measuring the size of bulky microscope at a special m.μworkshop with an accuracy of 1 Abrasive grain structure studied was observed on a JEOL JSM scanning electron microscope type LV-5510 coupled with the desktop computer. Densities were determined using abrasives pycnometer in a traditional way. The content of magnetic fraction was determined using a magnetic analyzer production of the USSR. However, ductility abrasive resistance was determined by a special

grinding ball mill followed by sieving on sieves FRITSCH GmbH. Chemical compositions of tested abrasives determined using X-ray spectrometer, and was determined by Vickers microhardness. The compressive strength determined on the hydraulic press using a special device made in CP. Capacity indicator machining abrasive grains determined by formulas (1) referring machining weight material (microchip) for weight loss abrasive material after from the socket smelting honing.

Fig.4. General view of the position to determine the ability of abrasive grains machining

2. Test results

The obtained experimental results are presented below in the form of histograms [5].
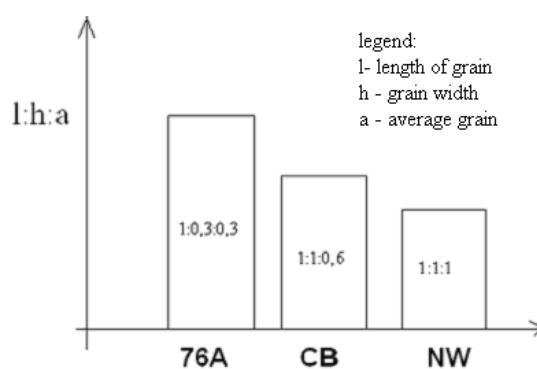

Fig.5. Comparison of grain shape indices
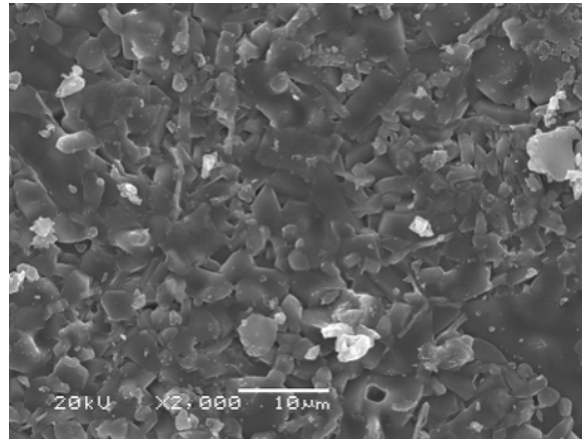
Fig.6. Microstructure grit 76A alumina sintered ordinary (pow.2000x)
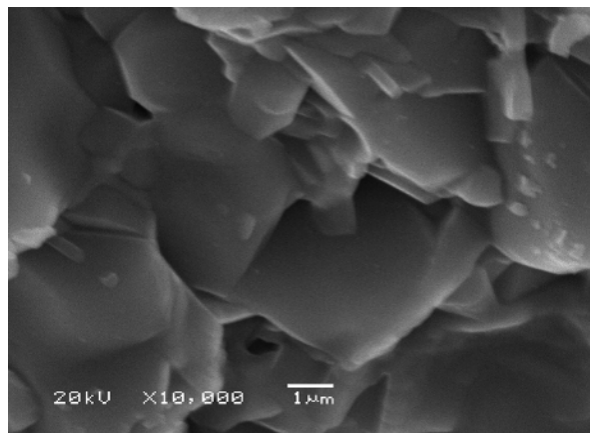
Fig.7. Microstructure grit 76A alumina sintered ordinary (pow.10000x)
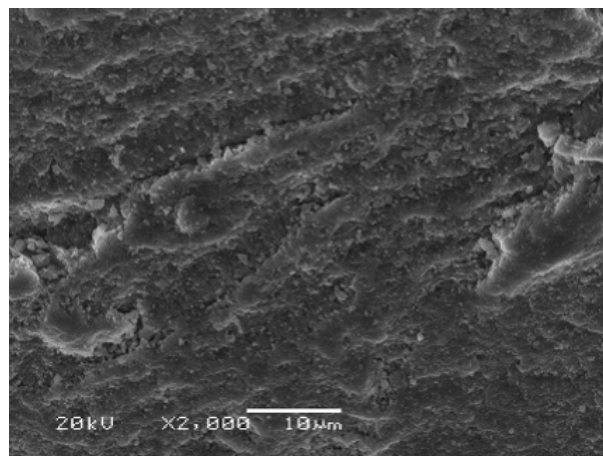
Fig.8. Microstructure grit Cubitron (CB) from s submicrocrystalline sintered corundum (pow.2000x)

Photo microstructure grit NanoWin (NW) is not given in the paper due to the fact that, with the greatest magnification scanning electron microscope could see only a black background with gray points.
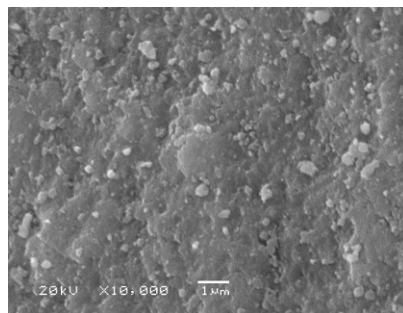
Fig.9. Mikrostruktura grain ściernrgo Cubitron (CB) of alumina submicrocrystalline Sintered (pow.10000x)
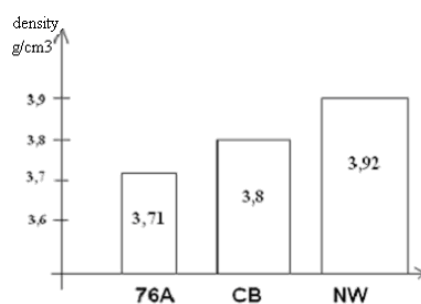
Fig.10. Comparison of the density tested abrasives
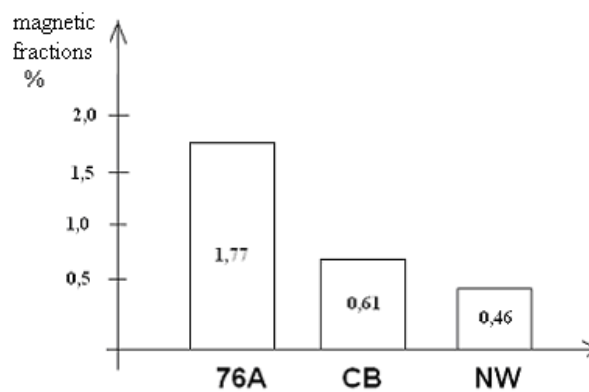
Fig.11. Comparison of the magnetic fraction tested abrasives

Table 1 - Comparison of chemical compositions investigated abrasives

Compound	76A	CB	NW
Symbol	% mass	% mass	% mass
Al_2O_3	87,5	94,5	98,0
ZrO_2	------	Scanty	Scanty
TiO_2	3,5	Scanty	Scanty
SiO_2	4,0	--------	------
Fe2O3	4,5	1,5	0,6
MgO	--------	3,4	1,3
CaO	Scanty	Scanty	--------
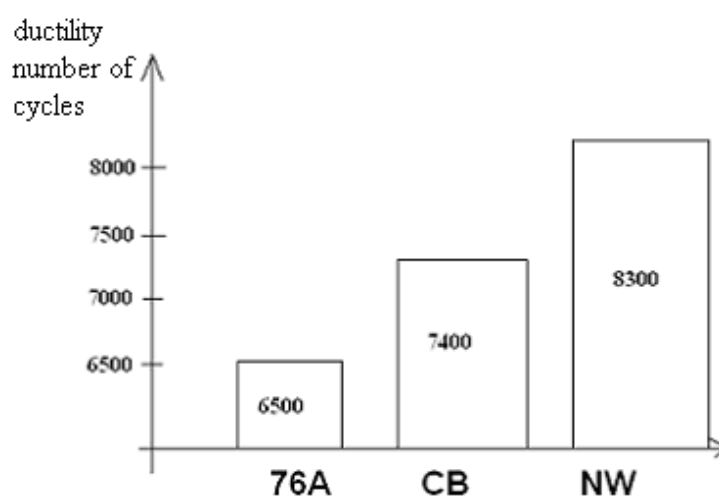
Fig.12. Comparison of toughness tested abrasives
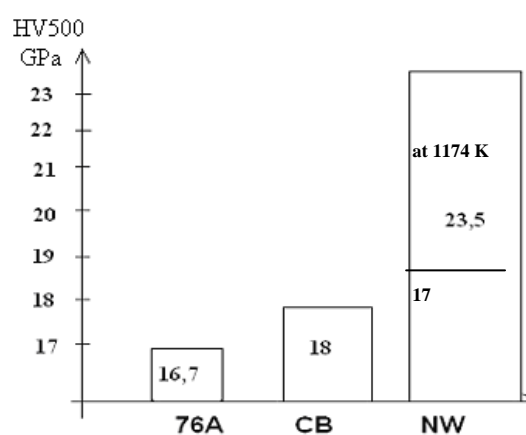
Fig.13. Comparison of microhardness test of abrasive grains.
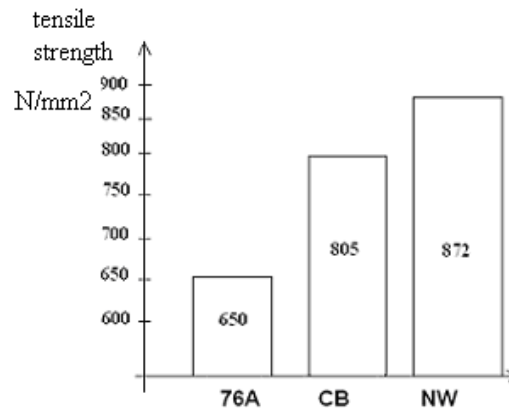
Fig.14. Comparison of compressive strength abrasives tested

The ability of abrasive grains machining respondents identified in the process of turning toughened to the hardness of HRC 42 ± conical cylinders of alloy steel construction, designed specifically for the manufacture of the equipment loaded. As the blades of cutting tools used abrasive grain abrasive test soldered on the frame honing onegrain flange (after checking the angles of corners)

Carried out on a high speed turning, precision lathe with stepless speed control spindle. Cutting speed varied from 4 to 10 m/s at 2 m/s.

Microchipmass and weight loss cutting abrasive grains (after smelting) was measured using laboratory balance.
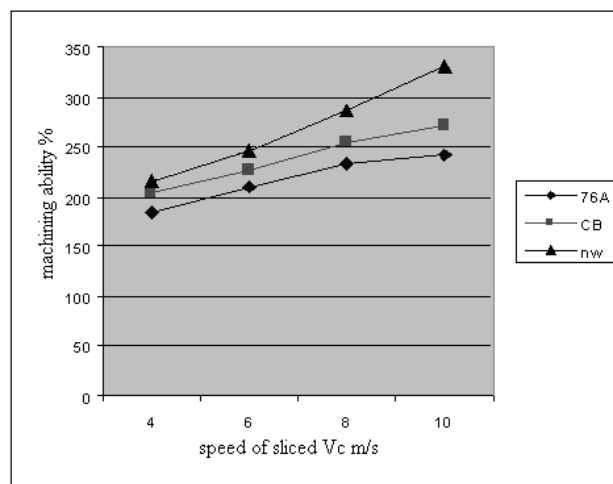
Fig.15. Comparison of the capacity of machined respondents abrasive grains according to the speed micromachining
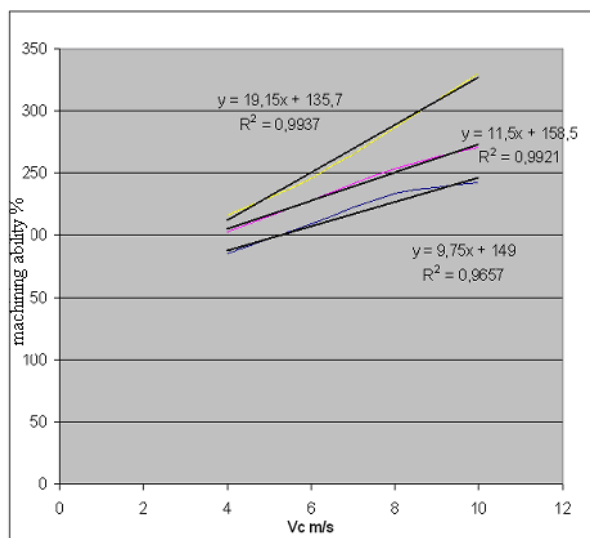
Fig.16. Comparison of the machining ability respondents abrasive grains according to the speed micromachining

On the basis of experimental results determined following function test objects:

• the machining ability grit 76A alumina sintered ordinary

$$Z = 149 + 9.75 \text{ vc.} \tag{2}$$

With a coefficient of determination

$$R^2 = 0{,}9657. \tag{3}$$

• the ability to grit machining CB

$$Z = 158{,}5 + 11{,}5 \text{ } v_c \tag{4}$$

With a coefficient of determination

$$R^2 = 0{,}9921 \tag{5}$$

• the ability to grit machining NW

$$Z = 135.7 + 19.15 \text{ Vc} \tag{6}$$
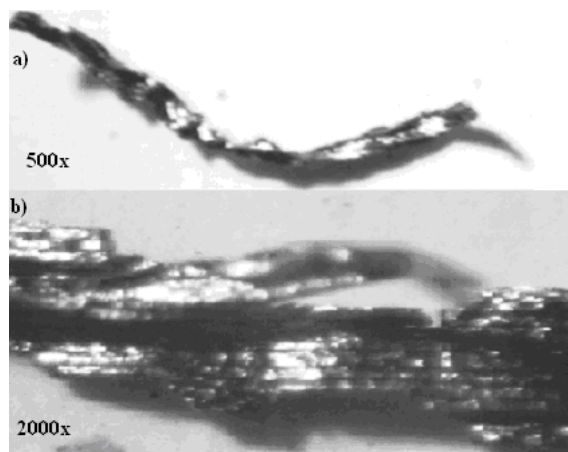
Fig.17. Chips obtained by micromachining sintered corundum grains in the process of rolling

With a coefficient of determination

$$R^2 = 0,9937 \tag{7}$$

Characteristic bands on the surface of the chip flow traces of the many submicroedges (crystallite) sintered alumina abrasive particles.

Conclusion

The results of experimental studies permit the following conclusions:

• together with the reduction of crystallite size of abrasive grains of alumina sintered getting better all the properties of abrasive grains,

• differences in the shapes of abrasive grains examined and small differences in their chemical compositions resulting from the manufacturing technology,

• the ability to spark sintered alumina abrasive particles increases with cutting speed. This increase is all the more intense their magnitude crystallites forming the structure of the grains is lower. Therefore NanoWin abrasive type is preferably used only at high cutting speeds

References

1 Niżankowski Cz. ,Badania właściwości ściernic typu Cubitron 3M. Podstawy i technika obróbki ściernej. Wyd.WSI Ksz.,Koszalin 1993 str.17-22 [2] Niżankowski Cz.,Właściwości skrawne ściernic z korundu spiekanego. Monografia 205.Zakł.Graf.PK, Kraków 1996.

3 Staniewicz – Brudnik B.Wodnicka K.,Jaworska L.,Wilk Wl., The effect of the high energetic milling on the polymorphic Changes of submikrocrystaline sintered korundum grains. Współczesne problemy obróbki ściernej . Wyd.Ucz. PKSz., Koszalin 2009 str 43-52.

4 Katalogi firmy Rappold 2008.

5   Niżankowski Cz. Properties, structure and machnining capabilities sintered corundum abrasives. Archives of Foundry Engineering, Vol. 8, No. 27 Gliwice 2010, p. 57-62

5.1.2 ROLA PRĘDKOŚCI W PROCESACH SKRAWANIA
Liubymov V.[1], Cwanek J.[1]

Wpływ prędkości na przebieg procesu skrawania potrzebuje specjalnego rozważania. To jest tym bardziej ważne ponieważ współczesny przemysł wchodzi w strefę obróbki z dużymi prędkościami (High Speed Machining).

Prędkość jest najbardziej wpływowym parametrem procesu obróbki skrawaniem. Od niej, bowiem, zależy w dominującym stopniu bilans cieplny w obszarze skrawania, zużycie narzędzia skrawającego, stan i struktura powierzchni obrobionej. Ale to jest wpływ na przebieg wtórnych procesów w strefach 2 i 3 (rys. 2). Co do procesów pierwotnych mających miejsce w strefie 1, to tu wpływ prędkości skrawania, jak to nie dziwnie brzmi, jest minimalny. Spróbujmy to wyjaśnić.
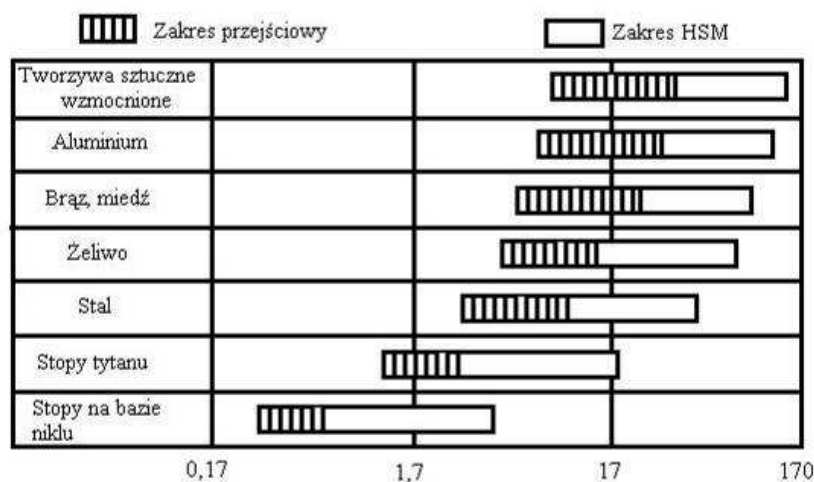
Rys.1. Prędkości skrawania (m/s) przy obróbce konstrukcyjnych materiałów

---

[1] Politechnika Rzeszowska

Podstawowymi i jedynymi procesami w strefie 1 są procesy odkształceń plastycznych i procesy pękania: kruchego, plastycznego (ciągliwego) lub mieszanego. Ważnym jest to, że inicjacja pękania nie zależy od prędkości inicjacji, ale tylko i wyłącznie od działających w miejscach inicjacji naprężeń.
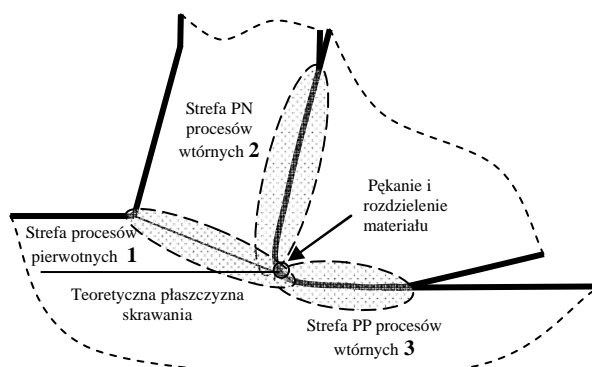
Rys.2. Strefy odkształceń plastycznych w obszarze skrawania

Odkształcenia plastyczne cechują się poziomem ε. Poziom odkształceń ε= ctgφ + tg(φ − γ) zależy wyłącznie od parametrów geometrycznych strefy skrawania, mianowicie, od kąta ścinania φ i kąta natarcia γ narzędzia skrawającego. Natomiast prędkość (gradient) odkształceń w strefie poślizgu zależy od dwóch parametrów: prędkości poślizgu v_{sh} i grubości pasma poślizgu ΔX. Przypomnijmy sobie ten wzór: $\dot{\varepsilon} = v_{sh}/ \Delta X$. Biorąc pod uwagę, że moduł prędkości $m_v \approx 10^1$, moduł grubości pasma poślizgu $m_{\Delta x} = 10^{-8}$, otrzymujemy moduł zależności prędkości odkształceń od prędkości skrawania, (związanej z prędkością ścinania $v_{sh} \approx v_c \cdot 1,2$) jako $m_{\Delta \varepsilon} = 10^{-7}$ Błąd takiego rzędu można traktować jako błąd znikomo mały w porównaniu z obserwującym się doświadczalnie wpływem prędkości skrawania na procesy odkształceń i pękania w strefie procesów pierwotnych. A to znaczy, że objaśnienie związków skutkowo – przyczynowy tego zjawiska trzeba szukać gdzie-indziej.

Opór materiału odkształceniom plastycznym zależy od stopnia realizacji dwóch konkurujących między sobą procesów: umocnienia odkształceniowego, jakie zależy bezpośrednio od prędkości odkształceń, i osłabienia cieplnego, przy czym zwiększenie prędkości tłumi procesy osłabienia.

Wpływ ciepła zewnętrznego na procesy odkształceniowe w strefie skrawania 1 jest znikomy (patrz rys. 3). Pozostaje tylko prędkość.
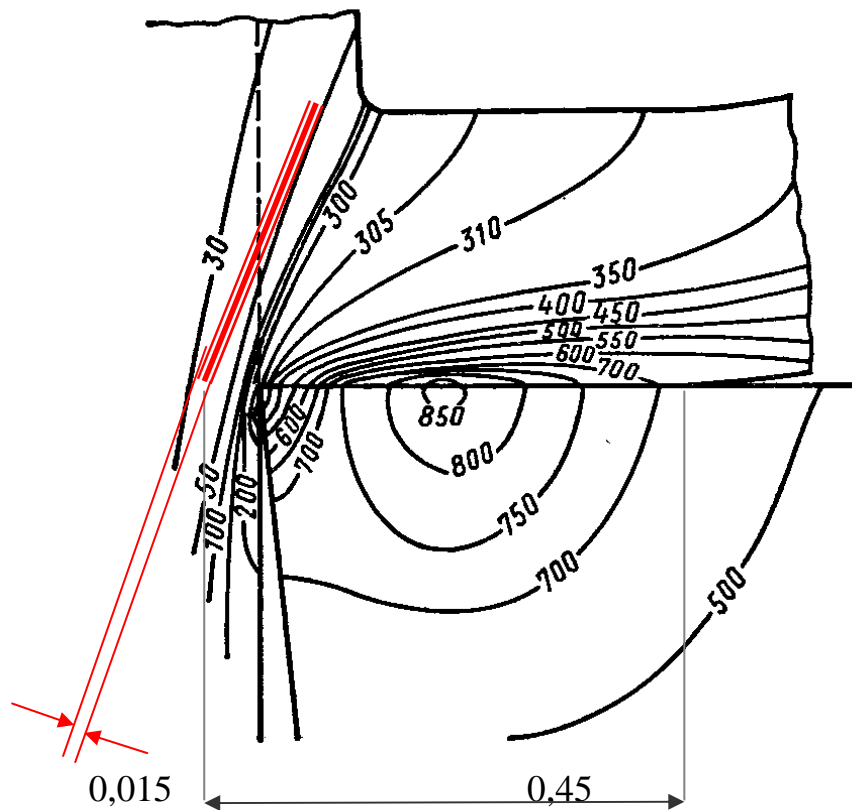
Rys.3. Rozkład temperatur w obszarze skrawania.
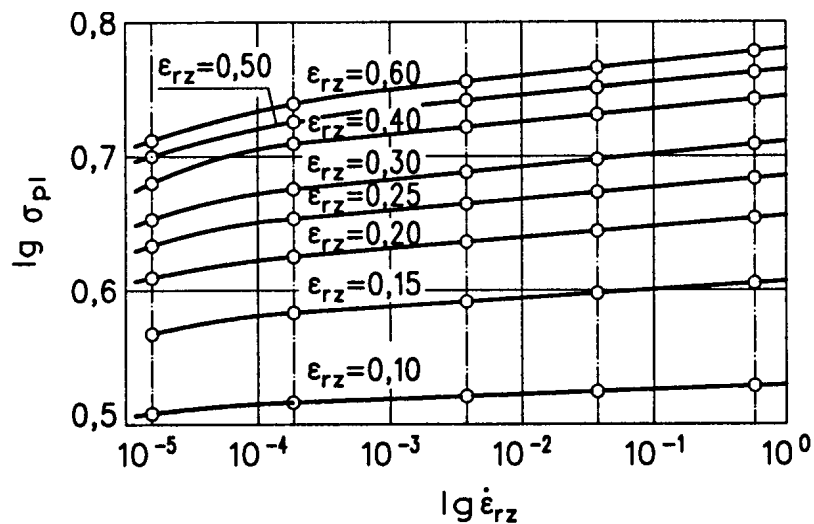
Rys.4. Wpływ prędkości odkształceń na naprężenie uplastyczniające przy różnych odkształceniach rzeczywistych ε$_{rz}$ wg J. Sieniawskiego i J. Klepaczki, materiał – aluminium.

411

Z fizycznej teorii plastyczności wynika, że wzrost prędkości odkształcenia plastycznego powoduje zwiększenie współczynnika umocnienia odkształceniowego i wskutek tego – naprężenia płynięcia plastycznego (rys.4).

Z tego można wyciągać kilka wniosków wśród których podstawowe są:

• razem ze wzrostem prędkości odkształcenia wzrasta naprężenie uplastyczniające,

• biorąc pod uwagę moduł skal, przychodzimy do wniosku, że wpływ $\dot{\varepsilon}_{rz}$ na σ_{pe} jest prawie nieznaczący.

W pewnym sensie to się potwierdza badaniami prof. W.Grzesika wpływu prędkości skrawania na wskaźniki odkształceń plastycznych w strefie skrawania (rys.5).

Przebiegi 1, 2, 3a na rys.5 dotyczą toczenia stali 45, a przebiegi 3b, 3c i 3d – odpowiednio stali ZH15, aluminium i miedzi.

Interesującą informację o wpływie prędkości na procesy odkształceń i pękania zawierają badania dynamicznej wytrzymałości prof. G. I. Pogodina-Aleksiejewa w próbach udarności.
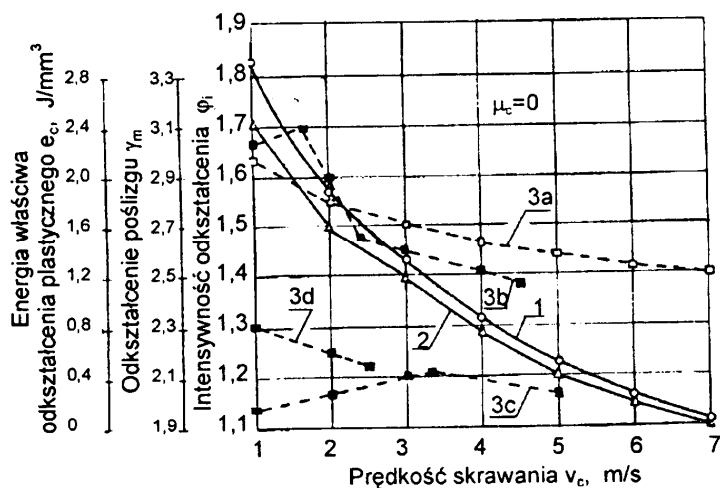
Rys.5. Wpływ prędkości skrawania na wskaźniki odkształceń plastycznych: 1-intensywność odkształceń, 2 – odkształcenie poślizgu, 3 – energia właściwa odkształcenia plastycznego.

Po-pierwsze, sama metoda badań stwarza warunki obciążeń w pewnym stopniu zbliżające się do warunków procesu skrawania, np. strugania lub okrawania na prasach. Po-drugie, próby udarności na młotach prowadzą się z prędkościami do 100 m/s, takimi samymi, jak i obróbka skrawaniem. Spróbujmy

skorzystać się z wyników badań kruchości na zimno. Zbadano wpływ prędkości uderzenia młótu udarowego (analog prędkości skrawania v_c) na poziom progu kruchości. Rezultaty przytoczono w tablicy 1.

Table 1 - Temperatura progu kruchości na simno dla stali St5.

Parametr chropowatości Ra,μm	Temperatura progu kruchości w ^{0}C dla prędkości, m/s		
	5	50	75
5,80-6,20	- 97	- 61	- 52
2,20-2,50	- 105	- 71	- 62
0,90-1,12	- 105	- 97	- 71

Pierwszy wniosek z przytoczonych w tablicy wyników jest taki, że temperatura progu kruchości zmniejsza się razem z wzrostem chropowatości próbki. Wniosek jest interesujący, logiczny, ale nie dotyczy procesu skrawania. W kontekście naszych rozważań znacznie bardziej interesujący jest drugi wniosek, mianowicie: zwiększenie prędkości badania wyraźnie przesuwa przedział kruchości w stronę wyższych temperatur, a to znaczy czyni próbki bardziej kruchymi. Takie stwierdzenie w zasadzie swojej, nie jest sprzecznym z dyslokacyjnym podejściem do problemu wpływu prędkości na procesy odkształceń i pękania. Udowodniono, bowiem, że wzrost prędkości powoduje wzrost liczby pasm poślizgu i skrócenie ich długości, co tworzy dość efektywną barierę do propagacji dyslokacji. Przykładowo, dla miedzi średnia długość przemieszczenia dyslokacji podczas odkształceń jest dwu – trzykrotnie mniejsza niż podczas odkształceń statycznych. Z tego można byłoby wnioskować, że w procesie skrawania wzrost prędkości skrawania powołuje zmniejszenie plastyczności materiału w strefie obróbkowej. Ale w rzeczywistości to nie jest dokładnie tak. Zatem, pamiętamy, że kruchość na zimno jest raczej anomalią plastyczności.

Zwykle uważa się, że prędkość deformacji i temperatura okazują przeciwny wpływ na wartość naprężenia płynięcia, ale wskutek tego, że na płaszczyźnie ścinania obydwaj te parametry przyjmują duże wartości, efekty ich działania są wzajemnie zrównoważone. I tu zakrada się błąd. Faktor temperatury bowiem nie odgrywa w strefie ścinania żadnej roli (patrz rys.3). Pozostaje tylko prędkość odkształceń.

W swoich fundamentalnych pracach A.H.Cottrell przeanalizował zjawisko płynięcia plastycznego przy dużych prędkościach odkształceń $\dot{\varepsilon}$ i pokazał, że po przekroczeniu pewnej krytycznej wartości naprężenie płynięcia staje niezależnym od prędkości deformacji. W tym przypadku odkształcenia zaczynają katastrofalnie rosnąć przy jakiejkolwiek wartości przyłożenia naprężenia (zjawisko nadplastyczności). Kabajaszy i Tompsen udowodnili, stosownie do warunków skrawania, że naprężenia poślizgu przy dużych prędkościach nie zależą od temperatury, i umocnienia materiału, co znów nie do końca wyjaśnia rolę prędkości w procesach skrawania oraz jej wpływ na przebieg odkształceń plastycznych i pękanie materiału w strefie procesów pierwotnych.

Indze, trzeba szukać innych możliwych objaśnień. Zwróćmy się do kryterium Yoffe"a. Wg niego stan materiału zależy od ilości naładowanej do materiału energii zewnętrznej. W przypadku skrawania materiał przyjmuje dawkę energii zewnętrznej jedynie w postacie energii mechanicznej $E = v_c \cdot F$. Siła skrawania przy stałym przekroju warstwy skrawanej w zależności od prędkości skrawania zmienia się nieznacznie (proporcjonalnie $v_c^{-0,15}$), a to znaczy, że ilość skoncentrowanej w strefie skrawania energii zależy praktycznie tylko od prędkości skrawania. Z tego wynika interesujący wniosek: w szerokim zakresie zwiększenia prędkości skrawania (np. w procesach HSC) materiał obrabiany może zmieniać swój stan z kruchego poprzez mieszany do plastycznego. Oczywistym jest, że próg kruchości zależże przede wszystkim od właściwości materiału obrabianego, jak to pokazano na rys.6.
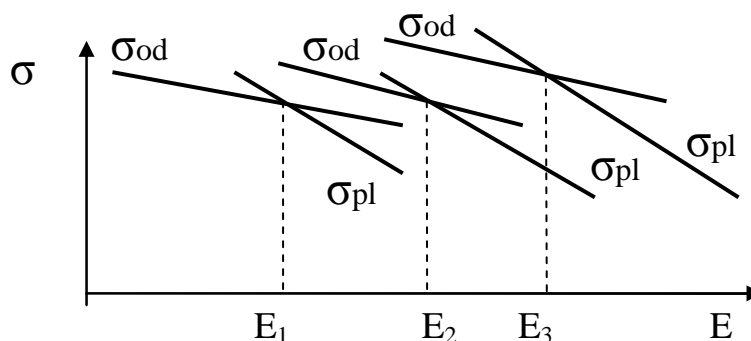
Rys.6. Schemat Yoffe"a dla materiałów o różnych progach kruchości, E- energia zewnęczna, σod- naprężenie pękania kruchego, σpl- granica plastyczności

Próg kruchości jak i samo pojęcie „kruchość materiału" trudno określić precyzyjnie i wyznaczyć jego znaczenie. Dla stali takim progiem może być próg kruchości na zimno, który to w cale nie jest określony jednoznacznie. Jak widać z tablicy, na jego położenie wpływa w znacznym stopniu struktura geometryczna powierzchni i jej amplitudowe parametry, jak również prędkość odkształceń plastycznych. Znaczny wpływ na stan materiału ma charakter struktury: zwiększenie wymiaru ziaren (np., po odpowiedniej obróbce termicznej) powoduje zwiększenie kruchości. Jeżeli chodzi o kruchości metali, przykładowo, stali, nie można nie wymienić wpływu składu chemicznego, w szczególności wpływu siarki. Obecność siarki nawet w znikomych ilościach powoduje gwałtowny wzrost kruchości stali, przesuwając temperaturę progu kruchości nawet w strefie temperatur dodatnich. Ta właściwość siarki wykorzystuje się w stalach automatowych celem ułatwienia ich skrawalności. Trzeba też przyjąć pod uwagę, że przejście ze stanu kruchego do stanu ciągliwego nie jest procesem gwałtownym, lecz płynnym.

Celem sprawdzania możliwości stosowania koncepcji Yoffe"a przy analizie procesy skrawania realizowano badania doświadczalne przy toczeniu stali 45, żeliwa szarego 200 oraz marmuru metamorficznego z kopalni Sidi Bel-Abbes (Algeria). Badania przeprowadzono z głębokością skrawania 0,5mm przy posuwie f = 0,1 mm/obr. W badaniach przyjęto założenie, że morfologia powierzchni obrobionej odzwierciadla stan materiału w trakcie obróbki. Wyniki badań zawiera rys.7.

Fraktogram na rys.7a obrazuje powierzchni ukształtowane po obróbce ze stosunkowo niewielką energią skrawania, przy czym stal znajdowała się w stanie plastycznym. Dla znormalizowanej stali 45 z numerem wielkości ziarna 4 (średni wymiar ziarna 80µm) próg kruchości znajduje się w granicach między – 60^0 C i - 80^0 C. Warunki eksperymentu można traktować jako skrawanie plastyczne z narostem, czemu odpowiada charakterystyczny fraktogram powierzchni. Natomiast żeliwo i marmur okazują cechy materiału w stanie kruchym.

Przejście do skrawania szybkościowego zmienia charakter powierzchni obrobionej próbek ze stali i żeliwa. Powierzchnia obrobiona stali wykazuje cechy płynięcia plastycznego zbliżającego do odkształcenia płynnego.

Powierzchnia żeliwa nabiera cechy powierzchni po odkształceniach plastycznych ze znikomymi oznakami pęknięć kruchych. Natomiast powierzchnia marmuru zachowuje kształt charakterystyczny dla pękania kruchego i praktycznie nie różni się od poprzedniej powierzchni "a".
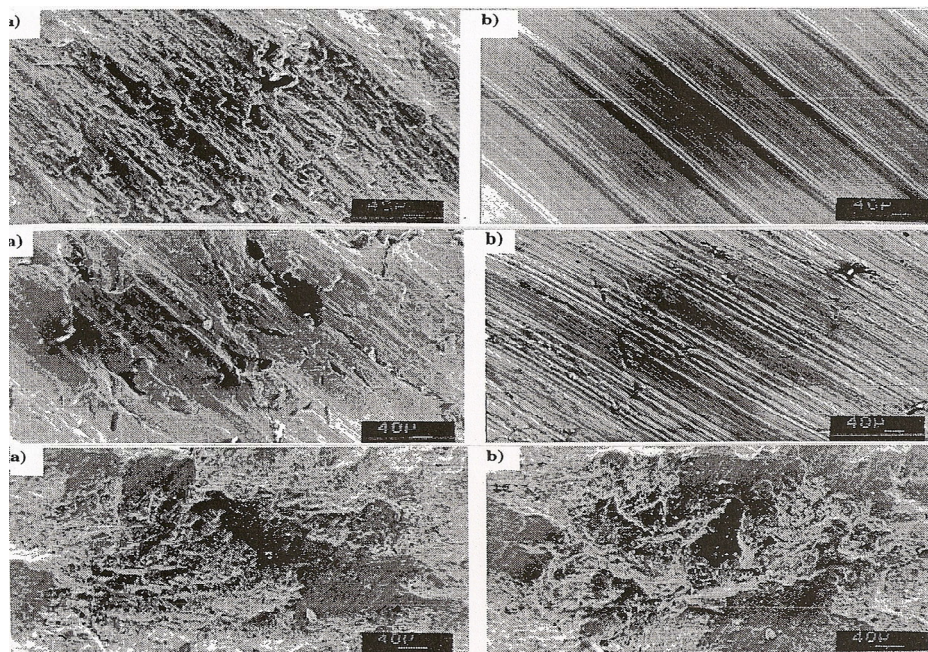
Rys.7. Fraktogramy powierzchni obrobionych (z góry w dół) stal 45, żeliwo 200, marmur, f = 0,1mm/obr, a) - v_c = 1,4 m/s   b) – v_c = 20 m/s, dla marmuru – v_c = 8,6 m/s (ze względu na BHP), D = 200, pow. 100x, badania własne.

Ewentualnie objaśnienie rys.7 można szukać na schemacie z rys.6. Przyjmiemy, że punkty E_1, E_2 i E_3 należą do stali, żeliwa i marmuru odpowiednio. Z uzasadnioną pewnością można założyć, żę stal w obydwóch przypadkach znajdowała się w strefie decydujących naprężeń σ_{pl} i wzrost prędkości skrawania sprzyja wyłącznie intensyfikacji procesów pękania i zbliżeniu pękania plastycznego do pękania płynnego . Żeliwo, prawdopodobnie, w strefie swego krytycznego punktu E_2 zaczyna przejście do stanu plastycznego. Natomiast marmur znajduje się znacznie niżej swego punktu E_3 i w cale nie spieszy zmieniać swój stan z kruchego na plastyczny.

Mnie nie udało się znaleźć jakichkolwiek wzmianek dotyczących przejścia krucho-plastycznego dla tych materiałów. Prawdopodobieństwo przytoczonych wyżej rozważań można jedynie potwierdzić pośrednie przez

porównanie temperatur ich topienia: żeliwo ≈ 1250 – 1280^{0}C, marmur – grubo ponad 3000^{0}C.

Porównanie między sobą powierzchni obrobionych celem analizy procesów przejścia od stanu kruchego do stanu plastycznego kryje w sobie pewne niebezpieczeństwo. Mianowicie, powierzchnia obrobiona kształtuje się pod wpływem procesów wtórnych w strefie 2, które-to, swoim rzędem, znajdują się w mocnej zależności od prędkości skrawania.

Spróbujmy podejść do tego zagadnienia z wykorzystaniem badań kształtowania się wióra w procesach obróbkowych materiałów o różnych właściwościach krucho-plastycznych.

Materiały w stanie łupliwym i kruchym. Celem badań eksperymentalnych wybrano:

- szkło hutnicze jako materiał łupliwy amorficzny w kształcie płytek o wymiarach 20 x 10 x 5 mm,

- galena jako materiał łupliwy krystaliczny o regularnym układzie krystalograficznym w kształcie monokryształu sześcianowego o wysokości 10 mm z regionu Donieckiego (Ukraina).

Galena potrzebuje bardzo ostrożnego i delikatnego obejścia. Brak akuratności może doprowadzić do łatwego rozłupania kryształu na drobne kostki. Skąd ja to wiem?

- marmur jako materiał polikrystaliczny kruchy pochodzeniem z kopalni Sidi Bel – Abbes (Algeria) w kształcie pociętych płytek o wymiarach 20 x 10 – 8 mm.

Proces obróbkowy- struganie. Wyniki badań przytoczonych na rys.8 łatwo było prognozować, a badania doświadczalne dokładnie potwierdziły apriorne prognozy.

Otrzymane ułamki materiału trudno nazwać wiórem. Szkło jest materiałem łupliwym, powierzchni łupliwości rozprzestrzeniają się z szybkością ≈ 2/3 szybkości dźwięku (w szkle ≈ 6000 m/s) w sposób nieprzewidzialny tworząc przy tym wiór o kształtach również nieprzewidzialnych od ułamków igiełkowych do dużych ułamków o kształtach losowych.

| Szkło,pow2x | Galena, pow8x | Marmur, pow30x |

| Szkło,pow5x | Galena, pow5x | Marmur, pow30x |

Powierzchnie separacji (rozłamu):

nominalnie płaska   schodkowa   zygzakowata
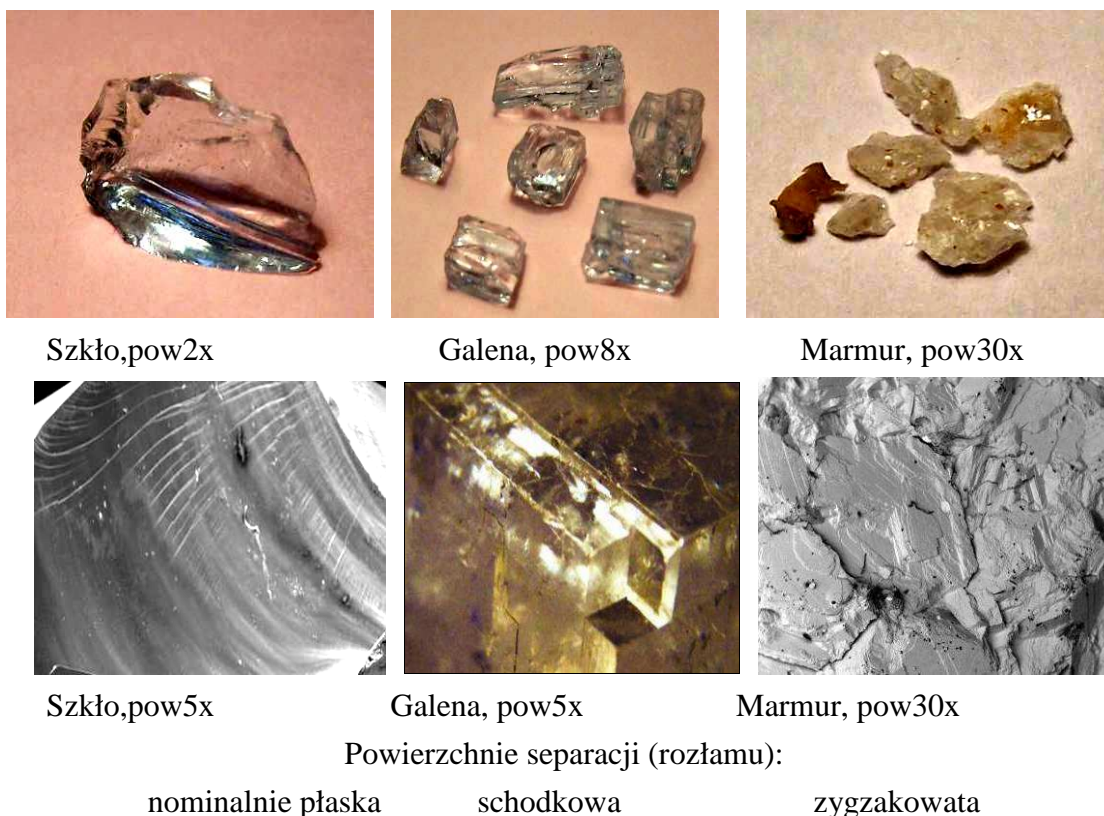
Rys.8. Odseparowane elementy i fraktogramy powierzchni rozłamu przy obróbce materiałów łupliwych i kruchych, próba strugania, badania własne .

Przy próbach strugania krystalicznej galeny fonom naprężeń przed nożem powoduje rozłupanie materiału wzdłuż płaszczyzn łatwego poślizgu 100 z ukształtowaniem prostokątnych bryłek o zbliżonych miedzy sobą wymiarach. Powierzchnia separacji schodkowa powtarzająca układ krystaliczny materiału.

Polikrystaliczny marmur jest materiałem łatwo obrabianym praktycznie we wszystkich procesach obróbkowych: toczenie, wiercenie, frezowanie, obróbka ścierna. Warstwa skrawana oddziela się w kształcie nie spojonych ułamków losowej formy tak samo polikrystalicznych o podobnych wymiarach. Powstająca zygzakowata powierzchnia obrobiona jest charakterystyczną powierzchnią kruchego przełomu przez cięcie ze śladami przełomu tak międzykrystalicznego, jak i trans krystalicznego. Przy obróbce wszystkich materiałów w stanie łupliwym lub kruchym ani charakter wióra, ani wymiary elementów nie zależą od prędkości skrawania.

Materiały w stanie plastycznym. Nieco inaczej wygląda wpływ prędkości na proces skrawania materiałów w stanie plastycznym. Ten wpływ ilustrują od lat znane schematy, zgłady i zdjęcia wiórów przytoczone na rys.9.

| Bronz | Stal 20, | Stal 45 |

Stal 3, v_c= 0,4m/s,   **Stal 20. v_c= 1,6m/s,**   **Stal 40H, v_c= 15-18m/s,**

a_p =2mm, f=0,5mm/obr a_p =2mm f=0,5mm/obr a_p = 2-10mm ,f=0,2-5mm/obr
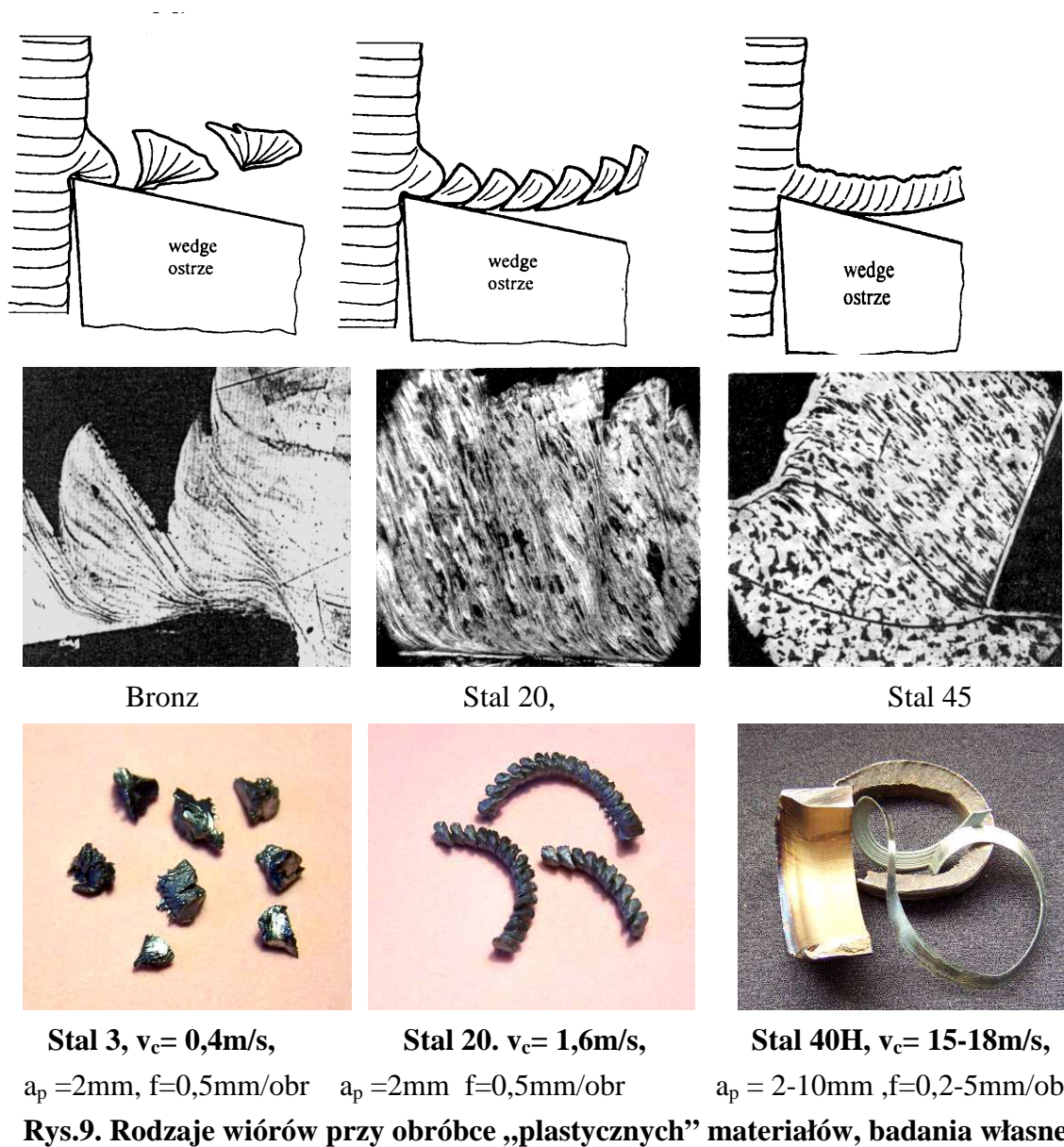
Rys.9. Rodzaje wiórów przy obróbce „plastycznych" materiałów, badania własne

Przytoczone na zdjęciach wióry otrzymano w warunkach toczenia nożem z węglika spiekanego z powłoką T i N, $\gamma = 0^0$. Według tradycyjnej klasyfikacji wióry dzielą się na trzy rodzaje: elementowy, segmentowy i ciągły (wstęgowy). Co do wióra segmentowego, to jego, moim zdaniem, można traktować jako rodzaj przejściowy od wióra elementowego do wióra ciągłego (pękanie plastyczne).

Przytoczone na rys.9 rodzaje wiórów związane są ze zmianą prędkości skrawania i, jakby potwierdzają koncepcję Yoffe"a. Szczególne temu potwierdzenie można odnaleźć na rys.10.

Rys.10. Wiór ciągły (śrubowy stożkowy), materiał obrabiany – żeliwo szare 200, vc = 31,2 m/s, F = 0,1 mm/obr., γ = 0⁰, badania własne.

Rys.11. Kształt wióra przy obróbce stali w warunkach kruchości na zimno, badania własne.

Rzeczywiście, podczas obróbki żeliwa przy prędkościach skrawania powyżej 20 m/s zaczyna powstawać wiór należący do wiórów ciągłych śrubowych stożkowych.

Celem dodatkowej weryfikacji przydatności koncepcji prof. Yoffe"a do warunków skrawania postawiono eksperyment toczenia stali ochłodzonej poniżej progu kruchości na zimno. Celem zwiększenia temperatury progowej wybrano stal 5 o wielkości ziaren 3 wg wzorców ASTM (125 μm) o oczekiwanym górnym progiem kruchości ≈ - 20^{0}C. Warunki obróbki: nóż z k = 90^0, γ = 0^0, a$_p$ = 2mm, f =0,3mm/obr, v$_c$ = 12m/s, temperatura próbki t = -28 ÷ -20^{0}C. Wyniki badań przedstawiono na rys.11.

W zasadzie swojej plastyczna stal przy temperaturach poniżej progu kruchości jest, faktycznie, materiałem o właściwościach stanu kruchego, chociaż i zachowującym cechy stanu plastycznego. Przy zbadanych parametrach skrawania, szczególnie prędkości skrawania $v_c = 12m/s$, w konwencjonalnych warunkach temperaturowych kształtuje się wiór ciągły. Natomiast przy obróbce stalowej próbki schłodzonej do temperatury poniżej progu kruchości powstaje wiór elementowy z dość wyraźnymi cechami wióra segmentowego, do złudzenia przypominający wiór żeliwa sferoidalnego. Badania fraktograficzne potwierdzają ten fakt, jak to widać na zdjęciu skaningowym fragmentu strefy skrawania (rys.12).
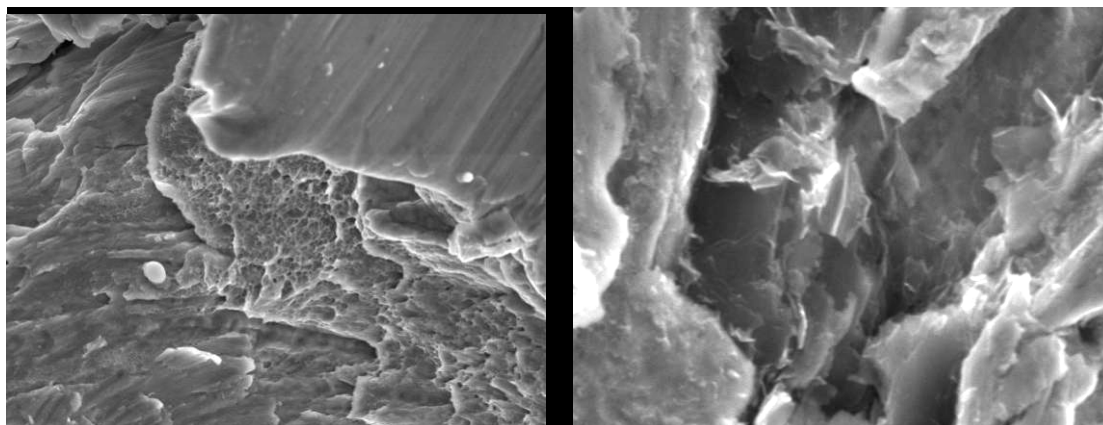
Rys.12. Fraktogramy powierzchni separacji wióra w strefie skrawania stali 5 przy temperaturze – 28^0C, $v_c = 12$ m/s, pow. 1800x, badania własne.

Na powierzchni pęknięcia występują dominujące fasety łupliwości na tle charakterystycznych oznak pękania plastycznego.

Przytoczony materiał w pewnym sensie wspiera słuszność stosowania hipotezy Yoffe"a do warunków skrawania. Ale tylko w pewnym sensie. Pozostaje sporo niejasności, na przykład, dotyczących stali z progiem kruchości, który znajduje się w granicach do -150^0C.

W pewnych warunkach, w zależności od stanu materiału, od jego poprzedniej obróbki termicznej , wymiaru ziaren itd. próg kruchości stali może przesuwać się nawet do temperatur dodatnich rzędu + 20^0C. Przykładowo, górny próg kruchości na zimno dla stali chromowo- manganowo- krzemowej 35HGS wynosi +25^0C, zaś dla stali chromowo-niklowej H3NM – 60^0C. Zatem kruchość na zimno stali jest raczej anomalią plastyczności [35].

Istnieje jeszcze jedno zjawisko rola którego w procesie skrawania stali nie jest badana. Ma się na uwadze tzw. kruchość niebieskiego przełomu. Zjawisko to wykryto w 1880 r przy próbach rozciągania stali w obszarze temperatur 100–250^{0}C odpowiadających niebieskiej barwie zgorzeliny. Dla stali o wysokiej zawartości węgla (do 0,72%) próg kruchości niebieskiego przełomu może przesuwać się do 400 – 500^{0}C, co odpowiada strefie „obniżonych" temperatur w obszarze skrawania (rys.13,14).

Co prawda, wpływ tego interesującego zjawiska może występować na powierzchniach styku narzędzia z wiórem i powierzchnią obrobioną, tzn. w strefach 2 i 3, co wychodzi poza granicy obecnego opracowania.
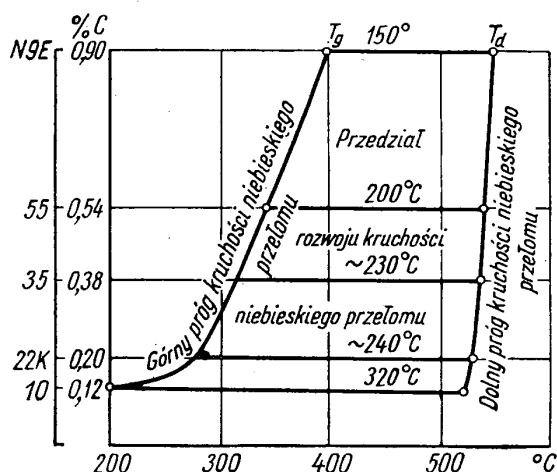
Rys.13. Przedział temperatur rozwoju kruchości niebieskiego przełomu dla stali o różnej zawartości węgla wg G. I. Pogodina-Aleksiejewa.
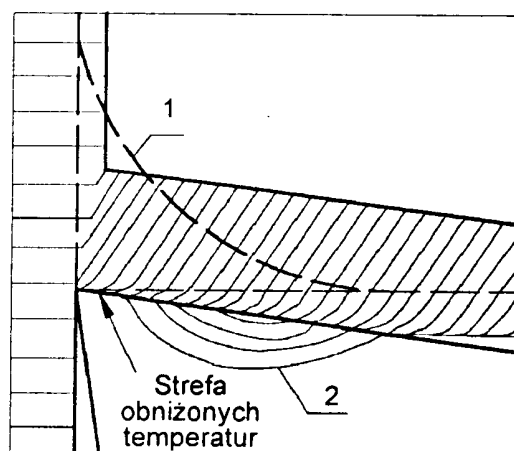
Rys.14. Naprężenie (1) i temperatury (2) w obszarze skrawania wg E.M. Trent'a.

Literatura

1.   Cotrell A. H.: Dislocations and plastic flow in crystals. Clarendon Press, Oxford 1963

2.   Grzesik W.: Advanced machining processes of metallic materials. Elsevier, Amsterdam 2008.

3.   Liubymov V. (red), Kovalenko V.: Sprawocznik po obrabotke metallow rzezaniem. Technika, Kiev 1983

4.   Liubymov V. Stachowicz F.: Wybrane zagadnienia z fizyki kształtowania struktur geometrycznych powierzchni. OWPRz, Rzeszów,2010

5.   Ostafiew V., Ostafiew D., Mazur N., Liubimov V.: Analitical method for chip ratio determination. Proc. Int. Conf. „OM 2000", t. 1, Kraków 2000, 231-240.

6.   Pogodin-Aleksiejew G. I.: Wytrzymałość dynamiczna i kruchość metali. Warszawa, WNT, 1969

7.   Trent E. M.: Metal cutting. London, Butterworths 1989

8.   Wasin S. A., Wereszczaka A.,S., Kuszner W.,S.: Rezanie metallow. MGU,Moskwa 2001

9.   Zorev N.N.: Mechanics of metal cutting. Pergamon Press, London 1996.

5.2. TEXTILE AND POLYMERIC MATERIALS

5.2.1 DYNAMICS OF ULTRASONIC OF TECHNOLOGICAL SYSTEMS

Paraska G.[1], Aly-Yafai Nasr[1], Rubanka M.[2], Misiats V.[2]

Working process of ultrasonic technological machine [1, 2] carried out by a working organ, which except for shape-generating motion of serve in relation to the processed good the high-frequency (to the ultrasound) vibrations of certain direction, frequency and intensity are reported. Ultrasonic technological machines behave to the general class of oscillation machines, however they are distinguished in a separate group on next principal reasons.

The first is determined by the educed numerous experiments by the fundamental features of conduct of materials and environments in the ultrasonic field. These features show up in the radical change of looked after in the experiment of their descriptions of resilient- plastic and reologik properties. So, for example, a dry friction in the area of contact of two surfaces under act of ultrasonic vibration will grow into viscid. At cutting of materials a knife which get ultrasonic vibrations is the substantial diminishing of cutting [3].

The second reason is conditioned by the specific of construction of basic elements of machine, which are cored shake by systems, made, as a rule, from heterogeneous areas and that work in the mode of waveguides. On this account at description of vibrations separate elements are designed by the systems with the up-diffused parameters and described by differential equalizations with the derivatives of part. As such oscillating systems have high good quality, ultrasonic machines can effectively work only in the resonance modes which allow to get sufficient for realization of technological process of amplitude of vibrations of working organ.

Two types of nonlinear effects take place during work of ultrasonic technological machine. The first is related to the mentioned higher looked after change of descriptions of material in the ultrasonic field. These nonlinear effects got explanation by means of nonlinear dynamic descriptions of these

---

technological processes. The second type of nonlinear effects is related to reverse influence of technological process on dynamic descriptions of the oscillating system. These effects appear as a result of consideration of dynamics of the system which works on the nonlinear technological loading. As a result the basic parameters of process, putting in the middle speed his flowing, which characterize the productivity of machine, her output-input ratio and efficiency succeeds to be bound to the basic parameters of machine.

On rice. 1 two generalized charts of ultrasonic technological machines are shown. Here 1 is some ultrasonic oscillating system, working organ 2 which co-operates with the technological loading 3, that designs a working process. Charts differ in the method of serve of the system. In a chart on Fig. 1, and a serve is carried out with permanent speed v from the occasion of serve. Such serve will name a kinematics.
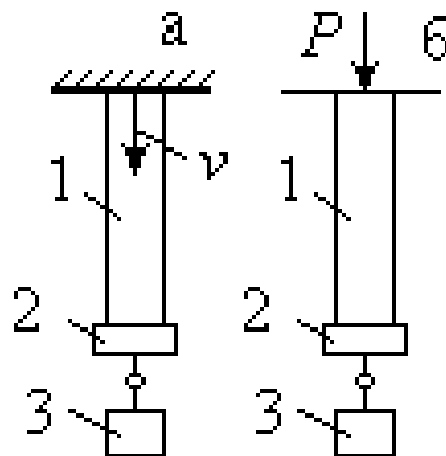
Fig. 1. Generalized charts of ultrasonic technological machines

In a chart on Fig. 1, a serve is carried out by permanent force P. Such serve will name power. In the end methods differ in that in first case the force P of serve created by an occasion, and in the second is middle speed of process v depend on the parameters of vibrations and dynamic description of process.

The oscillating system is considered linear with the known dynamic descriptions. The technological loading is created as a result of co-operating of working organ with the processed good. Force of co-operation will present as power dynamic description $f = f(u,\dot{u})$ of working process which binds

operating on good force of f to moving u and speed $\dot{u}$ of working organ. Examining motions of working organ of kind

$$u(t) \approx vt + u^0(t) = vt + \hat{a}\exp(j\omega t), \qquad (1)$$

where v is middle speed; $u^0(t)$ - periodic to composition of process, $\hat{a}_l$ - complex amplitude of vibrations of working organ.

Will conduct the harmonious linearizing of nonlinear description:

$$f_l\left(u_l, \dot{u}_l\right) \approx P_l(v, a_l) + [k(v, a_l) + j\omega b(v, a_l)]u^0.$$

Here $P(v, a)$ is a permanent constituent of force of co-operation of instrument with good. Coefficients $k(v, a)$ and $b(v, a)$ the equivalent characterize resilient and dissipative constituents of the nonlinear loading and determine influence of technological process on the dynamics of the oscillating system.

The coefficients of linearizing are calculated on formulas:

$$P(v, a) = \frac{1}{T}\int_0^T f\left[u(t), \dot{u}(t)\right]dt, \qquad (2)$$

$$k(v, a) = \frac{2}{Ta}\int_0^T f\left[u(t), \dot{u}(t)\right]\cos\omega t\, dt;$$

$$b(v, a) = -\frac{2}{T\omega a}\int_0^T f\left[u(t), \dot{u}(t)\right]\sin\omega t\, dt. \qquad (3)$$

A formula (2) gives connection of permanent component force P of co-operation and speed of v process depending on the parameters of vibrations.

At any method of serve the effect of influence to the ultrasound is arrived at the values of speed of serve $v < a\omega$ and force of serve $P < D$. These results comport with data of experiments. The most effect of decline of static force of cutting is arrived at treatment of hardly-plastic material $k_0 \to \infty$.

Will consider the dynamics of ultrasonic technological machine now. Let the vibrations of working organ of machine in default of the technological loading be known $u^*(t) = \widehat{a}^*(\omega)\exp(j\omega t)$, where $\widehat{a}^*(\omega)$ is complex amplitude of vibrations on idling. Then oscillation in an operating condition will describe next equalization:

$$u(t) = u^*(t) - L(p)f(u,\dot{u}), \qquad (p = \partial/\partial t) \tag{4}$$

where $L(p)$ is an operator of dynamic pliability of the system in the point of action of loading;

Taking into account character of these motions (1), conducting the harmonious linearizing (3) and considering $p = j\omega$, for complex amplitude of vibrations of working organ on-loading will get:

$$\widehat{a} = \frac{\widehat{F}(\omega)}{W(j\omega) + k(v,a) + j\omega b(v,a)}, \tag{5}$$

where $W(j\omega) = L^{-1}(j\omega)$ - dynamic inflexibility is known; $\widehat{F}(\omega) = a^*(\omega)W(j\omega)$ - the force over of excitation of the system brought to the working organ.

Coefficients k and b it is possible to present in a kind:

$$k(v,a) = \frac{D\omega}{\pi v}K\left(\frac{v}{a\omega}\right) \quad , \quad b(v,a) = \frac{D}{\pi v}B\left(\frac{v}{a\omega}\right) \tag{6}$$

In any case equalization for being of amplitude of vibrations of working organ comfortably to present in a kind:

$$a\omega = \left|\frac{\omega \cdot F(\omega)}{U(\omega) + k(v,a\omega) + j[V(\omega) + \omega b(v,a\omega)]}\right|, \tag{7}$$

where $U(\omega) = \mathrm{Re}\,W(j\omega), \; V(\omega) = \mathrm{Im}\,W(j\omega).$

At most resonance curve coincides with the intersection of skeletal curve lines of maximum amplitudes, equalizations of which look like, :

$$U(\omega) + k(v, a\omega) = 0,$$

$$a\omega = \frac{\omega F(\omega)}{V(\omega) + \omega b(v, a\omega)}.$$

On the set force P there is a corresponding value of size $(v/a\omega) = C_P$ .which gives the corresponding values of sizes $K = K_P$ and $B = B_P$. Now formula (6) for the coefficients of linearizing assume an air :

$$k(a) = \frac{D}{C_P \pi a} K_P;$$

$$b(a) = \frac{D}{C_P \pi a \omega} B_{P,}.$$

$$(8)$$

and equalization (7) for amplitude of vibrations of working organ:

$$a = \left| \frac{F(\omega)}{U(\omega) + k(a) + j[V(\omega) + \omega b(a)]} \right|. \qquad (9)$$

There is a dramatic change of type of resonance curve at exceeding of critical value of force of serve. Thus an output on the resonance mode can be carried out or tightening of vibrations from an area higher frequencies, or by a hard start, revealing to the system additional energy. Continuous striolas are show skeletal curves and that rounds resonance amplitudes.

From the brought general picture over of change of gain-frequency characteristics those difficulties which must be overcame at excitation of the resonance modes by an external action are obvious. Exactly these difficulties and ununderstanding of physical picture of processes, which take place, and are the basic obstacle of practical deployment of ultrasonic technological machines.

References

1. Ультразвук. Маленькая энциклопедия. / Под ред. И.П. Голяминой. -М.: Советская энциклопедия, 1979. - 400 с.

2. Марков А.И. Ультразвуковая обработка материалов. – М.: Машиностроение, 1980. - 237 с.

3. Кумабэ Д. Вибрационное резание. – М.: Машиностроение, 1985. - 424 с.

5.2.2 TESTS OF PTFE COMPOSITES FOR SEALING RINGS OF CONTACTING FACE SEALS

Kundera Cz.[1], Bochnia Je.[1]

Introduction

Constructional elements of slide bearings (particularly mechanical face seals) require usage of proper materials and proper selection of parameters of work, which assure tightness of the contact at the given rotational speed and the given pressure of the process liquid. The spectrum of the parameters of work, at which the sealing works properly, is restrained – for example – by the values of the unit pressures corresponding to the lower and upper border state [1, 2, 3, 4]. Determination of the characteristics of the border states has been described in the paper [5]. Experiments are carried out with appropriate measurement equipment, which emulates working conditions of the face seal.

The tests described in this contribution has been carried out on the stand SUM-1 [4, 6], which is able to measure moments of friction, unit pressures between the rings, temperature of non-rotating sliding ring at the sealing surface, working pressure of the process liquid, and smoothly adjusted rotational speed of the shaft. Therefore, the stand allows to carry out research in the scope of selection of appropriate materials designed for sliding mechanical seals.

1. Conditions of the tests

Running at the minimal unit pressures may result with sudden "opening" of the clearance and loosing the tightness. On the other hand, maximal unit pressures leads to quick wear, and short period of work, i.e. lowering the durability of the sealing. A minimal unit pressure corresponding to the maximal tightness is a state of balance of the forces, which may be named as a state of "unstable equilibrium". Any little external distortions appearing during the operation of the sealing may cause the system to loose that balance and result with a leakage. A way of preventing that from happening could be applying unit pressures slightly exciding the minimal values. Keeping the working parameters and the temperature smaller then the critical temperature is a protection form exciding the maximal values of the unit pressures.

---

[1] Kielce University of Technology, Poland

Indispensable experiments are curried out on a testing stand that models real conditions of work of seals. The testing enables [6]:

    −   easy exchange of sealing rings (samples);

    −   fluent regulation of rings load and rotational speeds;

    −   measurement of temperature in crevice (at friction surface) and in sealed chamber;

    −   measurement of force (moment) of friction.

Furthermore, the stand has visible (accessible) working zone, which is essential to curry out tests and determine minimum unit pressures.

The device for investigations of mechanical seals - SUM-1 is introduced on Fig. 1.

Fig. 1. The testing device for mechanical seals – SUM-1.

The device SUM-1 consists of the following main sub-assemblies and systems:

− testing head as sub-assembly that consist of pressurizing head and measuring head,

− spindle together with driving system,

− system of working liquid (system feeding seal in liquid),

− system loading the seal with axial force,

− block (system) of measuring,

− block (system) of regulation,

− pneumatic installation.

The part of testing device SUM-1 presented testing head is introduced on Fig. 2.
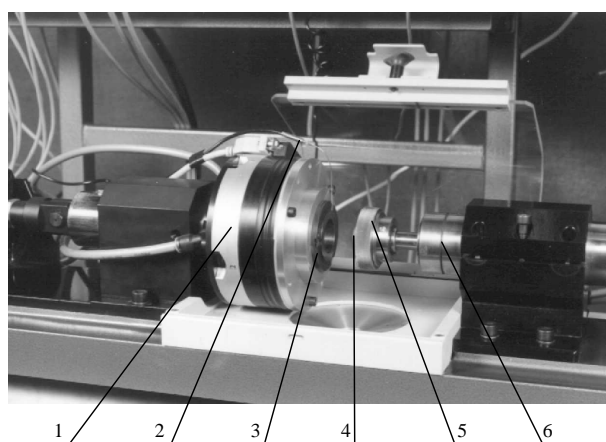
Fig.2. Side-head zone of testing device SUM-1: 1 – measure side-head, 2 – temperature-sensitive element, 3 – seat seal ring, 4 – rotational seal ring, 5 – casing rotational ring, 6 – spindle.

The testing head assures:

 – clamping the sealing face model,

 – presetting work parameters (unit pressures – pj, medium pressure – pc),

 – measurement of work conditions: values of sliding rings load – Fg, moment of friction – Mt, temperatures at surface of friction of solid ring –T.

Input parameters of work (input – factors) are preset through the pressurizing head. Pressurizing head can move along axis, so that one can install and uninstall sealing rings, and assure maintenance of given values of load during the work. In the vicinity of disk of the pressurizing head - meaning in the vicinity of non-rotational ring there is installed a sensor of medium pressure. The measuring head is attached to the disc of pressurizing head. The non-rotational ring of the tested face seal is installed in the seat of the measuring head. The head enables measurements of the output factors. Moment of friction and the rings load are measured by the means of extensometer sensors. The rings load is a preset value and it is a variable in formulas for calculation of unit pressures. Measurement of the temperatures in the vicinity of sealed surfaced is done with a thermocouple sensor introduced in the hole in non-rotational ring [1,7].

The tests of the sliding rings of the face sealing (Fig. 3.) have been carried out on the stand SUM-1 at the conditions of the lower border state. The rings were made of the following materials: stationary ring (seat) – NC10 steel thermally treated to the hardness of 60 HRC, rotational ring – composites PTFE and others. Water was used as the process liquid.

The sliding rings applied in the experiment were 43 mm in outer diameter and 37 mm in inner diameter. The stationary sliding ring was mounted in a clamping head. The surface of the stationary ring was polished in several stages - the last polish was finished with 1200 grain sanding paper to obtain a smooth (mirror) surface. The surfaces of the rotational sliding rings were polished in several stages as well. Additionally, after the last polish finished with 1200 grain sanding paper, the rings were grinded on a special cast-iron shield.

After mounting the rings in the measuring head and in the spindle, the load (the force), the rotational speed and the pressure of the process liquid, were gradually increased up to the values assumed in the experiment. The value of the load was adjusted in such a way, there was no leak (to small load), and the temperature at the sliding surface and the moment of friction were not to high (to high load). That kind of regulation allowed to maintain the conditions of the lower border state of work of the sealing rings. After a certain time – from a few up to a few dozens of minutes (depending on the preset parameters) – the working conditions were stabilizing. The whole process were recorded with a computer program.

In order to determine the minimal load on the sealing rings (minimal unit pressures) the test has to be carried out at assumed and maintained constant values of the rotational speed – n, liquid pressure – p, and the value of the load – Fg calculated from the balance condition of the forces acting upon the tested sliding coupling.

If for the calculated load – Fg and the rotational speed of the shaft – n = 0 (no rotation) there is a leakage, it is necessary to increase the load coefficient or grind again the sliding surfaces of the rings. The test should be carried out in such a way, that increasing the load on the rings is not causing significant increase of the moment of friction and the temperature.

Scheme of the face sealing and the parameters operating condition were presented in the Fig. 3.
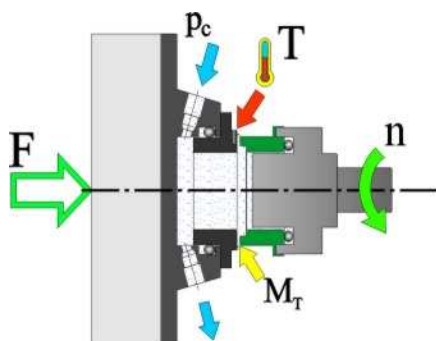
Fig. 3. Scheme of the measuring head and the model of the face seal.

(F – load on the sealing rings, p_c – pressure of the process liquid, T – temperature at the surface of the stationary ring, n – rotational speed of the shaft, M_T – moment of friction)

It is the best, when at the outer edges of the rings, there is a typical meniscus. Fluctuations of the temperature measured under the contact surface, and the moment of friction, appearing in the initial phase of the process, stabilize after certain time. Parameters of work measured in the state of stability characterize the materials that the sliding rings are made of.

2. Matching the range of admissible unit pressures

One of the basic characterizations of a given set of materials for sealing rings is the dependence of the admissible unit pressures (or sealing rings load) on sealed medium pressure and rotational speed of shaft (or relative sliding speed) $pj = f(p, v)$. Values of the admissible unit pressures correspond to so-called border-states of the working seal [1, 8]:

- the minimum unit pressure pj_{min} corresponds to a zero leakage condition i.e. condition in which intensity of leaking is equal to rate of medium evaporation from the friction zone - so-called lower border-state;

- the maximum unit pressure pj_{max} corresponds to the condition of maximum (critical) temperature for given set of materials, which exceeding ends up with "catastrophic" waste of sealing rings (in general the ring made of smaller hardness material) – so-called. upper border-state.

Exploitation of the sealing with minimum unit pressures may cause a sudden "opening" of the crevice and loss of tightness, while maximum pressures

may cause quick waste and shortening the period of work i.e. lowering the persistence sealing. The minimum unit pressure, corresponding to maximum tightness is a state of equilibrium of powers, which one can to call a state of "temporary" equilibrium. Even little external disturbances appearing during exploitation of the sealing may cause "knock:" the system out of that state and lead to leakage. Protection from this unprofitable (undesirable) state can be applying unit pressures that imperceptibly exceed the minimum values. Protection from the maximum (upper) values of the unit pressures is maintenance of work parameters at temperature smaller then the critical.

On the stand SUM-1 there where carried out tests in border-state condition of sliding rings of face sealing model made of the following materials: non-rotational ring (contra-specimen) – steel NC10 heat treated to hardness 60 HRC and rotational ring – composite PTFE of contents 4,5% of bronze, 18% of graphite, 0,8% of disulfide of molybdenum. As a sealed working liquid water was used. There were produced rotational sliding rings of external diameter Dz = 43 mm and internal diameter Dw = 37 mm. Non-rotational sliding ring was fastened in the pressurizing head.

After fastening the rings in the measuring head and spindle, one gradually enlarged the load, rotational speed and pressure of the working liquid up to the values assumed in the experiment. The value of the load was regulated so that there was no leakage (too little load) so that there was no temperature increment at surface of friction and moment of friction (too large load). This way of regulation allowed to hold the conditions of bottom border-state of work of the sealing rings. After a certain time - from several to tens of minutes (depending on kind of preset parameters) conditions of work were becoming stable. A computer program registered whole process.

The tests were curried out for the following values of preset parameters:

- for rotational speed n = 3000 r.p.m. pressure of working liquid (sealed) was equal to pc = 1,5 — 2 —2,5 —3 —3,5 —4 bar;

- for pressure of the working liquid pc = 3 bar the rotational speed was equal to n = 2000 —3000 —4000 —5000 —6000 r.p.m.

Measured output parameters are: temperature at surface of friction T, moment of friction Mt, and rings load Fg (program after processing the data converts load into unit pressures p_j).

Each of tests lasted about one hour. Exemplary results were introduced on graphs 4, 5, in coordinates - measured output parameter – time. The temperature of work at surface of friction was stable during the process attaining values of – at the beginning of test about 26°C, and at the latter part of test about 33°C. The biggest values of temperature of work – up to 39°C were recorded for rotational speeds 5000 and 6000 r.p.m. [8]. On the basic of data from the experiment in a stable state (it was assumed, that final 15 minutes of test sufficiently characterizes stable parameters of work) average values of measured quantities were calculated.
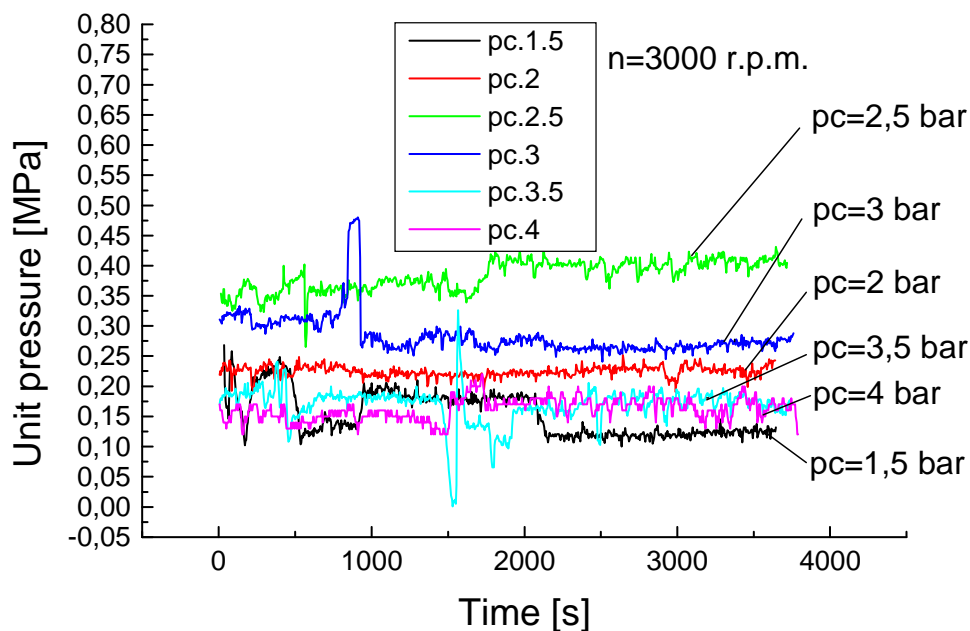
Fig. 4. Change of unit pressure at time for rotational speed n=3000 r.p.m. and different values of medium pressure (sealing rings: steel NC10 – composite PTFE).
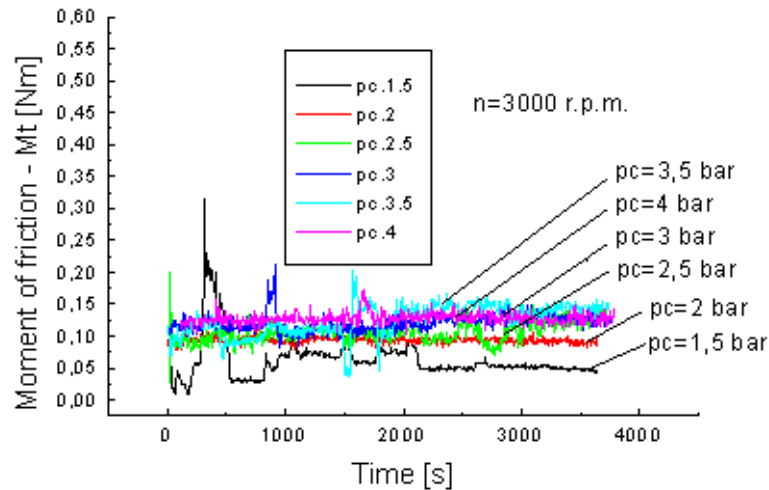
Fig. 5. Change of moment of friction at time for rotational speed n=3000 r.p.m. and different values of medium pressure (sealing rings: steel NC10 – composite PTFE).

After observing the runs (Fig. 4, 5) it was found that stabilization of majority of running parameters follows after about half an hour i.e. more-less at half of assumed cycle. It was assumed that bottom border-state would be characterized by parameters obtained in steady-state conditions. For statistical analysis the experimental data was taken from the last 15 minutes of run.

3. Findings of the research on composite materials

Figure 6 presents exemplary charts of changes of the moment of friction – Mt, unit pressures – pi, and pressure of the process liquid – pc, for sliding rings NC10 – PTFE 3 (composition according to the table 1.) It is possible to notice the initial phase of the process where there are fluctuations of the moment of friction and unit pressures. The fluctuations result from adjustment of the load – Fg, and the pressure of the process liquid, carried out to arrive at lower border state. After a certain time – usually a few or few dozens of minutes (in the figure about 2200 s) – the parameters of work stabilize. The parameters measured in this phase of the process are used in further analysis. Sliding rings which are well grinded – for example – rings which were tested few times, arrive at stable running state after much shorter time.

This contribution presents results of the tests of the sliding rings made of composites PTFE in the conditions of the lower border state. It was assumed:
- constant rotational speed of the shaft n = 3000 r/min
- constant liquid pressure pc = 1,5 bar.

436
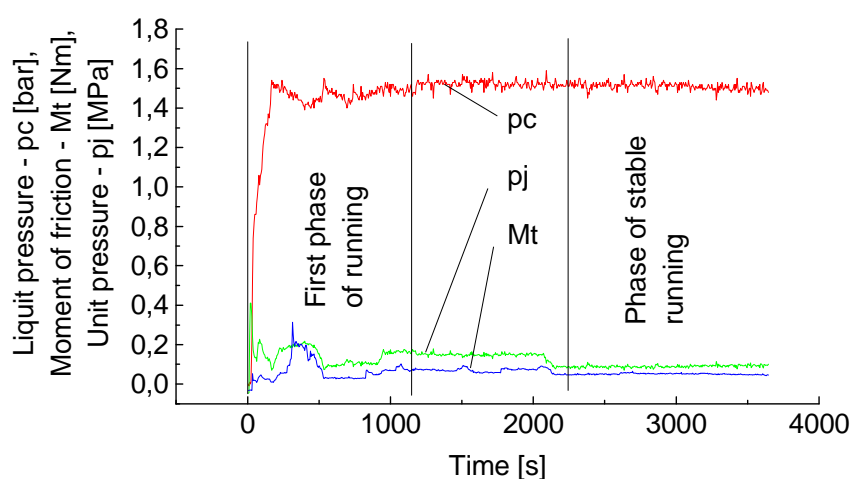
Fig. 6. Change of the operating parameters – pc, Mt, pj for sliding rings NC10-PTFE 3 (B4,5G18SMS0,8)

Values measured involved the load – Fg, moment of friction Mt, and the temperature at the surface of friction of the stationary ring. The tests were run on thirteen samples made of composite materials PTFE which contained bronze, graphite and molybdenum disulfide. The compositions of each composite is presented in table 1.

Table 1 - Composition of the composite materials PTFE.

Sample number	Bronze %	Graphite %	MoS$_2$ %	PTFE %
PTFE1	4,5	2,7	0,8	92
PTFE2	36,5	2,7	0,8	60
PTFE3	4,5	18	0,8	76,7
PTFE4	36,5	18	0,8	44,7
PTFE5	4,5	2,7	3,7	89,1
PTFE6	36,5	2,7	3,7	57,1
PTFE7	4,5	18	3,7	73,8
PTFE8	36,5	18	3,7	41,8
PTFE9	21	10,5	2,2	66,3
PTFE10	40	10,5	2,2	47,3
PTFE11	21	1	2,2	75,8
PTFE12	21	10,5	0,5	68
PTFE13	21	10,5	4	64,5

Table 2 - Operating parameters - working load Fg, moment of friction M$_t$, operating temperature T - of the sliding rings for stabilization low border condition for different composite materials PTFE.

PTFE	Fg [N]	M$_t$ [Nm]	T [^{O}C]
1	354	0,08	28
2	320	0,09	32
3	240	0,05	28
4	257	0,04	28
5	354	0,08	32
6	271	0,06	33
7	249	0,05	33
8	369	0,1	30
9	286	0,07	31
10	274	0,07	31
11	245	0,06	33
12	251	0,05	29
13	308	0,06	30

From the charts obtained for each composite material values of the operating parameters (in the state of stable running) were read, and presented in the table 2. Within the spec of the tests there are no great differences of the temperature, which varies in the range from 28 C to 33 C and is stable. The greatest loads no the sliding rings occurred with composites PTFE1, PTFE5 and PTFE8. The first two contain the smallest amount of components and obviously the greatest amount of clear PTFE i.e. 92% and 89,1%, and PTFE8 contain the greatest amount of components – thus the smallest amount of clear PTFE from the thirteen tested samples. This fact confirms the validity of the assumed border amounts of components. Greeted amounts of components may negatively influence the operating parameters – particularly the load.

The chart of moments of friction in stable conditions for each composite was presented in the Fig. 7.

The best effects were obtained with the materials containing 18% of graphite excluding previously mentioned PTFE8. Generally presence of graphite positively influenced on operating parameters of the sliding rings, particularly PTFE3, PTFE4 and PTFE7. Graphite particles, which are the products of wear, create a frictional film, which stabilizes the work of the sealing.
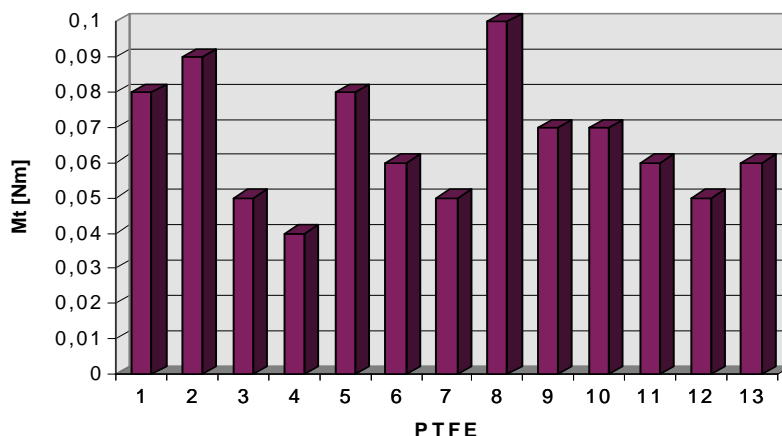
Fig. 7. Values of the moment of friction Mt of the sliding rings for stabilization low border condition for different composite materials PTFE.

Conclusion

Introduced in this paper way of testing sliding rings along with testing stand can be useful to estimate materials for sliding elements of mechanical seals, and qualification of their running parameters, especially in bottom border-state.

From the curried out tests it turns out, that changing such parameters as pressure of sealed liquid or rotational speed demands – in order to assure tightness – suitable change of rings load, and what follows, also change of unit pressures

Tests of models of the face seals carried out on the stand SUM-1 allowed to identify operational parameters of respective sliding couplings in the conditions of the lower border state. From the findings presented above, it results that non-active components significantly influence on operating parameters of the sliding rings – particularly the load. This piece of information allows for selection of the materials accordingly to assumed criteria – for example unit pressures or minimal moment of friction.

It was found that non-active components applied for modification of the PTFE improve its properties in respect of usefulness in application for sliding rings. However, the composition of the composite should be properly matched for the given operational parameters.

Acknowledgement

References

1. Kundera Cz., Rudol F.: Stan graniczny pierścieniowego uszczelnienia ślizgowego. Zagadnienia Eksploatacji Maszyn, Z. 1-2 (69-70), 1987, ss. 75-90.

2. Vizjak A., Vizintin J.: Experimental study on the relationship between lubrication regime and performance of mechanical seals. Lubrication Engineering, No.1, pp.17-22, 2001.

3. Nau B.S.: Mechanical seal face materials. Proc. of the Institution of Mechanical Engineers, Part J, Vol.211, No3, pp.165-183, 1997.

4. Kundera Cz., Bochnia J.: Tests of materials for sealing rings of mechanical seals. New Ways in Manufacturing Engineering, 17 – 18 June 2004, Prešov, Slovak Republic.

5. Kundera Cz.: Metoda badań i obliczeń konstrukcyjnych uszczelnień czołowych. SiNH, Zeszyt 5, 1992.

6. Bochnia J., Matecki K.: Stanowisko SUM-1 do badania mechanicznych uszczelnień czołowych, Problemy Eksploatacji, 4/1999, str. 275-283.

7. Lebeck A.O., Nygren M.E., Shirazi S.A., Soulisa R.: Fluid Temperature and Film Coeficient Prediction and Measurement in Mechanical Face Seals - Experimental Results. Tribology Transactions, Volume 41(1998), 4, pp. 411-422.

8. Matecki K., Kundera Cz., Bochnia J.: Method of testing work parameters of sealing rings. 10-th International Conference HERVICON-2002, Tom 1, Sumy State 2002, pp 216-233.

5.2.3 THE APPLYING OF NANOTECHNOLOGIES FOR OBTAINING ELECTROCONDUCTIVE TEXTILE MATERIALS WITH USING OF THE GETERO COAGULATION MECHANISM

Redko Ya.[1], Romankevich O.[1]

To the synthesis of electroconducting polymers, both in a clean kind and on different bases large attention is spared from unique properties of similar polymers [1–3].

A special case of conducting polymers is the synthesis of polyaniline on the fiber with the creation of conductive fiber materials using of

[1] Kiev national university of technologies and design

geterocoagulation mechanism dyeing process of oxidative condensation of aniline in the presence of surface-active substances (SAS) [3–6].

Synthesis of rigid-chain polymers – polyaniline by oxidation of aniline dissolved in the amorphous regions of fibers, which are changing the properties of the fibers until the appearance of fragility [3–6].

Necessary to develop a process for the synthesis of polyaniline on the fiber, which would polyaniline deposited on the fiber surface, but retaining sufficient strength to wet and dry friction.

Earlier [3–7] suggested that the deposition process is a process of geterocoagulation. For the development of technology for obtaining of conducting fibers, containing polyaniline, research of mechanism of flowings processes is needed.

Purpose of work: 1) study the dispersion of polyaniline obtained by oxidation of the dye bath in the presence of surface-active substances on the treatment of a similar mode of obtaining an electrically conductive polyamide fiber, containing polyaniline [3–6], 2) investigation of sorption of dispersion particles on fibre material.

1. Objects and methods of researches

The dispersion of polyaniline prepared by oxidative condensation of aniline, which was used previously to produce electrically conductive textile materials [3–6].

To determine the particle size distribution in the laser used sedimentograf Mastersizer 2000 (Malvern, UK) with appropriate software, which includes the Mie theory. Using the device allows to obtain the size distribution curves as a function of the numerical fraction of particles on their size.

2. Results and their discussion

Durability of connection of colloidal particles with a surface depends on its size, in the limit, the maximum interaction with the surface fibers in nano-sized particles of the dispersed phase. Fig. 1 and 2 show the distribution curves of particle size of polyaniline as a function of the numerical fraction of particles on their size the cumulative numerical fraction

The investigated dispersion refers to nanosystems: particles with size 100 nm about 30%, size more than 80% particles 60 ÷ 200 nm. With a middle size of ≈ 100 nm.
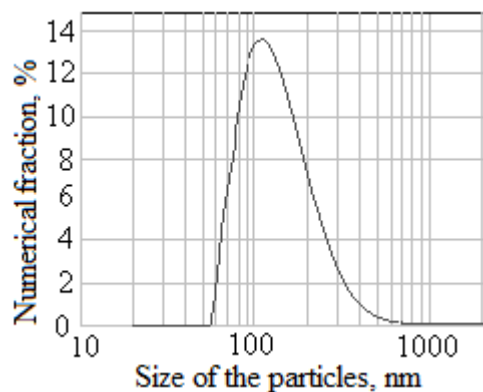
Fig. 1. Differential curve of polyaniline particles sizes distribution.
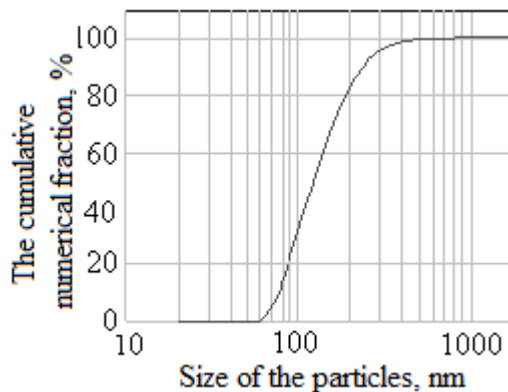
Fig. 2. Integral curve of polyaniline particles sizes distribution.

The investigated dispersion refers to nanosystems: particles with size 100 nm about 30%, size more than 80% particles 60 ÷ 200 nm. With a middle size of ≈ 100 nm.

As a result, at the modes of oxidization of aniline [7] used by us diffusion of particles of polyaniline deep into fibres impossible, and the basic mechanism of dyeing in this case is geterocoagulation of nanoparticles on the surface fibre.

The oxidation of aniline to polyaniline in the presence of polyamide textile material and a surfactant in the range 5 ÷ 15 minutes, depending on the concentration of aniline, which is not enough for molecular diffusion of aniline in the polyamide textile material (with subsequent oxidation) [3].

This is additional evidence of the possibility of obtaining an electroconductive fibers on the basis of polyaniline at the use of geterocoagulation mechanism, in the absence of dye sorption stage or semiproduct in a molecular form. In favor of geterocoagulation on the fiber surface is also indicated by the absence of changes in physical and mechanical properties of polyamide textile material also [3].

If sorption is described by the Langmuir equation, we find (for example, [8]), which formed a monomolecular adsorption layer. However, it is known [9, 10] that the deposition of nanoparticles on the surface may occur in the form of

monolayers by self-organization, in particular, the possible synthesis of polyaniline monolayers on films [11]. It is interesting to the equation describing the sorption of polyaniline nanoparticles with formation of monolayer.

For sufficiently weak interactions of particles with the surface fibers (parallel to the flow of mutually competing processes geterocoagulation and peptization) an equilibrium is possible between the processes of geterocoagulation and peptization. In the framework of the DLFO theory [12, 13], similar equilibrium between coagulation and peptization the more so probably, than less than depth of the second minimum (usually, $1 < U < 10kT$, U is potential energy of interaction; characterized by "long-range interaction" [13] or in the process of flocculation [12, 14]).

We will present an equilibrium between the processes of geterocoagulation and peptization (a sorption is a desorption) of colloid particles reversible reaction quasichemical. Similar approach sufficiently wide used for research of processes of molecular adsorption [15]. If the maximum possible concentration in a monolayer of dispersed particles deposited on the surface is equal C_∞, and a busy seating capacity during the concentration of particles in dispersion C_D is equal C_F, then the equilibrium constant of sorption:

$$K = \frac{C_F}{(C_\infty - C_F) \cdot C_D} \quad \text{and} \quad C_F = C_\infty \frac{KC_D}{(1 + KC_D)}, \tag{1}$$

In the coordinates $1/C_F = f(1/C_D)$ equation (1) will be transformed into a linear equation:

$$\frac{1}{C_F} = \frac{1}{C_\infty} + \frac{1}{KC_\infty} \cdot \frac{1}{C_D}. \tag{2}$$

Analysis of equations (1) and (2) shows that the formation of a monolayer of the dispersed phase in the process geterocoagulation sorption isotherm is similar in form to the Langmuir equation for monolayer adsorption of the interface.

The action of surfactants in the dye bath is multifaceted: on the one hand of surfactant influences on dispergating poorly water-soluble aniline in the dye bath, on the other hand – in a dispersed structure of polyaniline, which is formed

during synthesis, and the third – due to adsorption on the surface of the fiber to the possibility of geterocoagulation process and the durability of the interaction of the dispersed phase with the surface of the fibrous material.

In this regard, was investigated: the influence of anion surfactants on the sorption of polyaniline nanoparticles on the surface of the fibrous material on the geterocoagulation mechanism; influence anion surfactants on the value of resistance of polyamide knitting linen; influence of concentration of different types surfactants on the sorption of polyaniline nanoparticles on the surface of fibrous materials.

Character and degree of influence SAS, which are used in the processes of chemical technology of fibred materials, in a great deal depend on the first critical concentration of micelloforming (KKM). Is KKM of SAS (for an anion-active matter is a sulphonol) in the work [7] determined by a stalagmometrical method, equal $0,3 \div 0,5$ g/l.

The nature and degree of influence of surfactants, which are used as textile auxiliaries in the processes of chemical technology of fibrous materials depends largely on the first critical micelle concentration (CMC). In [7] is determined CMC surfactant (for anion substances – sulfonol) by a stalagmometrical method, which is equal to $0.3 \div 0.5$ g/l.

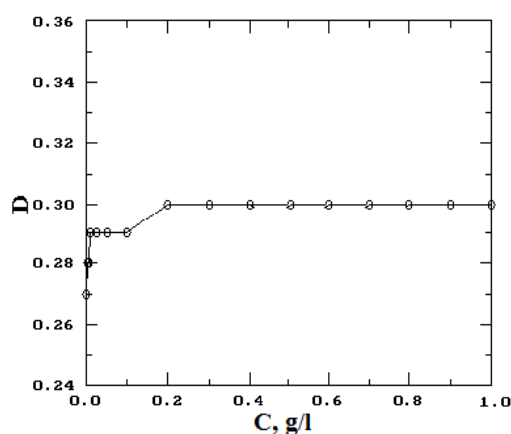**Fig. 3. The dependence of the optical density of solutions of polyamide materials, dyining polyaniline (D), from the concentration of sulphonol (C).**

Solutions of polyaniline in sulfuric acid, obey the law of Lambert-Buggere-Berr, as a consequence, the optical density of a solution dyed fiber material is proportional to the concentration of quantity dye on the fiber. The

introduction of anion surfactants – sulfonol (Fig. 3) at concentrations about $0.05 \div 0.1$ g / l <CMC causes a sharp increase in the quantity of polyaniline on the fiber.

Analysis of the dependence in Fig. 3 shows that the effective concentration sulfonol is within an order of magnitude smaller than the first critical micelle concentration (up to $0,3 \div 0,5$ g/l). Saturation is reached with the introduction of additives anion surfactant with a concentration of $0,01 \div 0,2$ g/l, that is, when the surfactant exists as a molecular solution, and when the surfactant concentration that is greater than its CMC and: $0.4 \div 1.0$ g/l, that is, when the surfactant exists in the form of a micellar solution.

On a Fig. 4 the estimation of dependence of polyamide knitting linen strip resistance is resulted, dyining by polyaniline, from the concentration of sulphonol in a dye bath. Analysis of dependence on a Fig. 4 does show that the value of resistance of polyamide knitting linen, dyining by polyaniline, reaching a limiting value at a concentration of sulfonol within $0.5 \div 1.0$ g/l.

A straight line on the curve dependence of resistance of polyamide knitting linen on the concentration of sulfonol in a dye bath (fig. 4) shows that over the subsequent increase of surfactant concentration brings to decreasing of polyamide linen resistance, namely, to the change of character of polyaniline distributing in the structure of fibrous material (quantity of polyaniline on a fibre at the change of containing surfactant in a dye bath in these limits does not change is a Fig. 3).
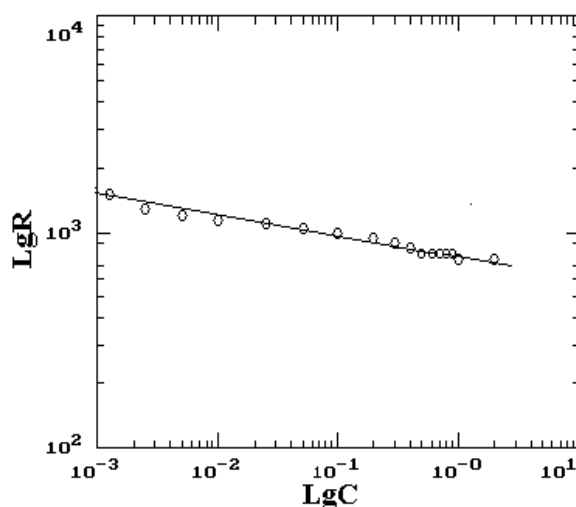
Fig. 4. Evaluation of polyamide textile material resistance (LgR), dyining polyaniline, depending on the concentration of sulphonol (LgC).

445

Line on a Fig. 4 answers a degree law, which is typical for statistical fractals[16].

Fig. 5. The dependence of the optical density of the solution of polyamide materials, dyining polyaniline (D) on the concentration of aniline (C) in the presence of: 1) sulfonol, 2) preparation OS-20, 3) alkamone OS-2. Adopted, the proportionality of the concentration of aniline to polyaniline concentration to the synthesis.

The sorption of polyaniline particles from colloid solution on the positively charged polyamide textile material on the mechanism of geterocoagulation most effectively occurs in the presence of anion surfactant (Fig. 5).

Equations (1) and (2), coinciding in form with the Langmuir equation, derived under the assumption that the reversible formation of a monolayer of particles on the surface of the variance, describes the process of geterocoagulation for non-ionogenic and kationaktive surfactant used as textile auxiliaries for the synthesis of polyaniline (Fig. 6).

Thus, the equation is the same form as the Langmuir equation can describe the various mechanisms of dyeing (dissolution [17] and geterocoagulation [18]), and the applicability of the Langmuir equation in its classical form can not be proof of the monolayer adsorption on the surface.

In the synthesis of polyaniline at a pH of dye bath about $2 \div 3$ in the sulfonol presenceof negatively charged particles of polyaniline deposited on the positively charged surface of the fiber. Electrostatic interaction of particles in this case very intensively for the irreversibility of the process.

As a result, at the use of sulphonol as a stabilizator, dependence of quantity of dye on the fibre from the concentration of aniline in the bath is not described equation, which coincides in form with the Langmuir equation.

The use of polymers for coating method for this application monolayers (layer on layer) was proposed earlier [11,19, 20]. Matrix successively immersed in a solution, containing polyelektrolites with different charges. Since then, the proposed variations of this approach – using different types of polymers, was replaced by one or more layers of polymer colloidal particles [9–11,19, 20].

Using a matrix of colloidal particles provides a much larger specific surface area than flat surfaces, which is essential for their application.

Fig. 7 shows the dependence of the conductivity of fibrous material on the number of stages of deposition of polyaniline with multi-stage dyeing process for the synthesis of polyaniline . Each successive stage of deposition was carried out with the change of type of surfactants, and as a consequence, the change of the charge of polyaniline nanoparticles.

Thus, during the deposition process was carried out classical geterocoagulation [12–14], when engaged in the process geterocoagulation oppositely charged surfaces (in our case, the surface of the particles of polyaniline and fibrous material). As the number of deposited layers increases the electrical conductivity of the textile material: almost 300 times.
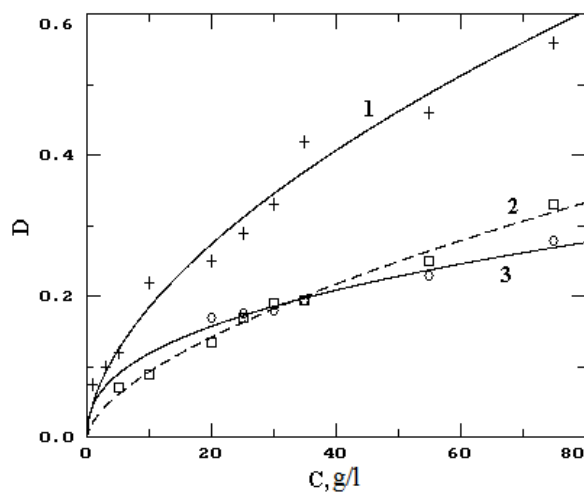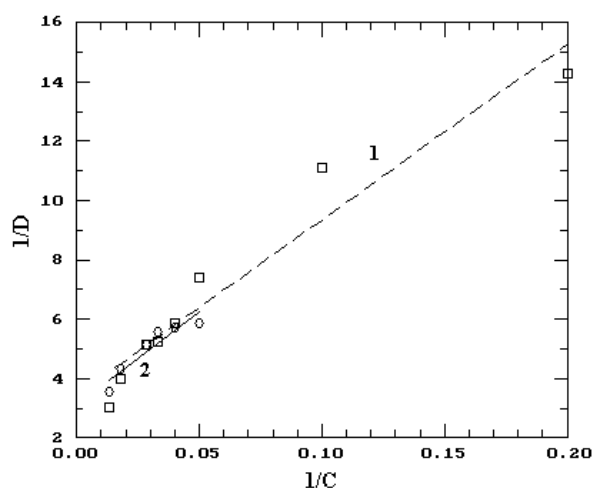

Fig. 6. The dependence of the optical density of the solutions of polyamide materials, dyining polyaniline (D), on the concentration of aniline (C) in a presence: 1) preparation OS-20 and 2) alkamone OS-2 is in the coordinates of Langmuir equation.

Fig. 8 shows the dependence of the conductivity of fibrous material on the number of stages of deposition of polyaniline with multi-stage dyeing process for the synthesis of polyaniline using only the anion surfactant (sulfonol). Using only the anion surfactant at different stages of deposition does not lead to proportional increase in conductivity with increasing the number of stages of deposition of polyaniline nanoparticles on the surface of the fibrous material.
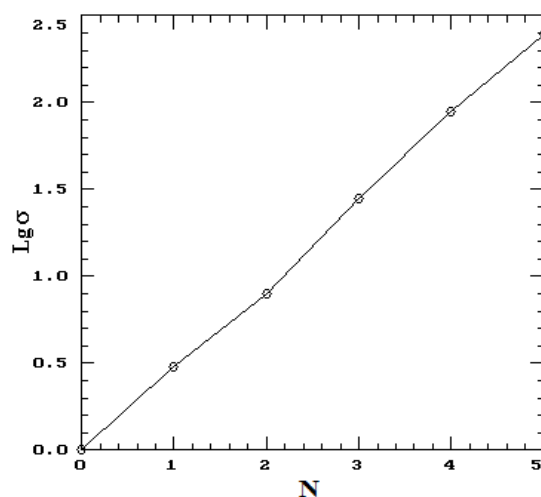
Fig. 7. The dependence of the conductivity of fiber material from the number of stages of polyaniline deposition (N).
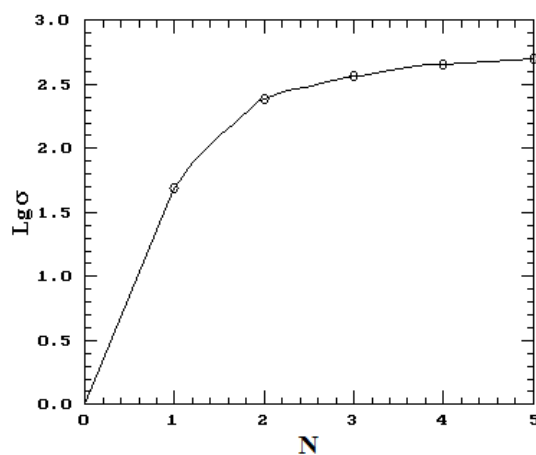
Fig. 8. The dependence of the conductivity of fiber material from the number of deposition stages of polyaniline with anion surfactant (N).

Thus, obtaining a linear dependence of the conductivity of fiber material coated on the number of deposition stages of polyaniline in the presence of different types of surfactants (Fig. 7) suggests that the oppositely charged nanoparticles of polyaniline stabilized by alternating anionactive and

kationactive surfactant to form electrically conductive layers through the implementation of self-assembly polyaniline nanoparticles, by forming a multilayer coating on the surface of a polyamide fiber material.

We can therefore say that the nanoparticles are capable of self-organization of polyaniline on the one hand, form stable ordered nanostructures on the surface of the fibrous material, and on the other – can easily change a form of self-organization when the parameters of the process.

Conclusions

- it is set that the sorption of polyaniline is carried out textile material from the nanosystem;

- by the basic mechanism of dyeing with formation of polyaniline in the process of oxidization of aniline is nanoparticles geterocoagulation of polyaniline on the fibre surface;

- equation (2) which is analogical in a due form to Lengmyure equation is got in supposition of convertibility of coagulation and peptization;

- equation (2) describes the sorption of polyaniline particles of fibre at the synthesis of polyaniline in presence kationaktive and non-ionogenic SAS;

- classic geterocoagulation of the particles with different charges of dispersible phase and surface of fibre results in irreversible coagulation – a process is not described equation (2);

- use layered process geterocoagulation particles of polyaniline can increase the electrical conductivity of dyed fibrous material is almost 300 times;

- obtaining a linear dependence of the conductivity of dyed fiber material from the number of stages of deposition of polyaniline in the presence of different types of surfactants shows the implementation of self-assembly of nanoparticles of polyaniline, which form a multi-layer coating on the surface of a polyamide fiber material.

References

1. Аксіментьєва О.І. Електрохімічні методи синтезу та провідність спряжених полімерів. – Львів: Світ, 1998. – 154 С.

2. Conductive electroactive polymers: intelligent materials systems. – 2nd ed. /Ed. Gordon G. et al. – London, CRC Press LLC, 2003.

3. Редько Я.В. Отримання електропровідних властивостей текстильних матеріалів в процесі опорядження: Дисс. канд. техн. наук: 05.18.19. – К., 2008. – 158 с.

4. Пат. (UA) 28451 U, МПК D06M 15/00. Спосіб отримання електропровідного волокнистого матеріалу / Романкевич О.В., Редько Я.В., Коваленко Р.В. (Україна). – № u200708676; Заявл. 27.07.2007; Опубл. 10.12.2007; Бюл. № 20. – 8 с.

5. Пат. (UA) 38517 МПК D06M 15/00. Спосіб отримання електропровідного волокнистого матеріалу / Романкевич О.В., Редько Я.В. (Україна). – № u200810005; Заявл. 01.08.2008; Опубл. 12.01.2009; Бюл. № 1. – 12 с.

6. Пат. 89070 Україна, МПК D06M 15/00. Спосіб отримання електропровідного волокнистого матеріалу / Романкевич О.В., Редько Я.В., Коваленко Р.В. – № a200708675; Заявл. 27.07.2007; Опубл. 25.12.2009. Бюл. № 24. – 8 с.

7. Редько Я.В., Романкевич О.В. Синтез поліаніліну за наявності різних типів поверхнево-активних речовин // Вісник КНУТД. – 2009. – № 5.– С. 168–174.

8. Кричевський Г.Е. Диффузия и сорбция в процесах крашения и печатания. – М.: Легкая индустрия, 1981. – 208 с.

9. Colloidal Particles at Liquid Interfaces // Ed. B. P. Binks and T. S. Horozov. – Cambridge – Cambridge University Press, 2006. – 503 p.

10. Self-Organized Morphology in Nanostructured Materials // Ed. K. Al-Shamery and J. Parisi. – Berlin – Springer–Verlag Berlin Heidelberg, 2008. – 175 p.

11. Travas-Sejdic J., Soman R., Peng H. Self-assembled polyaniline thin films: Comparison of poly(styrene sulphonate) and oligonucleotide as a polyanion // Thin Solid Films. 2006. – Vol. 497. – P. 96–102.

12. Зонтаг Г., Штренге К. Коагуляция и устойчивость дисперсных систем. – Л.: Химия, 1973. – 152 с.

13. Фридрихсберг Д. А. Курс коллоидной химии. – Л.: Химия, 1984. – 368 с.

14. Highlights in Colloid Science//Ed. Platikanov D. and Exerowa D. – Weinheim: WILEY-VCH Verlag GmbH & Co. KGaA, 2009. – 305 p.

15. Герасимов Я. И., Древинг В. П., Еремин Е. Н., Киселев А.В., Лебедев В. П., Панченков Г. М., Шлыгин А. И. Курс физической химии, т. 1. – М.: Химия, 1964.–624 с.

16. Шредер М. Фракталы, хаос, степенные законы. Миниатюры из бесконечного рая. – Ижевск: НИЦ «Регулярная и хаотическая динамика», 2001. – 528 с.

17. Романкевич О.В., Редько Я.В. Изотерма сорбции дисперсного красителя // Вісник Київського національного університету технологій та дизайну. – 2005. – № 4. – С. 35–40.

18. Песков Н. П. Физико-химические основы коллоидной науки. - М.: ОНТИ, 1934. – 325 с.

19. Li D., Jiang Y., Wu Z., Chen X., Li Y. Self-assembly of polyaniline ultrathin films based on doping-induced deposition effect and applications for chemical sensors // Sens. Actuators. B. – 2000. – Vol. 66. – P. 125 – 127.

20. Chiou N.-R., Lee L.J., Epstein A.J. Self-assembled polyaniline nanofibers/nanotubes // Chem. Mater. – 2007. – Vol. 19, Is. 15. – P. 3589–3591.

5.2.4 ATTRIBUTES OF COMPOSITE NONIONIC SURFACTANTS AND THEIR APPLICATION IN TEXTILE INDUSTRY

Paraska O.[1], Karvan S.[1]

For successful production development, in the context of fierce competition, great importance should be attached to the improvement of products quality and expanding the range. Detergents, textile chemicals for professional and domestic usage are convenience goods. The main manufacturers of detergents and textile chemicals (about 85 %) in Ukraine are such corporations, as: Procter & Gamble, S.C. Johnson, Unal ABC Chemicals Industry, Henkel, Interfil, Vinnytsia Pobutkhim, Milam, ONIKS [1]. The structure of usage of detergents is shown in the Figure 1.
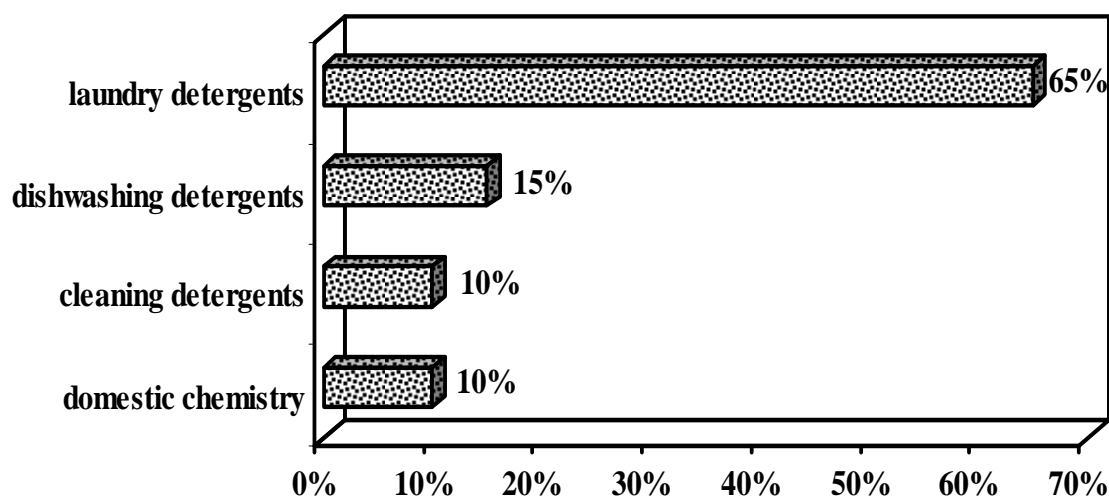
Fig. 1. The structure of usage of detergents

So, the biggest part of detergents (65 %) is detergents for clothes and textile goods care.

Development of detergents and textile chemicals market greatly depends on the living standards of population. Financial crisis negatively influenced on the development of the field: volume of domestic production and external trade has decreased, usage of comparatively cheap detergents has increased, usage of auxiliary products has reduced (rinses, conditioners, flavouring agents), product range has narrowed, the tendency to universal detergents usage has planned.

---

[1] Khmelnitsky National University, Ukraine

First of all, it is connected with the decrease of purchase power and fluctuation in the exchange rates. Small foreign companies have stopped delivery of detergents into Ukrainian market because the prices of detergents rise. At the same time, in crisis times, the portion of domestic detergents and textile chemicals usage has increased to 54 % from general amount.

Experts' researches [2,3] have shown, that notwithstanding strong competition, such segments of Ukrainian market as products for children, products in special selling forms (tableted, gel, sprays), organic products, industrial-use detergents are not saturated. Material costs make up almost 50 % of product's prime cost.

Surfactants are the basic components in the detergents and textile chemicals production [4,5,6]. The ability of surfactants to adsorption on the interface changes its characteristics, influences on important characteristics of dispersing systems and extensively uses in different technological processes. Depending on chemical nature, structure of phase boundary, surfactant molecules and conditions of their usage, this influence may de different. Surfactants, depending on their specific properties and characteristics can be used as wetting agents, conditioners, emulsifiers, dispersants, cleaning and antistatic agents, etc. Properties of surfactants in aqueous and non-aqueous mediums, and also their interaction with other components of washing system determine the efficiency of detergents. That's why, components of cleaning agents mostly determine products quality and influence on the efficiency of usage and on the products competitiveness.

At present, synthesis and production of detergents and surfactants [1,7] are organized in Closed Joint-Stock Company "Barva" (Ivano-Frankivsk region), Ltd "Lotos" (Kherson), Scientific and Technical Centre VNIIKHIMPROEKT (Kyiv), Open Joint-Stock Company "Krasytel" (Rubizhne), Open Joint-Stock Company "Crimean Soda Plant" (the Autonomous Republic of Crimea). But there is a problem of dependence on import and high price of raw materials for surfactants synthesis [8]. Moreover, the environmental and energy requirements to surfactants usage and processing become stricter every year.

Thereby, support and development of domestic raw materials on the basis of safe, effective, available and cheap substances with the aim of creation of competitive products for textile and other industry are conditined and necessary.

1. Problem definition

The peculiarity in detergents and textile chemicals production is creation of multifunctional products. Usage of such products allows to decide such tasks:

- to accomplish the direct removal of soils;
- to care about materials and protect the fabric surface;
- to impart special and functional properties.

At the same time, expenditures of chemical products, their amount and duration of processing are decreasing, and energy costs are reducing respectively.

Composition of detergents is formed empirically on the basis of research of washing and protective abilities of surfactants or the amount of removal soils, for washing of ones cleaning agent is used. Different artificial pollutants are used or exploratory wearing is conducted. Such reseachs not always give comparable results. That's why, for effective and optimal surfactants usage we should decide which colloid-chemical surface and bulk properties will be first-priority for the choosing surfactants as detergents.

The decision of this task is complicated by two facts. Firstly, there is the variety of surfactants, connected with their chemical composition, polarity, solubility and colloid-chemical properties of their solutions. Secondly, nowadays there are no unified and unambiguous assessment methods of some physical and chemical properties of surfactants. Emulsifying, wetting, solubilizing powers of surfactants, and also their washing power are determined empirically often with insufficient accuracy. It leads to impossibility of ambiguous assessment of surfactants efficiency in the specific technological process, including washing. That's why, first of all, we should solve the problem of estimation of surfactants efficiency and choose the most effective substances to the cleaning agents composition.

In our opinion, washing power can be estimated only by practical results of washing quality [9,10]: amount of removed soils from textile goods and their cleanness. On the other hand, there is strong interdependence between washing

power and the display of specific colloid-chemical properties of surfactants [11,12]: emulsifying, solubilizing, dispersive powers. So we can estimate the surfactants role on every stage of washing process and show interdependence between their functional and physical and chemical characteristics which can be estimated by known and widespread methods. The most important indicators of surfactants efficiency in washing process are given in Table 1:

- CMC [kg/m^3] – critical micelle concentration;

- $\Delta\sigma=\sigma_0-\sigma_S$ [mN/m] – decrease of surface tension of solution in surfactants presence (σ_S) in comparison with surface tension of solvent (σ_0);

- Γ [mmol/m^2] – adsorption of surfactants on the interface solution - air;

- Γ_{max} [mmol/m^2] – boundary absorption of surfactants on interface;

- W [J/m^2] – surfactants absorption work;

- a_m [m^2] – area per molecule in a filled monolayer;

- C_m [kg/m^3] – minimal concentration, at which stabilization effect of surfactants is shown;

- $\Delta\sigma$/CMC – maximal specific effect which can be achieved by surfactants micelle formation;

- θ [degree] – equilibrium angle of moistening of solid surface by surfactants solution at CMC;

- $\Delta\cos\theta=\cos\theta-\cos\theta_{water}$ – change of cosine of equillibrium contact angle on the paraffin surface in the presence of surfactants;

- $\Delta\cos\theta/\Delta\sigma$ – change of hydrophilic and lipophilic characteristics of the surface by means of surfactants adsorption on the interface of solid – liquid and $\Delta\sigma/\Gamma$, respectively for 2 nonmixed liquids interface;

- $\Delta\cos\theta$/CMC – maximal specific effect which can be achieved by moistening of solid surface;

- W_a [J/m^2] –work of adhesion to solid due to which strength of surfactants adsorption layers can be estimated;

- W_w [J/m^2] – work of surface wetting;

- HLB – hydrophilic-lipophilic balance of surfactants;

  − S_∞ – maximal surface, which can be stabilized by surfactants at the specific concentration;

  − K_s – stability factor of emulsion or dispersion which characterizes lifetime of dispersing system;

  − K_d – distribution coefficient of surfactants between emulsion phases;

  −   W.N. [ml] – water number (V_{water}), which characterizes hydrophilic properties of surfactants;

  −   E.N. [ml] – ethanol number ($V_{ethanol}$), which characterizes emulsifying properties of surfactants.

  The analysis of data in Table 1 has been shown, that all physical and chemical criteria of estimation of surfactants efficiency can be summarized to the such indexes: CMC, $\Delta\sigma$, $\Delta\cos\theta$, W, Γ, K_s, S_∞, C_m, K_d, molecular geometry, which can be determined on the basis of experimental study. Physical and chemical criteria in Table 1 can be used for preliminary estimation of surfactants efficiency as detergents.

  According to Peter Rebinder's theory [13], surfactants washing power is estimated by two main factors: their surface activity and surface strength of their films in aqueous medium, which, in turn, depend on the degree of dispersibility of washing agent in the solution and are described by curve with maximum. These two factors are initiators of surfactants washing activity, mostly, on the first two stages of washing process. In our opinion, third stage of washing process is limiting and long-time, especially the separation of soils from the fabric. This indicates that surfactants must have sufficient emulsifying, solubilizing and dispersive abilities. We think that taking into account of three properties of surfactants should be first-priority for choosing of detergents.

Table 1 - Estimation of surfactants efficiency in the washing process

№	Stages of washing process	Practical indexes of surfactants efficiency	Physical and chemical indexes of surfactants efficiency
1	Wetting of the material by washing solution	Increase of the penetration speed of washing solution into fabric	$\Delta\sigma$; θ; $\Delta\cos\theta/\Delta\sigma$; $\Delta\cos\theta/CMC$; W_a; $\Delta\cos\theta/\Gamma$; W_w
2	Adsorption of washing solution components on the surface of the fabric and the soils	Formation of surfactants adsorptive layers on the solid surfaces; distribution of the washing solution into the fabric	$\Delta\sigma$; Γ_{max}; W; W_a; S_m; δ; surfactants molecule geometry
3	Removal of soils molecules and particles from the fabric, as a result of:	Reducing of the soils amount on the fabric; increase of whiteness or purity of the color	
	dissolution	Raise of Washing power of solvent	Solubility, solvation of surfactants molecules in the solvent
	solubilization	Increase of the colloid solubility of soils in surfactants micelles	Solubility; CMC; HLB; W.N.
	emulsification	Formation of emulsions, the volume of emulsion, its lifetime, emulsion drops size regulation	HLB; K_S; S_∞; K_d; C_m; $\Delta\cos\theta/CMC$; W.N.; E.N.; surfactants molecule geometry
	dispersion	Facilitation of dispersion of particulate soils, decrease of adhesion between the fabric and the soil; lifetime and stability of dispersed system	$\Delta\sigma$; C_m; $\Delta\sigma/CMC$; $\Delta\cos\theta/CMC$; K_S
	foaming	Height of foam column and its stability	$\Delta\sigma/CMC$; C_m; K_S; S_∞
4	Stabilization of soils in washing solution	Protecive action; increase of dispersed system stability	$\Delta\sigma/CMC$; C_m; K_S
5	Removal of washing solution from the fabric	Reducing of the amount of soiled solution in the washing bath	$\Delta\sigma/CMC$; K_S; $\Delta\cos\theta/CMC$; viscosity and density of washing solution
6	Removal of the remnants of washing solution components from the fabric	Decrease of the amount of surfactants remnants on the fabric; number of rinses; volume of washing medium for rinse	$\Delta\sigma$; $\Delta\cos\theta/\Delta\sigma$; $\Delta\cos\theta/CMC$

2. Results of the research and discussion

Nonionic surfactants are used for a long time as components of cleaning agents [14]. These are products of combination of ethylene oxide to substances with developed hydrocarbon radicals: oxyethylated primary and second fatty alcohols, polyethylene glycol esters of fatty acids, oxyethylated alkylphenols. Saccharides, glucosides and glycerides also belong to nonionic surfactants. Nonionic surfactants are efficient when they are used in soft and hard water, in neutral, alkaline and acid mediums. Nonionic surfactants have strong solubilizing ability. Addition of nonionic surfactants into cleaning composition which are based on the anionic surfactants and their mixtures with ampholyte surfactants, allows to use the colouring agents, odorants, lipophilic antioxidants without any damage for consistence. The regulation of properties of nonionic surfactants by the change of the number of oxyethylene elements and low prime cost determine their mass production and common use.

Adsorption on the interface and creating aggregates of micelles play an important role in soils dispersion and solution, foaming, displaying of antibacterial effect. For understanding and prediction their effect, it is important to know the main interdependence between structure and properties of surfactants solutions, and to foresee the direction of properties change in multicomponent mixtures.

The main peculiarities of surfactants which determine their important qualities and common use, are:

- high surface activity;

- ability to free micelle formation – formation of liophilic colloid solutions with surfactants concentration higher some value (CMC);

- surfactants solutions ability to solubilization;

- high ability to stabilize disperse systems.

Research of colloid-chemical, technological properties of domestic nonionic surfactants on the base of oxyethylated products fibro-tex 4, fibro-tex 25, fibro-tex 6-25, fibro-tex 9-25 is presented by authors. The main component of the mentioned composite surfactants is Neonol AF 9-9 (9-10, 9-12) which belongs to oxyethylated nonilphenols with the general formula in Figure 2.
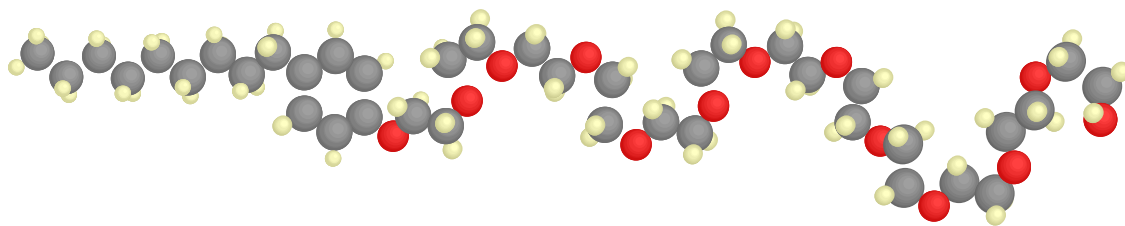
Fig. 2. General formula of Neonol AF 9-12

Surfactants surface activity determines their ability to lower surface tension, foaming, emulsification, dispersion, stabilization, wetting. Results of measuring of surface tension σ [mN/m] of the aqueous solution of the surfactant at critical micelle concentration and 20^0C are shown in the figure 3.
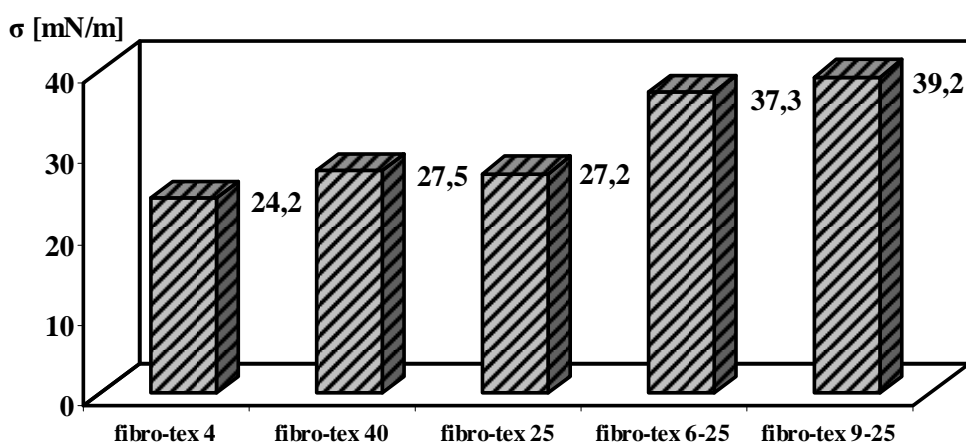
Fig. 3. Surface tension σ [mN/m] of the solution of surfactant

Among all investigated surfactants, fibro-tex 4 decreases the surface tension of water the most to 24,2 mN/m.

It is important to know CMC for assessment of surfactants activity and efficiency in different mediums and for foreseeing optimal additives to compositions in technological processes [15]. CMC values of surfactants aqueous solutions (see Table 2) at temperature 20 and 25^0C were estimated by different independent methods: estimation of surface tension on the interface solution – air (σ) according to Rebinder's method; measurement of solutions refraction index; estimation of optical density (turbidity) (D); measurement of solutions kinematic viscosity (υ).

Table 2 - Critical micelle concentration of surfactants

№	Properties	fibro-tex 4	fibro-tex 40	fibro-tex 25	fibro-tex 6-25	fibro-tex 9-25
1	σ	0.4/(1)	0.35	0.2/(1)	0.2	0.2
2	n	0.5	0.3	0.2	0.2	0.2
3	D	–	0.4	0.2	0.2	0.2
4	υ	0.4	0.3	0.25	0.2	0.2

Studies have shown that CMC of chosen surfactants solutions is observed at the concentration range $0.2 – 0.5$ kg/m^3. Another CMC of fibro-tex 4 and fibro-tex 25 at concentration area more 1 kg/m^3 are possible, that may be connected with complex micelles formation of other types.

Efficiency assessment of wetting power of surfactants is important in their usage in textile materials washing process. Surfactants hydrophilization occurs as a result of surfactants approximate adsorption on solid surfaces and increase of moistening by solvent respectively.

Examples of the dependence of contact angles of wetting of paraffin surface on their concentration in the solution is shown on the Figure 4.
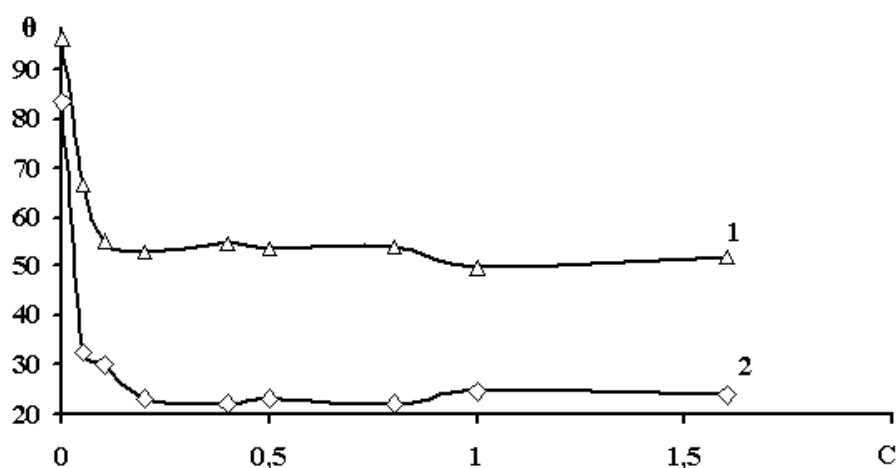
Fig. 4. Dependence of contact angles of wetting of paraffin surface on their concentration in the solution fibro-tex 25: 1 – the moment of contact of the solution with paraffin (θ_1), 2 –equilibrium angle of wetting (θ_2)

Contact angles were estimated at the moment of contact of the solution with paraffin (θ_1) and after 15 minutes, when thermodynamic equilibrium is attained (equilibrium angle of wetting (θ_2)). Both curves ($\theta_1=f(C)$; $\theta_2=f(C)$) have

identical character. The concentration of surfactant increase to $0,5 - 1$ kg/m^3, and it facilitates the increases of speed of drop spreading as well. It confirms the increase of solutions moistening power, after that contact angles reach maximum value.

Solubilization phenomenon [16] is commonly used in different processes which are connected with surfactants usage, e. g. in emulsion polymerization, emulsion lubricating liquids production, pharmaceutical preparations and foodstuffs production. Solubilization is the most important factor of surfactants washing power. Solubilization process is uncontrolled and inverse process. Completely determined saturation of the solution with solubilizer responds to the given surfactant concentration and temperature. As a result of solubilization, stable disperse systems (microemulsions, ultra and microheterogeneous emulsions) are obtained.

Analysis of the research results of oil-soluble red dye of Sudan III solubilization by surfactants in solutions show that this process is held in the wide range of concentrations (Figure 5).
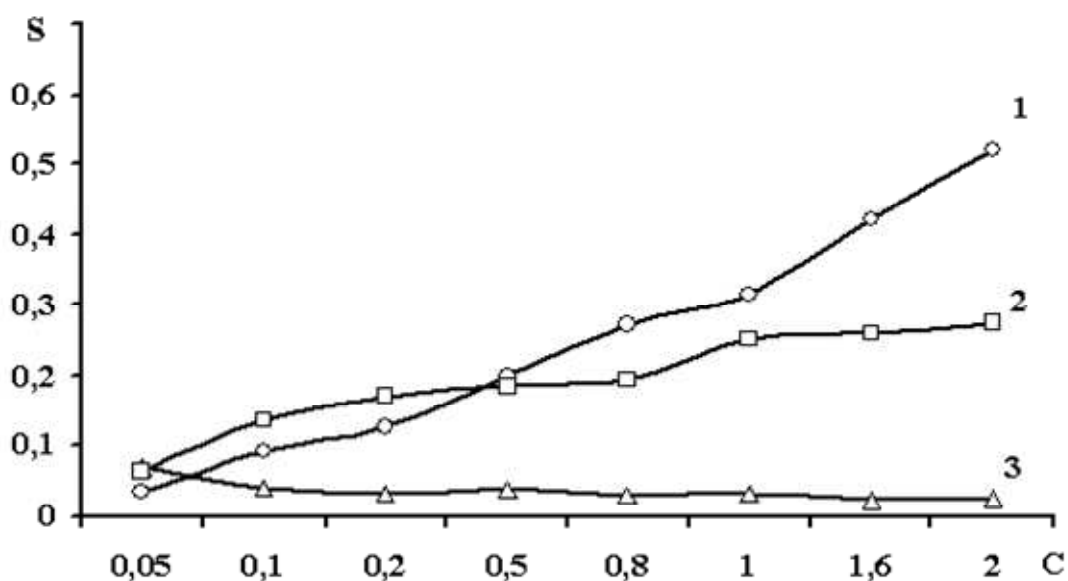

Fig. 5. Solubilization S [g/m^3] of the dye Sudan III:1 – fibro-tex 6-25; 2 – fibro-tex 9-25; 3 – fibro-tex 25

Minimal solubilizing effect responds to concentrations of CMC order, and it reaches the maximum value at concentrations which exceed CMC by $2 - 3$ times. The sharp rise of colouring agent solubilization by surfactants solutions

starts after CMC. Solubilizing ability of fibro-tex 40 and fibro-tex 25 occurs at higher a concentration that is explained by surfactants molecules adsorption on the colouring agent which is used for solubilization estimation.

Compositions of multicomponent washing systems [17 – 19] for processes of preliminary cleaning and for increasing of efficiency dry-cleaning have been elaborated on the basis of conducted research of colloid and chemical properties of surfactants.

The functional properties of fabrics: Ts [N] – tensile strength, S [%] – shrinkage, D [m] – fiber diameter, Δm [%] – weight change for textile materials after a single treatment (1 tr.) and fivefold (5 tr.) in perchlorethylene (PCE), in water (H_2O), in the composition have been determined [20, 21]. The changes of these properties are presented in Table 3.

Table 3 - The changes of properties of woolen fabrics

Treatment	Ts [N]		S [%]		$D \cdot 10^{-3}$ [m]		Δm [%]	
	1 tr.	5 tr.	1 tr.	5 tr.	1 tr.	5 tr.	1 tr.	5 tr.
PCE	9.44	9.31	0.13	0.54	0.531	0.677	0.49	-2.52
H_2O	9.43	8.89	2.11	4.16	0.778	0.834	0.57	-1.64
Composition	11.50	11.07	0.11	0.20	0.502	0.631	-0.23	-2.64

Studies have shown, that a sharp decrease of strength of fabric samples occurs after the first cycle of treatment.

Laser scanning the surface of woolen materials [22] showed that the thickness of fibers increases as the number and temperature of treatments increase (Fig. 6.).

Diameter fiber is $0.531 \cdot 10^{-3}$ m after a single cleaning and $0.677 \cdot 10^{-3}$ m after five circles of the cleaning at 60^0C in PCE. Significant increase of the diameter of the fiber is observed in the aqueous medium due to the swelling of the fibrous material and is $0.778 \cdot 10^{-3}$ m and $0.834 \cdot 10^{-3}$ m after a single treatment and fivefold, respectively. After processing in the compositions thickness of the fiber is $0.502 \cdot 10^{-3}$ m after a single treatment and is $0.631 \cdot 10^{-3}$ m after fivefold.
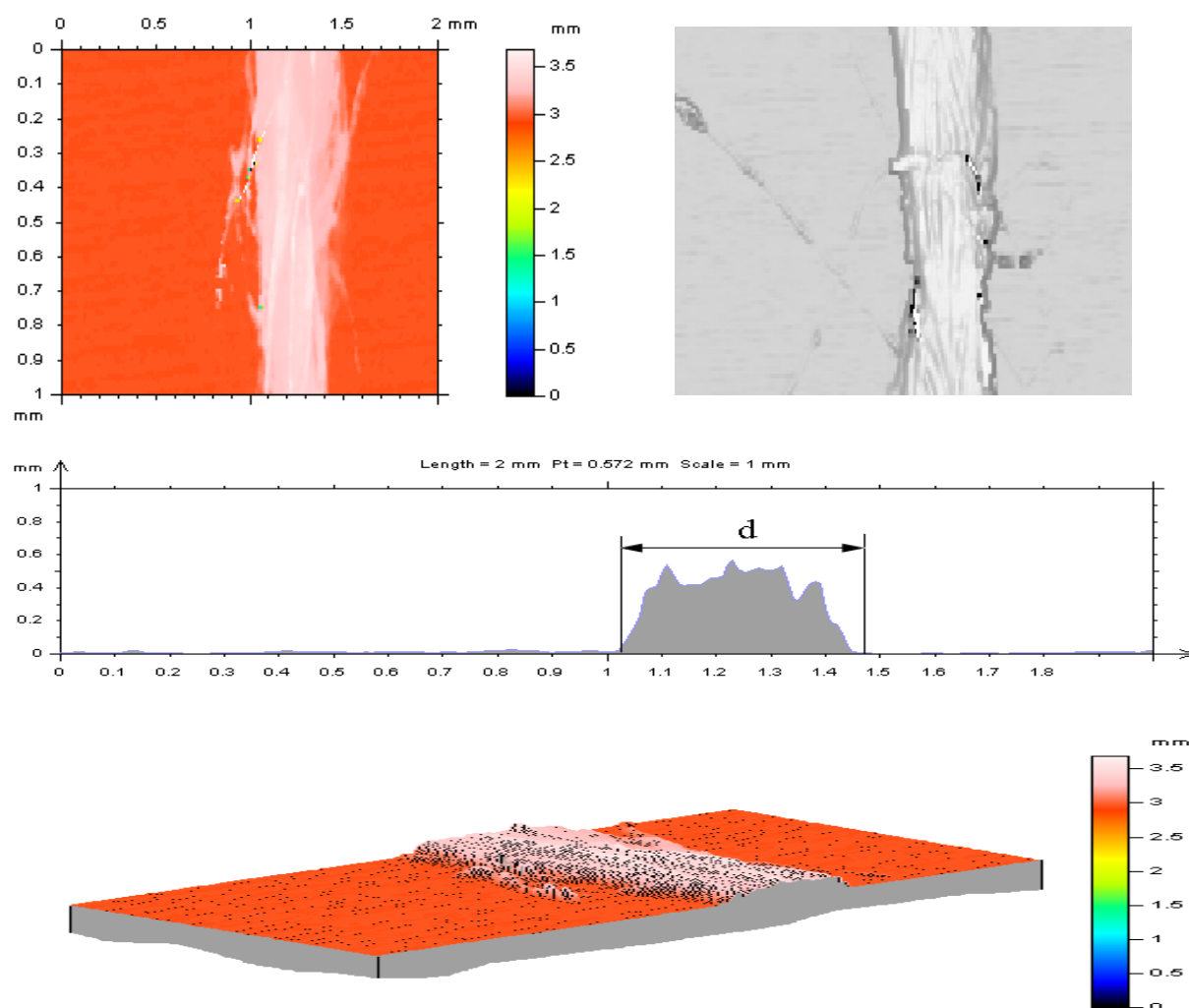
Fig. 6. Laser scanning the surface of woolen fibers after a fivefold in the composition

The study of the surface of woolen fibers after treatment in aqueous and non-aqueous environment indicates that the use of proposed compositions can increase resistance and antistatic properties of wool materials. Microphotograph of the surface of woolen fiber after treatment with the composition shows in Figure 7.
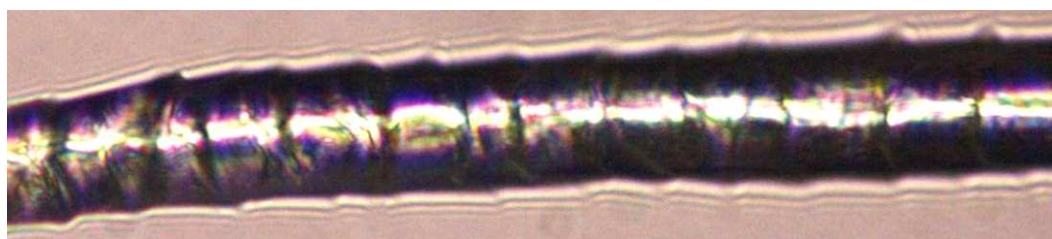

Fig. 7. The surface of woolen fiber after a fivefold in the composition

Conclusion

So, taking into consideration of experimental data, we can foresee surfactants efficiency in chemical-engineering processes of textile materials processing at their producing and usage in washing compositions.

Composition of multicomponent washing systems [17 – 19] for processes of preliminary cleaning and for increasing of efficiency of textile materials chemical cleaning has been designed on the basis of conducted research of colloid and chemical properties of surfactants. Also we have broadened the possibilities of their usage in goods processing processes according to the position of functionality and finishing effect.

References

1.   Chemistry of Ukraine 2 (248) (2010) 22 – 25.

2.   Gulenok, Yu.; Consumer Chemistry of Ukraine 7 (2003) 2 – 25.

3.   Chemical Industry of Ukraine 3 (92) (2009) 4 – 9.

4.   Durham, K.; Surface activity and detergency. – L., 1961. – 250 p.

5.   Detergency: Theory and Technology / Ed. By W.G.Gutler, E.Kissa. – N.Y., 1986. – 568 p.

6.   Volkov, V.A.; Surface-active substances in detergents and dry-cleaning. – M., 1985. – 200 p.

7.   Karvan, S.A.; Ukrainian Conference "Modern technologies in light industry and service", on May 18 – 19, 2011, Khmelnitskiy, p. 7 – 8.

8.   Business 31 (550) (2003) 22.

9.   Paraska, O.A.; Karvan, S.A.; Kulakov, A.I.; Visnyk KNUTD 2 (2006) 83 – 87.

10.   Karvan, S.A.; Bubenshchikova, G.T.; Paraska, O.A.; Problems of light and textile industry of Ukraine 1 (7) (2003) 37 – 39.

11.   Karvan, S.A.; Paraska, O.A.; Kulakov, A.I.; Visnyk KhNU 5 (2005) 98 – 101.

12.   Karvan, S.A.; Kulakov, A.I.; Paraska, O.A.; Light industry 4 (2008) 49.

13.   Rebinder, P.A.; Physics and chemistry of washing action. – M., 1935. – 158 p.

14.   Schoenfeld, N.; Nonionic detergents. – M., 1965. – 488 p.

15.   Paraska, O.A.; Karvan, S.A.; VII Ukrainian Conference "Scientific research of young people at the modern stage" on April 15 – 16, 2008, K, p.239.

16.   Paraska, O.A.; Karvan, S.A.; The work of scientific circles Rzeszów University of Technology (2008/2009) 169 – 176.

17.   Karvan, S.A.; Paraska, O.A.; Chryashchevskij, V.N.; Measuring and computer science in technological processes 2 (2009) 102 – 106.

18.   Karvan, S.A.; Paraska, O.A.; Kulakov, A.I.; Patent 25821, Ukraine 2007.

19.   Paraska, O.A.; Karvan, S.A.; Ksenjzuk, N.I.; Patent 43606, Ukraine 2009.

20.   Paraska, O.A.; Karvan, S.A.; Problems of light and textile industry of Ukraine №1(16) (2010) 35 – 38.

21.   Paraska, O.A.; Karvan, S.A.; Visnyk KhNU 4 (2010) 278 – 282.

22.   Paraska, O.A.; Light industry 3 (2010) 48 – 49.

5.2.5 DEVELOPMENT OF TECHNOLOGY FOR WOOL SCOURING ON THE BASIS OF COMPLEX PHYSICAL AND CHEMICAL METHODS OF INTENSIFICATION

Saribekova J.[1], Iermolaieva A.[1], Myasnykov S.[1], Myasnykova K.[1]

Introduction

Wool is an annually renewable natural resource grown on sheep. It is a planet friendly fibre as it has the ability to biodegrade without harm to the environment and can be recycled. These inherent advantages continue to underpin wool's heritage as today's best natural eco-fibre, just as they have done for many previous generations [1].

Wool is a high-tech fibre with a complex multi-layered structure that provides the key to wool's many and varied fibre properties. The structure and properties of fibers are shown in Figure 1 [2].

Wool is a multifunctional fibre with a range of diameters that make it suitable for clothing, household fabrics and technical textiles.

Its ability to absorb and release moisture makes woolen garments comfortable as well as warm. Two thirds of wool is used in the manufacture of garments, including sweaters, dresses, coats, suits and "active sportswear". Blended with other natural or synthetic fibers, wool adds drape and crease resistance.

Slightly less than a third of wool goes into the manufacture of blankets anti-static and noise-absorbing carpets, and durable upholstery (wool's inherent resistance to flame and heat makes it one of the safest of all household textiles).

[1] Kherson National Technical University, Kherson, Ukraine

Industrial uses of wool include sheets of bonded coarse wool used for thermal and acoustic insulation in home construction, as well pads for soaking up oil spills.
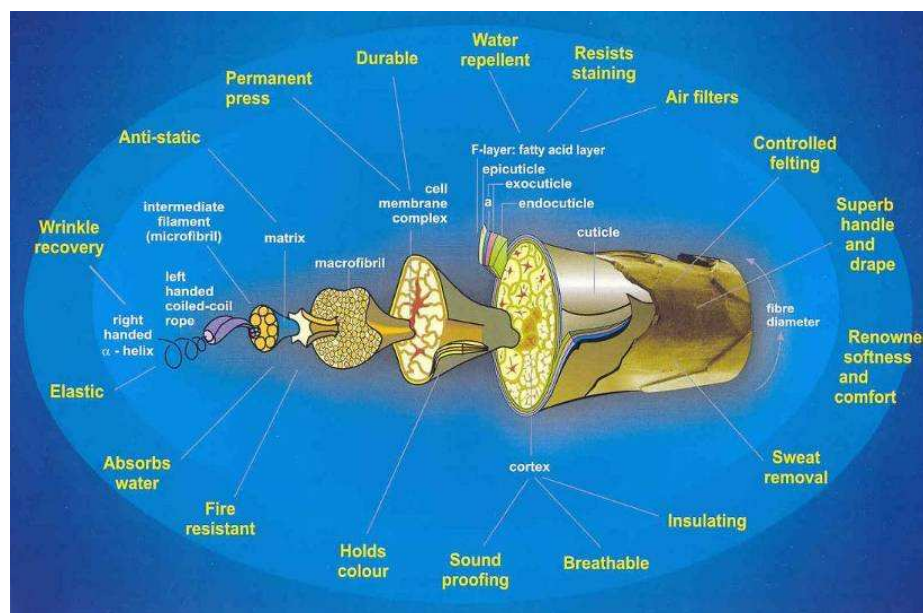
Fig. 1. The fibre of wool

Being a luxury fibre, demand for wool is sensitive to economic trends. The current global economic slowdown is expected to affect wool negatively, particularly by reducing demand in China, the world's biggest wool market. Also, falling oil prices may reduce the cost of synthetic fibers. To compete with synthetics, the wool industry continues to invest in new technologies which have made wool more attractive to consumers (e.g. crease resistance and wash ability) and given it a wider range of uses [1].

That's why all the more urgent the various ways to modify wool fibers that can improve the range of physical, mechanical and technological properties of wool.

This study is focused on the development of innovative technology of wool scouring with simultaneous modification of its surface structures (cuticle) by electro-bit nonlinear volume cavitations (ENVK).

Experiment

Studies carried out on fine merino wool Askanian breed – 70^s, III length.

Electro digit wool processing was carried out on an experimental installation "Vega - 6", which was established by researchers of the Institute of Pulse Processes and Technologies of the National Academy of Sciences of Ukraine (Nikolayev, Ukraine).
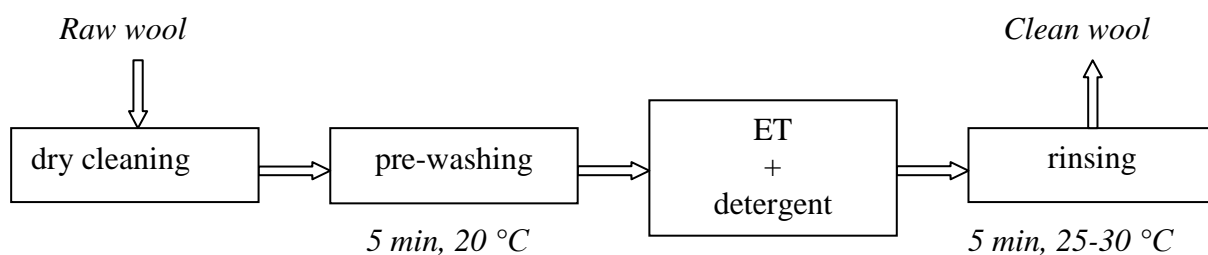
We have previously shown that a necessary condition for effective wool scouring and obtaining high-quality clean wool is the use of electric-treatment (ET) in combination with washing in detergent solution to remove wool grease [3]. In connection with the above, further investigation was carried out in two directions:

1. Study the possibility of using a single-stage wool scouring by the introduction of detergent into the ET reactor. The scheme of treatment is as follows:

Raw wool   *Clean wool*

dry cleaning	→	pre-washing	→	ET + detergent	→	rinsing
		5 min, 20 °C				*5 min, 25-30 °C*

In our view, with the possible following mechanism for the wool scouring: intensive mechanical action of ET contributes to the rapid destruction and dispersion of particles of greasy soils, which are separated from the fiber surface and pass into solution in the form of tiny droplets, enclosed in an adsorbed film of detergent molecules.

However, such a scheme would require treatment of frequent changes of washing solution to prevent pollution due to rapid resorption saturated solution of contaminants. Repeated deposition of pollution can also be caused by destruction of the solvate shells of detergent molecules due to intensive mechanical stress in the ET.

2. Study the possibility of using two-stage technology of wool scouring

The scheme of treatment of wool is as follows:

Raw wool   *Clean wool*

5 min., 25-30 °C

```
            ┌──────────────┐                    ┌──────────────┐
            │ dry cleaning │                    │   rinsing    │
            └──────────────┘                    └──────────────┘
                   │                                   ↑
            ┌──────────────┐   ┌──────┐   ┌──────────────────┐
            │ pre-washing  │ ⟹ │  ET  │ ⟹ │ washing with     │
            └──────────────┘   └──────┘   │    detergent     │
                                          └──────────────────┘
```

5 min., 20 °C
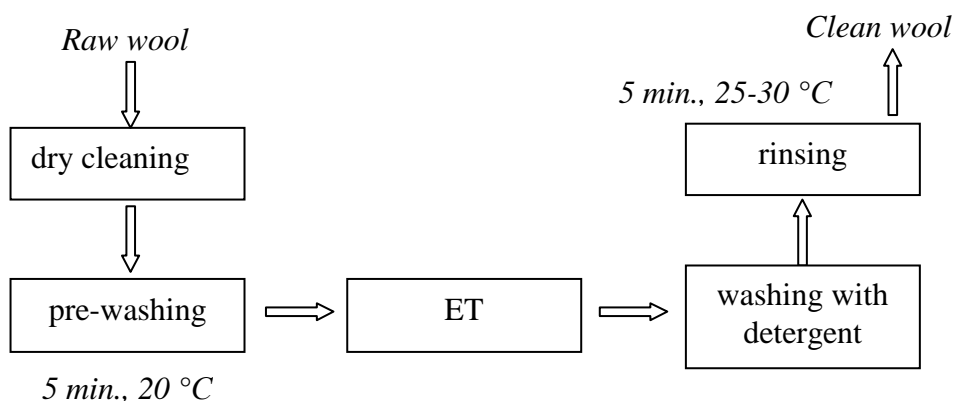
This scheme provides for the wool scouring following sequence of process steps: pre-cleaned wool goes to the ET reactor, where there is a removal of mineral and organic pollution, destruction of the film grease contamination on the fiber surface. Further wool goes to a wash solution of detergent composition, where there is the final cleaning of mineral, organic and grease substances.

To investigate the possibility of using single-stage technology of wool scouring the wool was treated according to scheme 1 by varying the concentration of the detergent and the treatment temperature from 20°C to 55°C.

The duration of treatment and the module of the bath were determined earlier [3].

As the detergent was used a composition of surfactants SULSID® we have developed earlier.

Data characterizing the degree of purification of wool on the concentration of the detergent and temperature of the solution are presented in Figure 2.

Increasing the concentration of the detergent composition with 1,5 g/l to 3,0 g/l with a simultaneous increasing of temperature contribute to more effectie removal of grease substances from the surface of wool fibers in ET.

The data presented in Figure 2, shows that increasing the concentration of the detergent composition with 1,5 g/l to 3,0 g/l within the range of temperatures 20°C, 45 C, 55°C reduces the content greasy pollution by 36,3%, 38,0% and 39,7% respectively.

Increasing treatment temperature from 20°C to 45°C significantly affects the process of wool scouring, helping to reduce grease impurities by 48,6% at 1,5 g/l and 50% at 3,0 g/l.
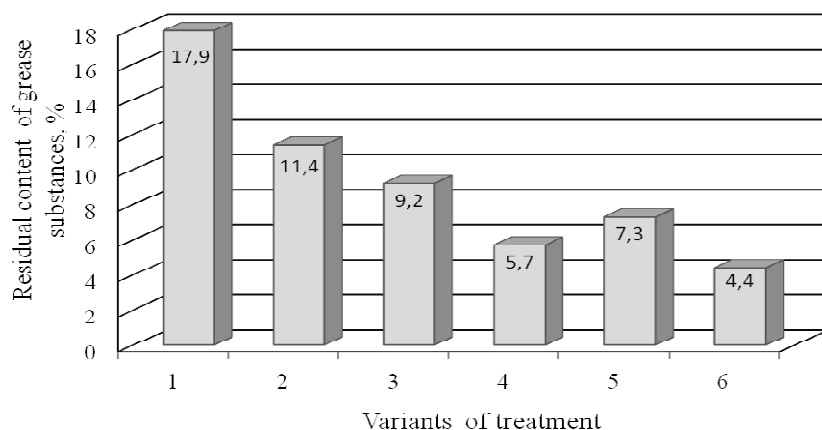
Fig. 2. Effect of concentration of the detergent composition and temperature of the solution in ET on the residual content of grease substances:
1 - 20°C, 1,5 g/l of detergent;
2 - 20°C, 3,0 g/l of detergent;
3 - 45°C, 1,5 g/l of detergent;
4 - 45°C, 3,0 g/l of detergent;
5 - 55°C, 1,5 g/l of detergent;
6 - 55°C, 3,0 g/l of detergent

Increasing the treatment temperature within 45-55°C has a lesser effect, reducing the impurity content by 20-23%.

Raising the temperature and the concentration of the detergent composition together with the mechanical action in ET promote emulsification and removal from the fiber surface most of grease soils, but not enough to get the clean wool that meets the requirements of standard (residual contamination of grease should not exceed 2% by weight raw wool).

Further increasing of the temperature can lead to increasing of wool fibers damage. In our view, increasing the concentration of the detergent composition is not desirable, because of difficulties in waste water treatment.

The results obtained formed the basis for investigating the possibility of a two-stage technology of wool scouring, carried out by the scheme 2.

In this case the probable mechanism of contamination removal of wool grease can be represented as follows:

1. Stage – the ET. Destruction and fragmentation of grease film on the surface of wool fibers due to the impact of the complex factors of cavitations:
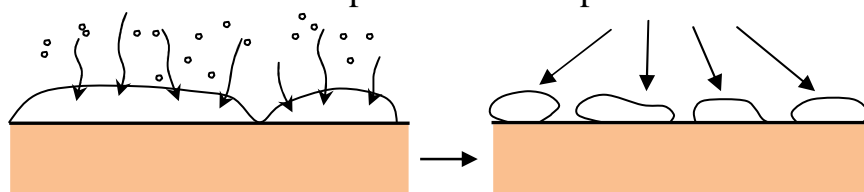
2. Stage – washing in a solution of detergent composition. Emulsification and removal from the surface of wool fibers milled particles of wool grease:
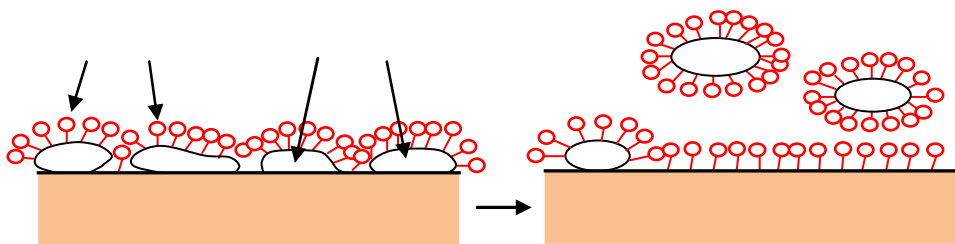
To determine the main technological parameters of ET and washing in a solution of detergent composition was carried out the optimization of wool scouring on the basis of mathematical experiment planning [4, 5].

To optimize the cleaning process is to determine the technological parameters of processing, which would ensure maximum optimization criterion ($\hat{Y}$), in this case - the residual content of grease substances.

It has been suggested that the effectiveness of the wool scouring based on ET is dependent on three main factors:

1. the concentration of detergent (C, g/l),
2. the temperature of washing (T, °C),
3. the time of electrical treatment (τ, min).

To obtain the mathematical effect of the concentration dependence of cleaning agents, temperature, washing, time of electrical treatment on the quality of clean wool conducted a full factorial experiment of type 2^3, consisting of eight experiments [5].

Factors, varying levels of factors and the variation intervals are presented in Table 1.

As a result of calculations we obtain the following equation:

$$\hat{Y} = 3{,}3 - 0{,}38 \cdot C - 0{,}36 \cdot \tau$$

According to the obtained regression equation in the investigated factor space dependence of the residual content of grease substances (Y) on the concentration of detergent treatment (C) and time of electrical treatment (τ) takes the form of three-dimensional plane (response surface), which is shown in Figure 3.

Table 1 - Factors and levels of varying factors

designation	Factors	Levels of variation			Variation interval, ε
		-1	0	+1	
C	Concentration of detergent, g/l	0,5	1,5	2,5	1
T	Temperature of washing, °C	40	45	50	5
τ	Time of electrical treatment, min	1	3	5	2

The resulting mathematical model of wool scouring indicates that the desired value of the optimization criterion - the residual content of grease substances - is within the investigated factor space. In this case, the optimal residual content of grease substances (1.63%) can be achieved with values of the factors corresponding to the zero level.

The resulting clean wool, treated by the developed technology, characterized by the following indicators of quality:

- residual content of grease substances - 1.63%;

- moisture content of wool - 15.6%.

Conclusion

It is established that the technology of wool scouring on the basis of consecutive operations ET and washings in a solution of a washing composition is most effective.

The method of planning of experiment receives mathematical model of process of wool scouring. It is shown that the criterion of optimization - a residual content of grease substances - in the chosen factorial space is influenced by two factors - concentration of a washing preparation and time of ET.

Optimum technological parameters of process of wool scouring are defined: concentration of a washing composition 1,5 g/l; temperature of water washing – 45 °C; time of ET - 3 mines.

References
1.   http://www.iwto.org/wool accessed August 13, 2011.
2.   http://www.csiro.au accessed August 13, 2011.

3.   Iermolaieva A., Saribekova J., Myasnykov S. (2008) Justification of the choice of two-stage processing technology of wool on the basis of an electric non-linear volume cavitation and optimization of its parameters, Herald of Khmelnitsky National University 1, 111-114.

4.   Vinogradov U.S. Mathematical statistics and its application in textile and light industry, Moscow, Light Industry, 1970, 370 p.

5.   Tihomirov V.B. Planning and analysis of the experiment, Moscow, Light Industry, 1974, 262 p.

5.2.6 FILM-FORMING POLYMER MATERIALS BASED ON AMIDE- AND URETHANE DERIVATIVES OF NATURE OILS

*Bubnova A.[1], Gudzenko N.[1], Barantsova A.[1], Sysyuk V.[1], Grishchenko V.[1]*

The investigations was done in the department of Chemistry of Oligomers and Ccross-linked Polymers IMC NASU under the direction of Corresponding Member, Prof. Valery Shevchenko

Mechanical properties of the polymers based on the plant oils possess excellent damping and shape-memory behavior over a wide range of temperature. Such materials have numerous applications in aircraft, automotive industry for the reduction of undesirable noises, for prevention of the vibrational fatigue failure, as well as in the building constructions, manufacturing, electronics etc. Research and investigation of the properties of plant oils and their potential to be used in polymer synthesis and modification attract very intensive scientific interest in the world.

Plant oils are the mixture of triglycerides of the saturated and unsaturated fatty acids. Their general structure is shown in Scheme 1:

The main characteristic fragments determining their chemical reactivity are ester groups of glycerol centers (marked by red in dot circles), unsaturated bonds of the fatty acid fragments (marked by pink) and functional hydroxyl groups (blue ones).

[1] Institute of Macromolecular Chemistry of National Academy of Sciences of Ukraine, Kyiv, Ukraine
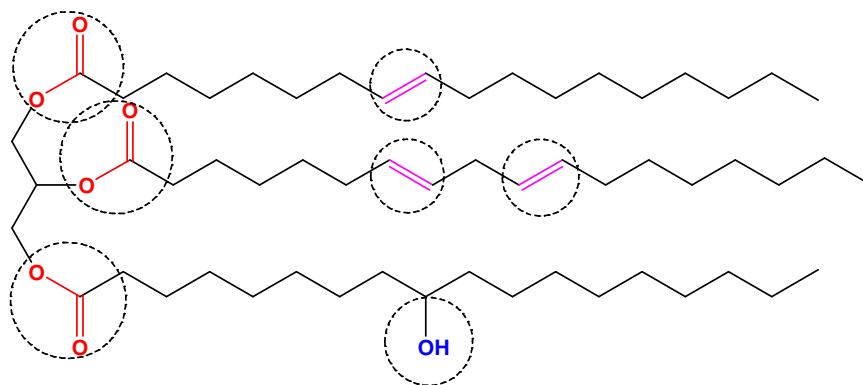
Scheme 1. General chemical structure of the plant oils.

The type and content of the fatty acid fragments (so called fatty-acid distribution) vary depending on the nature of a plant from which they are derived. For instance, linseed oil is based on the linoleic and linolenic acids, castor oil contains mainly the fatty ricinoleic acid, some of their characteristics are given in Table 1.1. Depending on the fatty-acid distribution each type of oil has its characteristic physical and chemical properties.

By the chemical structure, natural plant oils are mixture of the glycerin esters of different, mainly unsaturated, fatty acids, which differs from each other by a degree of unsaturation and a position of the double bond. Ability of the plant oils to "dry" in thin film under the air atmosphere increases at an increase of acid residues containing two or three double bonds. Moreover, presence of the conjugated double bonds significantly accelerates drying.

Degree of the unsaturation of the plant oils can be estimated by iodometry, when iodine number is given as mg of iodine reacted with one double bond. [6-9]. Depending on this parameter, plant oils are determined as drying (iodine number >130), semi-drying (iodine number is between 90 and 130) and non-drying (iodine number is less than 90). Linseed, tung, teak oils are drying oils, sunflower-seed, soybean oils are semi-drying, and coconut oil is non-drying oil.

Castor oil is intensively used in the polymer synthesis. Due to its hydroxyl functionality, it reacts easily with isocyanate compounds resulting in the formation of polyurethane elastomers of different structure including interpenetrating polymer networks (IPNs) [10-14]. Considerable effort is made

Table 1 - Fatty acid content of the plant oils

Fatty acid	Mn	Formule	ρ, g/cm^3	Iodine value	Oil
Linolic	280,44	$CH_3(CH_2)_4CH = CHCH_2CH = CH(CH_2)_7COOH$	0,92	181,1	All
Linolenic	278,4	$CH_3CH_2CH = CHCH_2CH = CHCH_2CH = CH(CH_2)_7COOH$	0,905	273,5	Drying oils
Olein	282,45	$CH_3(CH_2)_7CH = CH(CH_2)_7COOH$	0,898	89,9	All oils
Pal'mitiloinova	254,4	$CH_3(CH_2)_5CH=CH(CH_2)_7COOH$	-	298,8	Olive, woolen
	299	$CH_3(CH_2)_5CHOHCH_2CH=CH(CH_2)_7COOH$	0,95	85,1	Castor oil
Ricinoleva	278,4	$CH_3(CH_2)_3CH=CHCH=CHCH=CH(CH_2)_7COOH$	-	182	Tungova, yotsikova
Eleostearinova	338,56	$CH_3(CH_2)_7CH=CH(CH_2)_{11}COOH$	0,888	75	Mustard, rape, nut, rizhikova
Erukova	312,52	$CH_3(CH_2)_{18}COOH$	0,824	-	Peanut, corn, mustard, rape
Arachic	284,5	$CH_3(CH_2)_{20}COOH$	0,822	-	Woolen, copra, linen, palm
Behenic	228,36	$CH_3(CH_2)_{12}COOH$	0,844	-	Practically all
Miristinova	256,42	$CH_3(CH_2)_{14}COOH$	0,841	-	Practically all
Palmitic	284,5	$CH_3(CH_2)_{16}COOH$	0,845	-	Practically all
Stearin					

for the production of manufacturing varnishes, enamels, paints, lubricants and surfactants.

One of the plant oils derivatives being widely used in the paint and varnish industry are alkyd resins. They are the product of trans-esterification of plant oils with polyols and are the main film-forming component of enamels due to the oxidation reaction of the fatty acid fragments.

This article describes the modification of the plant oils such as soybean, linseed and castor oils by target functional groups, such as amide, amine and isocyanate ones, and application of such derivative products in the synthesis of polymer materials with improved exploitation properties.

1. Experimental part

As oil reagents castor, linseed, soybean, and sunflower-seed oils were used for the functionalization. As amide reagent hydrazine-hydrate was used. Chemical reaction was carried out at 50 °C at vigorous stirring for 6-8 hours. As amine reagents the following amines were used: monoethyle amine (MEA), 3-aminopropyle triethoxysilane (APTS), cyan-ethylated triethyl triamine (CETTA). Chemical reaction was carried out at 20 °C at vigorous stirring and acid catalyst. Isocyanate functionalization was carried out for the castor oil with 2,4-toluendiisocyanate (TDI).

Completeness of the reaction of functional groups was monitored by both Fourier-transform infrared (FT-IR) spectroscopy and potentiometric titration. The synthesized products were characterized by gel permeation chromatography (GPC) by Waters chromatograph with two columns (Srygel HR). The calibration was performed with polystyrene standards Shodex S-105, as an eluent tetrahydrofuran was used.Fourier transform infrared (FT-IR) spectroscopic measurements were performed on a Tensor-37 spectrometer (Bruker, Germany) between NaCl glasses.

FT-IR spectra were recorded in the transmission mode in the wavenumber range 4000-600 cm^{-1}.

2. Discussion

The general scheme of the chemical reaction of the amine/amide modification of the plant oils is shown in Scheme 2.
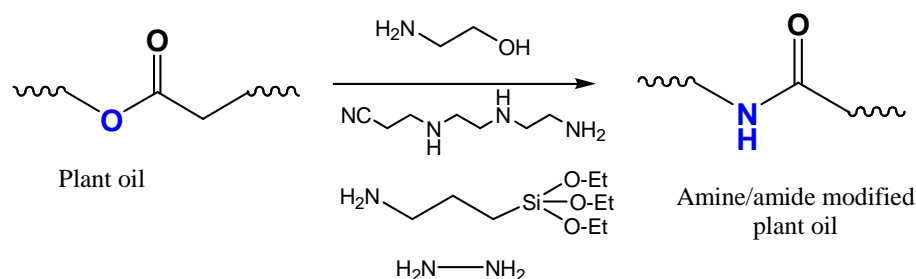
Scheme 2. Chemical scheme of the plant oils modification

Amide-modification

Structural characteristics of the products of the chemical reaction of plant oils with hydrazine-hydrate and their melting temperatures (T_m) are given in Table 2.

Table 2 - Structural characteristics of the amide-modified products

Reagent 1	Reagent 2	T_m, ^{o}C	FT-IR characteristic bands, cm^{-1}
Sunflower oil	Hydrazine-hydrate	70-75	$\nu_{C=O}$ hydrazide groups 1640 cm^{-1}, and ν_{NH} 3190 and 3330 cm^{-1}, δ_{NH} 1540 cm^{-1},
Linseed oil	Hydrazine-hydrate	85-90	$\nu_{C=O}$ hydrazide groups 1640 cm^{-1}, and ν_{NH} 3180 and 3340 sm^{-1}, δ_{NH} 1540 cm^{-1},
Castor oil	Hydrazine-hydrate	55-60	$\nu_{C=O}$ hydrazide groups 1630 sm^{-1}, and ν_{NH} 3220 and 3320 sm^{-1}, δ_{NH} 1540 sm^{-1},

As can be seen from the FT-IR data, the products of the modification contain amino-groups, indicating the chemical reaction with hydrazine-hydrate.

Amine-modification

The products of the amine modification by mono- and poly-amines are pastes from light-yellow to brown in color. Their melting point is 32-38 °C, they

are soluble in ketones, alcohols and most of the aromatic solvents. Their FT-IR spectra are presented in Figure 1.

As can be seen, the spectra of the modified products contain bands at 1638 та 1545 cm^{-1} which can be attributed to the bending vibrations of the NH groups. The double band with peaks at 3330 and 3380 cm^{-1} corresponds to the stretching vibrations of the NH groups. The main characteristics of the amine-modified plant oils are presented in Table 3.
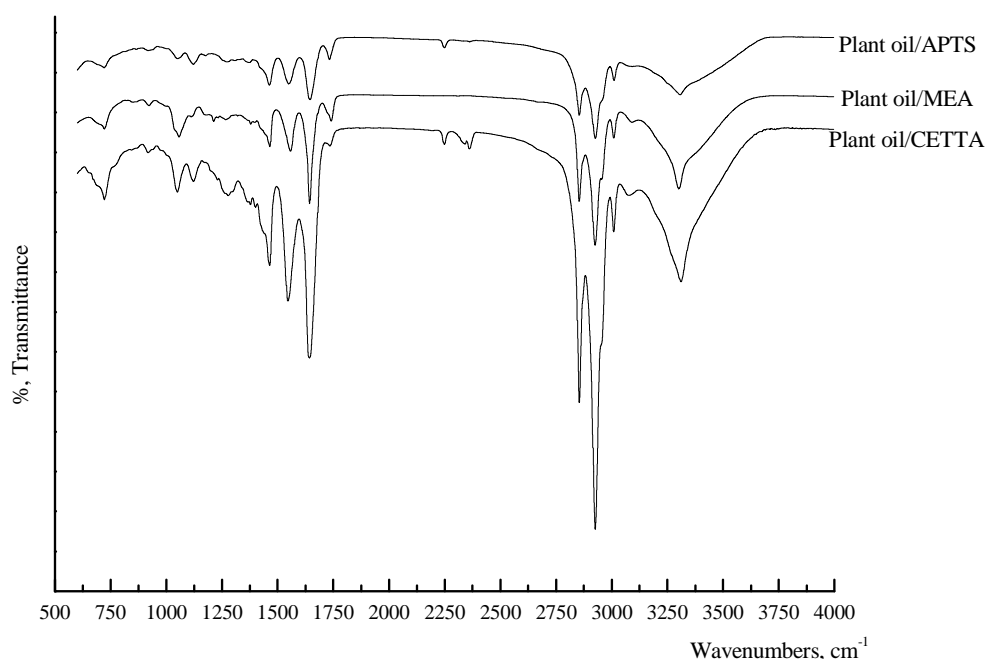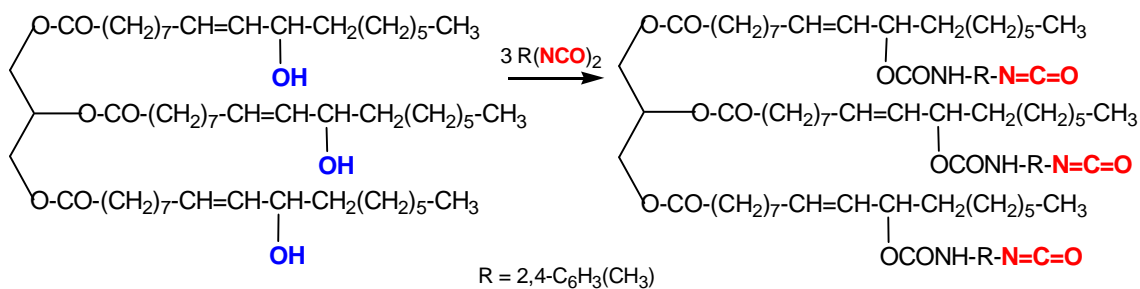

Fig.1. FT-IR spectra of the amino modified oils

Isocyanate-modification

For the isocyanate functionalization, castor oil was reacted with TDI (NCO/OH ratio 1:2) at temperature 70 °C at continuous stirring for 4-6 h. The product of the modification (oligourethane isocyanate, OUI) is a viscous liquid. The chemical reaction, FT-IR spectra are presented in Scheme 3 and Figure 2.

Table 3 - Characteristics of the amine-modified plant oils

Amine-modified plant oils	GPC			Molar ratio (amine/oil)	OH value, %	Iodine value, % mg J /100г	NH value, %
	Mn, g/mol	Mw, g/mol	M_w/ M_n				
Plant oils/CETTA (I)	452	660	1.46	3/1	3.0	126.4	3.54
Plant oils/CETTA (II)	550	617	1.12	2/1	5.7	126.3	4.8
Plant oils/MEA (III)	387	565	1.5	3/1	4.7	127.3	6.2
Plant oils/MEA (IV)	620	667	1.1	2/1	3.6	127.7	6.5
Plant oils/ATPS (V)	692	804	1.16	3/1	1.5	125.5	3.9
Plant oils/ATPS (VI)	810	891	1.09	2/1	3.0	127.6	3.0

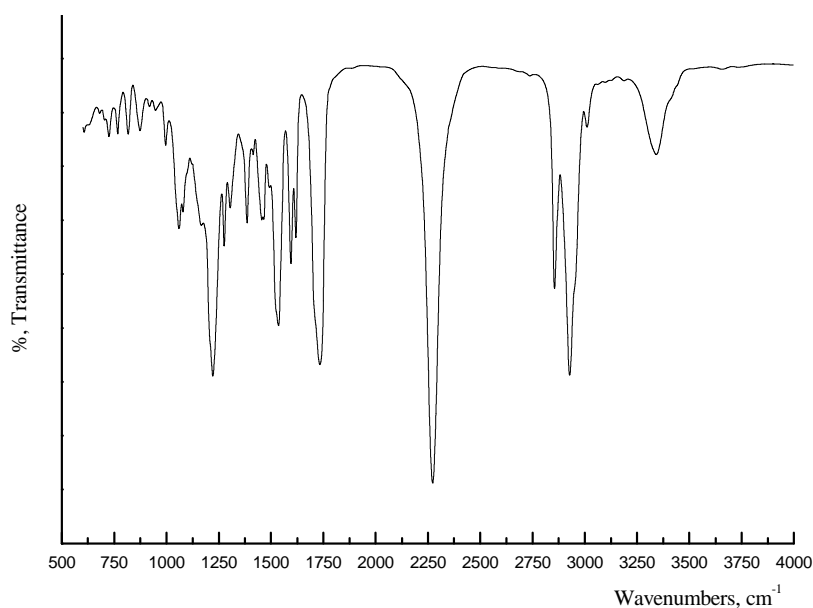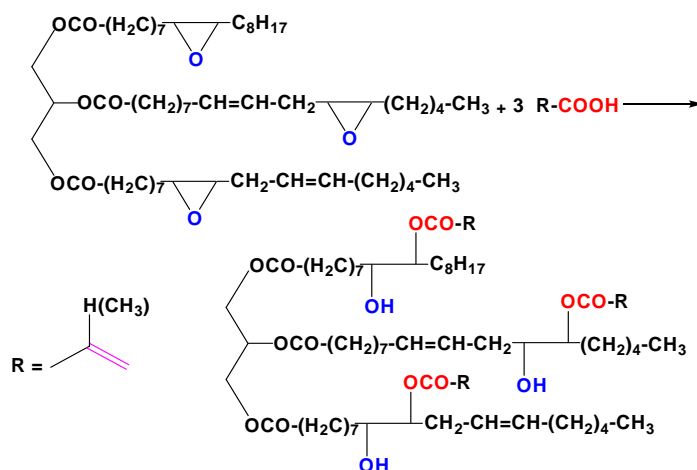**Scheme 3. Chemical scheme of the castor oil modification by TDI**

Fig.2. FT-IR spectra of the isocyanate castor oil

477

Esterification of the epoxy-modified oils

Apart from the neat plant oils, the reactions of the epoxy-modified plant oils were investigated in an esterification reaction with carbon acids, the chemical structure is shown in Scheme 4. The reaction with natural carbon acid compound, rosin, was carried out at 140 °C and acid catalyst.

Scheme 4. Scheme of the chemical reaction between epoxy-modified castor oils and carbon acids

The structure of the obtained products was investigated by FT-IR spectroscopy. As can be seen from their FT-IR spectra decrease of the intensity of the band corresponding to the epoxy groups at 930 cm^{-1} and increase of the band intensity of the ester groups at 1740 cm^{-1} indicates the reaction of epoxy groups of oil with carbon acids.

Polymer materials based on the amine- and amide-modified plant oils

Chemical modification of the plant oils by amine functional groups allows their application as a curing agent of the epoxy resins. Due to the plasticizing effect, use of the vegetable oils in the modification of epoxy resins improves the mechanical performance of such composites (flexibility, impact strength, scratch resistivity etc.). Moreover, introduction of double bonds within the fatty acid fragments brings additional reactive centers improving the curing reaction at ambient conditions.

CETTA modified sunflower-seed oil was used as a curing reagent for the epoxy resin DER-331. In order to improve wearing resistance of thin films, aromatic polyisocyanate was used for the introduction of the urethane groups. The condensation reaction was carried out using buthylacetate as a solvent.

Thin films were obtained in air atmosphere at ambient temperature, their main physico-mechanical characteristics are given in Table 4.

Table 4 - Physical-mechanical characteristics of the thin films based on epoxy resin and modified sunflower-seed oil

Parameter	Value
Appearance	Transparent, homogeneous
Time of drying to stage 3, hour	1.5
Hardness, a.u.	0.65
Glance, %	95
Elasticity, mm	1-2
Impact strength, kg	40

According to the data presented, obtained films are characterized by the accelerated drying, which is due to the presence of additional reactive centers introduced with fatty acid fragments of the plant oils. Mechanical properties of the films are quite high, which makes them promising materials for application as caulking compounds, sealant materials and protective coatings.

Alkyd resins modification by silan derivatives of plant oils

Alkyd resins are widely used in the synthesis of the protective coatings. Their important advantages are rapid drying at air atmosphere, good adhesion to the different substrates and high flexibility. However, their poor exploitation properties such as brittleness and instability toward aggressive media restrict their application. Modification of alkyd resins by silicone containing plant oils significantly reduce such disadvantages and improves protective properties of the coatings [15-17].

In our work, we used APTS-modified linseed oil for the modification of alkyd lacquer PF-060. The main characteristics of the produced films are presented in Table 5 and are compared to the coating based on the unmodified commercial PF-060.

Table 5 - Comparison of the physical-mechanical properties of the coatings based on unmodified PF-060 and silicon-modified linseed oil

Parameter	Coatings based on PF-060	Silicon-linseed oil modified coatings
Appearance	Transparent homogeneous film, light-yellow	Transparent homogeneous film, light-yellow
Time of drying to stage 3, hour	10	6
Hardness, a.u.	0,3	0,35
Glance, %	95	95
Adhesion,	1	1
Impact strength, kg	50	50
Elasticity, mm	1	1
Firmness of coverage to the action, hour: - water of technical; - hot 30% sodium solution; - 30% sodium solution;	Not proof Not proof Not proof	24 1-2 7 діб

As can be seen, introduction of the additional reactive centers within the functionalized derivatives of the vegetable oils, different polymer materials can be obtained with target properties. Such composite materials can find numerous applications in micro- and radio-electronic, as protective coatings, varnish, plasticizers and many others.

References

1. Vinay Sharmaa and P.P. Kundu. Addition polymers from natural oils // A review Progress in Polymer Science. – 2006. - Volume 31, Issue 11 , November, P. 983-1008.

2.F. Seniha Günera, Yusuf Yağcıb,, and A. Tuncer Erciyesa. Polymers from triglyceride oils // Progress in Polymer Science. -   2006. - Volume 31, Issue 7 , July, P. 633-670.

3. S.N. Khot, J.J. Lascala, E. Can, S.S. Morye, G.I. Williams and G.R. Palmese *et a.* Development and application of triglyceride-based polymers and composites // J Appl Polym Sci. - 2001, Volume 82, No 3, - P. 703–723.

4. Patent USA 7196124, Current US Class 523/457. Harry W. Parker, Richard W. Tock, Fang Qiao, Ronald S. Lenox. Elastomeric material compositions obtained from castor oil and epoxidized soybean oil. Publ. 27.03.2007.

5. Patent USA 7279448, Current US Class 508/491 , 554/102 , 554/124 , 554/149 , 554/24. Brajendra K. Sharma, Atanu Adhvaryu, Sevim Z. Erhan. Poly(hydroxy thioether) vegetable oil derivatives useful as lubricant additives. Publ. 09. 10.2007.

6. Firestone D (May-Jun 1994). "Determination of the iodine value of oils and   fats: summary of collaborative study". *J AOAC Int.* **77** (3): 674–6.

7. Weiss K. D. Paint and coatings: A mature industry in transition // Progress in Polymer Science. – 1997. – Vol. 22, №2. – P. 203-245.

8. Igwe O., Ogbobe O. Studies on the properties of polyester and polyester blends of selected vegetable oils / J Appl Polym Sci.- 2000.- Vol.75 .- P. 1441–1446.

9. Oyman Z.O., Ming W., Linde R. Oxidation of drying oils containing non-conjugated and conjugated double bonds catalyzed by a cobalt catalyst // Progress in Organic Coatings.- 2005.-Vol. 54, № 3.- P. 198-204.

10. Xie H.Q., Guo J.S. Room temperature synthesis and mechanical properties of two kinds of elastomeric interpenetrating polymer networks based on castor oil // European Polymer Journal.- 2002.- Vol. 38, №11.- P. 2271–2277.

11. Athawale V., Suresh K. Interpenetrating polymer networks based on modified castor oil polyurethane and polymethacrylate // Polymer Journal.- 1998.- Vol. 30, №10.- P.813–818.

12. Athawale V., Kolekar S. Interpenetrating polymer networks based on oil modified castor oil urethane and poly(methyl methacrylate) // Journal of Macromolecule Science—Pure Applied Chemistry.- 2000.- Vol. 37(A).- P. 65–79.

13. Athawale V., Pillay P.S. Interpenetrating polymer networks based on hydrogenated castor oil-isophorone diisocyanate and poly(butyl methacrylate) // Bulletin Chemistry Society Jpn.- 2002.- Vol. 75, №2.- P. 369–373.

14. Sanmathi C.S., Prasannakumar S., Sherigara B.S. Interpenetrating polymer networks based on polyol modified castor oil polyurethane and poly(2-ethoxyethyl

methacrylate)— synthesis, chemical, mechanical, thermal properties, and morphology // Journal of Applied Polymer Science.- 2004.- Vol. 94, №3.- P. 1029–1034

15. Horst H. Brüning. Utilization of vegetable oils in coatings // Industrial Crops and Products.- 1992.- Vol. 1, №2-4. – P. 89-99.

16. Rubber seed oil modified with maleic anhydride and fumaric acid and their alkyd resins as binder in water reducible coatings / Aibgodion A.I., Okieimen F.E., Ikhuoria E.U., Bakare I.O., Obazee E.O. // J. Appl. Polym. Sci.- 2003.- Vol. 89, №12.- P. 3256-3259.

17.Weiss K. D.. Paint and coatings: A mature industry in transition // Progress in Polymer Science. – 1997. – Vol. 22, №2. – P. 203-245.

5.2.7 A DESIGN OF PROCESS OF CAUSING OF POLYMERIC COVERAGE IS ON FABRICS

Petegerych S.[1], Paraska G.[1], Misiats V.[2]

The technological process of causing of thermoplastic polymeric material on the surface of fabric consists of two basic operations: causing of parts of polymer on the surface of fabric by the stream of the heated air forming of continuous layer of polymeric coverage by means of warmed-up rollers. The processes of rolling of polymers are investigational full enough, while the process of causing of hot-melt is difficult enough and investigational [1].

Will present the process of causing of parts of polymer a physical model. Parts of polymer move rectilineal in the streams of air which is heated to the temperature $T_{пов}$. Stream has speed v and sent to the plane of material under a corner α. During the blow of parts of polymer at the surface of material place is taken them common resiliently - flowage. A plastic constituent of deformation is remaining and results in the increase of area of contact of parts with material. Between parts of polymer and surface of material there are forces of adhesive contact. The resilient constituent of deformation after a blow recommences and causes the reverse impulse of parts, which results in diminishing of force of their co-operating with material and, at certain terms, even to their tearing away. At the defined value of corner α possible of slipping of parts of polymer is for the surfaces of material. Will accept next positions for simplification of model:

---

[1] Khmelnytskiy National University
[2] Kyiv National University of Technologies and Design

- the vectors of speed of parts of polymer are identical to direction and size which is permanent and equals speed to the stream of air;

- temperature of parts of polymer in the moment of contact with the plane of material equal to the temperature of current ($T_{пол} = T_{пов}$) of air;

- parts of polymer have identical mass m and form of bullet;

- correlation of resilient and plastic constituents of deformation of the system particle of polymer - material during a blow is determined by the coefficient of renewal κ, which depends on properties of polymer and material, temperature $T_{пол}$ and speed v.

Will consider the slanting resilient blow of particle mass m at an immobile surface taking into account a dry friction. In this case impulse of shock reaction of surface : $\overline{S} = \overline{S}_n + \overline{S}_\tau$, where $\overline{S}_n, \overline{S}_\tau$ - normal and tangent to composition of impulse. Coefficient of renewal: $K = \dfrac{S_{n2}}{S_{n1}}$, where S_{n1}, S_{n2} is a normal constituent of impulse of shock reaction in the phases of deformation and renewal accordingly, thus $S_n = S_{n1} + S_{n2}$. Constituent of impulse which takes into account a dry friction : $S_\tau = -f \cdot S_n \cdot sign(v_\tau)$, where f - the coefficient of sliding friction, $sign(v_\tau)$ is a function which takes into account sign of tangent component speed v_τ of point.

Speeds of parts before and after the blow (Fig. 1) accordingly: $\overline{v} = \overline{v}_n + \overline{v}_\tau$; $\overline{u} = \overline{u}_n + \overline{u}_\tau$.

Different possible motions of point are considered at a blow and terms which these motions will be realized at are certain.
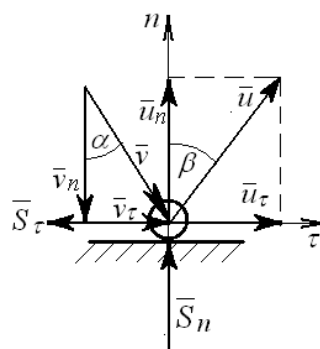

Fig. 1. Calculation chart of blow co-operation of particle of polymer and basis

1. A particle slides warpwise during all time of blow τ. Phase of deformation begins at $t = 0$ and closed at $t = \tau_1$. Component speeds of particle at the beginning of blow v_n, v_τ at the end of phase of deformation v_n^*, v_τ^*. Phase of renewal begins at $t = \tau_1$, and closed at $t = \tau$. Component speeds of particle at the beginning of phase of renewal v_n^*, v_τ^* at the end of blow u_n, u_τ.

On the basis of theorem about the change of amount of motion of point at a blow [2] certain terms at which possible sliding of point during all time of blow, id est when $v_\tau^* > 0$, $u_\tau > 0$: $tg\alpha > f(1 + K)$.

Modules of speed of particle after a blow and complete impulse of shock force accordingly levels:

$$u = \sqrt{u_\tau^2 + u_n^2} = v\sqrt{\left[\sin\alpha - f(1 + K)\cos\alpha\right]^2 + (K\cos\alpha)^2};$$

$$S = \sqrt{S_\tau^2 + S_n^2} = mv(1 + K)\cos\alpha\sqrt{1 + f^2}.$$

If in these formulas to put $f = 0$, then $u = v\sqrt{\left[\sin^2\alpha - K^2\cos^2\alpha\right]}$; $S = mv(1 + K)\cos\alpha$, id est get a decision for the case of blow of material point at an immobile surface without the account of friction.

2. Sliding of particle is closed in the phase of deformation. In this case the phase of deformation is divided into two stages: $0 - \tau'$ - is sliding of particle, $\tau' - \tau_1$ - is motion of particle without sliding (motion is for normals). In the moment of time $t = \tau'$ a tangent presents speeds of particle will become even to the zero (id est $v_\tau' = 0$) and sliding of particle will cease.

The first stage of phase of deformation begins at $t = 0$ (v_n, v_τ) and closed at $t = \tau'$ ($v_n' = 0, v_\tau' = 0$). The got equalizations look like:

$$S_{\tau1}^{(I)} = -mv_\tau = -mv\sin\alpha < 0;$$

$$S_{n1}^{(I)} = -\frac{S_{\tau1}^{(I)}}{f} = \frac{mv\sin\alpha}{f} > 0;$$

$$v_n' = -\frac{S_{n1}^{(I)}}{m} + v_n = v\left(\frac{\sin\alpha}{f} - \cos\alpha\right),$$

where $S_{n1}^{(I)}$, $S_{\tau 1}^{(I)}$ - normal and tangent to composition of impulse of shock reaction for time from 0 to τ', $S_{\tau 1}^{(I)} = -fS_{n1}^{(I)}$.

The second stage of phase of deformation begins at $t = \tau'$ (v_n', v_τ') and closed at $t = \tau_1$ $((v_n' = 0, v_\tau' = 0)$.

Equalizations of blow followings:

$$S_{\tau 1}^{(II)} = 0; \ S_{n1}^{(II)} = -mv_n' = mv\left(\cos\alpha - \frac{\sin\alpha}{f}\right),$$

where $S_{n1}^{(II)}$, $S_{\tau 1}^{(II)}$ - normal and tangent to composition of impulse of shock reaction on the second stage of phase of deformation.

For the phase of renewal, which begins at $t = \tau_1$ and closed at $t = \tau$, component speeds will be accordingly $v_n^* = 0, . v_\tau^* = 0$, $u_\tau = 0$, u_n. Equalizations of blow look like :

$$u_n = \frac{KS_{n1}}{m} = Kv\cos\alpha = -Kv_n;$$

$$S_n = S_{n1} + S_{n2} = (1 + K)mv\cos\alpha;$$

$$S_\tau = S_{\tau 1} + S_{\tau 2} = -mv\sin\alpha.$$

That sliding of point at a blow made off in the phase of deformation, necessary implementation of kinematics condition : $tg\alpha < f$. In default of sliding at the end of phase of deformation and at the end of blow the dynamic terms of sliding absence must be observed: $|S_{\tau 1}| < f \cdot S_{n1}$, $|S_\tau| < f \cdot S_n$.

3. Sliding of material point is closed in the phase of renewal. Will get at first a decision for the phase of deformation $(t = 0...\tau_1)$. Sliding in this phase is present, id est $v_\tau > 0$ and $v_\tau^* > 0$, and normal component speeds of point will be v_n, and $v_n^* > 0$. Equalizations look like :

$$S_{n1} = -mv_n = mv\cos\alpha;$$

$$S_{\tau 1} = -fmv\cos\alpha;$$

$$v_\tau^* = \frac{S_{\tau 1}}{m} + v_\tau = v\left(\sin\alpha - f\cos\alpha\right).$$

For a tangent and normal constituents of impulse of shock reaction have:

$$S_\tau = S_{\tau 1} - S_{\tau 2}^{(II)} = -mv\sin\alpha\,;$$

$$S_n = \left(1 + K\right)S_{n1} = \left(1 + K\right)mv\cos\alpha.$$

For realization of this case of blow necessary implementation of condition: $f \le tg\alpha \le f\left(1 + K\right)$, where $0 \le \alpha \le 90°$. On Fig. 2 built dependences $\alpha = arctg\left[f\left(1 + K\right)\right]$ at $K = 0,5$ and $K = 0$.

At $K = 0$ a curve $\alpha(f)$ is a general bottom limit for all cases of blow.

Curves divide areas And - III, in which a point moves at a blow variously. At $f = 0,5$ area And it is determined by a corner $\alpha = 26,6°$. At $\alpha < 26,6°$ sliding of point is closed in the phase of deformation.

At $f = 0,5$ and $K = 0,5$ the area of II is determined by a corner $\alpha = 6,9°$. At $26,6° < \alpha < 36,9°$ at the blow of material point at the rough shute of point closed in the phase of renewal.

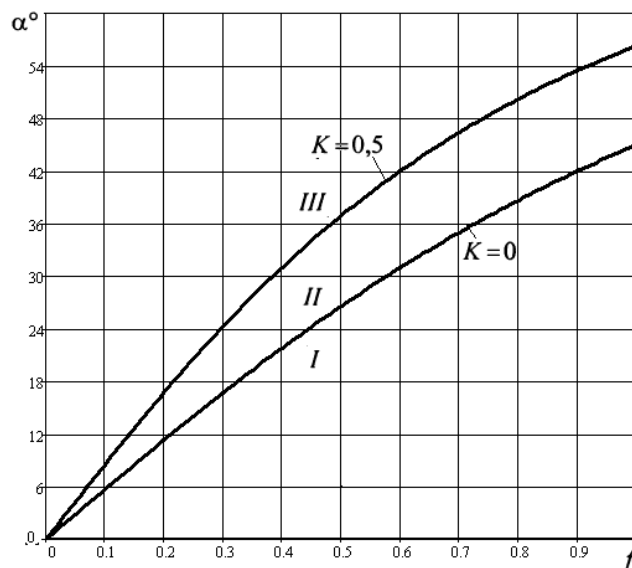**Fig. 2. Dependences** $\alpha = arctg\left[f\left(1 + K\right)\right]$

The area of *III* is determined by a change and within the limits of $36,9° < \alpha < 90°$. In this turn-down of angle of incidence of material point on the

rough shute of point at a blow does not cease to the end of blow. At the construction of curves the coefficient of sliding friction changed within the limits of $0 < f < 1$. However this range not often practically will be realized. At large values f this model can differ from the results of experiment.

The analysis of the got decisions in the case of stopping of sliding in the phases of deformation and renewal shows that the final values of speeds and impulses for them are identical, differences are observed in intermediate values.

For these cases have at $tg\,\alpha \le f\left(1+K\right)$: $u = Kv\cos\alpha$; $S = mv\sqrt{\cos^2\alpha\left(1+K\right)^2 + \sin^2\alpha}$. As $tg\,\beta = u_\tau / u_n$.

Then $tg\,\beta = \dfrac{tg\,\alpha}{K} - f\left(1 + \dfrac{1}{K}\right)$ at $tg\,\alpha > f\left(1+K\right)$; $tg\,\beta = 0$ by $tg\,\alpha \le f\left(1+K\right)$.

Dependence $tg\,\beta\left(\alpha\right)$ is brought around to Fig. 3 ($K = 0,5$; $f = 0,5$)
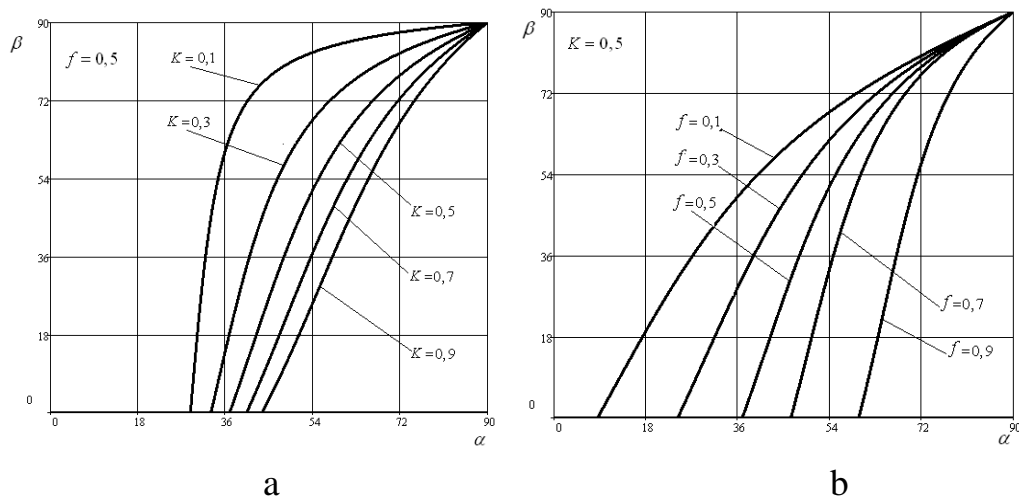

Fig. 3. Graphic arts of dependence of corner of reflection of particle β are from the corner of blow α at the different values of coefficients of renewal K (a) and friction f (b)

References

1. Сорокин М.Ф. и др. Химия и технология пленкообразующих веществ. М. Химия. 1989. – 480 с.

2. Дронг В.И., Дубинин В.В., Ильин М.М. и др. Курс теоретической механики: Учебник для вузов. МГТУ им. Н.Э. Баумана, 2005. – 736 с.: ил.

5.3. BUILDING MATERIALS

5.3.1 DRY FINE GRAINED AND POWDERED CONCRETE MIXES OF NEW GENERATION

Kalashnikov V.[1], Volodin V.[1], Valiev D.[1], Gulayeva E.[1]

Over the past 60 years, concrete common building purposes have been three stages of development. In the first phase from 1950-1970's, they may be called the concretes of the old generation, containing in the structure has four main components: cement, sand, gravel, and in-between. Chemical additives used primarily in concrete for special purposes: it is pozzolanic, heat from the mineral additives, sealing, antifreeze, US-koriteli and hardening retarders.

Natural loose, porous and water demand of pozzolan used in hydraulic engineering concretes. Although microsilica (MC) was already known, but due to the high dispersion and lack of strong plasticizers he has not found application in practice. As the plasticizers used in the RRT, UPB, PRS, lignosulfonates - LST, LSTM.

The second transition phase started from 1970 and, if we talk about the most effective Beto-tries, lasted until 1990 - the period of the start of the era of effective superplasticizers on naphthalene and melamine-based. This time period is arbitrary, as it continues today, along with the development of a new generation of concretes. In the third stage have been invented abroad giperplastifikatory highly functional new generation of on polyacrylic, polyglycolic and polycarboxylate-based, will strengthen vodoredutsirovanie in concrete mixtures, the old generation. Fundamental changes to the composition and structure of the concrete was cored activation of putstsolanicheskim mikrokremne-zemom, acidic ash and rock flour. Concrete since 1990, are multicomponent, involving 7.6 components through the use of MK-Charge of the dispersed filler - quartz (mikrokvarts) and rock flour (basalt, granite, limestone, etc.).

We can not say that powdered activated concrete was not used in the second transition period and early in the third period. But this activation did not

---

[1] The Russian Academy of Architecture and Building Sciences

pursue goals Kar dinalno change the rheology of concrete mixes with superplasticizer. Its main value to - to reduce cement consumption by active-fine fillers. Poly-structural theory, developed Solomatova VI and developed his scientific school, pre-envisions the introduction of fine fillers in an amount of 20-40% instead of cementite-ta. This sets the maximum strength as a function of volume content of filler peripheral devices.

The third period includes receiving high-strength and osobovysokoprochnye Be-tones by adding to cement a significant amount of powder dispersed in the filler, the required number of microsilica and fine-grained sand fraction 0,1-0,5 ÷ 0,16-0,63 mm.

Powder activation of fine gravel and concrete can be based on the finished dry cement-dispersed mixture.

A wide and varied nomenclature dry mixes, manufactured in Western countries and Russia, did not affect the production of dry concrete mixtures. Produce such a mixture of concrete in the traditional sense of him as a composite material comprising cement, sand and gravel are not reasonable and uneconomical. Transporting large volumes of Chiyah gravel and sand in the regions in which these components are available in sufficient quantities, is irrational. In addition, such mixtures can not be downloaded, unloading and trans-port pneumatic, moreover, they are separated when loading containers. The same applies to sand concrete, which contained medium and coarse sand with different measures of particles of 2-5 mm.

Recent advances in the technique of concrete in construction marked by the introduction of high-strength concrete and osobovysokoprochnyh samorastekayuschihsya of concrete mixtures with a strength of 150-200 MPa [1]. The establishment of such concretes are not used Supercement microwave brands and traditional cements marks 500-550 (42,5-52,5 classes CEM). Nai-more complete implementation of the special rheological properties samorastekanii and Self-sealing concrete mixtures achieved in fine mineral-cement-water systems with the latest generations of SE [2]. Adding to the mineral-cement dispersion reaction-active putstsolanicheskih supplements - microsilica (MC), finely metakao-ling (MTC), allowed to bind in concrete "ballast" Hydrolysis Ca (OH) 2 - portlan-leads to further cementing agent with

an increase in primary and normalized-term 28-daily strength with significant improvement of all physical and technical properties of concrete. This applies primarily to the powder concrete (PB), produces mym-of-fine-grained powder dry mixes. In such mixtures containing 50-60% in roshkovogo component (cement, ground rock, microsilica) and 40-50% fine-grained (sand fraction 0,1-0,6 mm).

Thus, the rheological matrix must be vodnodispersnoy, disperse phase of which is able to adsorb oligonucleotides or polyions GP, and dispersed in discrete nye particles from aggregates (clusters), formed by mixing powders of mineral water without surfactant.
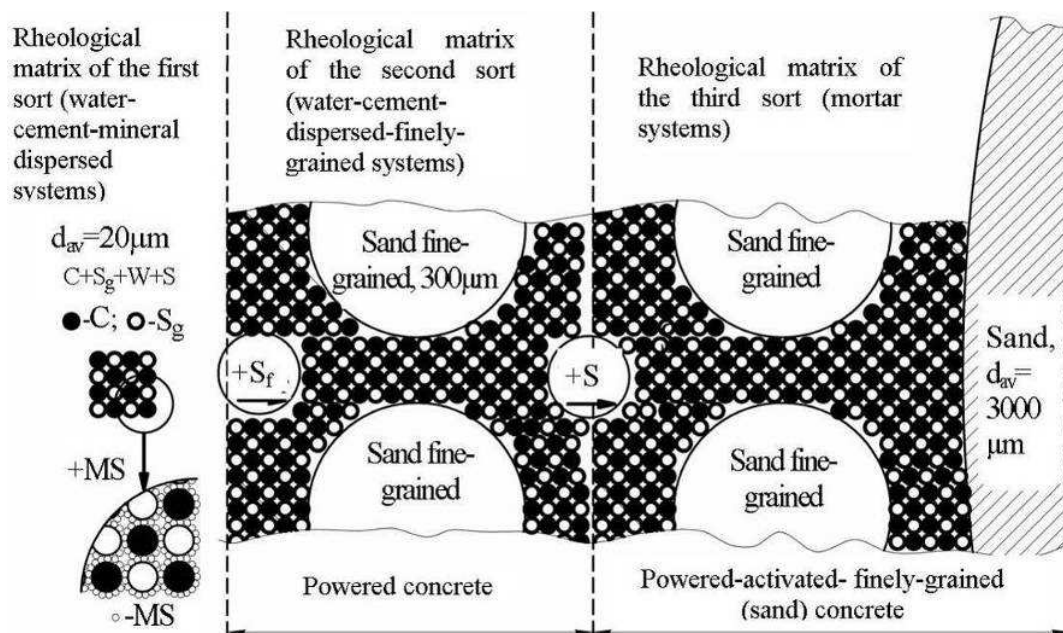

Fig.1. Topological structure powered-activated concretes of a new generation

All rheological matrix we classify into three kinds. In powder-activated gravel concrete of the new generation (Fig. 1), there are three rheological matrix. Matrix of the first kind consists of cement, ground quartz sand (rock flour), microsilica, superplasticizer and water matrix of the second kind involves math ritsu first kind and fine sand, the matrix of the third kind (mortar part of concrete) consists of matrices of the first and second kind and medium or coarse sand. In the concrete of the old generation of (Fig. 2) there is no matrix of the second kind, and the matrix of the third kind consists of cement, water, superplasticizer and raw sand
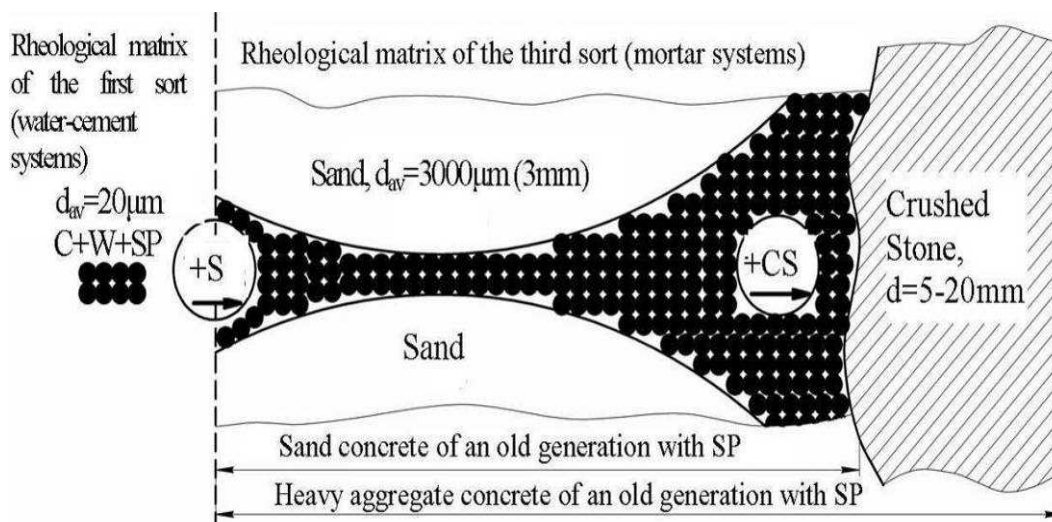
Fig.2. Topological structure concretes of an old generation (including SP)

Department of technology of concrete, ceramics and binders Penza State of the University of Architecture and Construction, about 15 years developing and Niemi study the properties of different types of high strength and osobovysokoprochnyh besschebenochnyh powder kovyh concrete [3], sand and gravel concrete with powder binder for other classes surface-B80 - V140. Made in the laboratory of the department in 2008, 2009. powdered concrete from the fine-grained, dry-powder mixed with cement content (C) within the 680-750kg per 1 m3 of concrete, microsilica from 7 to 15% by weight of C, ground sand to Ssp = 3200 3600sm2 / g - 350-375kg for 1 m3 of fine-grained sand francs. 0,16-0,63 mm - 700-750kg per 1 m3, giperplastifikatora brand Melflux (1641F, 2641F, 2651F) - 0,8-0,9% by weight of cement, with B / T = 0,10-0,13 , we have been tested for durability. Some concretes have-whether made with steel or acrylonitrile fiber. The test results are given in Table 1. Powder ligament was successfully tested for the production of conventional concrete GOVERNMENTAL M 200-800. In these types of concretes reached an all-time low specific consumption of cement per unit of strength - 3,4-4,5 kg / MPa, including the concrete without MK.

As can be seen from Table 1 concrete with compressive strength of 100-129 MPa at 28 days is normal, moisture-curing after natural hardening in air from one year to two years and substantially increase its strength. Increase in compressive strength ranges from 8.5 to 50%, the tensile bending - from 12.4 to

60%. Thus, high-quality concrete, Mr. microinhomogeneous "miracles " associated withloss of of strength was not found . PB-MC-21, PB-MC-46, PB-MK-53, PB-MK-54 had a lower strength of 100-110 MPa at 28 days showed a higher increase in compressive strength (34-50%). Thus, some new-generation concretes are subject to an annual strength of the logarithmic law: R365 = R28 · lg365 / lg28.

Thus, due to the extremely high strength of the cement binder of fine-grained powder, dry mix, it can be universal for manufacturing: powder high and osobovysokoprochnogo concrete, sand concrete in small, medium and coarse sand, gravel high-strength concrete and osobovysokoprochnogo betone strength at compression of 20-80 MPa.

The task of research was to develop formulations of dry concrete mixtures with the optimal ratio of cement, ground sand, microsilica, GP; determining the density of dry mixes, making PB, powder-activated gravel concrete (PASCHB) powder-doped fine-grained concrete (Pambou) , powdered adhesives, and to study their properties.

For the production of fine-grained, dry-powder concrete mix used: PC M 500 A0 Volsky, Krasnoyarsk and Topkinsky plants, white cement M 500 Xu-Doppler plants, ground quartz sand (PM) deposits with Ssp = 1400 4000sm2 / g sur-ray, Bashmakovskogo , Ivanovo deposits (Penza region), and metal-Achinsk storozhdeniya - (Krasnoyarsk Territory), fine-grained sand fraction 0,16 ÷ 0,63 mm (Fri), micro-granular rokremnizem (UA) ferroalloy plant Novokuznetsk and powdered- LIMITED - Lipetsk Metallurgical Combine; GP on the basis of polycarboxylate Melflux 1641, 2651, 5581F.

In some cases, we used stainless metal fiber d=0,15 mm, length l=7-9mm and poliakrilnitrilnaya Ricem MC 2,5 / 8 mm.

Cement due to the lack of effective mixer - activator mixed preliminarily with GP Melflux oversleeping on plastic film and a ball MBL laboratory mill with a small number of balls in 10 minutes without an increase in specific surface. Granular MK due to poor blooming in the water a short time (5-10 minutes) was dispersed with fine-grained sand in the mill. After co-mixing of

the components of a dry mixture is continuously poured into the mixer with a stirrer preliminarily otdozirovannym it plenty of water for 5-6 minutes at

Table 1 - Strength of reactive-powdered concretes depending on their hardening time

Indica-tors	Concrete Samples																				
	RPC-21*		RPC-30		RPC-36B **		RPC-46		RPC-52		PRC-53*		RPC-53A ***		RPC-54 ***		RPC-56		RPC-57 ***	
	Hardening Time, Days																			
	28	610	28	480	28	480	28	480	28	385	28	385	28	385	28	385	28	365	28	385
Strength - R_b, MPa	101	148	129	140	114	145	108	162	120	148	105	144	110	148	106	144	119	134	115	138
- R_t, MPa	10,5	14,1	10,0	13,2	12,2	19,7	9,3	12,8	12,4	15,3	12,1	13,6	12,6	17,6	12,4	16,4	11,3	12,9	13,4	15,8
Growth R_b, %	46,5		8,5		27,2		50		23,3		37,1		34,5		35,8		12,6		20	
Growth R_t, %	34,3		32		61,5		37,6		23,4		12,4		39,7		32,25		14,2		17,9	

* — reinforced by stainless steel fibers, d = 0,15mm; l = 8-9mm (1% of concrete volume);

** — reinforced by acrylonitrile fibers, d = 2,5mm; l = 4mm (0,3% concrete volume);

*** — reinforced by combined fibers (steel (0,9%) and acrylonitrile (0,1%)).

Table 2 - Component compositions and properties of concrete mixes, hardening time and strength of concretes manufactured with the use of dry reactive-powdered concrete mixture (DRPCM)

# of composition	Type pf concrete	Composition of concrete mix, kg/m³							Hyper-plastic izer, % from cement	Water/ cement (water/ solid)	Density of concrete mix, kg/m³	CS, cm; S,s	Compression (bending) strength, MPa, at the age of, days			Specific cement consumption, kg/MPa
		DRPCM				Sand	Cru shed ston e	Wat er					1	7	28	
		Ceme nt	Sg	Micr osili ca	Sf											
1	RPC	722	332	79	1046	—	—	218	0,9	0,3 (0,1)	2376	CS 26	52 (8,0)	126 (10,8)	147 (16,4)	4,9
2	RPC	738	380	73,2	1042	—	—	169	0,9	0,23 (0,08)	2285	CS 5-6	*After heat and moisture exchanger* 134 (13,1)			5,5
3	RPSC	497	374	—	400	1014	—	154	0,9	0,31 (0,06)	2365	S 10-15	52 (9,4)	94,8 (12,0)	114 (12,4)	4,4
4	RPSC	497	374	50	370	1014	—	154	0,9	0,31 (0,06)	2370	CS 2-3	—	93,2 (12,0)	120 (12,4)	4,1
5	RPCSC	480	260	52	485	300	800	157	0,75	0,33 (0,06)	2505	S 15-20	55,6 (7,2)	93 (13,2)	120 (17,6)	4,0
6	RPCSC	480	260	—	480	300	840	154	0,75	0,32 (0,06)	2530	CS 22	45,0 (7,3)	90,4 (11,3)	106 (13,1)	4,5
7	RPCSC	320	235	22,2	351	510	102 8	120	0,9	0,376 (0,048)	2534	CS 22	66 (8,6)	111 (12,1)	134 (15,0)	2,4

Hyper-plasticizer is a component of DRPCM

Table 3 - Density of dry finely-grained powder concrete mixes with different components ratio

Dry mix without microsillica, SSg=1,400cm²/g			Dry mix with microsillica, SSg=1,400cm²/g			Dry mix without microsillica, SSg=3,200cm²/g			Dry mix with microsillica, SSg=3,200cm²/g		
Components ratio	ρ_{nas}, kg/m³	ρ_{comp}, kg/m³	Components ratio	ρ_{nas}, kg/m³	ρ_{comp}, kg/m³	Components ratio	ρ_{nas}, kg/m³	ρ_{comp}, kg/m³	Components ratio	ρ_{nas}, kg/m³	ρ_{comp}, kg/m³
C : Sg : Sf 1 : 0,5 : 1,63	1376	1786	C : Sg : Sf : Mic 1 : 0,5 : 1,38 : 0,24	1324	1657	C : Sg : Sf 1 : 0,5 : 1,63	1336	1783	C : Sg : Sf : Mic 1 : 0,5 : 1,38 : 0,24	1277	1752

400 rpm. The mixture was poured, depending on the destination in the form of $40 \times 40 \times 160$mm, $100 \times 100 \times 100$mm $70 \times 70 \times 280$mm, $100 \times 100 \times 400$mm or plastic shapes for decorating plates with a size-mi $600 \times 300 \times 15$mm.

In the manufacture of sand concrete in the preparation of water-powder mixture was pre-diluted sand, followed by additional stirring, the manufacture schebe-night concrete - gravel fraction was added $5 \div 10$mm or a mixture of fractions $5 \div 10$ and $10 \div 20$mm.

Control the consistency of a mixture is based on their type and the desired compression technology: the spontaneous spreading diameter (Dr) cone from the jolt-tries on the glass table (cone Hagermanna GOST 310.4-81), and draft a standard cone (GC) or stiffness (M) on the instrument of the Red (GOST 10181.1-81).

Control the consistency of a mixture is based on their type and the desired compression technology: the spontaneous spreading diameter (Dr) cone from the jolt-tries on the glass table (cone Hagermanna GOST 310.4-81), and draft a standard cone (GC) or stiffness (M) on the instrument of the Red (GOST 10181.1-81).

The density of concrete was determined by weighing dimensional vessels after her self-sealing or vibration compaction. Yield concrete monitored very closely and checking hardened in sealed conditions of the samples in 12-14 hours after molding, weighing compacted concrete mix and the loss of vessels with the remnants of her. The actual density was compared with the theoretical value, calculated by the method of absolute volumes.

The test results are presented in Table 2. As can be seen from Table 2, using fine-grained, dry-powder concrete mixture can be made highly efficient

solid concrete powder, powder-activated and fine-grained powder-activated gravel concrete with specific cement consumption from 4,1 to 5,8 kg per Mpa strength. Currently, the figure for virtually all concrete product of irreducible in Russia, ranging from 7 to 14 kg per MPa at a grade of concrete from the M 200 and M 600.

It is important that as sand and gravel concretes not containing in its composition MK, have the strength to 5-15% lower than with the MC.

Dry mixture, containing in the structure of 6 components that determine the high strength of the cement matrix, when used on concrete plants and concrete increase Chiva dosing accuracy and greatly simplify the process of it. They are easily moved, pneumatic and have a bulk density of 20-25% more than the cement (Table 3).

By unique recipe blends with optimized versions of their in Krasnoyarsk in 45 in collaboration "New construction technology" were made of colored concrete grade M 1800-M 2000 "Victory Monument and Obelisk" Alley of Victory "

References

1.   Dallaire E., Bonnean O., Lachemi M., Aitsin P.-C. Mechanical Behavior of Consined Reactive Powder Concrete.// American Society of Civil Engineers Materials Engineering Coufernce. Washington. DC. November 1996, Vol. 1, pp. 555-563.

2.   Richard P., Cheurezy M. Composition of Reactive Powder Concrete. Scientific Division Bougies.// Cement and Concrete Research, Vol. 25. No. 7, 1995. - pp. 1501-1511.

3.   Kalashnikov VI Through rational rheology in the future of concrete.

Part 1. Types of rheological matrices in the concrete mix and strategies to enhance firm-STI concrete and save it in the construction / building materials of the XXI century, technology concrete. 2007. № 5. with. 8-10.

Part 2. Fine rheology of the matrix and powdered concrete next generation leniya. / / Technology of concrete. 2007. № 6. p.8-11.

Part 3. From high-strength concrete and osobovysokoprochnyh future to Superplast-skilled concretes general purpose of this / / Technology of concrete. 2008 № 1. from 22-26.

5.3.2 THE SYNTHESIS TECHNOLOGY FILLERS BASED ON DIATOMACEOUS EARTH FOR DRY CONSTRUCTION MIXTURES

Loganina V.[1]

Raw material base in the Volga region of Russia to bring about the production of building materials based on diatomite with an extensive distribution in its territory. That will allow not only rational use of mineral raw material base in the region, but also significantly reduce the cost of the construction materials.

At the present time in carrying out the construction or repair an increasing preference for dry mixtures. Efficacy of the dry mixtures uselargely depends on the economical use of all resources, in particular through the use of local raw materials.

Therefore, the promising direction is the production of dry mixtures with finely dispersed fillers on the basis of the local breeds.

Diatomite is composed mainly of the amorphous silica. In the fine condition in the presence of the moisture diatomite interacts with the lime binders, but the strength of such solutions at the air-dry hardening is small. It is therefore necessary to enhance the interaction of diatomite with astringent, which should increase the surface activity of the filler.

To date to improve the application of diatomite is proposed to conduct its activation by heat treatment at 900-950°S. However, this method of activation is associated with elevated energy costs. We propose activation technology for increase the content of the amorphous silica.

We used Inzenskij diatomite deposits. As an additive, increasing the content of amorphous silica in diatoms, used a sol of silicic acid [1] To obtain a sol of silicic acid was used a method based on ion-exchange chromatography. Liquid glass density of 1056 kg /m^3 was passed through the ion-exchange column with a cation exchange resin to give a sol of silicic acid with a pH of 4.5 … 5.0 density 1013-1030 kg/m^3. Turbidimetry method revealed that the radius of the sol particle density 1027 kg / m^3 to 5 days at 17 ... 25 nm, and 7 ... 19 days - 57 ... 140 nm. Sol of silicic acid is stable under the age of 15 days,

[1] Penza State University of Architecture and Construction, Penza, Russia

the electrokinetic potential of (-) 0,03 ... 0.103 V. In the future, a decrease of the electrokinetic potential. Thickness of the diffuse layer at the age of 1 day is 29.5 nm, which determines its stability.

The technology included the introduction of the sol mixture of the diatomaceous earth ground with a specific surface Ssp = 10982.58 cm^2 / g with a sol of the silicic acid in the ratio 1:1,1-1,8. The resulting suspension was maintained for 1 hour, then dried to the constant weight and milled to the same values of specific surface. The chemical composition of diatomaceous earth, made with a spectrometer firm «Thermo Scientific), was determined in Science and Technology Center (STC) Ltd. Diatom Plant. Established that the SiO2 content in the modified diatomite increased to 89.29%, while in the control group - 85.81%.

To characterize the hydrophilicity of the surface of diatomite was estimated heat of wetting of diatomaceous earth with water. Temperature measurement was performed using an electronic device "Ten 5. Heat of wetting was calculated using the formula

$$Q = cm\Delta t,$$ (1)

c - where c is the specific heat of mixture;

m-mass of the sample;

Δt - changes in temperature.

Specific Heat mixture (diatoms and water) was determined in accordance with the principle of additivity formula

$$c = \frac{c_1 P_1 + c_2 P_2}{P_1 + P_2},$$ (2)

c_1, c_2 – where the specific heats, respectively, diatomaceous earth and water;

P_1, P_2 - mass of diatomite, respectively, and water.

The results are shown in Table 1.

Table 1 - The heat of wetting of diatomite

Type of activation	The heat of wetting, KJ
Control (without activation)	0,012669
Processing of diatomite zolyu silica density = 1,027 g/cm^3, at a ratio of 1:1,1 1:1,125 1:1,5 1:1,7	 0,029 0,032 0,038 0,038
Treatment of calcined diatomite zolyu silica density = 1,027 g/cm^3 in a ratio of 1:1,5	0,042

Listed in Table 1 data indicate that the treatment of diatomite silica sol promotes its hydrophilization. Thus, the heat of wetting of the control composition is Q = 0,012669 KJ, and diatomite-modified sol of silicic acid in the ratio of diatomite: silica sol = 1:1,7 - 0,038 kJ.

To evaluate the local structure of the surface of the diatomite used methods of scanning probe microscopy (SPM), in particular, atomic force microscope working in contact mode using silicon cantilevers with tip radius 15 nm [2].

The characteristic form of the surface of diatomite shows the AFM image in Fig. 1. Analysis of the AFM - the image indicates the change in height of the surface topography, as evidenced

The fractal dimension of the fractal surface to surface is not activated diatomite is D = 2,52 (Fig. 1a).

a) b) c)
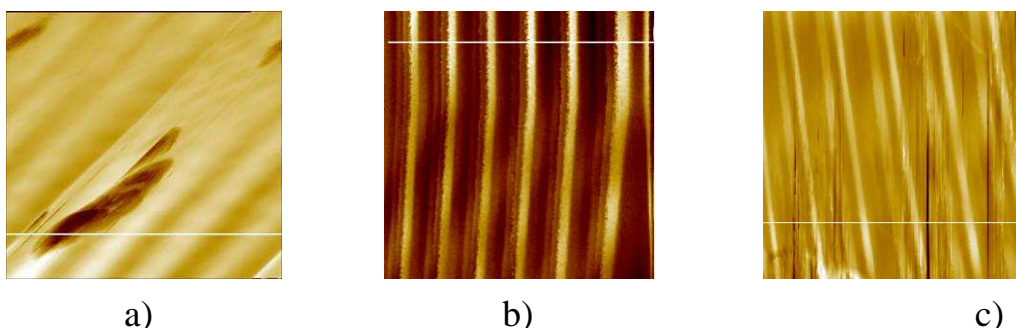
Fig. 1. AFM image of the surface of diatomite: a) not activated; b) the activated silica sol at a ratio of 1:1,5; c) activated silica sol at a ratio of 1:1,3 by periodic alternation of light and dark bands in the image.

The roughness of the surface of diatomite is Ra = 989 nm, and processed silica sol at a ratio of 1:1,5, - Ra = 55,9 nm. Elevation change on the smooth surface areas of diatomite treated with silica sol in a ratio of 1:1,5, less than 100 nm on a length of 2.88 micron, 50 ... 95% is the height of the surface relief component of 80.1 nm and 10 ... 50% - 128 nm. The fractal dimension of a fractal surface is D = 2,05. surface relief is 208 nm, and 10 ... 50% - 271 nm. Use of activated diatomite in the compositions of dry mixes promotes change their rheological properties. Fig. 3 shows the kinetics of plastic strength lime-diatom composites. Revealed that the formulations based on diatomaceous earth, activated silica sol, have a quick set of plastic strength. Thus, the plastic strength of lime-diatom composition with the use of diatomaceous earth, activated silica sol at a ratio of 1:1,5, at the age of 10 h after mixing is 0.5 kg / cm ^{2}, while the use of diatomite is not activated - 0.22 kg/cm^2. The growth of plastic strength, in our opinion, due to the increased amount of amorphous silica diatomite.

a)

b)
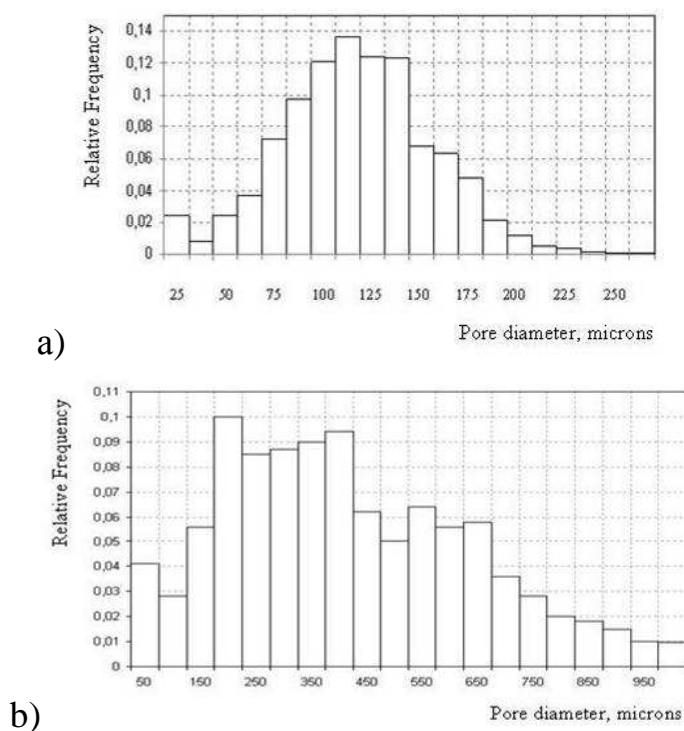
Fig. 2. Histogram of pore size of diatomite: a) activated kremnezolem at a ratio of 1:1,5; b) is not modified.
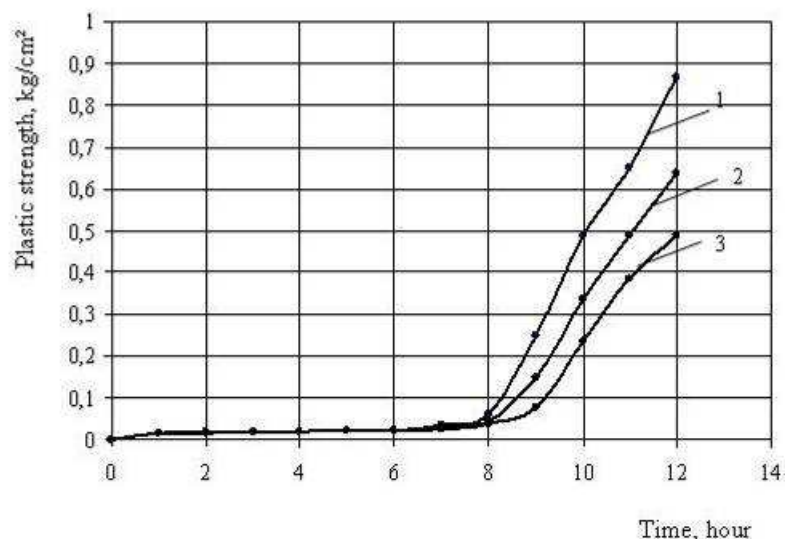
Fig. 3. Plastic strength of lime-diatom composition: 1 - diatomaceous earth, activated kremnezolem at a ratio of 1:1,5, 2 - diatomaceous earth, activated kremnezolem at a ratio of 1:1,1, 3 - control composition (without activation)

Use of activated diatomite in the structure of dry building mixtures promotes the formation of a dense structure of the material (Fig. 4). The structure of the lime-diatom sample is more homogeneous (Fig. 4b) with uniformly distributed pores.

To assess the structure of lime composite used XRD and differential thermal analysis (DTA). Established that the base composition of calc-diatom samples presented intense lines 10,059 Å, 3,353 Å, 3,042 Å, 2,456 Å, related to quartz and less intense lines, 1,797 Å, 1,685 Å, 1,542 Å, belonging to the calcium hydrosilicates. In addition, wasidentified i Portland (4,902 Å, 3,11 Å, 2,634 Å) and calcite (2,283 Å, 1,875 Å) (Fig. 5 a)

On radiographs lime-diatom samples with the use of diatomaceous earth, activated by silica sol, are identified lines belonging to hydrosilicate (4,256 Å, 3.037 Å, 1,481 Å), but compared with the control composition (without activation of diatomite) peak intensity increased. In addition, the intensity of the peaks related to portlanditu (2,634 Å, 1,796 Å, 1,685 Å) (Fig. 5 b).

Revealed that the composition of lime composite with diatomite treated with silica sol, an endothermic effect, accompanied by mass loss up to 3,13% occur when heated to temperatures of 114,6 ° C and are caused by removal of free water (Fig.6,a).. Endothermic effect at 420,4 – 423,1 ° C is associated with the removal of chemically bound water. The temperature of dehydration of
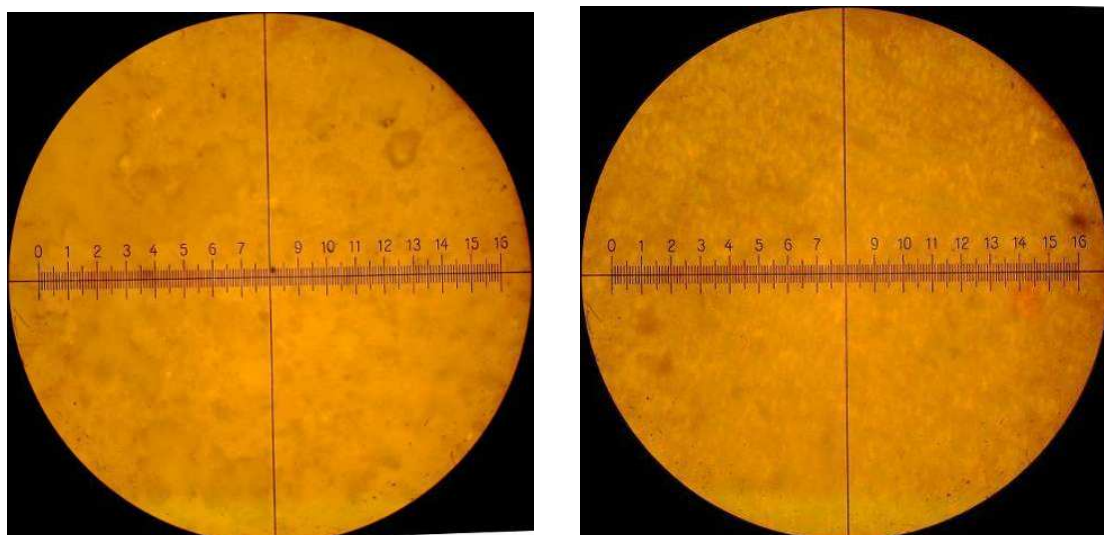
Fig. 4. The structure of the lime-diatom composite x200: a) controlling the composition, b) on activated sol composition of diatoms.

Ca (OH) 2 479,8 ° C indicates a more coarse particles portlandita. In compositions on the basis of diatomite, activated kremnezolem disappears stage endoeffect present in control samples. Also, the data obtained can be identified DTA decomposition CaCO3 - a small endothermic effect (885 - 887 ° C), further dehydration of the hydro calcium CSH - 692,3 - 689,1 ° C.

Additional endothermic effect at 650°S, absent in the thermogram of control samples, is associated with the dehydration of calcium hydro CSH, which testifies to their higher content of lime composite using diatomaceous earth, activated kremnezolem. The total mass loss of control samples is 20%, while the samples with the use of diatomaceous earth, activated silica sol, - 17,5%. The significant increase iof the endothermic effect in the region of 114.6 ° C, characterized by removing of the adsorbed water.. In the compositions with the non-activated diatomite the shift in temperature to 125°S, while the massof free water is 1.89% (Fig.6,b).

Endothermic effect in the temperature range from 420.4 to 423.1 °C corresponds to the decomposition of calcium hydroxide, while in the control samples the mass loss 4.33%; in the compositions activated silicic acid sol diatomite the mass lossis 1,38%. The findings suggest about the lower content of calcium hydroxide, which is also confirmed by XRD.
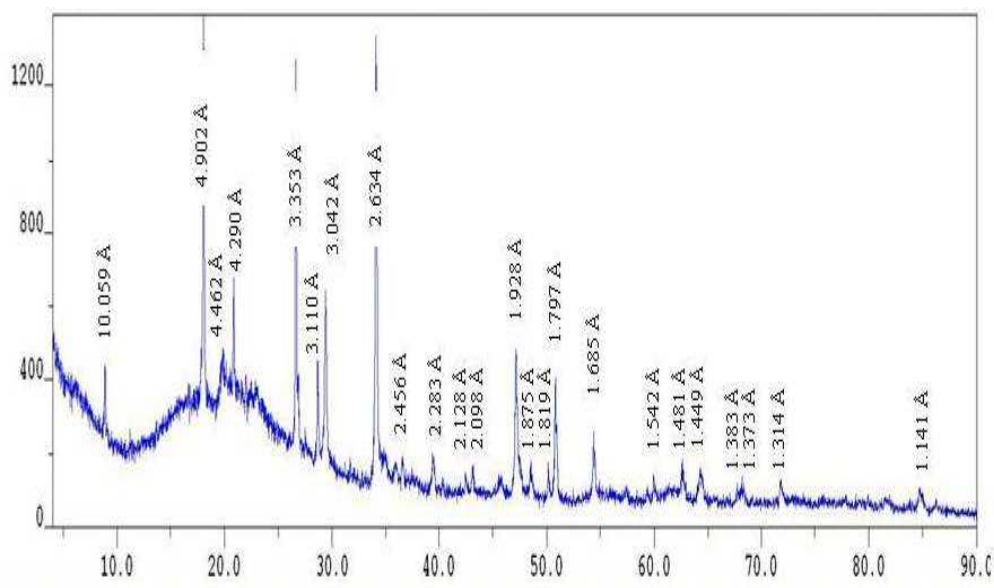
a)
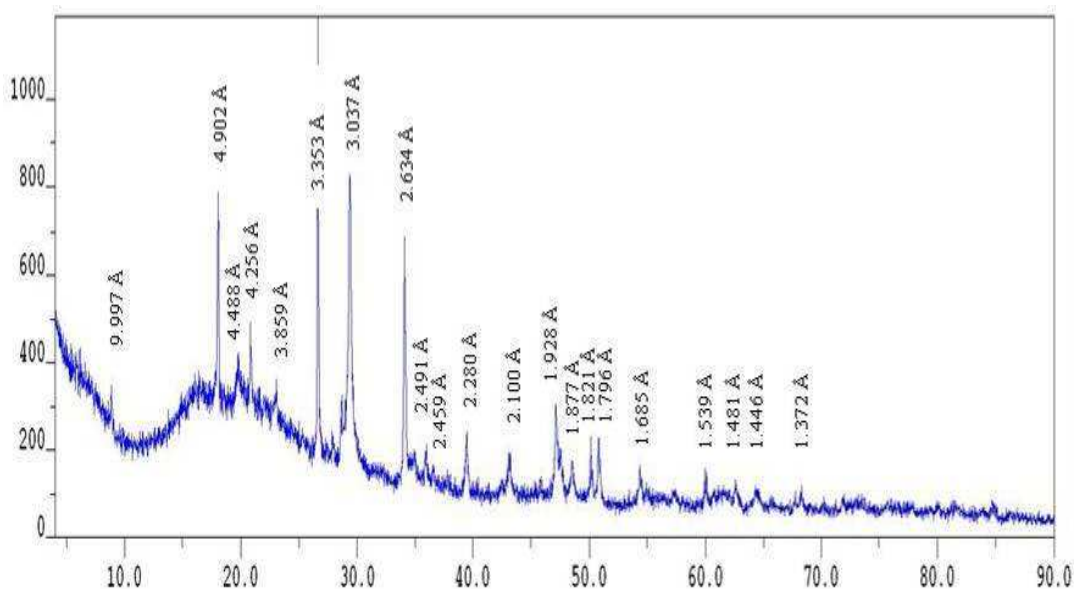
b)

Fig. 5. Radiograph izvestkovodiatomovyh composites; a) base composition; b) composition based on diatomite-modified kremnezolem.

The data obtained XRD and DTA indicate the formation of a more durable structure of lime-based composite activated kremnezolem diatomite, which is also confirmed by the indicators of strength with the helpofthe. Preliminary investigations we established that the optimum ratio of lime: diatomite, is 1:4. The samples were molded when the rations $(H_2O:Ca(OH)_2$ were equal to 2.8, 6.0 and werehardened in an air-dry conditions at ambient temperature 18-20C and atthe relative humidity of the air 60-70% (Table2).
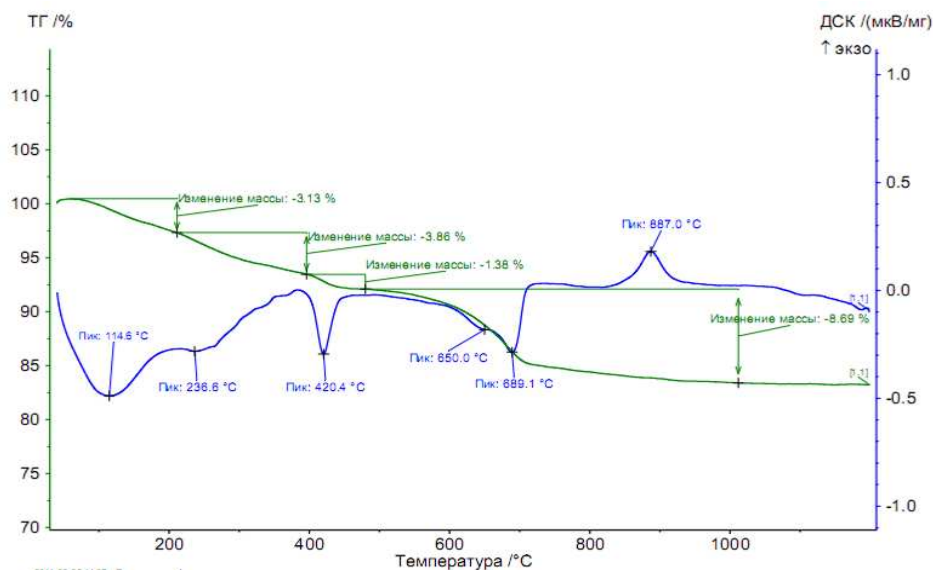
a)
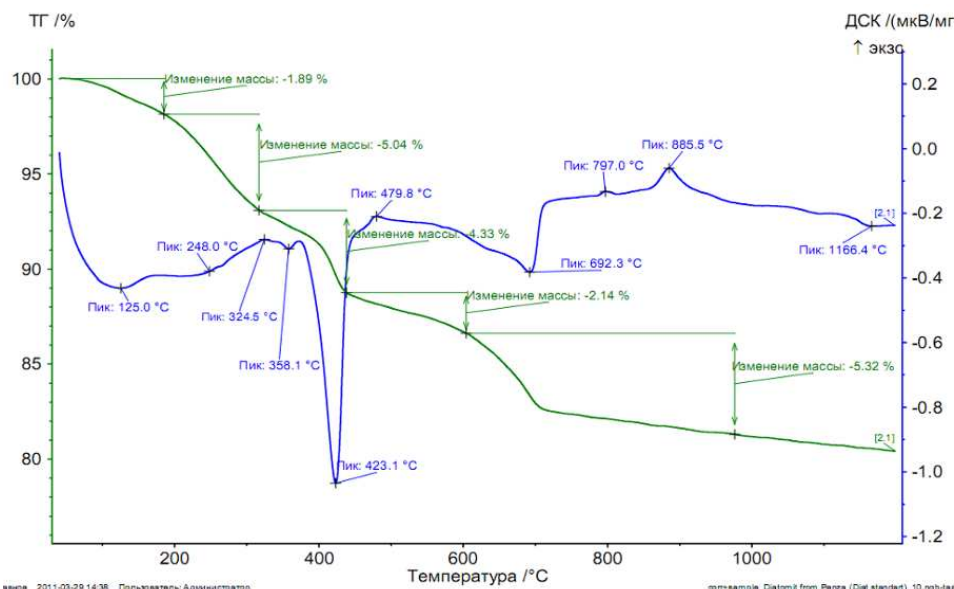
b)

Fig. 6. Thermograms of lime-diatom composite; a) diatomite treated with silica sol; b) is not activated diatomite.

Revealed that the formulations with the non modified diatomite have the compressive strength at 28 days of hardening wich is equal to 1,6 - 1,8 MPa, depending on $H_2O:Ca(OH)_2$ ratio, the and with the use of diatomaceous earth, activated silica sol, - 3,1 - 3 , 9 Mpa. Ie increase in strength is 1,9 - 2,2 times. In accordance with DIN 18550 such compositions are crack resistant.

Application of the proposed technology of the filler with the help of thediatomite for DCM will abandon the energy-consuming technologies firing.

Table2 - Compressive strength of lime-diatom compositions

Grade lime	ratio $H_2O:Ca(OH)_2$	Composition	Compressive strength. MPa		
			Age hardening, day		
			7	14	28
3	2,8	Control	1,2	1,4	1,6
2	2,8	diatomite, activated LIMITED in the ratio of diatomite: sol = 1:1,125	2,3	2,8	3,1
2	6,0	Control	1,3	1,5	1,8
2	6,0	diatomite, activated LIMITED in the ratio of diatomite: sol = 1:1,1	2,8	2,8	2,9
2	6,0	diatomite, activated LIMITED in the ratio of diatomite: sol = 1:1,3	2,8	2,9	3,7
2	6,0	diatomite, activated LIMITED in the ratio of diatomite: sol = 1:1,5	3,1	3,4	3,9

The work was done under government contract with the Ministry of Education and Science № 13.G25.31.0092.

References

1 Loganina V.I, Davydov, O. Lime finishing formulations based on sol-gel method // Building Materials. 2009, № 3.P.50-52.

2. Arutyunov, P.A, Tolstikhina A.L, Demidov V.I. system parameters for the analysis of surface roughness of materials in scanning probe microscopy / / Legislative and applied metrology. 1999. T. 65, № 8. P. 27-37.

5.3.3 HYDROIMPULSIVE TECHNOLOGY: PECULIARITIES OF DESIGN AND POSSIBLE APPLICATIONS

Rusanova O.[1], Semko A.[1]

Currently, due to the rise of malevolent and volatile human activity, various anthropogenic catastrophes happen more frequently. Sites of such catastrophes suffer a range of damage that its community is ill-prepared to repair itself. The areas of such catastrophes may be contaminated with radioactive or chemical materials, they may contain a lot of dust, there may be a risk of fire or explosions because of

[1] Donetsk National University, Donetsk, Ukraine

obstructions caused by destroyed buildings and damaged equipment. These areas need an inventive and effective means of cleaning within near impossible but necessary time restraints: the majority of the obstructions and safety hazards come from the large, unmovable fragments of destroyed buildings, and define these events as catastrophes ultimately providing the need for a means to make the clean-up of these catastrophes manageable. They need to be cut into smaller pieces suitable for transporting. In addition, the presence of victims and bystanders in the affected areas of special danger conditions should be strongly discouraged. With the proper controlled environment and an appropriate technology of cutting, catastrophes can be made manageable and effectively handled providing an immediate, proactive recovery.

The possible solution of this task is the further development of technological possibilities of ultrahigh pressure liquid jets. This technology provides high-capacity cutting of materials and elements of all different compositions, containing different mechanical characteristics and properties. Inversely, this technology is sensitive to the varying compositions as to make clean cuts void of fire or explosion risk for the particularly volatile elements [1-7].

The impulsive water jets can be used for the hydrodynamic destruction of rocks and coal [1 - 5]. The use of impulsive high-speed liquid jets used in mining and rock destruction is very inventive because of its high power, ecologically safe ability to destroy rock of any hardness and composition.

1. Methods of impulsive liquid jets production

The impulsive water-jet device and hydro-cannon are usually used to produce impulsive high-pressure liquid jets (ultra-jets).
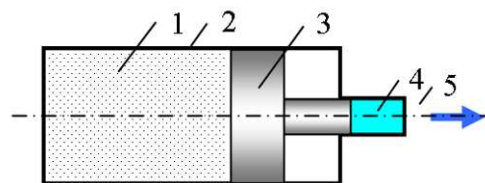

Fig. 1.The impulsive water-jet device.
1 – receiver, 2 – barrel, 3 –piston,
4 – water, 5 – nozzle.

The layout of piston water-jet device is based on the realized extrusion principle as seen in Fig.1. A heavy piston (3) is accelerated in barrel (2) by

compressed gas in receiver (1). At the end of acceleration, the piston compresses the small volume of water (4) and extrudes it through the small hole in the nozzle (5) as a pulsed high-pressure liquid jet. The pulsed water-jet device works by an electrical discharge energy or by energy of combustion products, the compression energy could also be transferred directly to the liquid without a piston.

The layout of the hydro-cannon is based on the inertial principle as seen at Fig. 2. A heavy piston (3) is accelerated by water (4) in the barrel (2) by compressed gas in receiver (1). The water reaches the narrowing nozzle (5) with an accelerating flow. The water acceleration arises due to the redistribution of energy
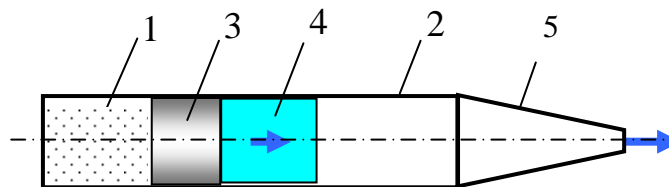
Fig. 2.The hydro-cannon.
1 – receiver, 2 – barrel, 3 – piston, 4 – water, 5 – nozzle.

between the particles of unsteady fluid liquid. The kinetic energy of the particles of liquid located near free surface significantly exceeds average energy through the volume. When approaching the edge of nozzle, water spurts from it as an ultra-jet.

Both a hydro-cannon and impulsive water-jet device have the same elements, but their different physical principles of jet forming lead to substantial quantitative and qualitative differences in their parameters. A hydro-cannon produces a jet with a speed up to 2-3 km/s that is much more then that of a water-jet device [6 -10]. However, the farther the target, the less efficient the hydro-canon becomes in destruction of the material which restricts the hydro-cannon application.

Y.Y. Lei (China) has reviewed the recent investigations of high speed (over 2000 m/s) impulse liquid jets and the prospects of their application [11]. Y.Y. Lei notes that the use of water-jet machines has rapidly increased in China. He also stresses the advantages of impulse jets in comparison with continuous water jets for cleaning and cutting of materials and points out the low reliability of equipment working under extremely high pressure.

The president of Water Jet Technology Association (WJTA) has analyzed the present situation of water jet technologies and has come to the conclusion that future possibilities of pulsed and impulse water technologies has great potential and an intangible demand [12]. These devices are compact, safe and require less energy than continuous jets. Further investigations in this field should be aimed at the increasing of reliability of the hydroimpulsive plants which work in the extreme modes, optimization of nozzle and other systems, and understanding of the mechanism of destruction of material.

2. Mathematical model of powder water-cannon .

The main property of the powder hydro-cannon shot in comparison with traditional construction is rapid decrease of jet outflow velocity immediately after the initial outflow.

The advantages of the powder hydro-cannon in comparison with pneumatic one are as follows: simple design, small outer dimensions and mass, and high specific power from a compact energy source. A powder hydro-cannon consists of combustion chamber (2), barrel (4), and nozzle (5) which ends with a collimator (6) (Fig. 3). Water charge (3) is in a barrel and is held by breech-block (7). The processes in powder hydro-cannon begin from the moment of powder ignition. Generated gunpowder gases accelerate the water charge in a barrel which then flows into a nozzle. The water continues to be accelerated and considerably increases its speed during flow in a narrowing nozzle. The water flows from the nozzle as an impulsive high-pressure liquid jet with speed up to 2000 m/s.

The following estimations are necessary for development of mathematical model of powder hydro-cannon. Reynolds number is equal to $4 \cdot 10^6$ if the barrel diameter is equal to 40 mm and water speed is equal to 100 m/s, permitting us to ignore fluid viscosity. The powder gases pressure reaches the value ca. 100 MPa; if a liquid mass is 0.5 kg then a liquid acceleration is $2 \cdot 10^5 \, \text{m/s}^2$ that in many times exceeds the free fall acceleration. The hydro-cannon shot is a brief process and lasts for about 2-3 ms.
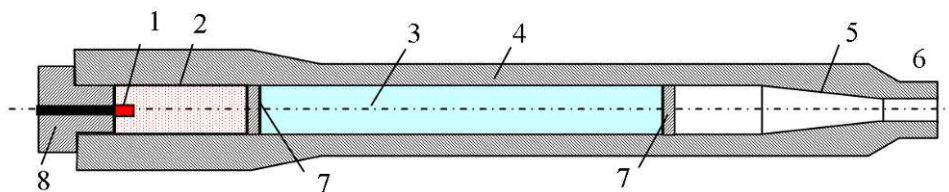
Fig.3.The powder hydrocannon.
1 – igniter, 2 – combustion chamber, 3 – water, 4 – barrel, 5 – nozzle, 6 – collimator, 7 – wad, 8 – breech-block

To elaborate on the mathematical model of powder hydro-cannon, one should accept the following assumptions: the liquid is assumed to be ideal and compressible. Its viscosity, heat conduction, and radial flow are neglected (quasi-one dimensional approximation) [1, 13]. An influence of the wads is also neglected. As the initial time, we take the time of ignition of the powder charge, the origin of coordinates is located at the entrance of the nozzle, and the *x*-axis is directed along the axis of the installation.

The quasi-one dimensional motion of water in the water-cannon is described by the system of equations of nonstationary gas dynamics [6, 13]

$$\frac{\partial \rho F}{\partial t} + \frac{\partial \rho v F}{\partial x} = 0, \quad \frac{\partial \rho v F}{\partial t} + \frac{\partial (\rho v^2 + p)F}{\partial x} = p\frac{dF}{dx}, \quad p = B\left[(\rho/\rho_0)^n - 1\right] \tag{1}$$

with the following initial, boundary conditions:

$$v(0,x) = 0, \ p(0,x) = 0, \ \rho(0,x) = 0, \tag{2}$$

$$p(t,x_f) = 0, \quad p(t,x_g) = p_g, v(t,x_g) = v_g, \tag{3}$$

where *t* – time, *x* – a coordinate, *v* – the velocity of water, *F* – the cross-sectional area of the nozzle, *p* – pressure, ρ – density, $B \doteq 304.5$ MPa, $n \doteq 7.15$, $\rho_0 = 1$ g/cm^3– constants in the equation of state of water in the Tait form, x_{g0}, x_{f0}, x_g, x_f – respectively, the initial and current coordinates of the contact and free surfaces, p_g, v_g – respectively, the pressure and velocity of powder-combustion gases on the contact surface.

The combustion of powder was considered in the quasi-stationary approximation under the following assumptions typical of the problems of internal ballistics in artillery [14]: the ignition of powder is instantaneous and its combustion is adiabatic (in parallel layers according to the geometric law), the

chemical composition of combustion products is constant, and their parameters are identical over the entire volume and obey the simplified Van-der-Waals equation taking into account only the volume of the molecules. The system of equations and initial conditions used to describe the process of quasi-stationary combustion of the powder have the form

$$\frac{dz}{dt} = \frac{u_1 p_g}{h_1} , \quad Q_g = m_{p0}\chi_1\sigma(z)\frac{u_1 p_g}{h_1} \tag{4}$$

$$\frac{1}{k-1}\frac{d(p_g V_g)}{dt} + p_g F u_g = qQ_g , \tag{5}$$

$$\frac{dV_g}{dt} = Q_g(1/\rho_p - \alpha) + v_g F , \quad v_g = \frac{dx_g}{dt} ,$$

$$z = 0, \; V_g = V_{g0}, \; p_g = p_{g0}, \; x_g = x_{g0} .$$

where h_1 – the half thickness of powder grains, z – the thickness of the burnt layer divided by h_1, u_1 – a constant of combustion rate, p_g – pressure of powder gases; Q_g – the velocity of delivery of powder-combustion gases, χ_1, $\sigma(z)$ – a coefficient and a function depending on the shape of the powder grains, α – the covolume (correction for the volume of molecules), m_{p0} – the initial mass of the powder, k – the exponent of the adiabat of powder-combustion gases, $q, \; p$ – the specific heat of combustion and density of powder, V_g – the volume of the powder-combustion gases, V_{g0}, p_{g0} – parameters of gas after the actuation of the igniter.

The axisymmetric mode of deformation of the barrel is described by the system of equations in the Lagrangian form

$$\frac{\partial\sigma_{xx}}{\partial x} + \frac{\partial\sigma_{xy}}{\partial y} + \frac{\sigma_{xy}}{y} = \rho\ddot{x} , \quad \frac{\partial\sigma_{xy}}{\partial x} + \frac{\partial\sigma_{yy}}{\partial y} + \frac{\sigma_{yy} - \sigma_{\theta\theta}}{y} = \rho\ddot{y} ,$$

$$\sigma_{xx} = -p + s_{xx} , \quad \sigma_{yy} = -p + s_{yy} , \quad \sigma_{\theta\theta} = -p + s_{\theta\theta} ,$$

$$\frac{\dot{V}}{V} = \frac{\partial\dot{x}}{\partial x} + \frac{\partial\dot{y}}{\partial y} + \frac{\dot{y}}{y} , \qquad \dot{E} = -p\dot{V} + V(s_{xx}\dot{\varepsilon}_{xx} + s_{yy}\dot{\varepsilon}_{yy} + s_{\theta\theta}\dot{\varepsilon}_{\theta\theta} + \sigma_{xy}\dot{\varepsilon}_{xy}) \tag{6}$$

$$\dot{s}_{xx} = 2\mu\left(\dot{\varepsilon}_{xx} - \frac{1}{3}\frac{\dot{V}}{V}\right) + \delta_{xx} , \quad \dot{s}_{yy} = 2\mu\left(\dot{\varepsilon}_{yy} - \frac{1}{3}\frac{\dot{V}}{V}\right) + \delta_{yy} , \quad \dot{s}_{\theta\theta} = 2\mu\left(\dot{\varepsilon}_{\theta\theta} - \frac{1}{3}\frac{\dot{V}}{V}\right) ,$$

$$\dot{\varepsilon}_{xx} = \frac{\partial\dot{x}}{\partial x} , \quad \dot{\varepsilon}_{yy} = \frac{\partial\dot{y}}{\partial y} , \quad \dot{\varepsilon}_{xy} = \frac{\partial\dot{x}}{\partial x} + \frac{\partial\dot{y}}{\partial y} ,$$

where x, y – the axial and radial spatial coordinates, ρ – density, V – volume fraction, p – hydrostatic pressure, E – internal energy per unit of volume, $\sigma_{ii}, s_{ii}, \varepsilon_{ii}, i = x, y, \theta$ – respectively, combined stress, component of stress and strain deviator, σ_{xy} – shearing stress, δ – rotation correction.

The point over the variables means time derivative in the line of the particle path. This system of equations is supplemented by following state equation

$$p = n B\left(\frac{\rho}{\rho_0} - 1\right) + E(n - 1)\rho \,,$$

where B – Tait constant, n – adiabatic index, ρ_0 – density under normal conditions.

It is considered that the matirial passes into plastic stage if the Mises condition is satisfied, are equivalent stresses equal to yield strength

$$\sigma_{eq} = \sqrt{\frac{1}{2}\left((\sigma_1 - \sigma_2)^2 + (\sigma_1 - \sigma_3)^2 + (\sigma_3 - \sigma_2)^2\right)} \leq [\sigma]. \qquad (7)$$

3. Powder hydro-cannon for field operation

Numerical methods are widely used for calculations. The problem of the liquid flow has been decided using Godunov and Rodionov's methods [6, 8, 15], the calculation of the stressed-deformed state was carried out using artificial viscidity method [16].

Based on this calculation the powder hydro-cannon has been designed and made for the field tests with the performance characteristics as follows: barrel radius R_c 16 mm, nozzle radius R_s 7,5 mm, nozzle length L_s 70 mm, collimator length L_k 50 mm, length of water charge acceleration L 110 mm, water charge mass m_w 230 gm, volume of combustion chamber V_{k0} 47 sm^3, mass of gunpowder m_p 30 gm, calculated speed of impulsive jet u_{max} 1100 m/s; maximal pressure in nozzle p_{max} 600 MPa; hydro-cannon mass m_c 15 kg; hydro-cannon length L_c 600 mm; shot energy E_0 100 kJ; jet impulse p_{jet} 130 N s; length of high-speed area of jet of L_{max} 100 mm.
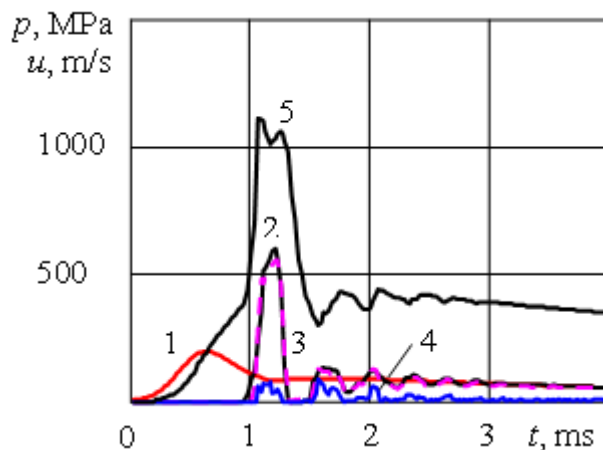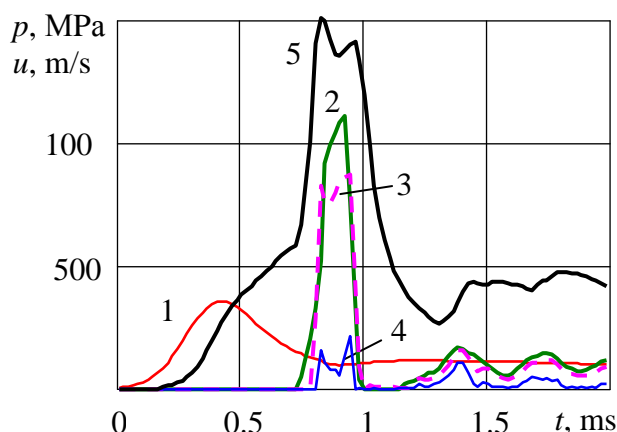
Fig. 4. Dependence of pressure and speed on time. Curves 1 – 4 pressure in the cross-sections of x_1 – x_4, 5 is speed of inflow and outflow, mass of m_p = 30 g.

Figure 4 shows the dependences of pressure and speed on time for this device if the mass of gunpowder m_p is equal to 30 g. Curves 1 – 4 indicate pressure in the cross-sections of $x_1 = -450$ mm (combustion chamber), $x_2 = -200$ mm (middle of barrel), $x_3 = 0$ (beginning of nozzle), $x_4 = 70$ mm (end of nozzle). Curve 5 indicates speed of inflow and outflow.

The shot of powder hydro-cannon lasts for 2 ms. The jet outflow begins with maximum speed $u_{max} = 1070$ m/s. During 0.3 ms speed of jet outflow changes insignificantly, but then it diminishes very quickly to 300 m/s. The high-speed sector of jet is formed during this time and its length is approximately 300 mm.

Fig. 5. Dependence of pressure and speed on time. Curves 1 – 4 pressure in the cross-sections of x_1 – x_4, 5 is speed of inflow and outflow, mass of m_p = 40 g.

511

The pressure reaches its maximum at the beginning of nozzle where jet outflows and its value is approx. p_{max} = 600 MPa. At the end of nozzle the pressure is considerably less than maximal (curve 4). The changes of pressure and speed have the pronounced impulsive character by duration 0.2 – 0.3 ms. Pressure of gunpowder gases reaches 200 MPa and changes rather fluently (curve 1).

The distribution of pressure and speed by length of the powder hydro-cannon at the end of outflow for different gunpowder charges is seen at Fig. 6. Curves 1 and 3 are pressure, 2 and 4 are speed, 1 and 2 – for 30 gm of gunpowder, 3 and 4 – for 40 gm. As the diagram shows, the pressure reaches its maximal values at the beginning of nozzle. The water speed changes on length considerably, and the flow is stabilized in collimator, speed gradient is small here.

The carried out examinations show that the processes in powder hydro-cannon are of complex character. The jet outflow from powder hydro-cannon begins with its maximum speed, which stays almost constant during a small period of time, and then quickly diminishes in 4-5 times. The high-speed sector of jet is formed at this time.

The offered model in which a liquid is considered to be ideal and compressible gives good results for description of processes in powder hydro-cannon.
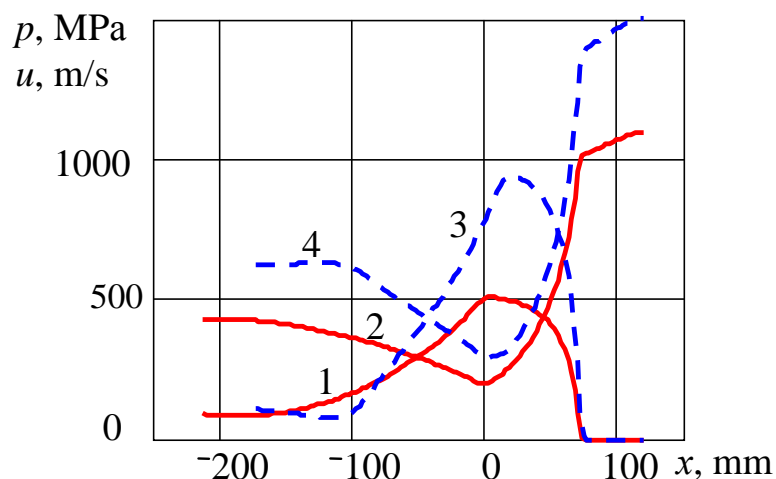

Fig. 6. Dependence of pressure and speed on length of powder hydrocannon. Curves 1 and3 are pressure, 2 and 4are speed,1 and 2 – for mass of m_p = 30 g, 3 and 4 – for mass of m_p = 40 g.

The hydrodynamic parameters of powder hydro-cannon substantially depend on a sort of gunpowder, sizes and form of gunpowder grain and mass of gunpowder charge. Therefore, the parameters of powder hydro-cannon should be calculated in a complex manner; i.e. taking into account energy characteristic of gunpowder, sizes and form of gunpowder grains, sizes of combustion chamber, length of acceleration of water charge, sizes and form of nozzle.

The stress-deformed state of powder hydro-cannon barrel can be described by equations (6) if taking into account elasto-plastic deformations. If Mizes inequality (7) is completed, material passes to the plastic stage, equivalent stresses become equal to the yield point and remain constant if the mentioned condition is met. The load is created by influent water and is variable, both by length of barrel and by time. The equations (6) are solved by a numerical method with artificial viscidity.

The equivalent stresses at the different moments of time are seen at Fig. 7. The results evidently demonstrate the dynamics of a process. At first, the pressure of gunpowder gases and layers of liquid adjoined to this area arises quickly. At the beginning the appeared pressure causes insignificant stresses and deformations of barrel in a small area. On the initial stage of a process equivalent stresses in the described area change from 400 to 1400 MPa (Fig. 7 a) and are far beyond the yield point.

By the moment of time of 0.7 – 0.75 ms which corresponds to the time of origin of maximal pressures of liquid into a barrel, maximal equivalent stresses arise in the body of powder hydro-cannon, which are equal to the yield point. The most dangerous part of the hydro-cannon body is a conjugation of its cylindrical and conical parts.

For time from 0.55 ms to 0.75 ms the area of large stresses expands and covers almost whole barrel (Fig. 7 b, c). This fact confirms the wave character of processes. Then from 0.8 ms the jet outflow begins, which is accompanied by diminishing of pressure that in turn led to diminishing of equivalent stresses in the hydro-cannon barrel (Fig. 7 d). Large-scale stresses in the middle of process result with appearance of residual deformations that can be considered as a spontaneous work-hardening of barrel by the autofrettage method.
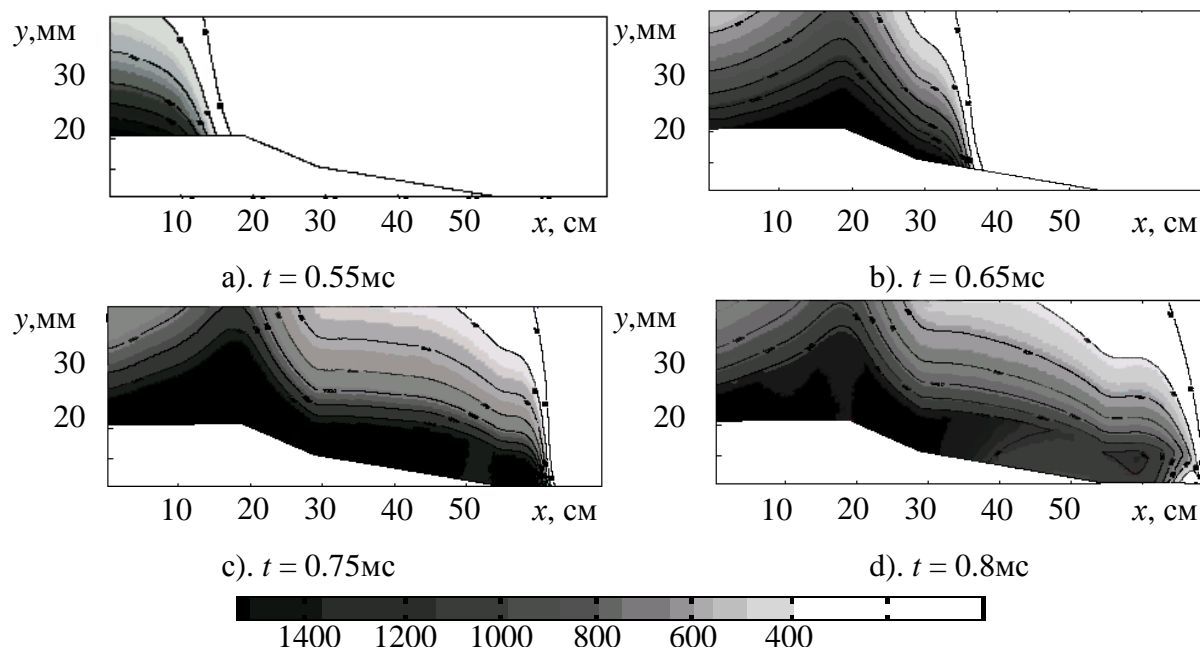
a). $t = 0.55$мс

b). $t = 0.65$мс

c). $t = 0.75$мс

d). $t = 0.8$мс

Fig. 7

The calculations have shown that stresses penetrate deep into cylinder in the area of stress concentration, and that may cause destruction of the body in this place in case of repeated loading. It is therefore expedient to create a preliminary tension of barrel by tightening it with the wire winding or ferrule.

4. Experimental examinations of the powder hydro-cannon

The series of experiments with the specially made powder hydro-cannon have been carried out to vivificate the developed mathematical models. The hydro-cannon parameters are as follows: barrel radius is 20 mm, nozzle radius is 10 mm, barrel length is 400 mm, nozzle length is 86 mm, collimator length is 70 mm, combustion chamber volume is 135 sm^3, water charge mass is 400 g. During the experiments, the pressure into hydro-cannon barrel and speed and impulse of jet have been measured. The pressure was measured by industrial device intended for research of internal ballistics of cannon barrels.
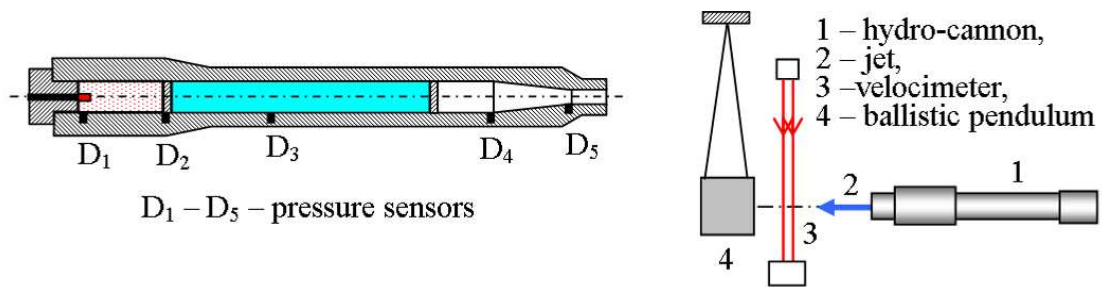
Fig.8.Experimental setting and scheme of experiment

There were five pressure sensors set along the length of hydro-cannon. Speed of jet head was measured by a non-contact laser measuring device specially developed for the field examination. The impulse of jet was measured by a ballistic pendulum with a special trap for a jet. The experiments on pressure measuring were carried out by V.A. Bigvava, A.V. Kochergin from «Iskra» enterprise and V.I.Gubskiy. The experimental hydro-cannon and scheme of experiments on measuring of speed and impulse of jet is seen at Fig. 8.
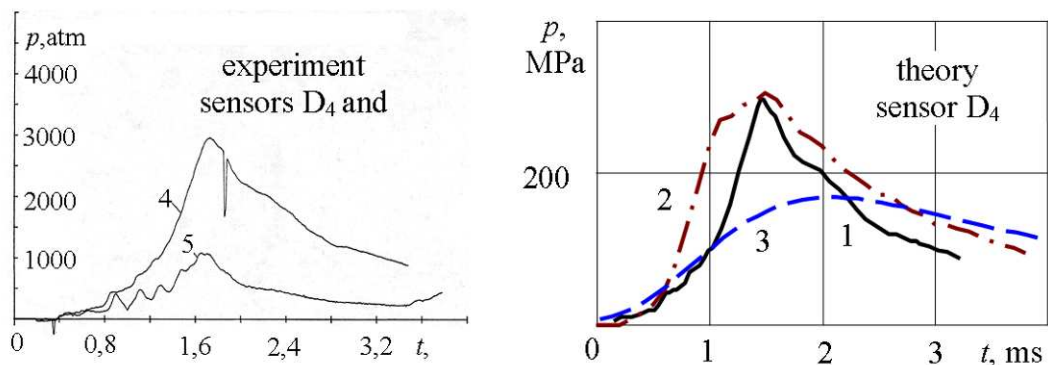
Fig. 9. Pressure inside powder water-gun

The experimental and theoretical dependences of pressure for the powder water-jet device and hydro-cannon are resulted at Figs. 9 and 10. Curves 1, 2 and 3 on a Fig. 9 indicate an experiment, calculations in the non-stationary and quasi-stationary statements. It is evident that the results of calculations in the non-stationary statement match with the experiment. The maximal speed of jet outflow, which was recorded during the experiment, is equal to 730 m/s and differs from calculated value of 4%.
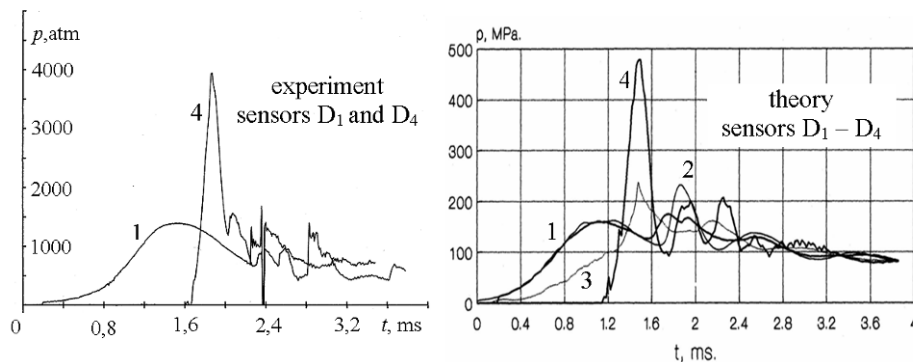
Fig. 10.Pressure inside powder hydro-cannon

The jet impulse was measured by a ballistic pendulum. It was a hollow steel cylinder filled with lead of weighing 110 kg. The pendulum was suspended on thin hawsers 1285 mm long. The comparison of the calculated and experimental data measuring the speed of the jet head and jet impulse of powder hydro-cannon is shown in Table 1.

Table 1 - Speed and impulse of jet

Value	Calculation	Measurement	Error, %
v, м/с	1070	1076 ± 49	0.75
P, Н·с	122	129 ± 11	5.7

It ensues from the analysis of results of calculations and experiments that processes in water-jet device and hydro-cannon differentiate substantially. The non-stationary quasi-one dimensional model of motion of liquid and quasi-stationary model of powder burning describe processes in the real powder water-jet device and hydro-cannon well.

The qualitative and quantitative results of calculations on this model coincide with the results of measurements of water pressure and gunpowder gases, speed and impulse of jet. If certain conditions are met, the quasi-stationary model of motion of liquid and burning of gunpowder gives acceptable precision for a powder hydro-gun. The average jet speed of powder hydro-cannon is equal to $v_{cp} = (1089 \pm 62)$ m/s. The calculation value of jet speed of hydro-cannon is equal to $v_s = 1070$ m/s and differs from the average value for 2 %. The rather precise matching of measured results and calculated values proves the adequacy of model of powder hydro-cannon and reliability of numeral

methods.

5. Application of hydro-jet technologies

Hydroimpulsive destruction. The experimental model of powder hydro-cannon was tested by destruction of concrete and ferroconcrete blocks, lumps, construction materials, liquidation of explosive devices, etc. The efficiency of destruction of concrete objects was estimated by the number and sizes of fragments that broke off from the concrete. The level of noise made by the shot of powder hydro-cannon and the distance of projectiles of broken fragments were also estimated in experiments. A noise level was measured by acoustic sensors which was located at 5, 10 and 20 m from the place of shot. The degree of scattering of broken fragments was estimated by sight, by video camera shooting and by measuring of distances from the destructed object to the fragments that flew away. Usually, after the first shot there was a network of cracks in the massive concrete block and scattering of fragments was insignificant. After subsequent shots, there was intensive destruction of the concrete block and distance of scattering was longer than anticipated.

The results of destruction of the non-reinforced and reinforced concrete slabs, which thickness is 180 mm, are seen at Figs. 11 and 12. The destruction was made by shot of powder hydro-cannon in a lateral direction. We can see that a slab has been cracked on two parts. The picture of destruction of ferroconcrete slab with 15 mm armature is seen at Fig. 12. The armature has not influenced on the degree of destruction of the slab. After the first shot the pieces of concrete broke off and the network of cracks appeared. After the second shot, the slab was completely destroyed.

Fig. 11   **Fig. 12**

The results of the experiment on destruction of ferroconcrete slab with a metal barrier before it are seen at Fig. 13. The n-shaped steel profile, which thickness is 6 mm, was placed before the ferroconcrete slab. The impulsive

water jet broke through the steel profile, punched a 3×5 cm hole in it, and split a concrete slab into a few fragments.

These experiments proved that the impulsive high-pressure water jet can effectively destroy concrete, ferroconcrete and construction materials made of reinforced concrete and steel.

The series of experiments by destruction of models of explosive objects were carried out to estimate the abilities of the potential application of impulsive high-pressure water jet. The scheme and results of the experiment on destruction of model of explosive objects is seen at Fig. 14. The object was a metal jar of 5 l volume which was filled up with dried out putty which looks like a gypsum or alabaster by its hardness and consistency. A 4 mm protective steel plate was placed in front of the object in the distance of 2 – 3 cm. A shot from the powder hydro-cannon was fired in the object through the steel plate from distance of 10 cm. The impulsive jet punched a 5×5 cm ragged hole in the steel plate. The metal jar with filler was split into small pieces (3×5 cm). The shards flew away in different directions on a distance up to 5 m from initial position of the jar. The bottom of the jar was only left on the ground.

The scheme and results of experiment on destruction of electronic explosive objects is seen at Fig. 15. The device was a box with a charge of explosive material and electronic circuit with a clock-work as a trigger for blowing up in a preset time. Furthermore, any attempt to mine clear the electronic circuit after the clock-work countdown was started led to blowing up of the device. The device was demolished by a shot from the powder hydro-cannon which stood in the distance of 15 cm from the object. As a result of experiment the device was split without detonation.

This paper observes the possibilities of application of the powder hydro-cannon and impulsive high-speed water jets (by speed of 1000 m/s and over). The powder hydro-cannon are compact; they are powerful and concise, small in size and weight, mobile and reliable. The physical and mathematical model of the shot of powder hydro-cannon is expounded; the hydrodynamic parameters of powder hydro-cannon are calculated. The powder hydro-cannons of different purposes were calculated, designed and made for the field tests.

Destruction of construction materials

Before a shot   After ashot

Destruction of reinforced-concrete blocks

Before a shot   After ashot

Destruction of reinforce-concrete blocks and construction

Fig. 14.Liquidation of model of explosive objects

Liquidation of explosive device

Fig. 15.Liquidation of model of electronic explosive objects

The results of calculations coincide well with experiments on measurement of speed of jet head. The full-scale tests of experimental samples of powder hydro-cannons have been carried out and successfully aimed at destruction of concrete and reinforced-concrete blocks, punching of steel plates of different thickness, demolishing of models of explosive objects and liquidation of explosive objects. It has been demonstrated that powder hydro-cannon can effectively destroy such objects with minimal risk.

The experiments proved availability of application of impulsive high-speed water jets in different technological processes. The positive results of this experiment provides need for further investigations regarding the interaction of impulsive spurts of liquid with certain objects, which depend both on the parameters of impulsive jets and on properties of objects.

References

1. G. A. Atanov, Hydroimpulsive Installations for the Destruction of Rocks [in Russian], Vyshcha Shkola, Kiev, (1987).

2. A.I. Petrakov and O.D. Krivorotko, "Destruction of Rocks by pulsed jets," Coal, No. 3, P. 12-15 (1982)

3. W.C. Cooley, "Advances in the Technology of Fluid Jets: Past, Present and Targets for the 21st century," in: Proc. of 5th Pacific Rim International Conference on Water Jet Technology, WJTSJ, Tokyo (Japan), P. 1–8 (1998).

4. W. C. Cooley and W. N. Lucke, "Development and Testing of a Water Cannon for Tunneling," in: Proc. of the 2nd Int. Symposium on Jet Cutting Technology, Paper J3, Cambridge, England (1974), P. 141–160.

5. G.A. Atanov, "The Impulsive Water Jet Device: a New Machine for Breaking Rock," International Journal of Water Jet Technology, Vol.1, № 2. – P. 85–91. (1991)

6. G.A. Atanov and A.N. Semko, "The powder hydro-cannon" in: Proc. of International Summer Scientific School "High Speed Hydrodynamics" (HSH 2002), Cheboksary, Russian/ Washington, USA: Cheboksary, Russian, June 16 – 23, 2002. P. 419 – 424.

7. G.A. Atanov, E.S. Geskin, A.V. Kovalev and A.N. Semko, "The powder hydro-cannon of broad action spectrum," Applied hydromechanics, Vol. 6 (78), No. 3. P. 3-9 (2004).

8. A.N. Semko, "Interior Ballistics of Powder Water-jet Device and Hydro-cannon", Theoretical and Applied Mechanics, Osnova, Kharkiv, Vol. 35. – p. 181 – 185 (2002)

9. O. Petrenko, E.S. Geskin, G.A. Atanov, A.N. Semko and B. Goldenberg, "Numerical Modeling of High-Speed Water Slugs," Transaction of the ASME. Journal of Fluids Engineering, Vol. 126. No 2, P. 206 – 209 (2004).

10. O.P. Petrenko, E.S. Geskin and A.N. Semko, "Mechanics of Powder Hydrocannon for Incompressible Fluid," in: Proc. of 2005 WJTA American Waterjet Conference (2005 WJTA, August 21-23, 2005). - Houston, Texas, - P. 1 – 14 (2005).

11. Y.Y. Lei, X. Wan, L. Yang and C.L. Tang, "Ultra-hight Speed Pulsed Water Jet – a Potential Tool for Stone Material Machining," Key Engineering Materials, Trans Tech Publications, Vols. 259–260, – P. 602–608 (2004).

12. M.M. Vijay, "Pulsed jets: fundamentals and applications," in: Proc. of the 5th Pacific Rim International Conference on Water Jet Technology, New Delhi (India). P. 610–627 (1998).

13. G. A. Atanov, V. I. Gubskii, and A. N. Semko, "Internal ballistics of a powder water cannon," Izv. RAN.MZhG, No. 6, 175–179 (1997).

14. G. A. Atanov, A. N. Semko, O. P. Petrenko, et al., "Peculiarities of the Powder Water Cannon Operation," in: Proc. of the ASME Int. Mechanical Engineering Congress & Exp. (November 16–21, 2003), Washington, ISMECE2003-42788.

15. V.V. Reshetnyak and A. N. Semko, "Application of Rodionov's Method for Calculation of Quasionedimensional Flow of Ideal Uncompressible Liquid," Applied hydromechanics, Vol. 9 (81), No. 3, P. 56 – 64 (2009).

16. O.A. Rusanova and A.N. Semko, "Stressed-deformed State of Powder Hydro-cannon Barrel during the Shot" Visnik Donetskogo yniversitety. Vol. 1, No. 1, P. 166 – 170 (2006).

6. NEW PRINCIPLES OF TECHNOLOGY OF MEASUREMENT

6.1 ANALIZA MOŻLIWOŚCI WYKORZYSTANIA CZUJNIKÓW SIŁY DYNAMICZNEJ DO OKREŚLANIA STANU NARZĘDZI W WYBRANYCH PROCESACH TECHNOLOGICZNYCH

Flaga S.[1], Konieczny J.[1]

Wstęp

Wpracy przedstawiono problemem trudnego do wykrycia uszkadzania się narzędzia wykonującego gniazdo pod wkrętak w procesie technologicznym produkcji śrub. Gniazdo to wykonywane jest w technologii tłoczenia na zimno w maszynie o nazwie spęczarka (zbijarka) dwuuderzeniowa. Część nazwy „dwuuderzeniowa" wywodzi się z technologii pracy: pierwsze uderzenie wykonuje spęczenie łba śruby (układ diagnostyczny nie analizuje stanu narzędzia spęczającego), drugie uderzenie wykonuje gniazdo dla narzędzia (wkrętaka).

W chwili obecnej wielu producentów śrub analizę stanu narzędzia przeprowadza wzrokowo, co nie jest łatwe ze względu na warunki pracy narzędzia. Narzędzie jest przewidziane na wykonanie określonej liczby gniazd. Ten problem rozwiązywany jest poprzez stosowanie automatycznych liczników wyłączających maszynę po określonej liczbie wykonanych sztuk.

Praca maszyny z uszkodzonym narzędziem przynosi wymierne straty ekonomiczne. Zakładając, że standardowa spęczarka produkuje 2 szt półproduktu (drut o średnicu 2 – 8 mm) w czasie 1 sekundy, co przy materiale o średnicy 5 mm (stal węglowa $\gamma \cong 7500 kg/m^3$) i długości półproduktu 50 mm daje straty materiału rzędu $6{,}8 \cdot 10^{-3} kg/s$. Zakładając, że producent posiada 10 takich maszyn pracujących na 2 zmiany, to jeżeli każda z nich w ciągu dnia roboczego wykona tylko 100 wadliwych półproduktów (w czasie 50 s) to straty materiału wyniosą 6,8 kg. Straty te są szczególnie istotne wtedy, kiedy śruby wykonywane są nie ze stali węglowej, ale ze stali szlachetnej.

---

[1] AGH w Krakowie, Wydział Inżynierii Mechanicznej i Robotyki, KAP

Wadliwie wykonane na spęczarce półprodukty są nadal obrabiane (walcowanie linii śrubowej, montaż specjalizowanej końcówki nawiercającej, obróbka cieplna, cieplno-chemiczna), ponieważ kontrola jakości dotyczy dopiero wyrobu gotowego. Należy zaznaczyć, że kontrola poprawności wykonania gniazda (sprawnym narzędziem) jest najbardziej czasochłonna.

Automaty diagnozujące stan narzędzia w nowych maszynach są stosunkowo skuteczne, natomiast nie sprawdzają się w starszych maszynach, które to stanowią większość na rynku. Dlatego też przeprowadzono badania i podjęto próbę stworzenia prototypu analizatora stanu narzędzia (nagłownika), co przedstawiono w niniejszym sprawozdaniu.

Opis badanego procesu technologicznego

Proces wytwarzania śrub i wkrętów walcowanych rozpoczyna się najczęściej na spęczarce dwuuderzeniowej czyli analizowanej maszynie (rys 1). Jej zadaniem jest odcięcie ze zwoju drutu odcinka zgodnego z projektem danego wyrobu. Następnie odcięty odcinek poddany jest dwuetapowej obróbce na zimno. W pierwszym etapie obróbki na zimno narzędzie o nazwie spęczak powoduje uformowanie łba śruby lub wkrętu, a w drugim wytłaczane jest gniazdo na narzędzie. Schemat kinematyczny maszyny pokazano na rysunku 1. Bardzo istotnym elementem tego urządzenia jest koło zamachowe magazynujące energię potrzebną do przeprowadzenia obróbki na zimno.
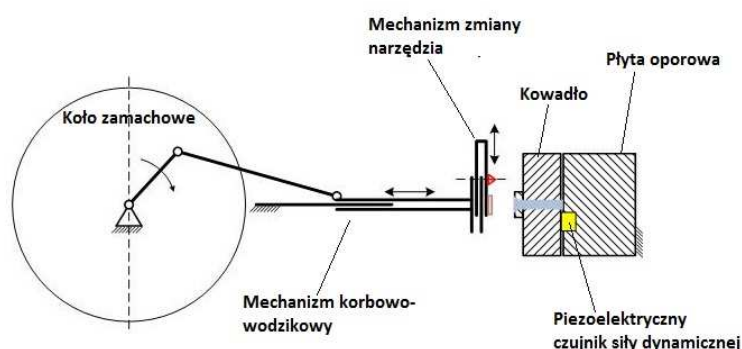
Rys. 1. Schemat kinematyczny maszyny

Wykonanie jednego półproduktu przeprowadzane jest w czterech fazach pokazanych na rysunkach od 2 do 5. Liczba faz wynika ze stopnia skomplikowania obróbki. Ponieważ proces spęczania łba śruby oraz wytłaczania
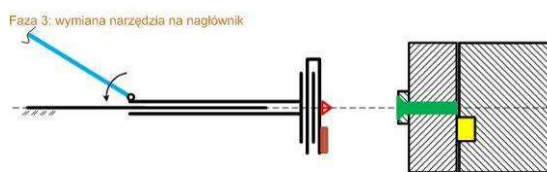
gniazda wymaga odpowiednio dużych energii to wykonanie tych dwóch czynności wymaga dwóch pełnych obrotów koła zamachowego.
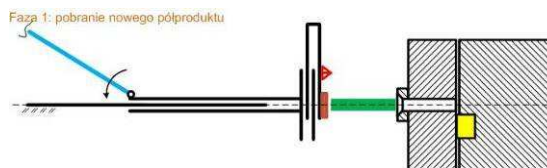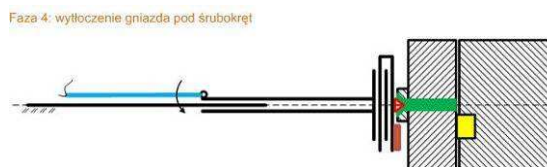

Rys. 2. Faza pobierania nowego materiału i wyrzutu gotowego półproduktu
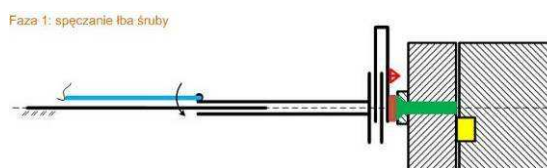
**Rys. 3. Faza spęczania łba śruby**

Rys. 4. Faza wymiany narzędzia na nagłownik

Rys. 5. Faza tłoczenia gniazda pod śrubokręt – narzędzie użyte do realizacji tej fazy produkcji podlega monitorowaniu przez projektowany system

Badania rozpoznawcze i ich analiza

Przed przystąpieniem do analizy możliwości diagnozowania stanu narzędzia z wykorzystaniem czujnika siły dynamicznej, określono sposób jego montażu w maszynie (rys. 6) i przeprowadzono badania wstępne. Niestety nie było możliwości, aby w badanej maszynie optymalizować miejsce montażu czujnika. Wynikało ono bardziej z możliwości konstrukcyjnych. Gniazdo na czujnik zostało wykonane z wykorzystaniem elektrodrążarki.
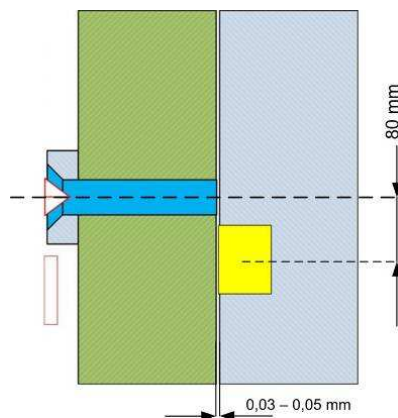
Rys. 6. Sposób montażu czujnika pomiarowego w maszynie

Głównymi zadaniami badań wstępnych były dobory parametrów kondycjonera sygnału i identyfikacja wpływu uszkodzenia nagłownika na otrzymany sygnał wejściowy. Analizując otrzymane wyniki stwierdzono, że do identyfikacji uszkodzenia wystarczy tylko część sygnału odpowiadająca ściskaniu – podjęto więc decyzję o jego jednopołówkowym wyprostowaniu. Do prostowania sygnału wykorzystano prostownik liniowy.

Typowe uszkodzenia badanego narzędzia

Narzędzie, którego stan jest badany może ulec uszkodzeniu na następujące sposoby:

−   wytarcie (po określonej liczbie cykli, wykonanych tłoczeń musi być dokonywany pomiar kontrolny nagłównika, i na tej podstawie podejmowana jest decyzja o jego wymianie), normatywna liczba wytłoczeń wynosi w zależności od wielkości narzędzia około 40 000 sztuk,

−   wyłamanie jednego zazębienia dla śrubokręta krzyżowego z odłamaną końcówką,

−   złamanie prawie całego nagłównika.

Najczęściej narzędzie ulega uszkodzeniu przy starcie lub nieumiejętnym (bez użycia hamulca) zatrzymaniu maszyny. Nagłównikiz odłamaną częścią tłoczącą pokazano na rysunku 7.Dla porównania sprawne narzędzie pokazano na rysunku 8.

Rys. 7. Nagłównik z odłamaną częścią tłoczącą

Rys. 8. Sprawne narzędzie

Na rysunkach 9 a, b, c, d pokazano półprodukty wykonane sprawnym i uszkodzonym narzędziem

a) b) c) d)

Rys. 9. Przykłady półproduktów wychodzących ze spęczarki dwuuderzeniowej: a) półprodukt wykonany sprawnym narzędziem, b) półprodukt wykonany narzędziem z uszkodzonym jednym wejściem, c), d) półprodukty wykonane narzędziem z odłamaną częścią tłoczącą

Koncepcja systemu diagnostycznego

Koncepcyjnie przyjęto, że analizie poddany zostanie sygnał mówiący o względnej szczątkowej energii uderzenia E_{szu} mierzonej między kowadłem, a płytą oporową. Uproszczony rozpływ energii w omawianym procesie pokazano na rysunku 10.

Przy założeniu, że analizujemy produkcję opartą na materiale o stałych parametrach i z użyciem jednego narzędzia (jeden rodzaj półproduktu) praca W_{gn} potrzebna do wytłoczenia gniazda na narzędzie będzie funkcją siły uderzenia $\vec{F}_u$ i przemieszczenia nagłównika w materiale $\vec{s}_u$ czyli możemy zapisać $W_{gn} = fF_u \cdot s_u$. Siła $\vec{F}_u$ jaka może być wygenerowana w układzie maszyny jest taka

sama dla każdego detalu (stała masa koła zamachowego, stałe parametry mechanizmu mimośrodowego, stałe parametry silnika napędowego). Natomiast przemieszczenie narzędzia w materiale będzie zależne od stanu narzędzia (zmiany jego długości, kształtu). Można więc w uproszczeniu przyjąć, że

$$W_{gn} = f_u s_u.$$
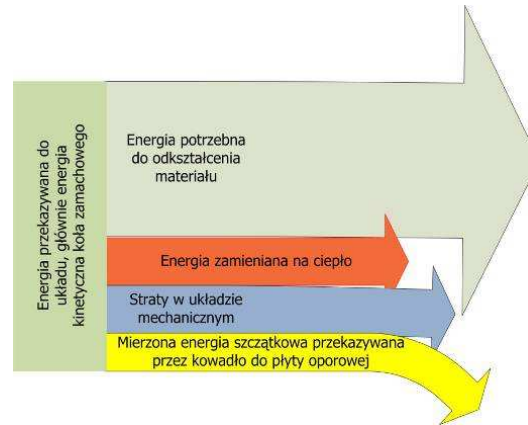
Rys. 10. Uproszczony rozpływ energii w procesie wytłaczania na zimno gniazda pod narzędzie wkręcające.

Problem nie jest jednak trywialny, ponieważ bezpośredni pomiar na ile nagłownik zagłębił się w obrabiany materiał nie jest możliwy. Założono więc pomiar pośredni polegający na pomiarze energii E_{szu}.

Oczywiście posiłkowanie się siłą $\vec{F}_u$ jest pewnym uproszczeniem, ponieważ nie możemy powiedzieć, że na podstawie wartości siły w pewnej chwili t możemy określić stan narzędzia. Dodatkowym utrudnieniem jest fakt, że na jednej maszynie może być wykonywanych kilka asortymentów ze względu na grubość drutu (wielkość narzędzia) i ze względu na rodzaj materiału. Z tego powodu postanowiono nie mierzyć bezwzględnych wartości energii, a jedynie dostrajać czułość urządzenia do aktualnie wyrabianego półproduktu. Mierzona wartość energii szczątkowej nie jest wyrażana w konkretnych wartościach. Analizę stanu narzędzia postanowiono określać na podstawie charakteru zmian względnej energii szczątkowej w czasie.

Jako przetwornik pomiarowy wykorzystano piezoelektryczny przetwornik siły dynamicznej, docelowo będzie to przetwornik wykorzystujący materiał z magnetyczną pamięcią kształtu (MSMA).

Przetwornik ten generuje ładunek elektryczny będący miarą siły. Pomiary wykonywane tego typu przetwornikami wymagają stosowania kondycjonerów sygnału działających na zasadzie wzmacniaczy ładunku elektrycznego.

Konstrukcja prototypu systemu diagnostycznego

Ideę urządzenia pomiarowego pokazano na rysunku 11.
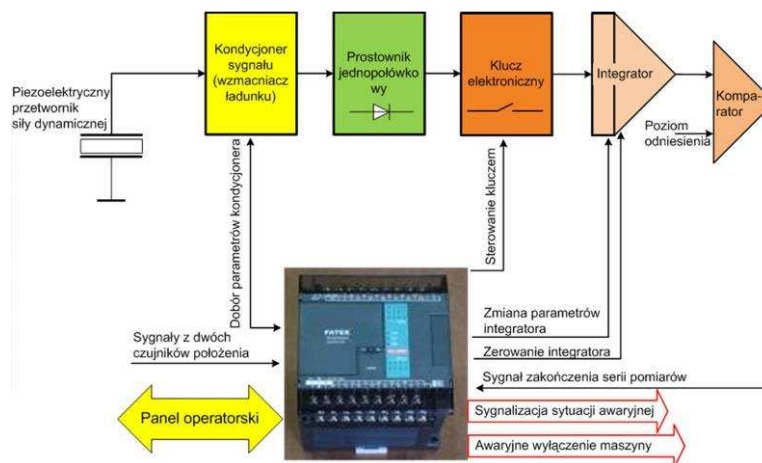
Rys. 11. Schemat ideowy urządzenia diagnostycznego.

Wszystkie obwody elektroniczne (oczywiście poza PLC) zostały zaprojektowane i wykonane przez autorów. W oprogramowaniu sterownika PLC zawarta jest cała idea detekcji uszkodzenia.Postanowiono wykorzystać klasyczny sterownik PLC zamiast systemu mikroprocesorowego ze względu na łatwość modyfikacji algorytmu jak i trudne warunki pracy urządzenia.

Badania rozwiązania prototypowego

Badania prototypu prowadzono zdalnie cowynikało z odległości od miejsca pomiarów jak i z czasochłonnością ich wykonania. Sto uszkodzeń na jednej maszynie to około miesiąc pracy na dwie zmiany. Część sygnałów pochodzących z zaprojektowanego i wykonanego obwodu elektronicznego była mierzona i archiwizowana przy wykorzystaniu LabView i karty pomiarowej. Do nadzorowania pracy (realizacji algorytmu identyfikacji uszkodzenia) wykorzystano arkusz kalkulacyjny Excel komunikujący się ze sterownikiem PLC poprzez OPC serwer. Wybór taki podyktowany jest łatwością zapisu w arkuszu excela wybranych (biorących udział w podejmowaniu decyzji) rejestrów sterownika. Z kolei na tak pobranych i zapisanych rejestrach, korzystając z mechanizmów arkusza, łatwo można przeprowadzać obliczenia

sprawdzające działanie programu w sterowniku PLC. Działanie arkusza kalkulacyjnego zostało zmodyfikowane poprzez odpowiednie skrypty w języku VBA. Takie sprawdzanie algorytmu wynika z zaimplementowaniu w PLC stosunkowo skomplikowanego (jak na PLC) algorytmu obliczeniowego. Arkusze z monitorowanymi danymi zapisywane były automatycznie, co pozwalało na analizę przypadków wykrycia bądź niewykrycia uszkodzenia narzędzia.

Podsumowanie

Badania wstępne oraz efektów pracy prototypu przeprowadzono w fabryce wyrobów złącznych. Ponieważ badania efektywności pracy prototypu są bardzo czasochłonne (prototyp podłączony do jednej maszyny przy średnio jednym lub dwoma uszkodzeniami dziennie) wykorzystano zdalne połączenie z komputerem nadrzędnym połączonym z prototypem. Pakiety danych zarejestrowane przez komputer nadrzędny mogą być analizowane w dowolnym miejscu z posiadającym dostęp do Internetu.

Zauważono problemy z dostosowaniem parametrów pracy urządzenia diagnostycznego przy zmianie średnicy drutu oraz przy zmianie prędkości obrotowej silnika napędowego spęczarki.

Skuteczność urządzenia mierzoną jako stosunek poprawnych wyłączeń maszyny (wykrycie uszkodzenia nagłównika) do wszystkich wyłączeń maszyny (uznanie sprawnego nagłównika za dobry) wynosi około 80 % przy próbie 140 wszystkich wyłączeń. W badanym okresie 5 złamanych nagłówników nie zostało wykrytych.

Urządzenie prototypowe wymaga dalszego badania i rozwoju w celu osiągnięcia większej skuteczności wykrywania uszkodzenia narzędzia.

References

1. Boguta A.: Identyfikacja parametrów modelu przetwornika piezoelektrycznego jako czujnika siły uderzeniowej, MOTROL, Lublin, 2006, s. 49-58

2. Flaga S., Kata D. Sapiński B.: (2010), Microstructure evaluation of Ni-Mn-Ga alloy, Mechanics and Control, no 1/2010, AGH University of Science and Technology, Cracow.

3. Górecki P.: Wzmacniacze operacyjne, BTC, Warszawa, 2003

6.2 MULTI-PHASE METHODS OF MEASURING DISTANCES
Shinkaruk O.[1], Lubchik V.[1]

This article focuses on the study phase methods of measurement of distances and the development of multi-frequency phase method of determining distances and sizes of nanoparticles. Shown that when probing at several frequencies, is able to write the system of equations whose solution allows you to find the phase shifts of signals reflected by multiple objects. Since the phase shifts are proportional to the distance, the distance can be determined. The accuracy of measurement of distances and the resolution of the proposed method is proportional to the phase accuracy of the phase shift, which allows to develop a method of multifrequency phase size measurements of nano-objects.

Depending on the tasks that are solved using different methods of measuring distances. The most widely used temporary methods, among which is necessary to allocate the pulse method.

Table 1

Parameters / Method	Temporal	Frequency	Phase
Distance	$D = \dfrac{c \cdot t_D}{2}$	$D = \dfrac{c \cdot T_u}{2} \cdot \dfrac{\Delta \omega_u}{\Delta \omega}$	$D = \dfrac{c \cdot \Delta \varphi}{2 \cdot \Omega}$
Min. distance	$D_{min} = \dfrac{c \cdot (\tau_u + t_a)}{2}$	-	-
Border unequivocal sample	$D_{min} = \dfrac{c \cdot T_u}{2}$	$D = \dfrac{c \cdot T_u}{2}$	$D = \dfrac{\pi \cdot c}{\Omega}$
Potential resolution	$\Delta D_{min} = \dfrac{c \cdot \tau_u}{2}$	$\Delta D_{min} = \dfrac{c \Delta \Delta_\phi}{4 F_M \Delta f_m}$	-

Table 1 shows the characteristics of a pulsed, frequency and phase measurement techniques distances. Comparative characteristics are shown in Table 2. A significant drawback of most methods is the low accuracy of measurement, only the phase lot of scale method has high accuracy. [1-3]

---

[1] Khmelnitsky National University

One of the tasks that can be solved with reflection methods have control of nanoparticle size. To solve this problem have use different methods. They are based on methods of scanning probe microscopy (SPM), X-ray diffraction, dynamic light scattering. SPM is divided into optical and non-optical metods. Moreover, these methods have a number of drawbacks. Such as accuracy of the nanoparticle size is determined visually, on screen scanning microscope. This significantly increases the measurement error of nanoparticle sizes. Methods of dynamic light scattering have several disadvantages: the dependence of results on the adequacy of the mathematical model, which is the basis of correlation analysis, estimated not the particle size distribution but the distribution of agglomerate particles by size.

Table 2

Method	Benefits	Limitations
Temporal	The ability to determine distances to an arbitrary number of objects The ability to determine the nature of the object	Resolution is dependent on the pulse duration With decreasing pulse duration increases the attenuation of the pulse
Frequency	The ability to determine distances to an arbitrary number of objects The ability to determine the nature of the object High accuracy	The complexity of the technical implementation The need to ensure the linearity of the modulation
Phase	Determine the nature of the object High accuracy The use of low-frequency signals	Lack of resolution

Let us consider the phase lot of scale method (Fig. 12). The technique of measurement is known that the accuracy of the angle of the phase shift does not depend on the frequency of the signal. But if the phase shift of exaggerating value 2π then a phase ambiguity, the fact that most phase meters measures phase shift from 0 to 2π (360 °). To eliminate the phase ambiguity, the distance measurement is carried out in stages. First, measuring the phase shift is carried out harmonic signal, whose wavelength is greater than or equal to the maximum measuring distance. Then measuring the phase shift signal is carried out at a frequency 10 times higher than the frequency of the first signal. And the value

of the phase shift obtained in the first dimension is used to determine the number of full phase cycles. The result is a phase shift value greater than 2π, with the same accuracy of measurement of the phase, whereas the accuracy of the measurement distance increases by 10 times. Increasing the signal frequency will further increase accuracy. A feature of this method is that to eliminate the phase ambiguity using measurement information obtained at several frequencies of harmonic signals.
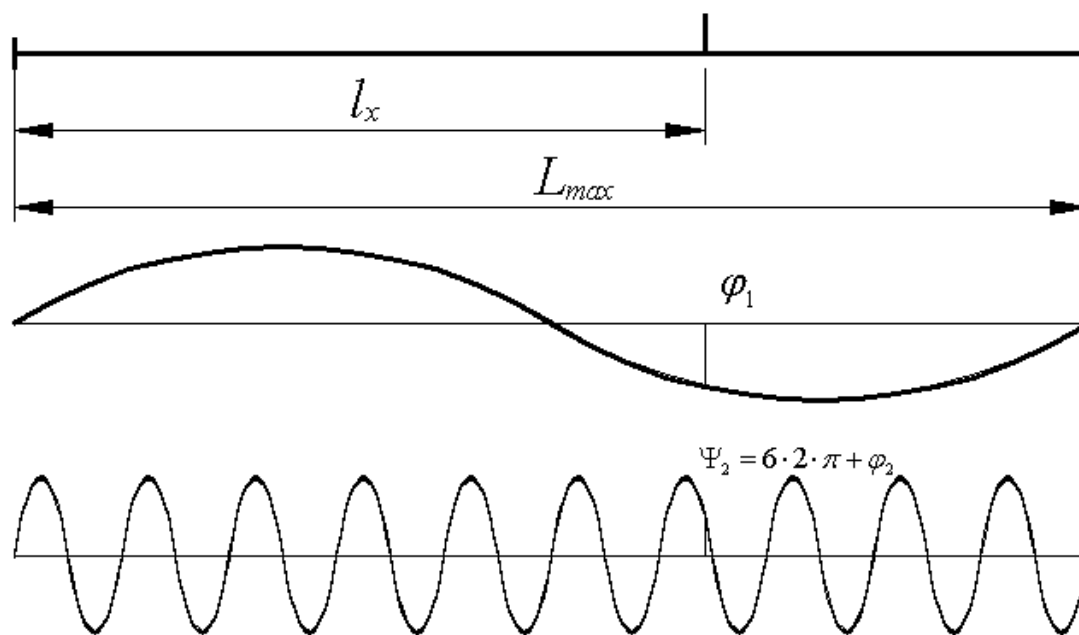

Fig. 1. Lot of scale phase method of measuring distances

Consider the passage of harmonic signals in the presence of multiple objects, in general, there can be any number. Fig. shows the three objects. If the wavelength of the harmonic signal is equal to the maximum distance, the phase ambiguity, the phase ambiguity, due phase incursion of more than $2\square$ can not occur. Upon reflection of the harmonic signal from each object, the starting point, there are three signals which are represented by the vectors a 1, 2 and 3, the phase shifts are represented by the vector angle, amplitude - the length of the vector. It is these values and describe objects - their distance and reflection coefficients. But because the system is linear, all these signals have the same frequency as the probe signal. Thus, we obtain a harmonic signal, whose vector is the geometric sum of the vectors of signals reflected from each object - . To find the sine, cosine and magnitude vector can be used the appropriate formulas.

But the split apart, all vectors of signals reflected from each object is not possible, as the total signal with a certain amplitude and a phase shift.

To solve the problem separating vector signal reflected from each object using an approach which is used in the phase lot of scale method, namely, obtaining measurement data on multiple frequencies and its general use.
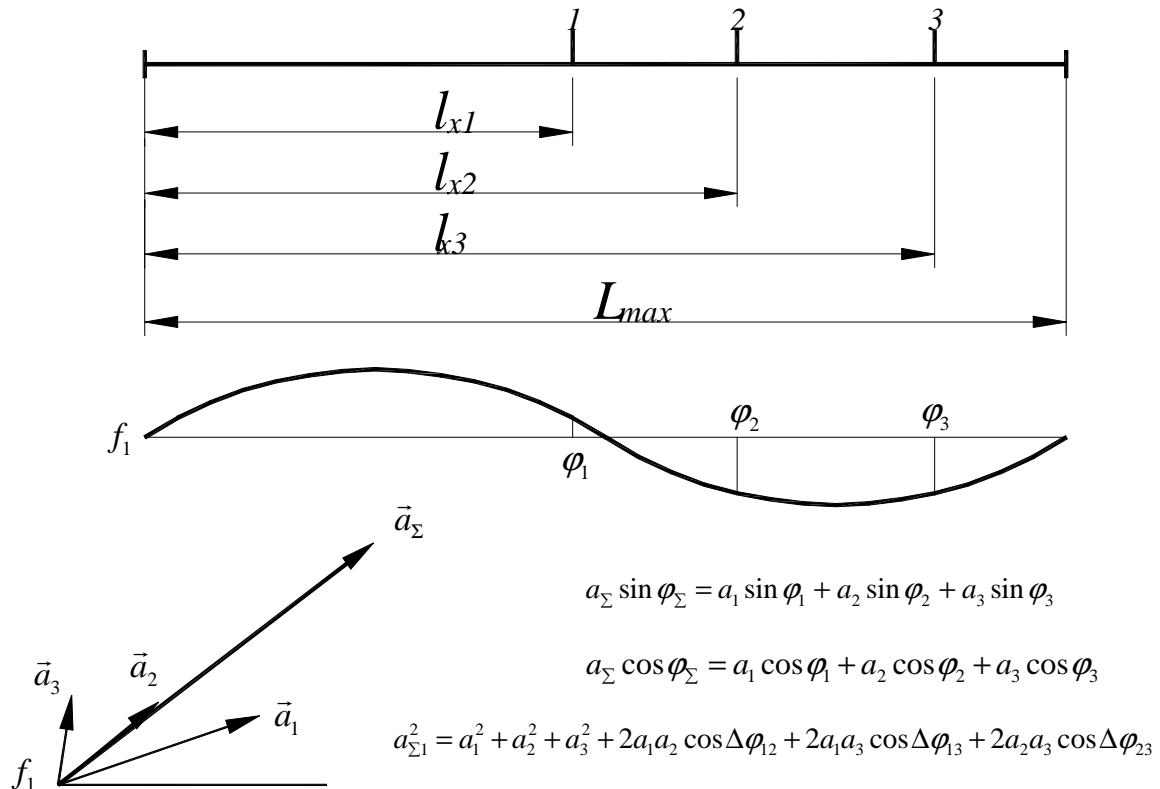
$$a_\Sigma \sin \varphi_\Sigma = a_1 \sin \varphi_1 + a_2 \sin \varphi_2 + a_3 \sin \varphi_3$$

$$a_\Sigma \cos \varphi_\Sigma = a_1 \cos \varphi_1 + a_2 \cos \varphi_2 + a_3 \cos \varphi_3$$

$$a_{\Sigma 1}^2 = a_1^2 + a_2^2 + a_3^2 + 2a_1 a_2 \cos \Delta\varphi_{12} + 2a_1 a_3 \cos \Delta\varphi_{13} + 2a_2 a_3 \cos \Delta\varphi_{23}$$

Fig. 2 . Total signal at a frequency f_1

Consider the passage of signals with frequencies of 2 and three times higher than the previous one (Fig. 3). The wavelengths of these signals in two or three times, respectively, less than the maximum measuring distance. Phase shift of each signal reflected from each object increases in two and three times, respectively, the relatively frequency of the first signal. In this case all vectors are rotated by an angle in two and three times more than on the first frequency. But total signals at these frequencies, as the statement indicates that their phase shifts do not vary linearly, and the amplitude decreases. If we consider the change in amplitude and phase shift of the frequency, we can construct the amplitude spectrum and spectrum of phase of the reflected signal. As can be seen with increasing frequency the amplitude decreases and increases, the phase

changes abruptly. The shape of these characteristics depends from number and ratio vectors signals reflected from all objects (phase and amplitude).
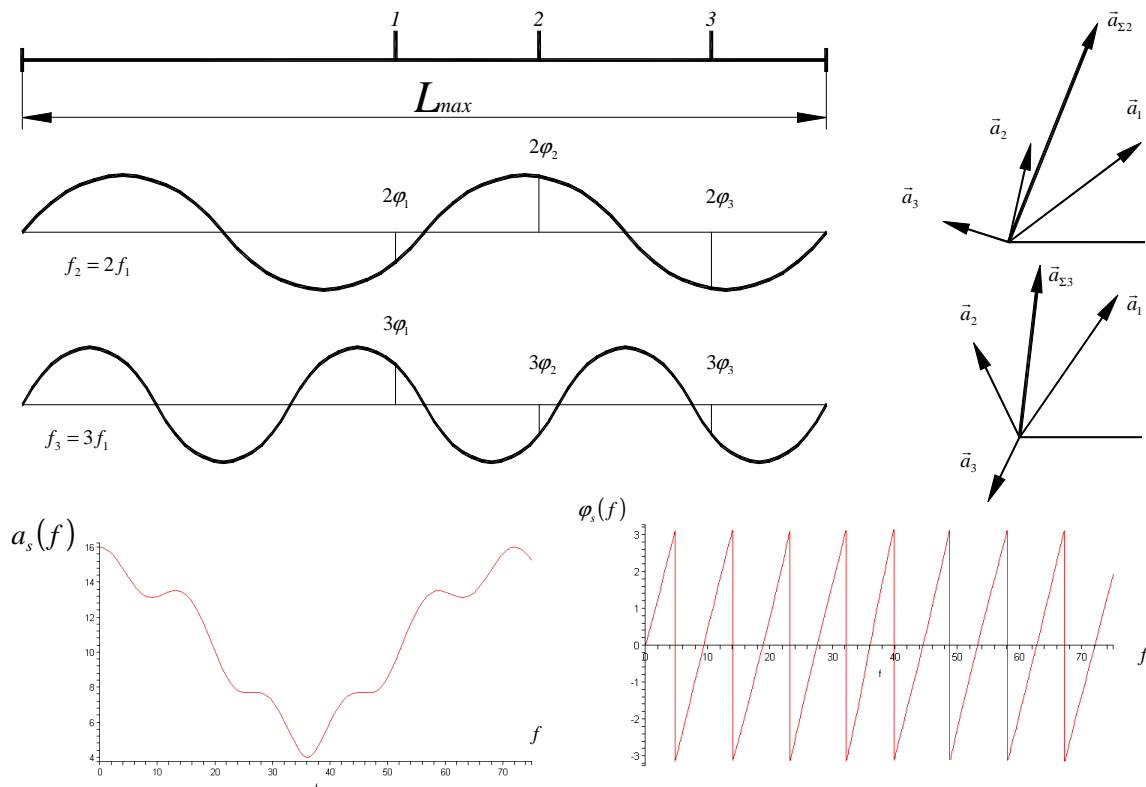

Fig. 3 . Total signals at frequencies f_2 and f_3

When measured, the frequency changing need to change with the uniform step. In this case we can write equations that will describe the relationship between the measured values of the vectors of the total signal at each frequency and the amplitudes and phases of signals reflected from each object. There are two options - the trigonometric (1) and exponential (2) form of writing.

$$
\begin{cases}
a_{\Sigma 1} \sin \varphi_{\Sigma 1} = a_1 \sin \varphi_1 + a_2 \sin \varphi_2 + ... + a_n \sin \varphi_n; \\
a_{\Sigma 2} \sin \varphi_{\Sigma 2} = a_1 \sin 2\varphi_1 + a_2 \sin 2\varphi_2 + ... + a_n \sin 2\varphi_n; \\
... \\
a_{\Sigma f} \sin \varphi_{\Sigma f} = a_1 \sin f\varphi_1 + a_2 \sin f\varphi_2 + ... + a_n \sin f\varphi_n; \\
a_{\Sigma 1} \cos \varphi_{\Sigma 1} = a_1 \cos \varphi_1 + a_2 \cos \varphi_2 + ... + a_n \cos \varphi_n; \\
a_{\Sigma 2} \cos \varphi_{\Sigma 2} = a_1 \cos 2\varphi_1 + a_2 \cos 2\varphi_2 + ... + a_n \cos 2\varphi_n; \\
... \\
a_{\Sigma f} \cos \varphi_{\Sigma f} = a_1 \cos n\varphi_1 + a_2 \cos n\varphi_2 + ... + a_n \cos f\varphi_n.
\end{cases}
\tag{1}
$$

$$\begin{cases} a_{\Sigma 1} \cdot e^{-j\varphi_{\Sigma 1}} = a_1 \cdot e^{-j\varphi_1} + a_2 \cdot e^{-j\varphi_2} + ... + a_n \cdot e^{-j\varphi_n} \\ a_{\Sigma 2} \cdot e^{-j\varphi_{\Sigma 2}} = a_1 \cdot e^{-j2\varphi_1} + a_2 \cdot e^{-j2\varphi_2} + ... + a_n \cdot e^{-j2\varphi_n} \\ ... \\ a_{\Sigma f} \cdot e^{-j\varphi_{\Sigma f}} = a_1 \cdot e^{-jf\varphi_1} + a_2 \cdot e^{-jf\varphi_2} + ... + a_n \cdot e^{-jf\varphi_n} \end{cases} \qquad (2)$$

$a_{\Sigma 1}, a_{\Sigma 2}, ..., a_{\Sigma f}$ - the total amplitude of signals at frequencies of 1, 2 ,..., f;

$\varphi_{\Sigma 1}, \varphi_{\Sigma 2}, ..., \varphi_{\Sigma f}$ - the total phase shift of signals at frequencies of 1, 2 ,..., f;

$a_1, a_2, ..., a_n$ - amplitude of the signals reflected from the 1, 2 ,..., n of the object;

$\varphi_1, \varphi_2, ..., \varphi_n$ - phase shifts of signals reflected from the 1, 2 ,..., n of the object.

Solutions of these systems will permit divide the vectors of signals reflected from each object. But these systems are nonlinear, and as you know, their solution is possible only in individual cases.

Was obtained by the method of solving system (2). The complete solution is presented in [4, 5].To solve the system need to perform measurements of vectors total signals at multiple frequencies, amount which is twice the amounts distances to be measured.

The study of multifrequency phase method of measurement of distances, permit obtain depending accuracy and resolution. Shown that the accuracy is mainly dependent on the accuracy of measuring the phase shift total signals at all frequencies. Since the accuracy measuring phase shift is independent of frequency [6, 7], it is possible to increase the accuracy of distance measurements by increase in the frequency. Which leads to increased accuracy in determining distances in proportion to the frequency. The error of measurement of distances and resolution will also decrease.

When measuring the size of nano-objects, you must use the probing signals whose wavelength is commensurate with the size of objects. These properties have a laser, whose wavelength lies in the optical range from 400 to 750 nm. This allows using laser light to measure the size of individual nanoparticles.

The experimental setup includes a laser light source, modulator, baseband signal generator, two semi-transparent mirror, the registrar of radiation, an

interferometer, the test specimen, computer system. Laser radiation is modulated by the modulator by the amplitude. Then, passing through two semi-transparent mirror, goes to the test specimen. Reflected signals from a first surface of nanoparticles and from a second surface, superposition each other, have formed the summarized signal. This signal is reflected in the opposite direction. Reflected from the semi transparent mirror, he goes to the registrar of the radiation and the interferometer. By measuring the amplitudes of the reflected signals and phase difference at different harmonic modulation signals is determined by the amplitude-frequency and phase-frequency characteristics. As a result of their mathematical treatment, are determined by the size of the nanoparticles.

References

1. Reference radar. Ed. M. Skolnick. With 74 New York City. 1970. Trans. from English. (Four volumes) under the general editorship. K.N. Trofimova. Volume 1. Fundamentals of radar. Ed. Y.S. Itskhoki - M., Sov. Radio, 1976. 456.

2. De Lano RH A Theory of Target Glint or Angular Scintillation in Radar Tracking // Proc.IRE.-1953.-V.41, N4 .- R.61-63.

3. Majewski S.M., Bazhenov V.G., Baturevich E.K., Kutz Y.V. Application of methods for precision measurement of the phase meter distances. - Kiev: Highest school. Univ at Kiev. un-te, 1983. 84.

4. Paraska G.B., Shinkaruk O.M., Lubchik V.R. Theore the basis of phase measuring distances to many objects. - Electronics and Communications, №3, 2010 - p.82-86.

5. Lubchik V.R., Senchishina J.V., Paraska G.B., Kilimnik O.M. Development of analytical method of phase measure distances up to three objects// News KNU, № 2, 2009 - p.146-151.

6. Lubchik V.R., Dem'yanyuk S.M. Research potential accuracy and speed of spectral-phase method of measuring the distance// ISTJ "Measuring and computer science in technological processes", Khmelnytsky, 2003. - №1(23), – p. 74-80.

7. Shinkaruk O.M., Lubchik V.R., Dementev T.O. Research potential accuracy and resolution multifrequence phase method measurement of distances - Electronics and Communications, № 3, 2011 - p.78-82.

6.3 ESTIMATION OF FLUCTUATION MODULATION
CONSTITUENTS OF SOUNDINGS RADIO-LOCATION SIGNALS ON
DEGREE OF THEIR DISTINCTION.

Shinkaruk O.[1], Chesanovskyi I.[1], Karpova O.[1]

One of variants of increase of degree of distinction of radio-location signals is considered in the article which isalternative to existing and is based on application of the not determined peak and angular modulation constituents in a signal as a coherent sign within the limits of period of sounding. It is shown in addition, that potential properties of impulsive radio-location signals on distinction, considerably higher, than those which in them are mortgaged at modulation, that explained by the presence of fluctuation constituents in bearing oscillation, which at the known form perceived as useful modulation.

Entry

Development of radio-location, as separate science, constantly accompanied by the search of ideal (optimal) methods and facilities of receipt of information about the objects of supervision. A key role development of perfect models of soundings signals played in this process; first of all, as exactly, their properties are determined potential possibilities of the systems on the whole. In parallel, the methods of their treatment were created development of theory of signals, however almost always in practice they didn't enable to realize those potential possibilities which was mortgaged in signals. Development and introduction of digital methods of treatment of signals which almost lifted restrictions on potential possibilities of receivers in regard to a discovery, so in regard to distinction they became a considerable breach in this part, as a result, potential limits on descriptions of the radio-location systems are laid on possibilities of signals.

To date plenty of effective models of signals [2,3], what differ on modulation and power properties, own high possibilities as compared to signals, however require application of the special facilities for their synthesis. Exactly through problematical character of realization of difficult signals range, considerable part of modern radio-locationfacilities built with ineffective simple

[1] Khmelnytsk national university

soundings signals. It lays on considerable limits on descriptions of facilities results in the further removal of efficiency of methods of treatment and potential possibilities forming of signals which stipulates the necessity of search of new engineering decisions at the construction radio-location integral systems.

1. Aim of work and generalraisingof task

By an aim hired, there are development and research of mathematical model of radio-location sounding signal, adequate to influence of casual fluctuation processes, operating in keyers and microwave oscillators. For gaining end, an analysis and theoretical generalization of mathematical model of sounding radio-location signal are in-process conducted taking into account not determined on period of sounding of peak and angular fluctuation constituents.

2. Basic part

In theory, possibilities of distinction of radio-location signals are determined breadthways their frequency spectrum. In case of application of simple impulsive radio-location signals, the width of their spectrum is determined breadthways the first petal of spectrum more than 90 percents of power in which consequently is to inversely proportional duration of sounding signal. However, as an analysis of structures of the impulsive radio-location systems shows, the width of frequency stripe of key-in of receivers is always accepted more wide. It is related to that pulsers, Over frequency is high (OFH) own high enough instability , scope of which both briefly and protractedly can exceed the width of spectrum such approach enables to realize maximal part of energy of signal, and on the other hand and hindrances which operate on the entrance of receiver increases proportionally. Obviously, that is nonoptimal, however in the conditions of existent indetermined fluctuation especially in regard to brief frequency instability), taking into account short duration of soundings impulses and impossibility of the greater stabilizing, it is only possible.

Other approach is potentially possible in actual fact perceive present brief fluctuations as angular, real possibilities of soundings signals, as shown in a numbers[1,4,5]of works, they become considerably higher. His realization is possible on those considering, that the transmitter of signal and receiver are mounted in one device, their work is synchronized and it is necessary only to

synchronize them on modulation. In-process [4] the structure of device is offered, the algorithm of work of which enables it to realize, is conducted sufficient estimation of the potential winning, which can be got from his application.

For the estimation of the winninganalyse physical processes which take place in a microwave oscillator during his work and to formulate the adequate to them mathematical model of sounding radio signal.

At certain assumptions and limitations, taking into account the action of destabilizing factors in a transmitter, generalized mathematical model limited in time and on the frequency axis of sounding signal can be presented in a kind:

$$s(t) = S(\chi_s(t), t)\cos(\omega_0 t + \varphi(\chi_\varphi(t), t)),$$
(1)

where $S(\chi_s(t), t)$ is peak modulating; $\chi_s(t)$ - it is a lawof distribution peak; $\varphi(\chi_\varphi(t), t)$ it is an angular modulating constituent; $\chi_\varphi(t)$ it is a law of angular fluctuation constituent.

In the case when a radio-location comes true by simple impulsive soundings radio signals an angular modulation constituent in which, and peak modulation comes true by the impulses of rectangular form,

$$\varphi(\chi_\varphi(t), t) = \varphi_0 + \chi_\varphi(t);$$

$$S(\chi_s(t), t) = S(t)\chi_s(t) = \begin{cases} S_0\chi_s(t), & |t| \le \tau; \\ 0, & |t| > \tau, \end{cases}$$

expression (1) will assume an air:

$$s(t) = \begin{cases} S_0\chi_s(t)\cos(\omega_0 t + \varphi_0 + \chi_\varphi(t)), & |t| \le \tau; \\ 0, & |t| > \tau. \end{cases}$$
(2)

As, cross-correlation properties of signal are determined by a form their complex circumflex, we will write down expression (2) in a complex kind and will distinguish here complex circumflex:

$$s(t) = Re\{\dot{s}(t)\} = Re\{\dot{S}e^{j\omega_0 t}\};$$

$$\dot{s}(t) = S_0\chi_s(t)e^{j\omega_0 t}e^{j(\varphi_0 + \chi_\varphi(t))}, \qquad |t| \le \tau;$$
(3)

For simplification further that $\varphi(\chi_\varphi(t), t) = \varphi_0 + \chi_\varphi(t)$. And consequently expression (3) will assume an:

$$\dot{s}(t) = \chi_s(t)e^{j\omega_0\tau}e^{jx\varphi(t)}, \qquad |t| \leq \tau_i \qquad (4)$$

Cross-correlation function complex circumflex such signal will look like :

$$B(\tau) = \int_{\frac{\tau_i}{2}+\tau}^{\frac{\tau_i}{2}} \dot{S}(t)\dot{S}(t-\tau)dt = \int_{\frac{\tau_i}{2}+\tau}^{\frac{\tau_i}{2}} \chi_s(t)\chi_s(t-\tau)e^{j[(x)\varphi(t)-\chi_\varphi(t-\tau))]}dt \qquad (5)$$

In default of fluctuation constituents, or if not to take into account them, cross-correlation function of complex circumflex, taking into account accepted in (4) assumptions of signs kind:

$$B(\tau) = \int_{\frac{\tau_i}{2}+\tau}^{\frac{\tau_i}{2}} \dot{S}(t)\dot{S}(t-\tau)dt = \int_{\frac{\tau_i}{2}+\tau}^{\frac{\tau_i}{2}} dt = \tau_i - |\tau| \qquad (6)$$

During realization of the concerted filtration in a receiver description of filter is synthesized according form complex circumflex signal, and consequently a reaction of filter on a signal, it will be his autocorrelation:

$$B'(\tau) = \int_{\frac{\tau_i}{2}+\tau}^{\frac{\tau_i}{2}} \dot{H}(t)\dot{S}(t-\tau)dt = \int_{\frac{\tau_i}{2}+\tau}^{\frac{\tau_i}{2}} \dot{S}(\tau_i-t)\dot{S}(t-\tau)dt = \tau_i - |\tau|. \qquad (7)$$

However, at presence of in the signal of the not determined constituents, they are not taken into account at the synthesis of filter, an autocorrelation function grows into the cross-correlation function of impulsive description of filter and actual complex circumflex signal

$$B'(\tau) = \int_{-\frac{\tau_i}{2}+\tau}^{\frac{\tau_i}{2}} \dot{H}'(t)\dot{S}(t-\tau)dt, \qquad (8)$$

Where

$$\dot{H}'(t) \neq \dot{S}(\tau_i-t).$$

Depending on the error of forming signal, the form of response of the concerted filter actually determined by the type of cross-correlation function (8) will change. As in practice peak and angular casual processes in sounding OFH signal are statistically independent, for the estimation of degree of transformation of response, it is necessary to set the laws of distributions of casual sizes $\chi_s(t)$ and $\chi_\varphi(t)$.

We will consider one of in-process pulsersOFH, namely when $\chi_s(t)$presents the reaction are chains with permanent to time of T on the impulse of rectangular form, that inherently to distortions the presence of Parasite reactive constituentsdurations of wavefronts and unevenness of top, and $\chi_\varphi(t)$it can be approximatedby a linear law, that inherently most pulsers OFH through dependence here changes of managing tension of feed.

Thus:

$$|nourishment, feeding|\chi_s(t) = \left(1 - e^{\frac{t}{T}}\right)\sigma(t) - \left(1 - e^{\frac{t-\tau_i}{T}}\right)\sigma(t - \tau_i), \tag{9}$$

where$\sigma(t)$ - function of Heviside.

$$\chi_\varphi(t) = bt^2, \tag{10}$$

Putting expressions (9) and (10) in (4), complex circumflex sounding signal of signs kind

$$\dot{s}(t) = \left(\left(1 - e^{\frac{t}{T}}\right)\sigma(t) - \left(1 - e^{\frac{t-\tau_i}{T}}\right)\sigma(t - \tau_i)\right)e^{jbt^2}, \tag{11}$$

Depending on the parameters of distributionstime of T and coefficient of steepness of frequency modulation b efficiency of algorithm of optimal treatment will be different, as a degree of «co-ordination» of transmission description of filter and signal depends on On fig.1 are dependences of form of complex circumflex and her autocorrelation function shown, at insignificant angular and peak distortions, namely at tightening at the level of 5% and relative instability of frequency of microwave oscillator at the level of $1{,}5\times 10^{-5}$. As be obvious from a picture, considerable deformation of form is complex circumflex and diminishing of interval to correlation on a level 1,34 times.

If to confront such properties of soundings signals and algorithm of their concerted treatment which does not take into account the presence of casual fluctuation constituents, the form of response of the concerted filter will be formed coming from a form peak circumflex and will not contain angular fluctuation constituents, however at application of quadrature detector or quadrature device of discretisation these constituents will result in appearance of sidelobes $f(b,\tau)$ amplitudes of which are limited to the form of autocorrelation function on peak circumflex.
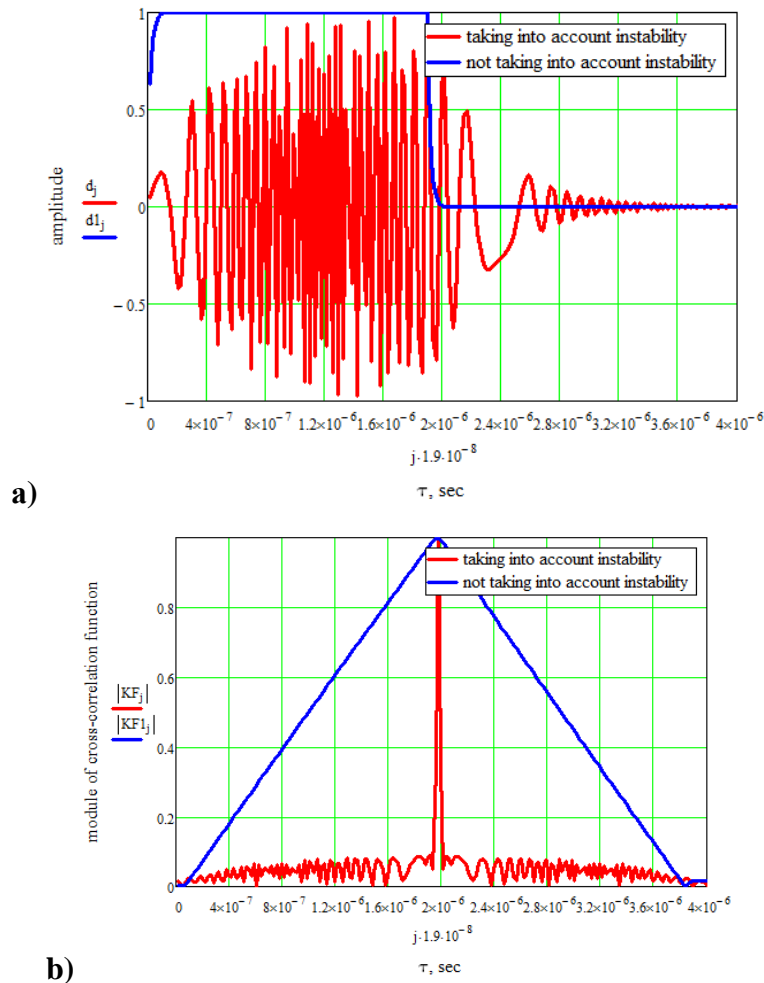
а)

б)
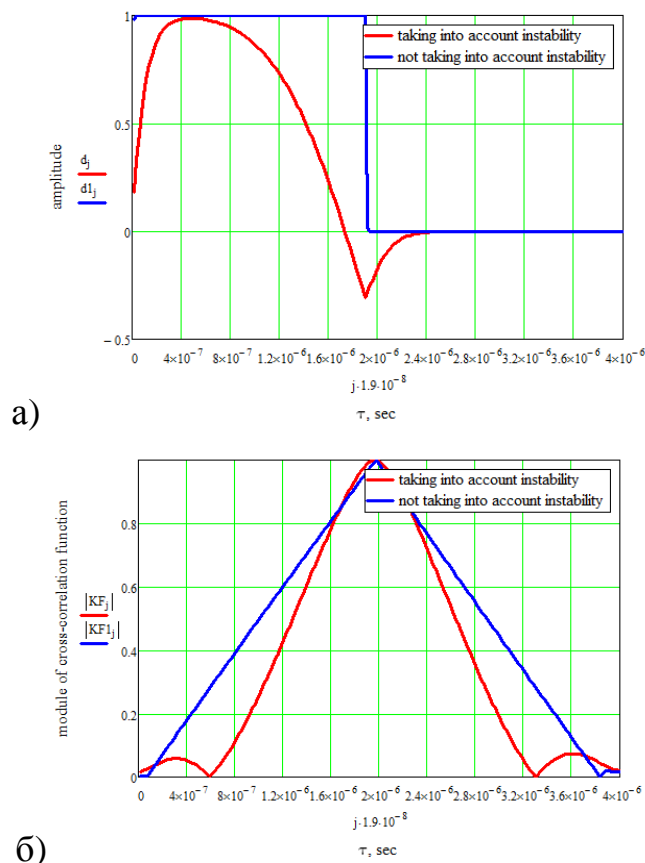
Fig. 1. Change complex circumflex a) and autocorrelation function of b) signal at an account peak and angular fluctuation making $\delta f = 1 \times 10^{-5}, T = 0.05\tau_i$ (radiotechnical systems with oscillators)

For pulsers OFH, providing such stability is enough difficult, as pulsers OFH type of magnetron, that used in majority impulsive radio-location facilities have relative stability of frequency at the level of 1×10^{-5}, and keyers provide duration at the level of 20-30% from duration of impulses. For such case (fig. 2) there are a considerable change of circumflex of her interval to correlation measured already by ten on a picture diminishes in times.

$$B'(\tau) = \int_{\frac{\tau_i}{2}+\tau}^{\frac{\tau_i}{2}} \acute{S}(t)\acute{S}(t-\tau)e^{jb(t-\tau)^2}dt = (\tau_i - |\tau|)f(b,\tau).$$

(12)

Actually in a receiver there signal processing with which he is concerted partly, that results appearance in a response, for the removal of which, algorithms (charts) of indemnification transmitter. However as be obvious from a fig. 2, the presence of angular and peak distortions results reduction of interval of autocorrelation, that at the synthesis of corresponding transmission

542

description of the concerted filter potentially increases the degree of their distinction/

a)

b)

Fig. 2. Change complex circumflex a) and cross-correlation properties of б) signal at an account peak and angular fluctuation making $\delta f = 1 \times 10^{-3}, T = 0.2\tau_i$

Conclusions

Thus frequencies of receiver by of modulation, winning on by a discriminability and to the relation signal/noise can take on a value a few ten of one times without making alteration in soundings signals and without complication of transmitter. Howev er determined nature of modulation requires additional algorithms of treatment, namely to permanent (dynamic out of limits of sounding period) adaptation of transmission description of the concerted de vice of treatment It is necessary to notice that at such approach potential possibilities of distinction of signals are also limited their duration and

breadthways stripes of key-in of receiver and by the laws of distribution of casual constituents in a peak and angular circumflex.

References.

1.Вопросы перспективной радиолокации. Коллективная монография/ Под редакцией А.В.Соколова. – М.: Радиотехника, 2003 – 512с.

2.Передающие устройства СВЧ: Учебное пособие для радиотехнических спец. вузов /Вамберский М.В., Казанцев В.И., Шелухин С.А.; под ред. М.В. Вамберского – М.: Высш. шк., 1984. – 448 с.

3.Кравченко В.Ф. Алгебра логики, атомарне функции и вейвлеты в физических приложениях/ Кравченко В.Ф., Рвачев В.Л. . – М.: ФИЗМАЛИТ, 2006. – 416 с.

4.Обробка радіолокаційних сигналів з урахуванням внутрішньоімпульсних фазочастотних нестабільностей/ О.М.Шинкарук, І.І. Чесановський// Зб. наук.пр. Військ. ін-ту Київського нац. ун-ту ім. Тараса Шевченко / за ред. С. В. Лєнкова. – Вип. № 17. – К.: ВІКНУ, 2009 с. 89-92.

5. Трансформування функції невизначеності радіосигналів з урахуванням внутрішньо імпульсної фазочастотної нестабільності/ І.І. Чесановський// Зб. наук. пр. Нац. акад. Держ. прикордон. служби України ім. Б. Хмельницького / за ред. В. О. Балашова. – Хмельницький: НАДПСУ, 2009. – № 50. с. 58-62

7. EXPERIENCE OF BIOENGINEERING TECHNOLOGIES

7.1 THE OUTSTANDING ACHIEVEMENTS IN THE SCIENTIFIC ACTIVITY OF THE INSTITUTE OF ENGINEERING MATERIALS AND BIOMATERIALS OF THE SILESIAN UNIVERSITY OF TECHNOLOGY IN GLIWICE, POLAND

Dobrzański L.[1]

The Institute of Engineering Materials and Biomaterials of the Silesian University of Technology in Gliwice, Poland is a strong international scientific centre of materials science and engineering, materials processing technologies and nanotechnology. Materials science was created in the 1950s as the fundamental branch of science and also materials engineering as the engineering knowledge applied in the industrial practice. The progress in the field of the advanced engineering materials is predicted and expected, including, among others, nanomaterials (with the particularly fine structure, ensuring the unexpected so far mechanical, as well as physical and chemical properties), biomaterials (as a group of the biomimetic materials and/or making it possible to substitute the natural human tissues and/or organs directly or designed into the purpose built devices), and infomaterials (as the most advanced group of smart- and self-organising materials), and also (functional or tool ones) gradient materials (in which properties change continuously or discretely with location because of the chemical composition, phase composition, and structure, or atomic orientation changing with the location), and light metals alloys (as materials of the particular importance, apart from the composite materials, in design and operation of the contemporary transport means), which issues decide about the development of materials engineering as one of the few areas of science and technology development most important nowadays in the contemporary World. A typical subject matter of materials science and engineering includes the description of phenomena and transformations occurring in technical materials, especially in the engineering ones, that is those

---

[1] Silesian University of Technology

manufactured in the purpose designed technological processes from raw materials available in the nature, in technological processes of manufacturing, processing, as well as forming of their structure and properties, for satisfying more and more complex practical requirements formulated by participants of the design process of products indispensable to the contemporary humans, including – among others - machines and devices.

Materials have to be manufactured on demand today, meeting the complex set of the specific demands. Manufacturing is expected of materials with properties ordered by products users. Those changes substantially the materials design methodology in general and the products materials design, as materials have to be delivered on demand of products manufacturers with the appropriately formed structure, ensuring the required set of physical and chemical properties, and not as before when the manufacturers were forced to select material closest to their expectations from the delivered materials with the offered structure and properties, yet – by assumption – not meeting them fully, which is not permitted by this design methodology. Therefore, the actual trends force classification of engineering materials based on their functional characteristics. Therefore, the type, and the chemical composition in particular, of the used materials are of less importance (to which materials engineers were used for decades, and especially the metallurgists), while its functionality is more important. This is so since the new engineering materials and manufacturing processes have been subordinated to customer needs and functional requirements of products. Manufacturing materials on demand fulfilling needs of market products manufacturers at the right time and place features a priority for new materials technologies and manufacturing processes, as the complementary base technologies (improvement of the existing solutions), alternative ones (taking advantage of synergy of various solutions), and original ones (new solutions being developed).

The Institute of Engineering Materials and Biomaterials takes the tradition one of the oldest internal units of this University launched after World War the Second in 24th May 1945 headed by Professor Fryderyk Staub and the tradition of the Physical Metallurgy created still 1844 in University of Technology in Lvov for long time continued by Professor Stanisław Anczyc. Today the main areas of

the scientific interests of the ca 150 persons' academic staff of the Institute are as follows:

- forming of structure and properties of engineering materials including biomaterials using advanced synthesis and materials processing technologies and nanotechnologies,

- engineering materials including biomaterials properties testing and microstructure characterisation using very advanced contemporary research methodologies including electron microscopy,

- modelling, simulation and prediction of properties and structure of engineering materials including biomaterials using advanced methods of computational materials science including artificial intelligence methods.

The results of the scientific activity of the Institute's staff are published in few hundreds papers yearly. In this paper the examples of the detailed scientific researches made in last years with the Author's participation are presented.

The new group of the sintered gradient tool materials manufactured by the conventional powder metallurgy method, consisting in compacting a powder in a closed die and sintering it, is presented firstly. The materials were obtained by mixing the powders of the HS6-5-2 high-speed steel, tungsten carbide (WC), and vanadium carbide (VC). The mixes were poured one after another into the die, yielding layers with the gradually changing volume ratio of carbides within the high-speed steel matrix. Structural research by using the scanning and transmission electron microscopes, X-ray microanalysis and density, hardness and porosity tests, are performed.

Structure and hardness of selected materials after heat treatment are also investigated. On the basis of the results of the research, it is found out that it is possible to obtain gradient materials by the powder metallurgy methods, in order to ensure the required properties (Fig. 1) and structure (Fig. 2) of the designed material. The gradient tool materials reinforced with the WC carbide are characterised by a higher hardness, and a lower porosity in relation to the materials reinforced with the VC carbide. It is found out that the desired structure and properties (density, porosity and hardness) has the material containing 25% of the WC carbide in the surface layer, after sintering at the temperature 1210°C, for 30 minutes. The heat treatment application causes a

significant increase of the surface layer hardness of the material. The highest surface layer hardness, equal to 71.6 HRC, shows the material austenitised at the temperature 1120°C, hardened and tempered twice at the temperature 530°C.
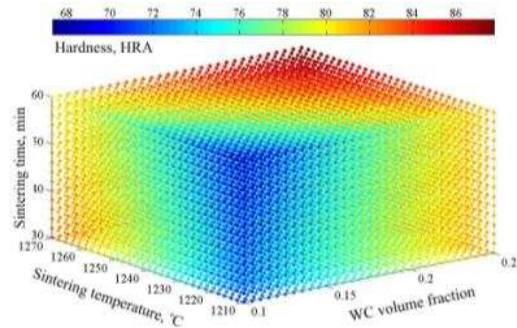

Fig. 1. The hardness of the sintered gradient tool materials on the HS6-5-2 high-speed steel matrix
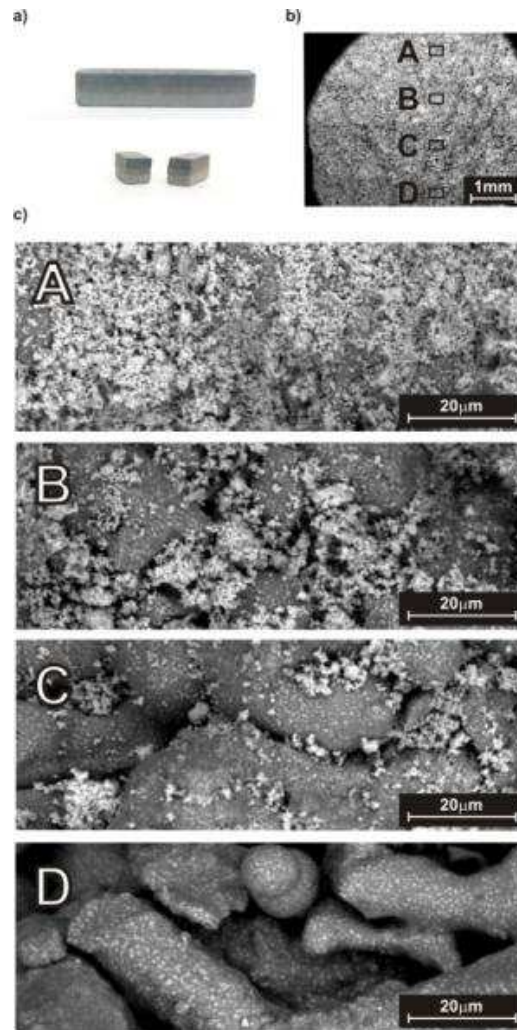

Fig. 2. The changes the structure of the sintered gradient tool materials on the HS6-5-2 high-speed steel matrix

The sintered tool gradient materials with cobalt matrix are presented next. Those addresses issues related to research of the new group of gradient tool materials developed by means of the powder metallurgy method. In this method, the subsequent layers of mixtures of different-composition powders are passed through a closed die, and then sintered too. The materials have been obtained from the mixture of tungsten carbide and cobalt powders. The analysis involves four-layer samples, where the subsequent transient layers were formed from the surface layer to the base layer. The volume fraction of the carbide hard phase in the transient layers. The analyses of the sintered gradient tool materials include structural analysis with scanning and transmission electron microscopes; X-ray microanalysis as well as density, hardness, porosity, abrasive wear and stress level K_{IC} tests. The results of the analysis show that it is possible to obtain sintered gradient tool materials WC-Co of the desired structure and properties by means of the new powder metallurgy method. It has been established that the new sintered gradient tool materials WC-Co consist of the tungsten carbide phase WC and cobalt matrix (Fig. 3). The cobalt matrix fills the space between WC grains, often as a thin layer between the vicinal tungsten carbide grains. An observation of thin foils structures has revealed many net defects in the tungsten carbide grains, especially dislocation. It has been determined that the desired structure of material is obtained due to sintering in 1460℃ for 30 minutes.
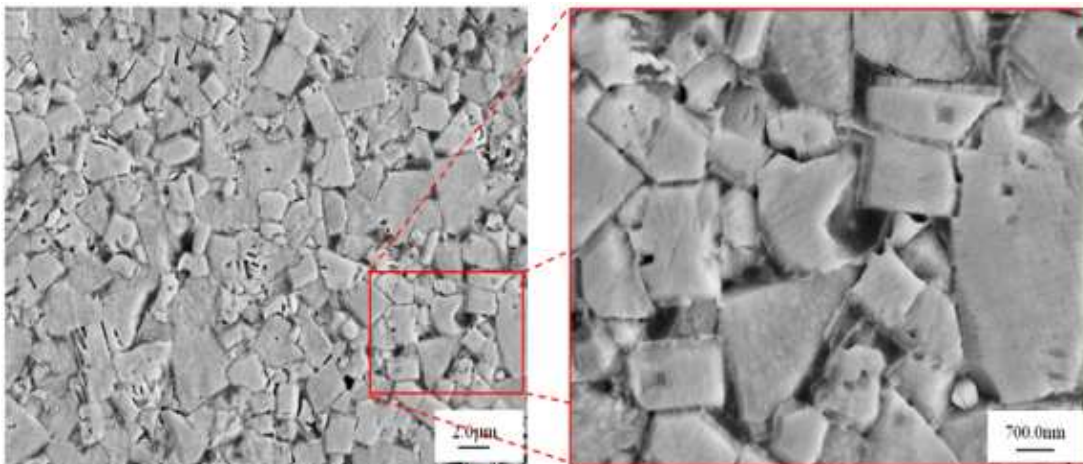
Fig. 3. Surface layer of gradient the material 3-9%Co/97-91%WC_4 sintered in a vacuum furnace at temperature T_{sp}=1430°C and subjected to hot isostatic condensation at the temperature T_{sp}=1425°C

Nanocomposite coatings deposited by cathodic arc evaporation will be presented next. The development of the deposition methods and the research of new types of coatings enable to produce coatings with better performance. Nanocomposite hard coatings are widely used due to their excellent mechanical properties that make them useful in a wide variety of industrial applications. Nanocomposite coatings comprise at least two phases, a nanocrystalline phase and a matrix phase, where the matrix can be either nanocrystalline or amorphous phase. The investigated coatings have nanocomposite character with fine crystallites, while their average size fitted within the range 8-15 nm, depending on the coating type (Fig. 4). The coatings demonstrated a dense cross-sectional morphology as well as good adhesion to the substrate, the latter not only being the effect of interatomic and intermolecular interactions, but also by the transition zone between the coating and the substrate, developed as a result of diffusion and high-energy ion action that caused mixing of the elements in the interface zone and the compression stresses values. The critical load L_{C2} lies within the range 55-85 N, depending on the coating type. The coatings demonstrate high hardness (4000 HV) and corrosion resistance.
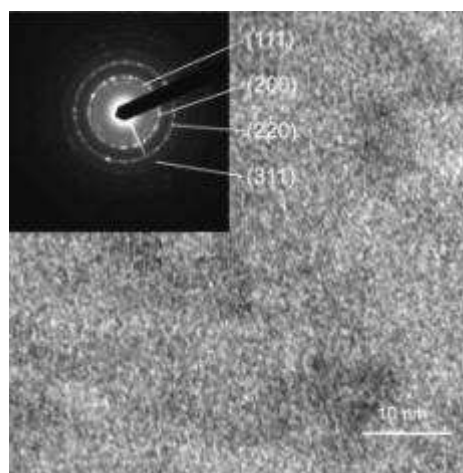
Fig. 4. TEM bright-field images and electron diffraction patterns of CrAlSiN coating

Structure and properties of the hard surface coatings depositing on sintered tool materials is the next presented research. They are presented investigations' results of the properties of the cemented carbides and cermets, both uncoated and coated with single and multiple hard surface layers in the

physical (PVD) and chemical (CVD) vapour deposition processes. It was found out basing on the metallographic examinations on the SEM (Fig. 5) and on the light microscope that all the investigated single- and multi-layer coatings developed in the PVD and CVD processes were put down evenly on the substrates of the cemented carbides and tool cermets. The coatings are compact without any visible pores and cracks and adhere tightly to their substrates. Only in case of the single-layer TiN coating put down using the PVD method on the CP20 cemented carbide substrate the coating thickness unevenness was encountered (Fig. 5). In case of the multi-layer coatings of the TiCN+TiN, TiCN+TiC+Al$_2$O$_3$, Ti+TiCN+TiN, TiCN+Al$_2$O$_3$+TiN/TiC types their laminar overlap was observed. Basing on the metallographic examinations on the LM and on the SEM no total delamination of coatings was found after the scratch test even at the maximum load. Basing on the adhesion tests it was found out that all the investigated single-layer and multiple-layer coatings are characterized by very good adhesion to the substrate. One can observe, comparing the values of critical loads obtained in scratch tests that the critical load for a particular coating increases with its microhardness. The microhardness tests of the coatings revealed that the highest hardness is displayed by the PVD multiple-layer coated cermet and cemented carbide, whereas, the lowest hardness displays the cemented carbide single-coated with TiN. The highest surface quality was obtained during machining with the multi-layer coated (TiCN+TiN) cemented carbide and with the cermet with the TiN+TiC+TiN coating, whereas, the lowest quality was observed after machining with the uncoated cemented carbide and cermet.

a)   b)
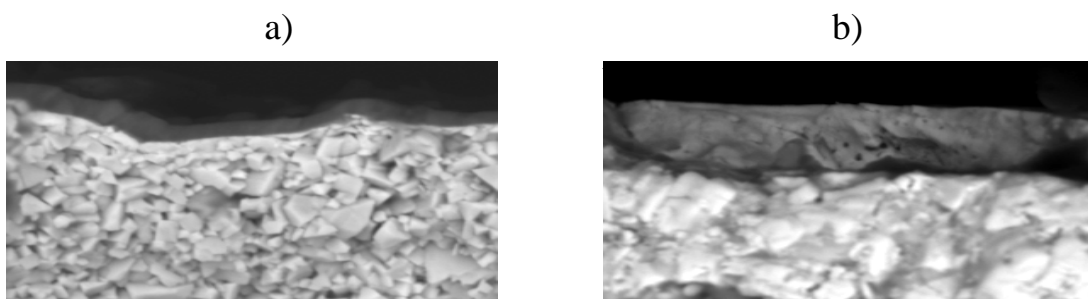
Fig. 5. Fractures of coatings deposited onto the cemented carbides substrate: a) TiN on CP20; b) TiCN+Al$_2$O$_3$ on TP100, magnification 5000x, SEM

A lot of research works carried out have been devoted to the problem of coating of tooling materials, including also the coating of tooling ceramics. PVD and CVD coating systems on oxide tool ceramics is the next solved problem. The aim of the work is the investigation of structure and properties of the Al_2O_3 based $Al_2O_3+ZrO_2$, Al_2O_3+TiC and $Al_2O_3+SiC_{(w)}$type based oxide tool ceramics coated with the anti-wear mono- and multilayers of the TiN, TiAlN, TiN+TiAlSiN+TiN, TiN+multiAiAlSiN+TiN and TiN+TiAlSiN+AlSiTiN types in the cathode arc evaporation CAE-PVD and with the multilayers of the TiCN+TiN and $TiN+Al_2O_3$ types obtained in the chemical deposition from the gas phase CVD process. The investigations were carried out on the multi-point inserts made from the $Al_2O_3+ZrO_2$, Al_2O_3+TiC, $Al_2O_3+SiC_{(w)}$ ceramics uncoated, coated in the PVD and CVD processes with thin coatings. Observations of the investigated coatings' structures were carried out on the transverse fractures on the scanning electron microscope. The diffraction examinations and examinations of thin foils were made on the transmission electron microscope (Fig. 6). The measurements of textures and phase composition were made. The macro-stress values were calculated. Tribological tests were carried out on the „pin-on-disk" tester. The microhardness and adhesion tests of coatings were made. Cutting ability of the investigated materials was determined basing on the technological continuous cutting tests. It has been demonstrated that the creation of the developed coatings by the use of the PVD and CVD methods on oxide ceramic tool materials causes the increase of coatings hardness and allows to improve application features of multi point cutting tools for high speed machining, tools for fine cutting coated with them and dry cutting without using the cutting fluids in comparison to the multi point cutting tools produced from the same uncoated materials. Putting down the anti-wear coatings onto the oxide ceramic tool materials is justified and the composite tool materials developed in this way may have the important application significance in the industry for cutting tools.

The research studies on the PVD and CVD coatings onto sialon tool ceramics and sintered carbides show that the deposition of thin coatings on the ceramic machining cutting edges is fully grounded, since it has been demonstrated that there is a rise of cutting abilities of ceramic tools covered by

the coatings obtained in the PVD and CVD processes. Both the coatings structure (Fig. 7) and mechanical properties deposited by PVD and CVD methods on sintered carbides and sialon tool ceramics substrates was an investigation. In the case of coatings containing AlN phase of the hexagonal lattice, there occur covalence bonds analogous to those in ceramic substrate, which in effect yields good adhesion of these coatings to the substrate. It means that the type of interatomic bonds presented in the material of substrate and coating has a great influence on the adhesion of the coatings to the substrate. It can be extremely helpful when selecting the coating material on ceramic cutting edges since the deposition of coatings on cutting edges in PVD processes is difficult due to their dielectric properties, because without the possibility to polarize the substrate during the deposition process it is difficult to obtain coatings which would have good adhesion to ceramic substrates. To define the influence of coating properties on the durability of cutting edges, artificial neural networks have been applied. Another relevant aspect of the research presented in the paper is the fact that the adhesion of the coatings contributes significantly to the durability of the cutting edge, whereas the microhardness of the coatings, their thickness and grain size have a slightly lower influence on the durability of the tool being coated (Fig. 8).

a)   b)
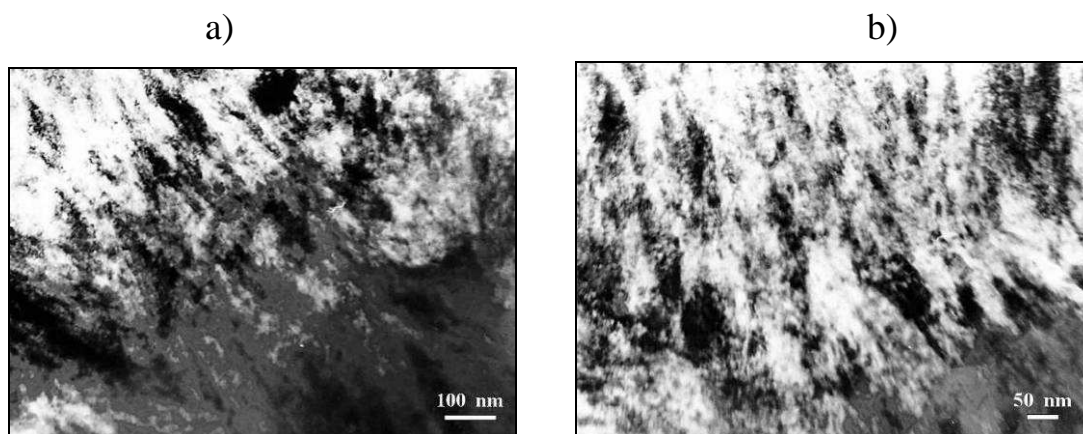
Fig. 6. a), b) TEM: Structure of TiAlN coating thin foil structure perpendicular to the layer surface at light field

Gradient PVD coatings deposited onto the sintered tool materials are presented by the investigation results of properties of the sintered tool materials: cemented carbides, cermets and Al_2O_3 type oxide tool ceramics with gradient

and single-layer (Ti,Al)N and Ti(C,N) coatings deposited with the cathodic arc evaporation CAE-PVD method (Fig. 9).
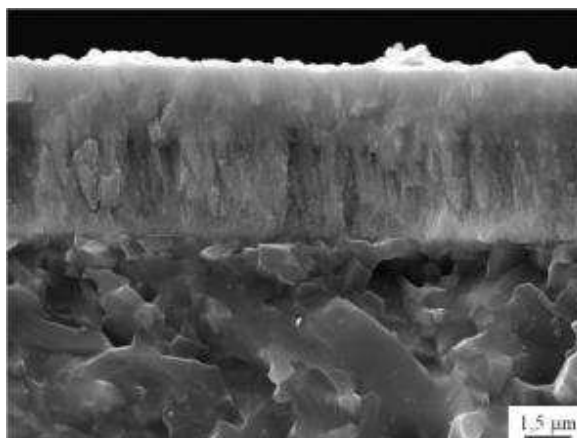
Fig. 7. Surface topography of the (Al,Cr)N coating deposited onto the sialon ceramics tools
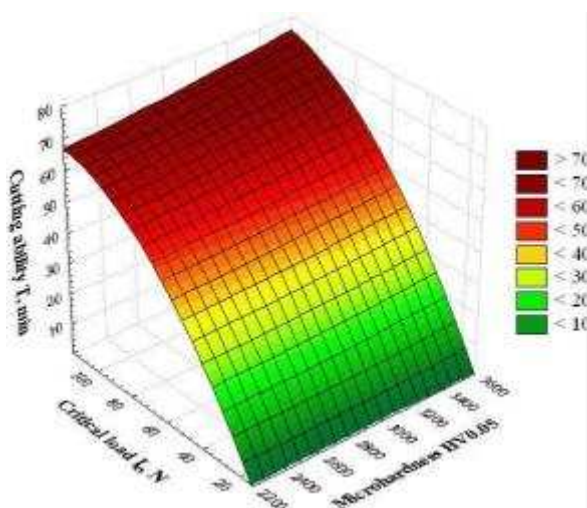

Fig. 8. Evaluation of the PVD and CVD coatings critical load and the microhardness influence of tool life T for sialon ceramics tools coated with PVD and CVD coatings determined by artificial neural networks at a fixed coating thickness 3.0 microns and particle size 8.2 nm

As a result of the metallographic and spectroscopy investigations the structure as well as chemical and phase composition of investigated materials has been characterised. On the bases of XPS and AES investigations of chemical composition it was ascertained that the increase of the substrates' elements concentration in the connection zone occurs simultaneously with decrease of the

coatings' elements concentration. Gradient character of the coatings was confirmed with use of Grazing Angle Incidence X-ray Scattering Geometry.
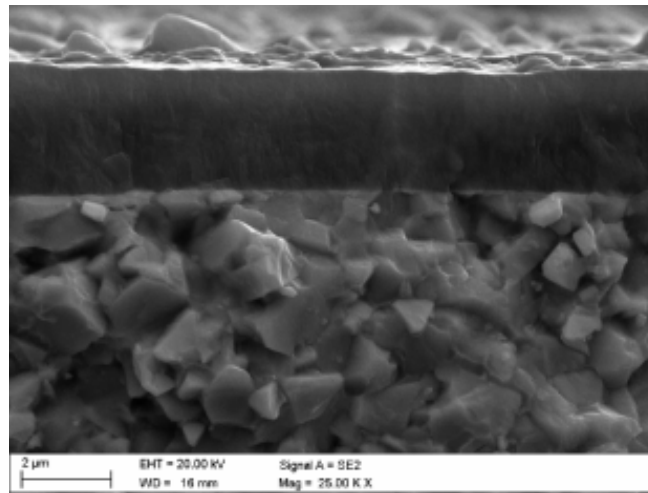
Fig. 9. Fracture surface of the gradient Ti(C,N) coating deposited onto the cemented carbides substrate

It is stated that deposition of (Ti,Al)N and Ti(C,N) gradient coatings on the investigated sintered tool materials causes the significant increase of microhardness in the surface zone. The influence of microhardness increase and good adhesion of coatings, achieved due to gradient structure of coatings, onto functional properties measured at cutting tests, was demonstrated. As a result of the functional properties it was found out that deposition of the both: single-layer and gradient (Ti,Al)N coatings onto investigated tool materials causes the tool life increase in comparison with Ti(C,N) coated tools. It is a result of high wear resistance of (Ti,Al)N coatings at elevated temperature. A better wear resistance of gradient in comparison with single-layer coatings was stated apart from the kind of substrate employed. Basing on computer simulated internal stresses of investigated coatings, verified by the experimental results, it was stated that more advantageous stress distribution of gradient coatings in comparison with corresponding single-layer coatings causes good mechanical properties of gradient coated materials. Especially stress distribution at the surface zone influence the microhardness and stress distribution at the connection zone have an effect on adhesion of coatings.

PVD coatings are deposited also onto plasma nitrited hot work tool steels. The paper presents the results of the project focused on the investigation of the

structure, mechanical and tribological properties of CrN, TiN and TiN/(Ti,Al)N PVD coatings deposited onto plasma nitrided hot work steel X37CrMoV5-1 type (Fig. 10).
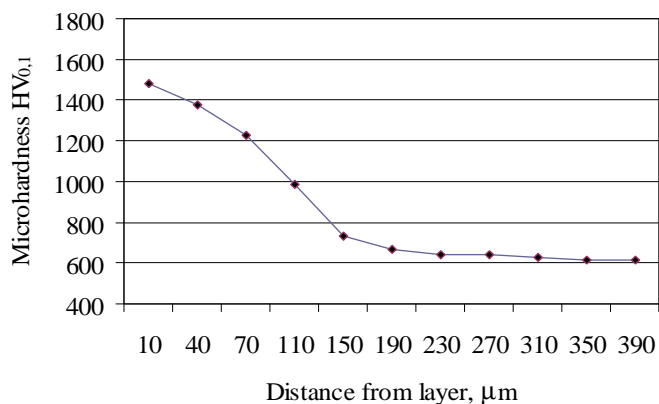

Fig. 10. Microhardness changes in the nitriding layer of the plasma nitrided hot work steel X37CrMoV5-1 type

The structure of TiN and TiN/(Ti,Al)N coatings is columnar while of the CrN coating – fine-crystalline. What decides about the roughness of the PVD coatings deposited onto plasma nitride steel is also the topography of the coatings with heterogeneous surfaces (Fig. 11). The roughness of the investigated coatings is between $R_a= 0.1$-0.32 μm for the TiN/(Ti,Al)N and TiN coatings adequately. With the increase of the hardness of the PVD coatings there is the increase of the wear resistance as well. The hardness of the investigated coatings is between 2443 $HV_{0.001}$ for the CrN coatings and 3354 $HV_{0.001}$ for the TiN/(Ti,Al)N coatings. The hardness of the examined PVD coating correlates with their adhesion to the substrate material. The PVD coatings deposited onto plasma nitride steel show the adhesion (L_c=51-62 N) of the CrN and TiN to the substrate respectively. As regards all the examined PVD coatings the failures begin with the double-sided chippings on the scratch edges and flakes on their bottoms. These damages appear at different loadings depending on the type of the coating. The increased hardness and resistance of the substrate in the plasma nitride layer contributes to the limitation of the fragmentation of coatings as a result of plastic deformation of the substrate, its conformal cracking, stratification, crumbling and delamination, what finally causes the increase of the adhesion parameters as a consequence of the scratch test. A very good adhesion of the TiN/(Ti,Al)N coating to the plasma nitride steel substrate and its

high hardness are connected with the good results of the pin-on-disc tribological test for this coating. The type of the damages of the coating and the substrate, arisen during the scratch test, is similar to the damages and the character of wear during the tribological test. During this test the coatings are worn in the adhesion-abrasive way, and the damage, in most cases, reaches the material substrate. It has been stated that the biggest resistance to the wear resistance at 20 and 500°C temperatures is characterized by the TiN/(Ti,Al)N coating, while the smallest resistance shows the CrN coating.
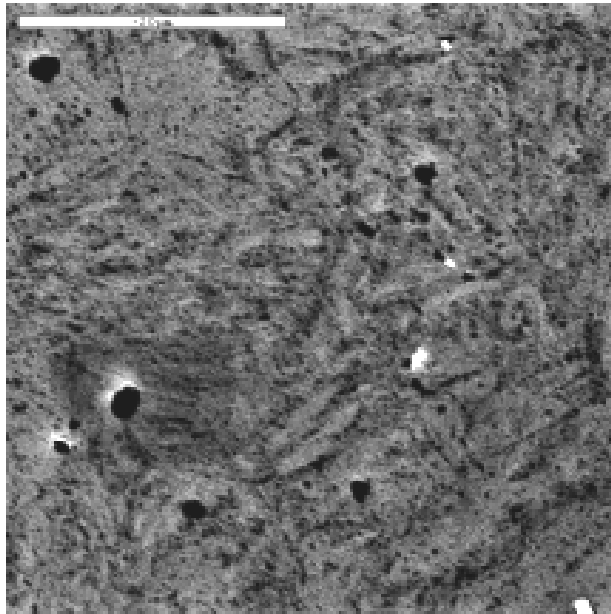
Fig. 11. Topography of the CrN coatings deposited onto plasma nitrided hot work steel X37CrMoV5-1 type

For PVD and CVD and generally surface engineering technologies development forecasting foresight methodology is applied. Foresight technology is the process concentrating scientists, engineers, industrialists, Government officials and others in order to identify areas of strategic research and the leading technologies, which in long term will contribute to the greatest economic and social benefits and sustain industrial competitiveness.

The main goals of foresight technology and ways of their realisation make the triangle in Fig. 12 presented. That approach is really important in the context of the European Union's priority strategy called Europe 2020 assuming that the development of the continent should be intelligent, supportive to social inclusion and sustainable.
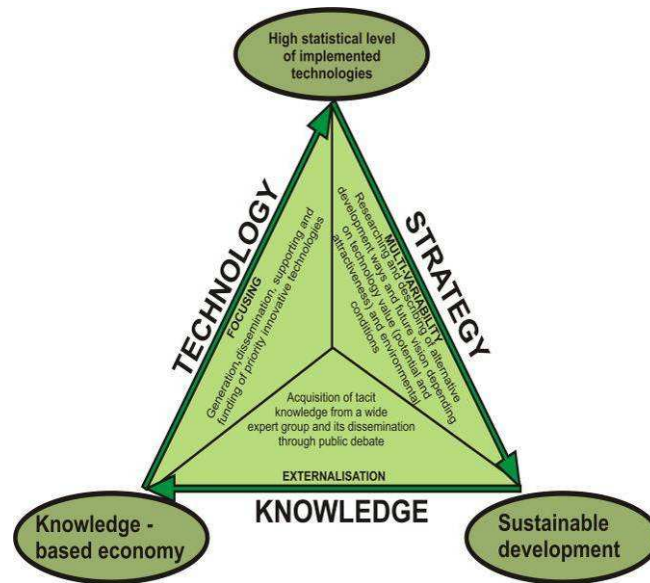
Fig. 12. Technology Foresight Triangle

The main goal of realised foresight research FORSURF is to identify the priority innovative technologies and strategic research directions whose development will be crucial during the next 20 years in the scope of surface properties formation leading technologies of engineering materials and biomaterials. It is feasible to put the so-defined objectives into life using the concept of e-foresight and a custom methodology of the Computer Aided Integrated Foresight Research that organises, streamlines and modernises the actual foresight research process. The approach proposed can be implemented practically by developing an information technology including: a virtual organisation, web platform and neural networks. The key methodological assumptions of the carried out research are illustrated graphically in Fig. 13. According to the handling procedure accepted, homogenous groups should be distinguished in the first place for the technologies assessed in order to subject them to the planned research of an experimental and comparative character. The dendrological matrix of technology value presents assessment results for the relevant technology groups according to the potential being the actual objective value of the specific technology and attractiveness reflecting the subjective perception of the relevant technology by potential users. Depending on the potential value and attractiveness level determined in an expert assessment, each of the analysed technologies is placed into one of the following matrix quarters: Quaking Aspen, Soaring Cypress, Rooted Dwarf Mountain Pine, Wide-

stretching Oak. The meteorological matrix of environment influence illustrates graphically the results of influence of external circumstances on the relevant group of technology grouped by the difficulties with negative influence and the opportunities with positive influence on the analysed technologies. Depending on the influence degree of positive and negative environment factors determined in an expert assessment, each of the analysed technologies is placed into one of the following matrix quarters: Frosty Winter, Hot Summer, Rainy Autumn, Sunny Spring. A ten-degree universal scale of relative states was used to assess the given technology groups for their value and environment influence degree. According to this scale the smallest value 1 corresponds to a minimum level, and the highest value 10 is the level of perfection. The results of expert studies visualised with a dendrological and meteorological matrices are applied in the next stage of research works applied onto the technology strategies matrix consisting of sixteen fields corresponding to the individual variants from the set of combinations of technology types with environment types. Mathematic relationships are formulated and a computer programme based on them is created enabling to transfer the specific numerical values from the dendrological and meteorological matrix dimensioned [2x2] to the strategy matrix for techno-logies dimensioned [4x4]. The matrix of strategies for technologies presents graphically the place of technology including its value and environment influence degree and indicates an action strategy to be adopted with reference to the specific technology considering the factors analysed earlier. The strategic development tracks are applied onto the technology strategy matrix consisting of sixteen fields reflecting the predicted situation of the given technology if positive, neutral or negative external circumstances occur. The forecast established concerns the time intervals of 2015, 2020, 2025 and 2030 and presents a vision of future events consisting of few variants.

The inherent part of the worked out methodology are detailed materials science experiments of surface layers structures created using the different kinds of surface treatment methods as well as research of mechanical and tribological properties and utility functions research under conditions of exploitation or similar ones. The results
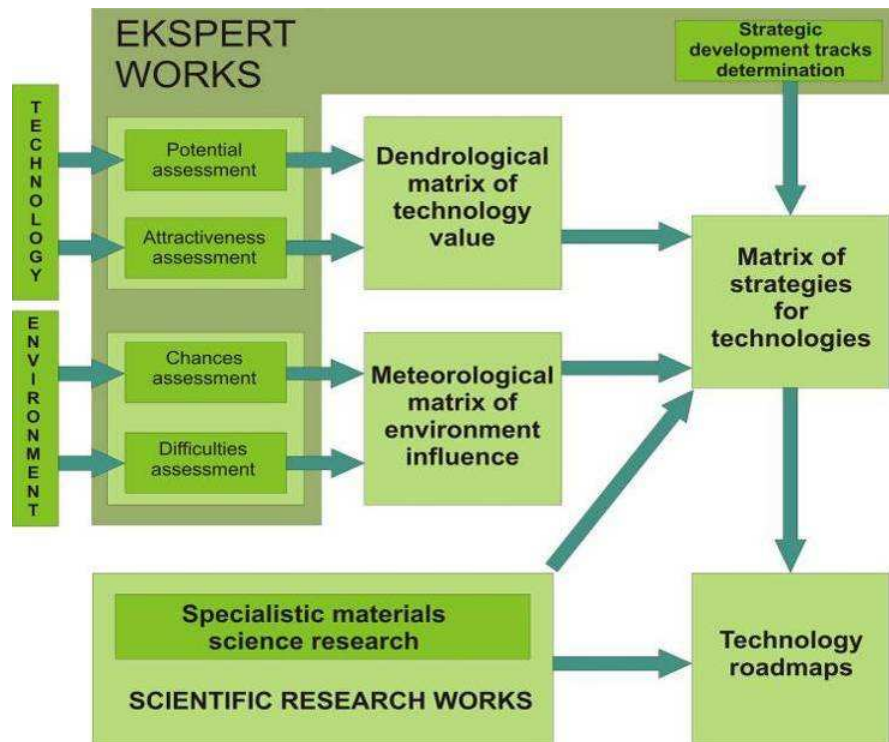
Fig. 13. Methodology of interdisciplinary foresight-materials science researches

of these investigations relating to technologies selected through the described technology valuating methods constitute an important premise for working out and experimentally verifying the evaluations made using the set of technology foresight matrices and they are necessary for creating the technology roadmaps. A technology roadmap is a graphical comparative analysis tool for choosing the best technology group in terms of selected criteria. The set-up of the custom technology roadmap corresponds to the first quarter of the Cartesian system of coordinates. Three time intervals for the years: 2010-11, 2020 and 2030 are provided on the axis of abscissa, and the time horizon for all the results of the research applied onto the map is 20 years. Seven main layers were applied onto the axis of coordinates of the technology roadmap answering subsequently to more and more detailed questions: When? Why? What? How? Where? Who? How much? The undisputed advantage of technology roadmaps is flexibility and, if needed, additional sub-layers can be added or expanded for the maps according to the circumstances of the industry, a size of enterprise, a scale of the company's business or an entrepreneur's individual expectations.

Table 1 - The technology roadmap for manufacturing of monolayer coatings by physical vapour deposition process onto the CuZn40Pb2 brass substrate

TECHNOLOGY ROADMAP	Technology name:	*Manufacturing of monolayer coatings by physical vapour deposition process onto the CuZn40Pb2 brass substrate*	Catalogue No.
	Research scope:	*PVD technologies*	*M2-12-2010/11*

When?	Time intervals	TODAY 2010-11	2020	2030
Why?	All-society and economic perspectives	Creating the Critical Technologies Book	Development of priority innovation technologies	Statistically high quality of technologies implemented in industry
		Creating future events scenarios	Using chances and avoiding difficulties	Sustainable development
		Development of information society and intellectual capital	Wide education and effective intensive cooperation between Science and Industry representatives	Knowledge- and innovativeness-based economy
	Strategy for technology Environment influence Technology value	Sunny spring / Wide-stretching oak	Strategy of an oak in string: Succeed. To develop, strengthen, implement attractive technology of a large potential in industrial practice in order to achieve outstanding success.	
What?	**Product**	Tools and machine parts working in the conditions of higher mechanical, thermal and corrosion loads, ultrathin layers for electronics and optoelectronics, photovoltaic equipment, artificial organs in clinical and experimental medicine, photovoltaic equipment		
	Product quality at the background of foreign competitors	Quite high (7)	High (8)	Very high (9)
	Substrate	Copper and zinc alloy (also alloys of non-ferrous metals, polymer materials, ceramic materials, glass, etc.)		
	Kind of surface coatings/ layers/ processes on substrate surface	Ti/CrNx1, Ti/ZrNx1, Ti/TiAlNx1, Mo/TiAlNx1 and other with similar properties		
	Improved material properties	Increasing mechanical properties (hardness), increasing resistance to corrosion agents and unique optical and electric properties		
	Diagnostic-research equipment	Scanning electron, transmission electron, atomic force microscopes, X-ray diffractometer, GDOS, Raman, Auger, XPS spectrometer, ultramicrohardness, device for testing coating adhesion, device for corrosion tests		
How?	**Technology**	Manufacturing of monolayer coatings by physical vapour deposition process onto the CuZn40Pb2 brass substrate		
	Life cycle period	Prototype (8)	Growth (7)	Early mature (6)
	Production type	Unit and small-scale serial	Small- and medium-scale serial	Medium-scale setial
	Production organisation form	Cellular	Cellular	Cellular
	Machine park modernity	Quite high (7)	High (8)	Very high (9)
	Automation & robotisation	Moderate (6)	High (8)	Very high (9)
	Quality and reliability	Quite high (7)	High (8)	Very high (9)
	Proecology	Quite high (7)	High (8)	Very high (9)
Where?	Organisation type	R&S centres, small-and medium- sized enterprises	Small-and medium- sized enterprises,	Large-and medium-sized enterprises, microenterprises
	Represented industry	Tool, machine-building, electrical, electronic, optoelectronic, medical ones		
Who?	Staff education level	Quite high (7)	High (8)	Very high (9)
	Engagement of scientific-research staff	Very high (9)	Quite high (7)	Moderate (6)
How much?	Capital requirements	High (8)	Moderate (6)	Quite low (4)
	Production size determining profitability in enterprise	Medium (5)	Quite high (7)	High (8)
	Production size in the country	Quite low (4)	Quite high (7)	Very high (9)

LEGEND: ⇒ Cause and effect connections ┄┄► Capital connections ┈┈► Time corelations ◄─► Two-way transfer of data and/or resources

561

Table 2 - The technology roadmap prepared for laser cladding of VC vanadium carbide particles in the substrate of Mg-Al-Zn casting magnesium alloys

TECHNOLOGY ROADMAP	Technology name:	*Laser cladding of VC vanadium carbide particles in the substrate of Mg-Al-Zn casting magnesium alloys*	Catalogue No.
	Research scope:	*Laser technologies in surface engineering*	M1-13-2010/11

When?	Time intervals	TODAY 2010-11	2020	2030
Why?	All-society and economic perspectives	Creating the Critical Technologies Book	Development of priority innovation technologies	Statistically high quality of technologies implemented in industry
		Creating future events scenarios	Using chances and avoiding difficulties	Sustainable development
		Development of information society and intellectual capital	Wide education and effective intensive cooperation between Science and Industry representatives	Knowledge- and innovativeness-based economy
	Strategy for technology Environment influence Technology value	Sunny spring / Wide-stretching oak	**Strategy of an oak in string: Succeed.** To develop, strengthen, implement attractive technology of a large potential in industrial practice in order to achieve outstanding success.	

What?	Product	Elements for automotive industry, which are friction, corrosive and/ or erosive worn, elements with quasi-gradient structure, MMCS composites, biomaterials, future yet unknown applications		
	Product quality at the background of foreign competitors	High (8)	Very high (9)	Excellent (10)
	Substrate	Casting magnesium alloys		
	Kind of surface coatings/ layers/ processes on substrate surface	Vanadium carbide VC		
	Improved material properties	Better mechanical properties of elements (hardness), better anticorrosive properties, better tribological properties		
	Diagnostic-research equipment	Light, confocal laser, scanning electron, transmission electron, atomic force microscopes, X-ray diffractometer, X-ray microanalyzer, GDOES spectrometer, hardness, microhardness, scratch testers, profilometer, potentiostat		

How?	Technology	Laser cladding of VC vanadium carbide particles in the substrate of Mg-Al-Zn casting magnesium alloys		
	Life cycle period	Prototype (8)	Growth (7)	Mature (5)
	Production type	Unit and small-scale serial	Small- and medium-scale serial	Small- and medium-scale serial
	Production organisation form	Cellular	Cellular	Cellular
	Machine park modernity	Excellent (10)	High (8)	High (8)
	Automation & robotisation	High (8)	Excellent (10)	Excellent (10)
	Quality and reliability	High (8)	High (8)	High (8)
	Proecology	Very high (9)	Very high (9)	Very high (9)

Where?	Organisation type	R&S centres, technological parks, large- and medium- sized enterprises	R&S centres, technological parks, large- and medium- sized enterprises	R&S centres, large-, medium-, and small- sized enterprises
	Represented industry	Medicine, automotive industry, military equipment, aviation, aeronautics		

Who?	Staff education level	Very high (9)	High (8)	Moderate (6)
	Engagement of scientific-research staff	Very high (9)	Quite high (7)	Moderate (6)

How much?	Capital requirements	Very high (9)	High (8)	Moderate (6)
	Production size determining profitability in enterprise	Medium (5)	Quite high (7)	Very high (9)
	Production size in the country	Very low (2)	Quite low (4)	Moderate (6)

LEGEND: ⇒ Cause and effect connections ·······▶ Capital connections ·······▶ Time corelations ◀──▶ Two-way transfer of data and/or resources

Two demonstration roadmaps prepared for manufacturing of monolayer coatings by physical vapour deposition process onto the CuZn40Pb2 brass substrate (Table 1) and for laser cladding of VC vanadium carbide particles in the substrate of Mg-Al-Zn casting magnesium alloys (Table 2) in that work are presented. The technology roadmaps supplement the technology information sheets, which include the technical information set being a compact compendium of knowledge making easier technology practical implementation in industry, especially in small and medium enterprises. The final results of advanced foresight-material science research is the Critical Technologies Book being the set of 140 roadmaps and 140 information sheets describing critical technologies in surface materials engineering area, three alternative versions of future events scenarios of surface materials engineering development as well as public debate concerning the significance of surface engineering development for the Europe 2020 strategy realisation.

The Finite Element Method is applied for modelling of the PVD coatings properties. On the basis of researches results, it was found out that using advanced technique of calculation among others thing the finite elements method FEM, can be exploited as tools usrd in surface engineering to characterise the coatings. This method allows to realise complex analysis proceeding during processes of coatings spread and also an analysis of phenomena occur as an effect of a final process.
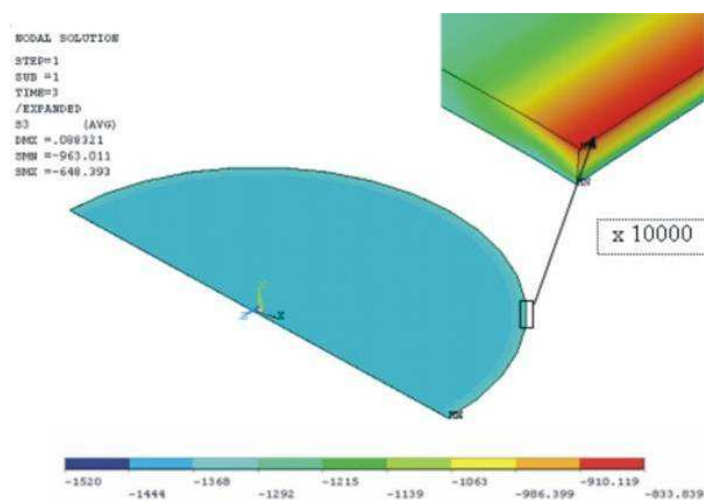
Fig. 14. Distribution of the simulated compression stresses in the TiN PVD coatings
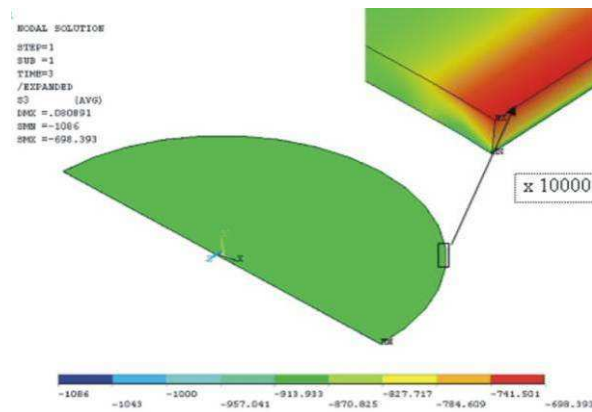
Fig. 15. Distribution of the simulated compression stresses in the TiC PVD coatings

One has to indicate that such an analysis needs knowledge of many quantities as physical and mechanical properties of substrate material and coating and also its parameters of spread. As a result of this abovementioned method allows to create a model which describes inner stresses in relation to parameters of process and also to a kind of substrate material and to coatings (Figs. 14 & 15). In addition, a developed model can eliminate the need for expensive and time-consuming experimental studies for the computer simulation to a large extent. Developing an appropriate model allows the prediction of properties of PVD coatings, which are also the criterion of their selection for specific items, based on the parameters of technological processes.

For predicting the properties of the PVD and CVD coatings the fractals as very interesting mode of the Computational Materials Science and Surface Engineering are used. The aim of the work is to establish a methodology elaboration, giving a possibility to predict properties of coatings reached in PVD and CVD processes on tool materials, based on fractal quantities describing their surface. Coatings' topography and its structure which has an impact on a shape of analysed objects' surface are characterised in a comprehensive way. Influence of a type of process and conditions of deposition over structure and shape of surface topography as well as mechanical and operational properties of the acquired coatings are determined. The coatings selection, represented in terms of types and conditions proceeding in deposition processes, types of substrates material as well as chemical and phase composition, and also a combination of applied layers provided diversity of their surface topography as well as mechanical and functional properties.

Methodology for precise description of coatings topography acquired in PVD and CVD process on tool materials including using of the fractal and multi-fractal geometry on the basis of images obtained on an atomic forces microscope is elaborated and verified. A modified methodology to determine fractal parameters of surface by means of the Projective Covering Method (PCM) is applied. Dependencies between fractal and multi-fractal parameters characterising analysed PVD and CVD coatings surfaces and their mechanical and operational properties are established. Values of the fractal dimension for coatings' topography received in the magnetron PVD process are correlated with microhardness and erosion resistance, whereas the fractal dimension values of coatings' topography obtained in the high-temperature CVD process (on a substrate made of Si3N4 ceramics and when the outer layer was made of Al2O3) and in the arc PVD process is correlated with tool life increase specified in the cutting ability test. It is shown that the presented interdependencies give a possibility to predict coatings' properties received in the PVD & CVD processes on tool materials based on fractal parameters defining their surface.

The next example of the application of the Computational Materials Science and Surface Engineering is methodology of high-speed steels design using the artificial intelligence tools. The main goal of the outcarried research is to develop the design methodology for the new high-speed steels with the required properties, including hardness and crack resistance expressed by fracture toughness. The adequate models are developed first, enabling computation of high-speed steel hardness and its crack resistance solely based on chemical composition of the steel and its heat treatment parameters, i.e., austenitising and tempering temperature. The outcarried research confirmed that using the catalogue data and standards is possible, which - supplementing the set of experimental data indispensable to develop the assumed model - improve its adequacy and versatility. Methodology of the multicriteria optimisation of the high-speed steel chemical composition, using the evolutionary algorithms, is developed to design the chemical composition of the new high-speed steels, demonstrating the required hardness and fracture toughness. It was used in the own computer programme, which enables design of the chemical composition of steel with the required hardness and fracture toughness in the specified search

area for the optimum high-speed steel chemical composition. Solutions presented in the work, based on using the adequate material models may feature an alternative in designing of the new materials with the required properties. The practical aspect, resulting from the developed models, which may successfully replace the above mentioned technological investigations, consisting in one time selection of the chemical composition and heat treatment parameters and experimental verification of the newly developed materials checking its properties and meeting the requirements has to be noted. It was also demonstrated that employment of computer tools enables especially efficient use of the existing materials data resources contained in publications, standards, catalogues, and data bases, and their integration in the material models form.

The Computational Materials Science and Surface Engineering methods especially the neural networks are applied among others for the prediction of continuous cooling transformation diagrams. The method of forecasting of Continuous Cooling Transformation (CCT) diagrams for steels by the use of neural networks has been presented. Input data are chemical composition and austenitising temperature.
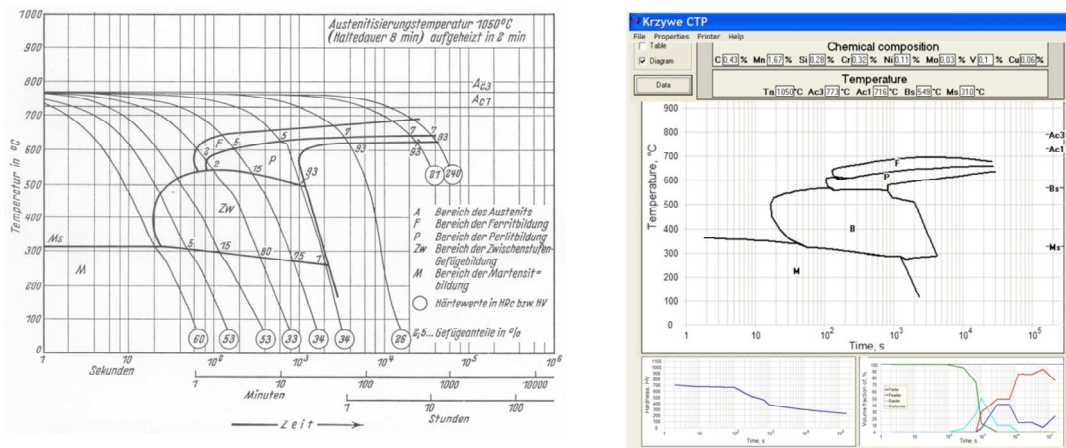
Fig. 16. CCT diagram for steel with concentrations: 0.43% C, 1.67% Mn, 0.28% Si, 0.32% Cr, 0.11% Ni, 0.03% Mo, 0.01% V, 0.06% Cu, austenitised at temperature of 1050°C: a) experimental, b) calculated by the neural network model

Results of calculation of neural networks consist of temperature of the beginning and the end of transformation in the function of cooling rate, the volume fraction of ferrite, perlite, bainite, martensite with the retained austenite and the hardness of steel cooled from austenitising temperature. Presented

quantities enable to draw the CCT diagram (Fig. 16). The developed neural network models make it possible to carry out computer simulation of the effect of chemical composition, austenitising temperature and/or cooling rate on a selected quantity describing austenite transformations in the CCT diagram.

The example of the Computational Materials Science and Surface Engineering methods is an analysis of alloying elements influence on the properties of the structural steels with the using of the materials science virtual laboratory. The paper introduces analysis results of selected alloying elements influence on the mechanical properties of the alloy structural steels for quenching and tempering. The investigations are performed in virtual environment with use of materials science virtual laboratory. Virtual investigations results were verified in real investigative laboratory. Materials researches performed with use of material science virtual laboratory in range of determining the mechanical properties are consistent with the results obtained during the real research in a real laboratory. For materials investigation alloyed structural steels have been selected. Material was manufactured in electric arc furnaces with devices for steel vacuum degassing (VAD). The material was supplied in the form of heat and plastic treated forged round rods. Material science virtual laboratory is, located in virtual environment, a set of simulators and trainers, which main objective is to simulate the research methodology of investigative equipment located in a real scientific laboratory. It allows for the mechanical properties prediction of non-alloy and alloy structural steels. On the basis of the input steels manufacturing conditions are possible to determine its mechanical properties without the need for real examinations (Fig. 17). Also the reversed inference is possible, namely on the basis of mechanical properties values steel's production conditions can be determined. For the description of structural steel, six mechanical properties presented in the metallurgical certificate have been selected. To describe the above properties a set of descriptors characterising steel in manufacturing process has been developed. In order to model and predict properties, material descriptors, such as chemical composition, heat treatment, plastic treatment and geometric parameters were inputted to a materials science virtual laboratory. To verify modelling correctness, results obtained during virtual examinations were compared with

the results of real material investigations performed on real steel samples in a real laboratory.

a)   b)

c)
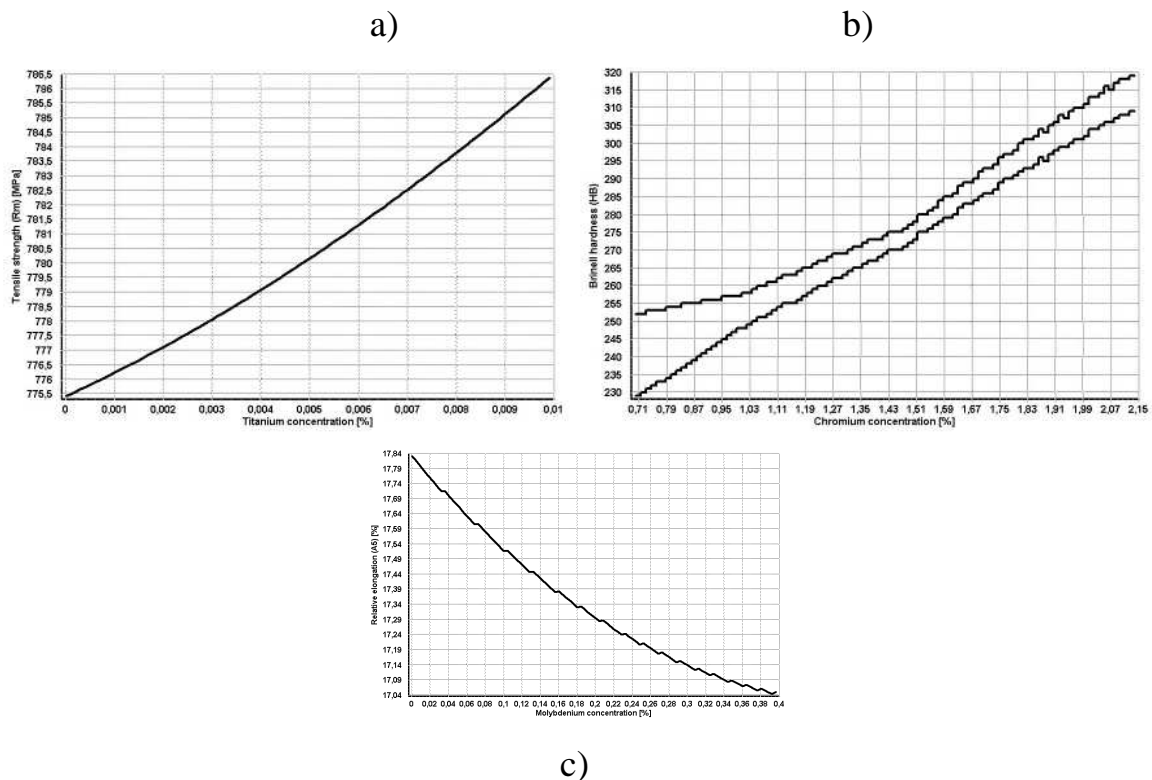
Fig. 17. Influence of: a) titanium concentration on tensile strength of 24CrMo4 steel; b) chromium concentration on Brinell hardness of 41Cr4 steel (minimum and maximum values); c) molybdenum concentration relative elongation of 30CrMo5-2 steel

Results of modelling were marked as correct, because all five types were recognised correctly. Differences among measured and predicted values of mechanical properties are very small and the values of the neural networks tolerances were not exceeded. Influence analysis was conducted to calculate how big the influence of the alloy addiction concentration on steels mechanical properties is. Dependence graphs were generated with the use of NeuroLab system among estimated mechanical properties and the concentration of chosen alloying additions. Materials researches performed in virtual environment with use of material science virtual laboratory in range of determining the mechanical properties of alloy structural steels are consistent with the results obtained during the real research in a real investigative laboratory. Results consistency was observed in the whole range of steel descriptor variation: of concentrations of chemical elements, heat and mechanical treatment conditions

and mechanical properties of examined structural steels for quenching and tempering.

In the field of dental engineering own researches directed on: structural effect occur in metallic materials, influence on useful properties like corrosion resistance and permanency of finished dentures which depends of ceramics adhesion to metallic substrate are performed. Also the study about crown and bridgeworks geometry modelling which is a criteria in tension minimalisation in constructions are provided. The last 25-30 years brought on huge development of metallic materials which are used in nowadays dentistry. An engineer may choose from hundreds materials from many world companies. Actually there is possibility to choose metallic materials using the American Dental Association classification (Fig. 18). The introduction to the alloys different additions has influence on forming metallic phases structure (Fig. 19), also affects on clinical characteristics, especially on biocompatibility and different possibility dental usage (Fig. 20).
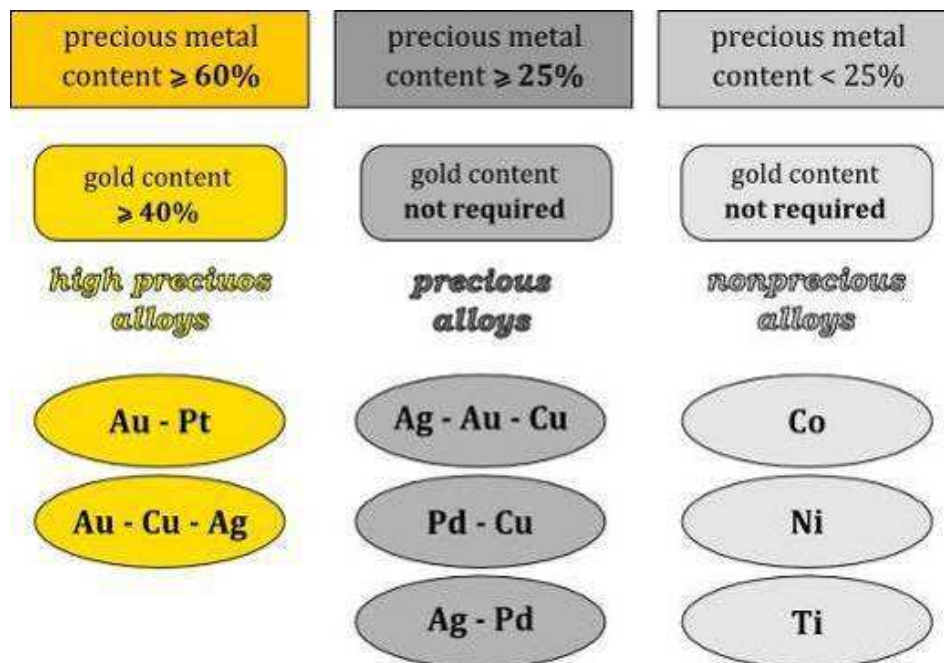
Fig. 18. Classification of the metallic materials used in dental engineering
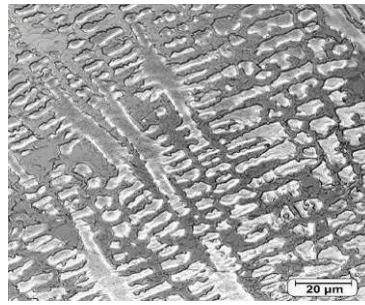
Fig. 19. Dendritic microstructure of Remanium 2000+ CoCr alloy, confocal microscope

Fig. 20. Dental work made by metallic materials

The outworked elastic aramid-silicone composite materials for the manufacturing of the internal oesophageal prosthesis (Fig. 21) has been applied. The aim of the work is to develop the prosthesis that could replace the natural oesophagous and perform its anatomical functions. The finished prosthesis will result in cognitive, constructional and technological effects, but first of all, it will enable the increase of comfort of life of the very sick people after resection of pathologically changed oesophagus. Within the framework of this work, the construction of the mentioned prosthesis has been developed, the structure and properties of the used material have been examined. It has been established that ourworked aramid-silicone composite material is characterised with specific properties against given group of laminated materials. Resilience of analysed material will decrease the risk of bedsore inside the human body after implementation of the prosthesis. Additionally, diversified degree of inner and outer surface roughness of the developed material (low at the inner side and high at the outer one) will positively influence on easy transport of food on the one side, on the other one, on better stabilisation of the prosthesis inside the body (Fig. 22). Properly prepared surface favours the living tissue development. The technological conditions of the material itself at the first stage and the prosthesis at the second one have been determined and optimised. The well-

known method of fibre with matrix winding onto previously prepared core has been chosen to prepare the prosthesis. This choice determined the necessity of a specific approach to a manufacturing process, it means, a methodological approach in the choice of the braid architecture proposed for the described prosthesis has been adopted. Present-day investigations are also of the biological character and are carried out in the Regional Blood-donor Centre – Tissue Bank. Those investigations consist on the culture and sowing of cells on the newly developed material in order to determine its influence on living organism. The application to Bioethical Committee has been also submitted, and its approval will allow the realization of planned clinical researches, which will enable the decision on further prosthesis modification. Realisation of this scientific work is enable to achieve research, constructional and technological results as well as, what is even more important, it will enable the effective help to very sick people.

Composite materials with controlled soft or hard magnetic properties are the next area of interesting. The search for the new soft magnetic materials has lead, among others, to the development of research on the Fe based metallic materials with the nanocrystalline structure, having the great soft magnetic properties.
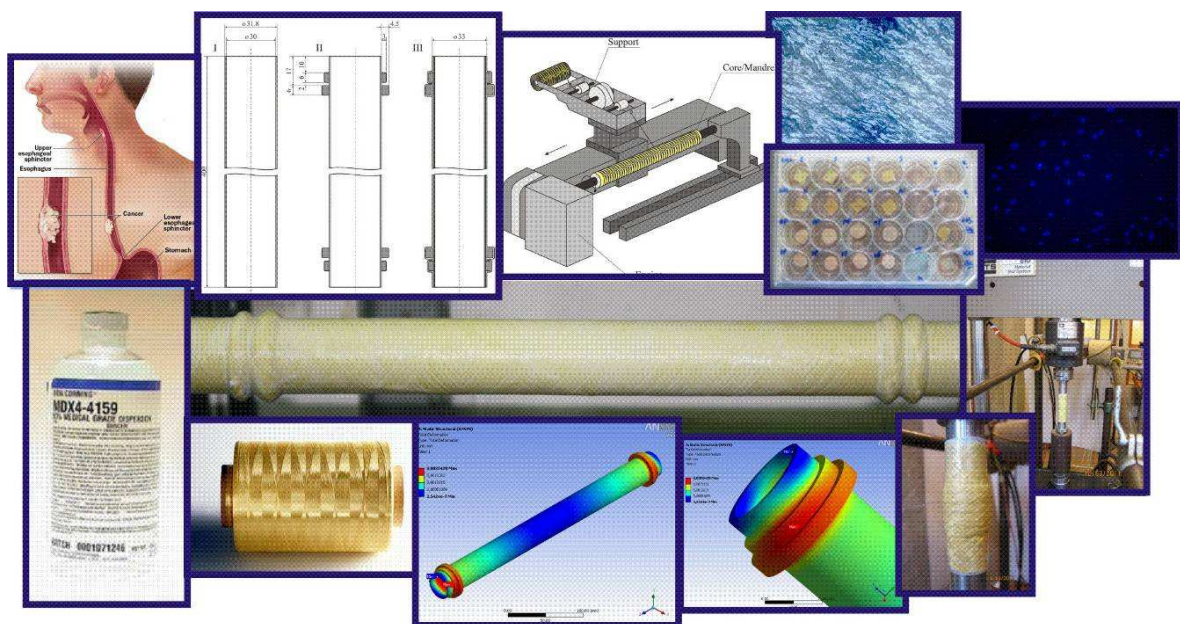
Fig. 21. The scheme of scientific activity for work out the elastic aramid-silicone composite materials for the manufacturing of the internal oesophageal prosthesis

Bonding of powders of Fe based nanocrystalline metallic materials with the polymers and low-melting alloys enables to obtain the composite materials (Fig. 23). The range of magnetic materials application growths with improvement of their magnetic, mechanical, electrical and thermal properties. The application of magnetic composite materials allows to miniaturise magnetic elements, construction simplification and lower both manufacturing and material costs.
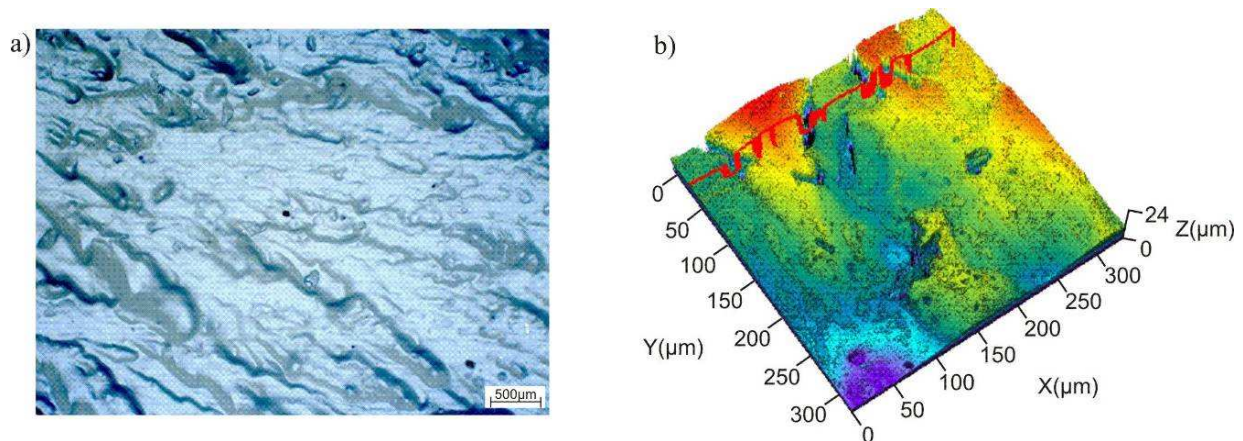
Fig. 22. The inner irregular surface of aramid-silicone material; a) MEF4A Leica Light microscope, b) LMS 5 Exciter Zeiss Confocal microscope

The work on the structure and properties of magnetically soft composite materials with the silicon matrix reinforced with the nanocrystalline powders of cobalt alloys, was dedicated to the investigation of the influence of high energy grinding process conditions on structure and magnetic properties of the soft powder material obtained from cobalt alloys and to the investigation of the effect of its heat treatment on its structure and properties. The obtained powders were consolidated and nanocomposite cores with the required properties were made from them. The examination of their magnetic properties were made on the FERROMETR-1 device; whereas, the examination of powders were carried out on the Lake Shore Cryotronics VSM vibration magnetometre and on the Moessbauer spectrometre. Structures of the amorphous strips and those isothermally annealed, and of the obtained powder materials were examined using the JEOL JEM 200CX and TESLA BS 540 electron transmission

microscopes and the DSM-940 electron scanning microscope with the Opton EDS LINK ISIS energy dispersive X-ray spectrometer.

a)

b)

H_c [kA/m]	B_r [T]	B_s [T]	μ_{max}	Min. [µm]	Max. [µm]	Mean [µm]	*Stdev.*
0.537	0.006	1.3	81	10.3	69.2	34.7	*6.5*

c)

d)

e)

	R_c [MPa]	A_c [%]	E_c [MPa]
mechanical properties	27.4	8.6	330.8
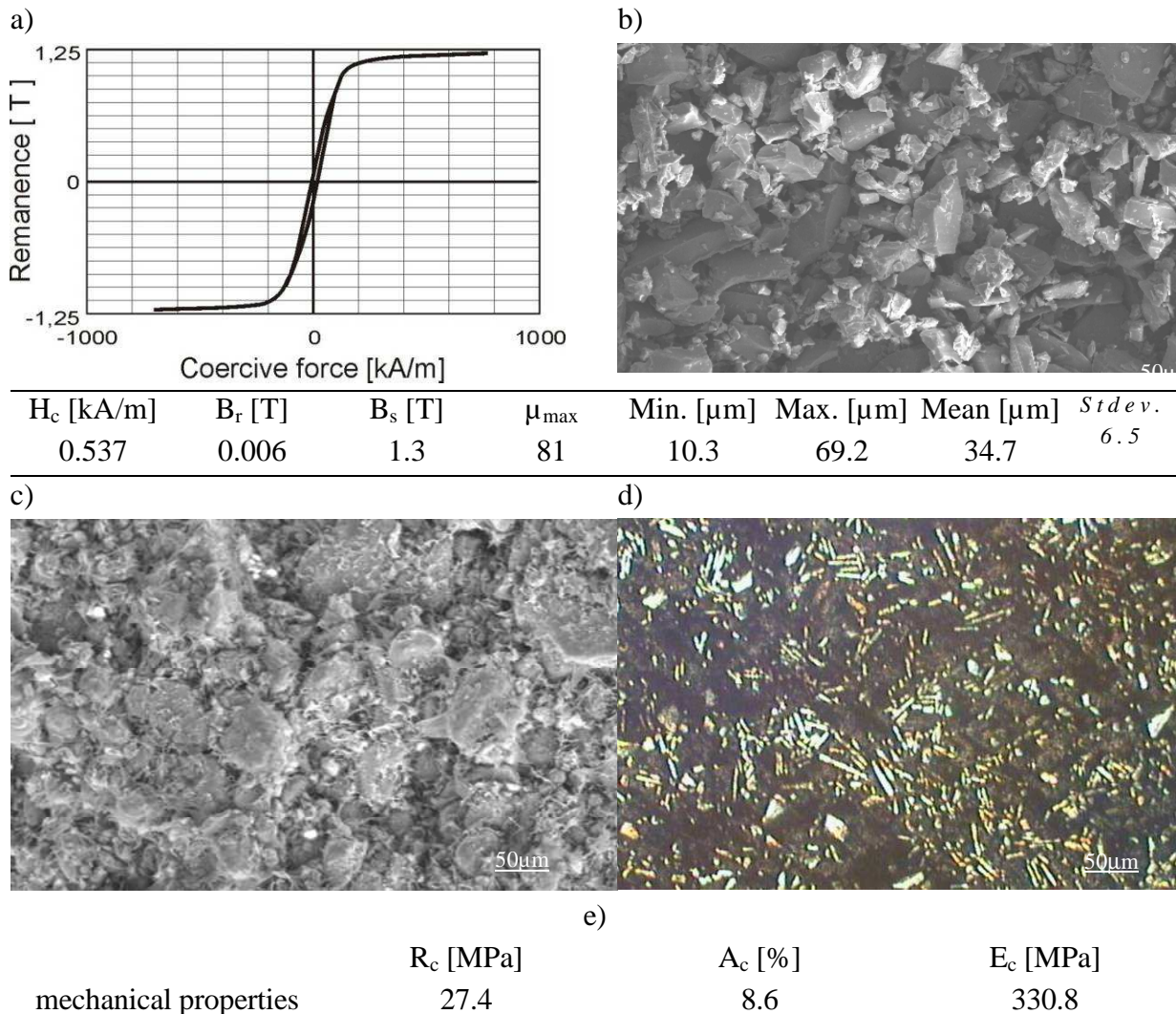
Fig. 23. FINEMET - PEHD composite material: a) hysteresis loop, b) powder Fe73.5Cu1Nb3Si13.5B9, c) fracture of composite material (SEM), d) structure of composite material (LM), e) mechanical properties

The soft magnetic powder materials are characterised by a relatively high value of coercion field (150-1200 A/m), which increased with the grinding time and magnetic saturation 0.6-0.87 T. There is a possibility to control these properties using heat treatment. Nanocomposite magnetic cores were made from the powder material obtained by high energy grinding and influence of the metallic powder fraction on soft magnetic properties were investigated along with the possibility to control these properties with the amount of powder fraction (Figs. 24 & 25). The nanocrystalline composite material with the mass

fraction of metal powder to silicone polymer of 6:1 has the most advantageous magnetic properties. Composite with the mass fraction of 2:1 has the worst properties. Mass fraction of the metallic powder in the nanocomposite decides the composite's mechanical properties. The highest ultimate tensile strength UTS is characteristic for the composite with the mass fraction of the metal powder to silicone polymer of 3:1 (UTS=1.18 MPa). As the mass fraction increases, the UTS value decreases. The elongation ε dependence of the powder mass fraction is similar – linear (proportional). The highest elongation of ε=212% is characteristic for the composite with the mass fraction of metallic powder to the silicone powder of 6:2. The determined high energy grinding parameters, high treatment conditions, and the metallic powder material consolidation methods may be employed in the electronic and electrotechnical industry.
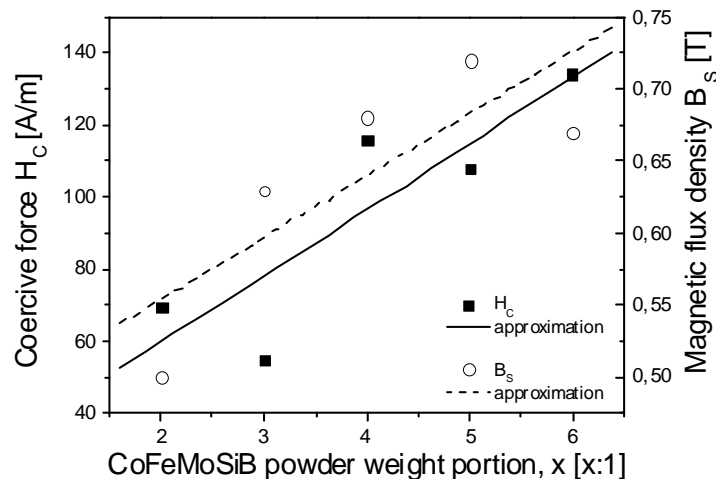
Fig. 24. Magnetic properties of the nanocomposite magnetic soft materials with the various metallic powder to polymer matrix weight ratios

Structure and properties of composite materials with polymer matrix reinforced Nd-Fe-B hard magnetic nanostructured particles were also investigated. The experiments were made with the polymer matrix hard magnetic composite materials reinforced with nanostructured particles of the powdered rapid quenched Nd-Fe-B strip MQP-B type made by Magnequench (Nd14.8Fe76Co4.95B4.25).
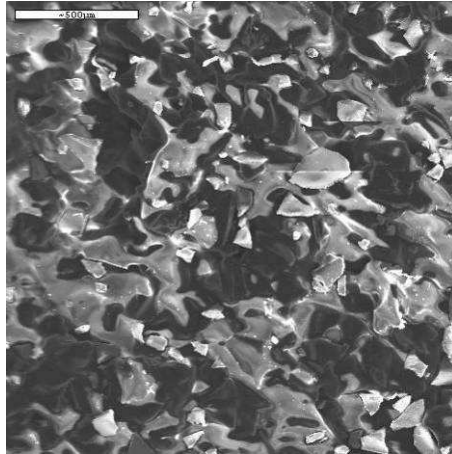
Fig. 25. Structure of the nanocrystalline composite material with the silicone matrix reinforced with the Co68Fe4Mo1Si13.5B13.5 alloy powder, powder to silicone in the composite weight ratio 3:1; SEM

Powders of metals and their alloys: iron, aluminium, CuSn10 casting alloy of copper with tin, and of the X2CrNiMo17-12-2 high-alloy steel (5, 10, 15% wt.) were added to the composite material. The heat-hardening epoxy resin was used as the matrix (2.5% wt.). The following compacting process parameters were used: unilateral uniaxial compaction, room temperature, pressure 800-900 MPa. The polymer matrix of the composite materials was cured at the temperature of 180°C for 2 hours after compacting (Fig. 26).
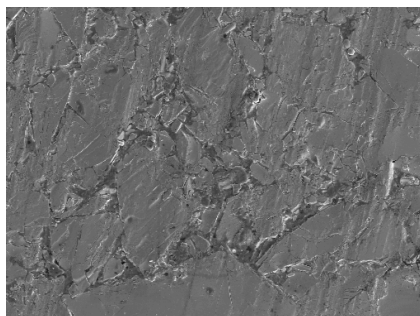
Fig. 26. Microstructure of composite material without addition powders

It is shown that additions of metal powders and their alloys to polymer matrix hard magnetic composite materials cause improvement not only of mechanical properties (Fig. 27) but also the application properties, including mainly corrosion resistance. Composite materials with no additions are characterised with good magnetic properties. Additions of metallic powders to those composite materials causes decrease of magnetic properties, but improves

mechanical properties of magnets. The highest influence on the increase of ultimate compression strength has iron powder, although the most advantageous influence on hardness increase has X2CrNiMo17-12-2 high-alloy steel powder. Corrosion resistance of composite materials increases thanks to additions of metallic powders. Materials including additions of aluminium powders are characterised with the greatest resistance, whereas including additions of iron provide the lowest one. The developed neural network model, verified experimentally, allows computer simulation of influence of metallic powder additions and/or the test duration on corrosive wear of magnets in corrosion environments assumed.
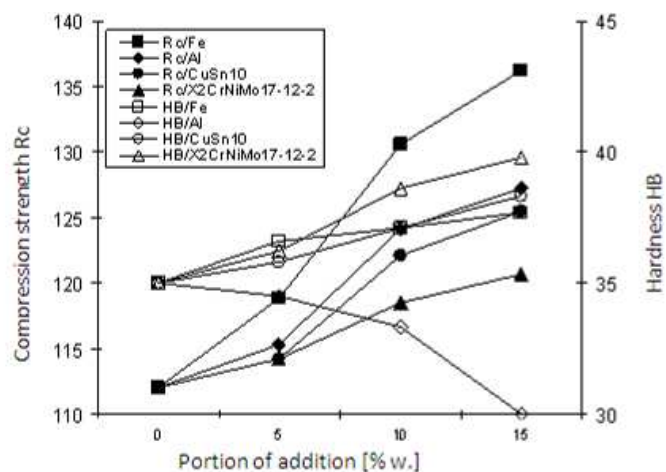
Fig. 27. Comparison of the hardness and compressive strenght of composite materials

Intelligent polymer matrix composite materials reinforced by Tb0.3Dy0.7Fe1.9 magnetostrictive particles were investigated. The Td0.3Dy0.7Fe1.9 alloy exhibits giant magnetostriction (800-1200 ppm) in a considerably low magnetic field (50-200 kA/m) at the room temperature. Unfortunately some factors – such as the development of eddy currents in high frequency applications, brittleness in tension, large magnetic fields required to induce strain and high price have limited its use. For potential applications in technological devices, such as sensors and actuators, it is desirable to form a composite system by combining magnetostrictive phases with passive matrix in order to have giant magnetostrictive effect and, at the same time, to reduce

disadvantages of monolithic material. In this work the relationships among the manufacturing technology conditions of composite materials, their microstructure, as well as their magnetic properties were evaluated as function of both bias field and frequency. It was shown that anisotropy of composite materials – arising from Tb0.3Dy0.7Fe1.9 particles magnetic alignment during curing of polymer matrix (Fig. 28) – causes low values of transverse magnetostriction but at the same time – the greater longitudinal response (Fig. 29) in comparison to non-oriented one. The obtained results show the possibility of manufacturing the magnetostrictive composite materials based on the Td0.3Dy0.7Fe1.9 particles with desired microstructure and magnetic properties, being a cheaper alternative for conventional giant magnetostrictive materials GMM.
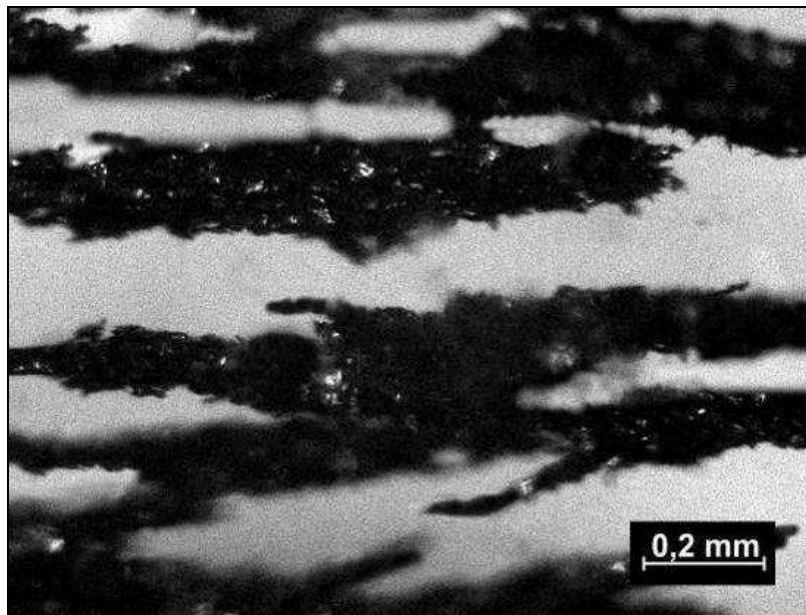
Fig. 28. Microstructure of composite materials with 10% volume fraction of Tb0.3Dy0.7Fe1.9 with aligning the particles in polymer matrix; 100x

The work on in-mould manipulation of injection moulded polymer nanocomposites investigates the structure development of polymer based nanocomposites. Nanofiller strongly influenced on mechanical behaviour and morphology of polymer composites. Polypropylene (matrix material) was blended with the organo-modified montmorillonite nanoclay in ratio of 97/3 wt% (polymer or polymer composite/nanofiller).
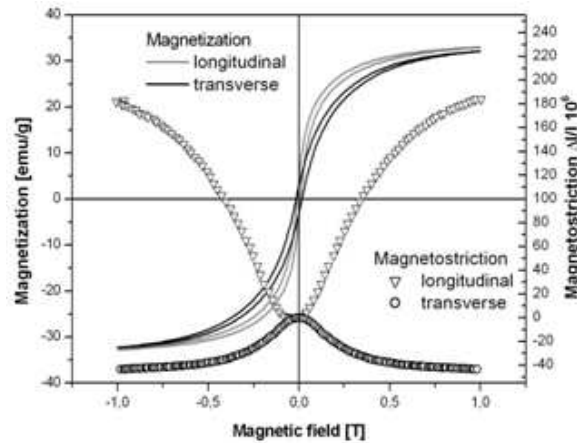
Fig. 29. Magnetic field dependence of magnetization and magnetostriction the external applied field longitudinal and transverse to the internal bias field for oriented composite materials with 10% volume fraction of Tb0.3Dy0.7Fe1.9

After blending in rotational drum, materials were injection moulded into cavity in special mould. Processing consists of two steps, where first one was traditional injection moulding process and second one started just after filling the cavity inside mould, where melt was manipulated by reciprocation movements, inducing multilayer zone and outer skin, and containing simultaneously small, spherullitic core. Diversified settings of the operative processing parameters were used according to the moulding set-up, basing on the design of experiments. Three main parameters (melt temperature, stroke time and number) were changeable during processing and their mutual combination brought series of interesting results. Mechanical tests were performed on universal testing machine on notched specimens and sharpened with razor blade, by 3-point bending test with crosshead speed 10 mm/min (according to the ASTM E399 standard) under constant room condition (23ºC and 50% of humidity). This mechanical characterization was prepared for comparison of the synergetic effects of polymer-polymer composites and processing conditions on the fracture behaviour. The best improvement of energy value has been obtained for pure polymer matrix reinforced by nanoparticles. Polymer nanocomposites as a new and interesting class of polymer composites derived from nano-scale particles are investigated worldwide, demonstrating a broad scope of material composition possibilities. A high aspect ratio of homogenously dispersed particles, which dimension

ranges from 1 to 1000 nm improve mechanical, thermal and barrier properties. Enriching composites by nanoparticles varies and is dictated by cost of nanofillers, generally reaching 5 and even 10 wt%. Production of polymer nanocomposites by compounding the nanofiller with polymer matrix (e.g. PC or PP) by melt mixing, in situ polymerization and other processes is widely and challenging investigating area. Nanoparticles inside polymer composites are disposed in two forms: intercalated and exfoliated ones. In reality both of these types are mixed simultaneously, unless special control during processing has been satisfied. The difference between these systems is the stacking – intercalated system contains stacked silicate galleries, while exfoliated system has fully separated particles, stochastically dispersed inside a polymer matrix. Good dispersion rises to enhance the properties (Fig. 30).

The purpose of the work on synthesis and characterisation of carbon nanotubes (CNTs) decorated with platinum nanoparticles is to obtain Pt/CNT composites. Platinum are widely used in many applications, especially as a catalyst for CO oxidation in catalytic converters and for fuel cell technology. It can also be used as a stable electrode material. Since Pt is particularly expensive, there is a real incentive to reduce the amount of Pt required in applied processes. With this end of view a lot of efforts is put to reduce the size of used Pt particles what additionally can significantly increase its specific surface area. Carbon nanotubes become the one of the mostly researched nanomaterial in the last decades because of their promising applications in any aspect of nanotechnology, result mainly from theirs high surface area, mechanical strength, chemical and thermal stability. Due to the possibility to combine the unique physical and chemical properties of CNT with innovative properties of noble (including Pt) metal nanoparticles in one discrete structure there is a great deal of interest in attaching nanoparticles to nanotube surface. The controlled coating without aggregation would be crucial for this issue and it was the main aim of the research.
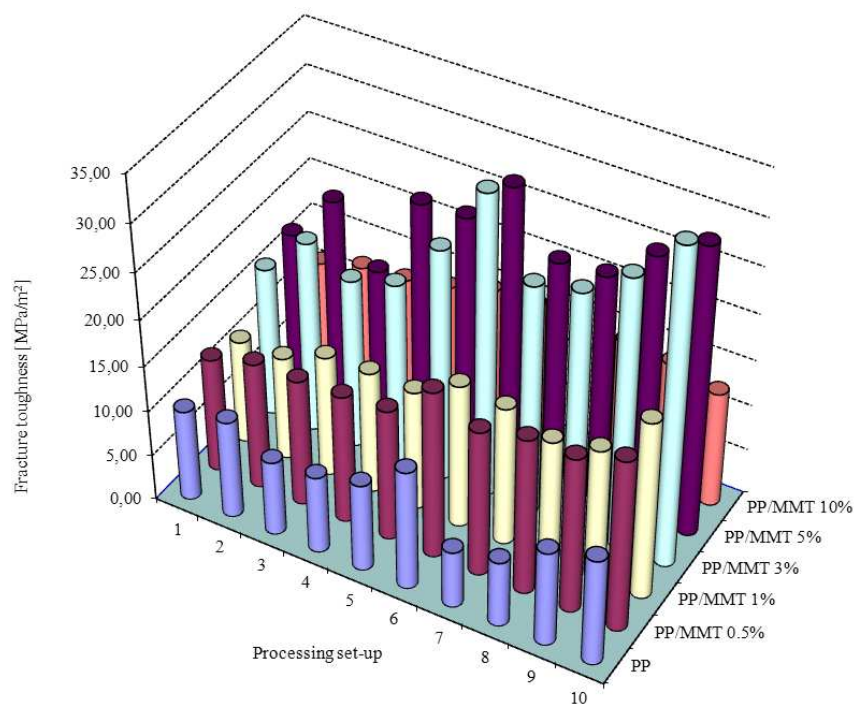
Fig. 30. Comparison of fracture toughness KIC of all nanocomposites performed by advanced injection moulding technique with different processing set-up of changeable parameters

To improve metal deposition onto CNTs in the experiments the purification procedure with a mixture of reduction reagents was applied. Carbon nanotubes decorated with platinum nanoparticles were synthesised by organic colloidal process as an example of direct formation of nanoparticles onto CNTs. Chemical composition and crystallographic structure of the obtained Pt/CNT composites were determined by energy dispersive X-ray spectroscopy (EDS) and by X-ray diffraction (XRD) measurements, while transmission (TEM) and scanning (SEM) electron microscopy were used for characterisation of the morphology of composite as well as the distribution of nanocrystals on the CNTs surfaces. High efficiency of proposed method was confirmed as well as possibility of the coating of Pt nanoparticles onto CNTs, without aggregation of these particles. Fabricated material is homogenous and contained mainly carbon nanotubes. The Pt phase appearance is convincingly confirmed by energy dispersive X-ray spectrometry. The side walls of CNTs with diameter of 10-50 nm are evenly decorated with Pt nanoparticles. The density of attached nanocrystals are high. Observed platinum particles appear to have a narrow size

distribution and they are durably attached to the nanotubes (Fig. 31). The diffraction peaks in XRD pattern indicating a good crystallinity of the supported nanoparticles. The average crystallite size of Pt calculated using the Debye–Scherrer formula was determined as about 4 nm, consistent with SEM and TEM observations. Obtained material can be employed in constructing various electrochemical sensors. As a result of increasing of the surface area of Pt caused by the reduction of the size of used particles, fabricated sensor are expected to be more sensitive.

The goal of the work on aluminium matrix composites reinforced by halloysite nanotubes consists in the elaboration of these composite materials, manufactured with the use of powder metallurgy technologies, including mechanical alloying and hot extrusion and in determining the influence of the share of halloysite – as the reinforcing phase on the structure and mechanical properties of fabricated composites. Halloysite being a clayey mineral of volcanic origin is built from flat surface plates, partially curled, or they are shaped like tubes made from curled plates (Fig. 32). Composite powders of EN AW6061 aluminium matrix reinforced with 5-15wt.% of halloysite nanotubes were produced by high energy ball milling using an centrifugal mill. The obtained powders were cold pressed in the cylindrical matrix with 300 MPa pressure and then extruded at 480°C without caning and degassing. Obtained
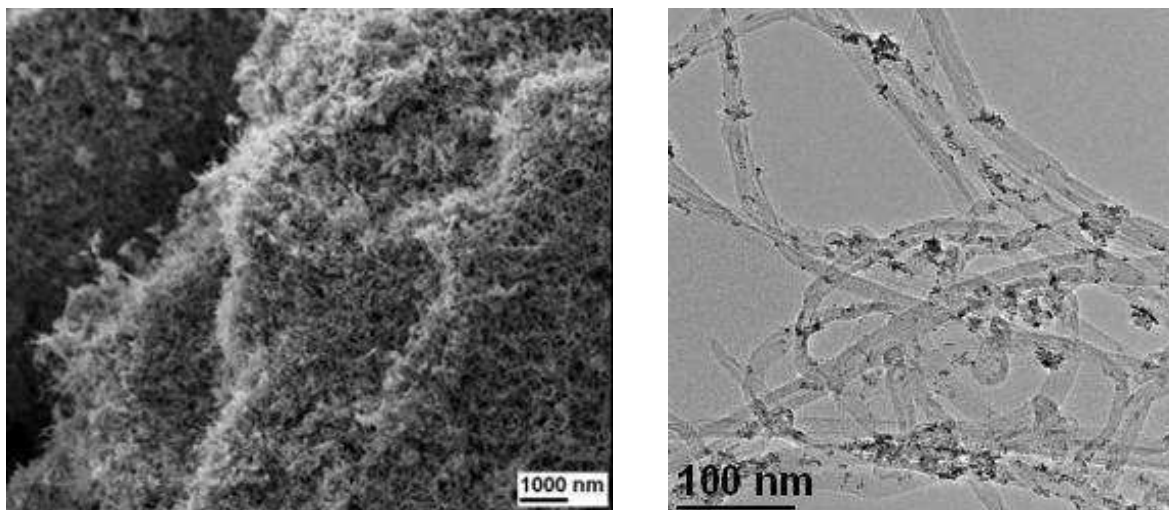
Fig. 31. SEM (left) and TEM (right) images of obtained Pt/CNTs composite

composite material was examined by hardness Vickers test in the parallel plane related to the extrusion direction. Microstructure observations were made by optical and scanning electron microscopy. It has been proven that the application of mechanical alloying method, which enables to fabricate nanostructural structure of the composite material, it is possible to regulate the size of the strengthening phase particles and to ensure its uniform distribution, which results in the rise of mechanical properties (Fig. 33). The presence of halloysite reinforcements particles accelerates the mechanical alloying process. It has been confirmed that halloysite nanotubes can be applied as effective reinforcement in the aluminium matrix composites (Fig. 34).
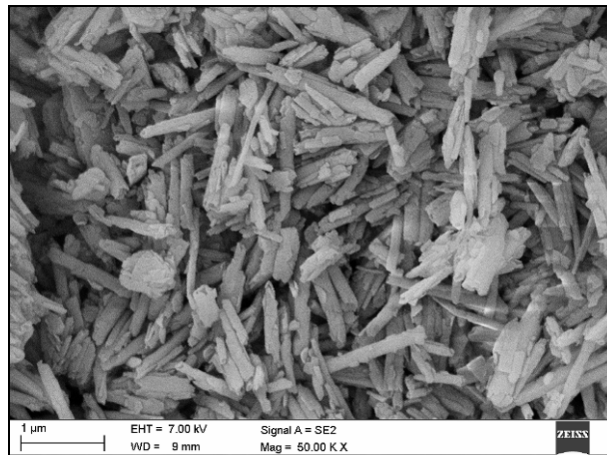
Fig. 32. Morphology of as received halloysite nanotubes, SEM
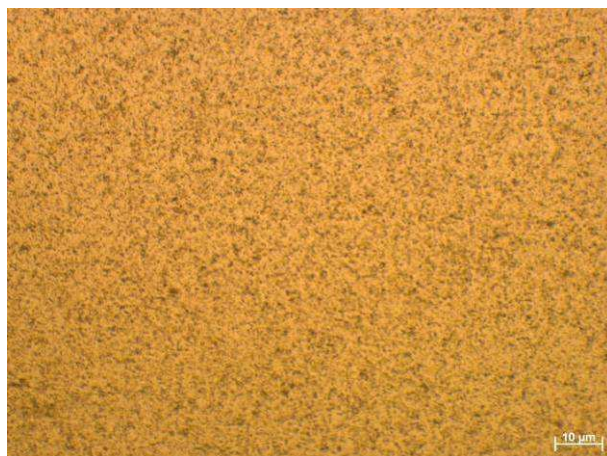
Fig. 33. Microstructure of extruded EN AW6061 with 15% addition of halloysite nanotubes
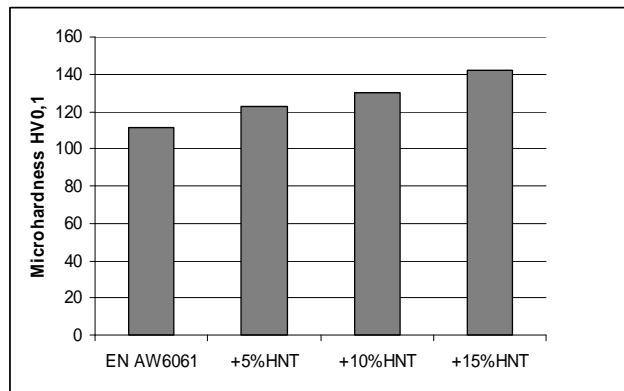
Fig. 34. Microhardness measurements results for obtained composites

Composite materials with the EN AW-AlCu4Mg1(A) alloy matrix (AlMMC) reinforced with Al_2O_3 and $Ti(C,N)$ ceramic particles are a group of materials which due to their properties (high specific elasticity modulus, high stiffness) are more and more frequently used in modern engineering constructions. Composites reinforced with ceramic particles (Al_2O_3 and $Ti(C,N)$, and also SiC and BN) are gradually being implemented into production in automotive, electronic or aircraft industries, first and foremost due to high resistance to friction wear. Basing on the outcarried structural examinations of the composite materials with the EN AW-AlCu4Mg1(A) aluminium alloy matrix reinforced with the Al_2O_3 and $Ti(C,N)$ particles the homogeneity of their distribution in the matrix was revealed, as well as the fact that during their extrusion the directed structure oriented according to the extrusion direction is developed. The employed heat treatment makes it possible to reduce significantly the sizes of the intermetallic phases' precipitations and results in a more homogeneous matrix structure (Fig. 35).

The influence of the heat treatment carried out on the corrosion resistance of the investigated composite materials was observed. Introducing the Al_2O_3 reinforcing particles into the matrix causes improvement of the corrosion resistance of the investigated materials. At the 5% and 10% portions of the reinforcing particles this resistance is better, and at their 15% portion a slight deterioration of the corrosion resistance occurs, compared with the matrix material. In case of the composite materials reinforced with the $Ti(C,N)$ particles, also at the 5% portion the corrosion resistance compared to the matrix

material corrosion resistance improves; whereas, at the 10% and 15% portions this resistance gets slightly worse.
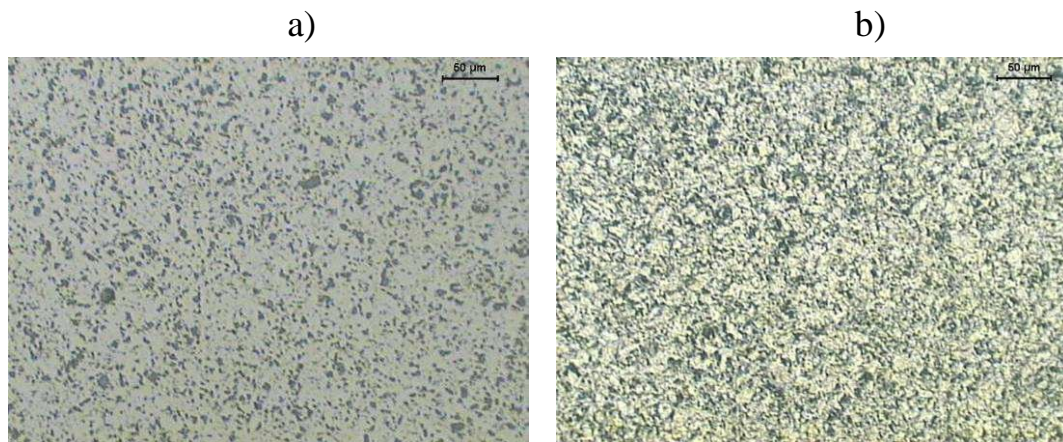
a)   b)

Fig. 35. Section of etched aluminium alloy matrix composite materials with particles: a) Ti(C,N), b) Al$_2$O$_3$, cross section

Thermal analysis of aluminium, magnesium and zinc alloys as a technique is used to evaluate the melt quality of these metals and their alloys. By this method, some characteristic values are extracted from a cooling curve and/or its derivative, and then a regression relationship is built up between the characteristics and quality indexes as for example grain size, eutectic structure and silicon morphology. The researchers shown that the thermal analysis carried out on UMSA Technology Platform is an efficient tool for collect and calculate thermal parameters. The formation temperatures of various thermal parameters, mechanical properties (hardness and ultimate compressive strength) and grain size are shifting with an increasing cooling rate (Figs. 36 & 37). For the improvement of the mechanical properties of the cast alloys, despite the heat treatment also modification of the alloy is applied, which causes change of the morphology and decrease of the inter-phase distance of the α+ β eutectic, as well as microstructure refinement. For this reason different kinds of modification additive are used. Improvement of the outcarried chemical modification and appliance of a proper cooling of the casts leads to the improvement of the mechanical properties of the produced casts. Therefore it is very important to have the knowledge about the microstructure modification of the casts according to the cooling rate or chemical composition change by addition of modifiers to the liquid metal.

The purpose of the work on heat treatment of casting aluminium alloys is to present influence of heat treatment on the microstructure of aluminium-silicon-copper casting alloys. Their chemical composition is not-standardised and contains approximately 7 and 9% silicon weight concentration and 1, 2 and 4% copper, respectively. The used heat treatment process is composed of solution treatment, quenching and artificial ageing. The samples are solution treated at temperature of 490°C for 2 hours, next quenched and artificially aged in various temperatures (130°C – 250°C) and times (1 h – 16 h). The microstructure of as-cast AlSi9Cu4 alloy is shown in Fig. 38. Most likely the dark grey plates are silicon phases while α matrix is light grey. Microstructure observed after precipitation hardening process is more dispersive, particles and intermetallic phases are spaced more evenly. Chemical composition of the samples has an influence on hardness of the as-cast material as well as at the parameters of the ageing process. In as-cast state copper content has bigger influence on hardness than silicon. Hardness of the samples changes from approximately 78 HRF (1% cooper weight concentration) to 88 HRF (4% cooper weight concentration). Hardness investigations after heat treatment shows that higher Si and Cu weight concentration results in higher hardness, for example AlSi7Cu4 has 95 HRF while AlSi9Cu4 – 98 HRF (ageing at 160°C for 4 h).
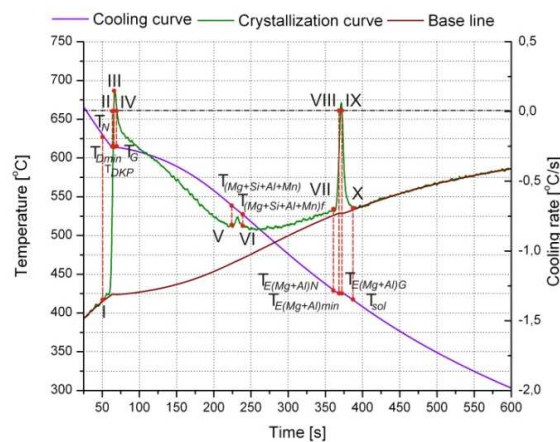
Fig. 36. Representative cooling, crystallization and calorimetric curves with characteristics points of crystallization process of MC MgAl6Zn1 alloy cooled at 0.6°C/s
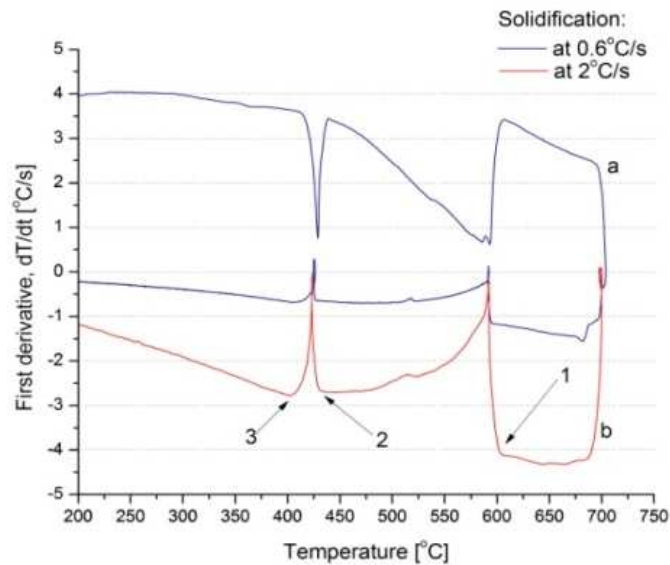
Fig. 37. First derivative (heating/cooling rate) vs. temperature curves of the test samples recorded during melting and solidification at 0.6°C/s (blue line) and 2°C/s (red line)
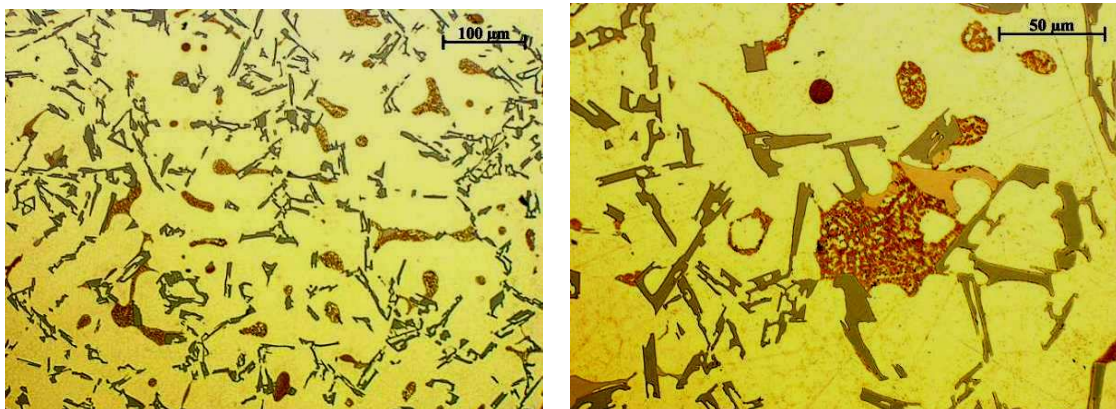

Fig. 38. Microstructure of as-cast AlSi9Cu4

Optimisation is very important for precipitation hardening process because dissolution of the all alloying elements is crucial during the solution treatment process. If time is too short and/or temperature too low than too little amount of alloying elements will be dissolved, while too long time and/or too high temperature may cause melting of the multi-component eutectic areas. Importance of these two factors during ageing process is great as well. Too long time and/or too high temperature will cause overageing of the alloy and in result mechanical properties would be much lower than expect.

Scientific aims of this work and the achieved results concerns the influence of phase transformation and precipitation processes of cast magnesium alloys. The magnesium alloys are one of the basic groups of metal alloys, which allows the realisation of the tasks mostly based on innovative constructional solutions as well as modern materials, which directly influence on mass, performances and fuel consumption of the contemporary cars. The most often pioneer solutions in this field there are applied light, strength materials with big projecting potentials in the dynamic development of the automotive industry. The investigations are made on the cast magnesium alloys MCMgAl12Zn1, MCMgAl9Zn1, MCMgAl6Zn1, MCMgAl3Zn1 with different concentration of alloying additives, particularly aluminium in the concentration range of 3 to 12% (in 3% steps) for achieving of desirable structure in the cast state and after heat treatment and its influence on the structure, mechanical properties, as well as the corrosion resistance. The selection of optimal heat treatment conditions that is temperature and heating time during solution treatment and ageing as well the cooling rate after solution treatment, is performed using criterion of maximal hardness calculated after the whole heat treatment process – solution treatment and ageing. For comparison of the achieved results on the basis of the performed investigations a computer neural network model was used for analysis of the aluminium content and heat treatment parameters influence on the properties of the worked out cast magnesium alloys. Based on the hardness measurement and modelling using neural networks can be stated that the optimal heat treatment type is solution treatment at a temperature of 430°C for 10 hours with water cooling and ageing in temperature at 190°C for 15 hours with air cooling (Fig. 39). Ageing with air cooling after solution treatment in water causes a precipitation of homogeny distributed $Mg_{17}Al_{12}$ phase in the matrix, which shows a following relationship with the matrix:

$(1\bar{1}01)$ α-Mg ∥ $(10\bar{1})$ $Mg_{17}Al_{12}$

$[11\bar{2}0]$ α-Mg ∥ $[111]$ $Mg_{17}Al_{12}$
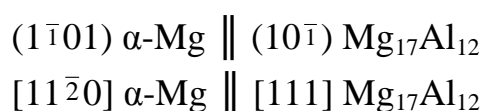
γ – $Mg_{17}Al_{12}$ phase precipitation have mostly a shape of rods and plates, a prevailing growing direction are the directions from the <110> family of the α-Mg phase (Figs. 40 & 41).Precipitation hardening has influence on mechanical

properties. The highest hardness increase, strength, yield point and the average mass loss value in tribologic investigations after ageing was found for the MCMgAl12Zn1 alloy. Corrosion resistance decrease of the investigated alloys occurs according to the increase of the phase content in magnesium matrix. The highest corrosion resistance has after the test in 3% water sodium chloride solution in as-cast material as well after heat treatment has the MCMgAl3Zn1 alloy.

The aim of the work on the effect of the laser surface melting microstructure and properties of the magnesium alloys is to achieve a quasi-composite MMCs structure onto the surface of elements produced from the magnesium alloys Mg-Al-Zn by appliance of high power diode laser (HPDL) remelting and alloying with carbide particles or ceramic particles like: TiC, WC, VC, SiC, NbC, Al_2O_3 . The aim is also to investigate the phase
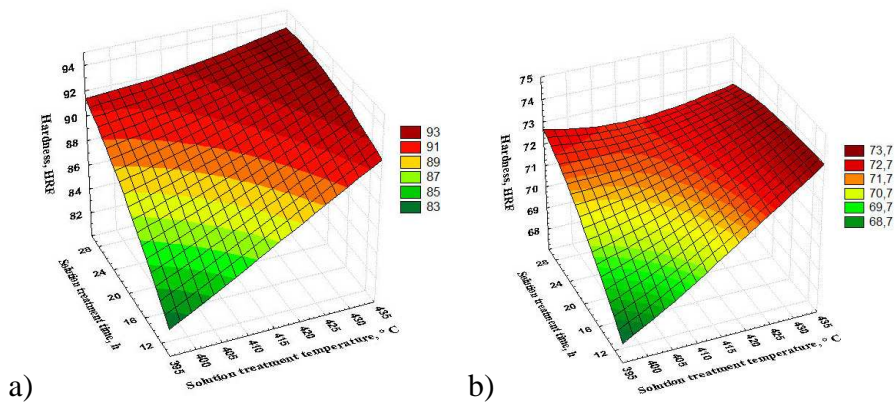
Fig. 39. Simulation of the temperature and solution heat treatment time influence on hardness of the: a) MCMgAl12Zn1, b) MCMgAl9Zn1 cast magnesium alloys by selected ageing temperature and time - 190°C and 15 hours, the results are achieved using a computer neural network simulation
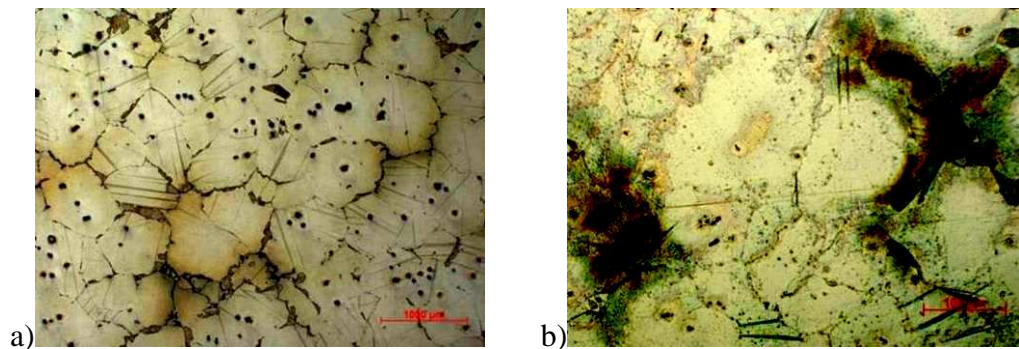

Fig. 40. Microstructures of a) MCMgAl9Zn1, b) MCMgAl6Zn1 alloys after aging treatment
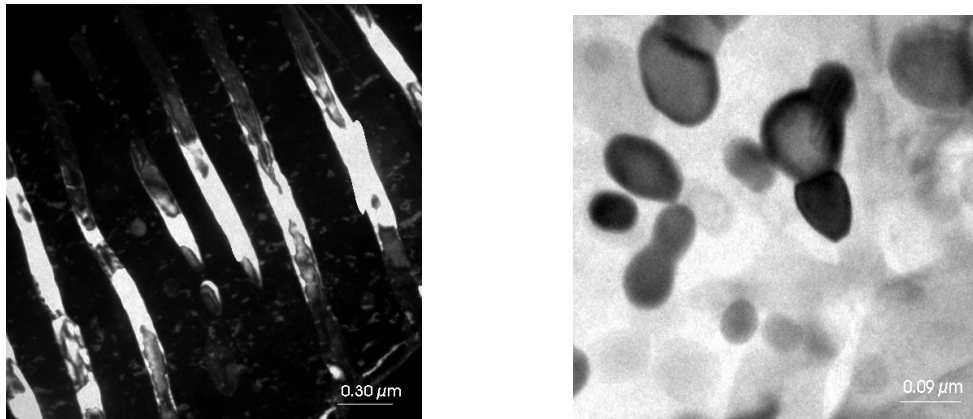
Fig. 41. TEM image examples of the intermetallic secondary phase γ – Mg₁₇Al₁₂ in the form of needle precipitations from the MCMgAl9Zn1 alloy after aging treatment

transformations and precipitations processes occurred after the laser alloying and remelting by properly chosen process parameters: laser power in the range between 0.5 to 2.2 kW, alloying/remelting rate in the range of 0.1 to 1 m/min as well as the type shielding gas. Investigations of the outcarried surface layers confirm that alloying of the surface layer of the Mg-Al-Zn casting magnesium alloys is feasible using the HPDL high power diode laser ensuring better properties compared to alloys properties after the regular heat treatment after employing the relevant process parameters. The structure of the remelted zone is mainly dendritic of primary magnesium with eutectic of phase α-Mg and intermetallic phase γ-Mg₁₇Al₁₂ (Figs. 42 & 43).
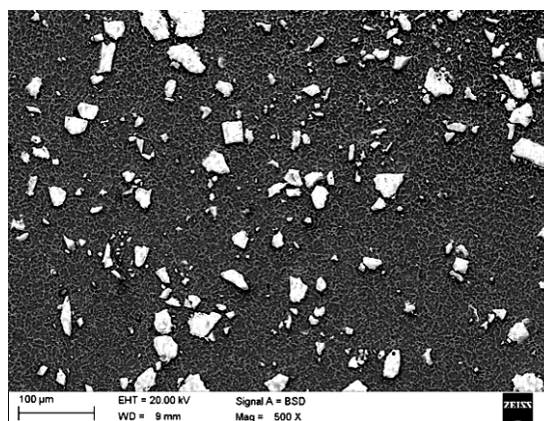

Fig. 42. Scanning electron microscope micrograph of laser modified surface of MCMgAl9Zn1 alloy with TiC particles of the central modified zone, scan rate: 0.75 [m/min], laser power: 1.6 [kW]
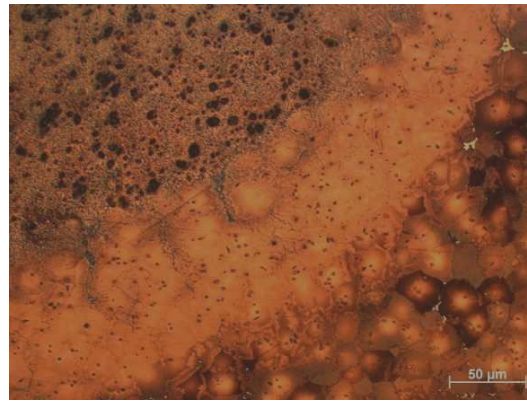
Fig. 43. Boundary between the RZ, HIZ and substrate of the MCMgAl12Zn1 alloy after alloying with WC powder, laser power 2.0 kW, scan rate 0.75 m/min

Magnesium alloys with aluminium concentration 9 and 12 wt. % reveal a heat affected zone in opposition to alloys with aluminium concentration 3 and 6 wt. %. Surface layers fabricated by alloying with VC, TiC, WC, SiC and Al_2O_3 the casting magnesium alloys (MCMgAl12Zn1 and MCMgAl9Zn1) demonstrate the clear effect of the alloyed material, parameters of the alloying process, and especially of the laser beam power and type of the ceramic particles on structure of the surface layers (Figs. 42 & 43). Due to laser alloying structure develops with the clear refinement of grains containing mostly the dispersive particles of the carbide and oxide distributed in the casting magnesium alloy matrix.

The purpose of the work on structure and properties of laser alloyed hot-work tool steels is focused on the X40CrMoV5-1, 32CrMoV12-28, 55NiCrMoV7, X38CrMoV5-3 hot work tool steels surface layers improvement properties using HPDL laser. Investigations indicate the influence of the alloying carbides on the structure and properties of the surface layer of investigated steels depending on the kind of alloying carbides and power implemented laser (HPDL). Laser alloying of surface layer of investigated steels without introducing alloying additions into liquid molten metal pool, in the whole range of used laser power, causes size reduction of dendritic microstructure with the direction of crystallization consistent with the direction of heat carrying away from the zone of impact of laser beam (Fig. 44). In the effect of laser alloying with powders of carbides WC, NbC, VC, TiC or TaC size reduction of microstructure as well as dispersion hardening through fused

in but partially dissolved carbides and consolidation through enrichment of surface layer in alloying additions coming from dissolving carbides occurs. Introduced particles of carbides and in part remain undissolved, creating conglomerates being a result of fusion of undissolved powder grains into molten metal base. In effect of convection movements of material in the liquid state, conglomerates of carbides arrange themselves in the characteristic of swirl. Remelting of the steel without introducing into liquid molten pool the alloying additions in the form of carbide powders, causes slight increase of properties of surface layer of investigated steel in comparison to its analogical properties obtained through conventional heat treatment, depending on the laser beam power implemented for remelting (Fig. 45).
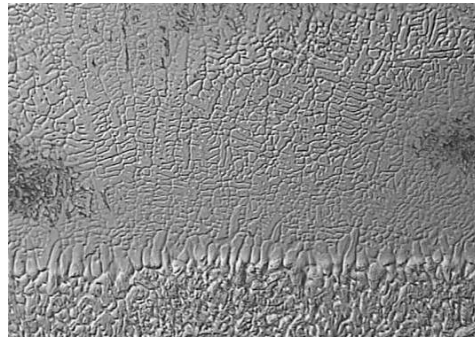

Fig. 44. Boundary of the remelted steel surface layer after alloying with parameters: scanning rate – 0.5 m/min, beam power – 1.5 kW, WC coating thickness – 0.11 mm
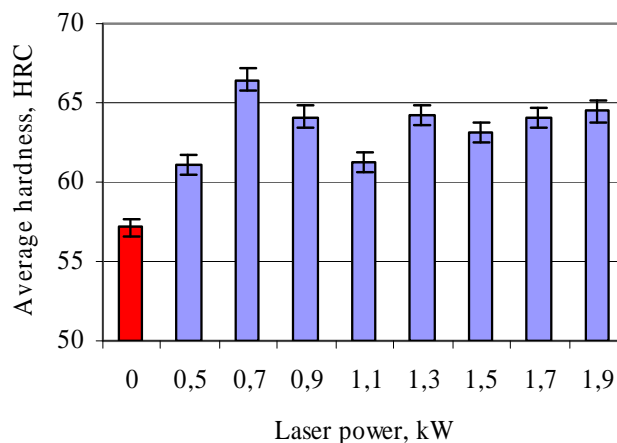

Fig. 45. Change of the average X40CrMoV5-1 steel surface layer hardness after alloying with the tungsten carbide of the 0.11 mm layer thickness with the variable power laser

The increase of hardness of surface layer obtained throughout remelting and alloying with carbides by high power diode laser is accompanied by increase of tribological properties, when comparing to the steel processed with conventional heat treatment. The artificial neural networks were used to determine the effect of the technological effect of laser alloying on hardness and resistance wear abrasion of the hot work tool steels. The outcome of the research is an investigation and proving the structural mechanisms accompanying laser remelting and alloying. It has the important cognitive significance and gives grounds to the practical employment of these technologies for forming the surfaces of new tools and regeneration of the used ones.

The purpose of work on laser surface remelting and alloying of sintered austenitic stainless steels deal with the microstructure and properties of laser remelted surface of wrought and sintered austenitic stainless steels type 316L. The laser treatment was performed with the use of high power diode laser (HPDL) and the influence of beam power of 0.7-2.1 kW on the properties of the surface layer was evaluated. The remelting process influences the microstructure refinement and formation of cellular-dendritic crystals with the microsegregation at the solidified cell boundaries in microstructure of stainless steel. The microsegregation of chromium at cell walls was not sufficiently high to form delta ferrite phase, as confirmed by performed X-ray analysis. The increase of laser beam power of LSR process resulted in the increase of hardness of sintered stainless steel due to strain hardening of refined microstructure and porosity reduction. In case of the wrought material the remelting results in remarkable decrease of roughness while in case of sintered material it slightly increases with the laser beam power. The corrosion resistance of remelted surface increased for sintered material when remelted at 2.1 kW. The wrought stainless steel revealed impairment of pitting corrosion when remelted at lower beam power and also comparing to the initial state. Taking into account the obtained results, the additional surface finishing treatment is indispensable to ensure the proper corrosion resistance of remelted surfaces. The studies of the effect of laser surface alloying with Cr on the

microstructural changes and properties of vacuum sintered 316L have been also performed. The influence of laser alloying conditions, both laser beam power and powder feed rate (1.0-4.5 g/min) at constant scanning rate of 0.5 m/min on the width of alloyed surface layer, penetration depth, microstructure evaluated by LOM, SEM, X-ray analysis, surface roughness and microhardness are performed. The microstructures of Cr laser alloyed surface consist of different zones, starting from the superficial zone rich in alloying powder particles embedded in the surface; these particles protrude from the surface and thus considerably increase surface roughness. The next one is alloyed zone enriched in alloying elements where both ferrite and austenite simultaneously occur. The following transient zone is located between properly alloyed material and the base metal and can be considered as a very narrow HAZ zone.

The optimal microstructure homogeneity of Cr alloyed austenitic stainless steel was obtained for powder feed rate of 2.0 and 4.5 g/min and laser beam power of 1.4 kW and 2 kW. Obtained results are very promising in respect of possible application of HPDL laser in surface alloying for sintered stainless steels. Despite of lower thermal conductivity of sintered steel comparing to wrought one they are still easy to process by laser treatment. Produced alloyed layers are uniform and flat without any visible undercuts or superficial cracks. The high surface roughness requires the application of final surface finish treatment but obtained penetration depth is sufficient to perform it. The microstructure of alloyed layer is composed of austenite and maximally 38% of ferrite with variable Cr content between 22-29%. The alloying process influenced the microstructure refinement and formation of cellular-dendritic crystals with the Cr microsegregation at the solidified cell boundaries. The fully alloyed Cr zone also consists of massive ferritic grains with the needle-like austenite precipitations on the grain boundaries (Fig. 46). Laser surface alloying can be an efficient method of surface layer modification of sintered stainless steel and by this way the surface chromium enrichment can produce microstructural changes affecting both mechanical and corrosion properties. Application of high power diode laser can guarantee uniform heating of treated surface, thus uniform thermal cycle across treated area and uniform penetration depth of chromium alloyed surface layer.

Austenitic steels, mainly high-manganese austenitic TWIP, TRIP and TRIPLEX steels, are the objects of interest in respect of application among others in the automotive industry. The aim of the work is to determine the high-manganese austenite propensity to twinning induced by the cold working and its effect on structure and mechanical properties, and especially on the strain energy per unit volume of ten new-developed high-manganese Fe – Mn – (Al, Si) investigated steels, including six selected high-manganese austenitic TWIP steels containing 25-27.5% Mn, 1-4% Si, 2-3% Al, two high-manganese TRIP
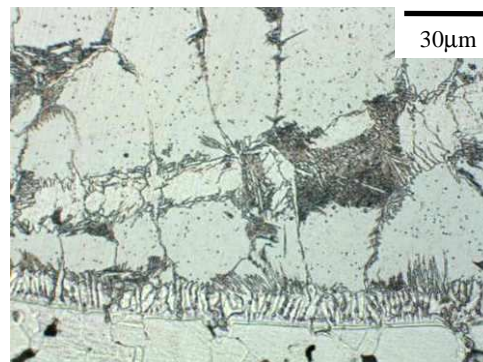
Fig. 46. The central zone of 316L laser alloyed with Cr at laser beam power 2.0 kW and powder feed rate of 4.5 g/min

steels containing 17-18% Mn, about 1% Si, about 3% Al and two selected high-manganese TRIPLEX steels containing 24% Mn and about 11% Al and some of that steels with Nb and Ti microadditions, with various structures after their heat- and thermo-mechanical treatments. New-developed steels achieve profitable connection of mechanical properties, i.e. (ultimate tensile strength) UTS~800-1000 MPa, (yield strength) $YS_{0.2}$ = 250-450 MPa, and plastic (uniform elongation) UEl = 35-90%, and moreover, particularly strong formability and strain hardening occurring during forming. The new-developed high-manganese Fe – Mn – (Al, Si) steels provide an extensive potential for automotive industries through exhibiting the twinning induced plasticity (TWIP) and transformation induced plasticity (TRIP) mechanisms for the fracture counteraction. TWIP steels not only show excellent strength, but also have excellent formability due to twinning, thereby leading to excellent combination of strength, ductility, and formability over conventional dual phase steels or transformation induced plasticity TRIP steels. In order to develop

automotive steels with excellent properties for CO_2 reduction into the environment and increased efficiency, thus, researches on identifying and understanding these mechanisms are highly required. The microstructure evolution in successive stages of deformation was determined in metallographic investigations using light, scanning and electron microscopes as well as X-ray diffractometre. Results obtained for new-developed high-manganese austenitic steels with the properly formed structure and properties in the heat treatment- or thermo-mechanical processes indicate the possibility and purposefulness of their employment for constructional elements of vehicles, especially of the passenger cars to take advantage of the significant growth about 25% of their strain energy per unit volume (Fig. 47) which guarantee reserve of plasticity in the zones of controlled energy absorption during possible collision resulting from activation of twinning for TWIP steels (Fig. 48), supported with martensitic transformation for TRIP steels, induced cold working which may result in significant growth of the passive safety of these vehicles' passengers.

The wide area of interests is photovoltaic materials and technologies. In laser technology it is possible to apply for texturisation of polycrystalline silicon surface for solar cells. Laser texturing constitutes an attractive alternative for other conventional texturing methods. The material used for experiments was commercially available boron doped p-type polycrystalline silicon wafers obtained from the ingot by wire sawing of thickness ~330 μm, area 5 cm x 5 cm and resistivity 1 Ωcm.
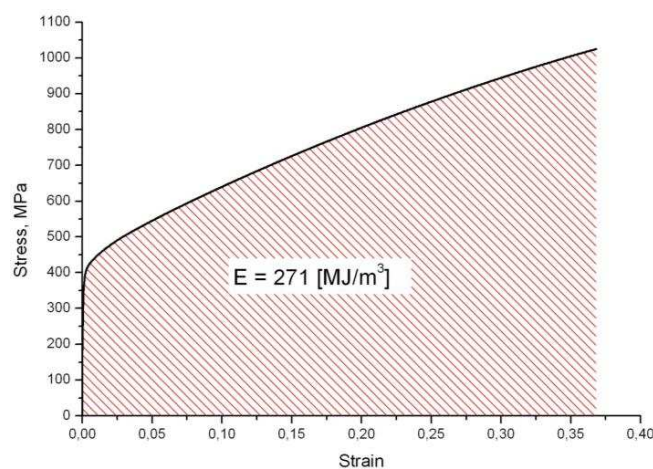

Fig. 47. Mechanism of twinning by the cold working of the high-manganese austenitic steels results in growth of the strain energy per unit volume
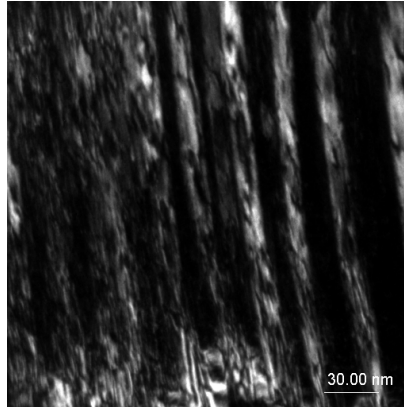
Fig. 48. Austenitic structures with mechanical twins obtained after hot-rolling with a true strain 0.29 and after static tensile test

To minimise reflection losses from the front surface texturisation of wafers by means of ALLPRINT DN50A Q switched Nd:YAG laser was performed. Successive grooves were scribed with constant spacing within consecutive scanning the wafer surface by laser beam in the opposite directions. Many trials for different values of laser parameters were carried out. It seems that presented laser texturing method may be successfully incorporated into production line of high-tech polycrystalline silicon solar cells. Solar cells (Fig. 49a) require good reflection control to minimise the amount of light lost at the front surface. This is typically achieved with combination of antireflection coating and surface texturing. Most conventional methods used for texturisation of monocrystalline silicon are ineffective when applied for texturing polycrystalline silicon. This is consequence of diversified susceptibility of regions of different crystalographic orientation to surface texturisation. As a result texture obtained by means of these methods is not uniform. Texturing of polycrystalline silicon surface using Nd:YAG laser makes it possible to increase absorption of the incident solar radiation. Moreover, the additional technological operation consisting in etching in 20 % KOH solution at temperature 80°C allows for significant improvement in their electrical performance compared to cells produced from the non-textured wafers after saw damage removal as well as wafers textured by etching in 40 % KOH:IPA:DIH$_2$O solution. With the appropriate selection of the laser processing conditions the uniform texture corresponding to parallel grooves and

criss-cross grooves can be produced (Figs. 49b & 49c). Solar cells produced from laser-textured polycrystalline silicon wafers demonstrate worse electrical performance than cells manufactured from the non-textured wafers after saw damage removal as well as wafers textured by etching in alkaline solutions. Those results from the laser induced defects introduced into the laser-processed layer that reduce electrical quality of textured silicon surface limiting performance of the cells. Etching of textured surface in 20 % KOH solution at temperature 80°C subsequent to laser processing shows to have a greatly increased impact on electrical performance of solar cells. However, continued etching to remove laser induced defects caused the texture to flatten out reducing its optical effectiveness.

The work on laser application in monocrystalline silicon solar cell fabrication shows that laser micro-machining of silicon elements of solar cells from different morphology monocrystalline silicon including selective laser sintering of the front contact to its surface using CO_2 laser influences the quality improvement by minimisation of the resistance of a joint between the contact and substrate. The influence of therefore obtained front contact on electrical properties of solar cells was estimated. This work investigates the front contacts formation using silver pastes (based on nano powder). Front metallisation is one of the process operations for the production of solar cells. Currently in the world different metal contacts fabrications methods in order to improve the electrical properties of contacts fingers are analysed. Selective laser sintering (SLS) is a manufacturing method that uses a high-heat laser to melt powder into a given before into a programme shape. The investigations were done on monocrystalline silicon wafers. In the Table 3 the material properties of silicon used in this work are presented. A special test structure to evaluate the contact resistance of the metal-semiconductor junction is prepared. Front contacts are formed on the surface with different morphology. Both surface topography using SEM (Fig. 50a) and CLSM (Fig. 50b) microscope and cross section of front electrodes using SEM microscope are investigated. The phase composition analyses of chosen front electrodes are done using the XRD method. The medium size of the pyramids was measured using the atomic force microscope (AFM).

Table 3 - The properties of silicon

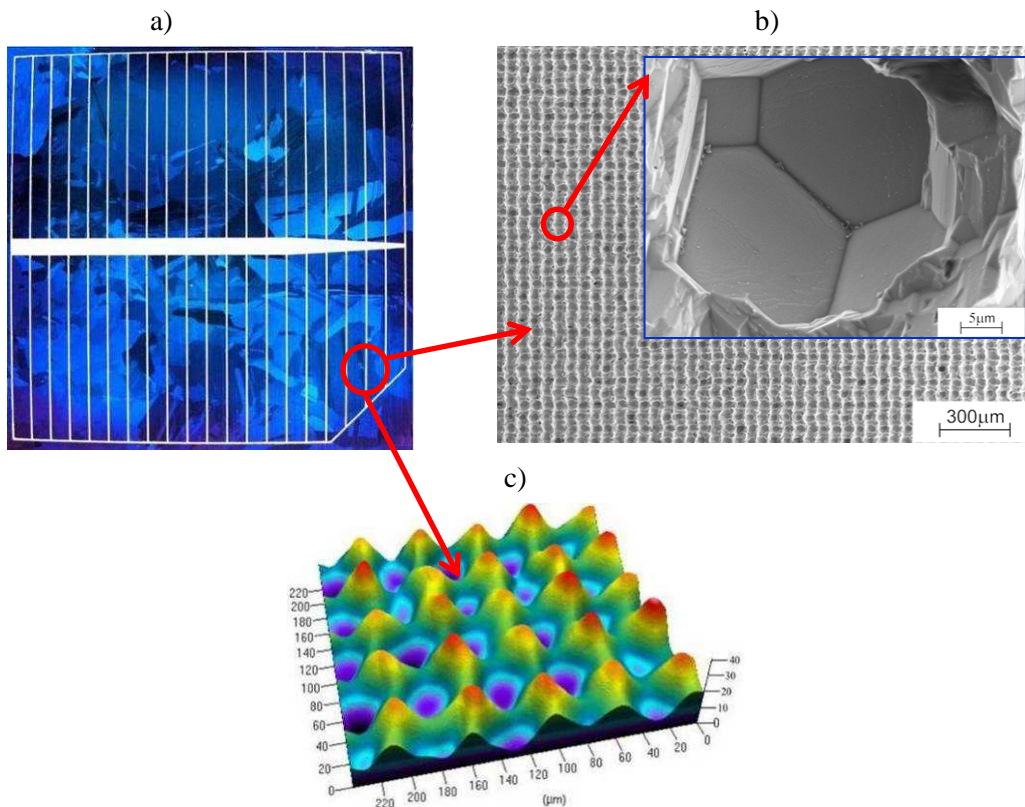| Type	p
Doped	boron
Thickness	200 ± 30 μm
Area	5 cm x 5 cm
Resistivity	1-3 Ω·cm

a)   b)

c)

Fig. 49. a) Polycrystalline silicon solar cells, b) SEM micrograph of texture corresponding to grid of grooves after removal of distorted layer of thickness 40 μm, c) 3D confocal laser scanning microscope topography of texture corresponding to grid of grooves after removal of distorted layer of thickness 40 μm

Resistance of front electrodes is investigated using Transmission Line Model (TLM). The following technological recommendations of the laser micro-machining technology such as optimal paste composition, the power and scanning speed of the laser beam, morphology of the silicon substrate, to manufacture the front electrode of silicon solar cells are experimentally selected in order to obtain uniformly melted structure well adhered to substrate, of a small front electrode substrate joint resistance value.
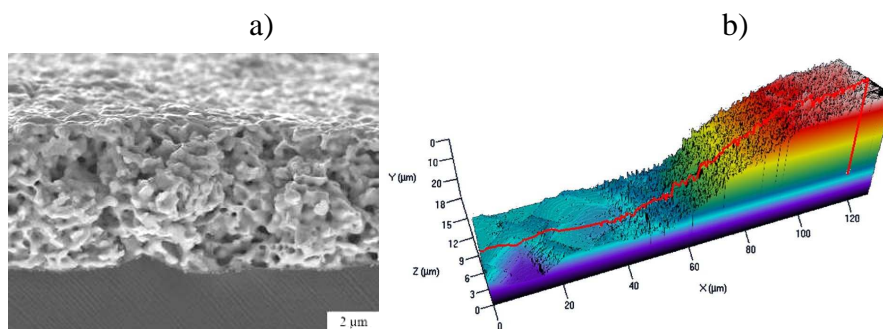
a)　　　　　　　　　　　　　b)

Fig. 50. a) SEM fracture image and b) CLSM three-dimensional surface topography of front electrode performed from standard PV 145 paste on the surface without texture and with ARC layer, co - fired in the furnace in 920°C temperature (chosen example)

The work on studying of thin films of organic compounds in photovoltaic applications presents the examined effect of the parameters of vacuum evaporation and chemical composition on the optical properties and surface morphology of the thin films of blends phthalocyanine - perylene derivative. These layers determine a bulk p-n junction which can significantly increase the efficiency of organic solar cells. The major aim of this work is to develop the technical conditions of fabrication bulk p-n junction in thin films using the thermal evaporation techniques. Thin films of organic mixtures composed of perylene-3,4,9,10-tetracarboxylic-dianhydride (PTCDA) and titanyl - phthalocyanine (TiO-Pc) or nickel -phthalocyanine (Ni-Pc) were deposited by vacuum thermal evaporation under vacuum of 10^{-5}hPa on glass substrate at room temperature (Fig. 51). Deposition technologies use evaporation from single and double sources. These mixtures of different proportions were evaporated using different temperatures. Obtained results indicate that surface topography and optical properties of layers obtained depend largely on the composition of the mixture derivative perylene - phthalocyanine, phthalocyanine type used and the evaporation rate. Research is led to the obtain of optimal parameters of evaporation process to obtain layers with the highest quality. The development of this technology also allows for material savings and minimising the cost of the process. To further study the organic layer blends composed of PTCDA and TiO-Pc or Ni-Pc that reveal the most promising properties of the surface topography and optical will be inserted between the

anode (ITO composition of PEDOT-PSS layer anda) and aluminium cathode in order to evaluate their photovoltaic properties.

Concluding this paper it is necessary to remark that the interesting area of the scientific researches of the Institute of Engineering Materials and Biomaterials of the Silesian University of Technology in Gliwice, Poland is very wide. In an opinion of the Author presented examples are representative for an explanation of a high level of the outworking researches and could give the imagination about the applied scientific methodology and about outstanding achievements of the Institute academic staff in the area of the forming of the structure and properties of engineering materials including biomaterials, their properties testing and microstructure characterisation and modelling, simulation and prediction of the properties and structure of these materials after selected materials processing technologies.
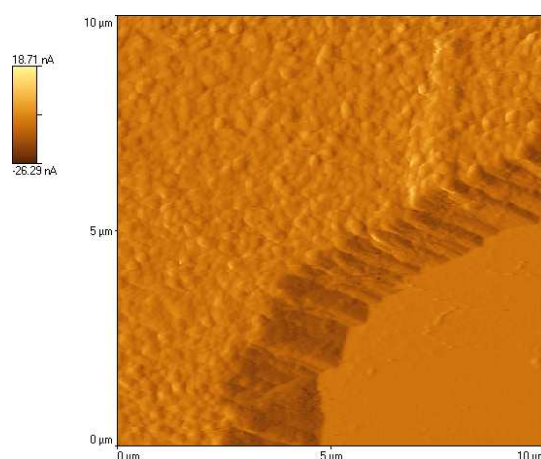

Fig. 51. AFM image of thin film composed of PTCDA/ TiO-Pc mixture

7.2 ILOŚĆ UWOLNIONYCH PRODUKTÓW ZUŻYCIA CEMENTU I TRZPIENIA SZTUCZNYCH STAWÓW BIODROWYCH WELLERA USUNIĘTYCH Z POWODU ASEPTYCZNEGO OBLUZOWANIA PANEWEK

Cwanek J.[1], Liubymov V.[1]

Wprowadzenie

Endoprotezy stawu biodrowego, w porównaniu z naturalnymi stawami znacznie szybciej ulegają zużyciu i nie regenerują.. Po przekroczeniu „bezpiecznego" progu zużycia, występuje aseptyczne obluzowanie stawu. Jest to najczęstsze niepowodzenie endoprotezoplastyki [4, 7, 8, 10, 17].

Zużycie endoprotez stawu biodrowego uzależnione jest od wielu znanych i nieznanych czynników biologicznych oraz biomechanicznych [1, 4, 6, 7, 9, 16]. Dotychczas nie udało się zminimalizować ilości wytwarzanych produktów zużycia oraz na trwałe połączyć elementów sztucznego stawu z żywymi tkankami [3 – 6, 10]. Poznanie mechanizmów zużycia cementu i trzpienia pozwoli na pogłębienie wiedzy z zakresu eksploatacji endoprotez oraz na poznanie niektórych z przyczyn aseptycznych obluzowań sztucznych stawów biodrowych.

W literaturze przedmiotu nie natrafiono na opracowania podające ilość uwolnionych produktów zużycia endoprotez Wellera, jak również innych modeli sztucznych stawów biodrowych eksploatowanych w warunkach naturalnych.

1. Cel pracy

Celem pracy jest podanie ilości uwolnionych produktów zużycia cementu i trzpienia endoprotez Wellera eksploatowanych w warunkach naturalnych oraz udzielenie odpowiedzi na pytanie - czy procesy zużycia trzpienia i cementu przebiegają z jednakową intensywnością podczas eksploatacji endoprotez w warunkach naturalnych.

2. Materiał badań

Materiał badań stanowiły 23 powierzchnie trzpieni sztucznych stawów biodrowych Wellera oraz 23 powierzchni cementów kostnych

---

[1] Wydział Medyczny Uniwersytetu Rzeszowskiego, Wydział Budowy Maszyn i Lotnictwa Politechniki Rzeszowskie

współpracujących z trzpieniami usuniętymi z powodu aseptycznego obluzowania polietylenowych panewek.

Uwzględniając okres eksploatacji sztucznych stawów Wellera, badany materiał podzielono na grupy:

- I grupa – czas eksploatacji endoprotez wynosił od 1 – 2 lat,
- II grupa – czas eksploatacji endoprotez wynosił od 6 – 8 lat,
- III grupa – czas eksploatacji endoprotez wynosił od 10 – 12 lat,
- IV grupa – czas eksploatacji endoprotez wynosił od 18 – 20 lat.

Przedstawiony podział na grupy podyktowany był pozyskiwanym materiałem przez autorów opracowania.

Dla celów porównawczych wykonano skaningi 5 nieeksploatowanych trzpieni endoprotez Wellera oraz 5 nieeksploatowanych cementów. Nieeksploatowane powierzchnie zaliczono do grupy 0 (zerowej), które. traktowano jako wzorzec podczas porównania z powierzchniami eksploatowanymi.

Liczbę zbadanych nieeksploatowanych i zużytych powierzchni trzpieni oraz cementu kostnego, w poszczególnych grupach, przedstawia tabela1. W nawiasach podano średni czas eksploatacji w grupie oraz odchylenie standardowe w latach.

Tabela 1 - Liczba skanowanych powierzchni trzpieni oraz cementów kostnych w grupach

grupa	czas eksploatacji endoprotez Wellera w latach (średni czas i odchylenie standardowe)	ilość badanych próbek	
		trzpieni	cementu
0	0 (0)	5	5
I	1 - 2 lat (x = 1,7; s = 0,5)	5	5
II	6 – 8 lat (x = 7,1; s = 0,8)	6	6
III	10 – 12 lat (x = 10,7; s = 1,0)	7	7
IV	18 – 20 lat (x = 19,2; s = 0,8)	5	5
suma		28	28

3. Metodyka wykonywania pomiaru parametru Smmr

Bezpośrednio po operacyjnym usunięciu endoprotezy Wellera, trzpienie i cementy myte były miękką szczotką. Przeznaczone do badania powierzchnie

zabezpieczono taśmą chroniącą przed przypadkowymi mechanicznymi uszkodzeniami.

Przed skanowaniem wszystkie powierzchnie przecierano spirytusem i oglądano przez szkło powiększające w celu sprawdzenia, czy nie ma na nich zabrudzeń lub uszkodzeń. Badano parametr powierzchniowy i objętościowy Smmr [w mm^3/mm^2], który umożliwia na obliczenie, w sposób pośredni, ilości uwolnionych produktów zużycia podczas eksploatacji endoprotezy. Metodykę obliczenia materiału podano w rozdziale 5.

Badania powierzchni trzpieni i cementu kostnego wykonano w Katedrze Technik Wytwarzania i Automatyzacji Politechniki Rzeszowskiej aparatem Rank Taylor Hobson - model Talyskan 150 (rys.1).

Rys. 1. Aparat Rank Taylor Hobson, model Talyskan 150

Skanowano powierzchnie o wymiarach od 1,0 do 4,0 mm^2 (przy prędkości przesuwu czujnika 500 μm/s i kroku próbkowania 2 μm):

1. Trzpienie - pod kołnierzem endoprotezy (rys. 2).

2. Powierzchnie cementu współpracujące z trzpieniem pod kołnierzem endoprotezy.

Rys. 2. Badania powierzchni trzpienia endoprotezy Wellera

Wyniki profilogramów poddano obróbce komputerowej za pomocą programu TALYMAP Expert 2.0 firmy Taylor Hobson oraz za pomocą arkusza kalkulacyjnego Microsoft Office Excel 2003. Przedstawiono zależności zmian wielkości parametru Smmr trzpieni i cementu kostnego od czasu eksploatacji endoprotez, wyznaczono linie trendów oraz współczynnik korelacji. Obliczono średnie arytmetyczne oraz odchylenia standardowe parametru Smmr powierzchni trzpienia i cementu dla każdej grupy oraz ilość uwolnionych produktów zużycia w mm^3.

4. Metodyka obliczenia ilości uwolnionych produktów zużycia trzpienia i cementu

Miarą zużycia objętościowego Q_j na powierzchni 1 mm^2 jest różnica pomiędzy średnią wartością liczbową parametru nieeksploatowanych powierzchni [Smmr$_{(0)}$] a średnimi wartościami badanych grup [Smmr$_{(j)}$].

Przyjęto założenie, że intensywność zużycia na całej czynnej powierzchni głowy, trzpienia i cementu jest jednakowa. Dla sprawdzenia wiarygodności tej tezy, wykonano dodatkowo pomiary parametrów SGP w innych miejscach od podanych w rozdziale 4. Rozrzuty odchyłek parametrów wysokościowych nie przekraczał 10% i mieściły się one w granicach dopuszczalnego błędu [14, 18]. Ocenę ilościowego zużycia powierzchni przy pomocy parametru Smmr przedstawia rysunek 3.

Źródłem danych do obliczeń według wzoru (4.1) są wartości liczbowe średnich arytmetycznych trzpieni i cementów kostnych (tabela 2)

$$Q_j^{'} = Smmr_{(0)} - Smmr_{(j)}, \qquad (4.1)$$

a)

b)

c)
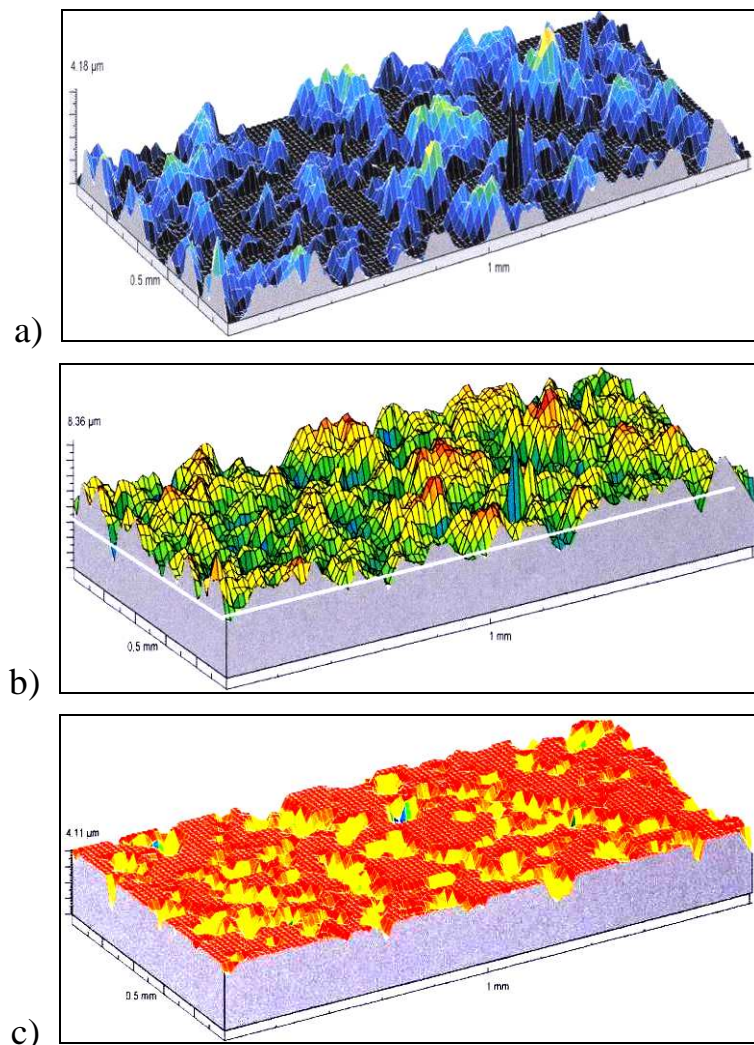
Rys. 3. Metodyka oceny ilościowego zużycia powierzchni: b) nieeksploatowana powierzchnia, a) materiał uwolniony w trakcie „i" lat eksploatacji (powyżej białej linii), c) powierzchnia zużyta w trakcie „i" lat eksploatacji (poniżej białej linii)

Sumaryczną objętość zużytego materiału obliczono ze wzoru:

$$Q_j = Q_j' \, S, \qquad (4.2)$$

gdzie S – jest powierzchnią eksploatowaną (zużytą).

Powierzchnie trzpienia i cementu, będące w bezpośrednim styku, są sobie równe. Obliczenie powierzchni wykonano wg wzoru:

$$S = S_1 \, k, \qquad (4.3)$$

gdzie S_1 – jest to powierzchnia styku cementu z trzpieniem obliczona na podstawie wymiarów trzpienia średniowymiarowego, k współczynnik uwzględniający niepełny kontakt trzpienia z cementem, który wynosi 0,65 [6]. Powierzchnia styku średniowymiarowego trzpienia z cementem zamyka się w granicach około 2.200 mm^2.

5. Wyniki badań

Średnie wartości oraz odchylenia standardowe parametru Smmr powierzchni cementu i trzpieni usuniętych z powodu aseptycznego obluzowania polietylenowych panewek endoprotez Wellera w badanych grupach przedstawia tabela 2.

Tabela 2 - Wartości parametrów Smmr [w mm^3/mm^2] trzpieni i cementu usuniętych z powodu aseptycznego obluzowania polietylenowych panewek endoprotez Wellera w grupach

badana grupa (średni czas eksploatacji endoprotez w latach)	trzpień		cement	
	x	s	x	s
0 (0)	0,0345	0,0037	0,0492	0,0034
I (1,7)	0,0151	0,0008	0,0372	0,0028
II (7,1)	0,0126	0,0012	0,030	0,0038
III (10,7)	0,0074	0,0013	0,0176	0,0024
IV (19,2)	0,0049	0,00026	0,0126	0,00221

Z danych zawartych w tabeli 2 wynika, że największe wartości średnich arytmetycznych parametru Smmr trzpieni i cementu stwierdzono na nieeksploatowanych powierzchniach, które zmniejszały się w miarę wzrostu czasu eksploatacji endoprotez Wellera. W pierwszych 2 latach eksploatacji sztucznych stawów stwierdzono największe zmniejszenie wartości parametru Smmr badanych powierzchni trzpieni cementu.

Objętość uwolnionego materiału z 23 powierzchni cementu i 23 powierzchni trzpieni usuniętych z powodu aseptycznego obluzowania panewek w średnim okresie eksploatacji endoprotez Wellera w grupach podaje tabela 3.

Ilość uwolnionych produktów zużycia trzpienia i cementu zwiększała się w miarę wzrostu czasu eksploatacji endoprotez Wellera. W pierwszych 2 latach

stwierdzono największe zużycie materiału (prawie 45 mm^3). Z trzpienia pochodziło znacznie więcej produktów życia (61%) aniżeli z cementu (39%).

Tabela 3 - Ilość uwolnionego materiału (w mm^3) z trzpienia i cementu kostnego w średnim okresie eksploatacji endoprotez w grupach

grupa (średni czas eksploatacji endoprotez w latach)	trzpień	cement	suma
I (1,7 lat)	27,7	17,2	44,9
II (7,1 lat)	31,3	27,5	58,8
III (10,7 lat)	38,7	45,2	83,9
IV (19,2 lat)	42,3	52,3	94,6

Po 2 latach eksploatacji endoprotez Wellera zaczęła wzrastać ilość uwolnionego cementu, zmniejszała się ilość uwolnionych drobin metalu z trzpienia. Po około 7 latach eksploatacji endoprotez objętość uwolnionego cementu była nieznacznie mniejsza w porównaniu z objętością uwolnionego metalu z trzpienia (z trzpienia pochodziło nieco ponad 53%, z cementu prawie 47%). Po około 11 latach eksploatacji sztucznych stawów ilość uwolnionego materiału z cementu była większa w porównaniu z ilością uwolnionych drobin metalu z trzpienia (z cementu pochodziło prawie 54%, z trzpienia ponad 46%). Po około 19 latach eksploatacji endoprotez z cementu pochodziło nieco ponad 55%, z trzpienia niecałe 45% objętości uwolnionych produktów zużycia.

6. Omówienie wyników badań i dyskusja

Podczas eksploatacji endoprotez wszystkie składowe sztucznego stawu ulegają zużyciu. Z danych przedstawionych w piśmiennictwie wynika, że najwięcej drobin pochodzi z panewki, według innych źródeł z cementu [3, 5, 8, 10, 12, 13]. Autorzy cytowanych prac nie podali objętości ani masy uwolnionych produktów zużycia.

Z przeprowadzonych badan wynika, że największa ilość produktów zużycia trzpienia oraz cementu uwolniona została w pierwszych 2 latach eksploatacji endoprotez Wellera. Koreluje to z badaniami zużycia technicznych węzłów tarcia ślizgowego w mechanice. W tym okresie znacznie więcej uwolnionych produktów zużycia pochodziło z trzpienia aniżeli z cementu.

Od 2 roku eksploatacji endoprotez Wellera wzrosła ilość uwolnionego cementu, zmniejszyła ilość uwolnionych drobin metalu z trzpienia. Tendencja ta utrzymywała się w późniejszych latach eksploatacji sztucznych stawów. Po około 7 latach eksploatacji ilość uwolnionych drobin z trzpienia było nieco większa od ilości uwolnionego cementu. Natomiast po11 latach eksploatacji endoprotez ilość uwolnionego materiału z cementu była większa w porównaniu z ilością uwolnionych drobin metalu z trzpienia.

Uzyskane wyniki badań potwierdzają spostrzeżenia poczynione przez innych autorów, że cement jest najsłabszym ogniwem endoprotez i nie spełnia stawianych mu wymagań [1, 9, 10, 15, 20]. Specyfika pracy sztucznego stawu wymusza przenoszenie bardzo złożonych i znacznych obciążeń wynikających z motoryki człowieka, co przyśpiesza zużycie cementu i prowadzi do osłabienie połączenia kość - cement - trzpień [2, 6, 20]. Następstwem tego jest aseptyczne obluzowanie trzpienia lub panewki endoprotezy [2, 6, 11,].

Prowadzone są badania mające na celu zwiększenie wytrzymałości zmęczeniowej oraz odporności na pęknięcia i ścieranie cementu [1, 9, 12, 15, 19, 20]. Poprawienie właściwości cementu wydłuży czas eksploatacji i zmniejszy ryzyko wystąpienia aseptycznych obluzowań endoprotez stawu biodrowego.

Uwolnione produkty zużycia nie ulegają neutralizacji, gdyż organizm człowieka nie posiada enzymów trawiących uwolnione drobiny trzpienia i cementu. Jedynie metale, w formie atomowej, wydalane są w niewielkich ilościach z moczem [19].

Uwolnione i zmagazynowane drobiny znajdujące się w płynie stawowym przyśpieszają resorpcję kości w okolicy sztucznego stawu oraz uruchamiają złożony łańcuch niezbyt dobrze poznanych reakcji niebakteryjnego zapalenia stawu oraz immunologicznych [3, 5, 16, 17, 19, 20]. Po przekroczeniu wydolności magazynowania produktów zużycia w przestrzeni stawowej, uwolnione drobiny naciekają otaczające tkanki, a następnie transportowane są przez naczynia krwionośne i chłonne do odległych narządów miąższowych (między innymi do wątroby, nerek, płuc i mózgu) [11, 16, 17, 19, 20].

Wnioski

1.   Największe wartości parametru Smmr stwierdzono na nieeksploatowanych powierzchniach trzpieni endoprotez Wellera oraz na nieeksploatowanych powierzchniach cementu, mniejsze na eksploatowanych powierzchniach. Proces ten nasilał się w miarę wzrostu czasu eksploatacji sztucznych stawów.

2.   Największa ilość produktów zużycia trzpienia oraz cementu uwolniona została w pierwszych 2 latach eksploatacji endoprotez Wellera. Więcej produktów zużycia pochodziło z trzpienia aniżeli z cementu.

3.   Po 2 latach eksploatacji endoprotez Wellera wzrosła ilość uwolnionych produktów zużycia cementu, znacznie zmniejszyła się ilość uwolnionych drobin z trzpienia.

4.   Wskazane jest poszukiwanie nowych materiałów do produkcji endoprotez stawów biodrowych oraz cementu w celu zminimalizowania ilość wytwarzanych produktów zużycia..

Referenses

1. Balin A.: Właściwości biomateriałów stosowanych jako wypełniacze w chirurgii kostnej, Biomechanika w Implantologii, Śląska Akademia Medyczna, Katowice 1999, supl. 29, 9.

2. Będziński R., Kędzior K., Kiwerski J., Morecki A., Skalski K., Wall A, Wit A.: Biomechanika i inżynieria rehabilitacyjna, Akademicka Oficyna Wydawnicza EXIT, Warszawa 2004.

3. Blanquaert D., Caton J.: Polyethylene in total hip prostheses wear, creep and ageing, Charnley Total Hip Arthroplasty, 33 years of world - wide experience, Groupe A.C.O.R.A., Lyon 1995, 117.

4. Clinical Review. Long term of the Charnley low – friction arthroplasty, proceed. Thackeray. Reconstructive Systems, Warsaw 1993.

5. Cooper J. R., Dawson D., Fischer J.: Macroscopic and microscopic wear mechanism in ultra – high molecular weight polyethylene, Wear, 1993, 162 – 164, 378.

6. Cwanek J.: Przydatność parametrów struktury geometrii powierzchni do oceny stopnia zużycia sztucznych stawów biodrowych, Wydawnictwo Uniwersytetu Rzeszowskiego, Rzeszów 2009.

7. Cwanek J., Czajkowski A.A., Lubimow W.: Overweight influence of patent body for aseptic loosening of Weller endoprosthesis, Journal of Vibroengineering, 2006, 2, 45.

8. Gierzyńska - Dolna M.: Oporność na zużycie materiałów stosowanych na endoprotezy, Mechanika w Medycynie, red. Korzyński M., Cwanek J., Rzeszów, Rzeszów, 1996, 3, 131.

9. Gierzyńska – Dolna M.: Biotribologia, Wyd. Politechniki Częstochowskiej, Częstochowa 2002.

10. Lee A.J., Ling R.S.M.M., Pearson G.P.: Fixation, in An introduction to the bio – mechanics of joints and joints replacement, red. Dawson D., Wright V., Mechanical Engineering Publication, London 1981, 17.

11. Marciniak J.: Biomateriały, Wyd. Politechniki Śląskiej, Gliwice 2002.

12. Maumy S. P.: The elastic prosthesis acetabulum. A new concept and design of an acetabular replacement, Hip International, 2001, 1, 42 – 46.

13. Nabrdalik M., Sobociński M., Gierzyńska – Dolna M.: Procesy zużycia zachodzące w elementach polietylenowych endoprotez, Mechanika w Medycynie, red. Korzyński M., Cwanek J., Rzeszów, 2006, 8, 151.

14. Oczoś E.K., Liubimov V.: Struktura geometryczna powierzchni, Oficyna Wydawnicza Politechniki Rzeszowskiej, Rzeszów 2003.

15. Palczewski D.: Właściwości mechaniczno – fizyczne cementu kostnego, Mechanika w Medycynie, red. Korzyński M., Cwanek J., Rzeszów, 2006, 8, 169.

16. Shanbhag A.S., Hasselman C.T., Jacobs J.J., Rubash H.E.: Biologic response to wear debris, w The adult hip, red. Callaghan J.J., Rosenberg A.G., Rubash H.E., Lippincott - Raven Publishers, Philadelphia 1998, 279.

17. Szmigiel A.: Rola produktów zużycia w patogenezie aseptycznego obluzowania endoprotez; skutki i implikacje kliniczne efektywnej przestrzeni stawowej, Kwartalnik Ortopedyczny, 2001, 1, 24.

18. Thomas T. R.: Rough surfaces, Imperial College Press, London 1999.

19. Wagner T.: Powikłania po artroplastyce i zmiany polekowe, w Patomorfologia stawów, red. Małdyk E., Wagner T., PZWL, Warszawa 1991, 199.

20. Włodarski J., Szyprowski J., Więckowski W., Szarek A.: Wpływ wypełniaczy na właściwości wytrzymałościowe kompozytowych cementów kostnych, Kompozyty, 2005, 4, 78.

7.3 SPEECH RECOGNITION BASED EVALUATION OF VOICE QUALITY IN TRACHEOESOPHAGEAL AND ESOPHAGEAL SPEECH

Mięsikowska M.[1], Radziszewski L.[1], Bień S.[2], Okła S.[2]

Introduction

Total laryngectomy is a surgical method that involves removal of the larynx, thereby depriving patients of the ability to generate speech sounds. Speech rehabilitation after laryngectomy is of paramount importance since the patient loses the ability to communicate verbally. The most common rehabilitation therapy involves teaching the patient how to produce an ESO voice. With the development of the tracheoesophageal puncture technique, the TRA speech has become a widely popular method of alaryngeal voice rehabilitation[1]. Both speeches use the pharyngoesophageal (PE) segment as the voicing mechanism, but differ in their air source. Traditional ESO speech is achieved by an intake of air into the pharynx through either injection or inhalation, causing the PE segment to vibrate. The TRA speech is achieved when pulmonary air is directed through prosthesis into the upper esophagus to vibrate the PE segment and to generate voice. This process provides increased air capacity and enables the TRA speaker to support speech with the respiratory system.

Voice quality is a perceptual phenomenon[2]. Apart from being expensive and time-consuming, another main disadvantages of perceptual evaluation is the fact that listeners differ in their opinion about the quality of voice. Acoustic measures computed digitally and obtained properly can form a valuable objective adjunct to perceptual evaluations, because they always produce the same result for the same signal input. Perceptual evaluations play a prominent role in therapy evaluation purposes in clinical practice[3]. Perceptual and acoustical analyses are the main methods of voice quality assessment. Traditionally, in voice assessment, perceptual analysis is considered a "proper standard" of voice quality evaluation[4]. Perceptual evaluations of laryngectomees have typically included measures of intelligibility, acceptability, or both. In general, acoustic time-based evaluations have included

[1] Kielce University Of Technology, Poland
[2] Holy Cross Cancer Centre, Poland

measures of duration, intensity, fundamental frequency, jitter, percentage of voiced, harmonics-to-noise ratio, glottal-to-noise excitation ratio, and band energy difference. Researchers have revealed that TRA speakers sustain longer phonation, produce more syllables per breath or insufflations, maintain faster speaking rates with less pause time, and speak with greater intensity than conventional ESO speakers[5]. Spectral analysis showed that formant frequencies play a key role in determining the intelligibility of natural speech and are likely to influence the perceived quality of TRA and ESO speeches[6]. On the basis of visual spectrographic characteristics four different types of TRA speech were distinguished[4].

In order to collect more information about different speech rehabilitation strategies, the aim of the research was to evaluate voice quality on the basis of speech recognition process. The process of speech recognition can be useful for the therapist in training the patient to achieve the high quality of voice. In addition, it allows the patient to check the percentage value of the recognition of their speech.

1. Methods

The samples of TRA and ESO speech signals were collected from patients of Holy Cross Cancer Centre - Department of Head and Neck Surgery in Poland. Patients aged 50-73, average age of 65 years old. Speech recordings were made in audiometric room in regular conditions. The speech sound was transmitted via a microphone with 22 kHz sampling rate, 16 bit signal resolution. Patients were in a sitting position; the mouth-to-microphone distance ranged from 0.35 to 0.40m. The speech samples for the purpose of the analysis consisted of six vowels /a, e, i, o, u, y/ repeated ten times. Three recordings were made of each patient. The research included vowels recognition, because the functioning of the vocal track can be evaluated on the basis of the articulation of vowels. The samples of NOR speech were collected from twenty students in regular conditions in the same settings as laryngectomized patients.

Voice quality was evaluated according to procedure presented on the block scheme illustrated in Fig.1.
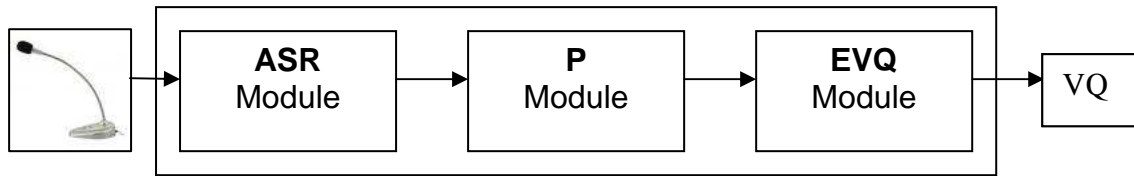
Fig. 1. The block scheme of evaluation model of voice quality.

The block scheme consists of three basic modules. The first module is responsible for the recognition of the vowels expressed by a speaker. It is called an automatic speech recognition (ASR) module. Second parameterization (P) module enables parameterization of recognition results obtained from the first module. Third module enables evaluation of voice quality (EVQ) on the basis of the parameters obtained from the second module.

The ASR module is based on cepstral parameters, DTW method as classifier and NOR speech pattern[7]. It consists of two parts. The first part enables extraction of cepstral features from a speech signal. The cepstral coefficients were calculated for a speech signal frame in the time domain. In this case the frame length was equal to 240 samples and the frame shift was equal to 180 samples. Twelve cepstral coefficients were calculated for each frame. The speech signal frame was multiplied by the Hamming window, which was followed by Fast Fourier transformation. The next step involved logarithmization of the spectral module with subsequent simple or reverse Fourier transform, which was expressed by the following formula:

$$c(n) = \frac{1}{N} \sum_{k=0}^{N-1} \ln | \sum_{m=0}^{N-1} w(m)x(m)e^{-j2\pi km/N} | e^{\pm j2\pi kn} , \qquad (1)$$

where:

$w(m)$ -Hamming Window, $x(m)$ - signal, N – the number of signal samples.

The second part consists of a DTW classifier, which assigns a definite signal of the alaryngeal speech to the NOR speech pattern[7]. The DTW method is based on the calculation of Euclidean distance matrix among every vector of cepstral parameters belonging to the phone recognized and every vector of the parameters of the pattern. The shortest path is sought in the matrix i.e. the path having the smallest accumulated value of the distance between the individual

vectors of the parameters of the phones recognized and the pattern along the road of the passage, joining the left, bottom take-off point with the right upper final point. The values obtained are the measure of the distance between the phones.

For example, if $C_s(n_s,k)=c_k^{(n_s)}$ is the phone matrix that has to be recognized

where $n_s=1...N_s$, $k=1...q$,

q - the number of calculated cepstral coefficients – in this case twelve,

and $C_w(n_w,k)=c_k^{(n_w)}$ is the pattern matrix

where $n_w=1...N_w$, $k=1...q$,

the new distance matrix $d(n_s,n_w)$ is calculated using formula (2). Each element of this new matrix equals to Euclidean distance between the phone cepstrum n_s and the pattern cepstrum n_w:

$$d(n_s,n_w) = \sqrt{\sum_{k=1}^{q}(C_s(n_s,k)-C_w(n_w,k))^2} \quad , \ n_s=1...N_s, \ n_w=1...N_w \qquad (2)$$

where N_s - the number of frames of the recognized phone,

N_w - the number of frames of the pattern.

The classification involves calculation of the shortest accumulated value between left, bottom take-off point and the right upper final point in the distance matrix. The accumulation means the sum of crossed values. The smaller the value, the closer is the phone to the pattern. The classifier allows the recognition of phones as well as words, and sentences.

Because of the variety of movements in the Euclidean distance matrix three limitations were introduced using formula(3):

- It is forbidden to move back.
- It is allowed to move only one position to the right, up or slant.
- It is allowed to limit the movements with lines.

$$g(n_s,n_w) = \min \begin{cases} g(n_s,n_w-1)+d(n_s,n_w) & up \uparrow \\ g(n_s-1,n_w-1)+2 \cdot d(n_s,n_w) & slant \ \nearrow \\ g(n_s-1,n_w)+d(n_s,n_w) & right \rightarrow \end{cases} \qquad (3)$$

The speech recognition system was implemented in a commercial programming language. The speech recognition results were estimated on the basis of descriptive statistics, punctual and interval estimators.

The efficiency of the proposed speech recognition system for each kind of speech was calculated with the following parameters:

1.   Speaker's Vowel Recognition Parameter (VR)– the value was calculated for each vowel of each speaker with formula (4):

$$V_{VR(S)} = \frac{numberOfrecognizedStatementsOfVowel}{numberOfAllStatementsOfVowel} \cdot 100\% \qquad (4)$$

where

$$V = a, e, i, o, u, y$$
$$S = 1, 2, ..., S_{max}$$

S_{max} – the number of speakers of analyzed speech.

For each speaker each vowel recognition results were calculated as follows:

$$a_{VR(S)} = \frac{\sum_{n=1}^{x} a_{VR}(n)}{n_{max}(=10)}, \; e_{VR(S)} = \frac{\sum_{n=1}^{x} e_{VR}(n)}{n_{max}(=10)}, \cdots, \; y_{VR(S)} = \frac{\sum_{n=1}^{x} y_{VR}(n)}{n_{max}(=10)} \qquad (5)$$

x – the number of correct recognized vowels, n_{max} - the number of vowels being recognized.

2.   Speaker Recognition Parameter(SR) - For each speaker the mean value was calculated for vowel recognition (each $V_{VR(S)}$ obtained for each vowel) – formula (6):

$$SR(S) = \frac{\sum_{v=a}^{y} V_{VR(S)}(v)}{6}, \qquad (6)$$

The efficiency of speech recognition system was evaluated by parameters

3.   SRVE (en. Speech Recognition - Vowel's Efficiency) calculated on the basis of the mean values obtained from the mean values of the each vowel's recognition results – formula (7a)

$$SRVE = \frac{\sum_{v=a}^{y} SRVE(v)}{6}, \ v = a, e, i, o, u, y \tag{7a}$$

where $SRVE(v)$ parameter for each vowel is calculated with formula (7b):

$$SRVE(a) = \frac{\sum_{S=1}^{S_{max}} a_{VR(S)}}{S_{max}}, \ SRVE(e) = \frac{\sum_{S=1}^{S_{max}} e_{VR(S)}}{S_{max}}, \cdots, SRVE(y) = \frac{\sum_{S=1}^{S_{max}} y_{VR(S)}}{S_{max}} \tag{7b}$$

or SRSE (Speech Recognition – Speaker's Efficiency) calculated on the basis of the mean values obtained from each recognition results of each speaker – formula (8)

$$SRSE = \frac{\sum_{i=S}^{S_{max}} SR(S)}{S_{max}} \tag{8}$$

4. The matrix expressed by formula (9) obtained from parameters calculated by first two modules is analyzed by the last EVQ module:

5.

$$\begin{bmatrix} a_{VR(1)} e_{VR(1)}, \ldots, y_{VR(1)} \\ a_{VR(2)} e_{VR(2)}, \ldots, y_{VR(2)} \\ \vdots \\ a_{VR(20)} e_{VR(20)}, \ldots, y_{VR(20)} \end{bmatrix} \begin{array}{l} \rightarrow SR(1) \\ \rightarrow SR(2) \\ \vdots \\ \rightarrow SR(S_{max}) \end{array} \tag{9}$$

$\downarrow SRVE(a), \ldots, \downarrow SRVE(y)$

Formula (9) presents also the idea of calculation of SR and SRVE parameter. The relationship between SRVE and SRSE parameter can be expressed by formula (10):

$$SRVE \cong SRSE \tag{10}$$

In this paper authors propose a new method of selecting the normal speech pattern based on speech recognition parameter (SRSE) applied to ASR module.

The pattern of normal speech was selected on the basis of the following criteria:

1. The highest value of the SRSE parameter with the smallest standard deviation.

2. There must be ten speakers who achieve 100% recognition (SR).

3. The acoustic parameters obtained for the sustained vowel /a/, such as mean fundamental frequency (mean pitch), Jitter value, Shimmer value, Noise-To-Harmonic Ratio must be similar to the parameters defined as normative. Normative values of parameters obtained for NOR speech signal gives for Jitter, Shimmer accordingly 1.040% and 3.810% as a threshold for pathology[8].

The evaluation of the voice quality by the EVQ module was based on the following parameters defined by the authors on the basis of speech recognition results:

1. High quality – means the correct voice that doesn't have to be rehabilitated – in this case the speech recognition results achieved by the speaker (SR) range between 70% and 100%. All values obtain by each speaker's vowel (VR) must equal at least 40%.

2. Medium quality – means the voice that has to be rehabilitated – in this case the speaker's recognition results (SR) range between 40% - 70%.

3. Low quality – means the voice that urgently needs rehabilitation – in this case the speaker's recognition results (SR) range between 0% - 40%.

In case that patient requires rehabilitation, the vowels recognition results can help the therapist train the patient in obtaining correct pronunciation of incorrectly classified vowels. In order to obtain vowels that are incorrectly pronounced by the speaker, the following parameters were defined by the authors on the basis of speech recognition results:

1. High vowel quality- means the correct vowel, valid pronunciation – in this case the speaker's vowel recognition results (VR) range from 70% to 100%.

2. Low vowel quality – means inacceptable vowel – in this case the speaker's recognition results (VR) range from 0% to 70%.

As a rule of thumb, one can assume that the closer is the speaker to the pattern, the better quality of the voice.

2. Results

In evaluation of voice quality the first step involves the selection of normal speech pattern. Mean values and trust levels of each speaker recognition (SRSE) obtained for each speaker applied as pattern were presented in Fig.2. The horizontal axis represents speakers applied as patterns. As illustrated in Fig.2 the third speaker (S3) obtained the best results.
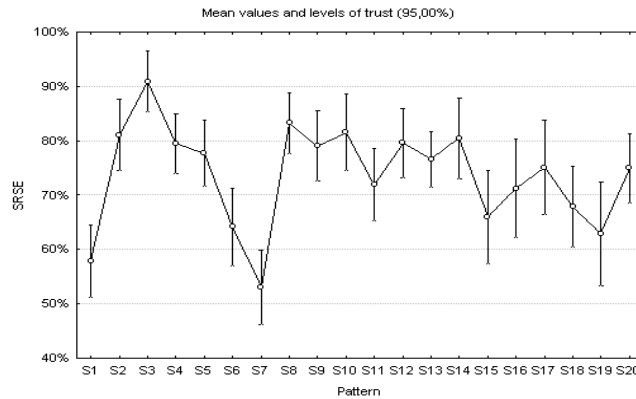

Fig. 2. SRSE value obtained for each speaker applied as pattern (S-Speaker).

The value of SRSE parameter of the third pattern (S3) equals 91% with 11% standard deviation between speakers, minimum 72% and maximum 100%. The values of parameter (SR) for all speakers, obtained by the third speaker (S3) applied as pattern are presented in Fig.3. Eleven speakers achieved 100% results of vowels recognition.
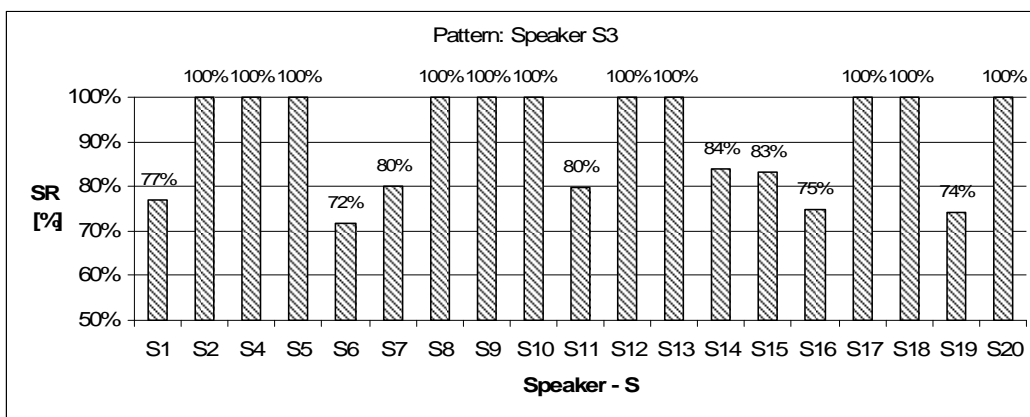
Fig. 3. Results of each speaker recognition (SR) obtained by the third speaker (S3) applied as pattern of normal speech (S mean speaker).

Acoustic parameters obtained from the third speaker (S3) were evaluated and are presented in Table 1.

Table 1 - Acoustical parameters of the sustained "a" vowel of the speaker (S3) selected as pattern.

Variable	Mean value	Trust -95%	Trust +95%	Min value	Max value	Standard deviation
Mean pitch [Hz]	108	104	112	105	110	2,79
Jitter (local)%	0,94	0,76	1,12	0,74	1,06	0,15
Shimmer (local)%	3,80	2,65	4,94	3,24	4,81	0,72
Mean NHR	0,24	0,20	0,28	0,22	0,27	0,02

The values are similar to normative one. The third speaker (S3) fulfilled all the criteria. The speaker (S3) can be regarded as normative one and be applied to the speech recognition system as pattern.

The best results of the vowel recognition of NOR, TRA and ESO speaker are illustrated in Fig.4.
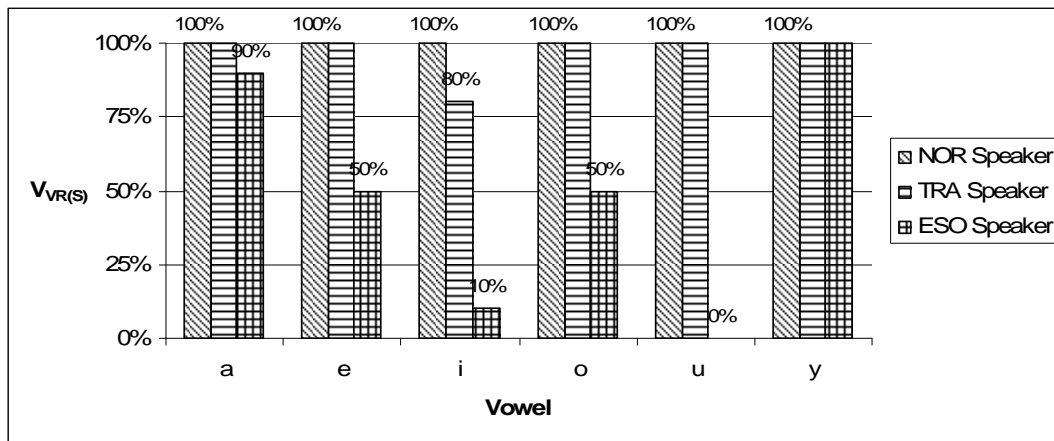
Fig. 4. The best obtained values of vowel recognition by NOR, TRA and ESO speaker.

Table 2 presents the evaluation of voice quality and the evaluation of vowel quality of the best recognized NOR, TRA and ESO speaker. The evaluations were estimated according to Fig. 4.

Table 2 - The evaluation of voice quality (VQ) and vowels quality (HQ-high quality, LQ-low quality) of the best recognized NOR, TRA and ESO speaker (SR). The value of standard deviation (S.D.) is obtained from the speaker's vowel recognition(VR) results.

Speaker	VQ SR	S.D. (VR)	Min VR	Max VR	HQ vowels	LQ vowels
NOR	100% HighQ	0%	100%	100%	a, e, i, o, u, y	-
TRA	97% HighQ	8%	80%	100%	a, e, i, o, u, y	-
ESO	50% MidQ	40%	0%	100%	a, e, o, y	i, u

The best TRA speaker was recognized in 97%. According to the defined parameters the speaker's voice can be evaluated as high quality (HighQ) voice. This TRA speaker doesn't require rehabilitation. All vowels were correctly pronounced. The best ESO speaker was recognized in 50%. The speaker requires rehabilitation, because the voice can be evaluated as medium quality (MidQ) voice, which means that the speaker has to improve pronunciation of those vowels that were recognized in less than 50% - Table 2, column LQ vowels.
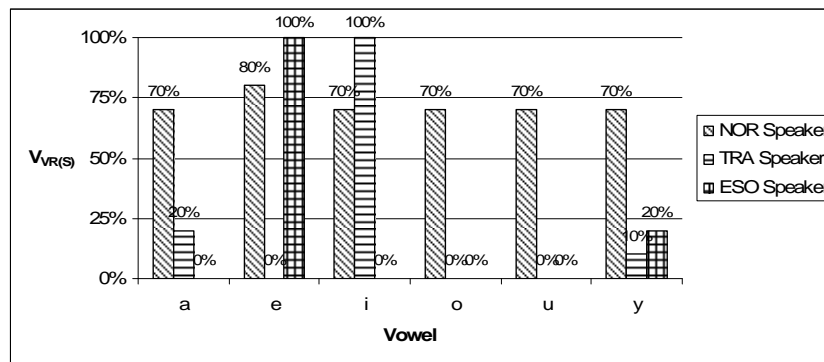
Fig. 5. The lowest results of vowel recognition of NOR, TRA and ESO speakers.

The lowest results of vowel recognition of NOR, TRA and ESO speakers are presented in Fig.5. Table 3 presents the evaluation of voice quality and evaluation of vowel quality of the lowest results of SR parameter obtained from NOR, TRA and ESO speakers. The evaluations were estimated according to Fig. 5.

Table 3 - The evaluation of voice quality (VQ) and vowels quality (HQ-high quality, LQ-low quality) of the lowest recognized NOR, TRA and ESO speaker (SR). The value of standard deviation (S.D.) is obtained from the speaker's vowel recognition results.

Speaker	VQ SR	S.D. (VR)	Min VR	Max VR	HQ vowels	LQ vowels
NOR	72% HighQ	4%	70%	80%	a, e, i, o, u, y	-
TRA	22% LowQ	39%	0%	100%	i	a, e, o, u, y
ESO	20% LowQ	40%	0%	100%	e	a, i, o, u, y

The NOR speaker was recognized in 72%. The TRA speaker was recognized in 22%. The ESO speaker was recognized in 20%. The TRA and the ESO speaker's voice can be classified as low quality (LowQ) voice group that requires rehabilitation. The correctly pronounced vowel by the TRA speaker was the /i/ vowel. In case of the ESO speaker the /e/ vowel was correctly pronounced.
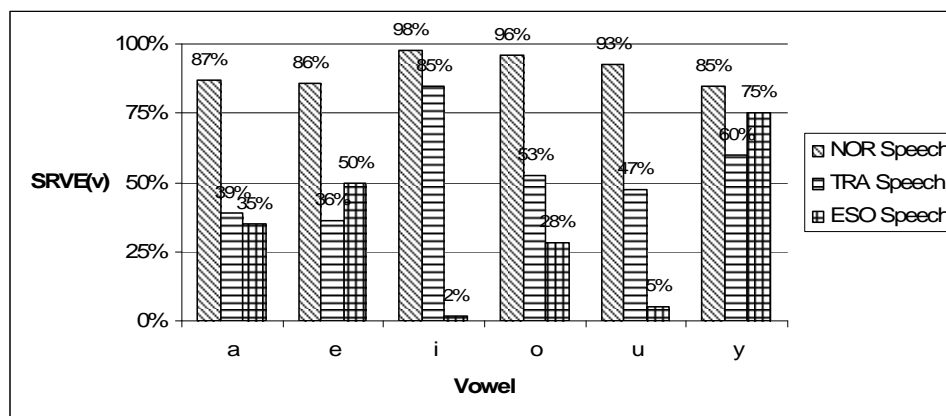
Fig. 6. Mean values of vowels recognition of NOR, TRA and ESO speech.

The mean values of vowels recognition of NOR, TRA and ESO-speech were presented in Fig.6.

Table 4 presents mean evaluation of voice quality and evaluation of vowels quality of the NOR, TRA and ESO speech. The evaluations were estimated according to Fig. 6.

Table 4 - The evaluation of voice quality (VQ) and vowel quality (HQ – high quality. LQ-low quality) of the NOR, TRA and ESO speech.

Speech	VQ SRVE	S.D. (SRVE(v))	Min SRVE(v)	Max SRVE(v)	HQ vowels	LQ vowels
NOR	91% HighQ	6%	85%	98%	a, e, i, o, u, y	-
TRA	53% MidQ	18%	36%	85%	i, y	a, e, o, u
ESO	33% LowQ	28%	2%	75%	y	a, i, o, u, e

The NOR speech is recognized in 91% and can be evaluated as high quality speech. The TRA speech is recognized in 53% and can be evaluated as medium quality speech. The ESO speech is recognized in 33% and can be evaluated as low quality speech. In general, TRA vowels that are correctly pronounced are the /i/ and /y/ vowels. In case of ESO speech, the correctly pronounced vowel is the /y/ vowel – Table 4, column HQ vowels.

Conclusions

The speech recognition process allows for an objective evaluation of the quality of NOR, TRA and ESO speech on the basis of the parameters defined. Automatic speech recognition method can be useful for speech therapist, who can evaluate voice quality of the speaker as well as the quality of vowels. TRA speech obtains better recognition results as ESO speech. In this case TRA speech is closer to the NOR pattern. The TRA speaker can achieve 100% of the vowel recognition. The results of the testing confirmed a similarity between the tracheoesophageal speech and the normal one.

In the recognition process of TRA and ESO speech the pattern of normal speech can be applied, as well as cepstral features can be used as parameters extracted from the signal. Therefore, the process of speech recognition based on cepstral features and DTW classifier with the normal speech pattern can be used for evaluating the quality of voice, and the method of rehabilitation. Acoustic measures computed digitally will always produce the same result for the same input, and when these measures are obtained correctly, they can form a valuable objective adjunct to perceptual evaluations in clinical practice.

References

1.   S. Bień, A. Rinaldo, C. E. Silver, J. J. Fagan, L. W. Pratt, Cz. Tarnowska, E. Topik, N. Weir, B. J. Folz and A. Ferlito, History of Voice Rehabilitation Following Laryngectomy*, The Laryngoscope* 118(3), pp. 453-458, (2008).

2.   C. D. L. van Gogh, J. M. Festen, I. M. Verdonck-de Leeuw, A. J. Parker, L. Traissac, A. D. Cheesman and H. F. Mahieu, Acoustical analysis of Tracheoesophageal voice, *Speech Communication* 47(1-2)*,* pp. 160-168, (2005).

3.   C. J. van As-Brooks, F. J. Koopmans-van Beinum, L. C.W. Pols and F. J. M. Hilgers, Perceptual evaluation of tracheoesophageal speech by naive and experienced judges through the use of semantic differential scales, *Journal of Speech Language and Hearing Research* 46(4), pp.947-959, (2003).

4.   C. J. van As-Brooks, F. J. Koopmans-van Beinum, L. C. W. Pols and F. J. M. Hilgers, Acoustic Signal Typing for Evaluation of Voice Quality in Tracheoesophageal Speech, *Journal of Voice* 20(3), pp.355-368, (2006).

5.   D. A. McColl, Intelligibility of Tracheoesophageal Speech in Noise, *Journal of Voice* 20(4), pp. 605-615, (2005).

6.   R. A. Kazi, V. M. N. Prasad, J. Kanagalingam, C. M. Nutting, P. Clarke, P. Rhys-Evans and K. J. Harrington, Assessment of the Formant Frequencies in Normal and Laryngectomized Individuals Using Linear Predictive Coding, *Journal of Voice* 21(6), pp. 661-668, (2007).

7.   T. Zieliński, P. Gajda, M. Stachura, R. Wilgat, D. Król, T. Woźniak and S. Grabias, Application of HFCC coefficients as Features in Automatic Detection of Pathological Pronunciation, *Measurements, Automatic and Monitoring (PAK)* No. 10Bis, (2006).

8.   P. Świdziński, Usefulness of acoustic analysis in diagnostics of voice disorders - postdoctoral thesis, Poznan University of Medical Sciences, Poland,(1998).

7.4 PROSPECTS OF APPLICATION ULTRASONIC TECHNOLOGIES ARE IN PHARMACEUTICAL INDUSTRY

Strokan A.[1], Burmistenkov A.[1], Misiats V.[1]

In pharmaceutical industry an ultrasound finds application at extraction, dissolution, receipt of emulsions, suspensions, making of microgranules , sterilization, production of ampoules, id est wherein an ultrasound directly

[1] Kyiv National University of Technologies and Design

contacts through a liquid phase with the molecule of matter. Taking into account it, the row of authors determined firmness of medications to the action of frequency vibrations [1].

Any technological process finds wide application in pharmaceutical industry, if he does not violate chemical firmness of medicinal matters. Ultrasonic waves are very specific from this point of view. One preparations under their action lose the properties, other remain neutral, third, opposite, become more active therapeutically. An ultrasound, passing through any environment, creates alternating pressure in him. As a result of molecule of solvent, medicinal matters, different parts and including which are in a liquid, must with frequency of wave repeat her motion. Most medicinal matters are difficult microobjects, which consist of undulating chainlets, rings, radicals. During passing to the ultrasound through such molecule her easy part will hesitate in resonance with frequency of wave, and heavy part will begin to fall behind. As a result there will be areas of tension, considerable forces of friction, which excel forces of chemical connection, the break of integral molecule of matter will happen. Thus, in solution there can be the phenomena of chemical depolymerization, education of new macroradicals, homogenization of snatches et cetera [2]. An ultrasound accelerates the processes of hydrolysis, breaking up, oxidization.

Processes of dissolution. In practice of pharmaceutical factories, plants, pharm productions of dissolution is the most widespread method of treatment of raw material, receipt of the prepared products [1, 2]. In plant terms, and also in large pharm establishments get different solutions of crystalline matters, solutions of dry and thick extracts, alcohols, fragrant water, solutions of colloids, other high molecular connections this method. At operating on the process of dissolution an ultrasound with large intensity in a liquid environment arise up alternating voice pressure, contributory infringement to penetration of liquid in cracks and capillaries of matter which dissolves, and also rapid flows, cavitation. Intensification of process of dissolution, and exactly and coefficient of diffusion depend on the values of amplitude and frequency of the forced vibrations of liquid. At operating dynamic viscidity of arctic liquids diminishes

on an environment to the ultrasound; microcracks and pores, present in a hard phase, branch, their sizes and depth increase.

At the use to the ultrasound as to the mean of intensification of process of dissolution the micropulsations of solvent have a substantial value, especially if a wave-length is equal or less size of hard part or linear sizes of microcracks, pores, capillaries. An ultrasound on two orders accelerates the stage of dissolution of solvends, in 10…30 times – difficult-soluble preparations, in 3…5 times - littlesoluble. For help to the ultrasound at an ordinary temperature 0.25°C) increases limit of solubility in a range difficult and practically nonsolutes, thus the concentration of satiation can exceed the known constants in 5...30 times.

Processes of extracting. Today very much biologically active matters get from natural raw material of vegetable or animal origin. Every third medicinal preparation, from present, in the arsenal of modern medicine is a product of phytogenous. It follows notices also, that in therapy of separate diseases preparations from plants occupy dominant position. An ultrasound in direction from an emitter forms in all wired for sound volume voice wind which creates a common flow (quiet or turbulent), and strength of wind depends both on intensity to the ultrasound and from the parameters of environment [1]. In a period extracting of raw material an ultrasonic effect shows up more clear in all. Powerful ultrasonic waves increase speed of impregnation of different materials which have a capillary structure considerably. It is explained by that the height of getting up of liquid under an action to the ultrasound increases and is in direct dependence on the diameter of capillary and surplus voice pressure. Звукокапілярний pressure regardless of position of source to the ultrasound is always directed for normals to the cut of capillary.

An ultrasound, creating a sound effect, not only accelerates expulsing of such bubbles of air but also creates terms for dissolution of him in liquids. A vacuum appears, id est there is the so-called effect of sponge. As a result time of soakage of raw material under an action to the ultrasound considerably grows short.

On speed of process of extracting biologically of active matters from a digister factors, dependency both upon the physic - mechanical state of raw

material and nature of solvent and from the parameters of wiring for sound, have influence for help to the ultrasound. Processes of making of emulsions. A receipt of emulsion is a labour intensive enough operation which consists in even distribution of one liquid in other. An ultrasound allows to get more proof emulsions as compared to the mechanical dispergating (in a mixer) or treatment a voice whistle. Frequency vibrations allow to get emulsions with the wide range of dispersion of emulsions parts from liquids and matters which do not yield to emulsion. However major other. The emulsions got an ultrasound are proof enough at the protracted storage, crushing of dispersible phase provides the receipt of parts with the sizes of 1…0,5 μm).

Processes of receipt of suspensions. A suspension is a liquid medical form which is kinetically the unsteady coarse-particle system, where a dispersible environment is a liquid (water, alcohol, butters), and a dispersible phase is thin dispersions of hard parts of medicinal matters by the size of not less than 103 нм [3]. Growing shallow for help to the ultrasound it is possible to attribute to the active growing shallow, as parts collapse regardless of their size and closeness. They are torn under the action of frequency vibrations and micro-shocking action of ultrasonic cavitation, thus the exception of large surfaces in a working chamber allows to save the cleanness of initial material.

There is mass disintegration of microbal cages at an action to the ultrasound. Mechanism of steralizing action to the ultrasound very difficult and not exposed fully. Obviously, a leading factor is cavitation which arises up first of all wherein durability of liquid is the least, id est on verge of division of environments cage-liquid. Thus sterilization can be conducted with less economic charges, economy of antiseptics, keeping active matters, enzymes, vitamins biologically, as ultrasonic sterilization is conducted at a subzero temperature.

References

1. Кардашев Г.А. Физические методы интенсификации процессов химической технологии – М.: Химия, 1990. - 208 с.

2. Молчанов, Г.И. Ультразвук в фармации – М.: Медицина, 1980, 176с.

3. Маргулис, М.А. Звукохимические реакции и сонолюминисценция – М.: Химия, 1986. – 300 с.

ALPHABETICAL INDEX OF AUTHORS